AN INVESTIGATION INTO VIBRATION CRITERIA FOR ROTATING MACHINERY.

by

Richard Woods B.Sc. (Hons)

Submitted in fulfilment of the degree of

Doctor of Philosophy.

The University of Aston in Birmingham.

December 1968

Faculty of Engineering

Department of Mechanical Engineering

Head of Department

Professor A. J. Ede.

Supervisor

Professor E. Downham.

S U M M A R Y

Concern had been expressed by engineers of the Shell Chemical Company regarding the validity of existing vibration criteria for rotating machinery.

A survey showed that existing criteria were based solely on the amplitude of vibration, normally of the bearing housings, with no allowance being made for the dynamic properties of the supporting structure.

The feasibility of measuring the mechanical impedance of bearing supports in order to assess the severity of vibration generated by a machine has been investigated. It is suggested that in many cases the oscillatory bearing force levels obtained from these measurements will provide a quantitative indication of severity.

Theoretical and experimental work has been conducted on a model rig, comprising a flexible shaft running in journal bearings housed in flexible, asymmetric supports. The accuracy with which the system behaviour could be predicted using measured support impedances is discussed together with the extraction of uncoupled support impedances from measurements on the complete rotating system.

Access was available to several industrial centrifugal compressors. To enable the bearing support impedances of these machines to be measured on site, considerable attention has been paid to the evolution of a technique involving the use of transient excitation. To develop this technique the model rig and a large rotary converter have been used as test structures. Methods have also been devised and developed for the analysis of the transient impedance data.

An extensive programme of experimental work on the compressors is reported in which support impedances, obtained using the transient approach, were used to estimate oscillatory bearing forces.

ACKNOWLEDGEMENTS.

The writer wishes to thank:-

Professor A.C. Walshaw and his successor as Head of the Department of Mechanical Engineering, Professor A.J.Ede, for permission to pursue the research reported here.

His Supervisor, Professor E. Downham, for advice and encouragement given throughout the course of this project.

The many members of the academic and technical staff who have given their help. In particular Mr.B.Muddyman, whose able and cheerful assistance for long hours under unpleasant working conditions was much appreciated during the field work.

Shell Chemicals U.K.Ltd., for the facilities provided at their Carrington, Manchester, plant. In particular Mr.R.LeWallace, Engineering Services Manager, and Mr.C.Hull for help given during the experimental work on the centrifugal compressors.

Mrs. D. Scott who typed the whole of this thesis.

NOMENCLATURE

b	Viscous damping coefficient.
b_{xx}, b_{xy} etc.	Journal bearing velocity coefficients.
c	Radial clearance.
d	Shaft deflection.
e	Journal eccentricity.
f	Frequency.
k	Linear spring constant.
k_{xx}, k_{xy} etc.	Journal bearing displacement coefficients.
l	Rotor/shaft system dimension.
m	Mass
q	Generalised co-ordinate.
r	Radius.
r	Attitude axis of journal.
s	" " " "
s	Exponent in Hertz relationship.
t	Time
x	Displacement along x axis
x_m	Maximax (absolute maximum) response.
x_R	Maximum response in residual era.
x_F	Maximum response in forced era.
y	Displacement along y axis.
$[A], [B], [X]$	Matrices.
B	Filter bandwidth.
C	Ockvirk's capacity number.
D	Dissipation function.
F	Force.
I	Inertia.
K	Constant in Hertz relationship.
L	Lagrangian Function.

Nomenclature - continued...

M	Rotor mass.
P	Radial load on ball bearing.
P	Load/unit breadth, journal bearing.
Px, Py	Dynamic journal bearing forces.
T	System natural period.
T	Kinetic Energy.
V	Potential Energy.
Z_{ij}	Impedance ($F_j/\ddot{x}_i$)
F(t)	Input time history.
$\overline{F(\omega)}$	Fourier spectrum.
Re	Real part of - e.g. Re ($\overline{F(\omega)}$)
Im	Imaginary part of -
α	Axial displacement of unbalance from rotor C.G.
δ	Approach of tracks, ball bearing.
ε	Journal eccentricity ratio ($= \frac{e}{c}$)
η	Oil viscosity
η	Whirl frequency ratio (App. III)
ψ	Journal attitude angle.
Θ	Phase angle.
θ	Inclination of principal plane (App.IV)
ζ	Viscous damping ratio.
τ	Transient duration.
ϕ	Angular displacement.
ω	Circular frequency.
ω_n	Natural circular frequency.
Δ	Determinant.
Δt	Small time increment.
Ω	Angular velocity of shaft.

NOTE:- Dots indicate differentiation w.r.t. time.

e.g. $\dot{x} = \frac{dx}{dt}$

INDEX

Index - continued...

Index - continued...

Index - continued...

Index - continued...

Index - continued...

Index - continued...

Chapter 1.

Introduction.

1.1 Outline of the Problem.

The work reported here was begun following discussion at The Hague with engineers representing the Shell Chemical Company. The problem discussed was that of ascertaining tolerances for permissible vibration levels on rotating machines. The investigation was concerned with vibration transmitted from the shaft to its bearings, such as that due to unbalance, bearing disturbances and coupling misalignment.

The Shell Company operates millions of pounds worth of rotating machinery in process plant throughout the world, and many of the machines are required to run continuously for periods of up to two years. Apart from the cost of the repair itself, the need to shut down a particular machine because of, for example, a bearing failure, often results in the loss of production from an entire plant. In two installations with which the writer has been concerned, the loss of a day's production was estimated to cost around £20,000. It was therefore of considerable economic importance to ensure, as far as possible, the trouble-free running of the machines involved.

It is conventional practice to use the measured amplitude of vibration at the bearing supports as a basis for the indication of satisfactory running. Various vibration acceptance criteria have been published with which the measured amplitudes may be compared. These criteria normally describe the level of vibration qualitatively in terms such as "very smooth" or, at the other extreme, "too rough to operate".

In writing specifications to be referred to during the commissioning of new plant, for instance, the problem of deciding on an acceptable level of vibration is usually overcome by referring

in turn to published criteria. However, in the original discussion, the Shell engineers had expressed a lack of confidence in existing vibration tolerances and had found that operating within the proposed limits was no guarantee against the failure of a machine.

A survey was therefore conducted by the writer into the means by which the existing, widely-used vibration criteria had been drawn up. It was found that, in all cases, the criteria were based on the subjective opinion of the author concerning the "severity" of vibration of a large number of machines of a similar class. No definite account was taken of the dynamics of the particular machines, and there was no evidence of attempts to relate the measured vibration levels to subsequent failure. In most cases the respective authors clearly stated that the tolerances proposed were but personal opinions of what should be deemed satisfactory.

In view of the considerable complexity of the structures involved it was clear that any pronouncement on whether or not a particular machine might be considered satisfactory would always involve an "assessment" rather than a categorical decision. However, it was considered that two main approaches might be made to obtain more reliable vibration criteria. These were, firstly, a statistical approach in which the vibration history and record of failures of many machines could be correlated over a long period of time. Although, with sufficient data, this approach would presumably yield more reliable vibration criteria, it was considered inappropriate for expensive machines of widely different capacities and types of construction. The second, more fundamental approach, and the one with which this thesis is concerned, was to try to interpret measured vibration amplitudes in terms of the dynamic properties of the particular machine concerned.

In a practical machine the shaft will often run in journal bearings, whose dynamic properties are complex and be supported in turn by a structure which deflects under the influence of shaft-generated forces. The latter effect is, of course, tacitly implied whenever reference is made to the measurement of vibration at the bearing supports.

Provisionally, it might be assumed that the dynamics of the shaft itself could be calculated with good accuracy, whilst, due to recent advances, the properties of the shaft bearings could also be approximately determined. However, except for the simplest of configurations, there seems little prospect of calculating at the design stage the dynamic stiffness, or impedance, of the structure interposed between the shaft bearings and 'earth'. The impedance of the bearing supporting structure occuring in practice is therefore largely fortuitous, as is the amplitude with which the supports vibrate due to the imposition of oscillatory bearing forces.

In an idealised situation, where the bearing supports were, in the absence of the shaft, uncoupled from each other, and in which the amplitude of vibration was measured in the principal planes of the support, a knowledge of the support impedances would allow the oscillatory forces imposed on the bearings by the shaft to be obtained directly. It is noted that for many machines, particularly those with shafts operating at speeds well removed from a critical speed, the maximum permissible bearing force will often be the limiting parameter for safe operation. That shaft bearings are frequently the first casualties of severe vibration supports this contention.

The possibility of measuring the bearing support impedances to enable the bearing forces to be estimated has therefore been investigated A technique has been evolved in which transient excitation was used to measure the support impedances.

For existing machines, and, in particular, several centrifugal compressors belonging to Shell on which the writer has conducted a series of experiments, the above proposal was attractive from a practical view-point since it did not involve any modifications to the machines.

Where new plant is to be purchased, consideration should be given in writing the specifications to instrumentation which will facilitate checks on satisfactory running. For example, transducers to detect the amplitude of vibration of the shaft itself might be installed. In the case of high speed machinery, however, experience suggests that the running frequency will often be close to a major resonant frequency of the bearing supporting structure. The interpretation of measured shaft amplitudes in terms of bearing forces or shaft stresses can therefore be very inaccurate if based on the assumption that the system dynamics are those of a simply supported shaft. Again, a knowledge of the bearing support impedance is required.

1.2 General Approach Adopted for Tackling the Problem.

The work carried out to date has covered the following main areas:-

(a) An investigation into the behaviour of a model rotating machine in which the impedances of the uncoupled bearing supports could be measured using standard, swept-sine techniques. The final configuration employed consisted of a flexible shaft running in hydrodynamic journal bearings housed in massive, flexible, asymmetric supports. It was considered that this system was of an order of complexity reasonably representative of practical machines.

In order to check the validity of the measured support impedances in determining the behaviour of the system, impedances were measured on the complete, assembled structure and compared with theoretical

predictions. Similar comparisons were made for the responses at the supports and at the shaft to unbalance forcing.

Despite the dynamic complexity of the model, good correlation was obtained between theory and experiment. As a general problem in the dynamics of rotating machinery, much of the work reported is believed to be unique - no published, quantitative comparison with analytic predictions being known for a system of the generality considered.

An investigation into the possibility of extracting the "uncoupled" bearing support impedances (i.e. those prevailing in the absence of the shafts) from measurements on the assembled, rotating model has also yielded encouraging results. It is anticipated that this approach may be of considerable value in measurements on full-scale machines where the information must be obtained under normal working conditions.

(b) Since, in general, the dynamic characteristics of bearing supporting structures cannot be calculated, the only practical expedient is to obtain these characteristics experimentally.

To obtain impedance data for the industrial compressors, the use of conventional, swept-sine techniques was precluded - partly due to the difficulties of transporting the large, electrodynamic vibrators and their associated power amplifiers. Also, the time required to set up such an experiment made this approach out of the question.

Early attempts to measure the support impedances of the compressors using a pneumatically-driven, rotary, out-of-balance vibrator also proved unsatisfactory, primarily because of the difficulty of obtaining excitation at the high frequencies required to be compatible with the compressor running speeds.

Attention was therefore turned to the possibility of using transient excitation as a method of measuring mechanical impedance. The advantages of this approach were that both the time required to obtain the "raw" data and the amount of equipment needed on site were minimal. An extensive programme of experimental and theoretical work has been undertaken to develop suitable techniques.

Methods investigated for generating the forcing transient have included the use of an ordinary hand hammer, a captive-bolt pistol and a large "pendulum" hammer. A variety of data-reduction techniques, some believed to be original, have been developed to obtain the Fourier spectrum of the force and response transients.

To provide a comparison between the values of mechanical impedance obtained using the transient approach and those obtained using conventional swept-sine procedures, the model rotating machine and a large rotary converter installed at the University have provided useful test structures.

Very encouraging results have been obtained using the transient approach and, except for certain limitations at low frequencies, the measured impedances agreed well with the swept-sine results.

(c) By using transient excitation, impedance measurements have been made on the bearing and casing supports of the centrifugal compressors. These measurements have demonstrated conclusively that existing vibration criteria, based on amplitude alone, are most unreliable.

Variations in support impedances of about 300:1 have been recorded from one machine to another, which imply corresponding variations in oscillatory bearing force levels per unit amplitude of vibration.

Measurements of shaft-frequency vibration levels over a range of shaft speeds have provided qualitative confirmation of the validity of the measured support impedances.

1.3 Layout of Thesis

This thesis is divided into ten chapters and seven appendices. Diagrams and graphs are included at the end of the chapter or appendix to which they refer. Fig.8.6, for example, is the sixth figure in Chapter 8, Fig.III.1 the first in Appendix III, and so on. A similar numbering system has been adopted for mathematical equations occuring in the text. References, listed numerically in Appendix VII, are indicated as follows:- (1), (27) etc...

The subject matter in each chapter and appendix is briefly outlined below.

Chapter 2.

Technical and historical survey of important literature on the dynamics of rotating machines, with reference to the problems encountered during the present work. In the final section the basis and validity of four existing vibration criteria are discussed.

Chapter 3.

Introduction to the concept of mechanical impedance, and to the interpretation and presentation of experimental impedance data.

Chapter 4.

Theoretical analysis of a rotating machine having massive, flexible, asymmetric bearing supports. The final system considered incorporates a flexible shaft running in journal bearings. The analysis has been used, primarily, as a basis for comparison with the observed behaviour of the model rotating machine.

An outline is given of the digital computer programmes written to obtain system impedances, unbalance response, and to extract the uncoupled support impedances from measurements made on the complete system.

Chapter 5.

Description of the transducers, instrumentation and data-analysis techniques that have been used for periodic and complex vibrations. A discussion of 'harmonic tracking' and swept-sine mechanical impedance measurement systems is included.

Chapter 6.

Experiments on a model rotating machine. Primarily a parametric exercise to investigate the validity of measured, uncoupled support impedances in determining the behaviour of the system. Results compared with analytic predictions of Chapter 4.

Chapter 7.

Experiments on a large rotary converter installed in the University's Electrical Engineering Department. The machine provided a useful test structure for the development of experimental techniques.

Bearing support responses to deliberately-introduced unbalance were compared with values of impedance previously obtained.

Chapter 8.

Theoretical basis for the measurement of mechanical impedance using transient excitation and description of a series of experiments conducted during the development of the method.

Chapter 9.

Outline the data-reduction techniques developed for the analysis of transients to obtain mechanical impedance.

Chapter 10.

Experiments on the six industrial, centrifugal compressor sets. General surveys of vibration behaviour. Bearing support impedances using transient method. Support responses interpreted in terms of machine-generated forces. Case histories of bearing failure and journal bearing instability discussed with reference to measured impedances. Comparison of measured impedances with those quoted in published literature.

Appendix I.

Theoretical analysis of non-linear effect on the measurement of bearing support impedances of a shaft lying stationary in journal bearings. A series of experiments on a simple model are also discussed.

Appendix II

Errors arising in the analysis of transients from filmed records. Effect on the Fourier spectrum of truncation of the response time history. Effect of trace misalignment. May also be important in digital sampling techniques.

Appendix III

Characteristics of ball and journal bearing disturbances encountered on model rig. Discussion of severity in terms of bearing force levels. Analytic prediction of threshold of unstable operation of journal bearing configuration.

Appendix IV

Illustration of the effect on bearing support impedances of coupling between planes of measurement. Coupling expressed in terms of angle of inclination with principal planes.

Appendix V

Tabulated details of the six centrifugal compressors. Running speed, makers' critical speeds, power requirements, casing mass, shaft mass, etc...

Appendix VI

Steady running design calculations for model rig journal bearings. Dynamic coefficients compared with other estimates.

Appendix VII

Numerical bibliography.

Chapter 2.

TECHNICAL AND HISTORICAL SURVEY

2.1 Scope of Survey

Ideally the formulation and application of meaningful vibration acceptance tests on a rotating machine should reflect the best available knowledge accumulated on the dynamic behaviour of rotating machines.

Since the first attempts by Rankine (1) nearly a century ago to explain the whirling behaviour of a shaft carrying a simple disc, an enormous volume of literature has appeared concerned with rotating machine dynamics. Some impression of the rate of growth of interest in the problem may be gauged from fig 2.1. This diagram shows the number of papers containing original contributions listed in three recent bibliographies between the years 1869 - 1967.

Despite the more obvious differences in function and design of industrial flexible shaft machines a similar overall, dynamical model may be considered for analysis purposes. The idealised layout of a typical machine from a vibration engineering standpoint is illustrated in fig. 2.2.

The assumed system in fig. 2.2. is seen to consist of a flexible shaft running in bearings which are in turn housed in some supporting structure, either integral with the stator of the machine or of the independent pedestal type. The machine may be mounted on a foundation structure of re-inforced concrete or, more recently, fabricated steelwork. For some arrangements, the support conditions of rafting or piling in the subsoil on which the foundation is constructed may influence the vibrational behaviour of the complete system.

Aside from the analytic convenience of this subdivision it also serves to emphasise the general categories into which the relevant literature may be placed. Section 2.2. of the discussion of important

literature that follows is therefore concerned with problems relating to the basic dynamics of shafts carried in 'ideal' bearings. In this section literature on the more important secondary vibration effects due to the detailed construction of the shaft is also reviewed.

Section 2.3 outlines the developments in methods for calculating flexural shaft behaviour. Papers on the nature of the supporting condition provided by both rolling contact and hydrodynamic journal bearings are briefly summarised in section 2.4, which also refers to some vibration problems which can be directly attributed to their use.

Section 2.5 is concerned with work on flexibly supported rotors and the effect of foundations, whilst the survey ends by considering the basis and validity of several existing rotating machine vibration criteria which are frequently referred to in specifications.

2.2 The Vibration of Shafts on 'Ideal' Supports.

2.2(i) Pioneering Writers.

Early observations on the behaviour of long line-shafting indicated that, as the rotational speed was increased, severe vibrations occured as some 'critical speed' was approached. It was widely believed, presumably due to lack of knowledge or instrumentation to effect useful reductions in residual unbalance of the flexible shafts, that failure would occur if the shaft was run through this critical speed. The first recorded attempt to explain the nature of the phenomenon was due to Rankine (1) in 1869. He advanced a theory which attributed the 'whirling' speed to a state of indifferent equilibrium, between the elastic restoring force of the shaft and a 'centrifugal' force, when the shaft was rotating at a speed corresponding to its natural frequency. Due to the limited accuracy of calculations and the relatively simple systems considered, the numerical coincidence between the natural frequency of the non-rotating shaft and the observed critical speed was accepted as confirmation of the correctness of Rankins's hypothesis.

These opinions were further hardened by the work of Greenhill (2) who extended the approach in his paper of 1883. The classic experiments of Dunkerley (3) on loaded shafts, reported in 1894, apparently supported the calculations of Osborne Reynolds based on the same pretext. These experiments also enabled him to put forward his empirically derived method for the approximate estimation of the fundamental natural frequency of such shafts.

Nearly thirty five years after Rankine's first publication on the subject, Chree (4) re-affirmed the correctness of the 'indifferent equilibrium' assumption, and devoted the remainder of his paper to the calculation of natural frequencies of shafts with various loadings and end conditions.

Historically, it is interesting to note that both Rankine and Greenhill were trying to explain a phenomenon which, to the best of their knowledge, produced failure of the shaft. Chree and Dunkerley, on the other hand, presumably published their work in the knowledge that the flexible-shafted, single-wheel turbines designed by De Laval (introduced at the Paris exhibition of 1883) ran through and operated well above their fundamental critical speeds.

It was not until 1919, however, that a satisfactory analysis of the whirling shaft was published by Jeffcott (5). In treating the case of light shaft with external damping carrying a single, unbalanced disc with negligible moment of inertia, Jeffcott discussed the geometric nature of the transition through a critical speed. His work was to form the basis of the modern treatment of whirling. Having clearly and satisfactorily explained the dynamics of the problem, other writers were able to investigate more complex behaviour.

The analytic and experimental work of Stodola, presented in his principal work (6), typifies the developments of the early nineteen-twenties. Stodola made many original contributions. He was the

first writer, for instance, to examine the influence of gyroscopic torques exerted by discs of appreciable inertia. His work, however, was often based on the earlier concepts of Chree.

In the same period several authors, such as Kimball and Hull (7), provided experimental verification of Jeffcotts analysis, or, like Morris (8), extended the theoretical analysis of shaft whirl.

A series of papers published by Robertson (10) between 1932 and 1935 summarised the known causes of whirling. To develop his theoretical treatment, Robertson used Jeffcott's approach but considered the motion of the shaft with reference to axes rotating at shaft-speed - a valuable innovation.

Once the pioneering writers had indicated the nature of whirling, subsequent contributors tended to concern themselves with more specific problems so that it is impossible to trace overall progress chronologically. Discussion regarding the behaviour of the shaft itself, followed one of two broad paths. On the one hand are found analyses of the geometric motion of the shaft, frequently with reference to stability criteria, whilst on the other hand methods of calculating speeds were continually being refined to simplify and improve the accuracy of design calculations.

2.2(ii) Secondary Disturbances.

In the first group the influence of internal damping on shaft behaviour has received much attention due to the possibility of unstable operation. The earliest assumption, that the internal damping force obeyed a viscous law, resulted in considerable mathematical simplification and led to the conclusion that rotor motion was stable below the critical speed and unstable at all speeds above it. It was shown, however, that the presence of external damping increased the boundary of instability in a manner directly dependent on the ratio between internal and external damping coefficients.

Various mechanisms of internal damping have been proposed which relax the idealisation of a viscous relationship. Newkirk (11) and Kimball (12) suggested that elastic hysteresis forces, consequent on the change of shaft strain, could act as a form of internal damping and drive the whirl in an unstable manner. A further proposal that a major contribution to internal damping could arise from the use of shrink fits for hubs, couplings and the like, was confirmed in a series of tests by the latter author. (13).

Various authors have proposed that internal damping in real shafts should be considered as arising from a combination of hysteretic, Coulomb and viscous forces. But, bearing in mind the known complexities of material damping alone, such as have been discussed by Pisarenko (16), it seems improbable that the magnitude of these effects could, in practice, be estimated with sufficient accuracy to justify the considerable analytic complications they introduce.

Concise, modern treatments of the influence of internal friction are provided by two authors, Dimentberg (17) and Tondl (18), in books containing translations of their earlier papers. (See also Tang and Trumpler (14), Alford (15)).

Smith (19) observed in his survey paper in 1965 that instability with internal friction as the primary cause had seldom been reported in recent years. Presumably this has been due to precautions taken during design and manufacture to remove established causes.

Flexural Asymmetry

An instability problem of considerable practical significance arises when the shaft has differing stiffness in its two principal planes. Such a condition is inevitable to some extent in all practical rotors, but it is of major significance in electrical machinery. Here, the provision of axial slots for conductors can

produce differences of 30% in the principal stiffnesses, and it has therefore been the practice of manufacturers in recent years to minimise these differences by machining compensating slots in the pole faces of their machines.

Stodola (6) was one of the first authors to consider the behaviour of such an asymmetric shaft carrying a single disc, whilst Smith in his 1933 paper (20) investigated more general aspects of the problem, including the possibility of ranges of shaft instability. Smith indicated that the nature of the resulting vibrations was described, in a stationary co-ordinate system, by linear differential equations with periodic coefficients. Recently published work by Tondl (18) included a treatment of asymmetric shafts having distributed mass, and an elegantly conducted investigation into the combined effects of factors causing shaft instability. He also re-investigated the phenomena of 'gravity whirl' in horizontal shafts and showed that the second-order forcing, arising from the shaft's weight, produced resonance at a shaft speed corresponding to roughly half the arithmetic mean of th. two primary resonant frequencies.

Of more academic interest is the possibility of negative static deflection of a horizontal asymmetric rotor. Tondl's analysis, and the experiments of Bishop and Mahalingam (21), showed that this effect was likely to represent much less than one per cent of the normal static deflection in practical rotors.

Non--stationary vibration.

Several writers have examined the non-stationary vibrations consequent on acceleration through a critical speed, using both experimental and analytic techniques.

The first writer to investigate the problem was Lewis (22), who considered a single-degree-of-freedom system with linear damping during linear acceleration and deceleration through its critical speed. To

solve the equation of motion thus formulated, Lewis resorted to a method of graphical integration. He was able to show that, for any non-zero acceleration, the resonant amplitude was always reduced, compared with the stationary vibration case, whilst the angular velocity at which resonance occured was increased during acceleration and reduced during deceleration.

With the wider availability of digital computers it is generally possible to examine by numerical techniques any system whose equations of motion can be written down. Such a facility has been used by Fernlund (23) for the numerical solution of the equation of motion of a linear system excited in a non-stationary manner (See also, Marples(24))

2.3 Methods of Calculating Flexural Behaviour.

At an early stage in the design of any rotating machine it is necessary to calculate the flexural critical speeds of the proposed arrangement. Improvements in the efficiency and accuracy of methods of calculation have occupied the attention of numerous writers. In cases where the natural frequencies of the rotating shaft are unchanged from the stationary case, the problem reduces to the calculations of those frequencies. For this reason the empirical methods advanced by Dunkerley (3), intended for the fundamental critical speed of shafts carrying concentrated loads, were still in use ten years ago. This despite the fact that they were first published before a satisfactory description of unbalance whirling had been formulated. Dunkerley's method gives the natural frequency accurate to within about five per cent, and is normally lower than the 'exact' value.

The work of Morris (8) (9), first published in 1929, was based soundly on Jeffcott's analysis and included the treatment of more complex systems having several critical speeds. The theoretical and experimental of Downham (25) included developments of Morris's analysis for the calculation of natural frequencies of several more complex rotating systems.

The majority of rotating machines incorporate shafts which have several abrupt changes in section. Some writers have considered each section of such systems in terms of the Euler-Bernoulli beam theory or its extensions. Such an approach has been used in Dimentberg, whilst Bishop (26) uses a similar technique to express the receptances of both uniform and non-uniform shafts in series form.

To overcome the complexities of the purely analytic techniques, and the lack of generality of methods such as Rayleigh's when used for criticals other than the fundamental, a method was put forward by Poritsky and published by Prohl (27) in 1944. Prohl's method for flexural critical speeds is analogous to that of Holzer for torsional vibrations, although necessarily more complicated since the former involves satisfying two boundary conditions at each end of the shaft. Because of its versatility and iterative nature Prohl's method has been widely used as the basis for digital computer programmes for obtaining critical speeds.

In the last ten years or so increasing interest has been shown in the precise notation of matrix algebra for formulating many problems in elasto-mechanics. The main spur to this development has again been the progress in digital computation. Of the various matrix methods evolved the transfer matrix approach is particularly suited to the evaluation of critical speeds. This technique is not new in principle and a paper by Uhrig (28) traces its development from the tabular methods of Holzer and Prohl. It involves deriving matrix equation defining the change in state vector from one side of an element to another, and successive multiplication of a series of such matrices to evaluate the end conditions.

A lengthy catalogue of transfer matrices for both lumped-parameter and distributed elements is given by Pestel and Leckie (29).

Numerical difficulties can occur during computations using transfer matrices since the accuracy of the solution sometimes depends on the difference of two nearly-equal, large numbers. These difficulties are particularly likely to occur where the system includes very stiff terminations (at shaft bearings for instance) or very flexible intermediate elements (e.g. shaft couplings). Such difficulties delayed the widespread practical application of Transfer Matrix techniques but they can now be overcome by the use of modified methods, such as the delta-matrix approach suggested by Fuhrke (30)

2.4 Influence of Shaft Bearings.

Each of the two most commonly used bearings, rolling contact and hydrodynamic journal, is capable both of influencing the whirling characteristics of the shaft and of acting as a source of vibration.

2.4 (i) Radial Rolling Contact Bearings.

These bearings act as spring-like elements interposed between the shaft and bearing support. Their finite stiffness arises primarily from deformation of the rolling element and track. The work of Hertz (31) has formed the starting point for all subsequent theoretical discussion on the contact of such solid elastic bodies. Hertz showed that the mutual approach, δ, of two contacting bodies was related to the compressive load, P, by

$$\delta = K.P^{s}. \qquad (2.1)$$

In equation (2.1) K is a constant for the particular configuration and dependent on the elastic properties of the material and the principal radii of curvature at the contact zone. The exponent s, has the value 2/3 for 'point' contact (ball bearings) and 0.9 for line contact (roller bearings).

The bearing radial stiffness is therefore non-linear, but for small perturbations is determined by the radial load P - normally due to the shaft weight.

In practice the bearing will contain several rolling elements and its load-deflection properties are therefore the result of several individual contacts of the type mentioned above. Longman (32) has published methods of calculating the effective stiffness of multi-element bearings together with a discussion of the effect of radial clearance, axial loading and tilt. Longman's methods give results sufficiently accurate for normal vibration analyses but simplify the geometry of contact in practical bearings.

Other writers have attempted to generalise the theoretical treatment. Recently, Japanese investigators have been particularly prolific, and amongst them Yamamoto, Aoki, Shimuzu and Tamura are of particular note. A paper by the last two authors (34) typifies the approach of several of their contemporaries. In that paper Shimuzu and Tamura, starting from the Hertzian theory, developed expressions for the stiffness of multi-element bearings, including allowance for the effects of varying ball diameter and irregularities in the inner and outer tracks. The applications of theoretical treatments of this type are, however, limited by the difficulties of determining the nature of any particular irregularities arising during normal engineering production. For the majority of cases in the calculation of flexural behaviour, first order approximations, such as Longman's, are adequate. In very high speed applications it may be necessary to consider, at least qualitatively, the secondary effect of centrifugal ball loading. This modifies the radial load carried by each rolling element and therefore alters the operating point on the non-linear force-deflection characteristic (33).

The presence of lubricant in a practical bearing suggests that a rigorous treatment would involve elasto-hydrodynamic contact conditions. But although these effects are of considerable importance to lubrication specialists the influence on effective stiffness appears to be slight (35).

Non-uniformities of rolling elements or tracks may also provide displacement excitation of the rotating shaft at a non-integer multiple of the shaft rotational frequency. Amongst the disturbances more commonly detected with conventional bearing designs are those related to the precessional frequency of the rolling elements ($f_e \simeq 2.4f$), to the cage velocity ($f_e \simeq 0.4f$) or to the passage frequency of individual balls or rollers. Such disturbances can give rise to 'critical speeds' which differ from the flexural criticals excited by rotor unbalance. A series of papers by Yamamoto (36) illustrated the mechanism of several such phenomena.

2.4 (ii) Hydrodynamic Journal Bearings.

Although suitable bearing design procedures are primarily problems in fluid dynamics, increasing interest has been shown by vibration engineers in the properties of journal bearings because of their significant effect on the vibrational behaviour of the shafts they support. The literature on these effects may be placed in one of two broad categories. In the first category are found papers dealing with the non-rigid support conditions provided by journal bearings, whilst in the second are found examinations of the nature of various self-excited and non-linear vibrations to which such bearings are subject.

Dynamic Characteristics.

Nearly half a century ago Stodola suggested that journal bearings might have a significant effect on the location of flexural critical speeds. It has since been established that their principal qualitative effect is to reduce the critical speeds as calculated on rigid supports. Since this phenomenon is particularly apparent at higher critical speeds it has assumed major importance in recent years.

In comparison with the linear elements normally considered in vibration analyses, the dynamic characteristics of journal bearings are extremely complicated. For amplitudes of the journal which are a

significant fraction of the working clearance they exhibit marked non-linearities. Even for very small disturbances they introduce strong coupling between orthogonal axes and differ from ideal elastic components in that their force-displacement properties are non-reciprocal. A general discussion of these effects has been given by Smith (37).

Providing only small journal amplitudes are considered, linear force-velocity-displacement relations in two mutually perpendicular radial planes, x and y, may be written:-

$$\left.\begin{aligned} P_x &= k_{xx}\, x + k_{xy}\, y + b_{xx}\dot{x} + b_{xy}\dot{y} \\ P_y &= k_{yx}\, x + k_{yy}\, y + b_{yx}\dot{x} + b_{yy}\dot{y} \end{aligned}\right\} \qquad (2.2)$$

In general, due to the non-reciprocal properties mentioned above, it is found that

$$k_{xy} \neq k_{yx}.$$

The earliest attempts to allow for the flexibility of hydrodynamic oil films (like that of Hummel (38)) supposed that this could be approximated by a simple linear spring between shaft and support. Such analogues are inaccurate because the velocity dependent forces, which in appropriate cases may be regarded as damping terms, are of the same order as the forces arising from displacements. Approximate representations envisaging single plane spring-viscous damper combinations are also inadequate since they neglect the effect of the coupling terms.

The first reliable estimates of journal bearing dynamic properties were obtained experimentally by Hagg and Sankey (39). They assumed that the bearing behaviour could be expressed by using only the four direct coefficients of qqn.(2.2) above.

i.e. that

$$\left.\begin{aligned} P_x &= a_{xx}\, x + b_{xx}\dot{x} \\ P_y &= a_{yy}\, y + b_{yy}\dot{y} \end{aligned}\right\} \qquad (2.3)$$

Hagg and Sankey's tests were performed on a rig incorporating a journal with its axis vertical and having some unbalance. The forcing appearing in eqn. (2.3) above therefore arose from the unbalanced condition and was at the frequency of rotation of the journal. Hagg and Sankey's coefficients therefore included the effects of the neglected cross-coefficients, and thus were only applicable for forces rotating at journal speed. Providing they are used in this sense, for example for unbalance excited critical speed calculations, no error is introduced.

No author has reported a successful attempt to measure all eight coefficients in eqn.(2.2).

Various approaches have been tried by different authors in analytically determining the linear dynamic coefficients for small journal motion. In recent years investigators have tended to favour a particular type of analysis based on certain assumptions. These papers start the calculation from Reynold's equation in the form

$$\frac{\partial}{\partial x}\left(h^3 \frac{\partial p}{\partial x}\right) + \frac{\partial}{\partial z}\left(h^3 \frac{\partial p}{\partial z}\right) = 6\eta U \cdot \frac{dh}{dx} - 12\eta U_o \ldots\ldots \quad (2.4)$$

Eqn.(2.4) relates the normal pressures, p, acting on the bearing surface in the circumferential (x) and axial (z) directions with the tangential velocity (U) of the upper surface and the film thickness (h) at any point. The term $12\eta U_o$ allows for the effect of transverse journal velocity U_o. This term is often referred to descriptively as the 'squeeze film' term.

In addition to the usual assumptions made in deriving eqn.(2.4) (see Barwell (40)) it is further assumed in this type of analysis that:-

(i) the dynamic characteristics may be expressed by linear relationships like eqn. (2.2) above.

(ii) the displacement dependent terms may be obtained by differentiation of the appropriate steady running conditions.

(iii) the velocity dependent terms are governed by 'squeeze film' effects.

Sternlicht (41), Holmes (42), and Morrison (43) typify this type of approach. Sternlicht concentrated on the dynamic properties themselves whilst Holmes discussed their influence on the behaviour of a rigid shaft. Morrison's work was inspired by a particular industrial problem in which the observed flexural critical speed of a turbine generator differed appreciably from that calculated assuming knife edge supports.

Both Holmes and Morrison assumed that Ockvirk's short bearing theory was applicable, and both considered the possibility of instability due to the non-conservative nature of the coefficients. Smith has given a qualitative description of the exchange of energy which produces such instability (37). Amongst his other contributions Smith has also extended the linear analysis to include the effect of lubricant inertia (44). He concluded in that paper that the inertia terms may be significant for short, stiff rotors carried in wide bearings.

Two recent papers by Morton (45, 46) discussed in much more general terms the formulation and solution of equations of motion for flexible shafts carried in journal bearings. Morton concluded from his theoretical and experimental work that journal bearings cause the appearance of pairs of critical speeds which, due to the effect of non-reciprocal coupling, may be detected anywhere in the system. He observed that both these critical speeds were lower than those obtained in the absence of journal bearings, and that they were heavily damped.

All the above writers concerned themselves with plain, cylindrical bearings in which the oilflow was laminar.

Morton and Sternlicht obtained the dynamic coefficients by numerical, finite-difference solutions of Reynolds equation. A similar procedure may be used for multi-section bearings with more complicated oil-film boundary conditions.

The journal bearings of the latest generation of turbo-generators operate well into the turbulent regime. It is probable that as the operating speed of other classes of machines are increased, turbulent oil film conditions will be encountered more frequently in the future. The available evidence (e.g. Smith (37)) suggests that at least there is no obvious discontinuity in dynamic behaviour during transition from one type of flow to the other, although measurements of power loss, oil film temperature etc., may indicate the transition.

Journal Bearing Instability and Non-linear effects.

The identification of self excited vibrations due to journal bearings was due to Newkirk (11) who, with Taylor (13), examined the problem experimentally and gave a much-simplified theoretical explanation. A similar, but more directly presented, analysis has also been given by Hagg (47). He showed, from considerations of flow continuity alone, that a journal bearing has a fundamental tendency to orbit in a forward direction about the bearing centre at a frequency half that at which it rotates about its own axis. Many apparently contradictory experimental and theoretical estimates of the location of the point of self-excited oscillations were subsequently put forward.

In recent years it has been recognised that the dynamics of the complete shaft-bearing system must be considered if quantitative estimates are to be obtained. In particular, the relative magnitudes of elastic shaft forces and hydrodynamic oil forces was emphasised by Hori (48). He also pointed out the need to distinguish between small-amplitude vibrations just below the threshold of self excited whirl and

the very large-amplitude motion occuring when the whirl had been established. Non-linear effects are of major importance in the latter.

The condition for stability for both small and large (non-linear) amplitude vibrations has been discussed by Soneya (49). He used numerical integration techniques to solve the equations of motion, including the non-stationary problem associated with the build-up of large amplitudes at the boundary of instability.

The characteristics which serve to identify self-excited bearing vibrations may be summarised as follows:-

(a) They are usually much more intense than those associated with the flexural critical speeds of well balanced rotors.

(b) For flexible rotors they only occur when operating above the first flexural critical speed.

(c) The rotational speed at which self-excited vibration is induced depends greatly on the particular bearing design, but under the most adverse condition is usually somewhat lower than twice the critical speed.

(d) The phenomenon is not a resonance and, once established, self-excited vibrations persist with almost equal severity as the speed is raised.

(e) The frequency of the resulting vibration, when first established, is close to the natural frequency of the rotor.

(f) Self-excited vibrations exhibit a 'hysteresis' effect - the boundary of instability is lower when decreasing speed.

Despite the wide theoretical attention the problem has attracted, the practical solution has been, for many years, the use of bearing designs which have been found, empirically, to prevent self-excited vibrations - or at least increase the speed at which they occur.

An extensive series of tests by Tondl (18) led him to conclude that almost any departure from plain cylindrical bushings improved resistance to self-excited vibration. He found that multi-element, 'tilting pad' designs were the most successful.

The non-linear bearing forces can give rise to sub- and super-harmonic resonances. 'Jump' phenomena due to the curved backbone of the response curves have also been detected. The most frequently occuring sub-harmonic is of order one half. Analogue computer solutions of Reynolds equation by Huggins (50) showed the possibility of a range of similar sub-harmonic vibrations of order one third, one quarter and so on.

Although sub-harmonic resonance has in the past been confused with self excited vibrations, the non-linear effects have very different characteristics, as outlined below:-

(a) They are true resonances, occuring over a limited speed range, and are normally much less intense than the corresponding first order vibration.

(b) Unlike self-excited vibrations, they are directly affected by the state of balance of the shaft.

(c) They are vibrations at an exact integer multiple or submultiple of the rotational frequency and therefore, unlike the self-excited type above, appear as periodic vibrations.

2.5 Non-rigid supports and Foundations.

For a simple system, consisting of a point mass mounted on a massless, flexible shaft, the introduction of flexible (spring) supports which are equally stiff in all radial directions normal to the shaft axis presents no analytic difficulty. The critical speed is lowered but the shaft motion is characterised by a direct extension

of the simple Jeffcott analysis. The single unbalance whirl has a forward precessional motion.

In practical machines it was very unlikely that the bearing supports will be perfectly symmetric. The complications arising from lack of symmetry have been examined for the case of a cantilever shaft, by Downham (25). He showed that there then existed two natural frequencies, corresponding to the direction of maximum and minimum stiffness, both of which could introduce a critical whirling speed. The region between the critical speeds was shown theoretically and experimentally to be characterised by precession in the opposite sense to the shaft rotation, consequent on the 180° phase change in the most flexible direction of vibration. Due to the lack of symmetry, criticals appeared as elliptic whirls.

The same conclusions were reached by both Dimentberg (17) and Yamamoto who discussed particular solutions of the equations of motion of a non-symmetrically supported shaft in terms of the vectors representing forward and reverse precession. Dimentberg also examined the stability of such a system under the action of various forms of internal damping. He showed that, although the elastic mounting itself could not produce instability, the possibility could arise where the ratio of external to internal damping was small. For real machines external damping is normally many times greater than the internal component and this type of instability is therefore unlikely.

Foundations

A more general treatment of flexibly supported shafts has been published by Tondl (18). After reviewing the case of a simple shaft on symmetric and non-symmetric supports, he then considered the behaviour of a frame foundation having a rigid table. He extended this work to a non-symmetrically supported shaft which itself was not equally flexible in all radial planes - a problem of considerable mathematical

difficulty. Tondl also analysed the vibration of shafts on non-linear foundations - work which the present writer believes to be unique.

Tondl's experimental and analytic investigation of the properties of a simple foundation led him to conclude that coincidence between shaft and foundation natural frequencies resulted in the beneficial use of foundation damping by limiting the relative shaft amplitude. He could find no simple relationship, however, between relative shaft-foundation amplitudes for different degrees of foundation tuning.

Since typical foundation designs may involve as many as twelve natural frequencies in one plane (51) (52) it seems unlikely that any detailed information could be extracted by representing their behaviour by a single natural frequency.

Attention to the design of foundations with regard to their dynamic properties has increased rapidly in the last fifteen years. A review of the major historical developments has been given by Haupt and Probst (52). They traced the changes in design from the early, solid concrete block foundations through the period when reinforced concrete foundations were first introduced, up to the latest practice of using prefabricated steel foundations.

Early patterns used well-established constructional methods, whilst the first attmpts to minimise vibration in rotating machines were the use of cork mats between the concrete block and supporting raft. To obtain a compromise between the ideal, very flexible foundation and the problems of alignment, modern reinforced concrete foundations incorporate a rigid table supported on flexible columns. This practice results in a very massive base for the machine which minimises the reduction in bearing forces that would otherwise be achieved. The recent introduction of all-welded steel foundations of cellular structure appears to be a useful technique in producing light, rigid supporting tables.

A paper by Fitzherbert and Barnett (53) concluded by recording the views of the Central Electricity Generating Board on the relative advantages of steel and concrete foundations. Despite the increased cost, at present, they favour the wider use of steel foundations, which offer a greater resistance to thermal distortion, more rapid construction on site, and a greater flexibility in design.

Because the density and elastic properties of steel are much more accurately known at the design stage than those of concrete, calculation of the dynamic properties of foundations manufactured from steel are more reliable. Adjustments in the stiffness of steel foundations can also be carried out after construction with relative ease. However, out-of-balance excited resonances are likely to be more severe for steel foundations because of their reduced damping capacity. Major (54) has stated that, for several foundations investigated, concrete foundations showed magnification factors about half that of steel foundations.

Many writers have reported methods for the measurement and calculation of foundation dynamic properties. Vesselowsky (55) has described experiments using out-of-balance exciters to estimate the modes and natural frequencies of a steel turbo-generator foundation, whilst Hull (56) discussed some experiments on non-rotating models which had been used to simulate the properties of full-scale foundations. A paper by Pust (57) advocated the use of scale models constructed from 'Perspex'. Pust obtained natural frequencies agreeing within 5% between scale model and full-scale structures. Weber (58) has outlined the application of transfer matrices in digital computation for calculating dynamic properties. He illustrated the efficiency of the method by sample computations for both model and full-scale foundations.

Most of the above writers concerned themselves primarily with estimating natural frequencies. Whilst there is no doubt that many natural frequencies may exist in the running speed range of practical installations, their significance in terms of severity of forced vibration is problematic. A series of papers by Schaff and Krieb (59) reported comparisons between steel and concrete turbine foundations. Their results indicated that many of the calculated natural frequencies were either undetectable or associated with very shallow resonances. Similarly, Morton (45) has tentatively suggested that the influence of reinforced concrete foundations on turbo-generator rotor behaviour was slight.

The effect of the soil on which the foundation stands has also been the subject of much discussion. Apart from the additional flexibility involved it is claimed that a significant fraction of the total energy dissipation is associated with soildeformation (see Eastwood for example (60)). One of the earliest papers dealing with soil dynamics, as applicable to machine-foundation vibrations, was that of Crockett and Hammond (61). They introduced the concept of 'soil natural frequency' and supported their argument with experimental results on several industrial installations. Although their concepts have been severly criticised on theoretical grounds, they do appear to concur with observed behaviour. More elaborate theoretical treatments which consider the soil as a semi-infinite elastic medium are also available (62).

2.6 Existing Vibration Criteria.

Several published papers present information on vibration levels which purport to represent the boundaries of satisfactory or unsatisfactory running conditions. Three such vibration criteria for rotating machines, which are frequently referred to in machine specifications, are reviewed below.

Rathbone 1939 (63)

The tolerances given in this paper were devised and used as a code of practice for insurance underwriters. In common with many published criteria, those proposed by Rathbone were presented in the form of a chart showing vibration amplitude against rotational frequency. Rathbone's chart is reproduced in Fig.2.3 from which it can be seen that areas are marked in order of assumed severity - 'smooth', 'slightly rough', 'too rough to operate' - and so on. The vibration tolerances presented were intended to be estimates of vibration likely to cause damage, as opposed to nuisance.

The information on which the chart was based had been obtained by tabulating the opinions of - 'several practical engineers and inspectors' - as to the smooth running or otherwise of a number of machines of various types. Rathbone compared each tabulated assessment with simultaneous vibration records taken with a hand-held vibrometer placed at the bearing supports of the machines.

Rathbone was aware both of the limitations of the vibration measuring equipment available to him at the time, and of the questionable validity of any assessment of satisfactory operation based on the measurement of bearing amplitude alone. He suggested that resonance of the structure could serve to allow increased tolerances and that machines particularly sensitive to unbalance vibration might require a criterion based on residual unbalance.

Rathbone's experience of machinery operating at speeds above 5000 r.p.m. was slight, but it appeared reasonable to him to extrapolate the proposed curves with amplitudes proportional to $f^{-1.7}$, where f was the rotational frequency. He observed that at frequencies between about 10c/s and 60c/s his proposed tolerance curves closely followed previously suggested criteria for permissible vibration levels in buildings. It is interesting to note that in this region they are also very similar to

several curves illustrating human sensitivity to vibration, such as those put forward by Reiher and Meister (64). Such an agreement might be expected, bearing in mind the subjective nature of the original assessments on which his chart was based.

At frequencies below 10 c/s Rathbone's tolerances approach constant amplitude, and he pointed out that any other relationship, dependent on frequency, would permit very large amplitudes at low frequencies.

Rathbone did not attempt to specify the cause of vibrations for which his criteria were to be applied and he made no reference to any form of wave-analysis on the vibrometer records. His criteria are, however, frequently interpreted as applying to first order unbalance vibration only.

Yates 1949 (65)

Yates suggested vibration acceptance criteria which, like those of Rathbone, were based on subjective opinions. He derived his values from many tests on marine geared turbines and it was specifically for that class of machine that the criteria were intended.

Yates proposed that the parameter to be used in assessing relative vibration intensity should be velocity, and he supported that argument with several examples of simple vibrating systems. In the examples he demonstrated that dynamically similar systems, having equal vibration velocities, were equally stressed when vibrating in the same mode.

Yates' tolerances are plotted in fig.2.3 (to the same scale as Rathbone's for the sake of comparison) and it can be seen that he used similar descriptive assessments to indicate the severity of vibration.

Although, by modern standards, the equipment for vibration analysis available to Yates was rather crude, he demonstrated the usefulness of accurate frequency analysis and the need to examine the vibration spectrum for successful diagnosis. He discussed the design of several

instruments he had found of practical value, including a highly selective wave analyser and an ingenious type of wave correlator, which functioned as a narrow band filter.

Yates' criteria were widely accepted and formed the basis of the P.A.M.E.T.R.A.D.A. scale which is also still in common use.

V.D.I. Directive 2056 (66) 1957

The German V.D.I. is one of few similar organisations who have attempted to catalogue opinions on acceptable vibration levels for rotating machines. The above directive is one of the most exhaustive. It was intended to provide guidance to manufacturer and customer in reaching agreement on both the vibration levels to be accepted and the method of measurement.

The directive was compiled from previously published criteria for five separate classes of machine. Those for power generating and process machinery on - 'heavy rigid foundations' - (Group G), were taken directly from Rathbone's work mentioned above. Rathbone's tolerance curves were approximated, however, by straight line, constant-velocity boundaries and the maximum rotational speed quoted was 12,000 r.p.m. - an increase of some 140 per cent on Rathbone's stated limit of experience (see fig. 2.4).

The directive placed no restriction on the type of vibration measured and suggested that, where several frequency components were present, an r.m.s. measurement of the complex signal should be taken and compared with the given criteria.

In opting for a criterion based on velocity, the directive cited Yates' conclusion that, on the basis of geometric similarity, such a standard also represented equal 'severity'. It was also observed that such vibrations were, from experience, felt to be of approximately equal value.

In applying the tests for severity presented in V.D.I.2056 the user was allowed considerable latitude. Twice as large vibrations were considered permissible in the horizontal direction and axial vibrations were also to be evaluated less stringently. The proposed criteria were only for an assessment of vibration on non-rotating parts (preferably the bearing housings) whilst the flexural vibrations of the shaft itself were excluded. Apart from observing that 'bearing disturbances' could be important no mention was made in the directive of possible causes of vibration in rotating machines.

Many companies who operate or manufacture rotating machinery have compiled their own standards for acceptable vibration levels. These are frequently based on criteria like those mentioned above or on a mean of several such published suggestions. Fig.2.4. shows a typical tolerance chart which is used by the Shell Chemical Company. The chart is referred to in day-to-day 'preventive maintenance' measurements and during the commissioning of new machinery. It can be seen that these tolerances represent a midway assessment between those of Rathbone and Yates (P.A.M.E.T.R.A.D.A.)

All the above vibration criteria are based on subjective opinion with no reference to subsequent failure of the machine concerned. The maximum level of vibration considered permissible varies appreciably from one criterion to the next - as might be expected in view of the different classes of machinery involved. For example, the point marked in figs.2.3 and 2.4., representing 10^{-2} in p.p at 22.5c/s (0.5 in/s r.m.s.), is judged 'slightly rough' according to Yates and 'rough - correct immediately' according to Rathbone. The rather vague description used for the level of vibration, and the fact that these criteria are often misquoted to apply to machinery of a class other than that for which they were intended, adds to the difficulties of applying them in practice.

Most important of all, apart from the most general of references in the original papers, no allowance is made for the dynamic properties of the

bearing supports on which the vibration is measured. From the method by which these tolerances were derived they appear to be more appropriate as criteria for the 'unpleasantness' of vibration.

Number of Papers Listed in Three Recent Bibliographies by J.L.Darker and A.Gommersall (I.Mech.E. Library Refs. May 1967 P 531.32016)

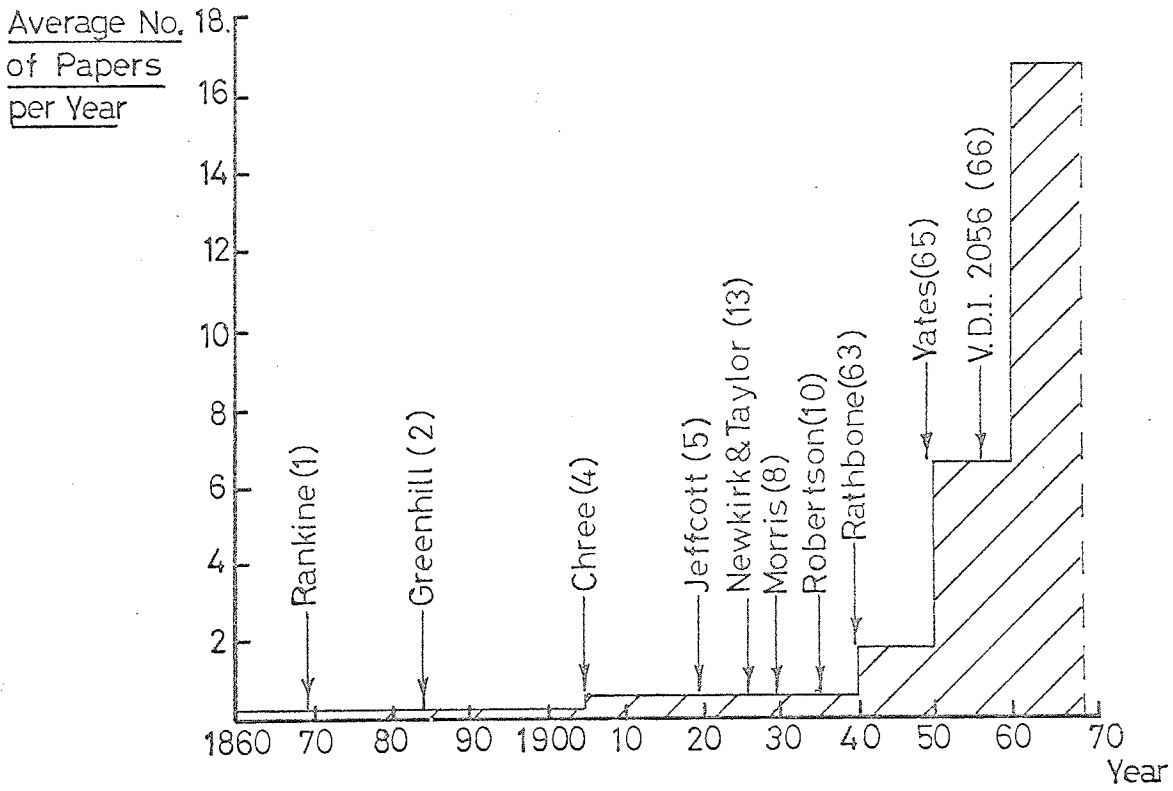

FIG. 2.1 INDICATION OF GROWTH OF LITERATURE ON VIBRATION OF ROTATING MACHINERY

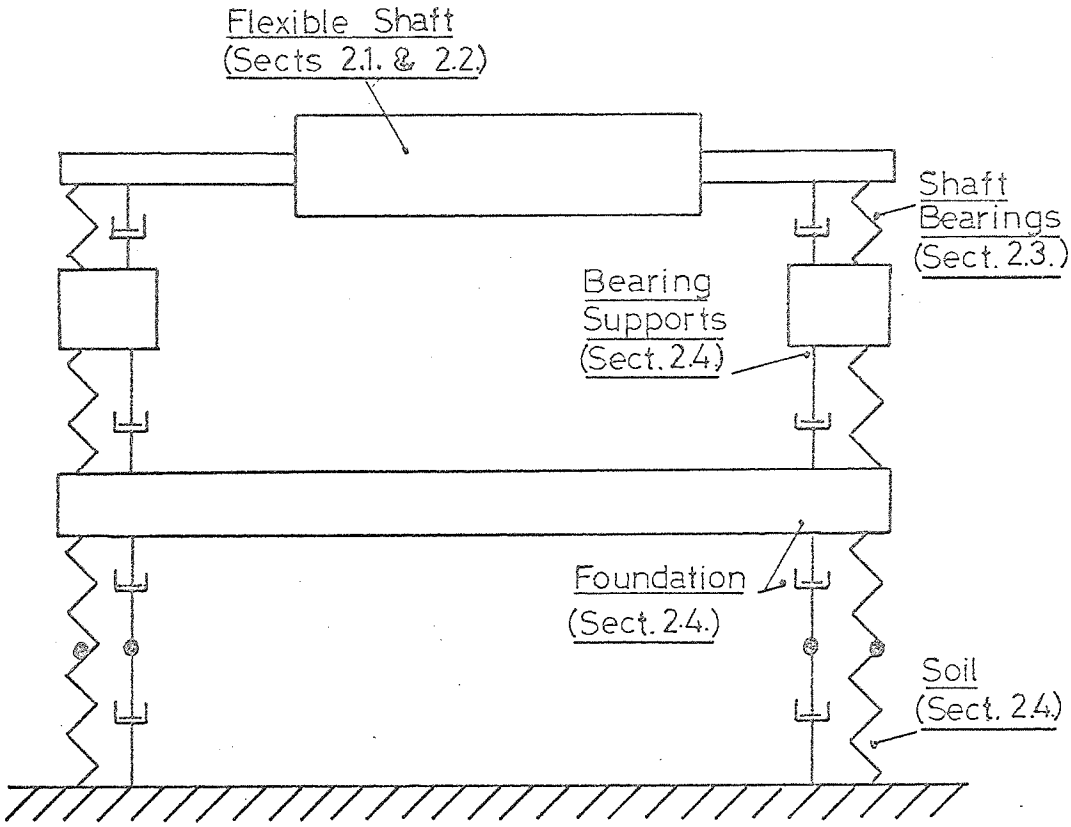

FIG.2.2 SIMPLIFIED MODEL OF ROTATING MACHINE FOR VIBRATION ANALYSIS.

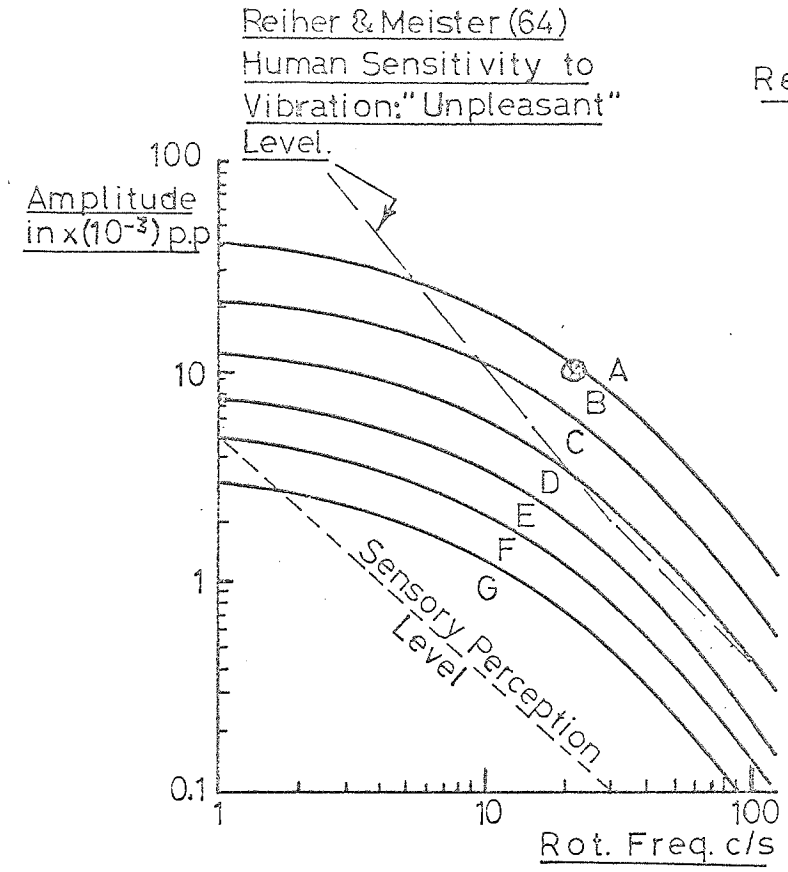

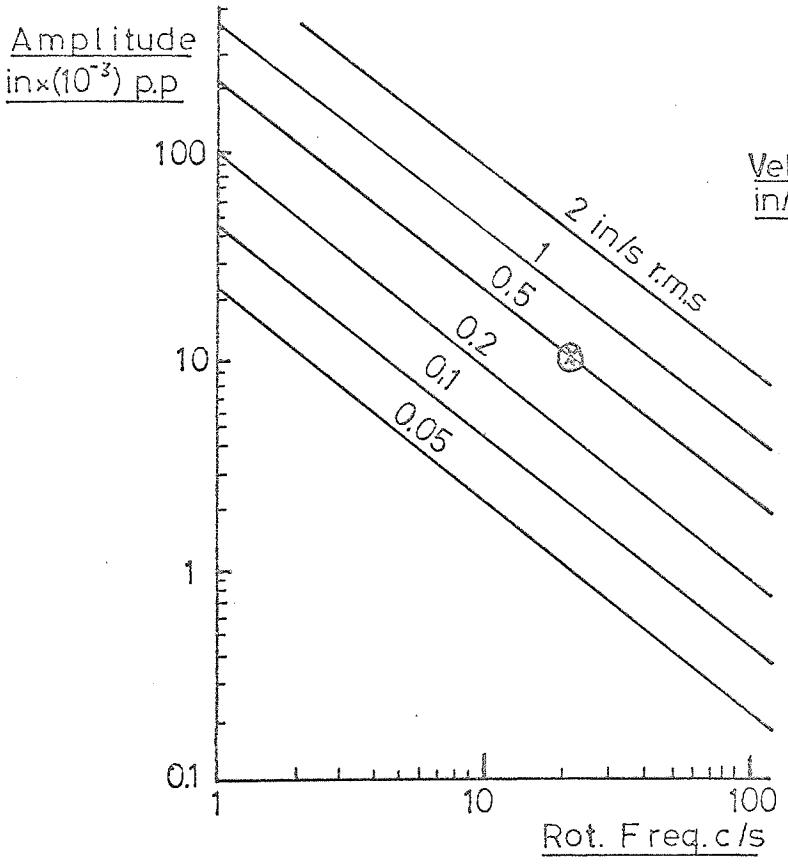

FIG.2.3 VIBRATION CRITERIA FOR ROTATING MACHINES PROPOSED BY RATHBONE AND YATES.

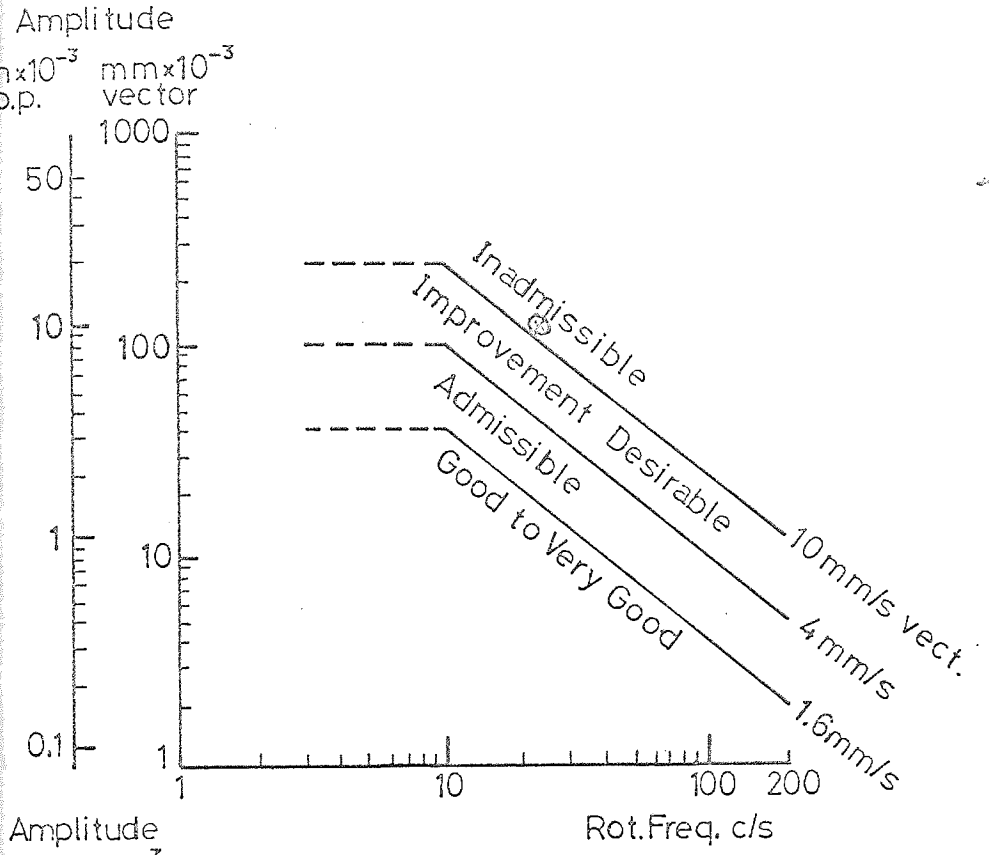

(a) V.D.I. 2056

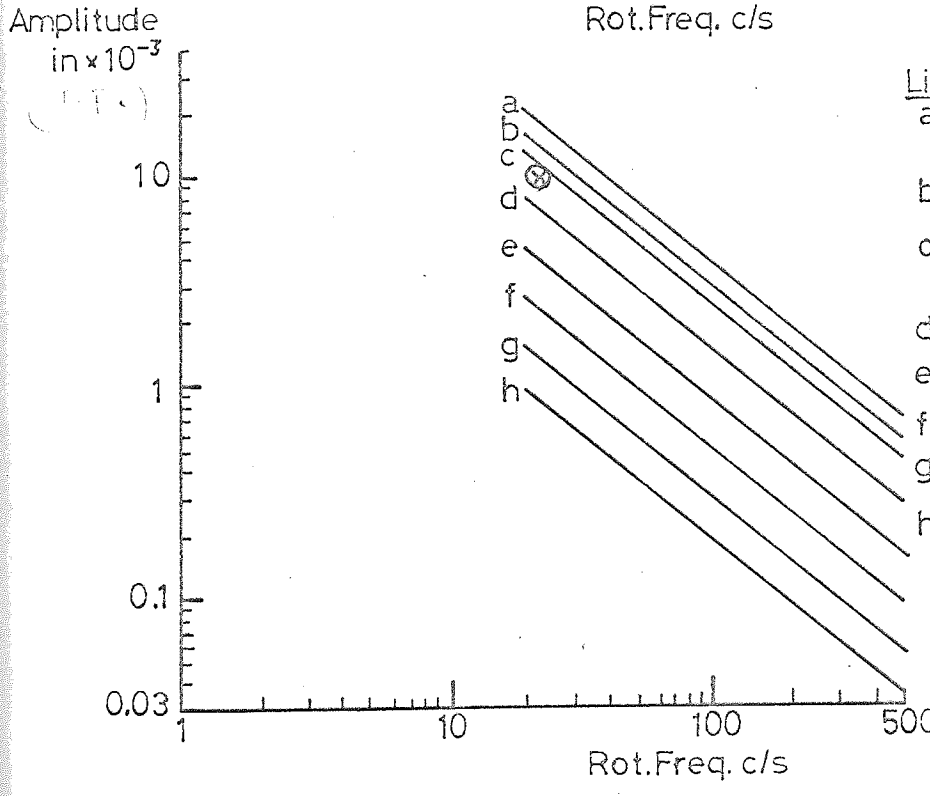

Line	Condition
a	Shut Down & Correct Immediately
b	Investigate & Correct
c	Limit of Continuous Operation
d	Slightly Rough
e	Fair
f	Good
g	Very Good
h	Spins Like a Top

(b) SHELL, CARRINGTON

FIG. 2.4 VIBRATION CRITERIA FOR ROTATING MACHINES. V.D.I. 2056 AND SHELL CHEMICALS, CARRINGTON.

Chapter 3.

Mechanical Impedance .

3.1. Outline of the Impedance Approach

During the last two decades considerable interest has been shown in the concept of mechanical impedance for the analysis of vibrating systems (67). Using this concept, the steady state behaviour to a sinusoidal excitation is described by the ratio of force to response. This ratio is, in general, complex, containing information regarding both phase and magnitude.

The earliest applications of impedance methods to mechanical systems relied on their conversion to analogous electrical circuits (69). The approach was later applied, using only mechanical properties, to the analysis of torsional vibrations. In recent years, a more comprehensive theory has developed, which enables the analysis of both lumped-parameter and distributed systems to be accomplished directly in terms of mechanical impedance. In particular, the network theorems and circuit transformations of electrical engineering theory have been translated into mechanical terms (70).

The main advantages claimed for mechanical impedance methods are:-

(i) the 'black-box' approach enables the effect of changing system parameters to be assessed without, as in traditional methods, re-writing the equations of motion.

(ii) A clear, physical picture of the behaviour of the system may be obtained - especially where the schematic circuit diagram notation is used.

(iii) Experimental data in graphical or numerical form may be introduced directly into the analysis.

Advantage (i) is certainly of importance in hand calculations for simple configurations, but for more complex arrangements this facility is common to many computational methods, for example the transfer matrix approach.

In the writer's opinion, the last two points are the most important in the examination of practical problems. Use is made of these properties in discussing the behaviour of the system considered in this thesis.

The measurement and presentation of impedance data may be made with reference to force per unit displacement ($^{F}/_{x}$), force per unit velocity ($^{F}/_{\dot{x}}$), or force per unit acceleration ($^{F}/_{\ddot{x}}$). Various terms have been suggested for ratios involving particular response parameters, a list of the more common ones being given by Salter (73). In this thesis, the term 'impedance' is used to signify the notion of a complex force-response ratio, normally frequency dependent, without reference to the particular response parameter used or its units. Since experimental measurements of response were invariably made using accelerometers, the ratio quoted is pounds-force per unit gravitational acceleration i.e. 'apparent mass'.

In accordance with convention, the results of impedance measurements or calculations are plotted against frequency on log-log graph paper. In these axes the characteristics of the normal, linear, lumped-parameter elements-spring, viscous damper and mass, - appear as straight lines having slopes -2, -1 and 0 respectively.

These characteristics are verified below and illustrated in fig.3.1

Ideal Spring

The ideal spring (fig.3.1(a)) is assumed to have linear force - displacement relationship such that

$$\frac{F}{(x_1 - x_2)} = \frac{F}{x} = k, \text{ the spring stiffness.}$$

If the applied force, F, is sinusoidal then

$$F = F_o\, e^{j\omega t}$$

$$\text{or} \quad x = \frac{F_o . e^{j\omega t}}{k}$$

$$\text{and} \quad \ddot{x} = -\omega^2 . \frac{F_o . e^{j\omega t}}{k}$$

The acceleration is therefore also sinusoidal and the vector acceleration amplitude $\ddot{x}_o$ is given by

$$\ddot{x}_o = -\omega^2 . \frac{F_o}{k}$$

Thus acceleration impedance, $\dfrac{F_o}{\ddot{x}_o} = \dfrac{-k}{\omega^2}$ (3.1)

i.e. a real quantity inversely proportional to the square of the excitation frequency. The negative sign indicates that the acceleration is in anti-phase with the applied force.

Viscous Damper.

Referring to fig.3.1(b), the applied force is

$$F = b(\dot{x}_1 - \dot{x}_2) = b\dot{x}$$

For a sinusoidal force, $F = F_o . e^{j\omega t}$

$$\text{then} \quad \dot{x} = \frac{F}{b} = \frac{F_o . e^{j\omega t}}{b}$$

which is also sinusoidal, and

$$\ddot{x} = j\omega . \frac{F_o . e^{j\omega t}}{b}$$

Thus the vector acceleration $\ddot{x}_o = j\omega . \dfrac{F_o}{b}$

whence the acceleration impedance, $\dfrac{F_o}{\ddot{x}_o} = \dfrac{b}{j\omega}$

$$\text{or} \qquad \frac{F_o}{\ddot{x}_o} = -j . \frac{b}{\omega} \qquad (3.2)$$

The apparent mass of viscous damper is therefore an imaginary quantity, indicating a quadrature phase relationship.

Mass.

In contrast to the spring and viscous damper, the ideal mass is a single ended element since it is a rigid body. It is conventional in impedance calculations to represent the ideal mass as shown in fig.3.1(c), having one end rigidly attached to an inertial frame of reference.

Since $F = m\ddot{x}$

for a sinusoidal force, $F = F_o e^{j\omega t}$

we obtain the acceleration impedance $\frac{F_o}{\ddot{x}_o} = m$ (3.3)

i.e. a real quantity in phase with the exciting force and independent of frequency.

An impedance terminology, distinction is made between two forms of impedance. The first of these is a driving-point impedance in which the response of interest is at the same point at which the force is applied. Using double suffix notation we write

Driving-point impedance at point 1. $Z_{11} = \frac{F_1}{\ddot{x}_1}$ (3.4)

The other impedance of interest is the transfer impedance, in which the force at point 1 is considered with respect to the response at another location, point 2.

Transfer impedance $Z_{21} = \frac{F_1}{\ddot{x}_2}$ (3.5)

3.2 Measurement and Interpretation of Test Data.

The most direct way of measuring the mechanical impedance of a structure is to excite the system harmonically at the frequency of interest and to measure both the resulting response and the phase relationship between it and the applied force. Fig. 3.3. shows a simple arrangement that could be used which employs a Lissajou figure technique for measuring the phase angle. Voltmeters 1 and 2 record the electrical analogues of force (F), and acceleration ($\ddot{x}$). The complex impedance is therefore obtained in terms of its magnitude, $|Z|$, and phase angle, θ.

$$\text{Thus } Z = \text{Re}(Z) + j\text{Im}(Z) \tag{3.6}$$

$$\text{and modulus of } Z = |Z| = \sqrt{\text{Re}^2(Z) + \text{Im}^2(Z)} \tag{3.7}$$

$$\text{whilst phase angle, } \theta = \tan^{-1}\left(\frac{\text{Im}(Z)}{\text{Re}(Z)}\right) \tag{3.8}$$

More elaborate impedance measuring equipment, available commercially, incorporates band-pass filtering of the force and response signals together with automatic plotting facilities. This type of equipment has been used by the writer and is discussed in Chapter 5. The use of transient excitation to obtain mechanical impedance has also been investigated by the writer. These techniques are reported separately in Chapters 8 and 9.

The type of impedance plot obtained from two simple systems is now discussed to illustrate the information they contain.

System (a) Damped Single-degree-of-freedom.

The arrangement under consideration is shown in fig.3.2 in both conventional and impedance representations. Since the elements of the system have identical accelerations at point 1 they are connected in

parallel. The resultant impedance is therefore obtained by adding the impedances of the individual elements.

$$\text{Thus } Z = Z_m + Z_k + Z_b \tag{3.9}$$

$$\text{or } Z = m - \frac{k}{\omega^2} - \frac{j.b}{\omega} \tag{3.10}$$

$$\text{whence } |Z| = \sqrt{(m - k/\omega^2)^2 + \left(\frac{-b}{\omega}\right)^2} \tag{3.11}$$

$$\text{and phase angle, } \theta = \tan^{-1} \frac{-b}{\omega(m - k/\omega^2)} \tag{3.12}$$

The impedance and phase angle curves that would be obtained for this arrangement are also shown in fig.3.2. At low frequencies it can be seen that the impedance modulus approaches the line

$$\frac{F}{x} = \frac{-k}{\omega^2} \tag{3.13}$$

and the system is then said to be 'spring controlled'. At high frequencies the impedance curve is asymptotic to the line

$$\frac{F}{x} = m, \tag{3.14}$$

when the system is 'mass controlled'

If the system is excited at its natural frequency, the damping force controls the behaviour of the system. The impedance at this frequency therefore indicates the value of the damping coefficient, b.

System (b). Two degree-of-freedom analogy of a Rotor-Bearing Support Arrangement.

The interpretation of impedance plots may be extended for more complex systems. Consider, for example, the two mass configuration shown in fig.3.3(a) which is assumed to represent a flexible rotor supported by massive flexible bearing-supports. Suppose that it is

required to find the driving point impedance, Z_{BB}, at the bearing support mass, m_b. In impedance notation this is represented by the model shown in fig.3.3(b), which emphasises that elements m_b and k_b are in parallel. The sub-system comprising k_R and m_R is also parallel with k_b and m_b. In this case, however, k_R and m_R are themselves in series.

The driving point impedance Z_{AA} at point of A of the sub-system (in the absence of the remainder of the system) is given by

$$\frac{1}{Z_{AA}} = \frac{1}{m_R} - \frac{\omega^2}{k_R} \qquad (3.15)$$

or $$Z_{AA} = \frac{m_R k_R}{(k_R - m_R \omega^2)} \qquad (3.16)$$

The driving point impedance of the complete arrangement at point B, is now obtained by adding the impedance of the individual parts, thus

$$Z_{BB} = Z_{AA} + Z_{k_b} + Z_{m_b} \qquad (3.17)$$

Substituting $Z_{k_b} = \frac{-k_b}{\omega^2}$; $Z_{m_b} = m_b$;

then $$Z_{BB} = \frac{m_R k_R}{(k_R - m_R \omega^2)} - \frac{k_b}{\omega^2} + m_b \qquad (3.18)$$

whence $$Z_{BB} = \frac{m_R k_R \omega^2 - k_b (k_R - m_R \omega^2) + m_b \omega^2 (k_R - m_R \omega^2)}{(k_R - m_R \omega^2) . \omega^2} \qquad (3.19)$$

The type of impedance plot that would result from measuring Z_{BB} is shown in fig.3.3(c). It can be seen from this diagram that there are two frequencies at which the impedance approaches zero, ω_{n_1} and ω_{n_2}. These are the natural frequencies of the system which are the roots of the frequency equation obtained by equating the numerator in eqn. (3.19) to zero.

At the frequency ω_{A_R} the driving point impedance approaches infinity, which represents an 'antiresonant' condition, the point B being a node. The antiresonant frequency may be evaluated analytically from eqn. 3.19 by noting that

$$Z_{BB} \longrightarrow \infty$$

when the denominator $(k_R - m_R\omega^2).\omega^2 = 0$ (3.20)

Eqn.(3.20) is satisfied when $\omega^2 = 0$; (3.21)

and when $\omega^2 = \frac{k_R}{m_R}$ i.e. $\omega = \sqrt{\frac{k_R}{m_R}}$; (3.22)

The first condition is trivial and arises because the acceleration impedance of the parallel spring element, k_b, is infinite at zero frequency. However, the second condition shows that Z_{BB} is antiresonant when the excitation frequency coincides with the natural frequency of the rotor on rigid supports. The proximity of the lower resonant frequency of the complete system, ω_{n_1}, to the antiresonant frequency, ω_{A_R}, is therefore a measure of the reduction in the critical speed of the rotor caused by the non-rigid support. This type of behaviour is referred to in tests reported later in the thesis.

The curve, fig. 3.3(c) also shows that at low frequencies Z_{BB} is controlled by the bearing support stiffness, k_b, whilst at high frequencies the impedance of mass m_b predominates.

3.3 Impedance Matching: Applications to Rotating Machinery.

Consider two undamped sub-systems in parallel as shown in fig. 3.4 (a). The driving point impedances of the uncoupled systems at points 1 and 2 are assumed to be Z_1 and Z_2 respectively. The condition for the coupled arrangement to be resonant is that the impedances throughout the system should be zero. In particular, the driving point impedance at A, Z_{AA}, must be zero.

But $Z_{AA} = Z_1 + Z_2$, since the subsystems are in parallel.

Therefore, for resonance,

$$Z_{AA} = Z_1 + Z_2 = 0 \qquad (3.23)$$

or $$Z_1 = -Z_2 \qquad (3.24)$$

If the condition indicated by eqn.3.24 holds good, the sub-systems are said to have 'matched impedances'.

The principle of mechanical impedance matching was first used in the calculation of torsional critical speeds of aircraft engine-propeller systems. More recently, it has been used for flexural critical speed calculations for rotating machines. (See Church (71), for example). The impedances involved are those of the rotor and of the bearing-support arrangement.

For example, the symmetric rotor shown in fig.3.4(b) might be represented by a single mass-spring combination m_R, k_R. Where $\omega_{n_R} = \frac{k_R}{m_R}$, the flexural critical angular frequency of the rotor when rigidly supported. The dynamic behaviour of oil films and supports might be approximated by the spring-mass-spring arrangement shown in fig.3.4(c). The schematic impedance diagram for the rotor and supports is shown in fig.3.4(d).

The impedance 'looking into' the rotor is Z_{RR},

$$\text{where } Z_{RR} = \frac{m_R k_R}{(k_R - m_R \omega^2)}$$

Whilst the impedance looking into the bearing arrangement is Z_{BB}

$$\text{where } \frac{1}{Z_{BB}} = \frac{-\omega^2}{k_f} + \frac{1}{\left(\frac{-k_b}{\omega^2} + m_b\right)}$$

$$\text{or } Z_{BB} = k_f \cdot \frac{(-k_b + m_b \omega^2)}{\omega^2(k_b - m_b \omega^2) + k_f \omega^2} \qquad (3.25)$$

The functions Z_{BB} and Z_{RR} are sketched in fig.3.4(d) from which it can be seen that the two curves intersect at points A and B. At these points $Z_{BB} = -Z_{RR}$, and they therefore define the resonant frequencies of the combined system.

In the practical application of impedance matching technique a combination of calculated and measured data may be used. Since the dynamic properties of the rotor are normally accurately known, the rotor impedance function may be calculated. Caruso (68) has reported the use of known rotor characteristics and observed critical speeds in working backwards to the effective support impedance. For the steam turbine rotors with which Caruso was concerned, the first critical speed was normally reduced by about 10%, compared with the rigidly supported value. In this respect fig. 3.4(d) overemphasizes the separation between ω_{n_1} and ω_{n_R} that is normally encountered in practice.

The concept of impedance matching may be extended to include rotors having many degrees of freedom. It is then convenient to consider symmetric and non-symmetric modes separately. Dimentberg (17), Morton (46), Mahalingham (72) and Caruso (68) have applied this approach.

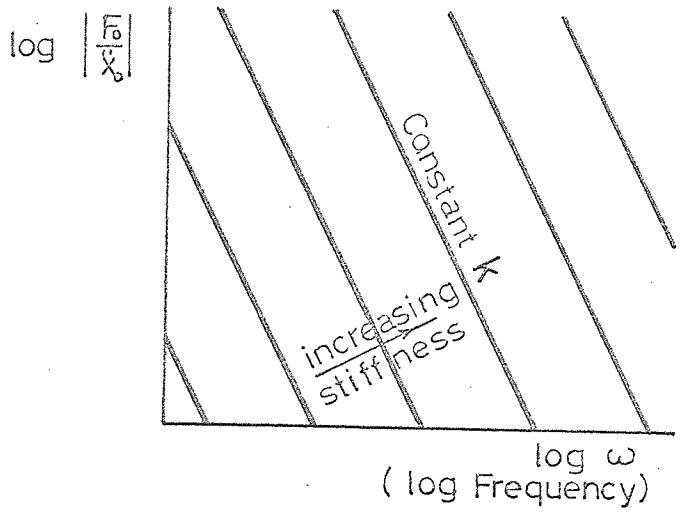

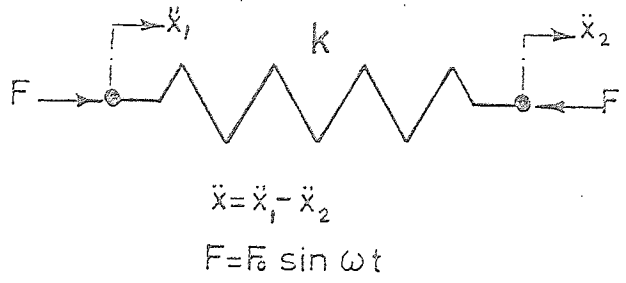

$\ddot{x} = \ddot{x}_1 - \ddot{x}_2$

$F = F_0 \sin \omega t$

(a) Linear Spring

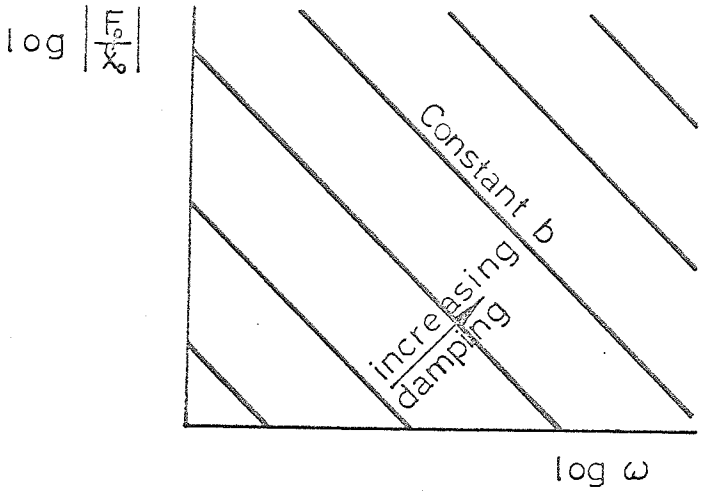

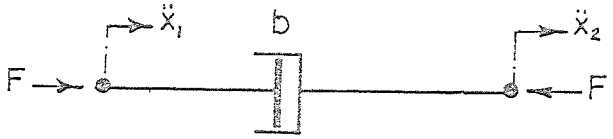

$\ddot{x} = \ddot{x}_1 - \ddot{x}_2$

$F = F_0 \sin \omega t$

(b) Viscous Damper

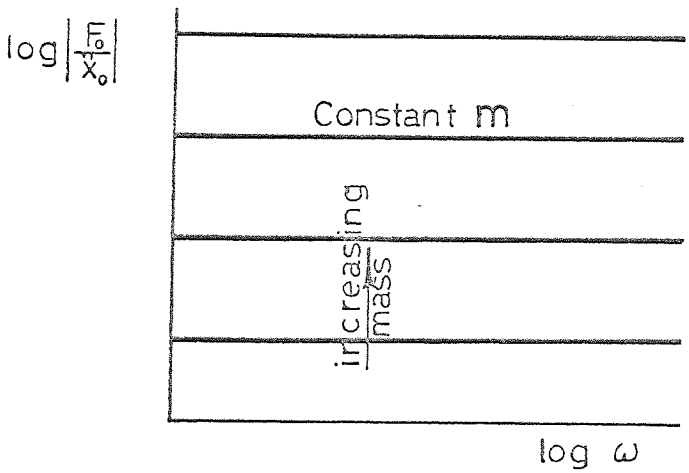

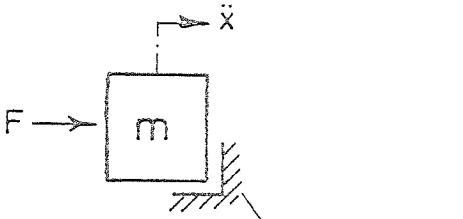

$F = F_0 \sin \omega t$

(c) Pure Mass

FIG. 3.1 ACCELERATION IMPEDANCE (APPARENT MASS) CHARACTERISTICS OF IDEAL LUMPED-PARAMETER ELEMENTS.

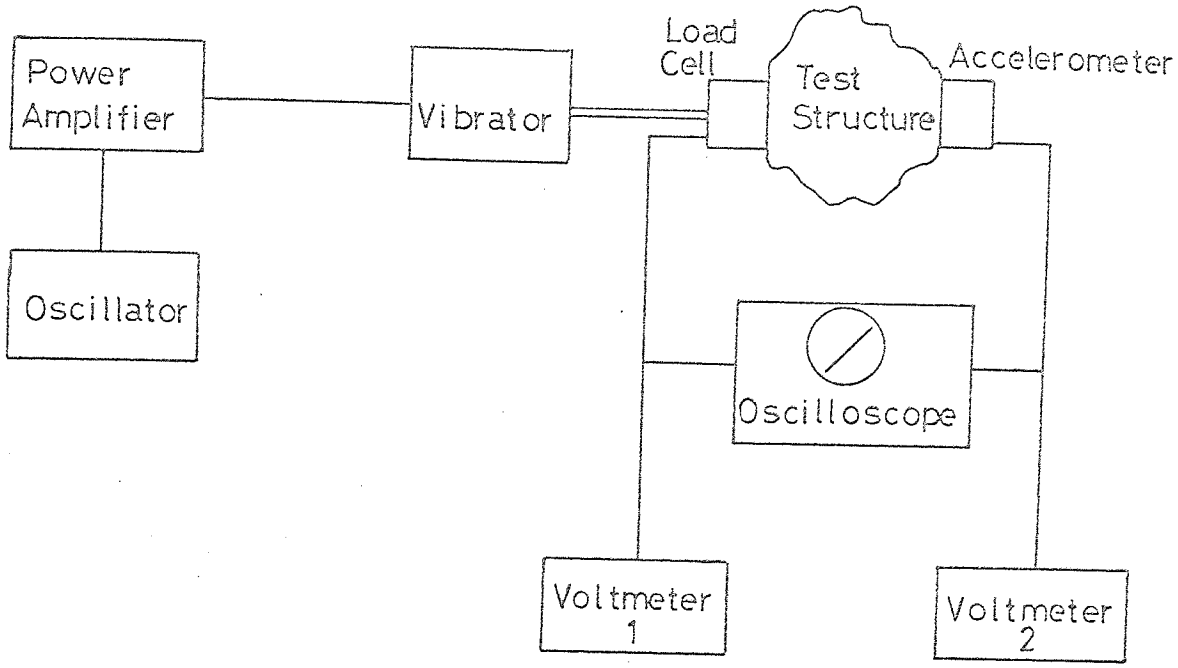

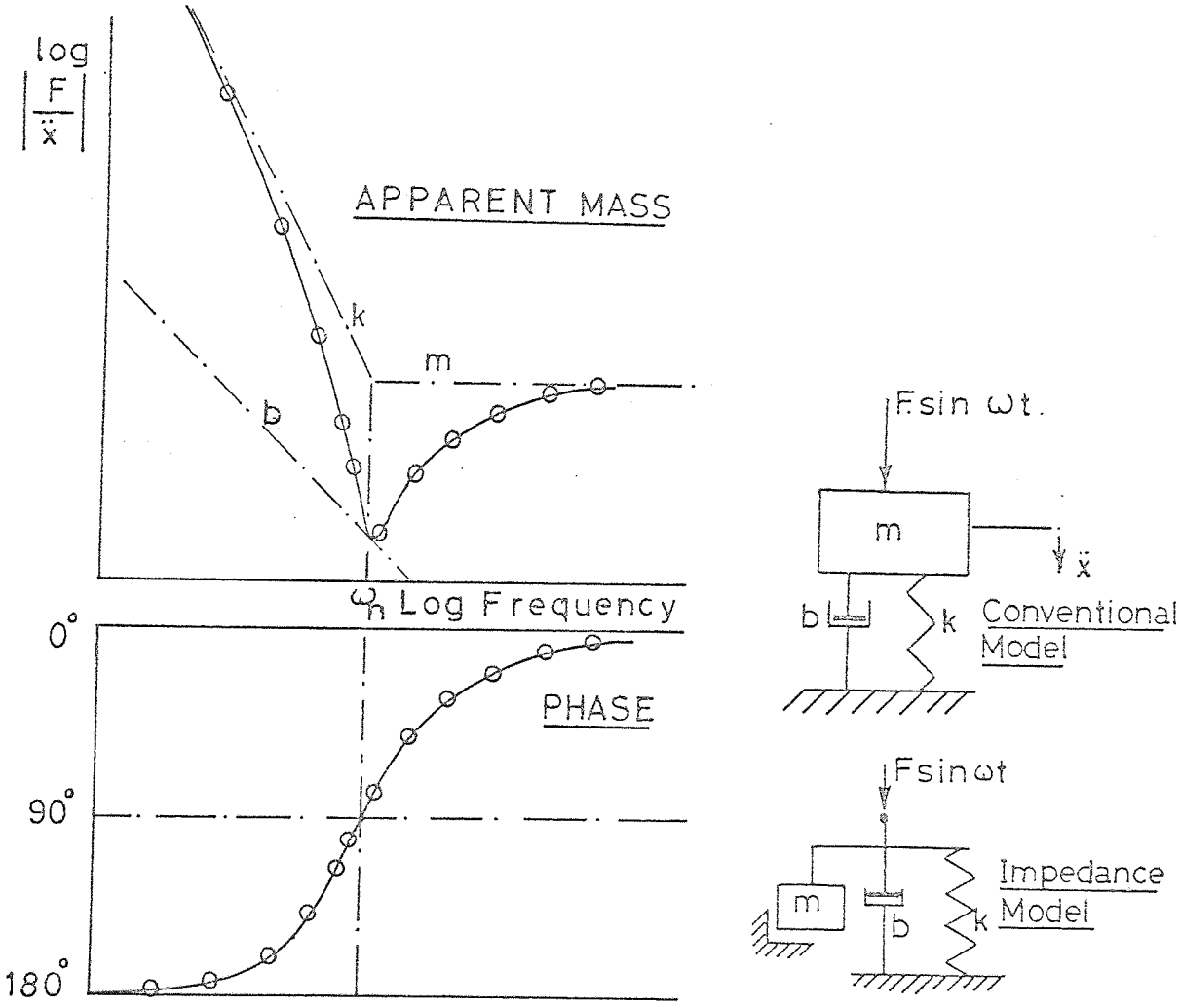

FIG.3.2 SIMPLE TEST ARRANGEMENT. IMPEDANCE AND PHASE PLOT SINGLE D.O.F. SYSTEM.

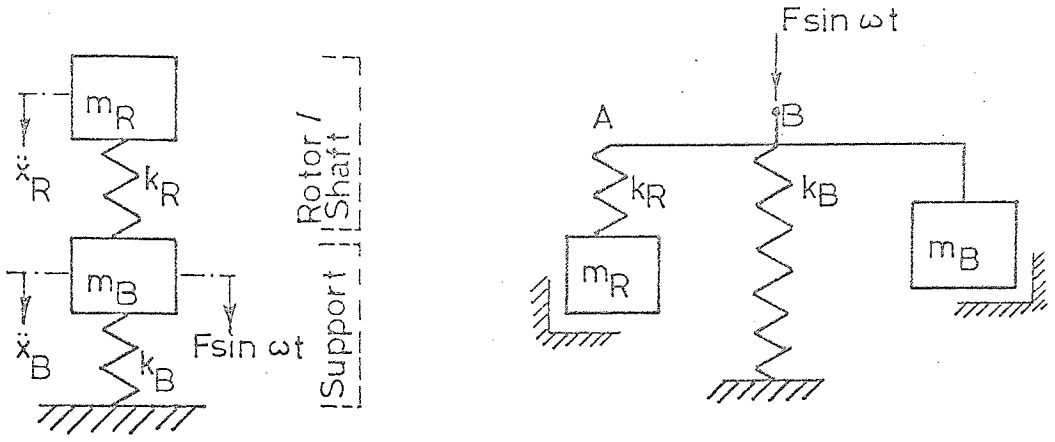

(a) Classical Notation

(b) Impedance Notation

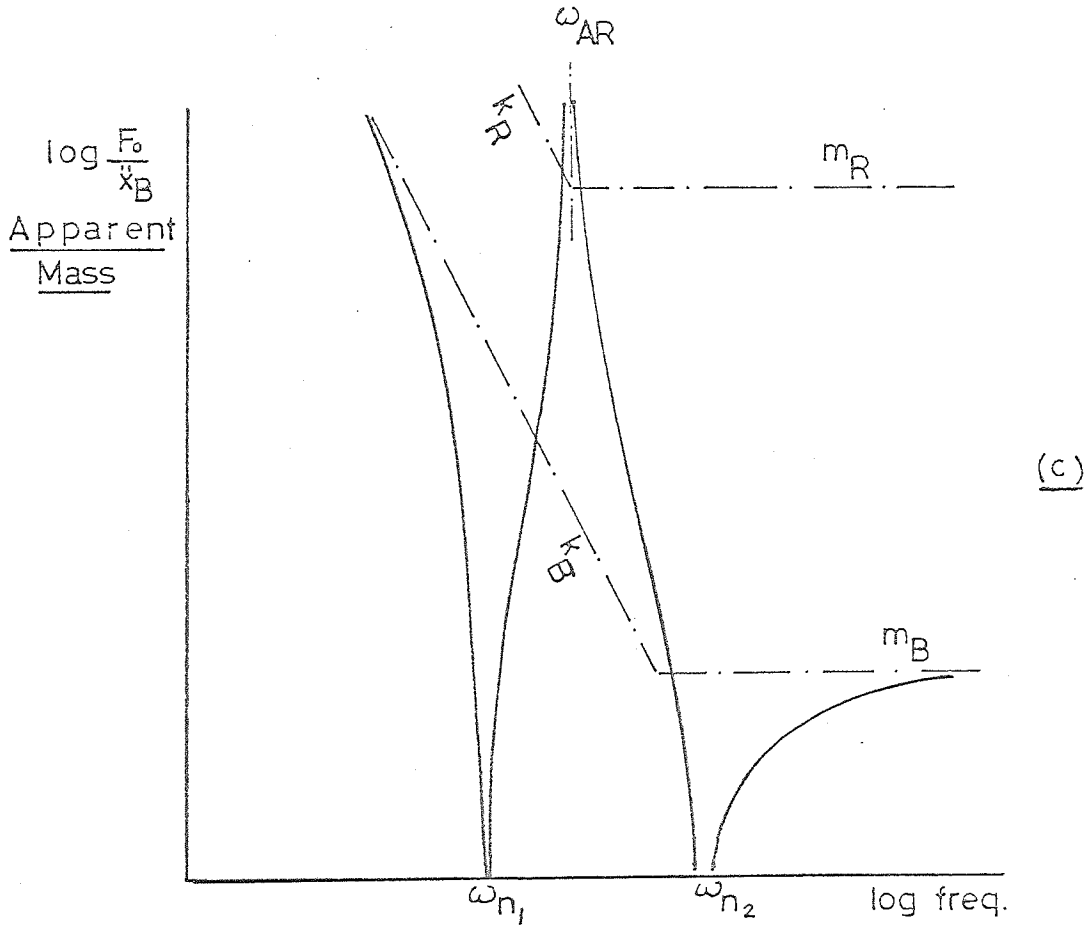

FIG.3.3 EXAMPLE: TWO D.O.F. APPROXIMATION FOR DRIVING POINT IMPEDANCE OF BEARING SUPPORT WITH ROTOR.

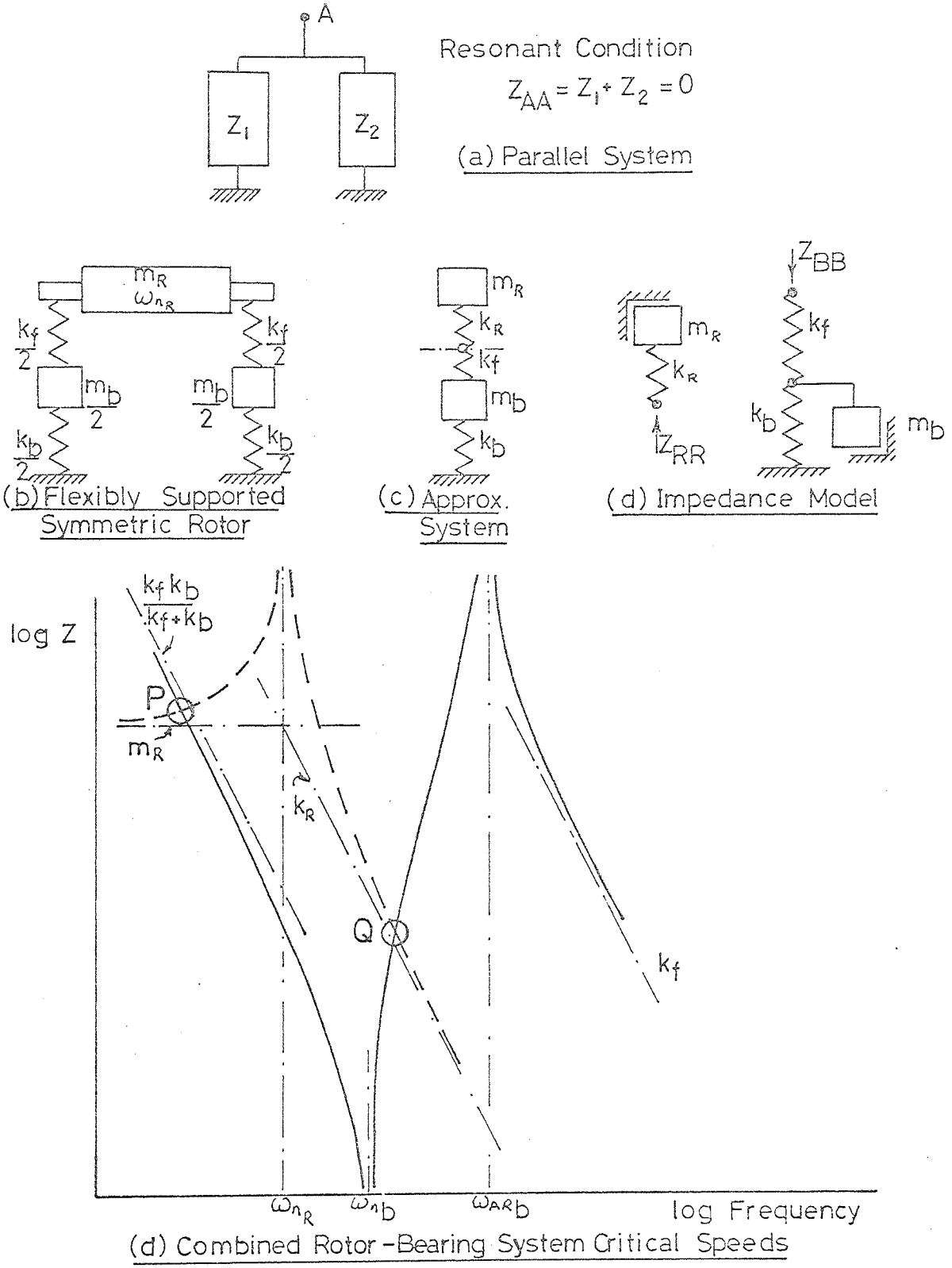

FIG. 3.4 IMPEDANCE MATCHING APPLIED TO CRITICAL SPEEDS.

CHAPTER 4.

Theoretical Considerations of a Typical Rotating Machine Structure

4.1 Introduction

In Chapter 1 it was proposed that, in order to establish more reliable vibration criteria for rotating machines, a knowledge of bearing support impedances was required. A better interpretation of measured vibration levels could then be obtained and, in particular, a quantitative estimate of oscillatory bearing force amplitudes would be available.

In all but the simplest supporting structures it seemed unlikely that attempts to calculate their effective impedance would yield results much more accurate than an order of magnitude. The practical expedient was therefore to measure the impedances of interests. The ideal state of affairs would permit measurement of the unknown support impedances with the shaft removed from its bearings. Then, the correlation between vibration amplitudes measured whilst the machine was running, the measured impedances and the shaft-generated oscillatory forcing would be independent of both the dynamics of the shaft itself and the manner in which the forces were generated.

This 'ideal' situation is illustrated in fig.4.1(a) in which it is assumed that the shaft is supported in two bearings located at axial planes 1 and 2. It is further assumed that the bearing supports have principal directions, normal to the shaft axis, such that motion in any of the planes is uncoupled from motion in any other. It is then possible to represent the dynamic characteristics of the supports in these planes by driving point impedances Zxx_1, Zxx_2, Zyy_1 and Zyy_2.

If the impedances Zxx_1, Zyy_1 etc. have been measured, then on installing and running the rotor, fig. 4.1 (b), the oscillatory forces Fx_1, Fy_1, Fx_2, Fy_2 in the principal planes of the supports may be found from the measured vibration levels in the same planes.

Thus $Fx_1 = x_1 . Zxx_1$

$Fx_2 = x_2 . Zxx_2$

$Fy_1 = y_1 . Zyy_1$

$Fy_2 = y_2 . Zyy_2$

In practice however, although it would normally be possible to measure impedances in two mutually perpendicular directions at each support (conveniently horizontally and vertically), in general these would not be principal directions. In addition, the two supports themselves would normally be coupled to some extent by the foundations or the machine casing.

Theoretically no assumptions need be made regarding the position of the principal planes of the individual supports or the coupling between them. But the number of impedance measurements required and the subsequent work involved in extracting the impressed bearing forces rapidly increases such as to make procedure impractical except, perhaps, under laboratory conditions.

An important objective of the experimental work on the model machine (Chapter 6) was therefore to examine the accuracy with which the system behaviour could be predicted when using approximate values for the support impedances. For this purpose the response to added unbalance and the impedance characteristics of the assembled system have been used for assessment.

It was anticipated that measurements on industrial machines on site would often have to be made with the rotor already assembled in its bearings and even with the machine running. Attention has therefore been paid to methods of extracting the support impedances from equivalent measurements on the complete shaft-support system.

The following sections present the theoretical analysis of a representative rotating machine which will subsequently be referred to as a basis for comparison with experimental results.

4.2 Undamped System: Ball Bearings.

The first arrangement considered is one in which no damping is present. All acceleration impedances are therefore real quantities whilst responses are either in phase or anti-phase with an assumed harmonic exciting force. Such an approximation is reasonable for a lightly damped system providing frequencies close to resonant or anti-resonant conditions are not considered. The model machine, when supported in ball bearings, was very lightly damped and the following analysis is therefore intended to provide an approximate description of that system's behaviour.

The structure examined has eight degrees of freedom and is shown diagramatically in fig.4.2. It consists of a rotor-shaft arrangement having two flexural natural frequencies in the range of interest when considered to be simply supported. The shaft is assumed to be equally stiff in all radial planes, whilst the rotor is considered to be a rigid cylinder. Initially, it is assumed that the shaft-rotor system rotate with angular velocity Ω . Two massive, flexible bearing supports are assumed, each having a single, uncoupled resonance in both horizontal, x, and vertical, y, direction. The driving point support impedances in these directions are assumed dissimilar.

i.e. $Zxx_1 \neq Zyy_1 \neq Zxx_2 \neq Zyy_2$

where the suffices 1 and 2 refer to the bearing planes.

The equationsof motion are first derived using a classical approach before re-casting them in matrix form. The equations in this form are then ideally suited for digital computation since both impedances and responses to shaft-generated forces can be obtained by systematic manipulation of the resulting arrays. Steady state conditions are assumed throughout.

4.2 (i) Equations of Motion.

Referring to fig.4.2, in which the system is shown displaced a small amount in the positive sense of each of the eight generalised co-ordinates x_1, y_1, x_2, y_2, x_g, y_g, ϕ_1, ϕ_2:

The end deflection, d_1, of the right-hand shaft section relative to its fixing at the rigid rotor is, in the horizontal plane 0 X,

$$d_1 = x_g + \left(\ell_3/2 + \ell_2\right) \sin \phi_2 - x_2$$

or writing $\left(\ell_3/2 + \ell_2\right) = \ell_5$

$$d_1 = x_g + \ell_5 \sin \phi_2 - x_2 \qquad (4.1)$$

Similarly the deflection in the Z 0 Y plane, d_2 is

$$d_2 = y_g - \ell_5 \sin \phi_1 - y_2 \qquad (4.2)$$

For the left hand shaft section the deflections d_3 and d_4 in the 0X and 0Y planes respectively, are

$$d_3 = x_g - \ell_4 \sin \phi_2 - x_1 \qquad (4.3)$$

$$d_4 = y_g + \ell_4 \sin \phi_1 - y_1 \qquad (4.4)$$

where $\ell_4 = \left(\ell_3/2 + \ell_1\right)$

The potential energy, V, of the system is therefore given by

$$2V = kx_1 x_1^2 + ky_1 y_1^2 + kx_2 x_2^2 + ky_2 y_2^2$$
$$+ k_1 \left((x_g - \ell_4 \sin \phi_2 - x_1)^2 + (y_g + \ell_4 \sin \phi_1 - y_1)^2 \right)$$
$$+ k_2 \left((x_g + \ell_5 \sin \phi_2 - x_2)^2 + (y_g - \ell_5 \sin \phi_1 - y_2)^2 \right) \qquad (4.5)$$

The kinetic energy T, of the complete system may be conveniently considered in two parts, T_1 and T_2. T_1 arises from motion of the supports and the translatory motion of the rotor, whilst T_2 is the rotational kinetic energy of the rotor.

T_1 may be written down directly as

$$2T_1 = m_1 \left(\dot{x}_1^2 + \dot{y}_1^2\right) + m_2 \left(\dot{x}_2^2 + \dot{y}_2^2\right) + M \left(\dot{x}_g^2 + \dot{y}_g^2\right) \qquad (4.6)$$

The kinetic energy T_2 may be obtained from

$$2T_2 = (I_1\omega_1^2 + I_2\omega_2^2 + I_3\omega_3^2) \qquad (4.7)$$

where I_1, I_2, I_3 are moments of inertia about principal axes 1, 2 and 3 and ω_1, ω_2, ω_3, are angular velocities about these axes.

The orientation of the three axes with respect to the XYZ planes is illustrated in fig. 4.3. The co-ordinate angles ϕ_1 and ϕ_2 conveniently describe the system - they are, in fact, Eulerian angles. In terms of ϕ_1, ϕ_2, their time derivatives, and the rotational angular velocity Ω are obtained:-

$$\omega_1 = \dot{\phi}_1$$

$$\omega_2 = \Omega + \dot{\phi}_2 \sin\phi$$

$$\omega_3 = \dot{\phi}_2 \cos\phi_1$$

Also, since the rotor is cylindrical $I_2 = I_1 = I$, say.

Substituting these values in equation (4.7) gives

$$2T_2 = I\left(\dot{\phi}_1^2 + \dot{\phi}_2^2 \cos\phi_1\right) + I_3\left(\Omega^2 + 2\Omega\dot{\phi}_2 \sin\phi_1 + \dot{\phi}_2^2 \sin^2\phi_1\right)$$

writing $\cos^2\phi_1 = 1 - \sin^2\phi_1$ in the first term this equation becomes

$$2T_2 = I\left(\dot{\phi}_1^2 + \dot{\phi}_2^2\right) + (I_3 - I)\dot{\phi}_2^2 \sin^2\phi_1 + 2I_3\Omega\dot{\phi}_2 \sin\phi_1 + I_3\Omega^2 \qquad (4.8)$$

For the small perturbations with which we are concerned the second term will be negligible since $\sin^2\phi_1 \ll 1$ and $\sin\phi_1 \simeq \phi_1$

$$\text{whence } 2T_2 = I\left(\dot{\phi}_1^2 + \dot{\phi}_2^2\right) + 2I_3\Omega\ddot{\phi}_2\,\phi_1 + I_3\Omega^2 \qquad (4.9)$$

The total kinetic energy, T, may now be obtained from eqns.(4.6) and (4.9):-

$$2T = 2(T_1+T_2) = m_1(\dot{x}_1^2+\dot{y}_1^2) + m_2(\dot{x}_2^2+\dot{y}_2^2) + M(\dot{x}_g^2+\dot{y}_g^2) + I(\dot{\phi}_1^2+\dot{\phi}_2^2) + 2I_3\Omega\dot{\phi}_2\sin\phi_1 + I_3\Omega^2 \qquad (4.10)$$

The appropriate Lagrange Equation may now be used to derive the equations of motion. This is

$$\frac{d}{dt}\left(\frac{\partial L}{\partial \dot{q}}\right) - \frac{\partial L}{\partial q} = 0 \qquad (4.11)$$

where q is the generalised co-ordinate under consideration and $L = T - V$ is the Lagrangian function.

$$\frac{d}{dt}\left(\frac{\partial L}{\partial \dot{x}_g}\right) = m\ddot{x}_g \qquad (4.12)$$

and $$-\frac{\partial L}{\partial x_g} = k_1(x_g - x_1 - \ell_4\phi_2) + k_2(x_g + \ell_5\phi_2 - x_2) \qquad (4.13)$$

whence, combining eqns. (4.12) and (4.13) according to eqn.(4.11) the equation of motion in x_g is obtained as

$$M\ddot{x}_g + (k_1 + k_2)x_g + (k_2\ell_5 - k_1\ell_4)\phi_2 - k_1x_1 - k_2x_2 = 0 \qquad (4.14)$$

Similarly the equations of motion in the remaining seven co-ordinates (y_g, x_1, x_2, y_1, y_2, ϕ_1, ϕ_2, respectively) are

$$M\ddot{y}_g + (k_1+k_2)y_g - (k_2\ell_5 - k_1\ell_4)\phi_1 - k_1y_1 - k_2y_2 = 0 \qquad (4.15)$$

$$m_1\ddot{x}_1 + (k_{x_1}+k_1)x_1 - k_1x_g + k_1\ell_4\phi_2 = 0 \qquad (4.16)$$

$$m_2\ddot{x}_2 + (k_{x_2} + k_2)x_2 - k_2x_g - k_2\ell_5\phi_2 = 0 \qquad (4.17)$$

$$m_1\ddot{y}_1 + (k_{y_1} + k_2)y_1 - k_1y_g - k_1\ell_4\phi_1 = 0 \qquad (4.18)$$

$$m_2\ddot{y}_2 + (k_{y_2}+k_2)y_2 - k_2y_g + k_2\ell_5\phi_1 = 0 \qquad (4.19)$$

$$I\ddot{\phi}_1 + (k_1\ell_4^2+k_2\ell_5^2)\phi_1 - I_3\Omega\dot{\phi}_2 - (k_2\ell_5 = k_1\ell_4)y_g - k_1\ell_4y_1 + k_2\ell_5y_2 = 0 \qquad (4.20)$$

$$I\ddot{\phi}_2 + (k_1\ell_4^2+k_2\ell_5^2)\phi_2 + I_3\Omega\dot{\phi}_1 + (k_2\ell_5 - k_1\ell_4)x_g + k_1\ell_4x_1 - k_2\ell_5x_2 = 0 \qquad (4.21)$$

Since only steady state conditions are considered, particular solutions to the above set of simultaneous equations are sought when generalised forces of the form $F\sin\omega t$ act in one or more of the co-ordinates.

The following trial solutions are found to satisfy equations (4.14) to (4.21).

$x_g = X_g \cos\omega t$ whereupon $\ddot{x}_g = -\omega^2 X_g \cos\omega t$

$y_g = Y_g \sin\omega t$ $\ddot{y}_g = -\omega^2 Y_g \sin\omega t$

$x_1 = X_1 \cos\omega t$ $\ddot{x}_1 = -\omega^2 X_1 \cos\omega t$

$y_1 = Y_1 \sin\omega t$ $\ddot{y}_1 = -\omega^2 Y_1 \sin\omega t$

$x_2 = X_2 \cos\omega t$ $\ddot{x}_2 = -\omega^2 X_2 \cos\omega t$

$y_2 = Y_2 \sin\omega t$ $\ddot{y}_2 = -\omega^2 Y_2 \sin\omega t$

$\phi_1 = \underline{\Phi}_1 \sin\omega t$ $\dot{\phi}_1 = \omega . \underline{\Phi}_1 \cos\omega t$ $\ddot{\phi}_1 = -\omega^2 \underline{\Phi}_1 \sin\omega t$

$\phi_2 = \underline{\Phi}_1 \cos\omega t$ $\dot{\phi}_2 = -\omega \underline{\Phi}_2 \sin\omega t$ $\ddot{\phi}_2 = -\omega^2 \underline{\Phi}_2 \cos\omega t$

Substitution of the above particular solutions into the equations of motion yields eight, simultaneous algebraic equations. These are conveniently written in matrix terminology in the form

$$A . \bar{x} = \bar{b} \qquad (4.22)$$

where A is a square matrix whose elements are impedances

$\bar{x}$ is a column vector of the system co-ordinates

and $\bar{b}$ is the vector of the generalised forces.

Thus :-

$$\begin{bmatrix} (k_1+k_{x_1}-m_1\omega^2) & 0 & 0 & 0 & -k_1 & 0 & 0 & k_1 l_4 \\ 0 & (k_2+k_{x_2}-m_2\omega^2) & 0 & 0 & -k_2 & 0 & 0 & -k_2 l_5 \\ 0 & 0 & (k_1+k_{y_1}-m_1\omega^2) & 0 & 0 & -k_1 & -k_1 l_4 & 0 \\ 0 & 0 & 0 & (k_2+k_{y_2}-m_2\omega^2) & 0 & -k_2 & k_2 l_5 & 0 \\ -k_1 & -k_2 & 0 & 0 & (k_1+k_2-M\omega^2) & 0 & 0 & (k_2 l_5 - k_1 l_4) \\ 0 & 0 & -k_1 & -k_2 & 0 & (k_1+k_2-M\omega^2) & -(k_2 l_5 - k_1 l_4) & 0 \\ 0 & 0 & -k_1 l_4 & -k_2 l_5 & 0 & -(k_2 l_5 - k_1 l_4) & (k_1 l_4^2 + k_2 l_5^2 - I\omega^2) & I_3 \Omega \omega \\ k_1 l_4 & -k_2 l_5 & 0 & 0 & (k_2 l_5 - k_1 l_4) & 0 & I_3 \Omega \omega & (k_1 l_4^2 + k_2 l_5^2 - I\omega^2) \end{bmatrix} \begin{bmatrix} X_1 \\ X_2 \\ Y_1 \\ Y_2 \\ X_g \\ Y_g \\ \underline{\Phi}_1 \\ \underline{\Phi}_2 \end{bmatrix} = \begin{bmatrix} F_1 \\ F_2 \\ F_3 \\ F_4 \\ F_5 \\ F_6 \\ F_7 \\ F_8 \end{bmatrix} \qquad (4.23)$$

4.2 (ii) System Impedances

The system response in a generalised co-ordinate, q, is obtained From:

$$q = \frac{\Delta q}{\Delta A}$$

where Δ_A is the determinant of the square matrix A in eqn.(4.22)

Δ_q is the determinant of A with the column containing the coefficients of q replaced by the generalised force vector $\bar{b}$.

Acceleration impedances of the system are of the form $F/\ddot{q}$, where F is the generalised force in one of the co-ordinates. The driving point impedance at q is therefore obtained by including only a generalised force F in q, whereupon

$$Z_{qq} = \frac{-F_q}{\omega^2 q} = -\frac{\Delta A}{\Delta q} \cdot \frac{F_q}{\omega 2} \qquad (4.24)$$

4.2 (iii) Unbalance Response.

For small, unbalance masses added at radii large compared with the resulting whirl amplitudes (see inset fig.4.2) forces appear on the R.H.S. of eqns. (4.14) to (4.21) of the form

$(m_b \cdot r_b \cdot \Omega^2) \begin{matrix}\cos \\ \sin\end{matrix} \Omega t$ in the rotor translational co-ordinates x_g and y_g

and

$(m_b \cdot \alpha \cdot r_b \cdot \Omega^2) \begin{matrix}\cos \\ \sin\end{matrix} \Omega t$ in the rotational co-ordinates Φ_1 and Φ_2,

where α is the axial distance of the place of the unbalance mass from the plane of the rotor centre of gravity.

In this case particular solutions $x_g = X_g \cos\Omega t$, $y_g = Y_g \sin\Omega t$, etc. are applicable and the forcing angular frequency ω is replaced by the rotational frequency Ω in eqns. (4.23).

4.2 (iv) Digital Computer Solution

A programme has been written to solve the system equation (4.23) for both impedances and unbalance response. This programme, the

operation of which is shown diagramatically in fig.4.4, was written in the Elliott 803 Autocode language to obtain the fastest possible computation on the University's own machine without resorting to basic machine code. Typical times to evaluate a given impedance for 100 frequencies were around 1 hour 15 minutes.

4.3 System Supported in Hydrodynamic Journal Bearings

All the industrial machines to which the writer had access and on which it was hoped to perform tests were carried in oil lubricated journal bearings. The theoretical work in this section is therefore concerned with the analysis of the representative rotating machine considered in section 4.2 when supported in this type of bearing. The configuration is illustrated in fig. 4.5.

Although only intended and used for the present investigation into the influence of support impedances on system behaviour, the methods of analysis and solution presented and general enough to form the basis for tackling a much wider range of rotating machine problems. For example, they provide a method of examining in more detail some of the problems of critical speeds and 'modal' balancing recently discussed by Morton (46).

4.3 (i) Bearing steady running conditions.

The operating condition of journal bearings are normally described in terms of the steady running position of the journal relative to the bearing. (see fig.4.6(a)). In the following analysis, Ockvirk's 'short bearing' theory is used to obtain the steady running conditions (in terms of assumed lubricant properties, bearing clearances and loadings).

Ockvirk (76) showed that for plain, circular bearings whose length to diameter ratio was small (i.e. ℓ/d about 1.5), it was reasonable to neglect the effect of circumferential pressure gradient on circumferential flow. Consider the appropriate form of Reynold's equation for steady running.

$$\frac{\partial}{\partial x}\left(h^3 \cdot \frac{\partial p}{\partial x}\right) + \frac{\partial}{\partial z}\left(h^3 \cdot \frac{\partial p}{\partial z}\right) = 6\eta U \cdot \frac{dh}{dx} \qquad (4.25)$$

This equation gives the relationship between, on the R.H.S. a flow quantity related to the tangential journal velocity, U, and on the L.H.S. the pressure gradients in the circumferential, x, and axial, z, directions (see fig. 4.6 (b)). Ockvirk's assumption for short bearings enables the first term on the L.H.S. of eqn(4.25) to be neglected whence the equation becomes

$$\frac{\partial}{\partial z}\left(h^3 \cdot \frac{\partial p}{\partial z}\right) = 6\eta U \cdot \frac{dh}{dx} \qquad (4.26)$$

It should be remarked here that the usual assumptions made in the derivation of eqn. (4.25) still apply - i.e. constant lubricant viscosity, laminar flow, non-deformable bearing material and film thickness, h, small compared with radius (see Barwell (40) for full derivation).

In his analysis Ockvirk also demonstrated that running conditions could be expressed by a single, non-dimensional group which will be referred to as the Ockvirk capacity number, C, where

$$C = \frac{P}{\eta U}\left(\frac{c}{r}\right)^2\left(\frac{b}{d}\right)^2 \qquad (4.27)$$

By assuming a 180° oil film he was able to integrate equation (4.26) analytically to obtain the expression

$$C = \frac{\pi\varepsilon}{(1-\varepsilon^2)}\,(1 + .622\varepsilon^2)^{\frac{1}{2}} \qquad (4.28)$$

which relates the eccentricity, ε, to the capacity number C.

4.3(ii) Bearing Dynamic Characteristics.

The journal bearings of the system shown in fig.4.5 are assumed to have linear dynamic characteristics of the type discussed in Chapter 2. That is, that the bearing forces P_p, P_q in any two perpendicular axes p, q may be written:-

$$\left.\begin{aligned} \Delta P_p &= k_{pp}.\,p + k_{qq}.\,q + b_{pp}.\,\dot{p} + b_{pq}.\,\dot{q} \\ \Delta P_q &= k_{qq}.\,q + k_{qp}.\,p + b_{qq}.\,\dot{q} + b_{qp}.\,\dot{p} \end{aligned}\right\} \qquad (4.29)$$

Various methods have been suggested (41), (42), (44) for obtaining the displacement coefficients (k_{pp}, k_{qp} etc.) and the velocity coefficients (b_{pp}, b_{qp} etc.). Here they are derived using a method first proposed by Morrison (43). His approach applies to short bearings, i.e. those conforming to Ockvirk's assumptions, and gives the dynamic coefficients with respect to axes parallel and at right angles to the attitude or load line of the bearings. That is in the axes s and r in fig. 4.6(a). By making the approximation that the journal deflection path under varying load in semi-circular then the eccentricity ratio, ε , is given by

$$\varepsilon = \cos\psi \qquad (4.30)$$

This assumption is a reasonable one based on the published evidence, for example that of Ockvirk himself, and yields relatively simple algebraic expressions for the coefficients as follows:-

$$\begin{aligned} k_{ss} &= \frac{W}{C} \qquad k_{sr} = \frac{W}{C}\,(4.6\sin\psi - \cot\psi) \\ k_{rs} &= \frac{-W}{C}\tan\psi \qquad k_{rr} = \frac{W}{C}\,(4.5\cos\psi + 1) \\ b_{ss} &= \frac{-2}{\Omega}\,k_{rs} \qquad b_{sr} = \frac{2}{\Omega}.\,k_{ss} \\ b_{rs} &= \frac{2}{\Omega}\,k_{ss} \qquad b_{rr} = \frac{2}{\Omega}\,k_{sr} \end{aligned} \qquad (4.31)$$

4.3 (iii) Transformation of Axes

However, the axes s, r are not convenient for the present analysis since their position in space is itself a function of the steady running conditions. It is therefore necessary to transpose the coefficients to the horizontal and vertical axes x, y. This transposition may be accomplished, with reference to fig.4.6(a) as follows.

Consider a small displacement, x, of the journal relative to the bearing along the axis Ox. Such a displacement has components in the s, r axes system.

$$r = x \sin\psi \qquad s = -x \cos\psi$$

A similar displacement, y, along Oy has components

$$r = -y \cos\psi \qquad s = -y \sin\psi$$

The total resultant radial force acting on the journal is, according to equation (4.29),

$$P_r = k_{rr}(x \sin\psi - y \cos\psi) - k_{rs}(x \cos\psi + y \sin\psi) \quad (4.32)$$

whilst the tangential force is

$$P_s = -k_{ss}(x \cos\psi + y \sin\psi) + k_{sr}(x \sin\psi - y \cos\psi) \quad (4.33)$$

The forces P_r, P_s have components in the Ox direction

$$P_x = P_r \sin\psi - P_s \cos\psi$$

or, from equations (4.32) and (4.33),

$$P_x = k_{rr}(x \sin\psi - y \cos\psi).\sin - k_{rs}(x \cos\psi + y \sin\psi)\sin\psi$$

$$+ k_{ss}(x \cos\psi + y \sin\psi).\cos\psi - k_{sr}(x \sin\psi - y \cos\psi)\cos\psi$$

$$P_x = (k_{rr}\sin^2\psi - (k_{rs} + k_{sr})\sin\psi\cos\psi + k_{ss}\cos^2\psi)\,x$$

$$+ (-k_{rs}\sin^2\psi + (k_{ss} - k_{rr})\sin\psi\cos\psi + k_{sr}\cos^2\psi)\,y \quad (4.34)$$

Since only displacements are considered in the above derivation, $\dot{y} = \dot{x} = 0$ and equation (4.29) gives

$$P_x = k_{xx}\,x + k_{xy}\,y \quad (4.35)$$

By comparing the coefficients of x and y in equations (4.34) and (4.35)

$$k_{xx} = (k_{rr}\sin^2\psi - (k_{rs} + k_{sr})\sin\psi\cos\psi + k_{ss}\cos^2\psi) \quad (4.36)$$

and $$k_{xy} = (-k_{rs}\sin^2\psi + (k_{ss} - k_{rr})\sin\psi\cos\psi + k_{sr}\cos^2\psi) \quad (4.37)$$

Which, on substituting from equations (4.31), reduce to

$$k_{xx} = 2 \tag{4.38}$$

$$k_{xy} = \tan \phi - \cot \psi \tag{4.39}$$

By similar reasoning for the resultant force P_y, the remaining two displacement coefficients are obtained:-

$$k_{yx} = (k_{rs} \cos^2\psi + (k_{ss} - k_{rr}) \cos\psi \sin\psi - k_{sr} \sin^2\psi) \tag{4.40}$$

and

$$k_{yy} = (k_{rr} \cos^2\psi + (k_{sr} + k_{rs}) \cos\psi \sin\psi + k_{ss} \sin^2\psi) \tag{4.41}$$

Again, substituting from eqns (4.31), these reduce to

$$k_{yx} = -4.6 \sin \phi \tag{4.42}$$

$$k_{yy} = \frac{W}{C} \cdot 4.6 \cos \phi \tag{4.43}$$

The velocity coefficients in the axes x, y are likewise found by considering the forces due to journal velocities in these axes. They are:-

$$b_{xx} = (b_{rr} \sin^2\psi - (b_{rs} + b_{sr}) \sin\psi \cos\psi + b_{ss} \cos^2\psi) \tag{4.4 }$$

$$b_{xy} = (-b_{rs} \sin^2\psi + (b_{ss} - b_{rr}) \sin\psi \cos\psi + b_{sr} \cos^2\psi) \tag{4.45}$$

$$b_{yx} = (b_{rs} \cos^2\psi + (b_{xx} - b_{rr}) \cos\psi \sin\psi - b_{sr} \sin^2\psi) \tag{4.46}$$

$$b_{yy} = (b_{rr} \cos^2\psi + (b_{sr} + b_{rs}) \cos\psi \sin\psi + b_{ss} \sin^2\psi) \tag{4.47}$$

Substituting from eqns.(4.31) these coefficients may be expressed as:-

$$b_{xx} = \frac{2W}{C} \quad (4.6 \sin^3 \phi - 2 \cos \phi \sin \phi) \tag{4.48}$$

$$b_{xy} = b_{yx} = \frac{2W}{C} \quad (-4.6 \sin^2 \phi \cos \phi + 2 \cos^2 \phi) \tag{4.49}$$

and

$$b_{yy} = \frac{2W}{C} \left((4.6 \sin\phi - \cot\phi) \cos^2\phi + 2\cos\phi\sin\phi + \tan\phi\sin^2\phi \right) \tag{4.50}$$

Like the corresponding coefficients in the axes s, r, the coefficients derived in axes x, y have the following properties

(i) the displacement dependent coupling terms are non-reciprocal

i.e. $k_{xy} \neq k_{yx}$.

(ii) the velocity dependent coupling terms are reciprocal.

i.e. $b_{xy} = b_{yx}$

4.3 (iv) Equations of Motion

By referring to equations (4.15) to (4.21) of section 4.2 for the undamped system together with fig. 4.5 the equations of motion ((4.51) to (4.62)) are found to be:-

$$M''_{xg} + (k_1 + k_2)x_g + (k_2\ell_5 - k_1\ell_4)\phi_2 - k_1 x_{j_1} - k_2 x_{j_2} = 0 \qquad (4.51)$$

$$M''_{yg} + (k_1 + k_2)y_g - (k_2\ell_5 - k_1\ell_4)\phi_1 - k_1 y_{j_1} - k_2 y_{j_2} = 0 \qquad (4.52)$$

$$I\phi''_1 + (k_1\ell_4^2 + k_2\ell_5^2)\phi_1 - I_3\Omega\phi'_2 - (k_2\ell_5 - k_1\ell_4)y_g - k_1\ell_4 y_{j_1} + k_2\ell_5 y_{j_2} = 0 \qquad (4.53)$$

$$I\phi''_2 + (k_1\ell_4^2 + k_2\ell_5^2)\phi_2 + I_3\Omega\phi'_1 + (k_2\ell_5 - k_1\ell_4)x_g + k_1\ell_4 x_{j_1} - k_2\ell_5 x_{j_2} = 0 \qquad (4.54)$$

$$m_1 x''_1 + k_{x_1} x_1 - P_{x_1} = 0 \qquad (4.55)$$

$$m_2 x''_2 + k_{x_2} x_2 - P_{x_2} = 0 \qquad (4.56)$$

$$m_1 y''_1 + k_{y_1} y_1 - P_{y_1} = 0 \qquad (4.57)$$

$$m_2 y''_2 + k_{y_2} y_2 - P_{y_2} = 0 \qquad (4.58)$$

$$k_1 (x_{j_1} - x_g) + k_1\ell_4\phi_2 + P_{x_1} = 0 \qquad (4.59)$$

$$k_2 (x_{j_2} - x_g) - k_2\ell_5\phi_2 + P_{x_2} = 0 \qquad (4.60)$$

$$k_1 (y_{j_1} - y_g) - k_1\ell_4\phi_1 + P_{y_1} = 0 \qquad (4.61)$$

$$k_2 (y_{j_2} - y_g) + k_2\ell_5\phi_1 + P_{y_2} = 0 \qquad (4.62)$$

Where P_{x_1}, P_{x_2}, P_{y_1}, P_{y_2} are the oil forces acting on the bearing given by:-

$$P_{x_1} = k_{xx_1}(x_{j_1} - x_1) + k_{xy_1}(y_{j_1} - y_1) + b_{xx_1}(\dot{x}_{j_1} - \dot{x}_1) + b_{xy_1}(\dot{y}_{j_1} - \dot{y}_1) \quad (4.63)$$

$$P_{x_2} = k_{xx_2}(x_{j_2} - x_2) + k_{xy_2}(y_{j_2} - y_2) + b_{xx_2}(\dot{x}_{j_2} - \dot{x}_2) + b_{xy_2}(\dot{y}_{j_2} - \dot{y}_2) \quad (4.64)$$

$$P_{y_1} = k_{xy_1}(y_{j_1} - y_1) + k_{yx_1}(x_{j_1} - x_1) + b_{yy_1}(\dot{y}_{j_1} - \dot{y}_1) + b_{yx_1}(\dot{x}_{j_1} - \dot{x}_1) \quad (4.65)$$

$$P_{y_2} = k_{yy_2}(y_{j_2} - y_2) + k_{yx_2}(x_{j_2} - x_2) + b_{yy_2}(\dot{y}_{j_2} - \dot{y}_2) + b_{yx_2}(\dot{x}_{j_2} - \dot{x}_2) \quad (4.66)$$

Steady state solutions are sought to the equations of motion when generalised harmonic forces of the form P.sinωt appear on the R.H.S. of equations (4.51) to (4.62). The following general, particular solutions are found to satisfy these equations:-

$$x_g = X_{g_c}\cos\omega t + X_{g_s}\sin\omega t \quad (4.67)$$

$$y_g = Y_{g_c}\cos\omega t + Y_{g_s}\sin\omega t \quad (4.68)$$

$$x_{j_1} = X_{j1_c}\cos\omega t + X_{j1_s}\sin\omega t \quad (4.69)$$

$$x_{j_2} = X_{j2_c}\cos\omega t + X_{j2_s}\sin\omega t \quad (4.70)$$

$$y_{j_1} = Y_{j1_c}\cos\omega t + Y_{j1_s}\sin\omega t \quad (4.71)$$

$$y_{j_2} = Y_{j2_c}\cos\omega t + Y_{j2_s}\sin\omega t \quad (4.72)$$

$$\phi_1 = \Phi_{1_c}\cos\omega t + \Phi_{1_s}\sin\omega t \quad (4.73)$$

$$\phi_2 = \Phi_{2_c}\cos\omega t + \Phi_{2_s}\sin\omega t \quad (4.74)$$

$$x_1 = X_{1_c}\cos\omega t + X_{1_s}\sin\omega t \quad (4.75)$$

$$x_2 = X_{2_c}\cos\omega t + X_{2_s}\sin\omega t \quad (4.76)$$

$$y_1 = Y_{1_c}\cos\omega t + Y_{1_s}\sin\omega t \quad (4.77)$$

$$y_2 = Y_{2_c}\cos\omega t + Y_{2_s}\sin\omega t \quad (4.78)$$

Substitution of the solutions Eqns.(4.67) to (4.78) and their appropriate time derivatives into eqns.(4.51) to (4.62) yield the simultaneous algebraic equations for the form

$$A.\ \bar{x} = \bar{b}$$

which are given in full on the next page.

$$
\begin{bmatrix}
K_1+K_2-M\omega^2 & 0 & 0 & 0 & -K_1 & 0 & -K_2 & 0 & 0 & 0 & 0 & 0 & 0 & 0 & (K_2\ell_2-K_1\ell_1) & 0 & 0 & 0 & 0 & 0 & 0 & 0 & 0 & 0 \\
0 & K_1+K_2-M\omega^2 & 0 & 0 & 0 & -K_1 & 0 & -K_2 & 0 & 0 & 0 & 0 & 0 & 0 & 0 & (K_2\ell_2-K_1\ell_1) & 0 & 0 & 0 & 0 & 0 & 0 & 0 & 0 \\
0 & 0 & K_1+K_2-M\omega^2 & 0 & 0 & 0 & 0 & 0 & -K_1 & 0 & -K_2 & 0 & (K_1\ell_1-K_2\ell_2) & 0 & 0 & 0 & 0 & 0 & 0 & 0 & 0 & 0 & 0 & 0 \\
0 & 0 & 0 & K_1+K_2-M\omega^2 & 0 & 0 & 0 & 0 & 0 & -K_1 & 0 & -K_2 & 0 & (K_1\ell_1-K_2\ell_2) & 0 & 0 & 0 & 0 & 0 & 0 & 0 & 0 & 0 & 0 \\
-K_1 & 0 & 0 & 0 & K_1+K_{xx_1} & \omega b_{xx_1} & 0 & 0 & K_{xy_1} & \omega b_{xy_1} & 0 & 0 & 0 & 0 & K_1\ell_1 & 0 & -K_{xx_1} & -\omega b_{xx_1} & 0 & 0 & -K_{xy_1} & -\omega b_{xy_1} & 0 & 0 \\
0 & -K_1 & 0 & 0 & -\omega b_{xx_1} & K_1+K_{xx_1} & 0 & 0 & -\omega b_{xy_1} & K_{xy_1} & 0 & 0 & 0 & 0 & 0 & K_1\ell_1 & \omega b_{xx_1} & -K_{xx_1} & 0 & 0 & \omega b_{xy_1} & -K_{xy_1} & 0 & 0 \\
-K_2 & 0 & 0 & 0 & 0 & 0 & K_2+K_{xx_2} & \omega b_{xx_2} & 0 & 0 & K_{xy_2} & \omega b_{xy_2} & 0 & 0 & -K_2\ell_2 & 0 & 0 & 0 & -K_{xx_2} & -\omega b_{xx_2} & 0 & 0 & -K_{xy_2} & -\omega b_{xy_2} \\
0 & -K_2 & 0 & 0 & 0 & 0 & -\omega b_{xx_2} & K_2+K_{xx_2} & 0 & 0 & -\omega b_{xy_2} & K_{xy_2} & 0 & 0 & 0 & -K_2\ell_2 & 0 & 0 & \omega b_{xx_2} & -K_{xx_2} & 0 & 0 & \omega b_{xy_2} & -K_{xy_2} \\
0 & 0 & -K_1 & 0 & K_{yx_1} & \omega b_{yx_1} & 0 & 0 & K_1+K_{yy_1} & \omega b_{yy_1} & 0 & 0 & -t_1\ell_1 & 0 & 0 & 0 & -K_{yx_1} & -\omega b_{yx_1} & 0 & 0 & -K_{yy_1} & -\omega b_{yy_1} & 0 & 0 \\
0 & 0 & 0 & -K_1 & -\omega b_{yx_1} & K_{yx_1} & 0 & 0 & -\omega b_{yy_1} & K_1+K_{yy_1} & 0 & 0 & 0 & -K_1\ell_1 & 0 & 0 & -\omega b_{yx_1} & K_{yx_1} & 0 & 0 & -\omega b_{yy_1} & -K_{yy_1} & 0 & 0 \\
0 & 0 & -K_2 & 0 & 0 & 0 & K_{yx_2} & \omega b_{yx_2} & 0 & 0 & K_2+K_{yy_2} & \omega b_{yy_2} & K_2\ell_2 & 0 & 0 & 0 & 0 & 0 & -K_{yx_2} & -\omega b_{yx_2} & 0 & 0 & -K_{yy_2} & -\omega b_{yy_2} \\
0 & 0 & 0 & -K_2 & 0 & 0 & -\omega b_{yx_2} & K_{yx_2} & 0 & 0 & -\omega b_{yy_2} & K_2+K_{yy_2} & 0 & K_2\ell_2 & 0 & 0 & 0 & 0 & \omega b_{yx_2} & -K_{yx_2} & 0 & 0 & \omega b_{yy_2} & -K_{yy_2} \\
0 & 0 & (K_1\ell_1-K_2\ell_2) & 0 & 0 & 0 & 0 & 0 & -K_1\ell_1 & 0 & K_2\ell_2 & 0 & (K_1\ell_1^2+K_2\ell_2^2-I\omega^2) & 0 & 0 & -I_y\Omega\omega & 0 & 0 & 0 & 0 & 0 & 0 & 0 & 0 \\
0 & 0 & 0 & (K_1\ell_1-K_2\ell_2) & 0 & 0 & 0 & 0 & 0 & -K_1\ell_1 & 0 & K_2\ell_2 & 0 & (K_1\ell_1^2+K_2\ell_2^2-I\omega^2) & I_y\Omega\omega & 0 & 0 & 0 & 0 & 0 & 0 & 0 & 0 & 0 \\
(K_2\ell_2-K_1\ell_1) & 0 & 0 & 0 & K_1\ell_1 & 0 & -K_2\ell_2 & 0 & 0 & 0 & 0 & 0 & 0 & I_y\Omega\omega & (K_1\ell_1^2+K_2\ell_2^2-I\omega^2) & 0 & 0 & 0 & 0 & 0 & 0 & 0 & 0 & 0 \\
0 & (K_2\ell_2-K_1\ell_1) & 0 & 0 & 0 & K_1\ell_1 & 0 & -K_2\ell_2 & 0 & 0 & 0 & 0 & -I_y\Omega\omega & 0 & 0 & (K_1\ell_1^2+K_2\ell_2^2-I\omega^2) & 0 & 0 & 0 & 0 & 0 & 0 & 0 & 0 \\
0 & 0 & 0 & 0 & -K_{xx_1} & -\omega b_{xx_1} & 0 & 0 & -K_{xy_1} & -\omega b_{xy_1} & 0 & 0 & 0 & 0 & 0 & 0 & K_{x_1}+K_{xx_1}-m_1\omega^2 & \omega b_{xx_1} & 0 & 0 & K_{xy_1} & \omega b_{xy_1} & 0 & 0 \\
0 & 0 & 0 & 0 & \omega b_{xx_1} & -K_{xx_1} & 0 & 0 & \omega b_{xy_1} & -K_{xy_1} & 0 & 0 & 0 & 0 & 0 & 0 & -\omega b_{xx_1} & K_{x_1}+K_{xx_1}-m_1\omega^2 & 0 & 0 & -\omega b_{xy_1} & K_{xy_1} & 0 & 0 \\
0 & 0 & 0 & 0 & 0 & 0 & -K_{xx_2} & -\omega b_{xx_2} & 0 & 0 & -K_{xy_2} & -\omega b_{xy_2} & 0 & 0 & 0 & 0 & 0 & 0 & K_{x_2}+K_{xx_2}-m_2\omega^2 & \omega b_{xx_2} & 0 & 0 & K_{xy_2} & \omega b_{xy_2} \\
0 & 0 & 0 & 0 & 0 & 0 & \omega b_{xx_2} & -K_{xx_2} & 0 & 0 & \omega b_{xy_2} & -K_{xy_2} & 0 & 0 & 0 & 0 & 0 & 0 & -\omega b_{xx_2} & K_{x_2}+K_{xx_2}-m_2\omega^2 & 0 & 0 & -\omega b_{xy_2} & K_{xy_2} \\
0 & 0 & 0 & 0 & -K_{xy_1} & -\omega b_{xy_1} & 0 & 0 & -K_{yy_1} & -\omega b_{yy_1} & 0 & 0 & 0 & 0 & 0 & 0 & K_{yx_1} & \omega b_{yx_1} & 0 & 0 & K_{y_1}+K_{yy_1}-m_1\omega^2 & \omega b_{yy_1} & 0 & 0 \\
0 & 0 & 0 & 0 & \omega b_{yx_1} & -K_{xy_1} & 0 & 0 & \omega b_{yy_1} & -K_{yy_1} & 0 & 0 & 0 & 0 & 0 & 0 & -\omega b_{yx_1} & K_{yx_1} & 0 & 0 & -\omega b_{yy_1} & K_{y_1}+K_{yy_1}-m_1\omega^2 & 0 & 0 \\
0 & 0 & 0 & 0 & 0 & 0 & -K_{yx_2} & -\omega b_{yx_2} & 0 & 0 & -K_{yy_2} & -\omega b_{yy_2} & 0 & 0 & 0 & 0 & 0 & 0 & K_{yx_2} & \omega b_{yx_2} & 0 & 0 & K_{y_2}+K_{yy_2}-m_2\omega^2 & \omega b_{yy_2} \\
0 & 0 & 0 & 0 & 0 & 0 & \omega b_{yx_2} & -K_{yx_2} & 0 & 0 & \omega b_{yy_2} & -K_{yy_2} & 0 & 0 & 0 & 0 & 0 & 0 & -\omega b_{yx_2} & K_{yx_2} & 0 & 0 & -\omega b_{yy_2} & K_{y_2}+K_{yy_2}-m_2\omega^2
\end{bmatrix}
\begin{bmatrix} X_{g_c} \\ X_{g_s} \\ Y_{g_c} \\ Y_{g_s} \\ X_{T_{1c}} \\ X_{T_{1s}} \\ X_{T_{2c}} \\ X_{T_{2s}} \\ Y_{T_{1c}} \\ Y_{T_{1s}} \\ Y_{T_{2c}} \\ Y_{T_{2s}} \\ \Phi_{1c} \\ \Phi_{1s} \\ \Phi_{2c} \\ \Phi_{2s} \\ X_{1c} \\ X_{1s} \\ X_{2c} \\ X_{2s} \\ Y_{1c} \\ Y_{1s} \\ Y_{2c} \\ Y_{2s} \end{bmatrix}
=
\begin{bmatrix} F_1 \\ F_2 \\ F_3 \\ F_4 \\ F_5 \\ F_6 \\ F_7 \\ F_8 \\ F_9 \\ F_{10} \\ F_{11} \\ F_{12} \\ F_{13} \\ F_{14} \\ F_{15} \\ F_{16} \\ F_{17} \\ F_{18} \\ F_{19} \\ F_{20} \\ F_{21} \\ F_{22} \\ F_{23} \\ F_{24} \end{bmatrix}
\qquad (4.80)
$$

4.3 (v) Systems Impedances.

Impedances throughout the representative rotating machine structure when supported in journal bearings may be found from eqn.(4.80). For example, the vertical driving point acceleration impedance at bearing support 1 (see fig.4.5), Z_{yy_1}, is

$$\overline{Z_{yy_1}} = -\frac{F_{y_1}}{\omega^2 \bar{y}_1} \tag{4.81}$$

The bars above the symbols in eqn.4181 indicate that these quantities are vectors and contain, in general, both in-phase and quadrature components. The impedance may therefore be obtained in terms of its modulus $\left|Z_{yy_1}\right|$ and phase θ

$$\left|Z_{yy_1}\right| = \frac{-F_{y_1}\ \Delta A}{\omega^2 \sqrt{\Delta y_{1_c}^2 + \Delta y_{1_s}^2}} \tag{4.82}$$

and $$\theta = \tan^{-1}\left\{\frac{\Delta y_{1_s}}{\Delta y_{1_c}}\right\} \tag{4.83}$$

In eqn. (4.82) and (4.83) Δ_A is the determinant of the square matrix A of eqn.4.80 and Δy_{1_c}, Δy_{1_s} are the determinants of the matrices obtained by replacing the coefficients of y_{1_c} and y_{1_s} in A by the column vector of the forces, $\bar{b}$.

A digital computer programme has been written to obtain the system impedances from the above equations. Although the programme was written in Elliott Algol, due to the size of the programme, and in particular the size of the matrix arrays to be handled, it was far too lengthy to be run on the University's own Elliott 803 machine.

Use was therefore made of the Atlas computer facilities provided by the Science Research Council at Didcot, Berkshire. The function and operation of this programme are shown diagramatically in fig. 4.7. It may be seen from this diagram that the programme made use of some of the Atlas 'library' matrix-handling procedures.

Provision was made for calculating the required impedances for three separate oil viscosity/shaft speed combinations over a range of excitation frequencies. The computing time required on Atlas for 100 different excitation frequencies was between 10 and 12 minutes. These times correspond very roughly to about 50 hours on the Elliott 803.

The biggest drawback experienced in using the Atlas machine was a difficulty of communication, for since it was not possible to check the programme on the Elliott 803 all the initial 'debugging' had to be done on Atlas. This was an awkward and time consuming operation.

4.3 (vi) Unbalance Response.

The responses of the system (fig.4.5) to unbalance excitation are obtained from the equations (4.80) considering generalised forces arising from small unbalance masses added at radii large compared with the resulting whirl amplitudes, as shown in the inset diagram, fig. 4.5.

If, for a particular rotational angular frequency (Ω), time (t) is measured from the instant when the unbalance mass is parallel to axis OX, then the forces acting on the rotor are:-

$m_b . r_b . \Omega^2 \cos \Omega t$ in co-ordinate x_g

$m_b . r_b . \Omega^2 \sin \Omega t$ in y_g

$m_b . \alpha . r_b \Omega^2 \cos \Omega t$ in ϕ_2

and $m_b . \alpha . r_b \Omega^2 \sin \Omega t$ in ϕ_1

The particular solutions are then of the same form as eqns. (4.67) to (4.78) except that the angular excitation frequency ω, is replaced by Ω.

Thus $x_g = X_{g_c} \cos \Omega t + X_{g_s} \sin \Omega t$ and so on.

A programme in the Elliott Algol language has been written to solve the resulting equations to find responses due to any combination of unbalance masses, located anywhere along the rotor/shaft combination.

Like the programme for finding system impedances mentioned in the previous section, this programme also had to be run on the S.R.C. Atlas computer because of its size and complexity. Many of the procedures used in the unbalance response programme were identical to those used in the impedance programme. In the former case, however, bearing coefficients had to be recalculated for each assumed rotational speed.

The computing time required on Atlas was about 7 minutes to calculate responses at three different points in the system for 30 rotational speeds. The equivalent computing time on the Elliott 803 is estimated to be about 30 hours.

4.4 Introduction of Experimental Impedance Data into the Analysis.

In the derivation of the equations of motion given above, it was assumed that the bearing support impedances could be represented by a single degree-of-freedom system in each plane. The support in plane 1, for instance, was assumed to have mass m_1 and stiffness k_{yy_1}, in the vertical plane i.e. a real acceleration impedance $\left(m - \frac{k_{yy_1}}{\omega^2}\right)$

Calculations for the model rig (Chapter 6) were initially based on such impedances, which were approximations to the experimentally determined support impedances. Calculations were also made in which the

measured impedance moduli, Z, and their associated phase angles, θ. were introduced directly into the computer analysis outlined in fig. 4.7.

To illustrate the procedure used, reference is made to the system equation, eqn. (4.80). It may be seen from this matrix equation that the undamped (real) support displacement impedances appear as elements in the leading diagonal in the form $(k - n\omega^2)$. In the more general case where, for example, the vertical driving point impedance of the uncoupled support in plane 1 includes the effect of damping, this would appear as contributions to the coefficients α and β, on and about the leading diagonal, in the form

$$\begin{aligned} \alpha Y_{1_s} - \beta Y_{1_c} &= F_o \\ \beta Y_{1_s} + \alpha Y_{1_c} &= 0 \end{aligned} \qquad (4.84)$$

where F_o is the magnitude of an external, harmonic force, and from eqn.(4.77), Y_{1_s} and Y_{1_c} coefficients in the assumed particular solution:-

$$y_1 = Y_{1_c} \cos\omega t + Y_s \sin\omega t \qquad (4.85)$$

An alternative form of this solution is:-

$$y_1 = Y_1 \sin(\omega t - \theta) \qquad (4.86)$$

where Y_1 is the vector displacement and θ the phase angle, ..

$$\text{or } y_1 = (-Y_1 \sin\theta) \cos\omega t + (Y_1 \cos\theta) \sin\omega t \qquad (4.87)$$

Comparing the coefficients in eqns.(4.85) and (4.87), it may be seen that

$$Y_{1_c} = (-Y_1 \sin\theta) \qquad (4.88)$$

$$Y_{1_s} = (Y_1 \cos\theta) \qquad (4.89)$$

Substituting these expressions into eqn. (4.84)

$$\left.\begin{aligned} \alpha(Y_1 \cos\theta) - \beta(-Y_1 \sin\theta) &= F_o \\ \beta(Y_1 \cos\theta) + \alpha(-Y_1 \sin\theta) &= 0 \end{aligned}\right\} \tag{4.90}$$

From the second of eqns. (4.90)

$$\alpha = \beta \cdot \frac{\cos\theta}{\sin\theta} \tag{4.91}$$

and substituting into the first of eqns.(4.90)

$$\beta = \frac{F_o}{Y_1\left(\frac{\cos^2\theta}{\sin\theta} + \sin\theta\right)} \tag{4.92}$$

$$\text{or} \quad \beta = \frac{F_o}{Y_1} \sin\theta \tag{4.93}$$

$$\text{But} \quad \frac{F_o}{Y_1} = -\omega^2 \cdot |Z| \tag{4.94}$$

$$\text{Whence } \beta = -\omega^2 \cdot |Z| \sin\theta \tag{4.95}$$

and from eqn. (4.91)

$$\alpha = -\omega^2 \cdot |Z| \cos\theta \tag{4.96}$$

By making a slight alteration to the computer programme of fig.4.7 it was therefore possible to 'read in' the measured impedance modulus, $|Z|$, and its associated phase angle, θ, and to allow for the contribution of the support by using the relationships of eqns.(4.95) and (4.96).

Similar modifications to the programme to enable the transfer impedances between the horizontal and vertical planes of the bearing supports, or between the each support could be incorporated with equal ease.

4.5 Extraction of Support Impedances from Measurements on the Complete, Rotating Systen.

Consider an impedance measurement made on the complete machine structure of fig. 4.5 whilst the shaft is rotating - for example, the

vertical driving point impedance, Z_{yy_2} at bearing support 2. It is required to find the value of the uncoupled support impedance, Z_{yy_2}, say, in the absence of the shaft when all other parameters are known or can be calculated.

Referring to the equations of motion of the system, these are, according to equation (4.79), of the form

$$A\,\bar{x} = \bar{b} \tag{4.97}$$

Eqn.4.97 may be written in general terms, as follows, to represent the physical state of affairs during the measurement of the impedance Z_{yy_2} - or any other transposing appropriate rows:-

$$\begin{bmatrix} e_{1,1} & e_{1,2} & \cdots & e_{1,n-1} & e_{1,n} \\ e_{2,1} & e_{2,2} & \cdots & e_{2,n-1} & e_{2,n} \\ \vdots & \vdots & & \vdots & \vdots \\ e_{n-1,1} & e_{n-1,2} & \cdots & e_{n-1,n-1} & e_{n-1,n} \\ e_{n,1} & e_{n,2} & \cdots & e_{n,n-1} & e_{n,n} \end{bmatrix} \begin{bmatrix} x_1 \\ x_2 \\ \vdots \\ x_{n-1} \\ x_n \end{bmatrix} = \begin{bmatrix} 0 \\ 0 \\ \vdots \\ b_{n-1} \\ b_n \end{bmatrix} \tag{4.98}$$

Consider the partitioning of eqn. 4.98 as follows

$$\left[\begin{array}{c|c} A_1 & B_2 \\ \hline B_1 & C \end{array}\right] \left[\begin{array}{c} X_1 \\ \hline X_2 \end{array}\right] = \left[\begin{array}{c} 0 \\ \hline B \end{array}\right] \tag{4.99}$$

$$\text{where } C = \begin{bmatrix} C_{11} & C_{12} \\ C_{21} & C_{22} \end{bmatrix} = \begin{bmatrix} e_{n-1,n-1} & e_{n-1,n} \\ e_{n,n-1} & e_{n,n} \end{bmatrix} \tag{4.100}$$

$$X_2 = \begin{bmatrix} x_{n-1} \\ x_n \end{bmatrix}$$

and
$$B = \begin{bmatrix} b_{n-1} \\ b_n \end{bmatrix} \tag{4.101}$$

Expanding the partitioned matrix equation (4.99) we obtain

$$\left.\begin{aligned} A_1 X_1 + B_2 X_2 &= 0 \\ B_1 X_1 + C X_2 &= B \end{aligned}\right\} \tag{4.103}$$

and eliminating X_1 from eqn. (4.103) and (4.104) gives

$$(C - B_1 A_1^{-1} B_2) X_2 = B \tag{4.105}$$

In eqn. 4.105, since all elements of the matrices B_1, A_1 and B_2 are known quantities, the function $-B_1 A_1^{-1} B_2$ may be evaluated to yield a 2 x 2 matrix. Using the symbol K for the elements of this matrix, to signify that they are 'known' quantities, we may write

$$-B_1 A_1^{-1} B_2 = \begin{bmatrix} K_{11} & K_{12} \\ K_{21} & K_{22} \end{bmatrix} \tag{4.106}$$

Also, due to the symmetry of eqn.4.80, it may be seen that in eqn.4.98

$$e_{n-1,n-1} = e_{n,n} \tag{4.107}$$

and
$$e_{n-1,n} = -e_{n,n-1}$$

So that eqn.4.100 may be simplified to read

$$C = \begin{bmatrix} C_{11} & C_{12} \\ -C_{12} & C_{11} \end{bmatrix} \tag{4.108}$$

In a similar manner, in eqn. (4.106),

$$k_{11} = k_{22} \tag{4.109}$$

$$\text{and } k_{21} = k_{12} \tag{4.100}$$

so that $$-B_1 A_1^{-1} B_2 = \begin{bmatrix} K_{11} & K_{12} \\ -K_{12} & K_{11} \end{bmatrix} \tag{4.111}$$

Expanding eqn. (4.105) using eqns.(4.101), (4.102),(4.108) and (4.111) gives

$$\left(\begin{bmatrix} C_{11} & C_{12} \\ -C_{12} & C_{11} \end{bmatrix} + \begin{bmatrix} K_{11} & K_{12} \\ -K_{12} & K_{11} \end{bmatrix} \right) \begin{bmatrix} x_{n-1} \\ x_n \end{bmatrix} = \begin{bmatrix} b_{n-1} \\ b_n \end{bmatrix}$$

In the case of the impedance Z_{yy_2} measured on the complete system,

$$x_{n-1} = Y_{2_c} \tag{4.113}$$

$$x_n = Y_{2_s} \tag{4.114}$$

and for a sinusoidal forcing frunction $F = F_o \sin \omega t$,

$$b_n = F_o \tag{4.115}$$

$$b_{n-1} = 0 \tag{4.116}$$

So that eqn. (4.112) becomes

$$\begin{bmatrix} C_{11} + K_{11} & C_{12} + K_{12} \\ -C_{12} + K_{12} & C_{11} + K_{11} \end{bmatrix} \begin{bmatrix} Y_{2_c} \\ Y_{2_s} \end{bmatrix} = \begin{bmatrix} 0 \\ F_o \end{bmatrix} \tag{4.117}$$

Solving eqn.(4.117) for the elements C_{11} and C_{12}, it is found that:-

$$C_{11} = \frac{\left(F_o/Y_{2_s}\right)}{\left(F_o/Y_{2_s}\right)^2 + \left(F_o/Y_{2_c}\right)^2} - K_{11} \tag{4.118}$$

$$C_{12} = \frac{\left(F_o/Y_{2_c}\right)\left(F_o/Y_{2_s}\right)^2}{\left(F_o/Y_{2_s}\right)^2 + \left(F_o/Y_{2_c}\right)^2} - K_{12} \tag{4.119}$$

But the quantities (F_o/Y_{2_c}) and (F_o/Y_{2_s}) are related to the impedance measured on the complete system, Z_{yy_2}, by

$$\left| Z_{yy_2} \right| = \frac{F_o}{\sqrt{Y_{2_s}^2 + Y_{2_c}^2}} \qquad (4.120)$$

$$\text{Phase, } \theta = \tan^{-1} \left(Y_{2_c} / Y_{2_s} \right) \qquad (4.121)$$

Eqns. (4.120) and (4.121) give

$$\left(F_o / Y_{2_c} \right) = \left(\left| Z_{yy_2} \right| / \sin \theta \right) \qquad (4.122)$$

$$\left(F_o / Y_{2_s} \right) = \left(\left| Z_{yy_2} \right| / \cos \theta \right) \qquad (4.123)$$

From eqns. (4.122) and (4.123), eqns. (4.118) and (4.119) may be solved for the elements C_{11} and C_{12}.

C_{11} contains the 'real' (in-phase), part of the uncoupled support impedance Z_{yy_2} that it is required to find, together with the journal bearing dynamic coefficient k_{yy_2}, i.e.

$$C_{11} = R_e \left| Z_{yy_2} \right| + k_{yy_2} \qquad (4.124)$$

Similarly

$$C_{12} = I_m \left| Z_{yy_2} \right| + b_{yy_2} \qquad (4.125)$$

Solution of Equations

For the system under consideration (fig.4.5) the equations of motion are such that the matrix A in eqn.4.97 is a 24 x 24 array. The matrices A_1, B_2 and B_1 in the partitioned eqn.4.99 are therefore of dimensions 22 x 22, 2 x 24 and 24 x 2 respectively. The inversion of A_1 to form the expression $-B_1 \ A_1^{-1} \ B_2$ in equation 4.90 is therefore only practical if digital computer facilities are available.

At the time of writing, a provisional computer programme for the S.R.C.Atlas machine has been written to obtain the elements of $-B_1 \ A_1^{-1} \ B_2$, the remaining manipulation being left for hand calculation. The structure of this programme is shown in fig. 4.8 from which it can be seen that use is made of several matrix algorithms from the Atlas library.

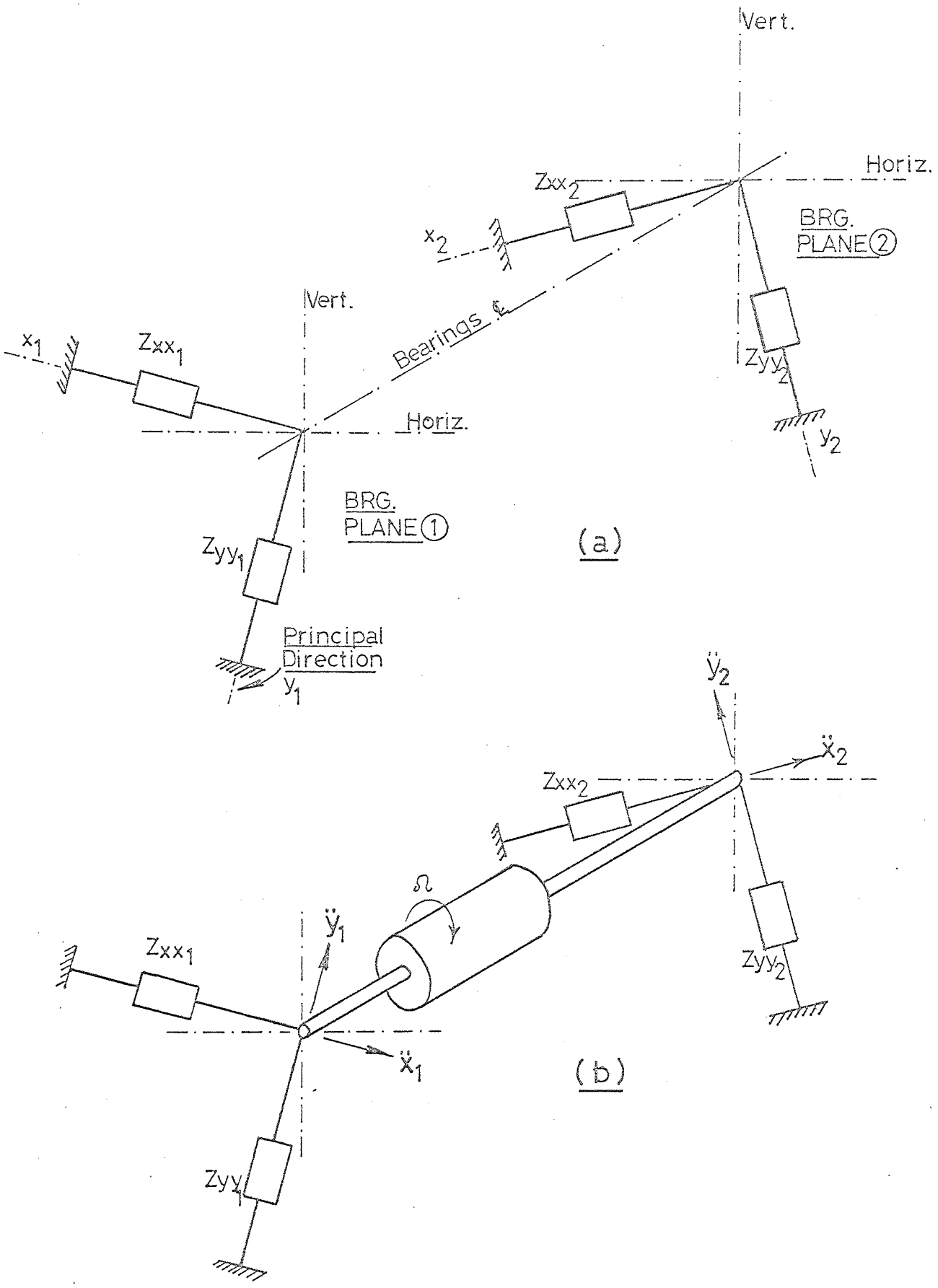

FIG.4.1 BEARING SUPPORT IMPEDANCES AND VIBRATION LEVELS OF IDEAL SYSTEM.

FIG. 4.2 UNDAMPED ROTATING MACHINE SYSTEM REFERRED TO IN CHAP. 4 SECTION 4.2.

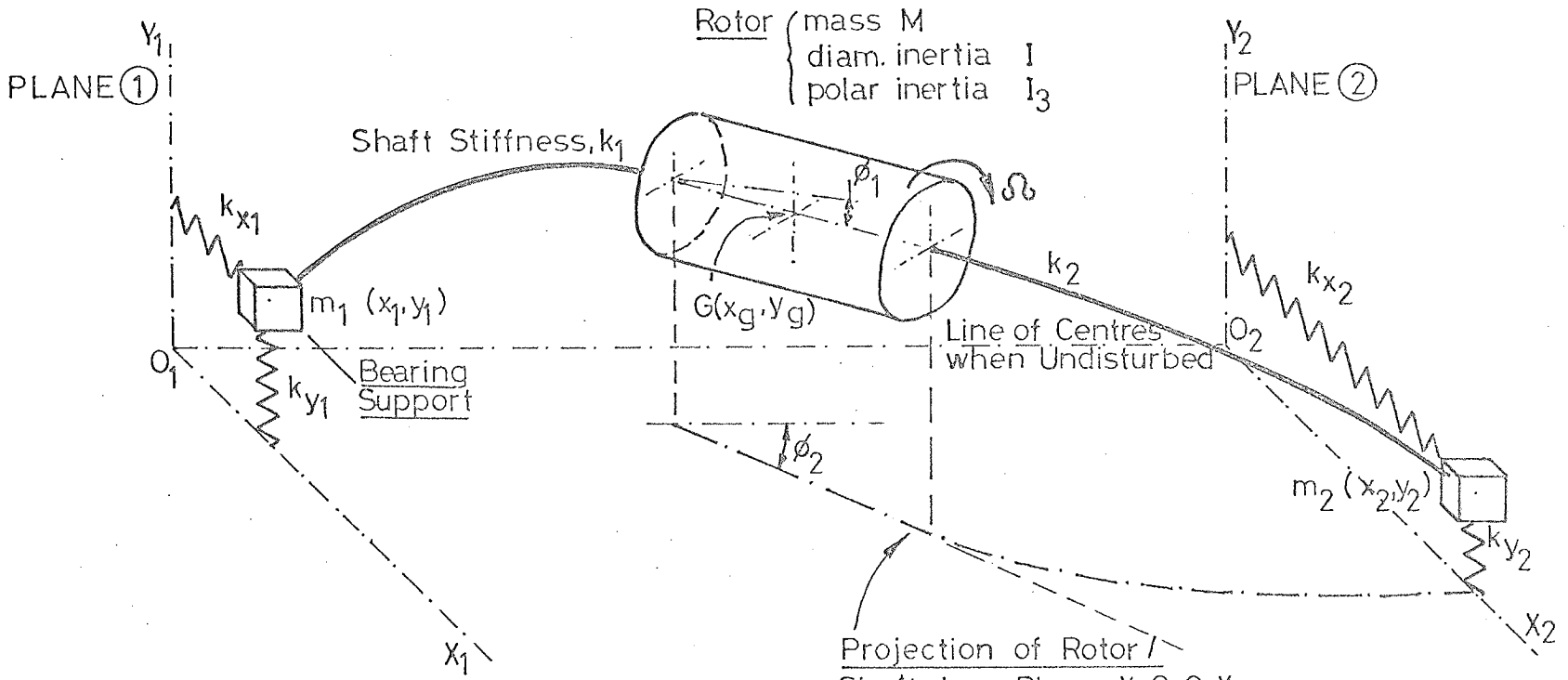

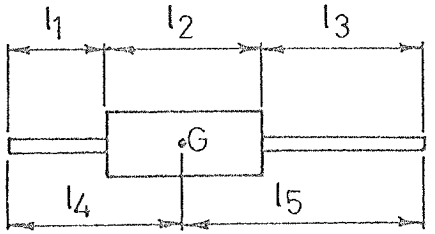

Rotor/Shaft Axial Dimensions

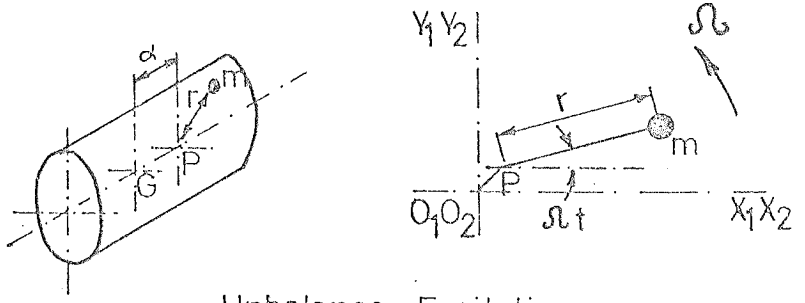

Unbalance Excitation

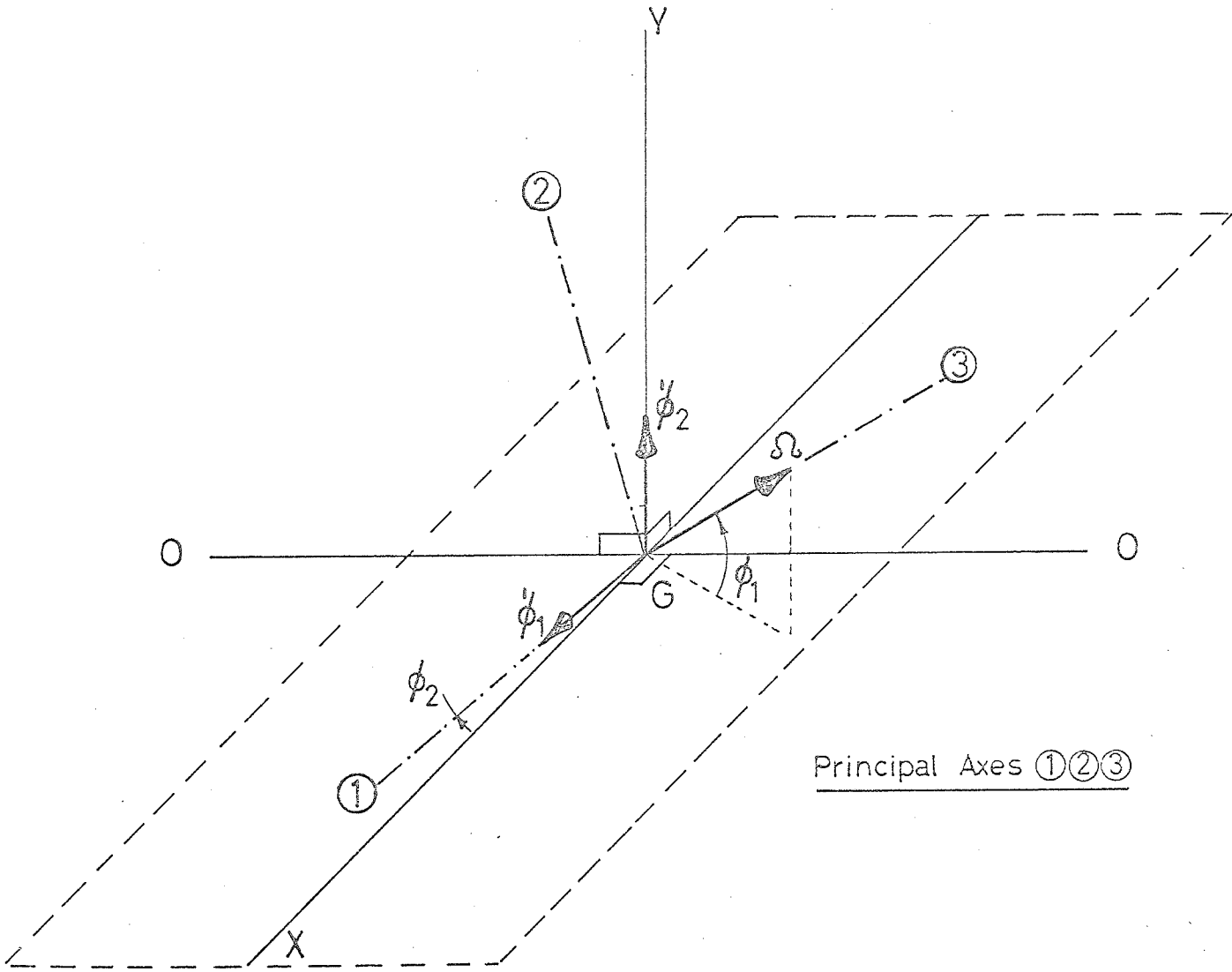

FIG.4.3 ORIENTATION OF ROTOR AXES.

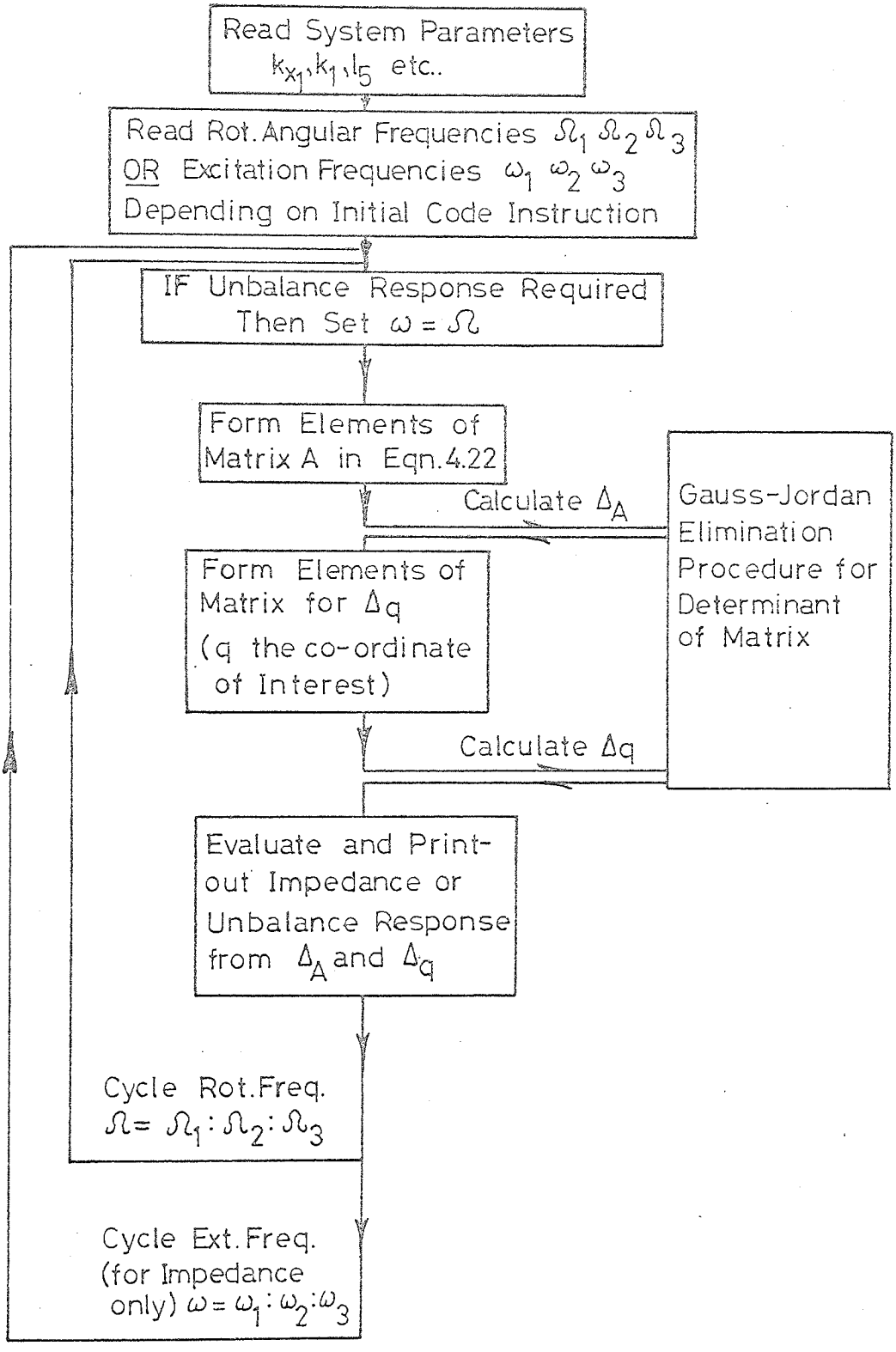

FIG.4.4 SCHEME OF DIGITAL COMPUTER PROGRAMME FOR UNDAMPED ROTATING SYSTEM.

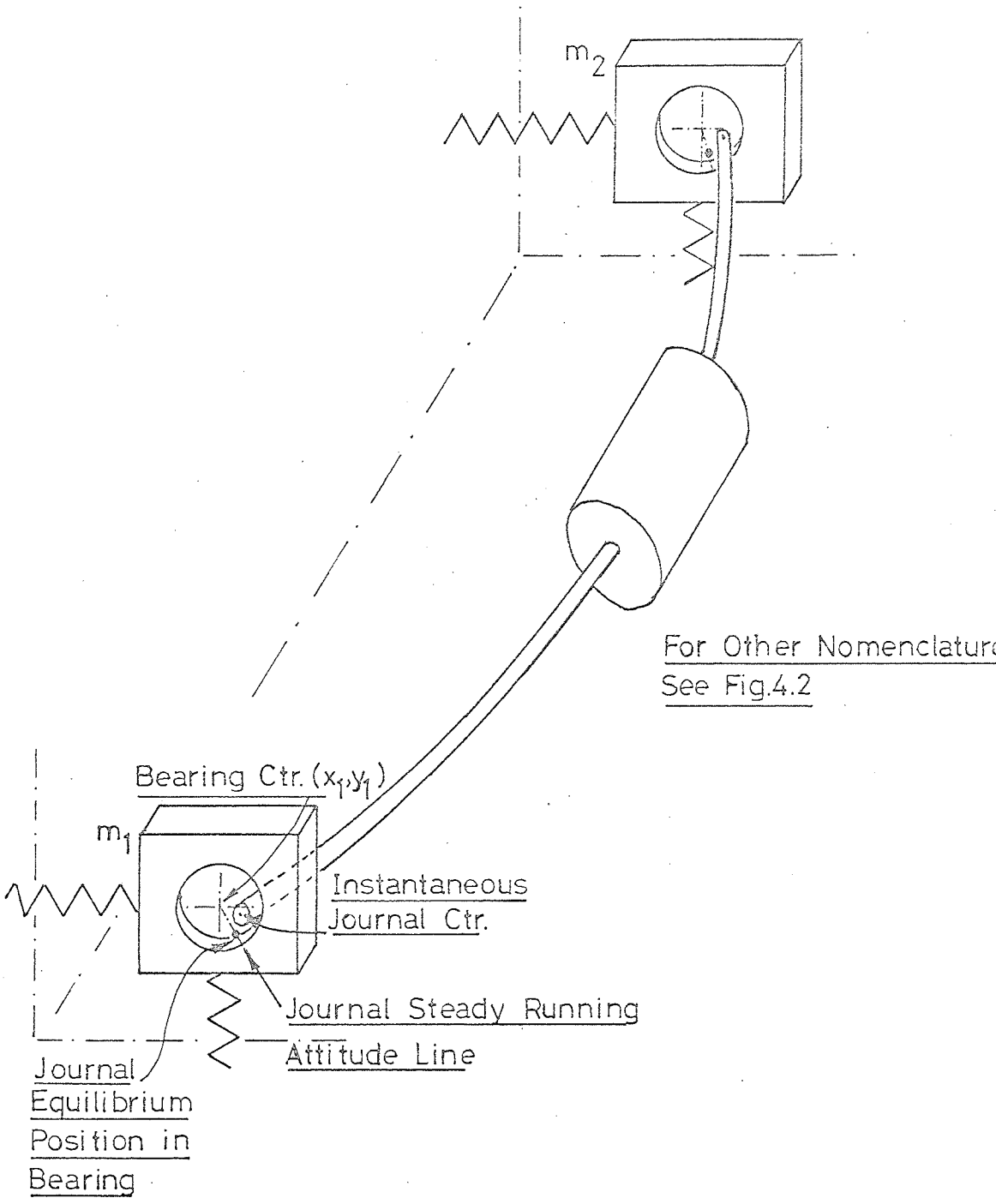

FIG.4.5 ROTATING SYSTEM IN JOURNAL BEARINGS.

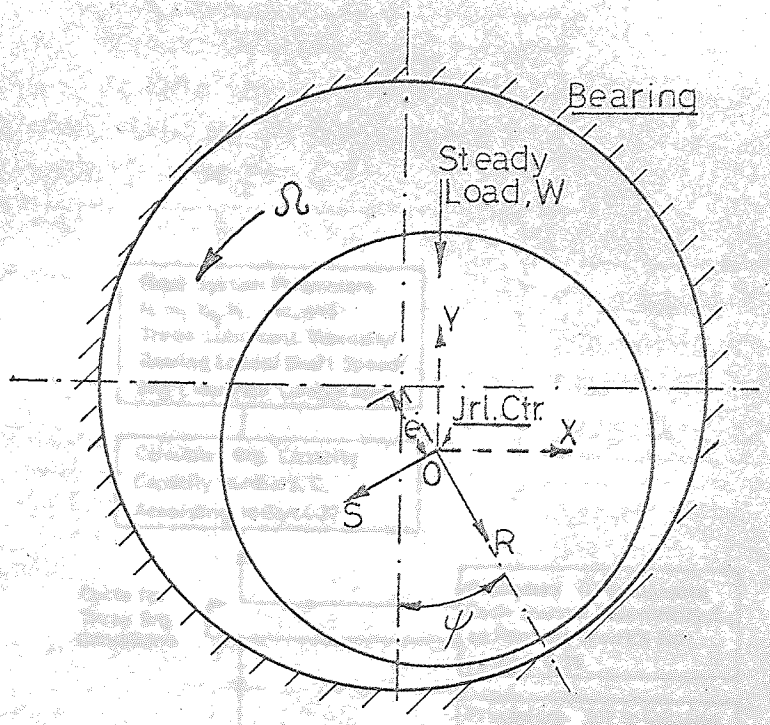

(a) Attitude Axes S, R

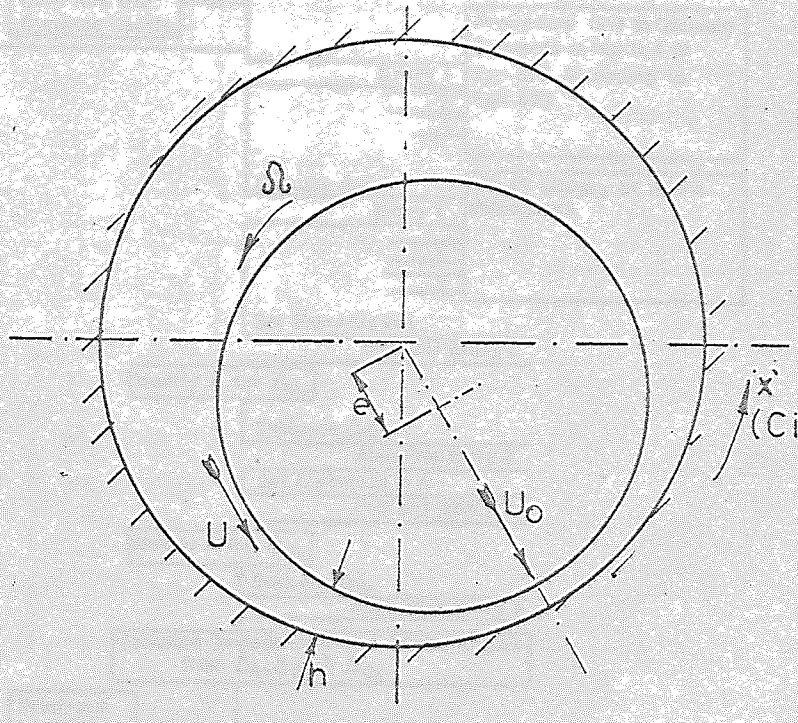

(b) Notation for Eqn. 4.25 — Reynolds Equation

FIG.4.6 JOURNAL BEARING GEOMETRY.

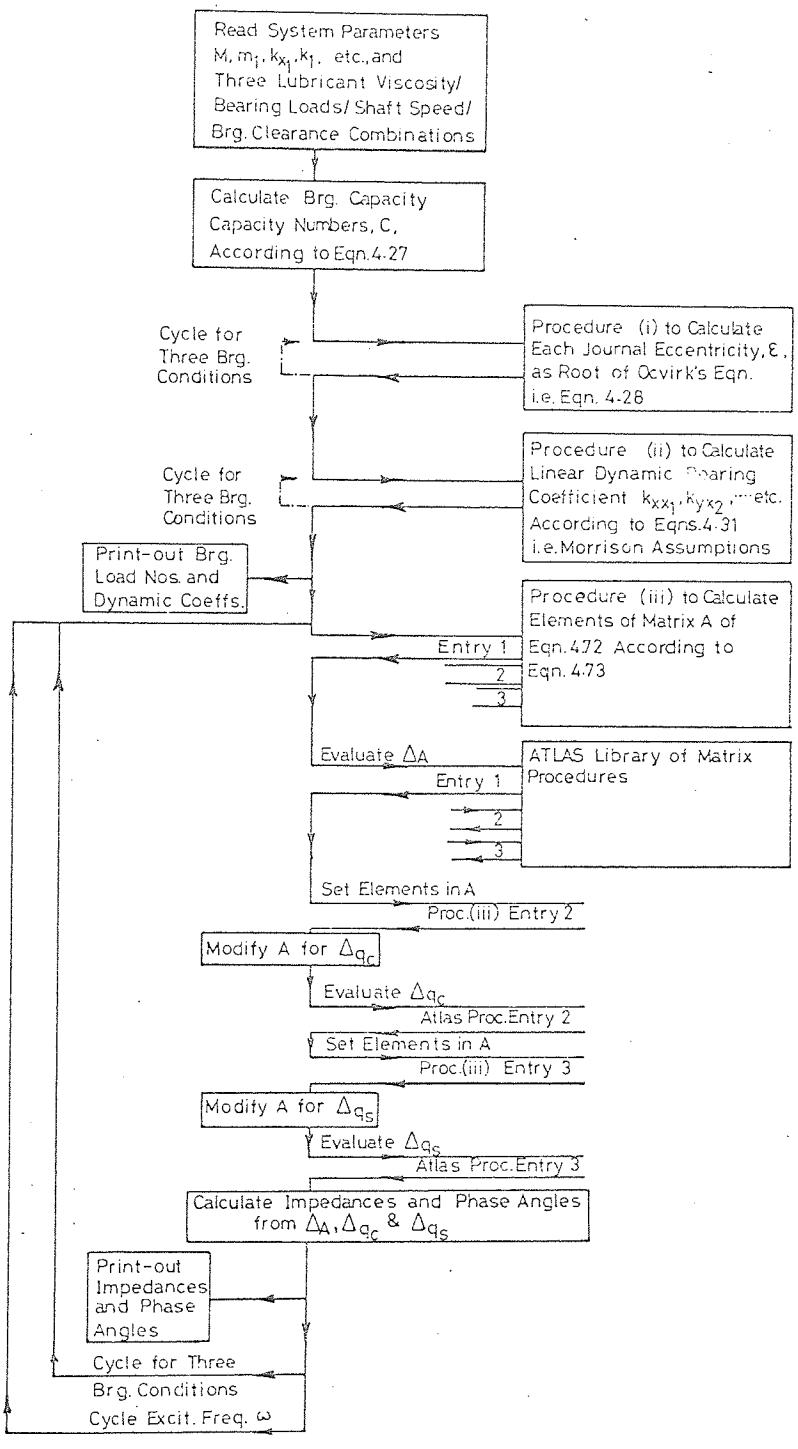

FIG. 4.7. LAYOUT OF PROGRAMME TO CALCULATE IMPEDANCES AT BEARING SUPPORTS OF SYSTEM WITH JOURNAL BEARINGS.

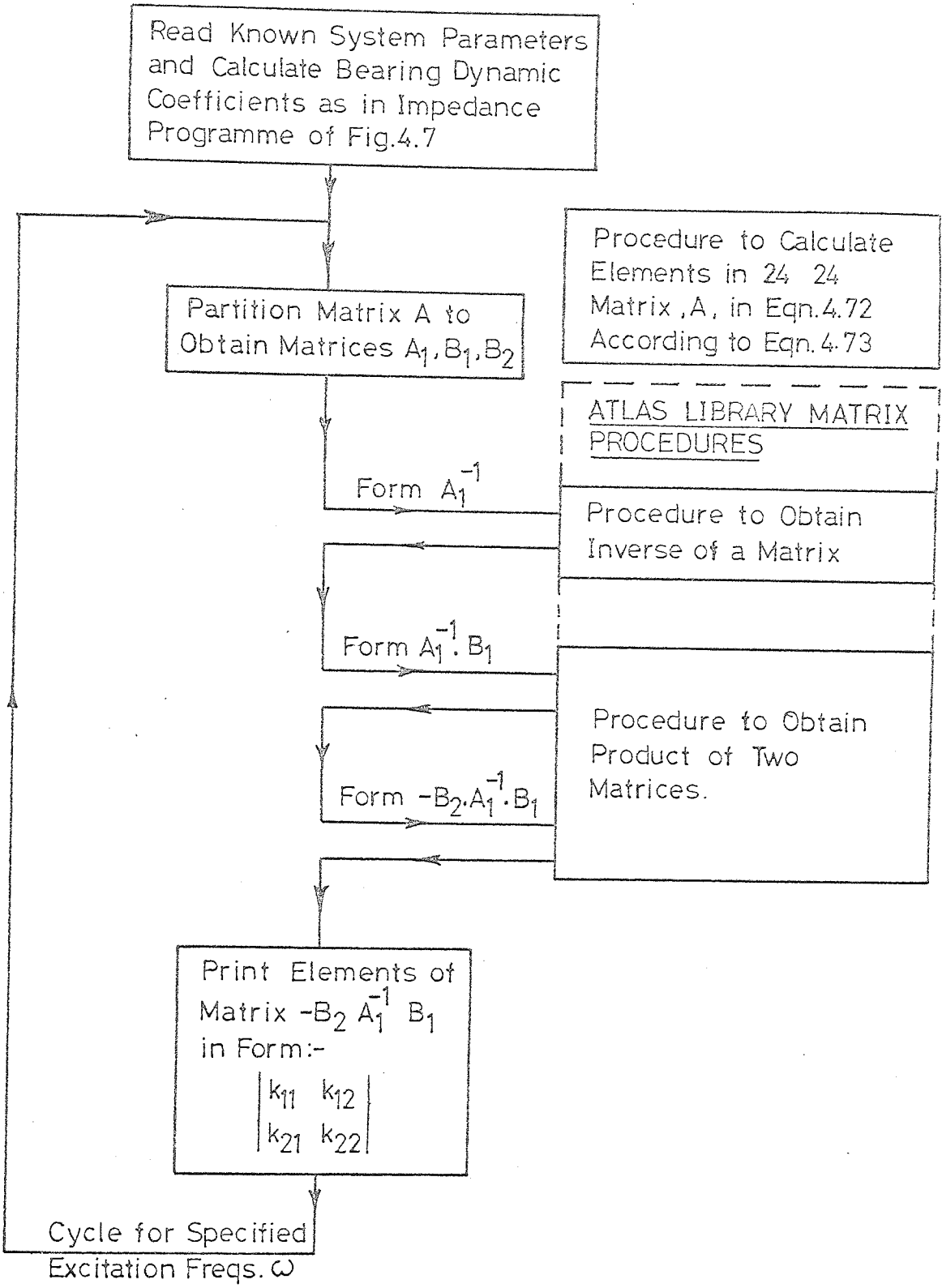

FIG.4.8. SCHEME OF PROGRAMME FOR EXTRACTION OF UNKNOWN SUPPORT IMPEDANCE FROM MEASUREMENT ON COMPLETE SYSTEM.

Chapter 5.

Techniques Used for the Analysis of Periodic and Complex Vibration

Introduction

The writer was fortunate in having access to a wide variety of modern vibration data-analysis equipment. But, like all technologies which are largely reliant on electronic instrumentation, that concerned with data-analysis methods is continually developing. During the course of this project, therefore, new instruments were, from time to time, bought by the Department for general use.

Often it was found worthwhile to incorporate these new instruments in an existing analysis system to improve either or both its speed and accuracy. In this chapter the relevant characteristics of key instruments are discussed but no attempt is made to cover all the minor variations in technique that have been used. Where such minor modifications had a bearing on the interpretation or accuracy of the results obtained, these modifications are pointed out during discussion of the appropriate experiments.

In sections 5.1 to 5.4, below, the properties of the main instruments are discussed whilst sections (5.5 (i),(ii) and (iii) describe complete systems that have been used for performing line spectrum analysis, harmonic tracking and the measurement of mechanical impedance using harmonic excitation.

5.1 Transducers.

Apart from the inductive displacement transducers used on the model rotating machine (Chapter 6), all vibration measurements were made using compression-type piezo-electric accelerometers. These were light and rugged and had a wide frequency range. They were of conventional design consisting of a small, concentrated mass mounted on a piezo-electric crystal which, in turn, was attached to the case of the accelerometer. J.Langham Thompson (J.L.T.) model XA2 or Kistler

model 812 accelerometers were normally used, these having natural frequencies of the crystal-mass combination of 11 kc/s and 18 kc/s, respectively, when they were rigidly mounted. They therefore had linear characteristics up to at least 3.7 kc/s and 6 kc/s respectively. The charge sensitivities of the J.L.T. accelerometers were around 12 pc/g, whilst those for the Kistler instruments were about 6 pc/g, the exact figures for each instrument being checked in the laboratory from time to time. The transverse (cross-axis) sensitivities of all accelerometers were less than 4% of the direct value.

Where possible a single-screw fixing was used for the accelerometers, although on site it was normally more convenient to use small, magnetic mounts. Providing a clean, flat surface was available, this type of mounting was found to be satisfactory up to sinusoidal accelerations of about 2.5g r.m.s. The cases of the J.L.T. accelerometers were electrically connected to one side of their crystals, so small 'Tufnol' insulating strips were always used to prevent earth-loop conditions.

The force transducer (load cell) normally used was a Kistler model 910, which was of the piezo-electric type. This transducer had a maximum load rating of 220 lbf in tension (limited by the strength of the bonding between crystal and case), a charge sensitivity of 20 pc/lbf, and was capable of resolving changes in applied force of about .002 lbf.

5.2 Charge Amplifiers.

The above piezo-electric transducers were invariably used with very high input impedance, capacitive-feedback 'charge' amplifiers. As their name implies, these amplifiers produced voltage outputs proportional to the electrical charge present at their inputs, and hence proportional to the quantity being measured. Using this

configuration, the overall sensitivity was very nearly independent of any capacitance shunted across the transducer terminals (see (7) Chapter 16). This property meant that the transducer cable capacitance was immaterial and very long leads could be used with no loss of performance. Miniature, low-noise coaxial cables, nearly 200 yards long, were frequently used on site.

The charge amplifier normally employed was a six-channel unit, manufactured by Environmental Equipment Ltd. type CVA6, which had, on each channel, continuously variably gain between 0 and 30 mv/pc. When used in conjunction with the J.L.T. accelerometers, overall sensitivities of up to about 360 mv/g were therefore obtainable with no additional amplification. The CVA6 amplifiers had frequency response characteristics which were flat within 5% between 2 c/s and 15 kc/s.

5.3 Magnetic Tape Recorders.

Two magnetic-tape recording systems were widely used for data acquisition and analysis. For site recordings, or whenever it was not feasible to use on-line analysis techniques, an Ampex FR 1300 transportable recorder was used. For laboratory analysis of pre-recorded signals an E.M.I. 2500 loop-deck was available.

5.3 (i) Ampex FR 1300 Recorder.

This instrument was a high-quality instrumentation recorder conforming to the I.R.I.G. (Inter-Range Instrumentation Group) specifications. It had been designed for use with 1" magnetic tape on which 14 channels of information could be recorded. An F.M. (frequency modulation) record/replay system was used on this particular machine, so that high-quality recordings down to zero frequency (D.C.) were possible with little dependence on the properties of the tape itself.

In accordance with the I.R.I.G. specifications, the FR 1300 operated with a 108 kc/s carrier frequency at the fastest tape speed of 60 in/s, whilst it was normally adjusted such that either a 1v r.m.s. or 0.5 v r.m.s. signal produced a 40% frequency deviation. Built-in filtering limited the maximum recording frequency to 20 kc/s at a tape speed of 60 in/s so that intermodulation distortion between this modulating frequency and the lowest significant sideband harmonic was precluded. Tape speeds of 30, 15, $7\frac{1}{2}$, $3\frac{3}{4}$ and $1\frac{7}{8}$ in/s (with appropriate filters) were also available with maximum recording frequencies pro rata the 60 in/s speed. Using standard 3,600 ft reels of tape, recording times from 12 to 384 minutes were obtainable at the fastest and lowest speeds respectively.

The makers quoted figures for signal to noise ratio of 44db and for flutter about 1% p.p. Both these figures were found to be conservative.

5.3 (ii) E.M.I. 2500 Loop Deck.

Continuous tape loops, of any length between about 4ft and 30 ft, could be used on this F.M. deck to produce repetitive (periodic) signals. These were normally obtained from initial data previously recorded on the Ampex FR 1300. The tape transport mechanisms was designed for 1 in wide tape and conformed to the I.R.I.G. specifications regarding head-and track-spacings. One record head and one replay head gave seven data channels, any two of which could be used simultaneously by using plug-in record and replay amplifiers. The fastest tape speed available was 120 in/s at which speed the recording frequency bandwidth was D.C. to 40 kc/s, corresponding to a carrier frequency of 216 kc/s.

To obtain the best performance from the loop deck, particular attention was paid to the quality of the tape splice used to form the continuous loop. It was found from experience that poor reproduction and reduced tape life resulted from imperfect splicing. The aim was

to produce a clean, flat butt-joint and this operation was simplified by using an E.M.I. type 100 tape splicer. This device helped to ensure that the tape on either side of the joint was in line and enabled it to be held firmly during cutting and splicing.

For a tape loop with a well-made joint it was found that around 1000 passes were obtainable before mechanical wear resulted in an unacceptable increase in signal-to-noise ratio. This represented rather more than 5 hours running time when using a 30 ft tape loop and a speed of 15 in/s.

5.4 Tunable Filters

Tunable filters, which discriminate in favour of information within a particular frequency band, form a key part of all vibration data-analysis systems. In the last few years a significant development in this field has been the introduction of electronic 'tracking' filters, which may be aligned by applying an external tuning signal. This facility makes such instruments extremely versatile and they may be used as 'building blocks' in a wide variety of configurations.

Two filters which could be operated in a tracking mode have been used extensively for both laboratory testing and data analysis. These were a Quantech Model 304 Wave Analyser and a Spectral Dynamics SD101A Analyser. Both these instruments had constant filter-bandwidth characteristics and both were of the heterodyne receiver type. (The principal advantage of analysers of the heterodyning type being that, by always translating the data signal to a fixed frequency, greater attention can be paid to the design of the constant centre frequency filters, and their characteristics can be made to approach those of the 'ideal' rectangular filter).

5.4 (i) Quantech 304 Wave Analyser.

Three filter characteristics were available on the Quantech having constant bandwidths of 1, 10 and 100 c/s when measured at the-3db points. Within these bandwidths, the filters had very nearly flat-topped responses, whilst the 'skirts' of the characteristics gave attenuations outside the passband of about 24 db/octave. The filter circuits were active R.C. networks which, by virtue of the heterodyning arrangement, operated at zero centre-frequency.

Input signals having frequency components within the range 0 to 5000 c/s could be analysed, either by manual tuning or by using an automatic, linear sweep. A simplified block diagram of the circuit is shown in fig. 5.1. from which it can be seen that two stages of amplitude modulation were employed. The incoming signal was first used to modulate the output of a variable-frequency voltage-controlled sweep oscillator whose output was between 10 and 15 kc/s. The first intermediate frequency (I.F.) stage allowed only the lower sideband of the modulated signal to pass and the resulting output was then split into two separate channels. The signal in each channel was subsequently used to modulate, respectively, the quadrature-phase outputs (r and j) of a fixed 10 kc/s oscillator. Thus, providing the original input signal was in the range of 0 to 5 kc/s, the lower side-band resulting from this second stage of modulation could be made of zero frequency by adjusting the variable frequency oscillator.

After passing through the constant bandwidth filters, the r and j channels were then chopped and summed to give a meter indication of the amplitude of the data signal within the effective passband.

By way of example, the intermediate frequencies and sidebands are shown in fig.5.1. for an assumed input signal of 1000 c/s with the variable frequency oscillator tuned to 11000 c/s. The latter frequency is seen to result in a zero frequency signal at the constant bandwidth

Several important auxiliary inputs and outputs were available on the Quantech, these being listed below.

Beat-frequency Oscillator; Tuning Frequency & Meter Analogue outputs.

A pure, sinusoidal signal at the tuning frequency was available from the Quantech (O/P 1, fig.5.1.) this being generated using a beat-frequency oscillator (B.F.O.) principle. It was obtained internally by amplitude modulation of the 10-15 kc/s sweep oscillator signal with that from the 10 kc/s fixed oscillator and low pass filtering the result to obtain the lower sideband. By using this output to drive a vibrator during conventional resonance testing, the response analogue of the system under test (derived from an accelerometer, say) could be fed back to the analyser. The centre frequency of the analyser was then always identical to the excitation frequency and therefore the analyser functioned in a tracking mode.

Linear, D.C. voltage analogues of both the meter deflection and the swept frequency were also provided (O/P 2 and 3). These were normally used to drive an X-Y plotter to obtain curves of input signal amplitude within the pass band against filter centre frequency.

'Restored' filtered output.

This output (O/P 4) provided a signal identical in frequency and proportional in amplitude to that part of the data signal within the passband. It was obtained by modulating the sweep oscillator output with the unrectified (10 kc/s chopped) meter signal and low-pass filtering to obtain the lower sideband only.

The instrument could therefore be used as a narrow band-pass filter, but, since both beat frequency oscillator and filtered output channels used the same modulator, it was not possible to monitor the filtered input signal during, for example, resonance tests using the B.F.O.

External Sweep Programming Input.

External control of the sweep oscillator, and hence the tuning frequency, could be achieved by applying a D.C. signal to this input (I/P 2. Fig.5.1.). By varying the input voltage between 0 and 5v, the tuning frequency could be varied from 0 to 5000 c/s.

5.4(ii) Spectral Dynamics SD 101 A Tracking Filter.

Two Spectral Dynamics data analysis systems have been used in the experimental work as discussed in sections 5.5(i) and (iii). Both these systems employed Spectral Dynamics SD 101 A tracking filters.

This tracking filter had a useful frequency range of 2c/s to 25 kc/s and used a hetrodyning frequency of 100 kc/s. A choice of plug-in crystal, lattice-type filters was available having-3db bandwidths of 1.5, 5, 10, 20 and 50 c/s respectively. All these filters had shape factors of 4, indicating that their bandwidth at the 60 db attenuation points was four times that at the 3db points. An internal, mains-frequency calibration signal could be switched to the input of the crystal filters to check that their gain was unity within the passband.

Unlike the Quantech discussed above, the SD 101 A could be tuned directly by an external sinusoid without the need for a frequency-to-voltage converter.

The simplified block diagram (fig.5.2) shows the principle of operation, the effect of the varying stages of modulation being indicated for assumed data and tuning signals of 20 c/s. The side-band frequencies are all shown, those passed by the filters being underlined.

The SD 101 A had three analogue outputs, all functions of that portion of the data signal within the passband, as follows:-

Filtered Signal Output (O/P 1. Fig.5.2)

'Reconstructed' analogue of filtered data signal.

Meter Analogue (O/P 2)

A linear, D.C. analogue giving 1v for full scale meter deflection. This output was normally used to provide a signal for the 'Y' axis of an automatic plotter.

100 kc/s Filter output (O/P 3)

Crystal filter output, whose modulation envelope was the data signal within the passband.

In addition to the above, a further output was available giving a constant-amplitude, carrier-frequency signal (100 kc/s reference oscillator and tuning frequency). This could be used to tune further SD 101 A tracking filters in the analysis system to an identical frequency, without the need for these to have their own carrier converters.

5.5 Typical, Complete Data-analysis Systems Used.

5.5 (i) Line Spectrum Analysis Using Spectral Dynamics.

SD 1001 System

This equipment, having automatic filter-bandwidth switching and variable averaging time facilities, was bought primarily for power spectral density (P.S.D.) analysis of random waveforms. It was equally suitable, however, for line spectrum analysis of periodic and complex signals.

For the sake of example, the method of analysing a recording of machine vibrations taken during constant speed running will be considered - such as were obtained during the vibration survey of the industrial compressors of Chapter 10. A portion of the original site recording, considered to be representative, was played from the

Ampex FR 1300 and re-recorded onto a continuous magnetic tape loop on the E.M.I. 2500 deck. Referring to fig.5.3. it may be seen that the resulting repetitive signal was connected to the input of the SD 101 A tracking filter incorporated in the analysis system.

The tuning signal for the tracking filter was derived from a Spectral Dynamics sweep oscillator which would be swept through the frequency range of interest. Normally, the frequency range chosen was 20 to 1200 c/s, this including up to the fifth-order running frequency of the fastest machines encountered.

By connecting the analogue outputs of oscillator frequency (i.e. filter centre frequency) and filter response to the X and Y channels of the Electro Instruments plotter, a plot of signal amplitude within the passband versus centre frequency was obtained - that is the line spectrum of the data signal.

A Hewlett-Packard logarithmic converter could be used to provide a logarithmic amplitude scale for the filter response whilst a logarithmic frequency scale was also available by using a 'D.C. $\propto$ log.frequency' output from the sweep oscillator. It was also possible to sweep the oscillator at either a linear or logarithmic rate, although the former was preferable since constant-bandwidth filters were being used.

Different filter bandwidth and sweep rate combinations could be automatically switched in at up to three, pre-selected frequencies.

As in all such analyses, some compromise was sought between the theoretically ideal process and that consistent with reasonably fast analysis times. Although there were no inherent statistical uncertainties or sampling errors associated with periodic data reduction, the following factors had to be considered:-

(a) Resolution

To provide the maximum resolution of close frequency components, and to accurately identify their respective frequencies, a very narrow filter bandwidth would be required. However, the time required to perform an analysis increases with decreasing filter bandwidth, as discussed in sub-section (c) below. The object was therefore to select filters which adequately resolved the spectrum without unnecessarily lengthening the analysis time. To be infallible, such a selection would require a prior knowledge of the spectrum to be analysed. In practice it was found that, for the majority of analyses of rotating machinery vibration, a 5 c/s bandwidth filter provided adequate resolution, whilst at higher frequencies this could often be increased to 20 c/s.

(b) Tape loop period, Tp

By recording a portion of the original data signal onto the tape loop a fictitious fundamental frequency, that of the loop passage frequency. f_p, was introduced. In general, therefore, the line spectrum of the signal from the loop deck would contain all harmonics of the loop passage frequency - f_p, $2f_p$, $3f_p$ and so on.

It may be shown (Burrow (101)) however, that providing the loop period T_p is greater than about ten times the period corresponding to the lowest data frequency present, little error is introduced since harmonics of the loop frequency away from the data frequencies are insignificant.

It was always ensured, therefore, that

$$T_p \left(= \frac{1}{f_p}\right) > \frac{10}{f_1} \qquad (5.1)$$

An alternative method of arriving at a suitable minimum record length is by considering it to be an isolated data sample to which the analyser filter must respond. The speed of response of a filter

depends inversely on its bandwidth, B, the exact properties depending on the filter's design.

For the crystal filters used in the SD 101 A analysers, and, approximately, for all narrow, constant-bandwidth filters, the signal must be applied for about 4/B seconds before the output reaches 98-99% of the steady state value (see Burrow (101)). Thus the criterion to be satisfied under these assumptions was that the loop period T_p exceeded the value given by

$$T_p \quad (= \frac{1}{f_p}) > \frac{4}{B} \qquad (5.2)$$

Since the lowest data frequency of interest was normally around 25 c/s (induction motor running frequency), using the 5 c/s filter the relationships given in eqn. 5.1 and 5.2 suggested minimum loop periods of 10/25 = 0.4 seconds and 4/5 = 0.8 seconds respectively.

For the majority of tests it was possible to obtain several minutes of stationary vibration data. Sufficient information was then available to make loop recordings of about 25 seconds duration, corresponding to a tape loop length of 30 ft with a tape speed of 15 in/s, i.e. much longer than the required minimum periods calculated above.

(c) Analysis Sweep Rates

To obtain accurate line spectra, it was necessary to sweep the analyser through the frequency range of interest at a sufficiently slow rate to enable the complete measuring system to respond to discrete data frequency components as they were encountered. As a given component came within the filter bandwidth, the filter itself, the detecting circuit, logarithmic converter and X-Y plotter had to reach the full steady-state level. For the overall system, the response times of each item must be added to obtain the total rise time, T.

(contrary to the advice offered by many papers and instrument handbooks on the subject).

Considering the filter and detecting circuits alone, the sweep rate should not be faster than one bandwidth every $(\frac{4}{B} + T_d)$ seconds, where T_d is the detector circuit response time and $4/B$ that due to the filter (see section (b) above). With no added averaging the value of T_d for the D.C. analogue output of the SD 101 A tracking filter was less than 0.1 secs. Sometimes, however, - for instance when the machine speed has been fluctuating slightly during the original site recording - small amounts of R.C. averaging were switched in to obtain clean, readable traces on the X-Y plotter. Under these conditions estimates of the fastest permissible sweep rate, R, could be obtained from

$$R = \frac{B}{(\frac{4}{B} + 4RC)} \qquad (5.3)$$

It should be mentioned here that the combined response time of the filter and averaging circuits, as given in eqn. (5.3) was independent of signal amplitude. The effective response times of the logarithmic converter and X-Y plotter, however, were functions of their response rates and of the signal amplitude. The makers figure for the response rate of the logarithmic converter was 60 db/s (absolute maximum) whilst that for the Electro-Instrument plotter was 15 in/s for the Y axis. These responses often governed the choice of maximum permissible sweep rate.

Other Line Spectrum Analysis Systems

The Quantech 304 analyser (sect. 5.4(i)) was also used for line spectrum analysis in conjunction with a Moseley X-Y plotter. In this arrangement no external sweep oscillator was required but only linear amplitude-frequency plots could be obtained without additional equipment. Of the three sweep times available on the Quantech, one was selected which allowed for the response rates of filter and plotter as discussed above.

5.5 (ii) 'Harmonic Tracking' of Rotating Vibration using Quantech 304 Wave Analyser.

In tests on the model rig and on the industrial machines (Chapters 6, 7 and 10) it was often required to plot the variation in vibration level at particular multiples of running frequency versus machine speed. For example, in the investigation into bearing instability of the ethylene compressor K 107 (Chapter 10, Section 10.4 (i) (b)) the multiple of interest was about 0.5 times running frequency.

One data analyser method that has been used is illustrated diagrammatically in fig.5.4., from which it can be seen that a reference signal was derived from the rotating shaft. Sometimes this signal was obtained from an existing A.C. tacho-generator, whilst on other occasions a magnetic inductive pick-up was used to generate pulses as a small, ferrous marker attached to the shaft passed the pole of the pick-up. A further method used for obtaining a reference signal made use of a pulse output from an E.M.I. Stroboscope. The stroboscope was triggered photo-electrically from reflective markings on the shaft, normally alternate strips of black and white P.V.C. adhesive tape, and delivered a square-wave output at half the triggered frequency.

In the case of site tests, the reference signal, together with the required accelerometer charge-amplifier outputs, were recorded simultaneously on the Ampex FR 1300 tape recorder as the machine speed was varied.

During subsequent analysis the reference signal was used to drive a Vidar frequency-to-D.C.voltage converter, which in turn was used to tune the Quantech 304 analyser via its external programming input.

The Vidar converter would operate quite satisfactorily from almost any repetitive input signal waveform, and its frequency to voltage sensitivity could be continuously varied between 0 and 0.25 volts per c/s over the range 2 c/s to 20 kc/s. This meant that, in conjunction with the Quantech, ratios of tracking frequency (filter centre-frequency) to reference signal frequency between 0 and 250 could be achieved with no additional attenuation or amplification.

Where the relationship between reference frequency and shaft speed was accurately known, the required tracking ratio was set before analysis using an A.F. oscillator as input to the Vidar and a digital frequency counter to monitor the Quantech centre frequency (B.F.O. output). Otherwise the first-order running frequency vibration, present all machines, at full or other known speed was used to check alignment.

As for the swept frequency line spectrum analysis techniques discussed in section 5.5(i)(c), it would be necessary, for accurate analysis, to control the rate at which the above tracking process was performed. In the case of industrial machines, however, the writer rarely had any direct control over the machine speed and sometimes the run-up to full speed was executed at a rate faster than that consistent with accurate analysis.

In the case of data tape-recorded on the Ampex FR 1300 it was sometimes possible to compromise by using a slower replay speed, but this often meant that the adjacent harmonic rejection capability suffered. For example, consider the harmonic tracking, using a 10 c/s filter, of first order running-frequency vibration on a machine running up from standstill to 200 c/s. Slowing down the original recording by a factor of eight (60 in/s record speed - 7.5 in/s replay speed, say) would have meant that the new frequency range was 0 to 25 c/s.

If the 10 c/s filter had still been used to analyse this slowed-down data, vibration components of both first-and-second-order running speed would have been simultaneously within the filter bandwidth up to 10 c/s - i.e. 80 c/s original running speed.

Even where this process did effect some improvement in the accuracy of the analysis, no correction could be made for the effect of non-stationary excitation of the original machine structure. These problems did not arise during run-down of a machine since deceleration rates were always much smaller.

Other Harmonic Tracking Methods.

The Spectral Dynamics SD 1001 analysis system, mentioned in section 5.5 (i) above, had been modified to include a 'tracking frequency multiplier' (T.F.M.) unit. This device enabled the SD 101 A tracking filter to be tuned, in place of the sweep oscillator, to a multiple of an input tuning signal. This system had the advantage of preset tuning ratio calibration, but since the complete system was rack mounted it was only convenient for analyses from tape recorded data.

5.5 (iii) Spectral Dynamics Mechanical Impedance Measuring System.

Historically, this equipment was of some interest since it was one of several designs built by American firms to meet specification of the U.S.Defence Ministry for impedance testing. Its performance was favourably reviewed in a report on an extensive series of 'round-robin' test measurements organised throughout the U.S. by Remmers et al (103). The particular system used by the writer was the first to be imported into this country (1966).

The complete rack of equipment was too large to be moved conveniently, even from one laboratory to another. All relevant

signals taken during a test were therefore recorded on the Ampex FR 1300 tape recorder and analysed later on the Spectral Dynamics equipment. The techniques used are conveniently divided under the headings 'data acquisition' and 'data analysis' below. Figs.5.5. and 5.6. show, in simplified block diagram form, the main features of these two operations.

Data Acquisition fig.5.5.

As in conventional resonance testing, the arrangement used consisted of an oscillator - providing a pure, sinusoidal signal - driving an electromagnetic vibrator through a power amplifier. The vibrator normally used was a Goodman type V50, which had a rated thrust of 24 lbf, and this was coupled to the structure at the required point through a Kistler force transducer. One output from the charge amplifier associated with the force transducer was used to provide a force feed-back signal to an automatic gain control (compressor) circuit. The particular compressor used was a Dawe type 1437A and it was connected between the oscillator and power amplifier. Constant force excitation was thereby achieved, which was desirable to maintain checks on linearity of the test structure.

Outputs from force cell and accelerometer charge amplifiers were recorded on the Ampex tape recorder, together with a signal from the oscillator. This oscillator signal was subsequently used for tuning the Spectral Dynamics tracking filters during data analysis.

Any good quality A.F. oscillator would have been suitable for these tests but it was found convenient to use the B.F.O. output from the Quantech 304 analyser (section 5.4 (i)). It was then possible to sweep the Quantech through a particular range and to use the analogue meter and frequency outputs to plot a response curve on the X-Y recorder at the same time as the tape recording was being made. This provided

a check on the satisfactory operation of the instrumentation and sometimes indicated the need to examine particular frequency ranges more closely. Sweep rates of the Quantech oscillator had to be selected bearing in mind the filter response times etc. that were to be used in the analysis system.

With regard to the trasnducers, it should be mentioned that for driving-point impedance measurements (i.e. force and response at the same location) the Kistler accelerometer and force cell were originally coupled in series in an 'impedance head' configuration, as recommended by the makers. It was found, after several apparently meaningless tests had been performed, that the accelerometer was so designed as to be sensitive to axial loading. Also, the series mechanical impedance of the force transducer, which was stiffness controlled at low frequencies, was of a comparable order to the impedances being measured. In all subsequent tests, therefore, the accelerometer was used independently of the load cell. For driving point impedances it was placed either as close as possible to the point of force application or on the opposite side of the test structure, in line with the forcing axis. The latter method was valid providing the coupling impedance of the structure between force transducer and accelerometer was much greater than the driving point impedance being measured.

Data Analysis fig.5.6.

The Spectral Dynamics mechanical impedance measuring system provided a method of automatically plotting the force-response ratio (impedance modulus) and the corresponding phase angle between force and response. Since these quantities were required with respect to the fundamental frequency only, force and response signals were filtered to remove noise, distortion and extraneous vibration frequencies. For this purpose two Spectral Dynamics SD 101 A

tracking filters were used, in the force and response channels respectively, and these filters were tuned by a sinusoidal signal from the sweep oscillator. The oscillator was programmed by the tape-recorded tuning signal with the aid of the Vidar frequency-to-voltage converter. When the Vidar was correctly adjusted the tracking filters were therefore aligned to the recorded tuning frequency i.e. the original excitation frequency.

Each SD 101 A tracking filter operated in a servo-loop with a Houston Instruments potentiometric-ladder type logarithmic converter. This arrangement ensured that, within the response speed capabilities of the servo, the tracking filters always operated at a constant input signal level.

To obtain an analogue output proportional to the logarithm of impedance, the outputs from the log. converters (proportional to log force and log acceleration response) were subtracted electrically.

Thus:-

$$\log \frac{F}{\ddot{x}} = \log F - \log \ddot{x}$$

With this analogue output applied to the Y axis of the plotter, and a D.C. ∝ log. frequency signal from the sweep oscillator applied to the X axis, a plot of log. impedance versus log. excitation frequency was obtained.

An Acton phase meter received the 100 kc/s filtered-output signals from the SD 101 A tracking filters which were phase coherent with the corresponding data-frequencies within the filter passband. The phasemeter therefore operated at a constant high frequency of 100 kc/s, a situation which favoured accurate phase measurement. A D.C. analogue output of phase was available from the phasemeter which enabled plots to phase versus log.frequency to be obtained.

Built-in facilities were available for calibrating the complete system, including the X-Y plotter, - in two steps of 40 db for impedance and at 0 and 360 degrees for phase.

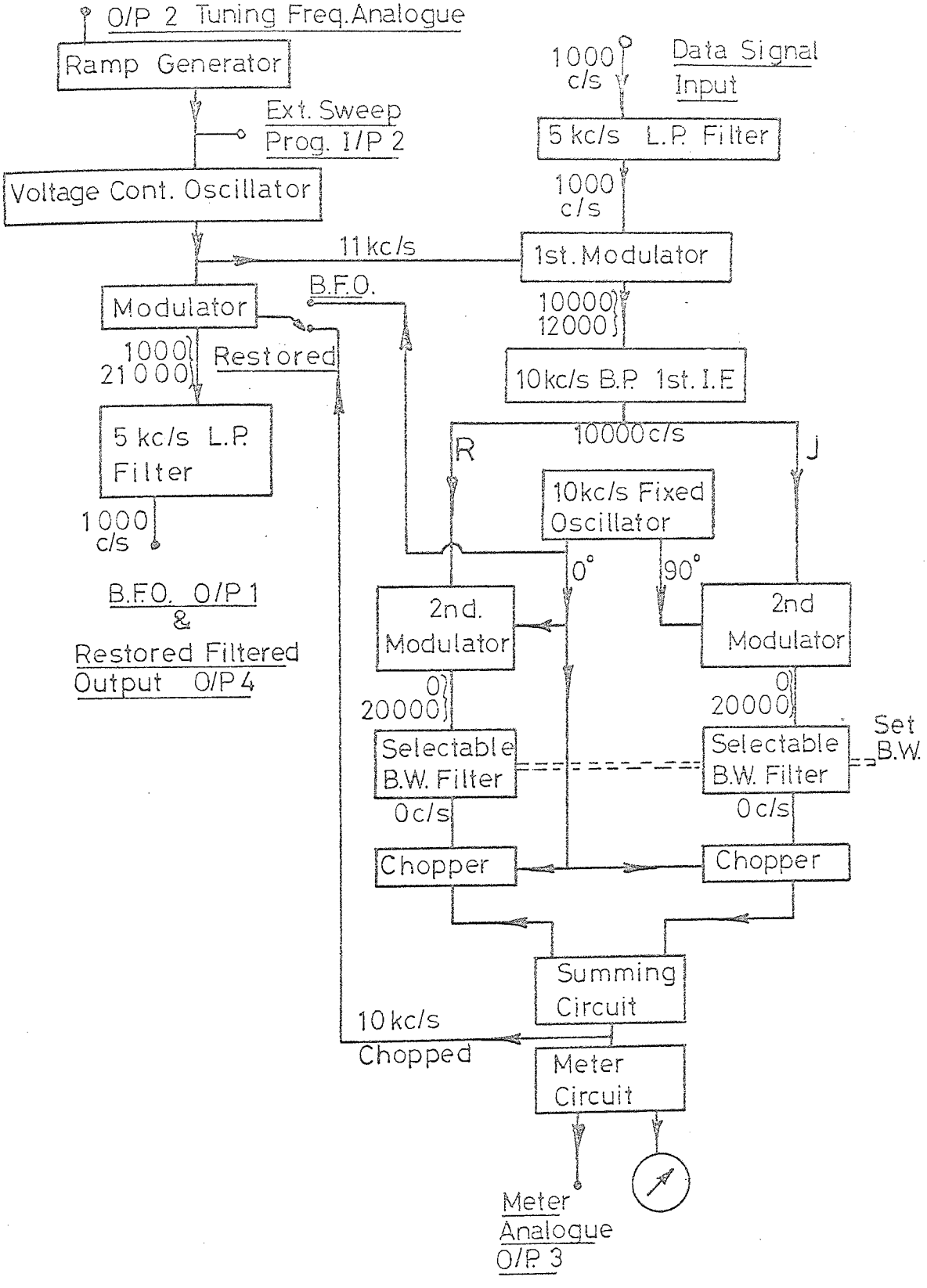

FIG. 5.1 QUANTECH 304 WAVE ANALYSER FACILITIES.

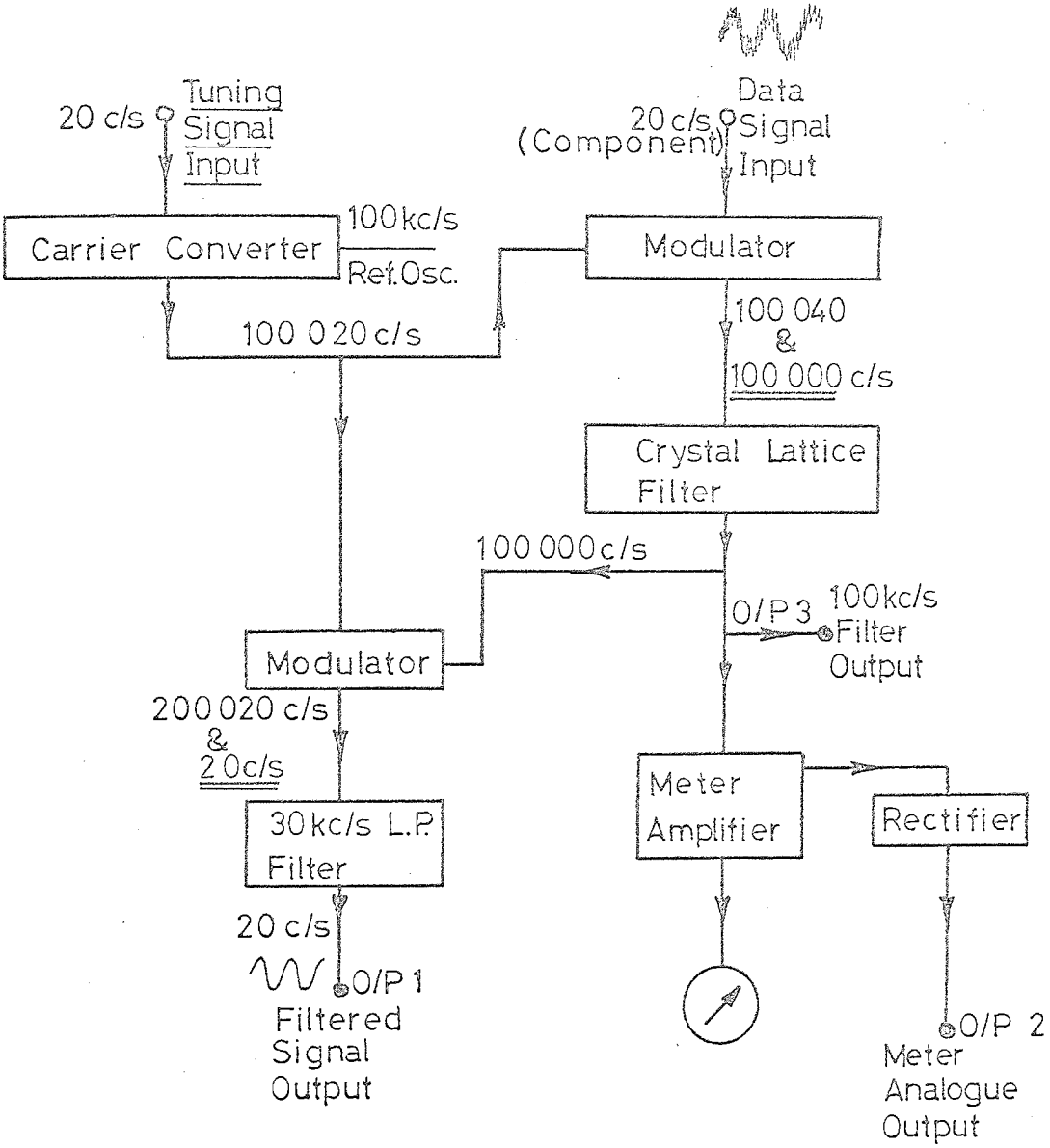

FIG. 5.2 'SPECTRAL DYNAMICS' SD101A
TRACKING FILTER FACILITIES

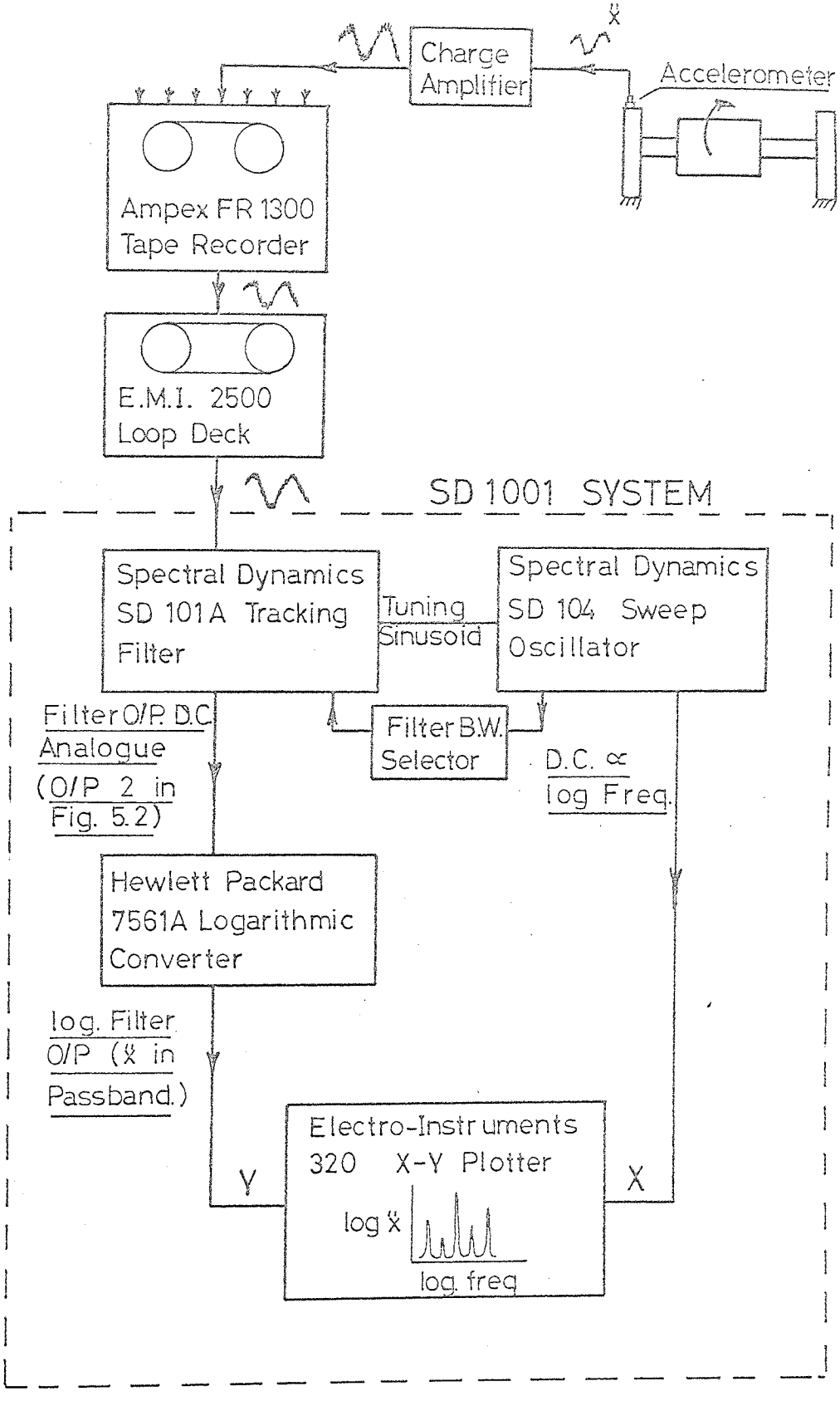

FIG. 5.3 LINE SPECTRUM ANALYSIS USING 'SPECTRAL DYNAMICS' SD1001 SYSTEM

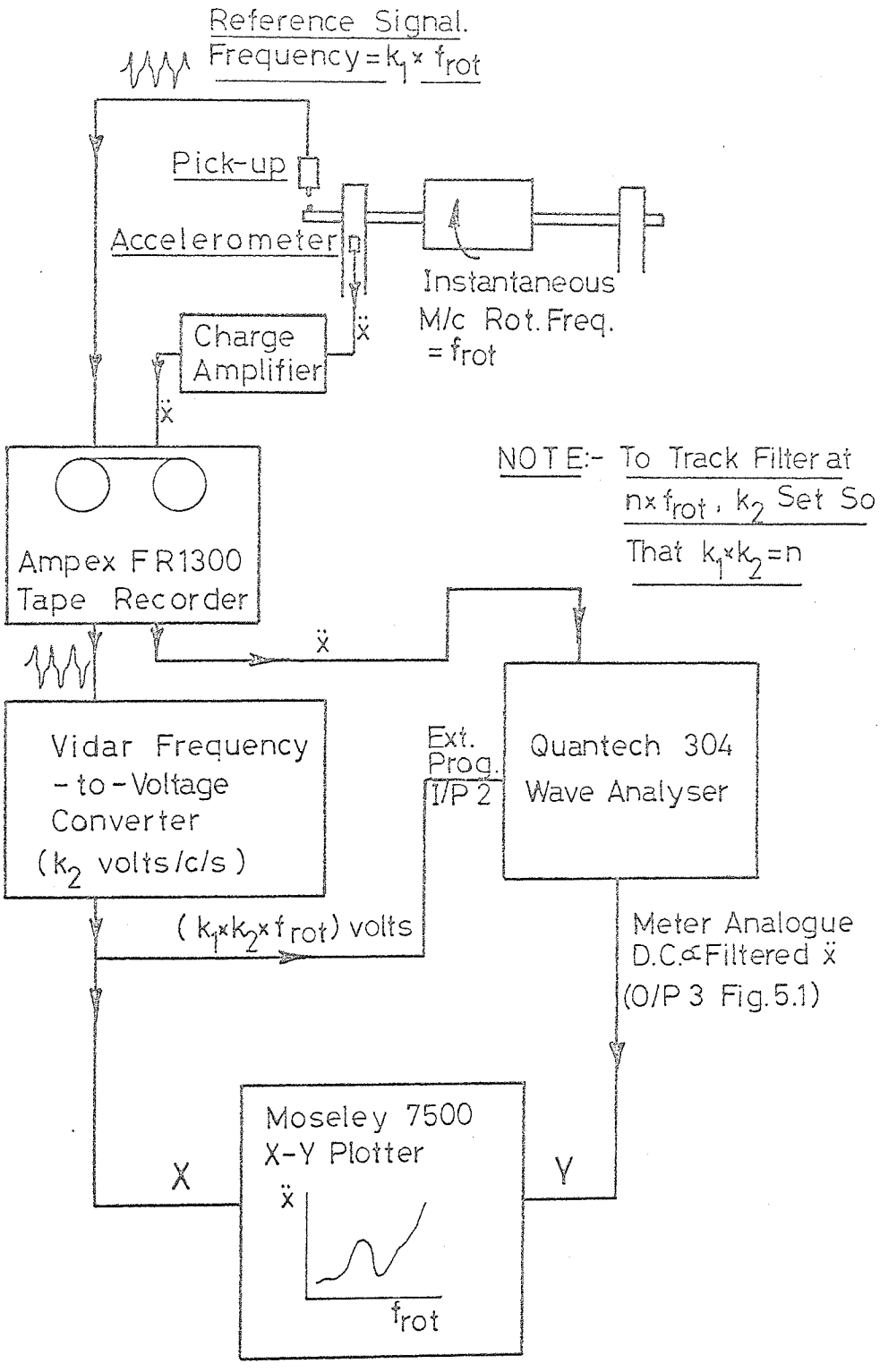

FIG. 5.4 HARMONIC TRACKING OF ROTATING MACHINE VIBRATION USING QUANTECH WAVE ANALYSER

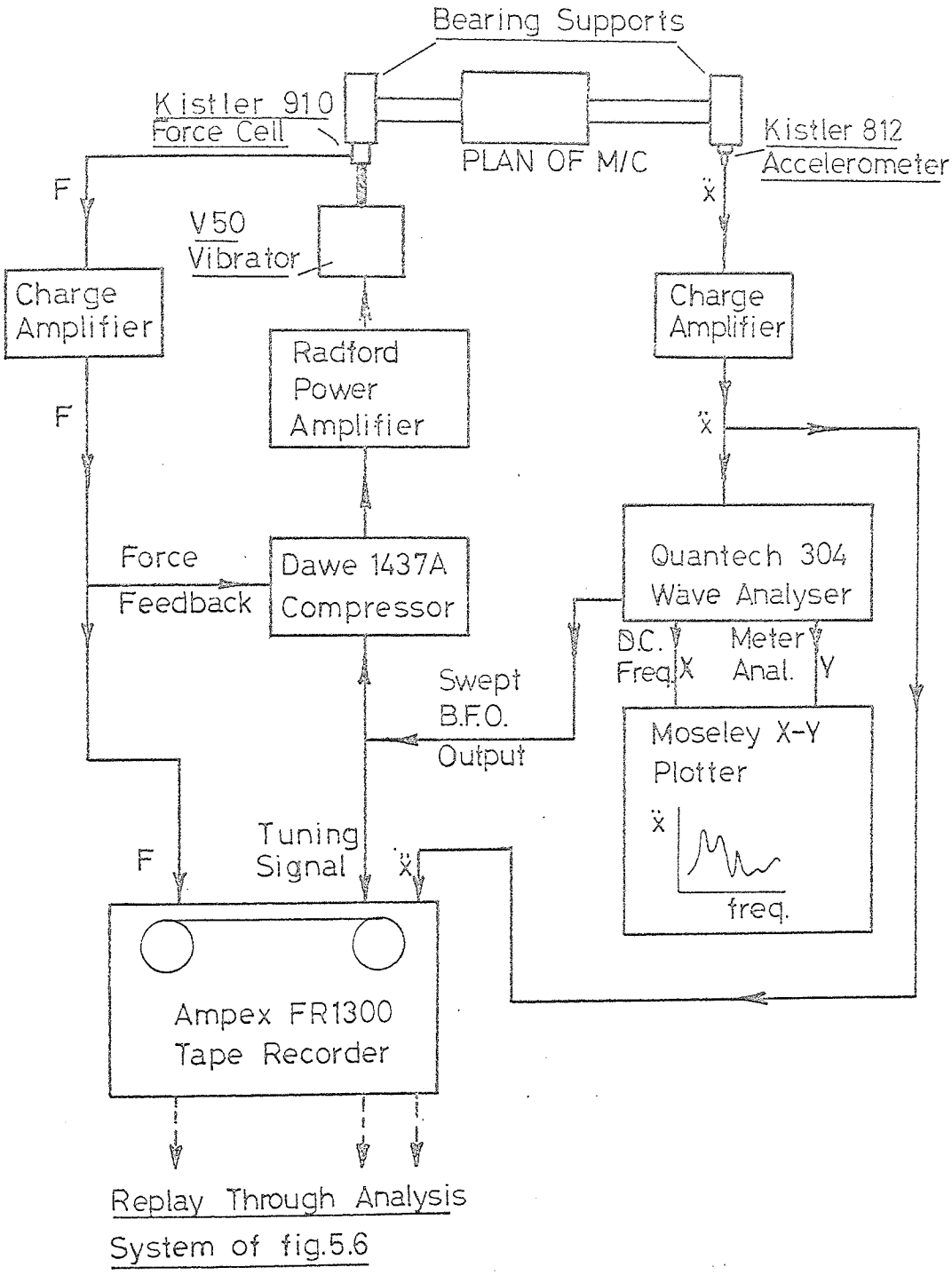

FIG.5.5 MECHANICAL IMPEDANCE MEASUREMENT USING HARMONIC EXCITATION: DATA ACQUISITION.

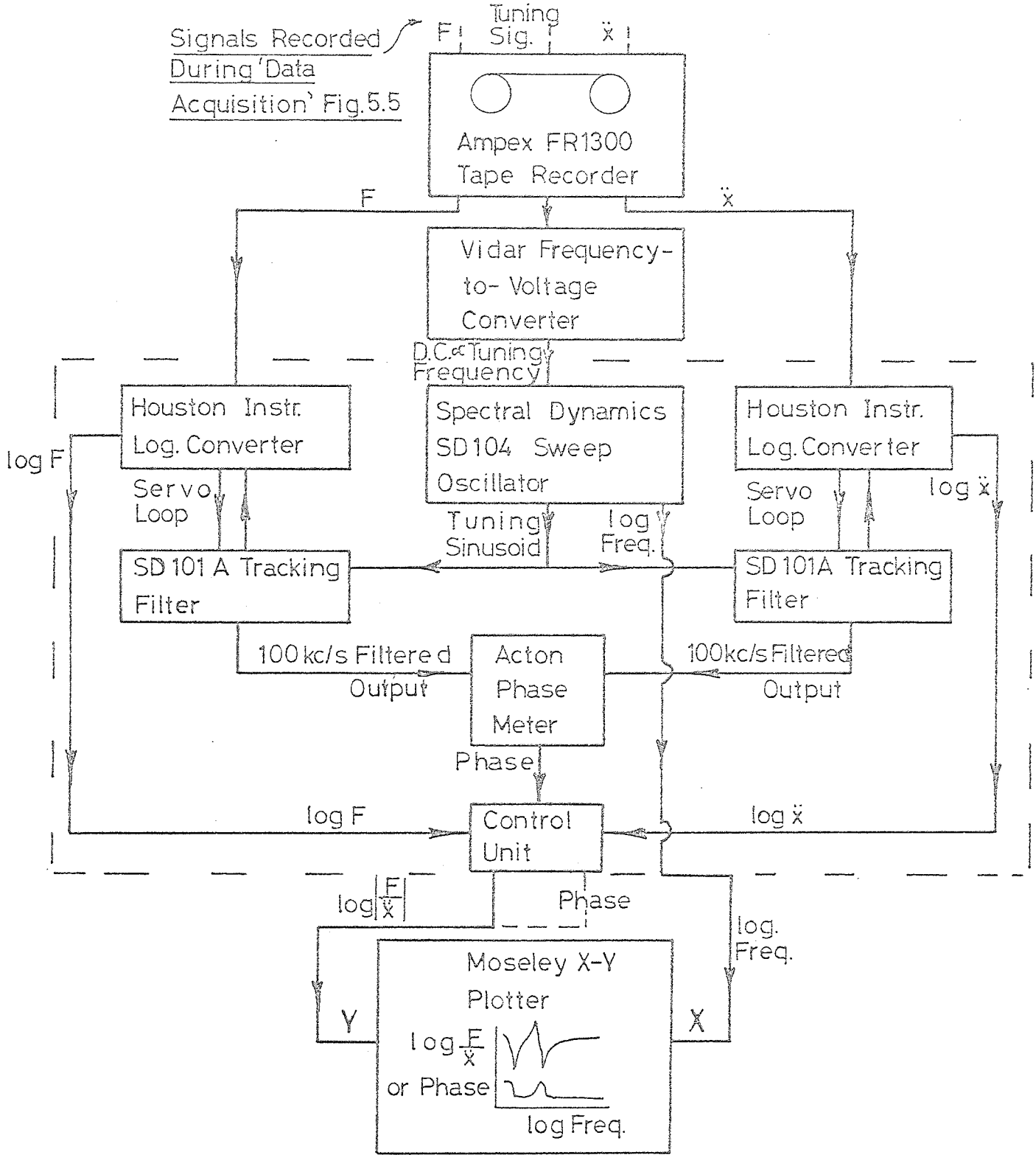

FIG. 5.6 MECHANICAL IMPEDANCE MEASUREMENT DATA ANALYSIS USING SPECTRAL DYNAMICS EQUIPMENT.

Chapter 6.

Model Rotating Machine Rig.

6.1 Introduction

This chapter presents the results of a series of investigations into the dynamic behaviour of a model rotating machine. The model was built to provide a proving ground for the theoretical proposals and experimental techniques which it was hoped to apply eventually to full scale machines. All work reported is original whilst that concerned with the rotating system in journal bearings is believed to be unique, no published quantitative comparison between theory and experiment being known for a system of the complexity considered. In this connection the final arrangement investigated was a flexible shaft supported in hydrodynamic bearings, the housings of which were supported by massive, flexible asymmetric supports.

Recalling the argument put forward in Chapter 1, any criteria for assessing the severity of machine vibration - based on measured vibration levels at the bearing supports for instance - must make allowance for the dynamic properties of the supports. For an 'ideal' system, such as is considered in Chapter 3, if the mechanical impedances of the bearing supports are known and the dynamic properties of the shaft/bearing system are known (e.g. can be calculated), then the measured vibration levels provide a quantitative measure of severity. In particular, the oscillatory bearing forces are directly obtainable. The question was whether this argument could be applied to real structures or whether an adequately accurate description of dynamic behaviour would require prohibitively accurate support impedance measurements.

The design and construction of the model rig are discussed in section 6.2 below. The arrangement was intended to be sufficiently general so as not to be of an unrepresentative order of simplicity, whilst the relative disposition of shaft critical frequencies, running

speeds and uncoupled support resonances were anticipated to be similar to those of the industrial compressors of Chapter 10. In this respect the published information reviewed in Chapter 2 section 2.5 provided some guidance.

The model shaft carried a rotor of mass 70 lb and had two flexural critical speeds, when simply supported, in the range 0 to 500 c/s. The maximum running speed was between the first and second critical speeds. The massive flexible bearing supports enabled either rolling contact or journal bearings to be used.

The experimental procedure adopted was to examine the behaviour of shaft and bearing supports separately, the former providing a comparison with calculated design values. The system was then assembled - first in ball bearings and finally in journal bearings - and the behaviour of the complete model compared with theoretical predictions based on the analysis given in Chapter 4. For this purpose mechanical impedances were measured at the supports with the machine rotating and with it stationary. Similar comparisons between theory and practice were made for unbalance responses throughout the system.

The initial tests on the rotor/shaft assembly to check its calculated characteristics are outlined in section 6.3. The properties obtained from these tests were subsequently assumed to be 'known' quantities - that is they were taken to represent information which would normally be available to the machine manufacturer in a practical case. Measurements made of the mechanical impedance of the bearing supports in the absence of the shaft are reported in section 6.4. These tests were performed before running the shaft in ball bearings and after the rig had been dismantled following the corresponding journal bearing experiments. In this section the validity of certain approximations to the dynamic behaviour of the supports is also considered.

Experiments on the assembled model rig are discussed in sections 6.5 and 6.6 for the cases where the shaft was supported in ball bearings and journal bearings respectively. In these sections, theoretical impedances and unbalance responses were based on the approximate driving point impedances of the bearing supports, whilst in section 6.7 the improvements in accuracy consequent on introducing the measured (complex) support impedances directly into the analysis are considered.

Having obtained reasonably accurate comparisons between theory and practice for the support impedances measured on the model when running in journal bearings, the more difficult problem of extracting the uncoupled support impedances from these measurements was attempted. At the time of writing various minor procedural difficulties in the digital computation discussed in Chapter 4 have meant that only a single set of results has been obtained. These, however, are encouraging and are presented in section 6.8.

The chapter ends with section 6.9 which summarises the general conclusions reached and puts forward suggestions for future work.

6.2 Design and Construction of the Model Rig.

6.2 (i) Rotor, Shaft and Bearing Supports.

Fig. 6.1 shows a general arrangement of the shaft system and bearing supports. The 8 in long, cylindrical steel rotor weighed approximately 70 lbf and on each side of it was bolted a flanged half-shaft. The half-shafts were hollow, so that they were comparatively light for a given bending stiffness, and each was 10 in long overall. To obtain a shaft assembly which was, as nearly as possible, concentric and balanced, the complete assembly was fine-ground along its entire length. Four rows of tapped 2B.A balancing holes were located around the rotor circumference at 30° intervals, whilst

grooves in each end face of the rotor were intended for coarse balancing. In the event, these grooves were not required.

Each bearing support consisted of a rectangular steel block bolted to a flexible cross-beam manufactured from $1\frac{1}{2}$ in wide x $\frac{1}{2}$ in deep tempered spring steel. The beam was supported at 14 in centres by bolting and dowelling it to a massive steel base, flame cut and machined from $1\frac{1}{2}$ in thick steel plate. The complete bearing support assembly was bolted to a large, cast-iron drilling table which weighed about 600 lbf.

It was not possible to calculate the dynamic properties of the bearing supports with any degree of accuracy, since the boundary conditions pertaining at the ends of the beam and the stiffening due to the bearing block were not precisely known. The supports were estimated, however, to have natural frequencies between 150 and 300 c/s in both horizontal and vertical directions at right angles to the shaft axis.

The axial position of each support could be altered over the full length of the half-shaft, the configurations used in the experiments reported here being 24 in and 20 in bearing centres. In the former arrangement the rotor was situated symmetrically between the supports, whilst with 20 in centres the 'non-drive end' (N.D.E.) support was moved towards the rotor as indicated in fig 6.1.

The preliminary design of the shaft assembly was based on the first and second critical speeds of the simply-supported, 24 in centre arrangement being approximately 4500 r.p.m. (75 c/s) and four times this value respectively. Final design calculations made on the University's Elliott 803 computer using a transfer matrix approach indicated the first and second simply-supported criticals to be 70.7 c/s and 330 c/s respectively.

6.2 (ii) Ball Bearings.

By boring out the bearing blocks to accept a standard-diameter adaptor, either rolling contact or journal bearings could be fitted. The ball bearing arrangement is shown in the upper drawing of fig. 6.1 the outer race of the bearing being fitted into the adaptor and the inner race onto the shaft. The tolerances of the shaft, housing and adaptor were so disposed as to provide a light interference fit between outer and inner tracks and their respective mating surface, with the minimum radial bearing clearance recommended by the makers. The bearings used were Hoffman, double-row, self-aligning ball races, type UMS 12. These bearings were grease-lubricated, the end location, grease seals etc. being of conventional design.

6.2 (iii) Journal Bearings.

The plain, circular journal bearings were machined from phosphor-bronze bar to be a light press fit in the bearing blocks, the arrangement used being shown in the inset diagram of fig.6.1.

The bearing dimensions were designed to give similar load numbers and eccentricities to those used in normal practice, the detailed calculation being given in Appendix VI. The bearing design finally chosen had a length of 0.788 in, a nominal diameter of 1.25 in, and a radial clearance of .0075 in.

The oil inlet to the bearings was positioned in the region of maximum running clearance (minimum film pressure), supply being through a $\frac{1}{8}$ in diameter drilled hole. In the bearing wall an axial groove $\frac{1}{2}$ in long was used to distribute oil over the length of the journal. No labyrinth bearing oilseals were used, deep, circumferential drain gutters being machined on each side of the bearing surface.

The total mass of the bronze bearing insert was designed to be equal to that of the ball bearing and adaptor assembly in an attempt to maintain the same effective support impedance for the two arrangements.

6.2 (iv) Oil Supply.

When the journal bearings were in use Shell 'Tapla 20' oil was supplied to each bearing from an overhead tank arranged to give constant head of about 4 feet (see fig. 6.2.). The tank overflow and the drains from the bearings were returned to a sump, circulation being maintained by a small gear pump.

6.2 (v) Oil Temperatures.

The oil temperatures at the inlet to each bearing block and at the drain outlets were measured using chrome-nickel thermocouples, the usual ice-water ($0^{\circ}C$) cold junction being employed. A digital voltmeter capable of resolving 50 μV (representing about $0.5^{\circ}C$) was used to measure the thermocouple e.m.f.'s. No attempt was made to measure the oil film temperature directly.

6.2 (vi) Shaft Drive Arrangement.

The model shaft was driven from a Heenan and Froude type ACM 903, 5 HP, eddy-current coupling with constant speed control (see fig 6.2). The maximum rated speed of this coupling was 1455 r.p.m. which was stepped-up by two stages of vee-belt driven pulleys to give a maximum final-drive shaft speed of about 7800 r.p.m. (130 c/s). The final-drive shaft was connected to the model shaft by a small flexible rubber coupling, which was intended to isolate the model system from any incidental vibration caused by the drive arrangement and to minimise any lateral constraint.

With the final-drive shaft connected to the rig, the maximum speed attainable was about 7200 r.p.m. (120 c/s), with infinitely variable control down to zero r.p.m. The speed could be set and maintained to better than 6 r.p.m. (0.1 c/s).

6.2 (vii) Guard Ring

For safety reasons a substantial guard ring, manufactured from $1\frac{1}{2}$ in thick steel plate, was located at the centre of the rotor as shown in fig 6.2. This had a radial clearance of about 3/32 in, which was adequate to preclude any accidental contact by the rotor during large-amplitude whirl.

When the journal bearings were in use the upper half of the guard ring carried a bridge-piece which served as an axial shaft stop, there being no thrust bearings to provide this location.

6.2 (viii) Shaft Displacement Transducers

Horizontal and vertical displacements of the two half-shafts at points immediately adjacent to the rotor (fig 6.2) were detected by four pairs of inductive transducers. These were 'home-made' devices consisting of a ferrite core around which was wound a coil of several hundred turns. Each transducer was carried on a standard .001 in/div. micrometer head, which in turn was supported from the drilling table by a stiff, steel framework.

Each horizontal and vertical pair of transducers were connected in series to form one arm of a balanced electrical bridge in an N.E.P. amplitude modulation system.

The oscillator (carrier) frequency of this arrangement was 3 kc/s which enabled disturbances of the rotor having frequencies from D.C. up to about 600 c/s to be detected- i.e. well above the frequency range of interest.

The four rotor displacement signals (two horizontal, two vertical) were displayed on an N.E.P. ultra-violet chart recorder which had provision for up to 12 galvanometers. In addition, a Nagard 4-channel

oscilloscope was available for direct observation. This had a Lissajous figure facility which enabled the motion of the shaft centre to be viewed in X-Y co-ordinates.

Calibration of each pair of transducers involved simulating a given rotor displacement, say .005 in, by moving the micrometer heads .005 in in the opposite sense. Overall sensitivities of galvanometer trace deflection to rotor deflection of 3000:1 (i.e. 3 in per .001 in) were readily obtained.

6.2 (ix) Shaft Speed and Phase Markers.

Southern Instruments (S.I.) permanent magnet inductive pick-ups were used to provide marker signals for the measurement of the shaft's speed and its instantaneous angular position or phase.

The speed marker was derived from a group of ten, equispaced, knife-edged, steel inserts carried in a hub on the final-drive shaft. The output from the S.I. pick-up was therefore a periodic signal whose frequency was ten times that of the shaft, and this was measured using a digital frequency-counter.

In a similar manner, a single insert at the non-drive end of the model shaft was used for phase measurements (see fig 6.2), the pick-up output being connected to the U-V recorder. The insert was fixed to a nut attached to the shaft - a brass insert diametrically opposite being used in an attempt to maintain balance without affecting the phase signal.

6.3 Initial Measurements on the Rotor-Shaft Assembly.

Both static and dynamic tests were conducted on the shaft assembly to check its calculated properties. The measured properties were subsequently used in all analytic estimates of the behaviour of the

complete model system. Since the main objective of the model rig was concerned with the influence of bearing support inpedances, these tests were intended to eliminate discrepancies due to the shaft which would otherwise have confused the issue.

(i) Static Tests

A series of simple static tests were performed to measure the shaft flexibility. Initial measurements with the rotor symmetrically supported at 24 in centres in vee-blocks indicated that the actual flexibility was about 37% greater than calculated. A typical test result is shown in fig 6.3.

Further tests were made with the rotor clamped to the machine table, as in the inset diagram of fig 6.4. Measurements of the half-shaft deflection along its length relative to the rotor body were made for incremental loads up to about 50 lbf. This load was estimated to be of the same order as that resulting on each half-shaft from the rotor executing circular unbalance whirl, under moderately well balanced conditions, at the calculated simply-supported critical speed (i.e. 16 gm.in.unbalance, $\zeta = 0.02$).

It was confirmed that the effective flexibility of the half-shafts was appreciably less than that calculated - assuming bending as a simple cantilever with built-in end conditions. The results from two separate tests on the D.E. half-shaft are plotted in fig 6.4 to compare measured and calculated deflected forms, those for the N.D.E. shaft being almost identical.

It was not immediately clear whether the increased flexibility was due to an error in the assumed stiffness (EI). However, by plotting the difference between measured and theoretical values, a linear relationship with distance along the shaft was found, as shown

in fig 6.4. The increased flexibility was therefore attributed to an additional flexibility at the flange fixing with the rotor, which resulted in a non-zero slope at the rotor end. No deflection of the flange relative to the rotor could be detected, however, and the mechanism involved was not discovered. The 'measured' half-shaft stiffness at 8 in from the rotor, that is at the bearing centre for the 24 in configuration, was found to be 1.42×10^4 lbf/in compared with the calculated value of 1.83×10^4 lbf/in. These results illustrate the need for care when relying on the calculated properties of shafts of built-up construction.

Following the discovery of the above discrepancies, further tests were made to detect any asymmetry in the shaft stiffness (for the significance of this see Chapter 2 section 2.2) and to ensure that its load-deflection properties were linear. In the first case, half-shaft deflections were measured for a given load as the shaft was rotated by 15° at a time, whilst in the linearity tests incremental end-loads of up to 100 lbf were applied. No evidence of asymmetric stiffness or non-linearity was detected.

(ii) Resonance tests

Using instrumentation of the type discussed in section 5, measurements of the natural frequencies of the shaft system were made under various conditions. Corresponsing modal shapes were also measured by traversing a Wayne Kerr capacitive proximity pick-up along the length of the shaft. These tests were performed primarily to provide confirmation of the shaft stiffness obtained in the static tests mentioned above.

The natural frequencies of the half shaft were measured when these were cantilevered from the rotor with the latter clamped to the machine table, as shown inset in fig.6.6. Good agreement was

obtained between the measured frequencies and those calculated using a transfer matrix approach in which the measured flexibility of the shaft/rotor flange joint was included. For the drive-end shaft for example, these frequencies were respectively 290 c/s and 286 c/s, the corresponding nodal shapes being shown in fig 6.6.

When the shaft assembly was supported in vee-blocks, however, to check its fundamental and first overtone 'simply-supported' natural frequencies, it was found impossible to obtain adequately rigid supporting conditions. Both the fundamental and first overtone modes occurred at frequencies lower than those calculated, the discrepancy in the case of the fundamental being about 4%. (Fundamental 62.1 c/s calculated, 59.7 c/s measured; first overtone 293 c/s calculated, 243 c/s measured). The effect of the non-rigid supporting condition may be seen in the measured fundamental nodal shape of fig 6.7.

Similar difficulties were encountered in attempts to measure the influence of the self-aligning ball races on the shaft natural frequencies. It was assumed, however, that this effect would be very slight since the radial stiffness of the bearing, based on Hertzian deformation when loaded due to the shaft's weight, was about 5×10^5 lbf/in i.e. approximately thirty-five times the shaft static stiffness in the 24 in bearing centre configuration. (See Chapter 2 section 2.4). The resulting effect on the shaft natural frequency would therefore be small, and in any case would be offset by the stiffening effect on the half shafts over the bearing width.

6.4 Tests on the Bearing Supports in the Absence of the Shaft Assembly.

6.4 (i) Procedure.

As outlined in the introduction to this chapter two main groups of tests were conducted on the rig in which the shaft was supported in ball and journal bearings respectively. In an attempt to keep the

support impedance constant for the two configuration the mass of the bronze journal bearings was designed to be equal to that of the corresponding ball bearing arrangement (see fig 6.1).

Measurements of the support impedances were made before assembling the model in ball bearings, and it was originally intended to repeat these measurements immediately before the corresponding journal bearing tests. In the event it was not possible to perform the repeat tests at that juncture and they were postponed until the rig was finally dismantled. No great importance was attached to this delay, since it was anticipated that the impedances would be nearly identical for both bearing arrangements. When the impedance measurements with the journal bearings in place were eventually carried out, however, very considerable changes had occured which are discussed below.

With both bearing arrangements horizontal and vertical driving point impedances were measured with the line of action of the excitation force passing through the bearing centre. These measurements correspond to the 'ideal' uncoupled impedances Zxx, Zyy discussed in Chapters 3 and 4. In addition the transfer impedances Zxy, Zyx were measured at each support, these representing, in effect, the deviation of the support from the ideal model. In all tests, steady state, harmonic excitation was used - the data acquisition and analysis techniques being as described in Chapter 5 section 5.5 (iii).

In figures 6.8 to 6.11, the moduli of the driving point impedances Zxx, Zyy are shown for the two bearing supports together with the corresponding phase angles. In each of these figures three separate curves are shown:-

(a) the measured impedances with the ball bearings in the housings

(b) a single degree-of-freedom impedance taken to represent, approximately, the measured values of (a)

and (c) the results of the repeat tests made on the supports with the journal bearings in place.

Examples of transfer impedances measured at the D.E. support are shown in fig 6.12. For the ball bearing configuration the impedance Zyx_2 is illustrated i.e. horizontal excitation and vertical response. For the journal bearing case both the (reciprocal) impedances Zyx_2, Zxy_2 are shown. Also sketched for the latter configuration are curves illustrating the maximum possible effect on the transfer impedance measurements of the cross-axis sensitivity of the Kistler accelerometer used, this being 3% of the 'direct' sensitivity.

6.4 (ii) Discussion of Support Impedance Measurements.

Referring to figs. 6.8 and 6.11 it can be seen that all driving point impedances had the same general characteristics in that at low frequencies (below about 100 c/s, say) their behaviour was spring controlled, whilst at high frequencies (above 300 c/s) they approached some value representing constant mass (see Chapter 3 for interpretation of impedance data). At intermediate frequencies both supports exhibited two main resonant impedance minima in both horizontal and vertical planes. These resonances were related to the approximate modal configuration shown in fig 6.13, the lower frequency mode being predominantly a vertical translation of the bearing block and the upper a 'rocking' mode. Had the supports possessed perfect symmetry the modes would have been uncoupled-motion at the bearing centre line in the horizontal direction being independent, for small amplitudes, from that in the vertical direction (see Appendix IV). Coupling between a predominantly axial resonance and both horizontal and vertical directions was responsible for the irregularities between 80 and 100 c/s.

Considering the results for the supports with the ball bearings in place (full line in figs 6.8 to 6.11) it may be seen that, despite the identical construction of the two supports, they varied appreciably in detailed behaviour. Thus for the D.E.support the controlling stiffness of the vertical driving point impedance at low frequencies was around 7×10^4 lbf/in, with the 'vertical' mode resonant at about 210 c/s (fig 6.10). For the N.D.E. support, however, the corresponding values were about 4×10^4 lbf/in and 165 c/s respectively (fig 6.8). Similar variations were apparent in the impedances measured in the horizontal plane.

Although some difference in the behaviour of the two supports was expected, the magnitude of the discrepancies was surprising. Preliminary checks on the mass of the bearing blocks, the dimensions of the spring beam, the tightening torques for the holding-down bolts etc. had shown no significant changes between supports. The results were also accurately repeatable, whilst the static stiffness in the vertical direction obtained from the impedance curves agreed closely with that obtained from previous dead-loading tests. Fig.6.14, for example, shows the measured static stiffness of the N.D.E. support in the vertical plane to be 4.3×10^4 lbf/in up to about 180 lbf, which agreed with the low frequency impedances of fig 6.8.

The approximate impedances (dashed lines fig 6.8 to 6.11) were based on the controlling stiffness at low frequencies, the effective mass of the bearing support ($\simeq$ 17 lb), and the resonant frequencies corresponding approximately to motion in the direction under consideration. These were subsequently used in the theoretical calculation for sections 6.5 and 6.6. For example the vertical driving point impedance at the D.E. support (Zyy_2) was represented by the undamped single d.o.f. system, having mass m_2 = 17 lb and stiffness $k_2 = 7.68 \times 10^4$ lbf/in or $Zyy_2 = m_2 - k_2/\omega^2$.

The results of the impedance measurements made on the supports after running the model in journal bearings are shown as chain-dotted lines in figs 6.8 to 6.11. Although the total mass of the bearing housing was constant within 3% for both bearing arrangements, and the support geometry was not altered in any way, significant differences in the measured impedances were apparent. It was concluded that these differences arose as a result of removing and re-assembling the bearing housing/beam assembly.

The changes apparent between the driving point impedances for the two bearing configuration showed no consistent pattern. Thus for the N.D.E. support the low frequency controlling stiffness was somewhat higher with the journal bearings in place (fig.6.8), the reverse being truefor the D.E. support (fig.6.10). Of particular significance was the greatly increased coupling at low frequencies between horizontal and vertical planes, as is illustrated in fig. 6.12. In this figure the transfer impedances Zxy_2, Zyx_2 approach a spring-controlled value of the same order as the driving point impedance Zyy_2, Zxx_2.

In all transfer impedances, however, good reciprocity was indicated (Zxy = Zyx) which supported the assumptions of linerarity.

If the differences in effective support impedances mentioned above were due to variations in the local stiffness at bolted joints - as appeared to be the case - it seems unlikely that attempts to calibrate particular bearing pedestal designs (as has been suggested by Caruso(68) Chapter 3) would be very successful.

6.5 Shaft Assembly in Ball Bearings

6.5 (i) Initial Alignment and Rotor Balancing.

Following the measurements of bearing support impedance discussed in section 6.4 the shaft was assembled in the ball races. Before running, the model shaft was aligned with the final drive shaft (fig 6.2) by

adjusting the horizontal and vertical centres of the latter until concentricity better than .001 in was obtained. Also, it was ensured that the bearing supports were square with the shaft axis in both planes. This procedure was repeated following each change of bearing centres.

Having aligned the system with the bearing supports at 24 in centres the rotor was balanced as accurately as possible. The initial unbalance of the shaft and rotor 'as machined' was of the order of 20 gm.in. This was reduced in stages to the final, 'balanced' state (subsequently referred to as 'fine' balance) in which the residual unbalance was estimated to be about 2 or 3 gm.in (.00007 in rotor c.g. eccentricity).

The balancing procedure was carried out in the conventional manner by running the rotor up to just below its fundamental critical speed and measuring the deflection and phase of the rotor using the inductive transducers (section 6.2 (viii)). Small balancing screws of mass 0.75gm (one 'unit') were then added to the rotor diametrally opposite the indicated unbalance.

It became apparent during the initial balancing runs that the rotor was running slightly eccentric to the bearing centres. This effect was largest at the D.E. of the rotor, representing about .00075 in radial eccentricity. It is thought that this eccentricity arose during final grinding of the shaft assembly and was probably unavoidable due to the flexible design.

In all subsequent measurements of the rotor amplitude and phase a correction was applied to allow for the initial eccentricity. This was achieved by measuring the eccentricity and its phase relative to the once-per-revolution shaft marker at a very slow speed, normally 2 or 3 c/s (120-180 r.p.m.), and subtracting the result vectorially from each measurement made at higher speeds (fig.6.24)

The need to correct all shaft amplitude and phase measurements reduced their overall accuracy, and for this reason the initial balancing of the shaft was only attempted with respect to its fundamental mode. (For a discussion on 'modal' balancing see, for example, Moore and Dodd (78) and Lindley and Bishop (77)), At shaft speeds above about 80 c/s, the effect of unbalance in the second mode (strictly pair of modes, one horizontal and one vertical) was becoming significant.

6.5 (ii) Impedance measurements on the complete model.

(a) General system properties.

The system under consideration was assumed to have - according to the theoretical proposals of Chapter 4 - four natural frequencies in both horizontal and vertical planes. When the shaft was not rotating it was also assumed that motion in the two planes was completely uncoupled, whilst coupling during rotation was due to the 'gyroscopic' effect consequent on the angular oscillations of the rotor axis.

To illustrate the nature of the system, the calculated modal shapes and natural frequencies in the vertical plane for the non-rotating case are shown in figs. 6.15 and 6.16, for the 24 in bearing centres and 20 in bearing centres respectively. These were obtained using a transfer matrix approach and were based on the approximate bearing support parameters discussed in section 6.4.

Although, theoretically, each natural frequency is a property of the complete system, it is convenient, since they are reasonably well separated, to relate each natural frequency to the corresponding uncoupled resonances of the component parts. For the fundamental mode in the 24 in centre configuration, for example, the natural frequency at 54.7 c/s corresponds to a simply supported mode at 62.1 c/s. The

next two calculated modes in fig. 6.15, at 155 and 208.4 c/s respectively, may be compared with the assumed resonances of the uncoupled supports at 157 and 210 c/s for the N.D.E. and D.E. supports respectively. The third overtone, calculated at 311.6 c/s, is at a considerably higher frequency than the simply supported case (293 c/s) due to the massive, flexible supports.

Typical results for impedances measured on the assembled rig are shown in figs. 6.17 to 6.23 those having been obtained using the technique of Chapter 5, section 5.5 (iii). In each case the measured results (full line) are compared with those obtained using the theoretical approach of Chapter 4 section 4.2. The shaft parameters used in these calculations were those obtained during the tests reported in section 6.3 above, whilst those for the supports were the approximate driving point impedances discussed in section 6.4.

(b) 24 in Bearing Centre Configuration.

Fig. 6.17 compares the theoretical and experimental results for the vertical driving point impedance at the N.D.E. support with the rotor stationary. In general good agreement between theory and practice is indicated, except in the immediate vicinity of resonances and anti-resonances where the absence of damping in the theoretical treatment is apparent.

All resonant and antiresonant frequencies agree within better than 5%, the only evidence of any coupling with the corresponding horizontal modes being around 250 c/s. This was encouraging and suggested that the effect of neglecting the transfer impedances of the supports (Zxy_1, Zyx_2 etc.) in the theory was small.

The impedance characteristics of fig 6.17 illustrate several general features of the type of system considered. At very low

frequencies the impedance at the bearing support of the assembled model was very close to that of the support alone (apparent masses of 450 and 430 lb at 30 c/s respectively) due to the 'pinned' nature of the bearing fixing conditions. As the excitation frequency was increased the fundamental mode was encountered (Res 1 in fig.6.17) followed immediately by the sharp antiresonance 2. As mentioned in Chapter 3, this antiresonance corresponded to the series resonance of the shaft system in the absence of the N.D.E. support - its frequency separation from the resonance 1 being a measure of the effect of this support.

The second resonance corresponds to that of the N.D.E. support alone. The resonances 3 and 4 of fig 6.17 relate to the second overtone of the system in the vertical plane (predominantly motion of the D.E. support) and the third overtone respectively (see fig.6.15) Above the main resonance at 159 c/s the impedance modulus tends to 'oscillate' about a mean horizontal line (e.g. a line of constant mass) and finally, above resonance 4, to approach the effective support mass of 17 lb.

It should be mentioned here that the close agreement in fig.6.17 in the region of the third overtone is somewhat misleading. In this respect the transfer matrix results shown in fig 6.15 predict a higher natural frequency (311.6 c/s) than the theoretical analysis of Chapter 4 (289 c/s) due to the neglect of the mass of the half shafts in the latter case. It was evident, therefore, that at these higher frequencies small errors in the assumed shaft parameters were becoming increasingly important. Fig. 6.18 shows the same driving point impedances at the N.D.E. support as in fig 6.17 but this time with the shaft rotating at 100 c/s (6000 r.p.m.). The effect of the gyroscopic coupling between horizontal and vertical planes is evident when comparing these two diagrams.

In Fig 6.18 the experimental resonant frequencies are indicated by the numbers 1 to 8 whilst the corresponding theoretical resonances are distinguished by a prime $1'$, $2'$, $3'$..... etc. Similarly the experimental antiresonances are marked A, B, C, etc. and the corresponding theoretical ones A', B', C', etc. These values are tabulated for direct comparison.

It may be seen from fig 6.18 that the bandwidths of the resonances and antiresonances are much narrower at higher frequencies, so that damping in the system reduces the overall variation in impedance to a greater extent than the corresponding stationary-shaft case. Nevertheless all theoretical maxima and minima can be identified and this test further suggested that the neglect of coupling at the supports (Zxy, Zyx) was not large in the case of impedance measurements.

This example also illustrates the advantage of using tracking filters in the analysis of vibration data containing extraneous signals (see Chapter 5 section 5.4). For the particular test shown in fig.6.18, the only interference with the impedance plot occured around the running frequency of 100 c/s and was due to the residual unbalance of the rotor. The next significant disturbance from the rig was due to ball bearing passage effects at 5.7 times running frequency (570 c/s) and was therefore outside the frequency range considered (see Appendix II for notes on this phenomenon).

A vertical transfer impedance is shown in fig.6.19 which was measured between supports (Zy_1y_2) with the shaft stationary. Again, good overall agreement between theory and experiment was obtained although there was some evidence of coupling with the 'horizontal' modes, for example around 195 c/s, which was assumed to be due to the bearing support characteristics.

Similar deviation from the theoretical curve was apparent at about 288 c/s in the form of a minor resonant minimum corresponding to the uncoupled 'horizontal' mode. In most cases evidence of the coupling of modes was normally more apparent in the phase plot than in the corresponding impedance modulus. This is illustrated in fig. 6.19 by the 'dip' in the phase around 70 to 100 c/s which was assumed to arise due to coupling with the axial support modes as observed in section 6.4 (ii) above.

When displayed in Kennedy & Pancu (79) type plots these effects due to modal coupling produce small 'modal circles' around the main resonance diagram. Where accurate identification of the corresponding natural frequencies is required this type of plot (or similar ones, like that proposed by Bishop and Pendered (80)) is the most useful. The more conventional modulus and argument diagrams are presented here, however, since they permit a wider dynamic range to be shown and are interpreted more readily in impedance terms.

Transfer impedances between supports, like fig 6.19, tend to give a more general basis for comparison with theory since they are less strongly conditioned by the properties of one particular support. The very sharp flanks of the impedance curve in fig 6.19 are characteristics of this type of inertia-coupled arrangement, in which the bearings provide 'pinned' end conditions. As such they indicate the departure of the system from the ideal in being sensitive to end fixing torques.

(c) 20 in Bearing Centre Configuration.

In the 24 in centre configuration considered above the N.D.E. half-shaft stiffness was relatively low compared with the support impedances. For instance the N.D.E. support had a vertical driving point impedance of about 4.3×10^4 lbf/in at low frequencies compared with a measured half-shaft stiffness of 1.42×10^4 lbf/in.

For the 20 in centre configuration, however, the N.D.E. half-shaft stiffness was 9.24×10^4 lbf/in (based on the results of the tests discussed in section 6.3) which was somewhat higher than both vertical and horizontal support controlling stiffnesses (7.37×10^4 lbf/in horizontal). The two configurations therefore provided a useful range of shaft-support parameters.

Figs 6.20 and 6.21 show respectively the measured vertical driving point impedances at the N.D.E. support with the shaft stationary and with it rotating at 100 c/s.

In the non-rotating case agreement between theory and experiment was obtained up to the third resonant frequency at 232 c/s which corresponded approximately to the vertical uncoupled resonance of the D.E. support. In this frequency range the largest discrepancy occurs around the first antiresonant frequency, measured as 80 c/s and calculated as 88 c/s, where errors in the estimated half-shaft stiffness were likely to be particularly important.

Above about 300 c/s larger differences were apparent. These were partly attributed to the omission in the lumped-parameter theoretical solution of the finite half-shaft masses, in particular that of the N.D.E. shaft which in this configuration was overhung from the bearing by about five inches. In this case the transfer matrix solution indicated a lower third overtone frequency as shown in fig.6.16. Fig.6.16 also shows the measured modal shapes of the system at the experimentally determined natural frequencies and emphasises the influence of the N.D.E. half-shaft in the third overtone mode.

In addition, from the theoretical approach of Chapter 4, the higher natural frequencies, at which motion of the rotor is largely governed by the rotational co-ordinates ϕ_1 ϕ_2, are dependent on the

function $(k_1 l_4^2 - k_2 l_5^2)$. Small errors in the assumed position of the bearing supports, and hence in l_4 and l_5, could therefore be significant.

The vertical driving point impedance at the N.D.E. bearing support made whilst the rotor was running (fig 6.21) gave a similar correlation with the theoretical analysis. Although the frequency errors in the higher modes were still evident, in all cases corresponding resonances and antiresonances could be identified which again supported the assumption that gyroscopic coupling would predominate.

In the horizontal driving point impedance at the D.E. support, shown in fig 6.23, a significant difference was apparent between the measured fundamental frequency (68 c/s) and the calculated value (77 c/s). This difference arose directly from the approximations made in the assumed support impedances in the horizontal plane. In particular the simple assumption made for the D.E. support impedance ($Zxx_2 = -k_2/\omega^2 + m_2$; $k_2 = 11.7 \times 10^4$ lbf/in; $m_2 = 17$ lb) was about twice as high as the measured value in the range 60 to 80 c/s. Thus, from fig 6.11, at 70 c/s the measured and assumed apparent masses of this support were 105 and 215 lb respectively.

Between 100 c/s and the 191 c/s resonant frequency evidence of modal coupling was apparent in the experimental impedance curve of fig 6.23. At about 110 c/s, for example, the resonant-antiresonant combination due to the coupled 'axial' support mode appeared (see Appendix IV), although much less pronounced and higher in frequency than the corresponding effect observed in the measurement made on the support alone (fig 6.11). Presumably the reduced influence was due to the axial constraint provided by the ball bearing.

6.5 (iii) Unbalance Responses with the Shaft in Ball Bearings

(a) Introduction.

Six examples of unbalance responses measured throughout the model rotating machine are given in figs 6.25 to 6.30. In each case a theoretical response is also shown based on the approximate support impedances considered in section 6.4 and the theoretical analysis of chapter 4.

Due to the need to correct all rotor amplitude and phase measurements for the initial shaft eccentricity (see section 6.5 (i)) the overall accuracy was decreased, particularly at whirl amplitudes of the same order as the eccentricity. Also, at higher shaft speeds the axial distribution of the unbalance became increasingly important, due to components in the first overtone (support) modes. Efficient correction for unbalance in these modes would have required balancing masses to be added along the half-shafts, which was not practicable due to their construction. In addition the accurate support response phase measurements required would, with the equipment available at the time, have been a very time-consuming procedure.

In the theoretical responses of figs 6.25 to 6.30 the absolute unbalance was therefore to be located at one end of the rotor and to be of magnitude equal to a simple multiple of the mass of one balancing screw used in practice (one balancing screw (0.75 gm) at the rotor radius of 3.31 in is subsequently referred to as one 'unit' of unbalance). In each figure the inset diagrams show the location of the balancing screws added to the rotor to achieve the qualitative state of balance indicated. The 'fine' balance condition, for instance, was the best balance that could be readily achieved (section 6.5 (i)) and required a total of eight balancing screws (units). The 'medium' balance condition was obtained by removing one balancing screw from the

D.E. of the rotor whilst 'coarse' balance involved removing a further unit from the N.D.E.

(b) 24 in Bearing Centre configuration.

Fig 6.25 shows the rotor response at the N.D.E. (plane 'A') and it may be seen that the fundamental critical frequency was noticeably lower than predicted theoretically (58 and 53 c/s respectively). This discrepancy was due to the high value assumed for the D.E.support impedance in the frequency range considered as was also observed in the impedance results of section 6.5 (ii). The plots shown emphasise the desirability of making comparison between theory and practice according to the overall pattern of the characteristics. In this respect measurements of vibration at a single rotational speed, such as is often done at full speed in the case of constant speed machines, can be completely misleading, and harmonic tracking techniques are much more satisfactory.

Comparing the 'fine' balance curve of fig 6.25 with the theoretical response, the bandwidth of the resonances and the amplitudes at higher frequencies suggested that residual unbalance in the fundamental mode was between 0.5 and 1.5 units (.38 and .75 gms at the rotor radius). These conclusions were borne out by a comparison between the 'fine' and 'medium' balance experimental curves. For, since these two conditions differed by one unit and the 'medium' state gave about twice the rotor amplitude of the 'fine' balance, the residual unbalance in the fundamental mode was assessed as being approximately one unit.

The phase plot of fig 6.25 shows the variation in the angular position of the maximum horizontal rotor amplitude with respect to the shaft marker. In this diagram a smooth, rapid phase change of nearly 180° was indicated on passing through the critical frequency range.

This contrasted with the somewhat irregular phase diagram of fig 6.26 in which the vertical rotor motion was considered. In this case the corresponding amplitude plot contained two significant peaks, which were roughly equispaced along the frequency axis, about a trough coinciding with the horizontal critical frequency of 53 c/s.

This type of behaviour is typical of the unbalance vibration of rotors in which coupling between orthogonal planes of measurement complicates the resulting whirl path. (see Morton (46) for example, and Appendix IV). In the case of unbalance excitation, unlike the impedance measurements, motion in the horizontal and vertical planes was coupled by external damping in the system. Since the impedance measurements of section 6.5 (a) had confirmed the theoretical effect of gyroscopic coupling to be of the correct order, and the neglect of the transfer impedances of the supports to have only slight influence, it was concluded that the main source of coupling apparent in fig 6.25 was in fact system damping.

Despite these complications it was still possible, by comparing theoretical and experimental bandwidths, to assess the residual unbalance in the 'fine' balance condition as about 0.5 units in the fundamental modes. On the basis of amplitude above the critical region, where the rotor behaviour was predominantly 'inertia controlled' in the fundamental mode, an estimate of between .5 and 1 unit residual unbalance could be made. These conclusions were in general agreement with those reached by considering the horizontal rotor amplitudes of fig 6.25.

Comparing the 'medium' balance curve of fig 6.26 with the 'fine' balance curve it may be seen that the frequency of the resonant peaks differs in the two cases, those for the 'medium' balance condition being more widely spaced. This effect was attributed to the slight

change in modal balance consequent on the change in axial location of the resultant unbalance between the two conditions.

The unbalance acceleration response in the vertical direction at the D.E.support is shown in fig 6.27. Both 'medium' and 'coarse' balance conditions show responses having a pronounced trough in the critical region due to coupling between horizontal and vertical planes. However, the bandwidth of the main resonance suggested absolute unbalances in the fundamental mode of about 1.5 and 3 units for the 'medium' and 'coarse' condition respectively i.e. similar to the estimates made by comparing measured and theoretical rotor responses.

In measurements of the bearing support responses at higher speeds, however, the limitations of the assumed unbalance distribution became more apparent. Fig.6.28 for example, shows the vertical response at the N.D.E. support to the 'coarse' balance configuration, and above a rotational frequency of about 70 c/s the experimental curve differs markedly from the theoretical. This discrepancy was attributed to the significant contribution of unbalance along the half shafts in the first overtone mode (similar to that calculated for the stationary, uncoupled case at 155 c/s and shown in fig 6.15). The zero theoretical amplitude at 109 c/s in fig 6.28 corresponded to the passage of a node through the assumed axial unbalance plane as the rotational frequency was increased.

The impression was gained in these experiments that much of the unbalance in the first overtone modes arose from the shaft phase marker assembly (see section 6.2 and fig 6.2). Although the latter was 'balanced' as nearly as possible by the addition of a brass insert opposite the knife-edged marker, the assembly was screwed to the shaft and therefore liable to appreciable eccentricity in terms of the unbalance tolerances under consideration.

(c) 20 in Bearing Centre Configuration.

Figs. 6.29 and 6.30 show typical measured unbalance responses of the rotor together with corresponding theoretical curves. As in the 24 in centre configuration above the calculated fundamental frequency (79 c/s) in the horizontal plane was higher than that observed in practice (69 c/s approx) due to the high D.E. support impedance assumed in the horizontal plane.

Although the theoretical curves clearly showed the effect of the gyroscopic coupling between the 'vertical' and 'horizontal' modes this was masked in the experimental results by the coupling influence of system damping and, to a lesser extent, coupling at the supports. The vertical response at the N.D.E. of the rotor (plane 'A'), shown in fig 6.30 illustrates the characteristic trough associated with this phenomenon.

6.6 Shaft Assembly in Journal Bearings.

6.6 (i) Introduction

The introduction of journal bearings considerably increased the complexity of the dynamics of the model system (see Chapter 4). However, despite the approximations made in the theoretical analysis, particularly those regarding the bearing support impedances and the journal bearing dynamic coefficients, encouragingly accurate results were obtained. This accuracy was further increased when the measured support impedances were introduced into the analysis, as is shown in section 6.6 (iv).

After initial difficulties with details of the digital computation on the S.R.C. Atlas computer it was also found that good approximations to the uncoupled support impedances (in the absence of the shaft) could be extracted from equivalent measurements on the complete system. This procedure is considered in section 6.8.

In the results presented in figs 6.32 to 6.44 the support impedances used in the theoretical analysis were the approximate values based on the initial measurements with ball bearings in the housings - as discussed in section 6.4 and illustrated in figs 6.8 to 6.12. The unexpected changes found in the support impedances with the journal bearings installed were not discovered until the rig was finally dismantled and after most of the Atlas computer calculations had been performed.

The calculated journal bearing coefficients - four displacement, four velocity for each bearing - were based on assumptions put forward by Morrison (43) as discussed in Chapter 4. They were expressed analytically as functions of the journal eccentricity ratio, ε, Alternatively they may be expressed in terms of the bearing load numbers which in the present analysis, was determined to Ocvirk's (76) 'short bearing' theory. However, since the eccentricity ratio varies rapidly with the load number, particularly at small journal loadings, it was originally intended to measure the journal eccentricities on the model rig directly, rather than relying on calculated values based on estimated oil film viscosities and bearing clearances.

The procedure initially adopted for obtaining journal eccentricities is illustrated in fig 6.31 (a), and involved measurements of the steady (D.C.) displacement of the rotor using the shaft transducers in conjunction with either an oscilloscope or the U.V.recorder. The corresponding journal locations were then determined from the geometry of the system. Unfortunately this method was found to be impractical, largely due to the difficulty of determining the zero (stationary journal) position with sufficient accuracy. Thus the journal centre position could only be determined within the limits of the initial shaft distortion mentioned in section 6.5(i).

Attempts were made to locate the journal centres by rotating the shaft by hand about 30^{o}, allowing it to come to rest and plotting a series of 'apparent' journal centres against angular rotation whose mean Was the required position. In these attempts, however, it was found that the journal would not take up a repeatable, stationary position for a given angular shaft rotation - presumably due to the effect of 'stiction' when the journals were near the bottom of the bearings. The usual problems of measuring small D.C. voltages over a period of time were also encountered, drift of the oscilloscope amplifiers being particularly noticeable.

The effect of the uncertainty of the exact position of the journals when stationary is illustrated in fig 6.31 (b). In this diagram the apparent locus described by the N.D.E. journal for increasing shaft speed is shown for the 20 in bearing centre configuration this being plotted from the horizontal and vertical displacements Xj_1, Yj_1. The locus is compared with semi-circular loci of the type assumed theoretically for radial clearances of .005, .006 and .007 in. Although the measured locus was approximately semi-circular its orientation within the bearing clearance could not be determined.

The above procedure was finally abandoned and bearing running conditions were estimated from the design clearance and the measured oil outlet temperatures. The assumption that the oil film temperature was equal to the outlet temperature was only an approximation, the outlet oil being partially derived from leakage past the top (unloaded) portion of the journal. Had time permitted it would have been better to redesign the bearings to include thermocouples in the loaded region.

Before each test the rig was run for at least one hour to allow oil temperatures to stabilise. In the case of impedance measurements at the bearing supports the model was run at a constant speed and oil

temperatures taken at the beginning and end of each test. The average time taken to record the basic impedance data (see Chapter 5 Section 5.5 (iii)) was about 5 minutes and during this interval oil outlet temperatures were normally constant within 1 C^{o}.

During the measurement of unbalance responses at the bearing supports the model was run up to speed and the amplitudes plotted during a controlled deceleration. Since this procedure again occupied about 5 minutes, it ensured the minimum oil temperature variation during the test.

For rotor whirl-amplitude measurements, however, obtaining the initial data took considerably longer since it was necessary to adjust the shaft speed, wait whilst it became steady and then take a U.V. recording of the shaft transducer signals. In some instances the oil temperature changed by up to $4C^{o}$ during the course of a test over the full shaft speed range. For the corresponding theoretical responses bearing coefficients were based on oil viscosities at the mean oil temperatures over the test. On this basis alone the agreement between theory and experiment would be expected to be closest at intermediate speeds i.e. in the region of the fundamental critical speeds.

The various qualities of rotor balance used in the tests with journal bearings were based on those referred to in the discussion of the ball bearing arrangement (section 6.5 (iii)(a)). Since no modifications to the rotor were involved in the change of bearing design, it was assumed that the absolute residual unbalances were the same for the same balancing mass distribution. Because the shaft assembly had previously been well balanced in its fundamental modes whilst carried in ball bearings, a much finer degree of balance was achieved than would have been possible using the journal bearings, due to the considerable 'damping' introduced by the latter.

The maximum shaft speed at which unbalance responses could be measured was limited by the onset of a violent bearing instability, which occurred at approximately 85 c/s in the 20 in bearing centre configuration and at about 75 c/s when the centres were set to 24 in. The appearance of this phenomenon was not entirely unexpected, in view of the plain, circular design of the bearings used (see literature Chapter 2 Section 2.4(ii)), but the low frequencies at which it occurred were interesting, these being only about 37% higher than those of the fundamental mode at the flexibly supported shaft in 'pinned' bearings. A discussion of this behaviour and the use of the theoretical work of Chapter 4 in predicting the boundary of instability is given in Appendix III.

6.6 (ii) Bearing Support Impedance Measurements.

(a) 24 in Bearing Centre Configuration.

Figs. 6.32 and 6.33 give typical driving point impedances measured on the model in this configuration. In fig 6.32 the calculated vertical impedance at the N.D.E. support below approximately 120 c/s is seen to be consistently about 30% lower than the corresponding experimental result. This discrepancy was attributed directly to the shortcomings of the assumed, approximate uncoupled N.D.E. support impedance which, from fig 6.8 differed from the measured value by the same order.

The fundamental shaft mode in this test was resonant at 50 c/s (for the running conditions shown) which was about 10% lower than that obtained with the shaft in ball bearings. The quality (Q factor) of the resonance and its associated anti-resonance was somewhat higher than that predicted theoretically, which effect was undoubtedly due in part to inaccuracies in the theoretical bearing coefficients.

Above about 140 c/s much larger discrepancies in the theoretical results were apparent, particularly around the resonances corresponding

to the first and second overtones (155 and 212 c/s respectively). The lack of system damping evident in both modulus and phase for the theoretical case was much greater than could be accounted for on the basis of errors in the journal eccentricities, and hence bearing velocity coefficients, alone. (This was established by running two further computations on the Atlas computer for assumed viscosities 20% higher and 20% lower than that at the oil film temperature initially used (190 c). The resultant changes in impedances modulus in the region of the 155 c/s resonances were found to be approximately 25%).

Similar differences at higher frequencies between the theoretical values based on the appropriate support impedances and the experimental results were found in measurements throughout the system. These differences were much greater than the comparitively minor variations found when the shaft was supported in ball bearings (section 6.5 (ii)(a)). Following the measurements of the uncoupled support impedances after the rig had been dismantled, however, all the major differences could be identified with regions where the assumed impedances were much too low.

The measured horizontal driving point impedance at the D.E. support, shown in fig 6.33, illustrates the above point. Thus in the region above 220 c/s the theoretical curve gave impedance moduli 2 to 3 times lower than the experimental values, in which frequency range the largest differences between the assumed and practical support impedance are apparent from fig 6.11.

(b) 20 in Bearing Centre Configuration.

In this configuration errors at the higher frequencies due to the approximate support impedances were again apparent, Fig.6.34 illustrates results typical of those obtained. In this figure the experimental impedance modulus and phase show very little evidence of the fundamental

shaft modes, whilst these are not detectable at all in the theoretical curve due to the high assumed uncoupled support impedance at the corresponding location. Similarly the 'third' overtone modes (one predominantly horizontal and one predominantly vertical) are not in evidence in either experimental or theoretical curves. Both cases illustrate the considerable damping effect due to the journal bearings.

The marked improvements in theoretical predictions of the system's behaviour consequent on the introduction of the measured (complex) impedances of the uncoupled supports into the analysis are discussed in section 6.7 below.

A problem which attracted the writer's attention because of its practical significance in measurements on full-scale machines was the behaviour of shafts lying stationary in journal bearings and the interpretation of support impedances measured on the assembled system. It was observed that such measurements on the modelrrig (and on the rotary converter discussed in Chapter 7) indicated very high levels of damping - of the same order as these encountered when the shaft was rotating in journal bearings. This type of behaviour is illustrated in the transfer impedance shown in fig 6.35. In this figure the full lines show the impedance modulus and phase measured with the rig in the 20 in centre configuration immediately after assembly and with the journal bearings chemically cleaned of all traces of oil. For comparison, the corresponding measurements made with the shaft rotating with the oil conditions indicated is also shown. The formulation and numerical integration of the non-linear differential equations describing the 'ideal' contact conditions occurring in this type of system are discussed, together with experimental work on a 'dummy' support - journal model, in Appendix I.

6.6 (iii) Unbalance Responses

(a) Introduction.

As far as is known the present work is unique in giving quantitative comparisons between theory and experiment for a rotating system of this generality (i.e. flexible rotor, journal bearings, massive flexible supports). Although the main aim was the examination of the accuracy with which support impedances could be incorporated to describe this behaviour a much wider interpretation could be attempted. In recent literature there has been a growing tendency to consider the behaviour of flexible rotor systems in their entirety - at least in general, analytic terms. This has been inspired largely by the increasing need for more complete descriptions as shaft speeds have risen. The problem of deciding satisfactory running conditions and of the balancing of flexible rotors are naturally closely linked - in both cases the need to interpret measured vibration levels arises with similar complications (see the contribution by Professor E.Downham and the writer to Morton's paper (46), just published at the time of writing).

Some impressions of the involved nature of the unbalance response of flexible shafts carried in journal bearings which themselves are not rigidly supported may be gained from fig 6.36. In this diagram the calculated unbalance whirl paths of the model machine, in the 20 in bearing centre configuration, are shown for a rotational frequency of 66.7 c/s i.e. close to the upper 'fundamental' critical speed. Since the journal bearing dynamic coefficients are assumed to be linear, the whirl path in each axial plane is an ellipse, but due to the displacement and damping coupling motion in the horizontal and vertical planes, the orientation of the axes of these ellipses differ along the length of the shaft. The instantaneous deflected form of the shaft is therefore not a plane curve, whilst the shape of this curve changes with time - that is with angular rotation of the shaft. Thus the whirl amplitude

and its phase relative to a given unbalance vector in a fixed radial plane of the shaft depends on the axial and radial planes in which it is measured. In fig 6.36, therefore, the phase angles α_1, α_2, α_3, α_4, α_5 and α_6 have values 90, 141, 126, 101, 195 and 61 degrees respectively in relation to the unbalance vector (shown horizontal at time t = 0).

Figs. 6.37 to 6.44 give examples of unbalance responses measured on the model for the 24 in and 20 in bearing centre configurations. For a given residual unbalance the systems was found to be five or six times less responsive in the region of the fundamental critical speeds compared with the ball bearing arrangement. As in the results for the latter arrangement the distribution of balancing masses added to the rotor is indicated in each figure by the inset diagram. In all cases the theoretical responses shown were obtained using the analytic approach of Chapter 4, and were based on the approximate driving point impedances of the bearing supports discussed in section 6.4. The unit of balance referred to is again .75gm at the rotor radius, corresponding to the effect of one balancing screw used in the experiments. In this respect the 'as machine' balance condition represented the removal of all eight balancing screws used to obtain the 'fine' balance condition discussed in section 6.5 (i).

(b) 24 in Bearing Centre Configuration

Fig. 6.37 shows the vertical response at the N.D.E. bearing support both experimental and theoretical curves of which show a heavily damped resonance in the region of the fundamental criticals. The experimental peak response occurred at a somewhat lower frequency (52 c/s) than the theoretical (54.1 c/s) but otherwise reasonable correlation was achieved in the region governed by unbalance in the fundamental modes. This agreement suggested reasonably accurate bearing coefficients.

In this region the experimental residual unbalance was apparently 2 to 4 times the theoretically assumed value (i.e. 3 to 6 balance units), the higher apparent unbalances being reached near the critical frequency. Above the critical region the apparent unbalance as based on the assumed theoretical distribution increases rapidly due to modal contributions in the first overtone modes outside the rotor's length. As in the case of the ball bearing configuration (fig 6.28, section 6.5 (iii) (b)) this effect was attributed to local unbalance in the shaft marker assembly.

The response at the D.E.support, shown in fig 6.38 indicated that the level of damping in the theoretical curve was of the right order. However, the apparent residual unbalance, based on the measured response below the critical region (i.e. predominantly in the fundamental mode), was about 9 to 10.5 units or roughly twice that predicted above from the N.D.E. support response. This high value was a direct effect of the high approximate support impedance assumed for the D.E.support in the vertical plane (fig 6.10).

A similar qualitative agreement between theory and practice is illustrated in fig 6.39 for the horizontal D.E.support response, the high assumed support impedance (fig 6.11) again increasing the apparent residual unbalance by a factor of 2.

It is of interest to note that the theoretical bearing coefficients appear to be good approximation to the actual conditions obtained even, as in the case of the particular examples of figs 6.37 to 6.39, where oscillatory bearing loads of up to 20% of the static value were induced. In fig 6.39 for instance, the acceleration response at 70 c/s was 0.04 g.r.m.s. which indicated an oscillatory force of 4.48 lbf r.m.s. or 6.34 lbf vector(based on the measured support impedance of 112 lb at the same frequency as shown in fig 6.11), compared with the dead load due to the shaft weight of 35 lbf.

Where much larger unbalances were introduced however, considerable errors became apparent. This is illustrated in fig 6.10 where an additional unbalance of 9.8 gms was added to the rotor in the place of its own inherent unbalance. In this case wider variations between the form of the theoretical and experimental rotor responses were evident, presumably due to the effects of non-linearity of the oil films.

(c) 20 in Bearing Centre Configuration

In this configuration good qualitative correlation between theory and practice was again obtained, the main quantitative differences in the responses being clearly due to errors in the assumed approximate support impedances. Examples of the results obtained are illustrated in figs 6.41 to 6.44.

Because the stiffness of the N.D.E. half-shaft was relatively high in this configuration, the unbalance behaviour was influenced to a greater extent by the dynamic characteristics of the journal bearings. Comparing the support acceleration responses of figs. 6.41 and 6.42 with the rotor amplitudes of figs 6.43 and 6.44 for instance, the character of the response is seen to vary considerably from location to location. In practice this emphasises that the complete system (shaft, bearings, supports) should be considered in interpreting measured vibration levels, amplitudes being no longer simply related as in the case of simpler, elastic whirling shaft arrangements.

At rotational frequencies up to about 55 c/s the residual unbalance in the 'V.coarse' condition is, from fig 6.41 apparently 5 times the theoretical value (i.e. 5 units). In the vicinity of the fundamental critical frequency the apparent unbalance increases to nearly 10 units which suggested that the theoretical bearing velocity coefficients were in error. At higher frequencies the apparent unbalance is again 5 to 6 units.

Similar quantitative values for absolute unbalance were also obtained from the D.E.support response shown in fig 6.42 when the high assumed support impedances were taken into account.

The rotor phase diagrams of figs 6.43 and 6.44 are interesting, the former showing a very gradual 180° change in the vertical motion as the speed increased from 30 to 80 c/s. In the horizontal plane (fig 6.44) the total phase change in this speed range was only about 100 degrees.

6.7 Impedance Measurements at the Bearing Supports (Compared with Theoretical Values Based on Measured, Uncoupled Support Impedances)

In the impedance measurements made on the complete rotating system (section 6.6 (ii)) large discrepancies at higher frequencies were found between the practical and theoretical results, when the latter were based on the support impedances originally measured with the ball races in the housings. The unexpected differences in the driving point impedances of the supports with the journal bearings in place - discovered when the rig was finally dismantled - indicated that these differences could account for the discrepancies in the behaviour of the complete system.

Modifications to the Atlas digital computer programme were therefore made, as outlined in Chapter 4, to enable the measured support impedance to be 'read in' as data for the calculations. Time has not permitted a full set of theoretical results to be obtained but those completed at present show that the above assumptions were correct.

Fig 6.45 for example, shows the horizontal driving point impedance measured at the D.E.support with the rig in the 20 in bearing centre configuration - the same experimental results as are given in fig 6.34. The improvement in the accuracy of the theoretical predictions in fig 6.45 in which the measured (uncoupled) support impedances were used may

be seen on comparison with the earlier figure. In particular the frequency and quality of the resonant minimum at 240 c/s is predicted much more accurately.

It is interesting to note that, in the region of this resonance, the impedance shown is quite critically dependent on oil film conditions. This is demonstrated by the theoretical points based on an oil film temperature 5 C^{o} higher than the outlet temperature considered in the main theoretical curve (circled points). The closest agreement between theory and practice in this case, however, was obtained by using the mean outlet oil temperature for estimating the oil viscosity.

Although discrepancies due to the neglect of the coupling between horizontal and vertical planes of the supports are evident in fig 6.45, particularly around the 'axial' resonance at 98 c/s, the differences are comparatively minor. It seems reasonable to conclude that the inclusion of the neglected transfer impedances (Xyx_1, Zxy_1, Zyx_2, Zyx_2) would yield even more accurate results.

Above 350 c/s the theoretical curve of fig 6.45 is lower than the measured results, this phenomenon being attributed to the neglected half-shaft mass in the lumped parameter representation. The effect of this simplification was more evident in the transfer impedance shown in fig 6.46, the theoretical results of which are again based on the measured support impedances. In this diagram the resonance corresponding to the 'third' overtones is at a lower frequency in the experimental curve (see discussion of corresponding effects in ball bearing specification, section 6.5 (ii)).

6.8 Extraction of Uncoupled Support Impedances from Measurements on the Complete Rotating System.

This procedure is discussed analytically in Chapter 4 section 4.5 Since it was the most exacting experimentally, and the most difficult from

the point of view of theoretical computation, it was not attempted until the remainder of the work had shown it to be a worthwhile proposition.

Detailed preparation of the Atlas computer programme to perform the necessary inversion of the system matrices have not yet been completed at the time of writing. One successful computation has been performed, however, the final somewhat lengthy calculations having been worked by hand.

Fig 6.47 shows eight points thus obtained for the vertical driving point impedance modulus of the D.E.support, together with the corresponding phase angles, extracted from an equivalent measurement on the complete system when it was rotating at 20 c/s in journal bearings at 20 in centres.

Considering the possible sources of error in this procedure, not least those arising from the use of calculated bearing dynamic coefficients, the results obtained are encouraging. It is hoped to perform further work in future, however, to investigate more closely the conditions governing the accurate extraction of support impedances. In this connection it was apparent during the hand calculations that under certain circumstances (when the phase angle was close to 0^{o}) relatively small errors in the measured phase angles could produce large errors in the corresponding extracted impedance. For this reason the accuracy of the point shown in fig 6.47 at 500 c/s is considered to be purely fortuitous and that a difference of about 5 degrees in the measured phase angle would have produced an increase in the impedance modulus shown of 100%

It is also tentatively suggested that this procedure may form the basis of a method for the indirect measurement of the full set of eight journal bearing dynamic coefficients - experimental determination of which, to the writer's knowledge, has not yet been attempted.

6.9 General Conclusions and Suggestions for Future work

All known existing vibration criteria for rotating machinery are qualitative and take no account of the dynamics of the particular machine under consideration. All appear to relate to levels of vibration which produce varying degrees of discomfort or annoyance to the person making the assessment (Chapter 2, Section 2.5). It has been proposed that, in order to interpret more realistically vibration levels measured on rotating machines, the bearing support impedances should be taken into account. One direct advantage of this procedure is that measured amplitudes at the supports may be translated into bearing force levels which, in the case of rigid rotors for example, would normally provide all the information required.

In the model rig the final system considered was a flexible shaft supported in journal bearings, the latter being housed in supports whose impedances had been determined experimentally. In a system of this nature the displacements measured at the supports are no longer simply related to those elsewhere. The work reported above has been concerned with the accuracy with which measured support impedances can be incorporated to describe the behaviour of the complete system.

Measurements on the shaft assembly and supports, and with the model assembled in ball bearings, were made before considering the journal bearing configuration. With the ball bearing arrangement (section 6.5) both impedance measurements on the complete system and unbalance response measurements indicated that approximations to the measured support impedances could be used to predict these properties with reasonable accuracy. Where discrepancies were apparent these could be identified with frequency ranges where the assumed support impedances were themselves inaccurate. The neglect of coupling at the supports was also shown to be justified.

At higher frequencies (above about 300 c/s) shortcomings of the lumped parameter representation of the system became apparent due to the effect of the neglected half-shaft masses. This was not considered to be a significant drawback, however, since extension of the existing analysis procedures would be a straightforward operation now the initial computer programme has been written and proved.

In the case of the unbalance responses of the model system in ball bearings (section 6.5(iii)), the assumption that the support impedances were real quantities (undamped) meant that the coupling between horizontal and vertical planes due to external damping occurring in practice was not taken into account. However, the use of the experimentally determined complex impedances in the analysis would be a straightforward procedure, this having already been accomplished for the theoretical impedance analysis of the journal bearing configuration (see below).

With the shaft running in journal bearings wide discrepancies in system behaviour were found when the approximate support impedances, based on those measured with the ball bearings in place, were used in the theoretical analysis. It was shown, however, that these discrepancies could be attributed to the unexpected variations in support impedances consequent on the installation of the journal bearings. For this purpose the measured complex driving point impedances were used at each frequency of interest in the subject.

The work performed to date on the extraction of support impedances from measurements on the complete rotating system (section 6.8) has given encouraging results. The main inference of this work in the present context is the possibility of extracting support impedances, and hence bearing forcing levels, from full scale machines whilst they are running. Further work on the problem is felt to be worth while since one of the drawbacks in trying to obtain experimental data from process machines

is the need to wait for the plant to be shut down.

It is also suggested that this technique may provide a method of measuring journal bearing dynamic coefficients - a problem not yet tackled experimentally and of considerable practical importance.

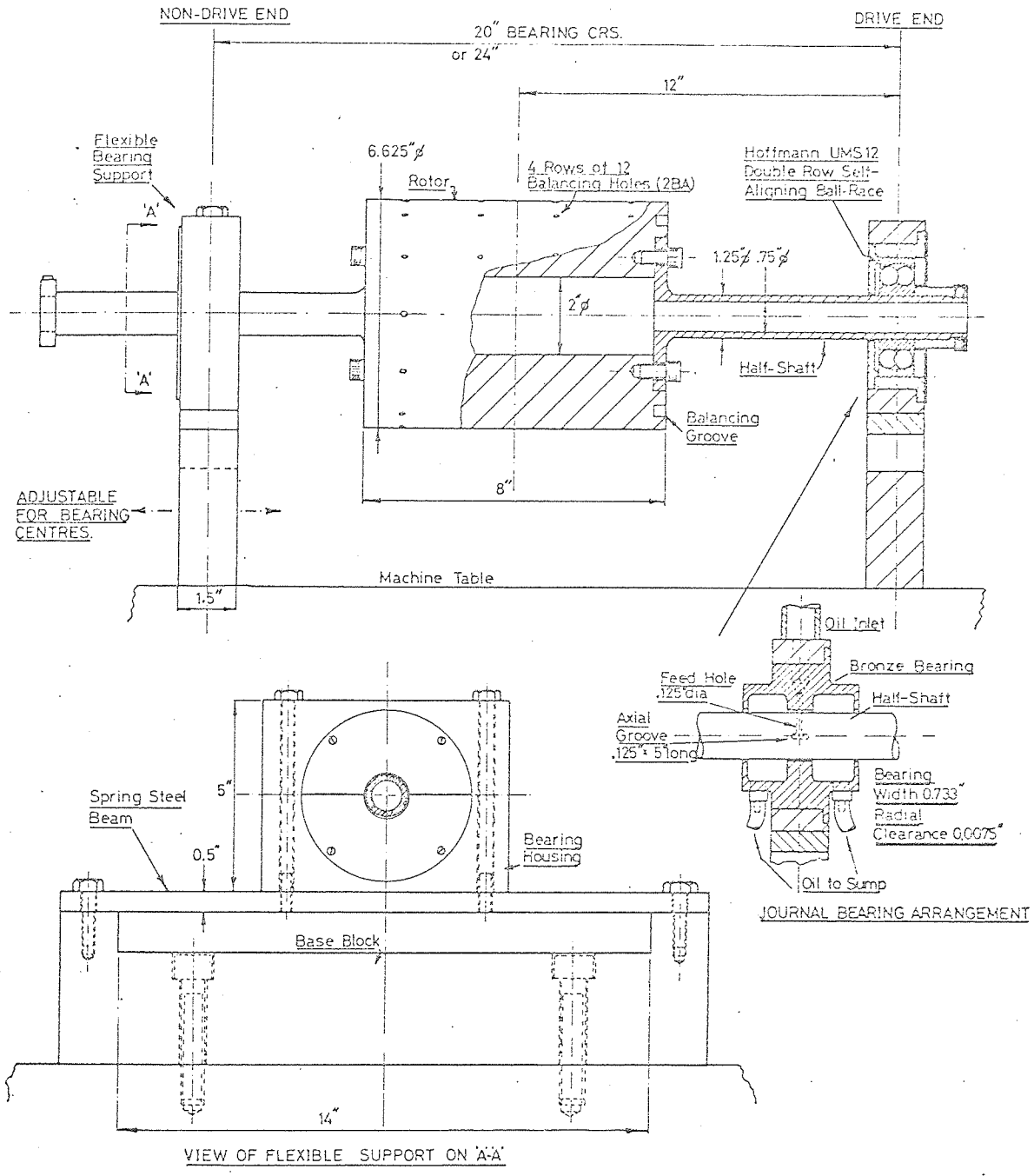

FIG.6.1. MODEL ROTATING MACHINE.

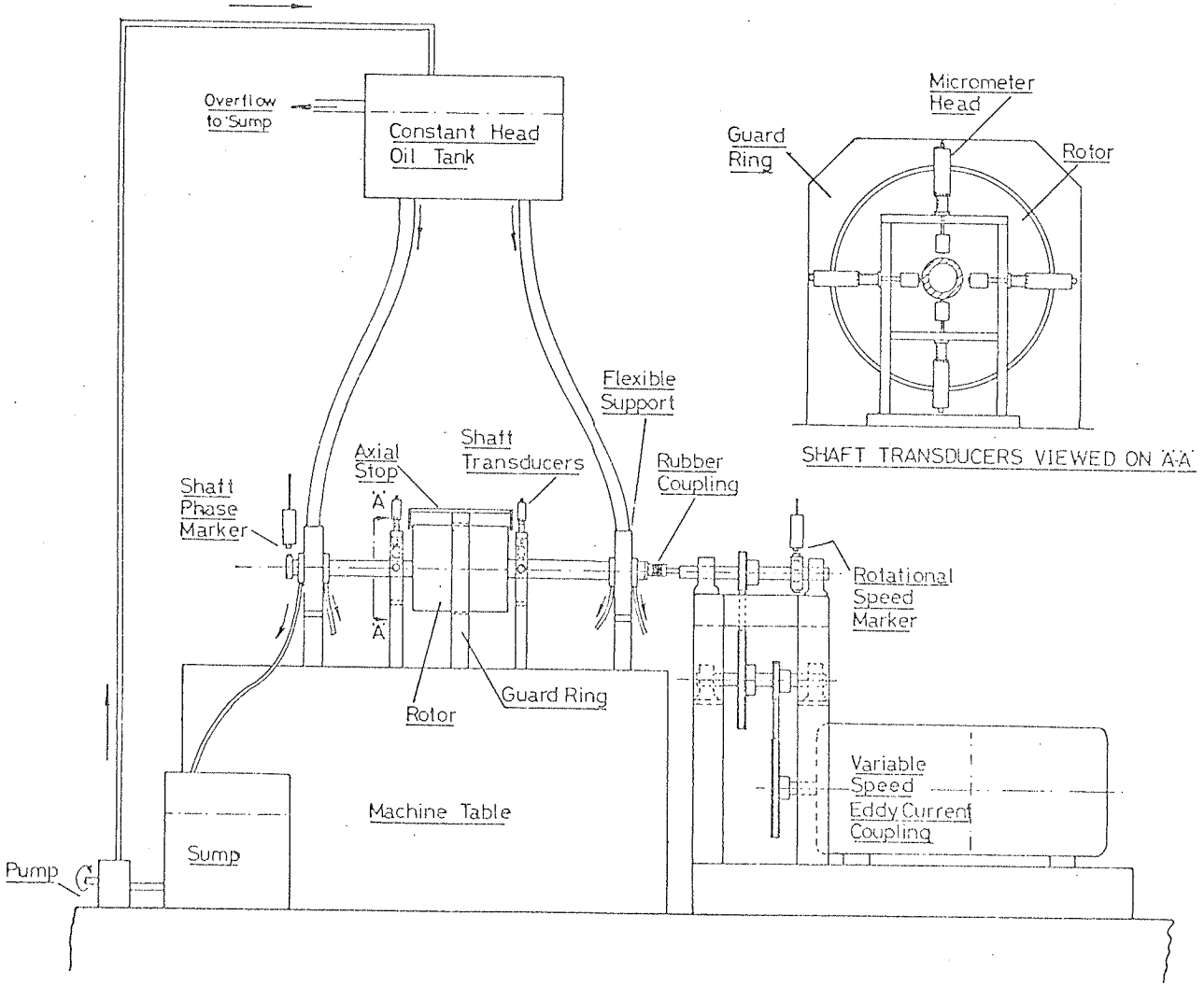

FIG. 6.2. MODEL RIG.

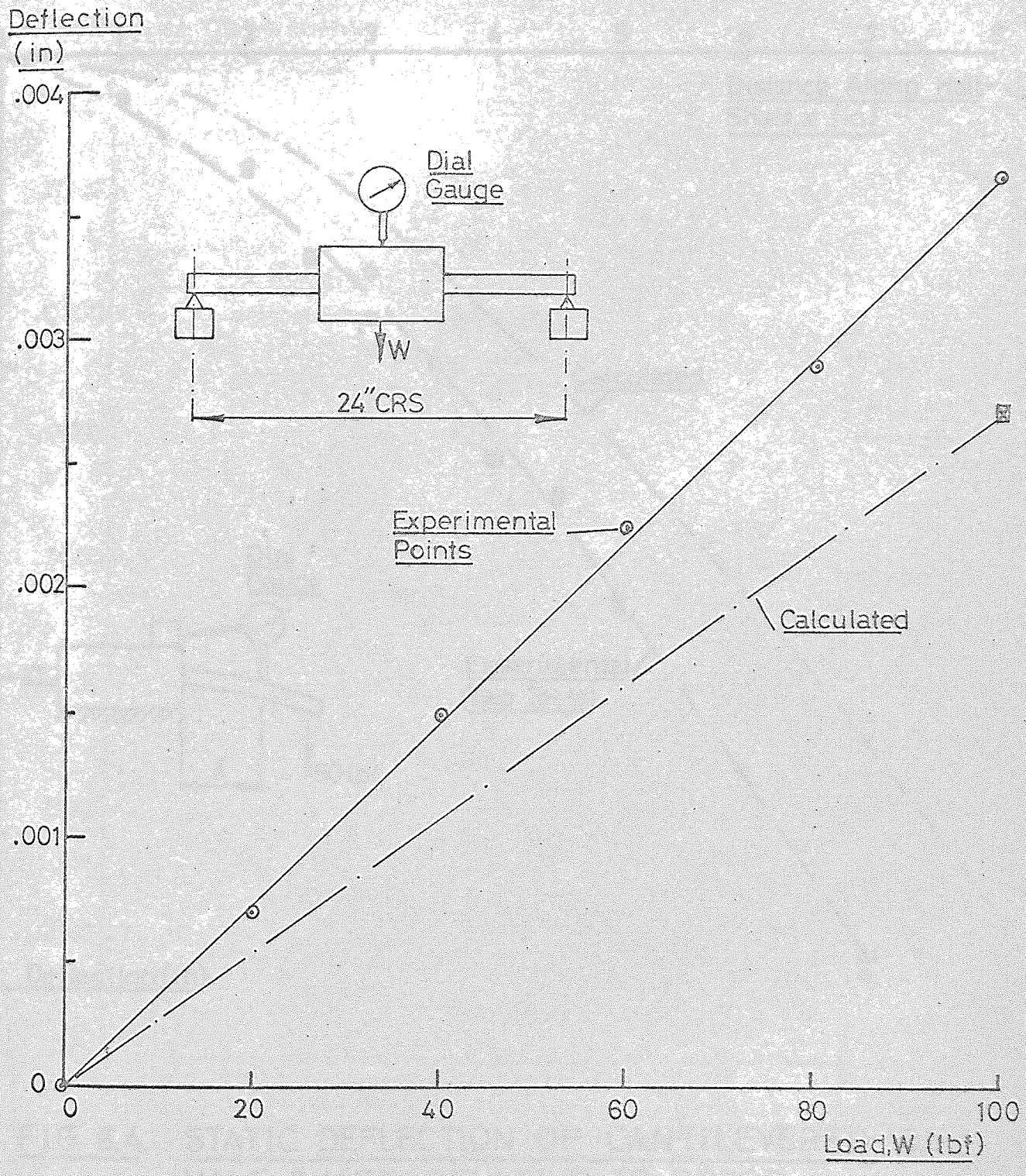

FIG. 6.3 STATIC STIFFNESS OF SHAFT ASSEMBLY

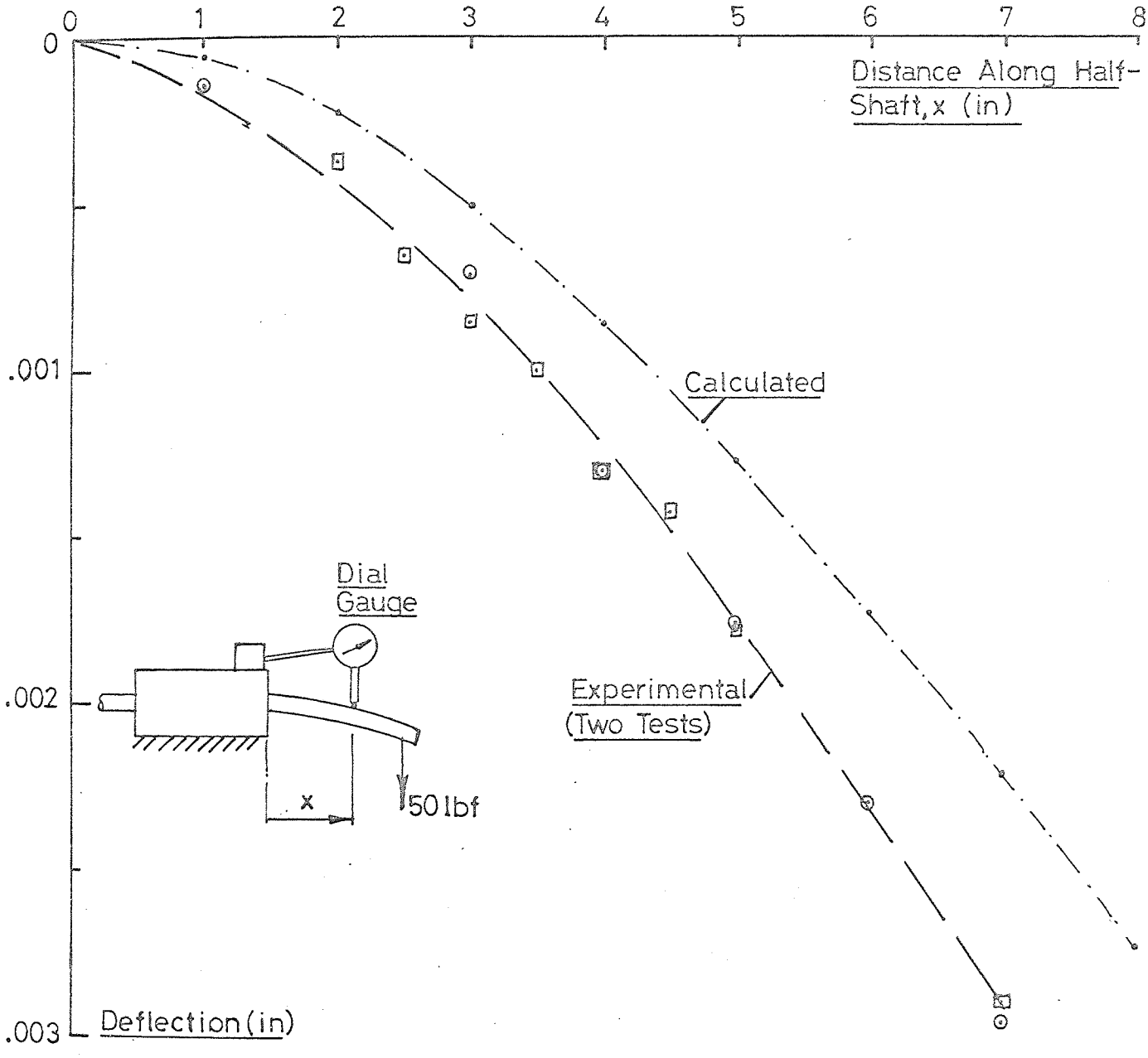

FIG 6.4. STATIC DEFLECTION OF CANTILEVERED D.E. HALF-SHAFT RELATIVE TO ROTOR.

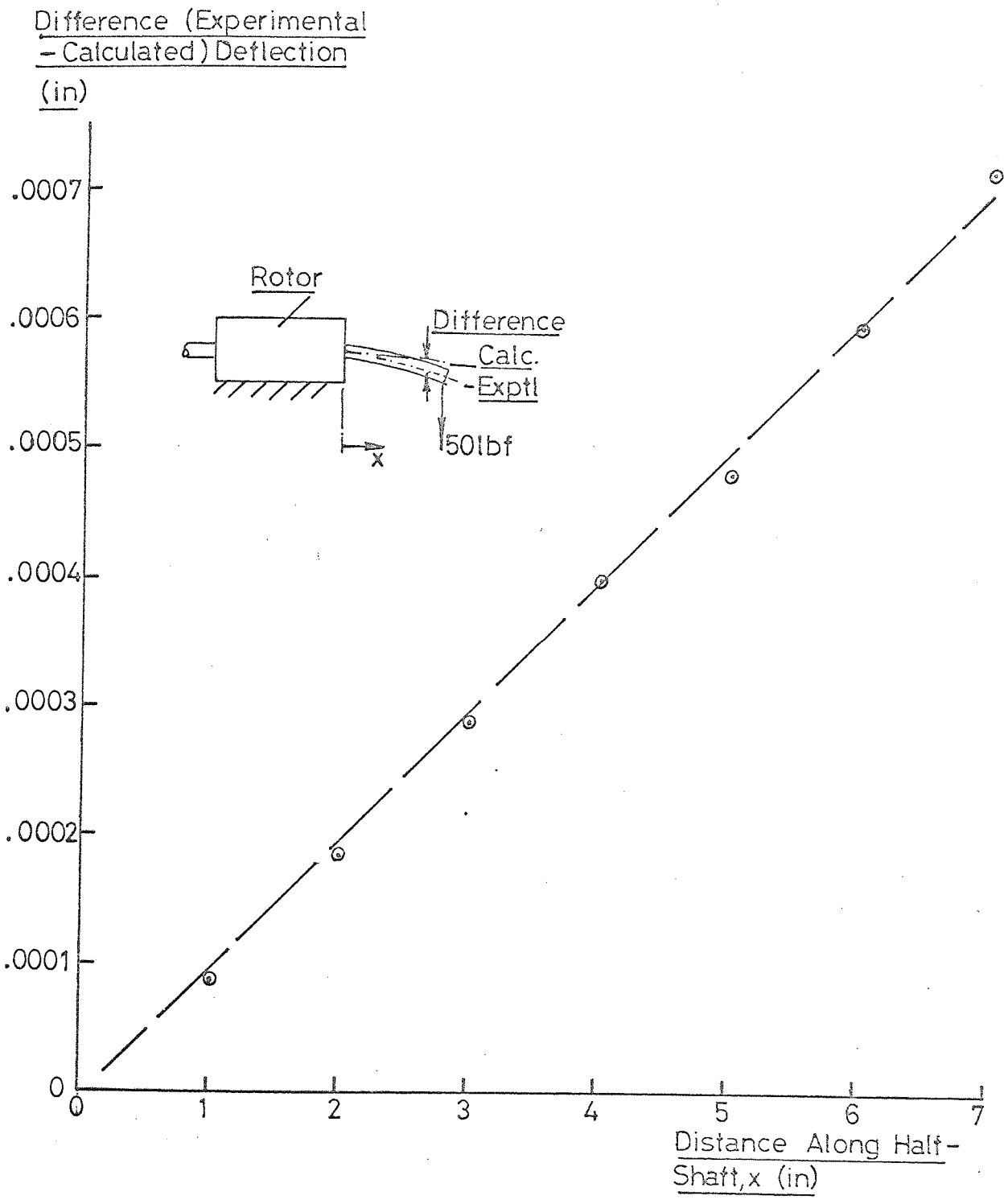

FIG. 6.5 LINEAR DIFFERENCE BETWEEN MEASURED AND CALCULATED D.E. HALF SHAFT STATIC DELECTION.

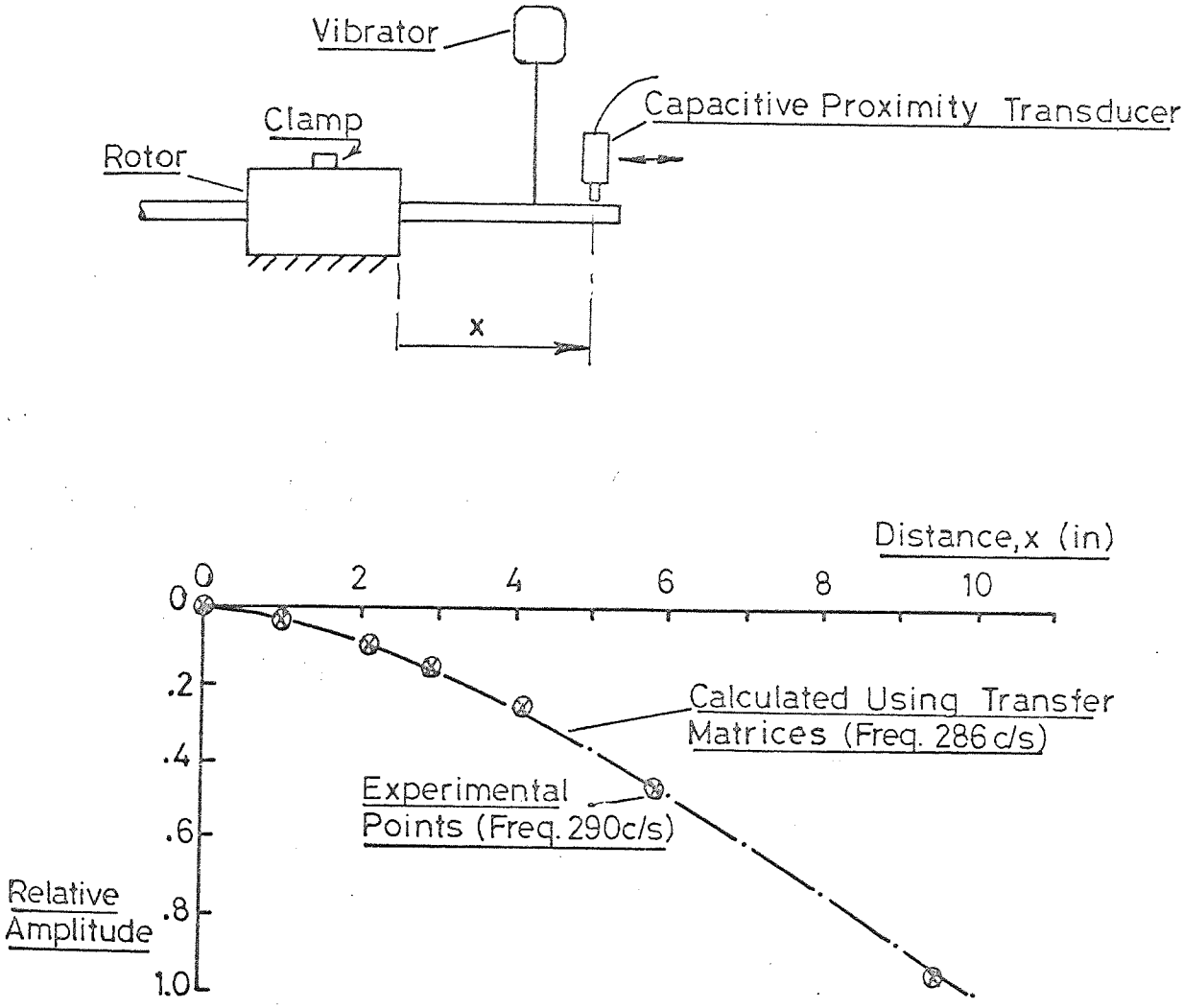

FIG.6.6 FUNDAMENTAL MODAL SHAPE OF D.E. HALF-SHAFT WHEN CANTILEVERED FROM ROTOR.

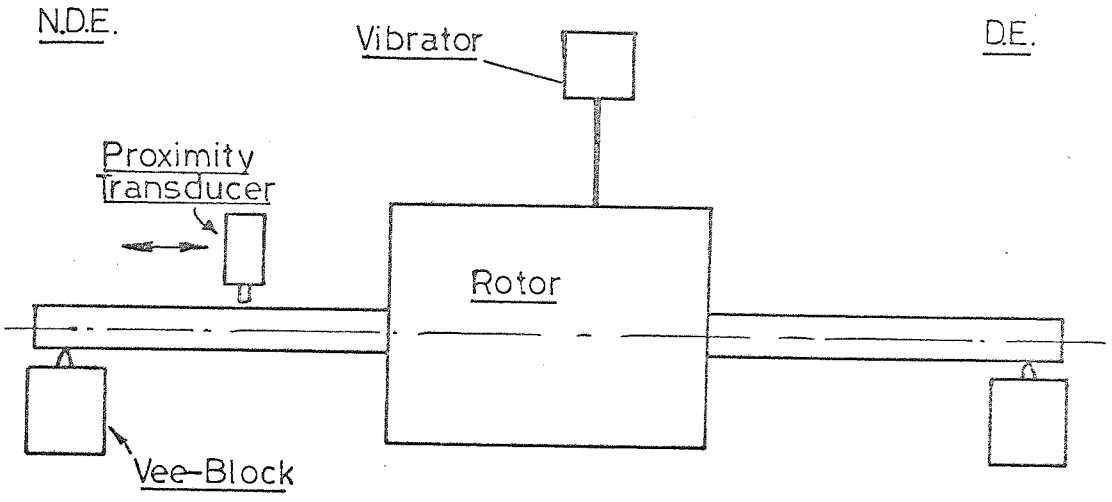

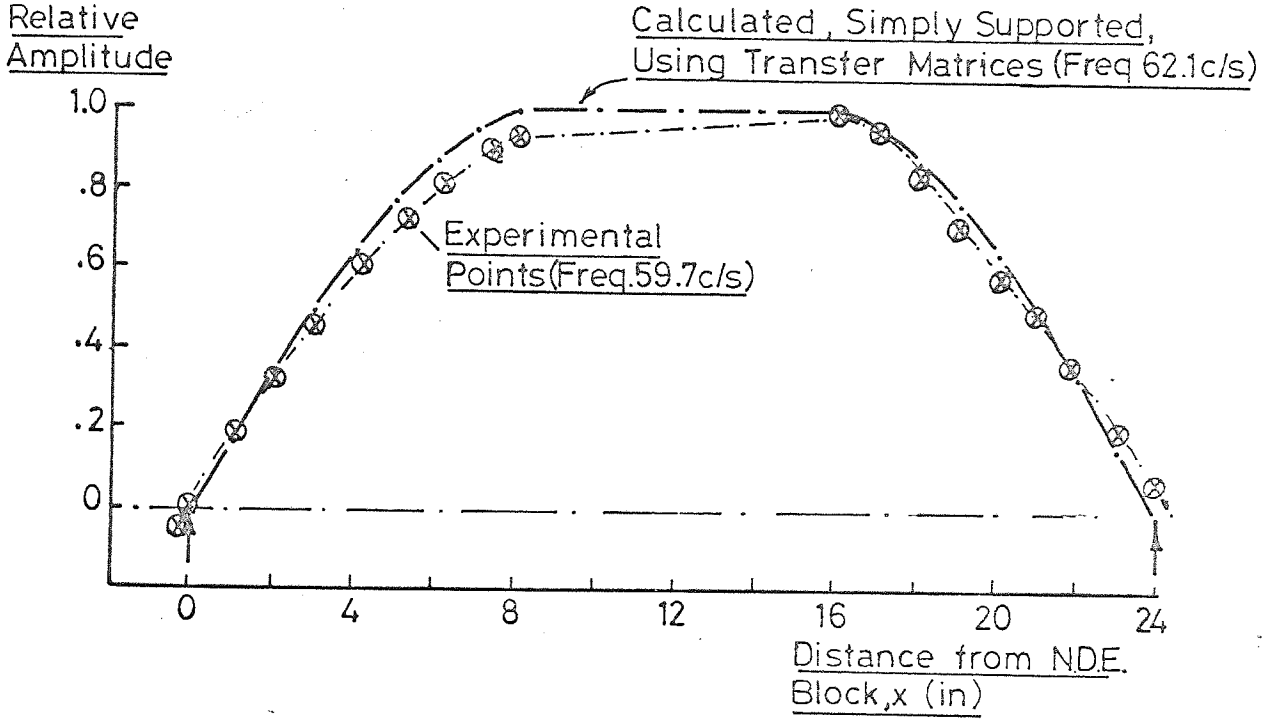

FIG. 6.7 FUNDAMENTAL SHAFT MODE. SUPPORTED ON VEE-BLOCKS AT 24" CRS

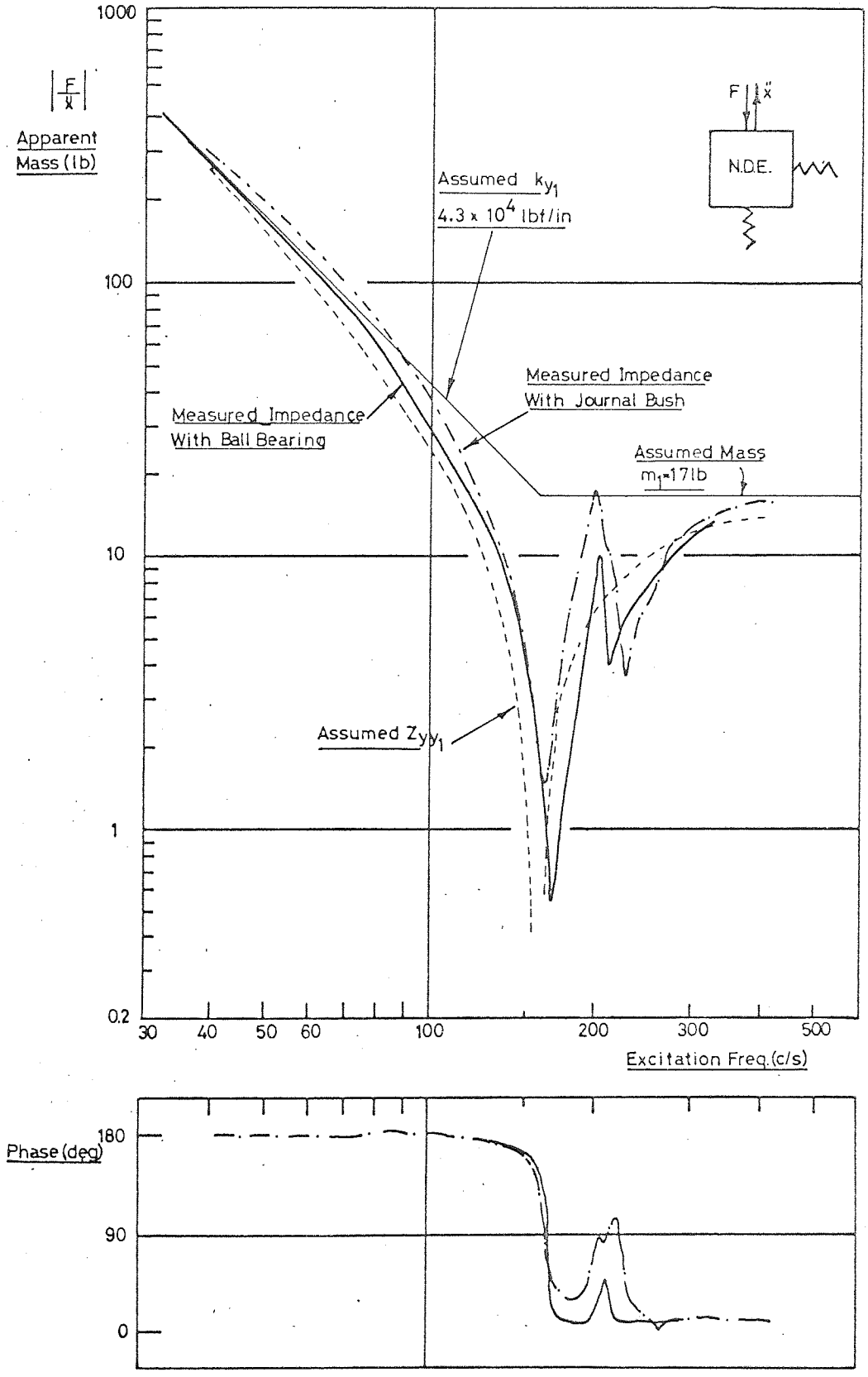

FIG.6.8 VERTICAL DRIVING POINT IMPEDANCE N.D.E. SUPPORT Zyy_1

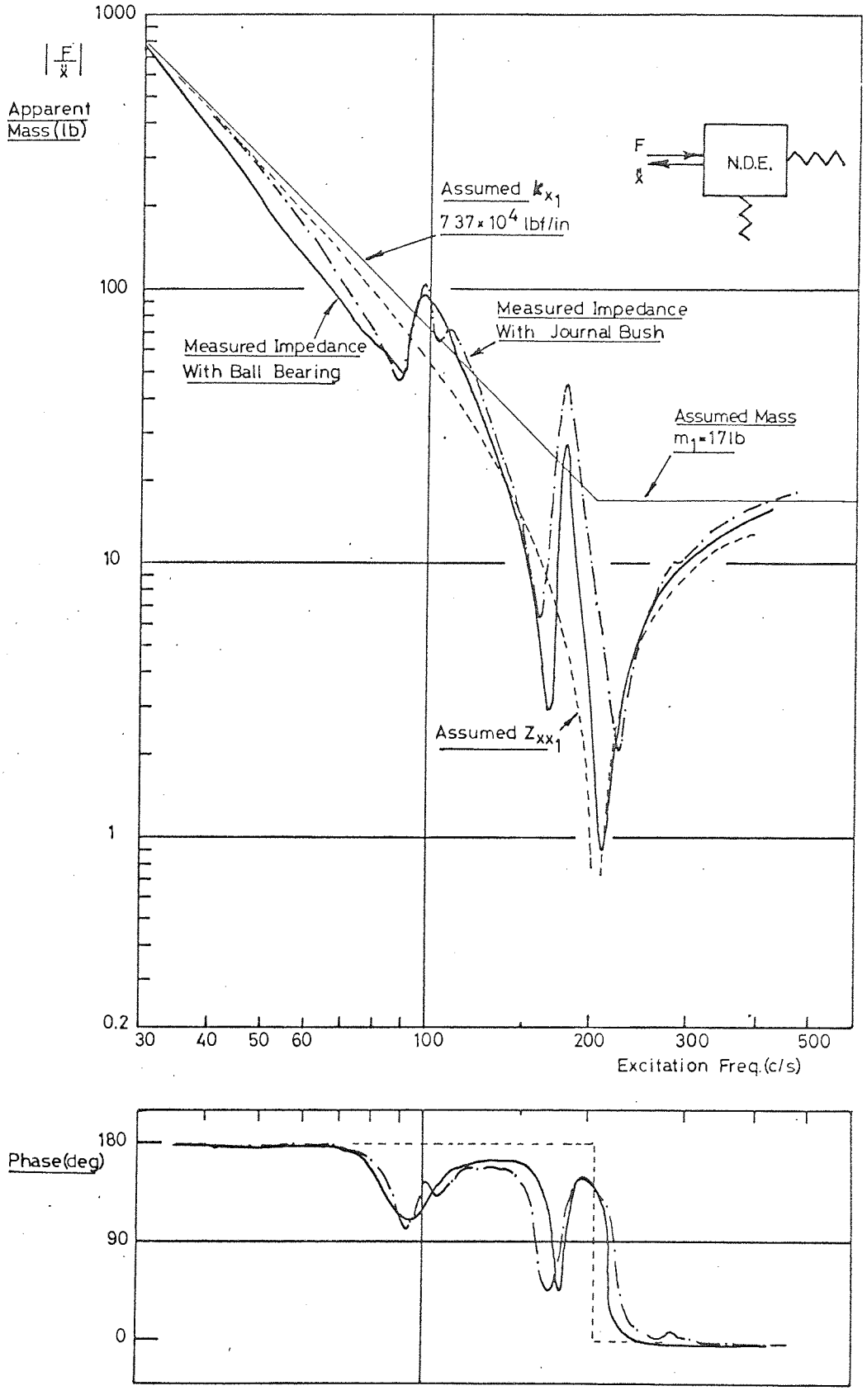

FIG. 6.9 HORIZONTAL DRIVING POINT IMPEDANCE N.D.E. SUPPORT Z_{xx_1}

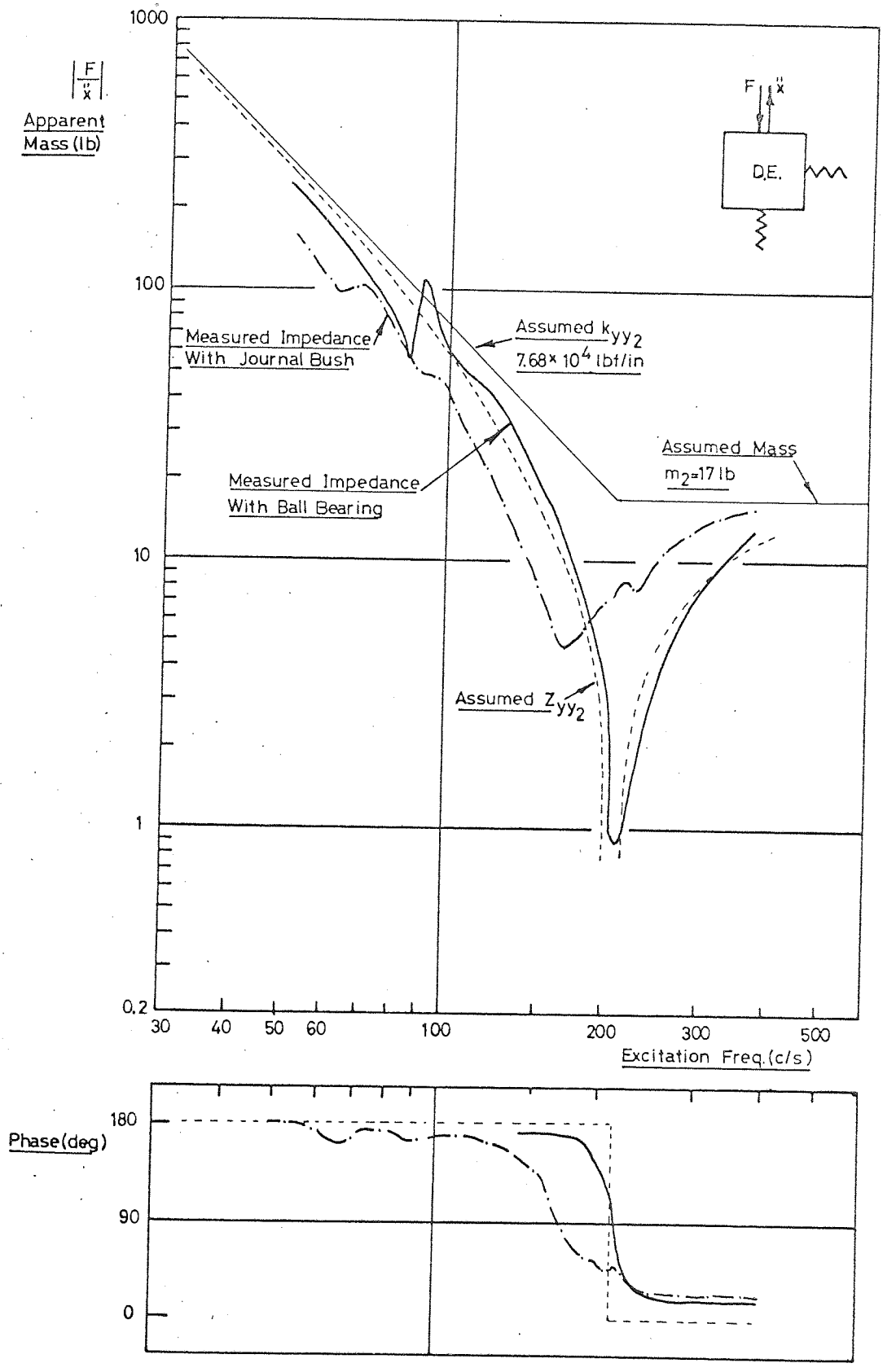

FIG.6.10 VERTICAL DRIVING POINT IMPEDANCE D E SUPPORT Z_{yy_2}

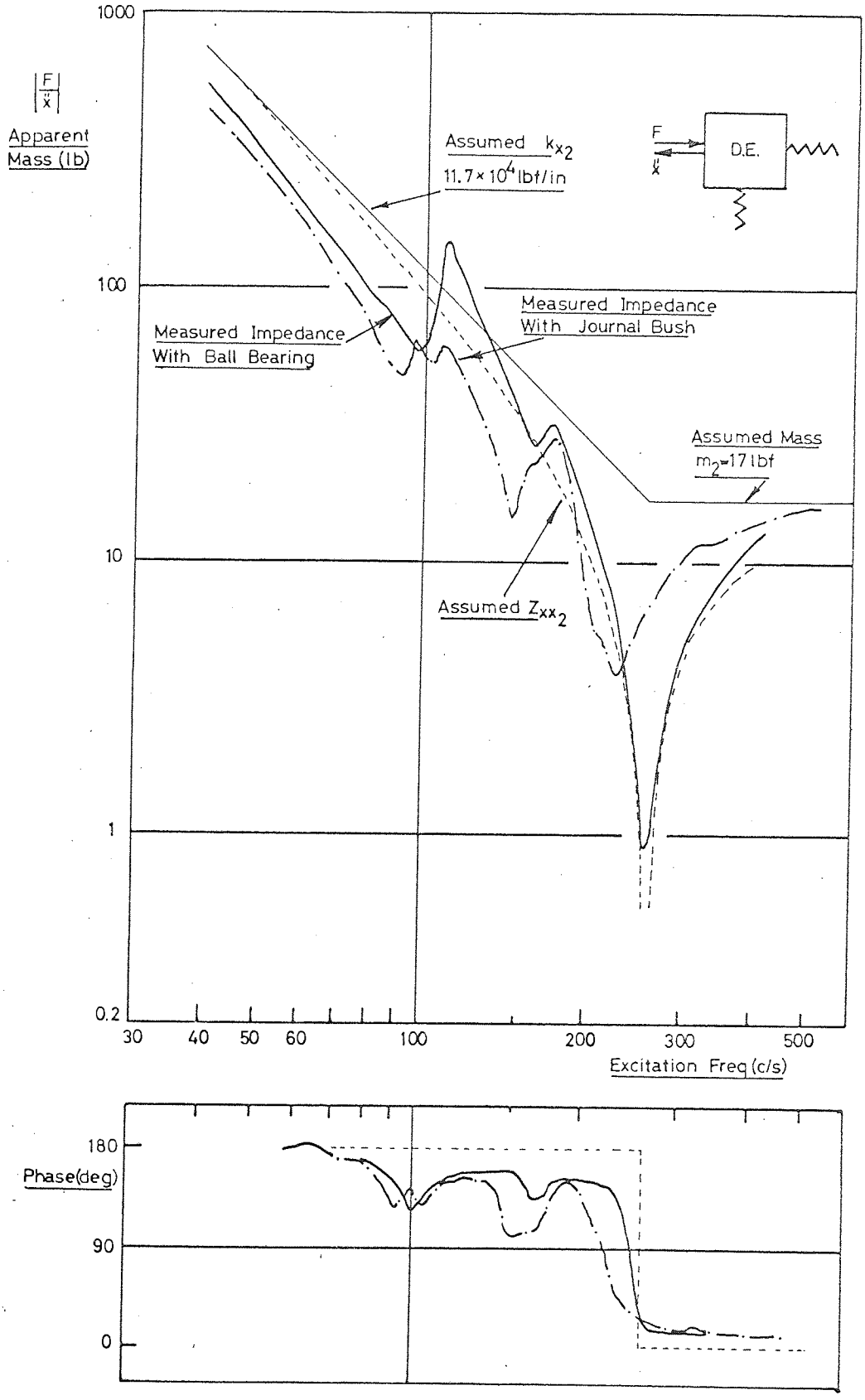

FIG. 6.11 HORIZONTAL DRIVING POINT IMPEDANCE D.E. SUPPORT Z_{xx_2}

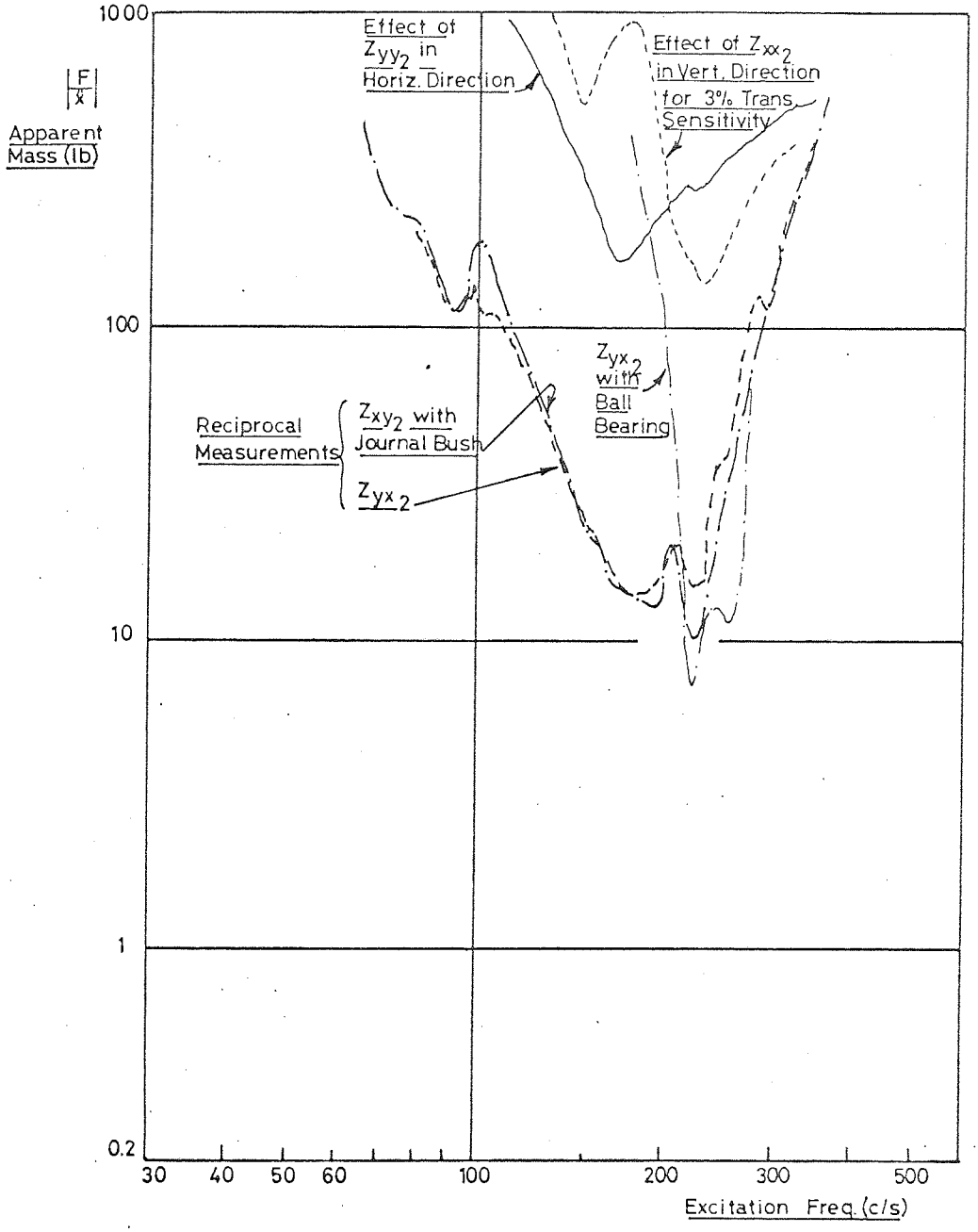

FIG.6.12 TRANSFER IMPEDANCES Z_{xy_2} Z_{yx_2} D.E. SUPPORT

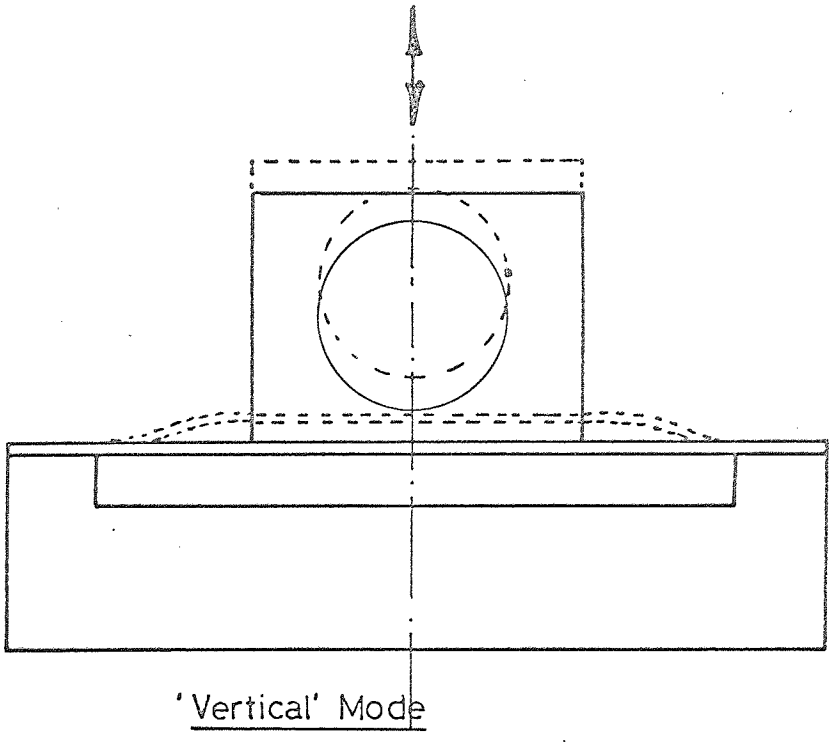

'Vertical' Mode

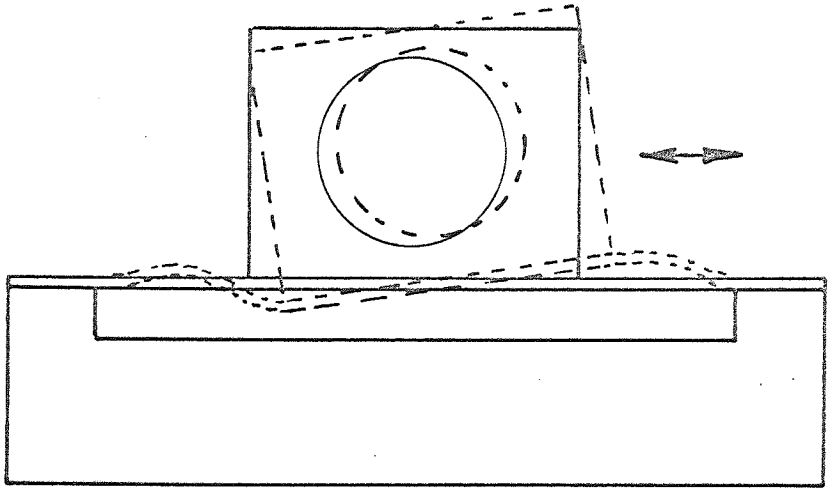

'Horizontal' (Rocking) Mode

FIG. 6.13. APPROXIMATE SUPPORT MODES MODEL RIG.

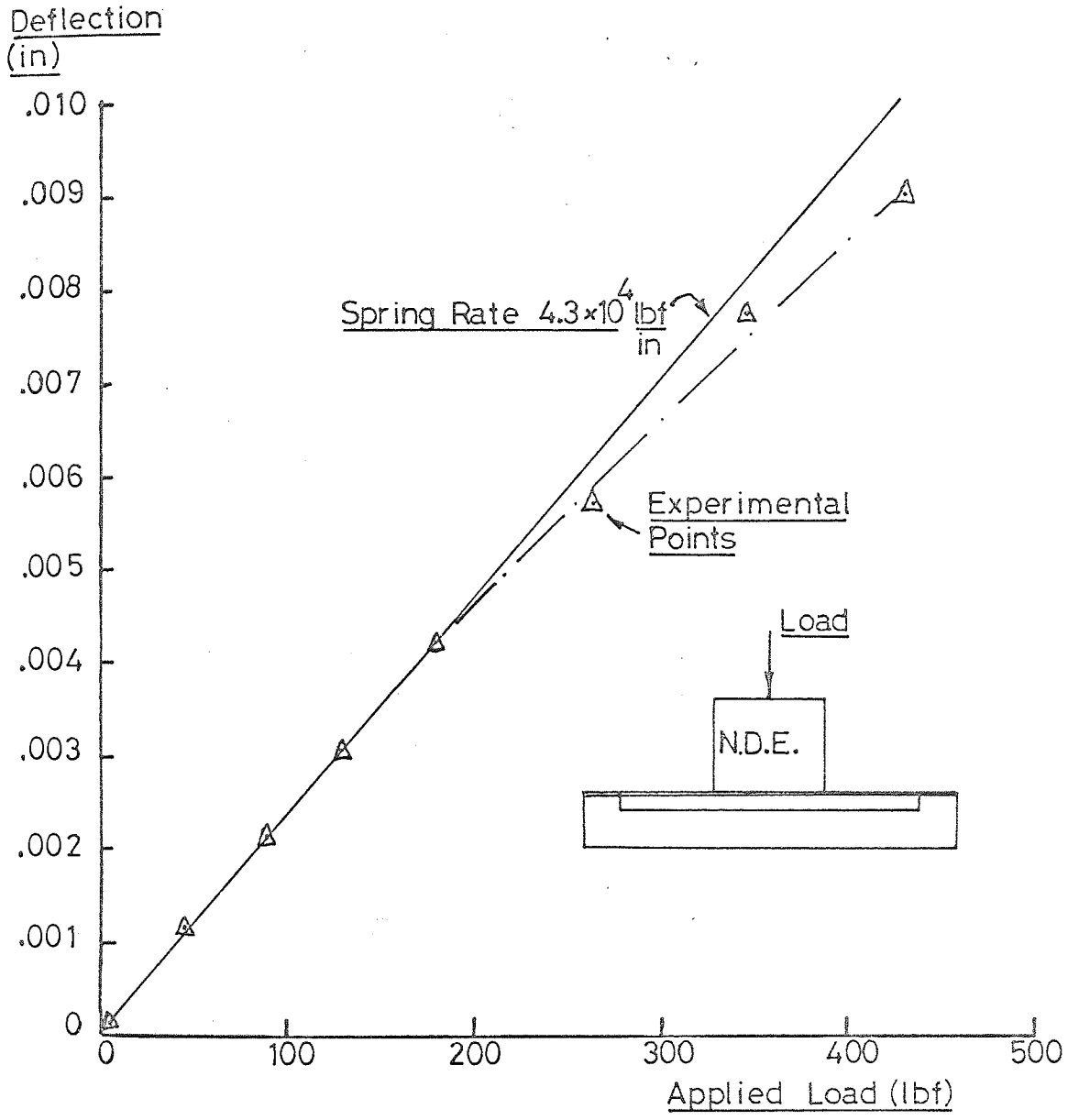

FIG.6.14. VERTICAL STATIC STIFFNESS. N.D.E. BEARING SUPPORT.

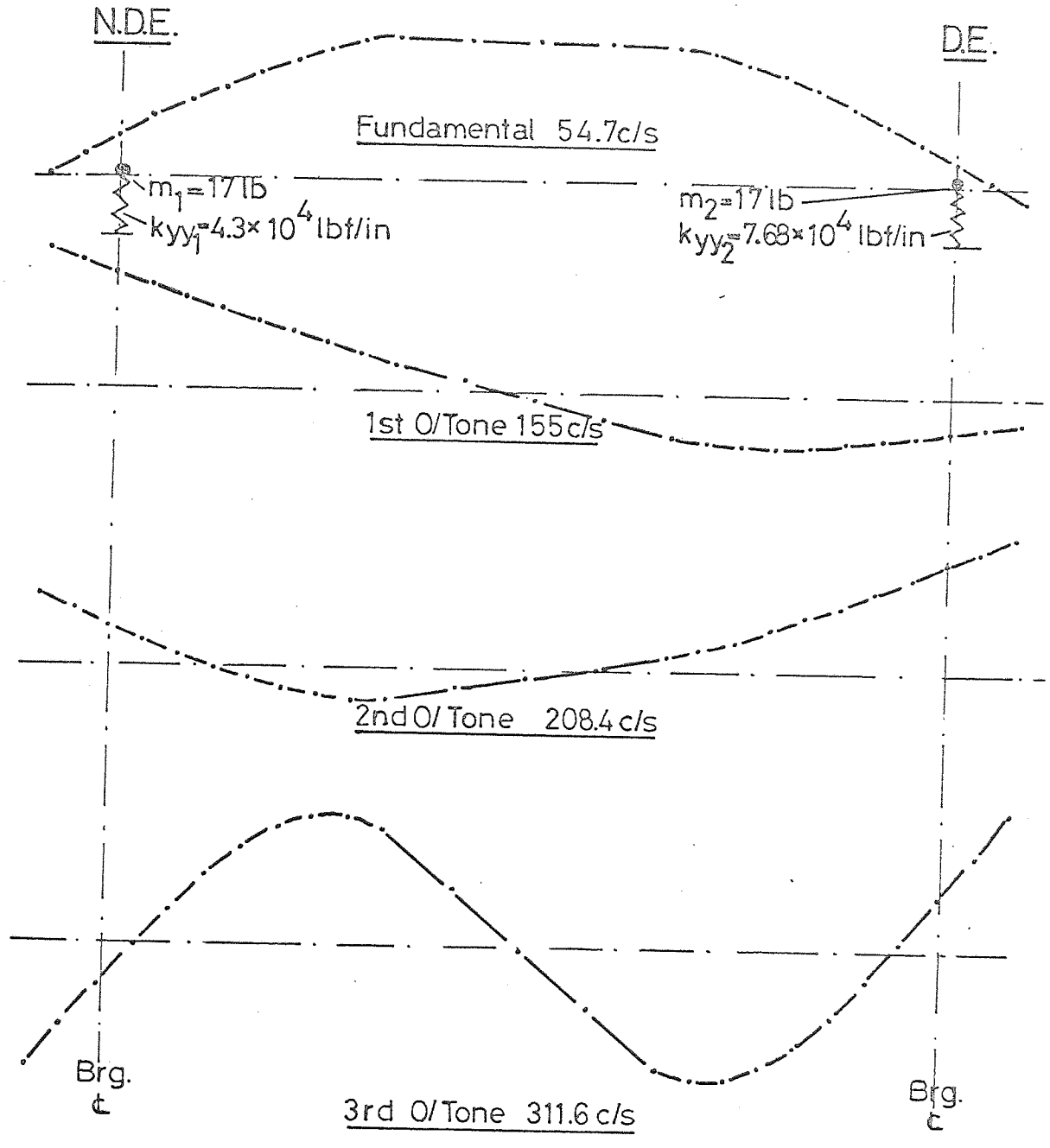

FIG. 6.15 FLEXIBLY SUPPORTED MODES IN VERTICAL PLANE CALCULATED FOR 24" BRG. CRS. USING TRANSFER MATRICES.

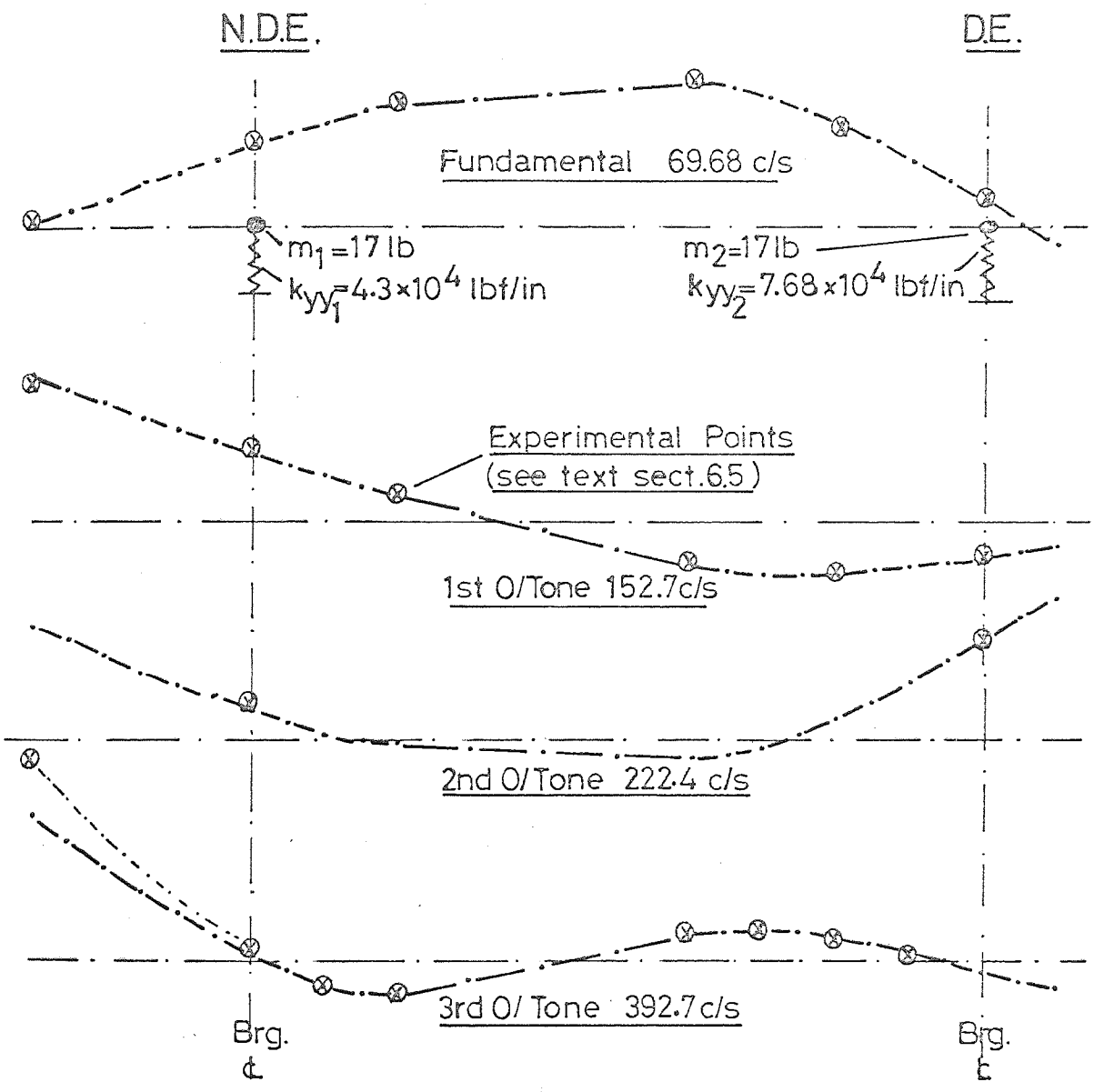

FIG 6.16 FLEXIBLY SUPPORTED MODES IN VERTICAL PLANE CALCULATED FOR 20" BRG. CRS. USING TRANSFER MATRICES.

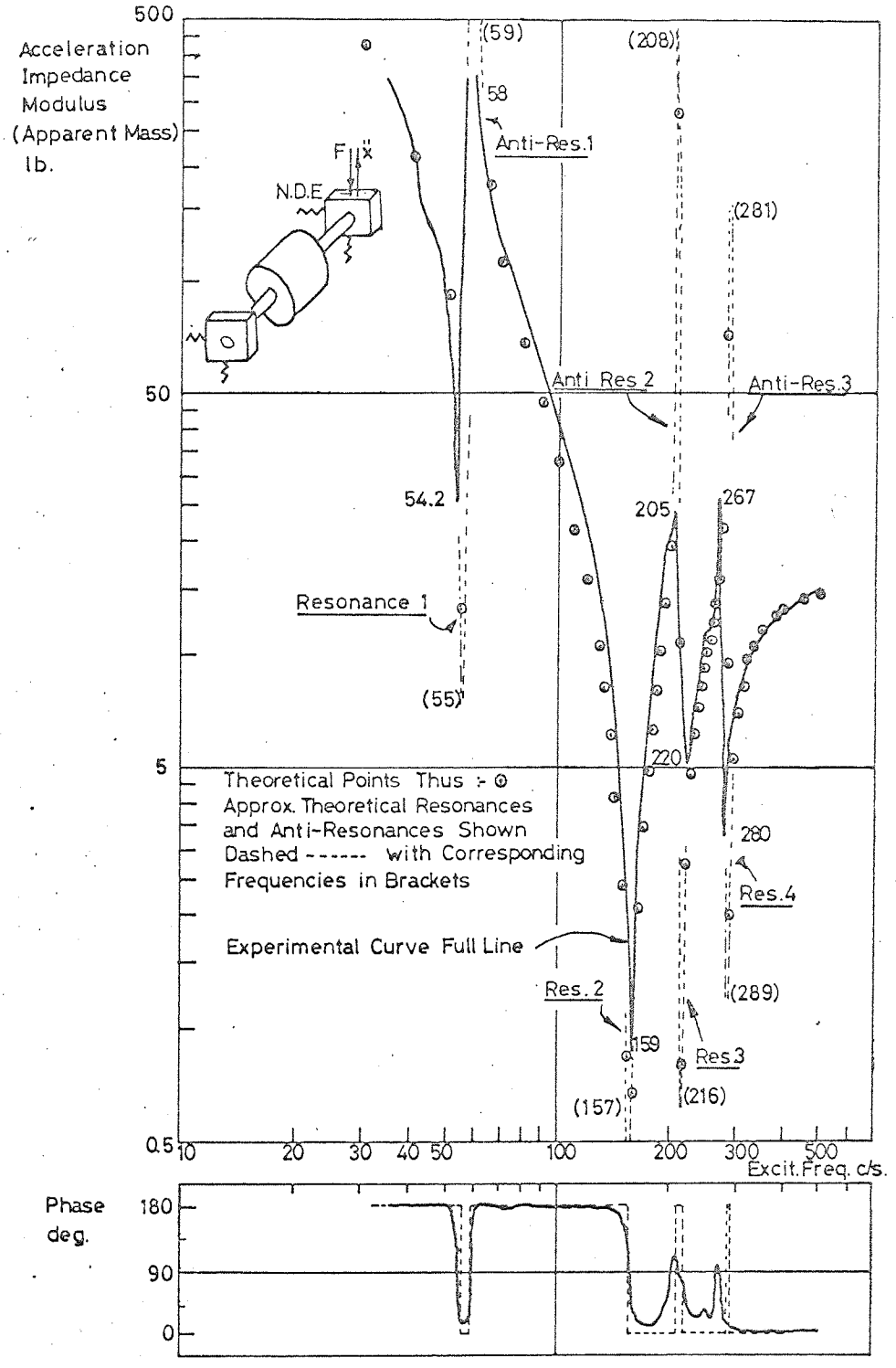

FIG. 6.17. VERTICAL DRIVING-POINT IMPEDANCE N.D.E. BEARING SUPPORT. MODEL RIG 24" CRS. ROTOR STATIONARY IN BALL BEARINGS

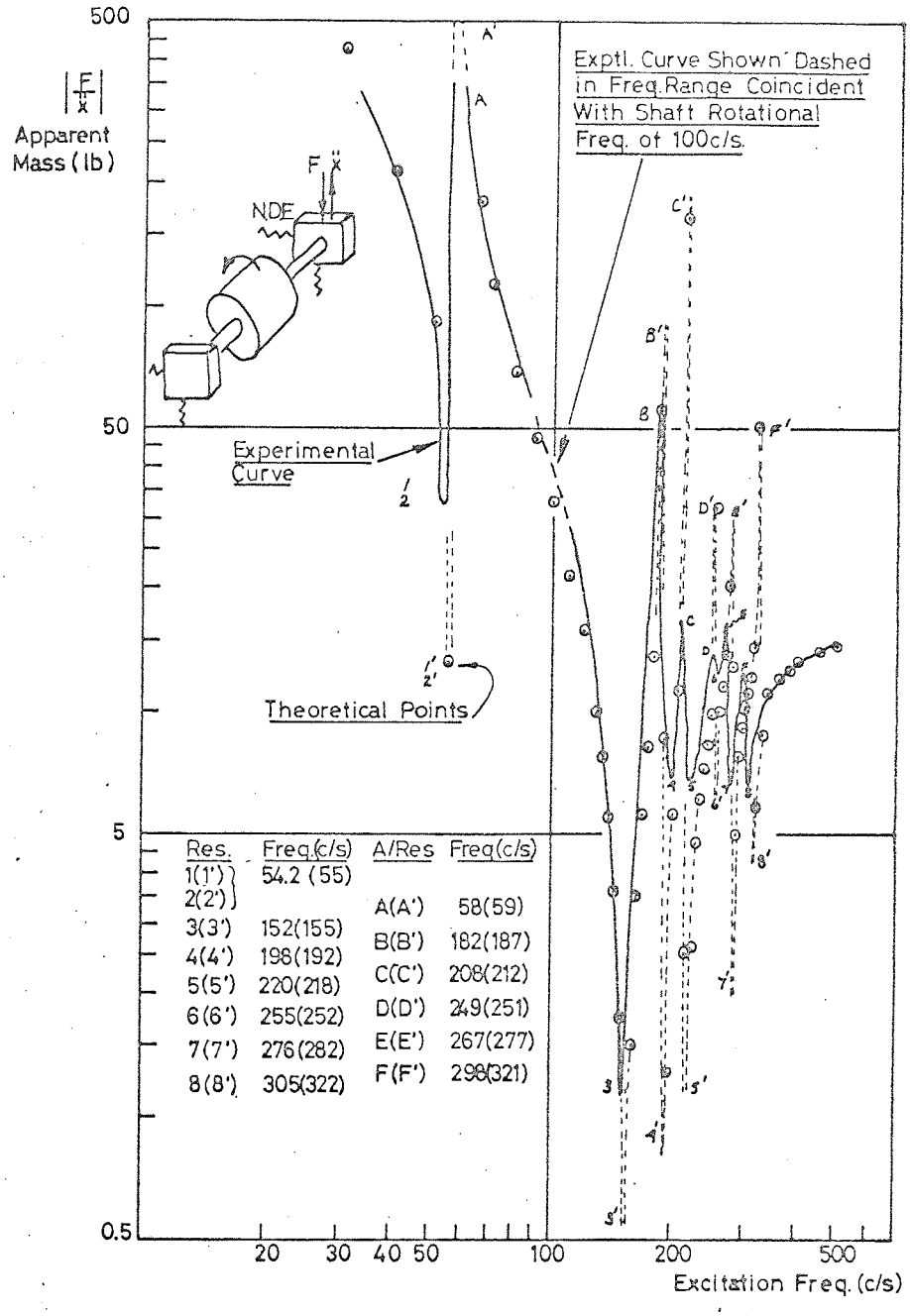

FIG.6.18. VERTICAL DRIVING POINT IMPEDANCE N.D.E. BEARING SUPPORT. MODEL RIG 24"CRS. ROTOR SPEED 100c/s (6000r.p.m.)

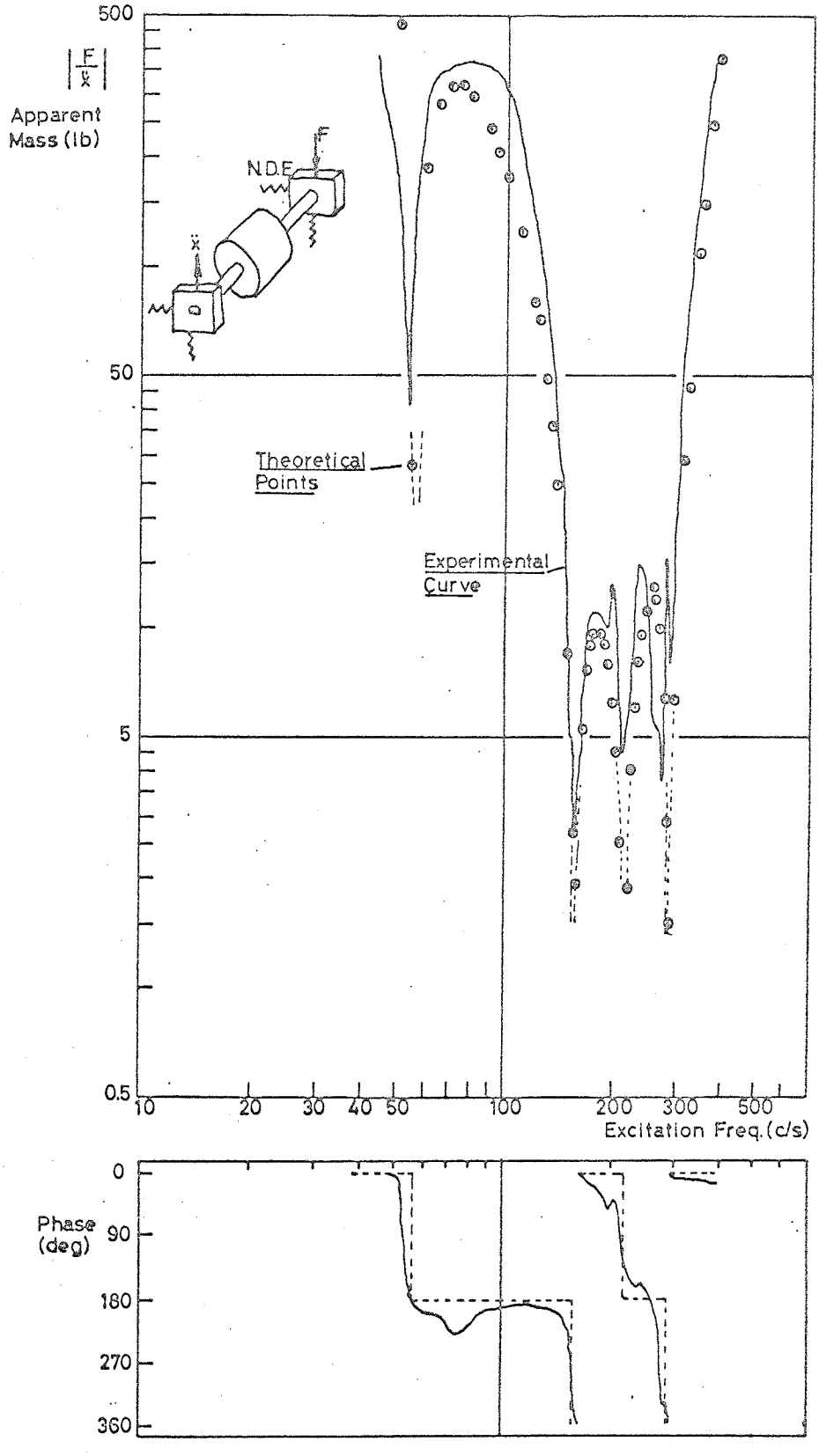

FIG. 6.19 VERTICAL TRANSFER IMPEDANCE. N.D.E. TO D.E. BEARING SUPPORTS. MODEL RIG 24" CRS. STATIONARY IN BALL BEARINGS.

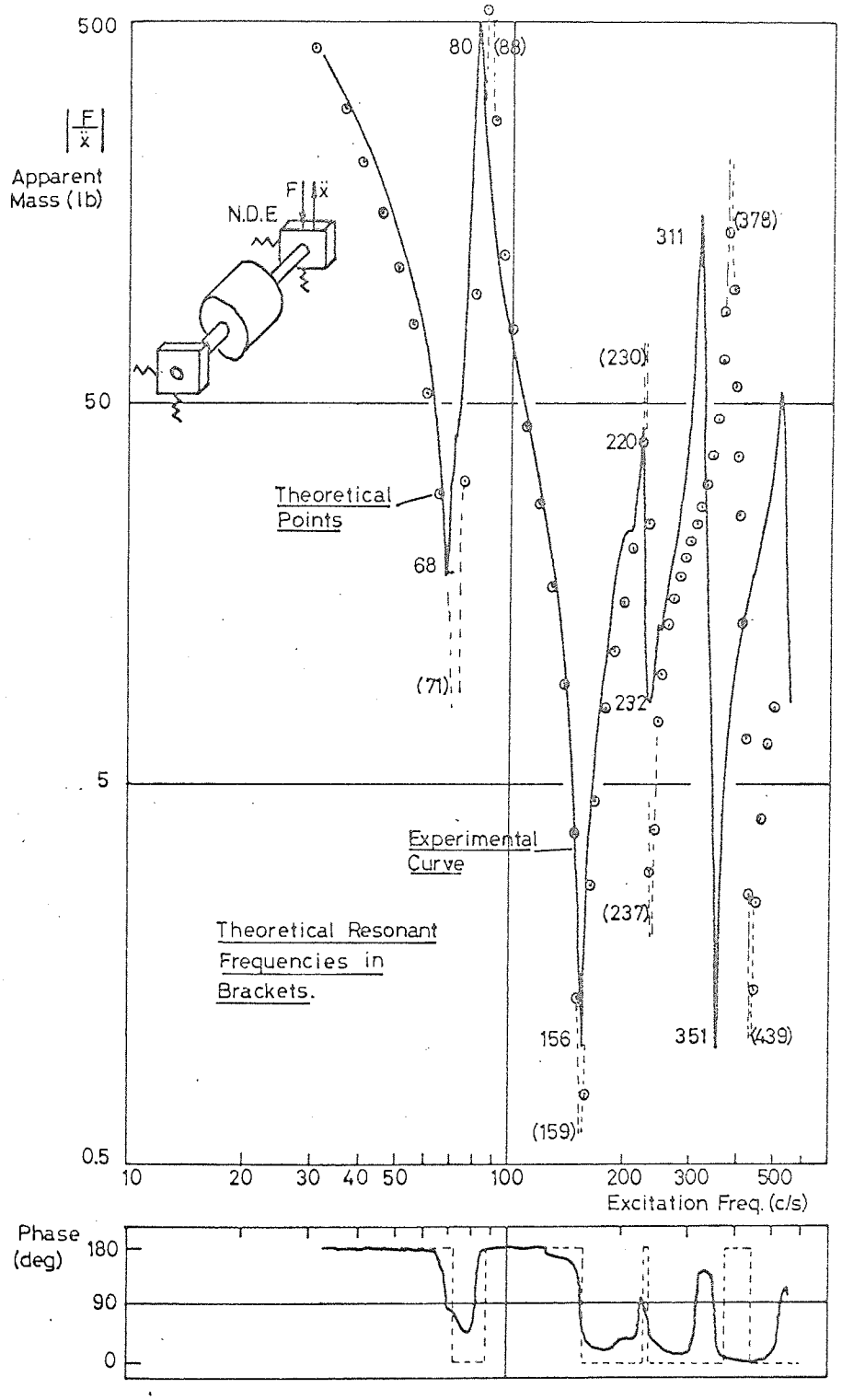

FIG.6.20. VERTICAL DRIVING POINT IMPEDANCE N.D.E. BEARING SUPPORT. MODEL RIG 20" CRS. ROTOR STATIONARY IN BALL BEARINGS.

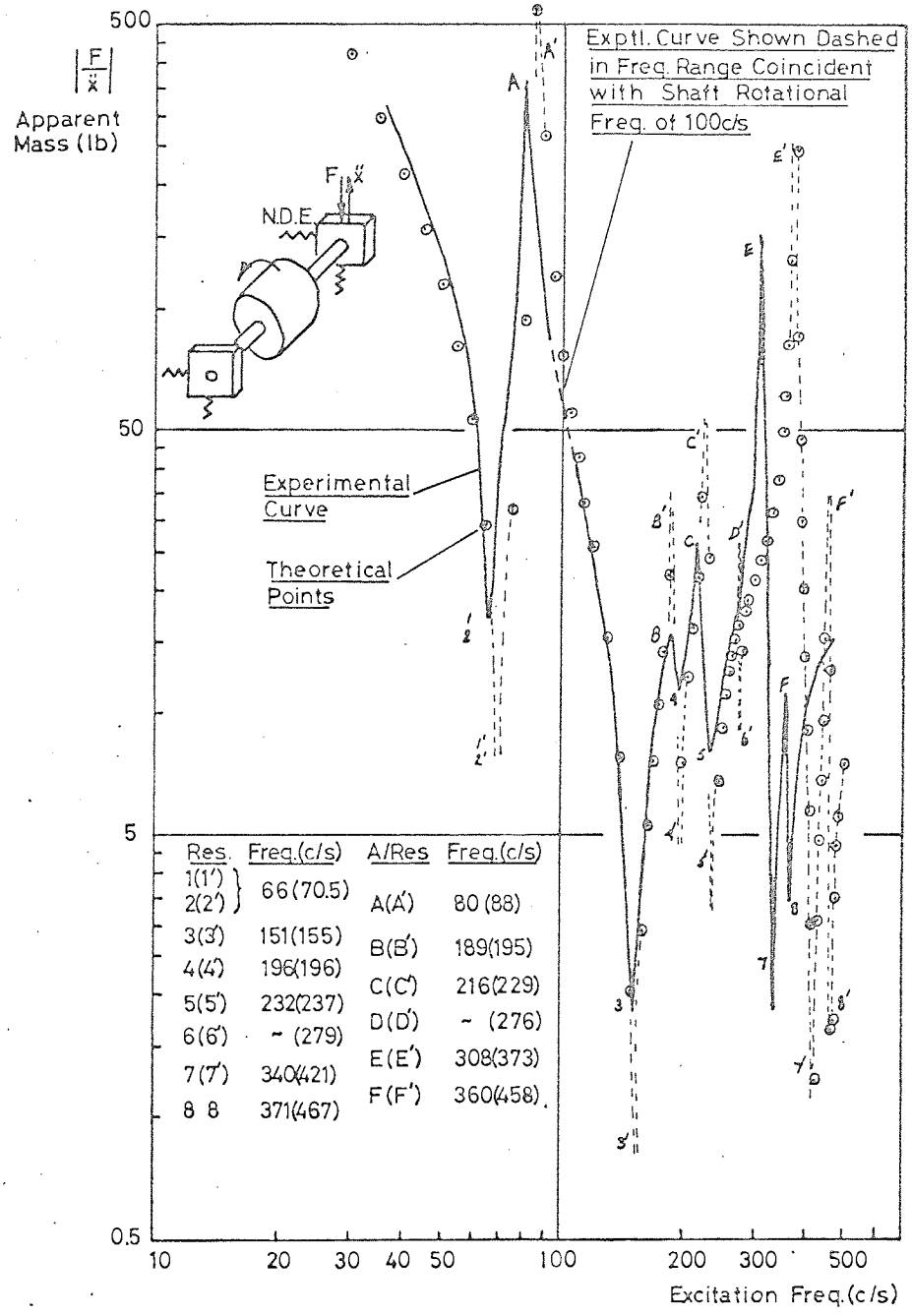

FIG.6.21. VERTICAL DRIVING POINT IMPEDANCE N.D.E. BEARING SUPPORT. MODEL RIG 20 CRS., ROTOR SPEED 100c/s (6000r.p.m.)

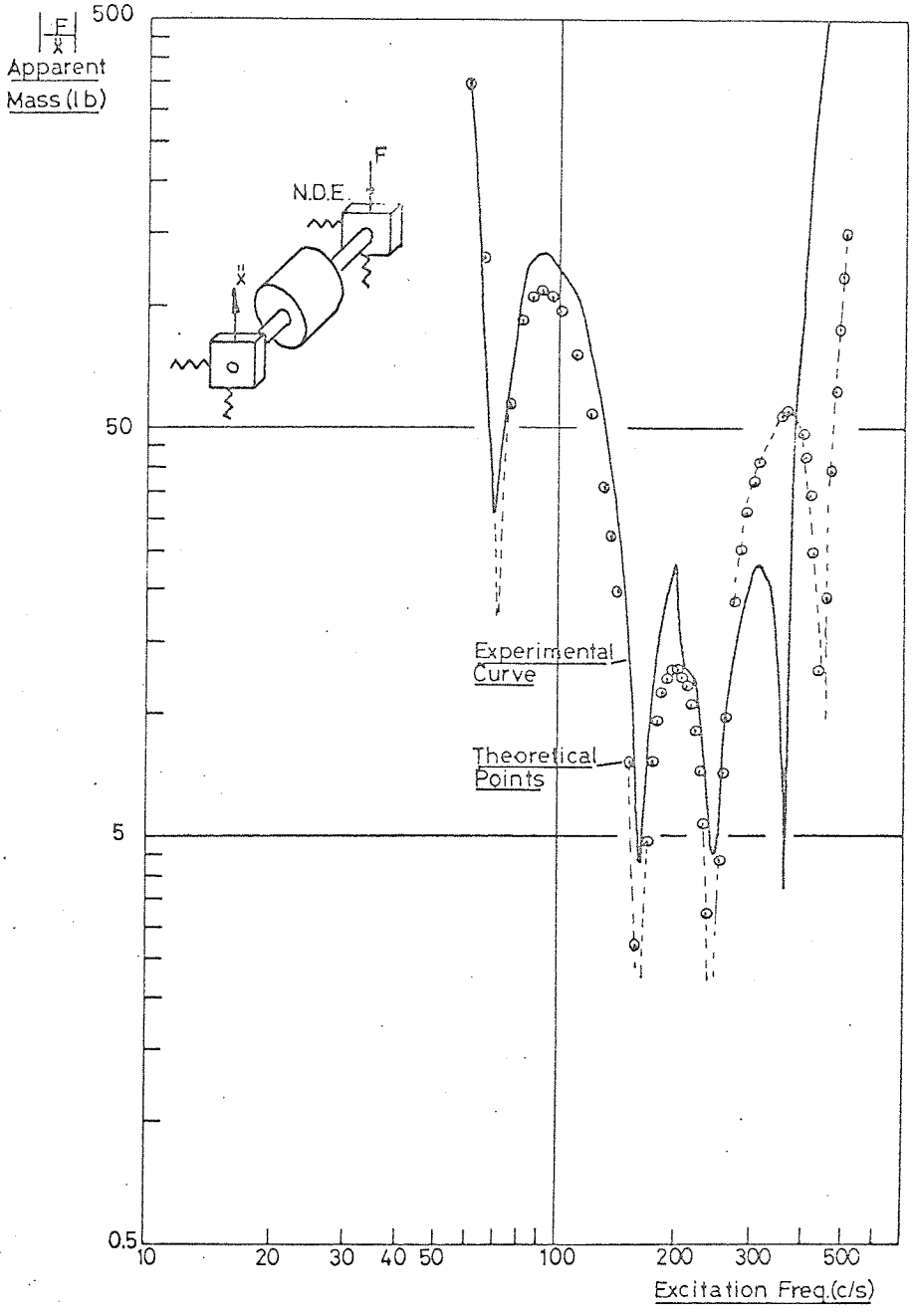

FIG.6.22. VERTICAL TRANSFER IMPEDANCE N.D.E TO D.E. BEARING SUPPORTS. MODEL RIG 20 CRS. ROTOR STATIONARY IN BALL BEARINGS.

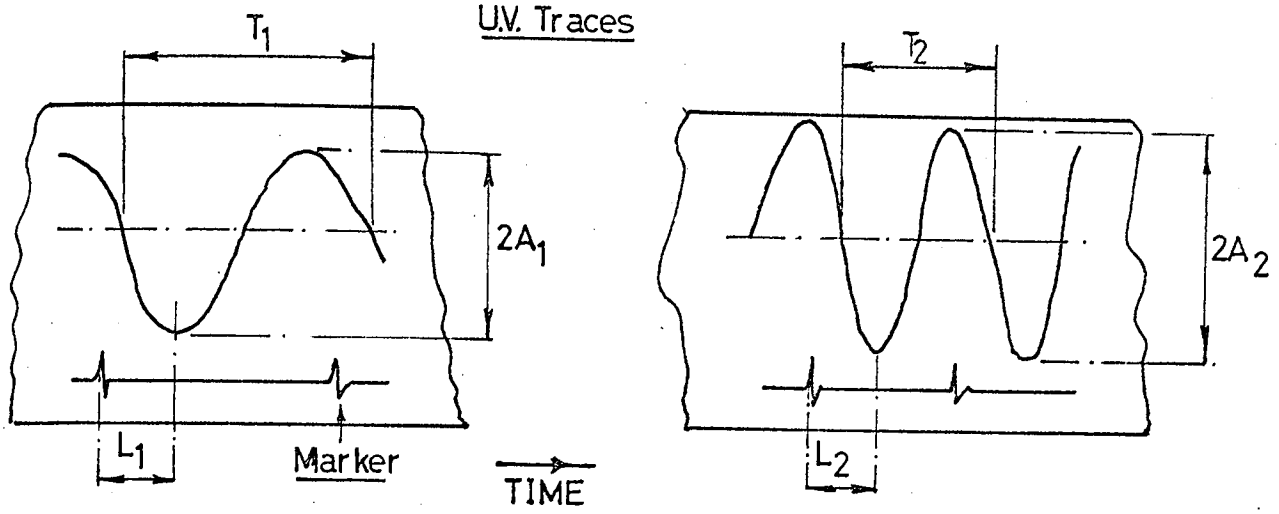

$\theta_1 = 2\pi . L_1 / T_1$

V. Slow Speed
Shaft Eccentricity Only

$\theta_2 = 2\pi . L_2 / T_2$

High Speed
Eccentricity+Whirl

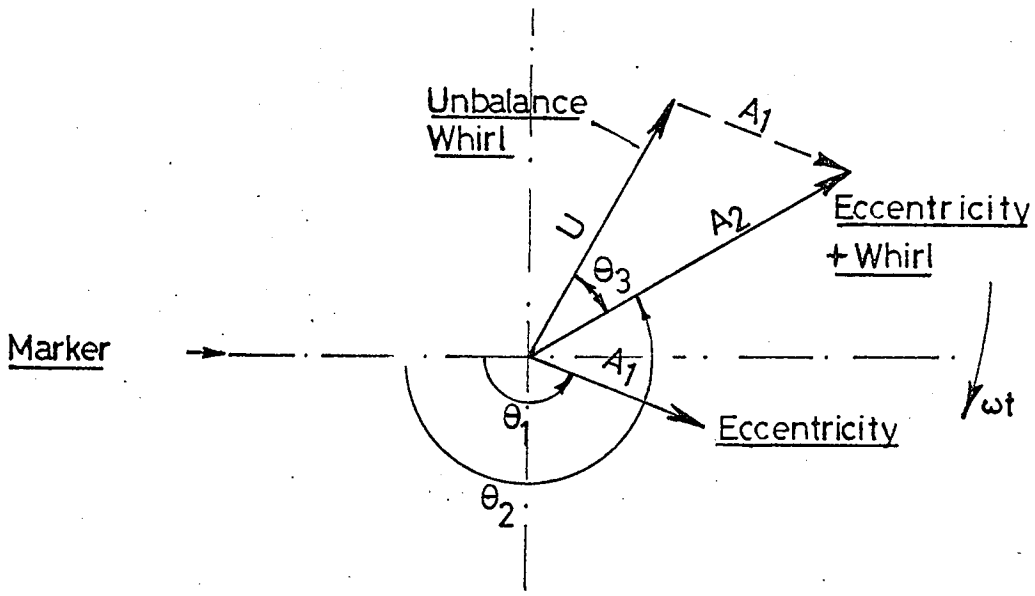

Unbalance Whirl Vector, $U = \sqrt{A_1^2 + A_2^2 - 2.A_1.A_2.\cos(\theta_1\ \theta_2)}$

Phase, $\theta_3 = \cos^{-1}((A_2^2 + U^2 - A_1^2)/(2A_2U))$

FIG.6.24 CORRECTION FOR SHAFT ECCENTRICITY.

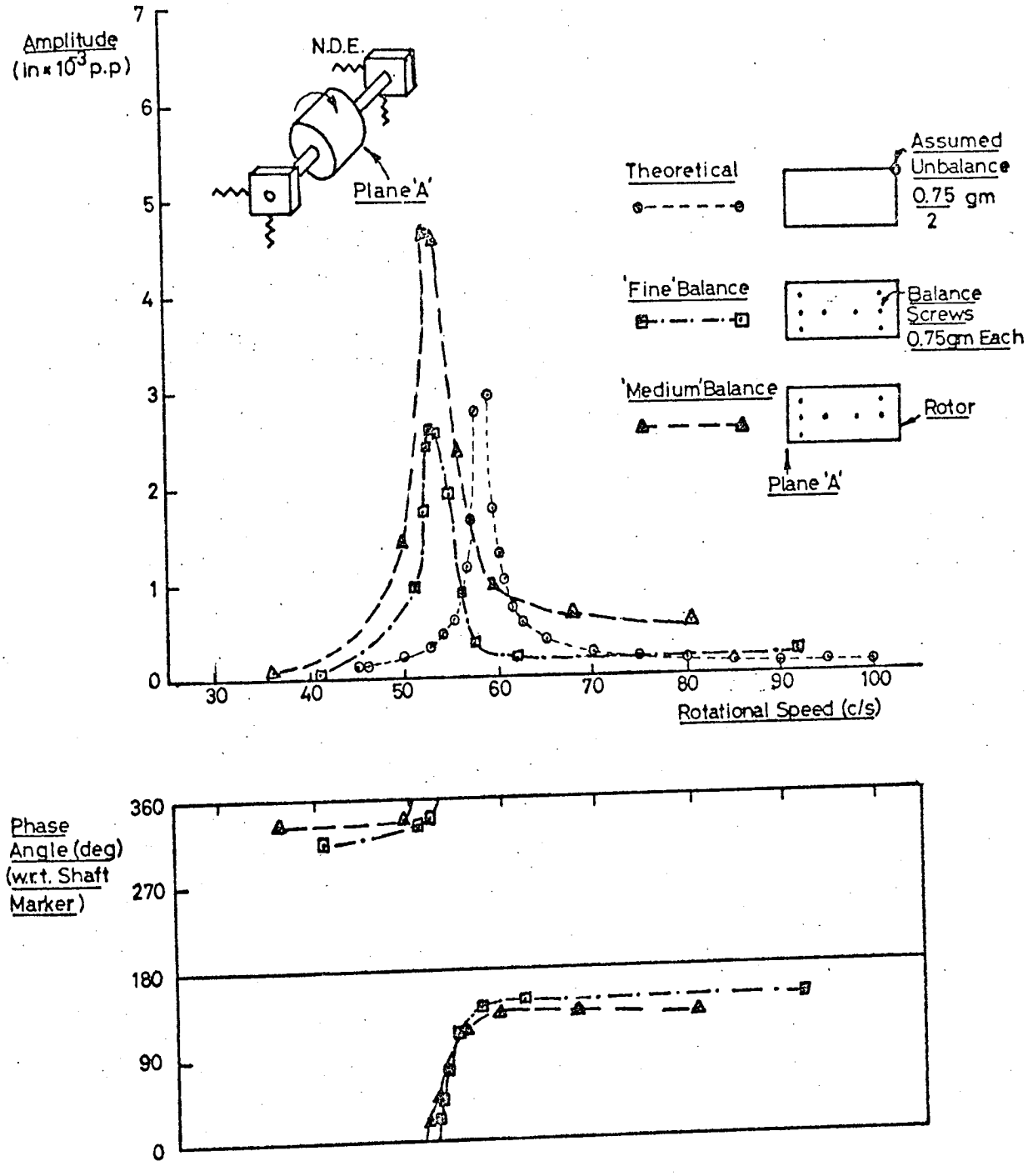

FIG.6.25. ROTOR UNBALANCE RESPONSE. HORIZONTAL, PLANE 'A'
MODEL RIG 24"CRS. IN BALL BEARINGS

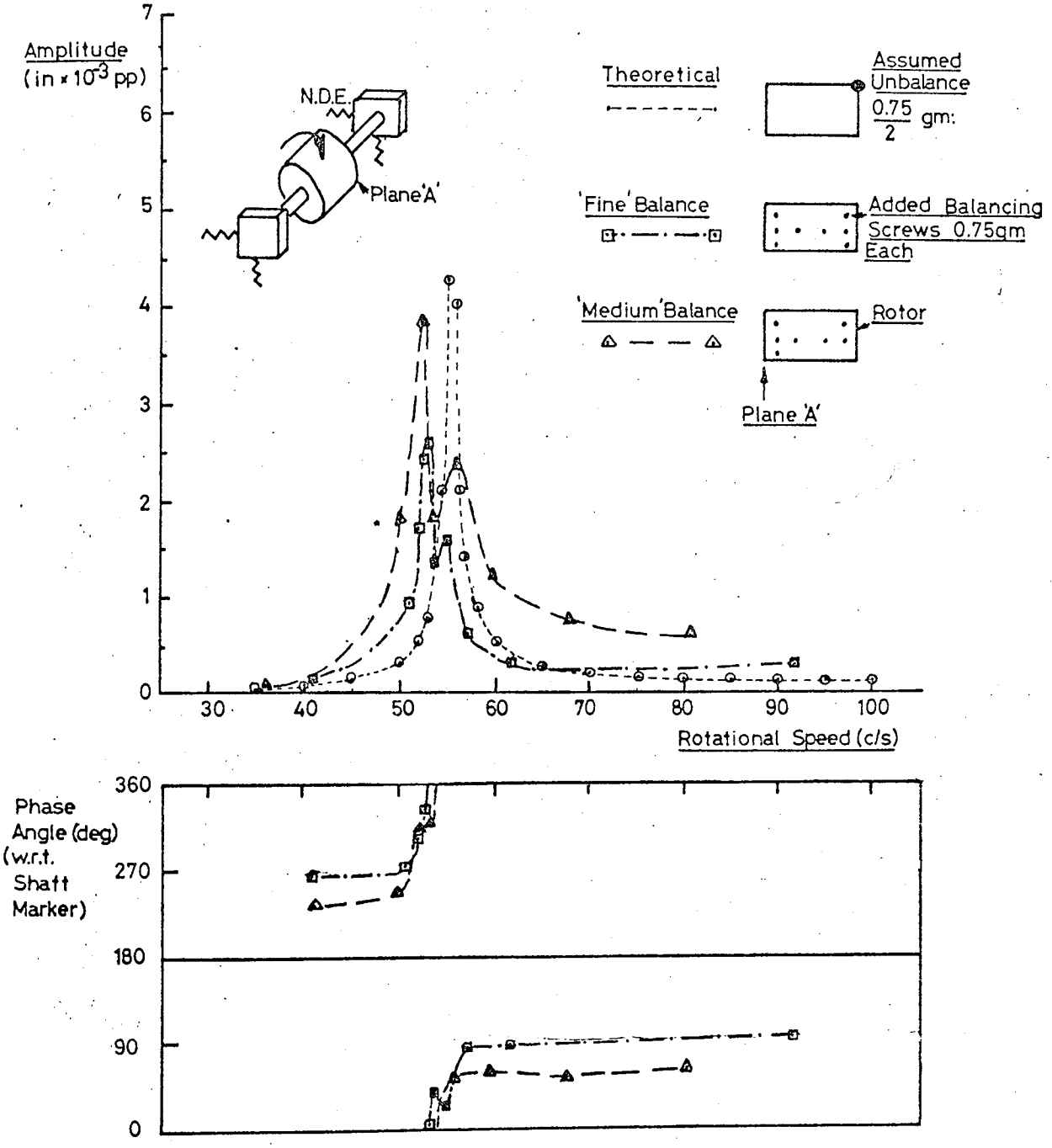

FIG. 626. ROTOR UNBALANCE RESPONSE. VERTICAL, PLANE 'A' MODEL RIG 24"CRS. IN BALL BEARINGS.

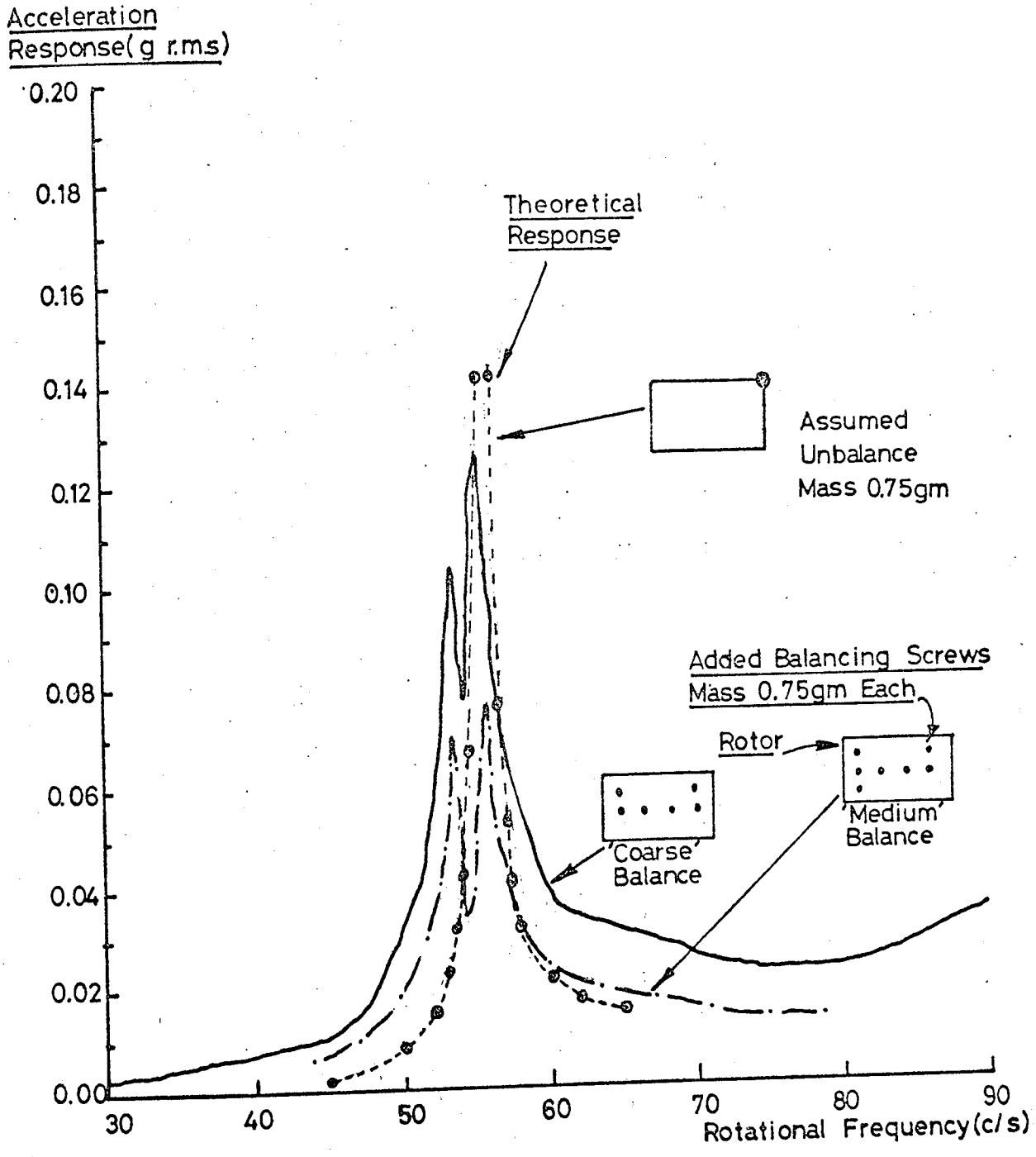

FIG.6.27. 24" CENTRE MODEL RIG IN BALL BEARINGS.
UNBALANCE RESPONSE. VERTICAL D.E. SUPPORT.

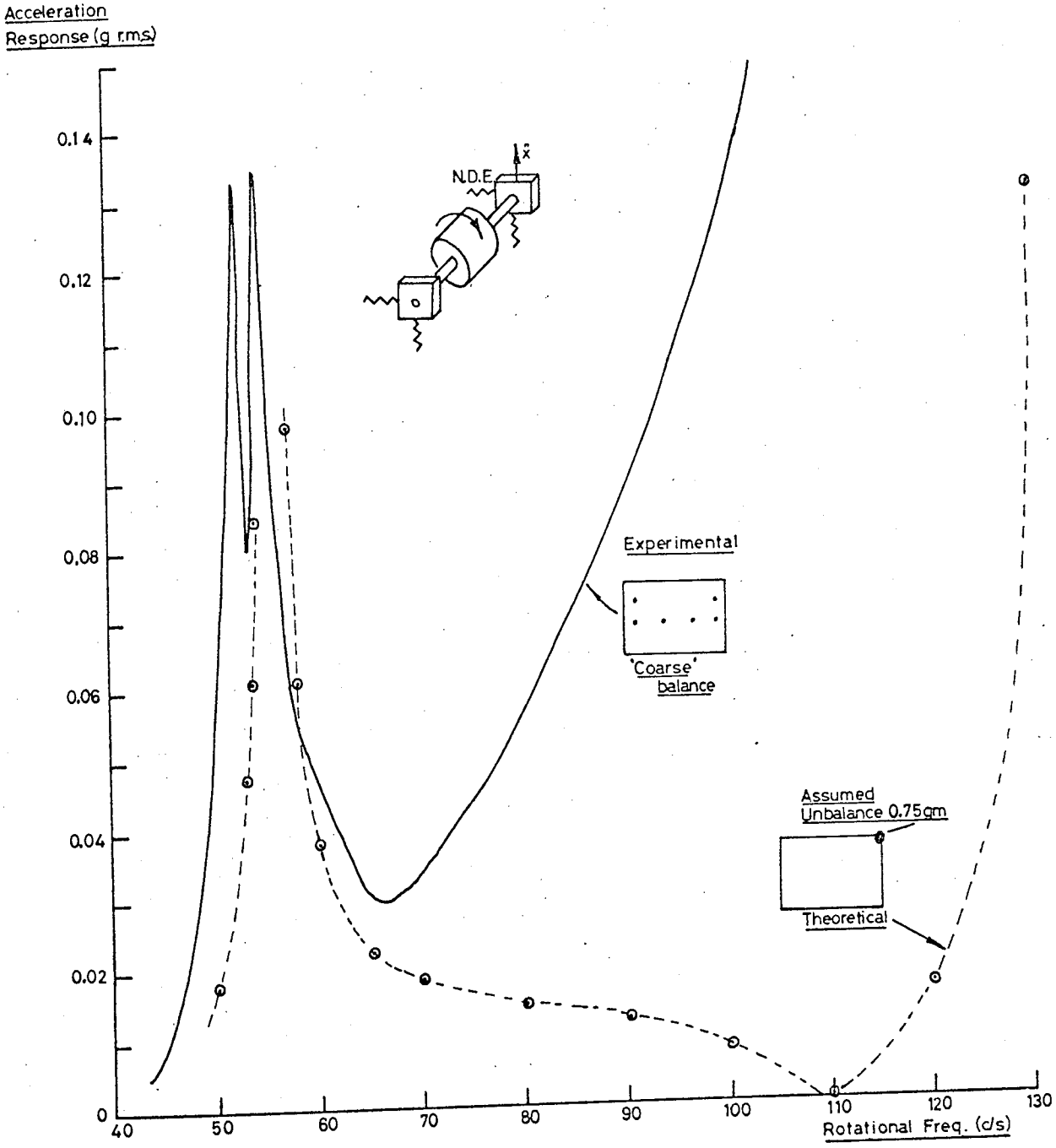

FIG.6.28. UNBALANCE RESPONSE . VERTICAL N.D.E. SUPPORT MODEL RIG 24" CRS IN BALL BEARINGS.

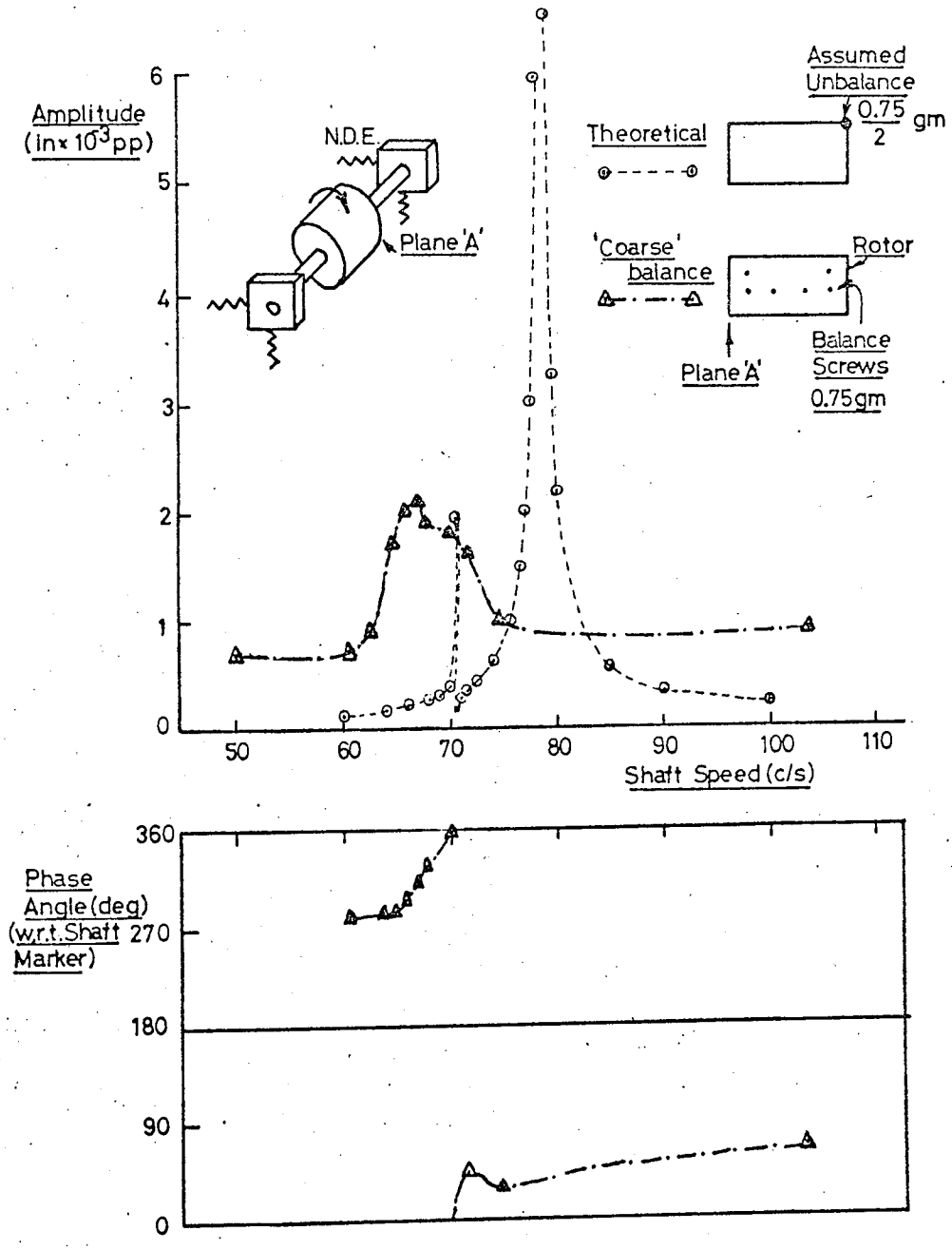

FIG. 6.29. ROTOR UNBALANCE RESPONSE. HORIZONTAL, PLANE 'A'. MODEL RIG 20"CRS. IN BALL BEARINGS

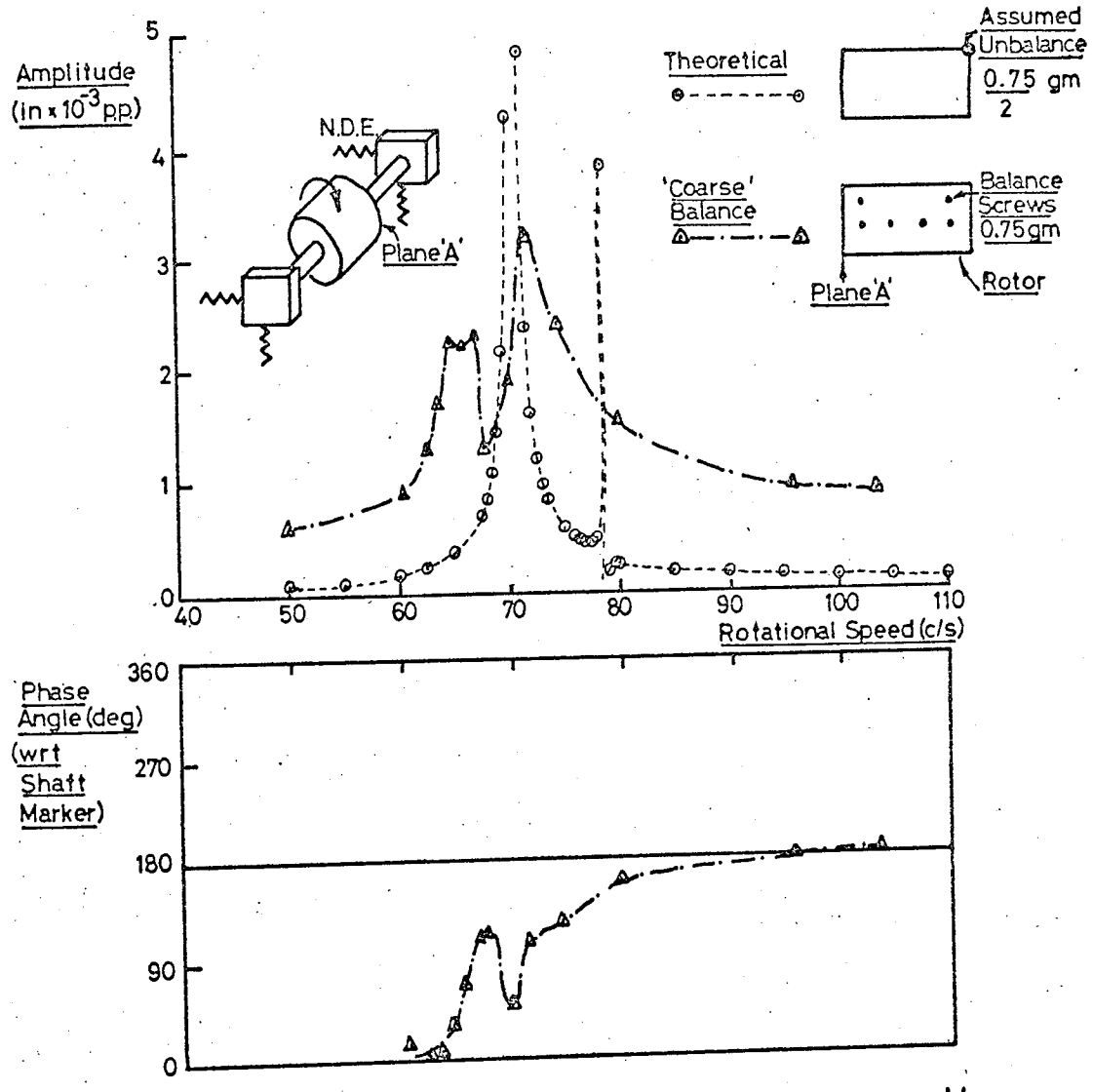

FIG. 6.30 ROTOR UNBALANCE RESPONSE. VERTICAL PLANE 'A'
MODEL RIG 20"CRS IN BALL BEARINGS

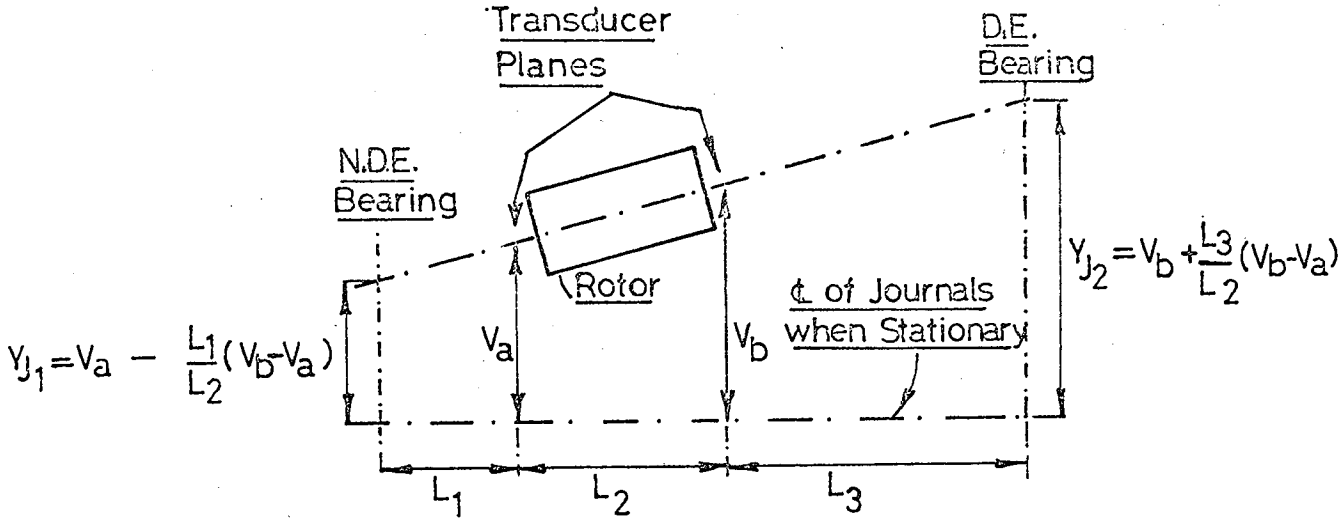

FIG 6.31(a) LOCATION OF JOURNAL STEADY RUNNING POSITION IN VERTICAL PLANE.

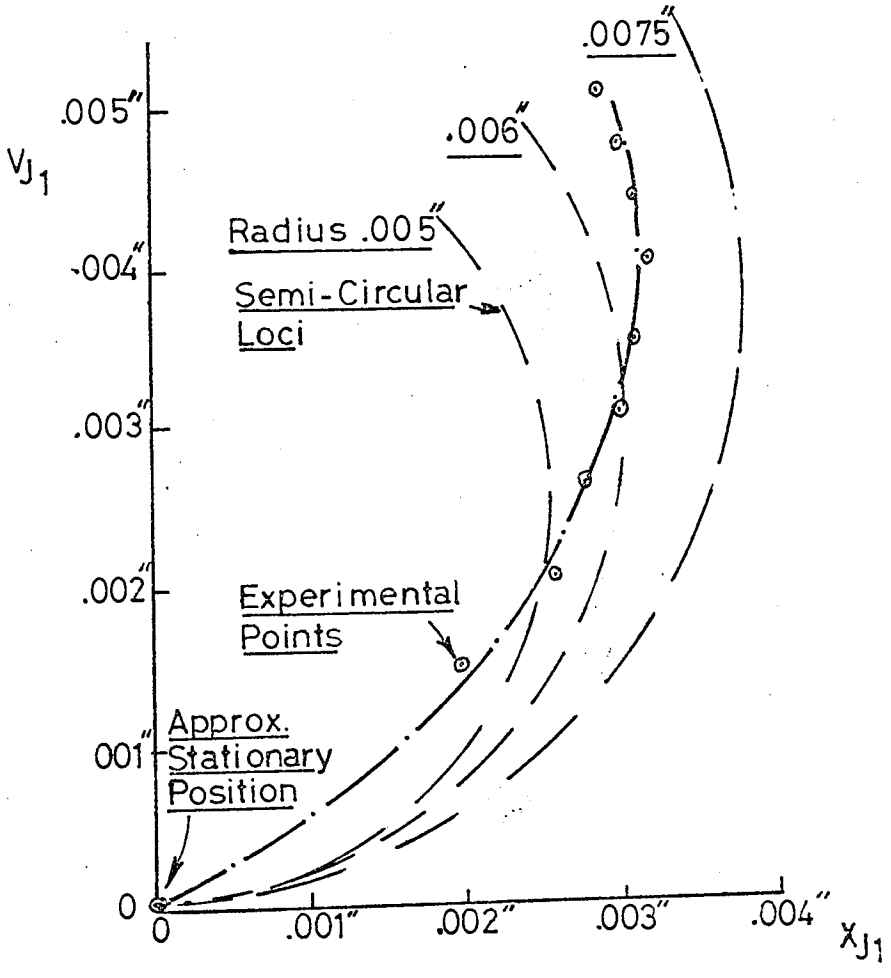

FIG.6.31.(b) JOURNAL LOCUS. N.D.E. BEARING. MODEL RIG 20"CRS.

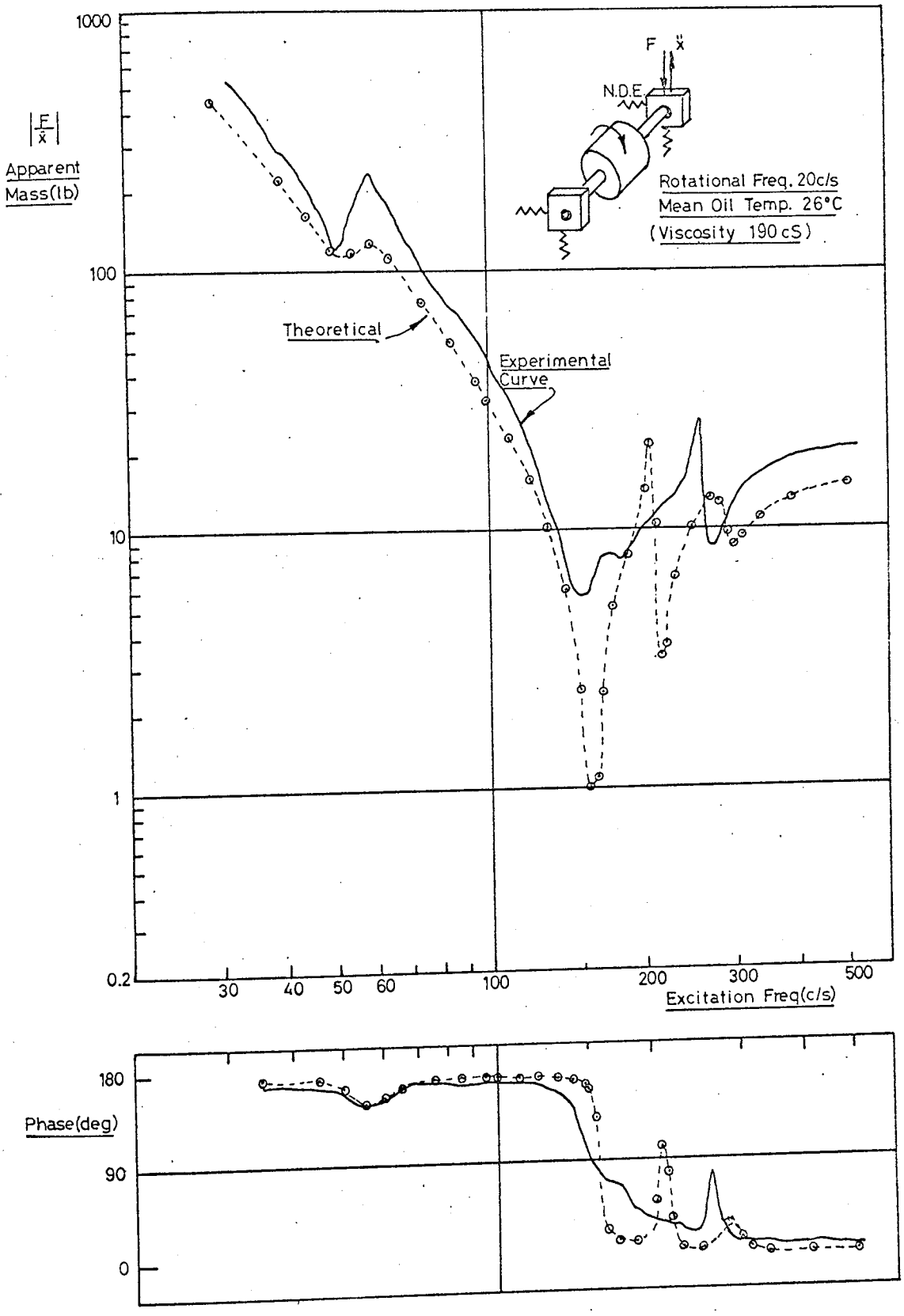

FIG. 6.32. VERTICAL DRIVING POINT IMPEDANCE. N.D.E. SUPPORT.
MODEL RIG 24 CRS IN JOURNAL BEARINGS.
ROTOR SPEED 20 c/s.

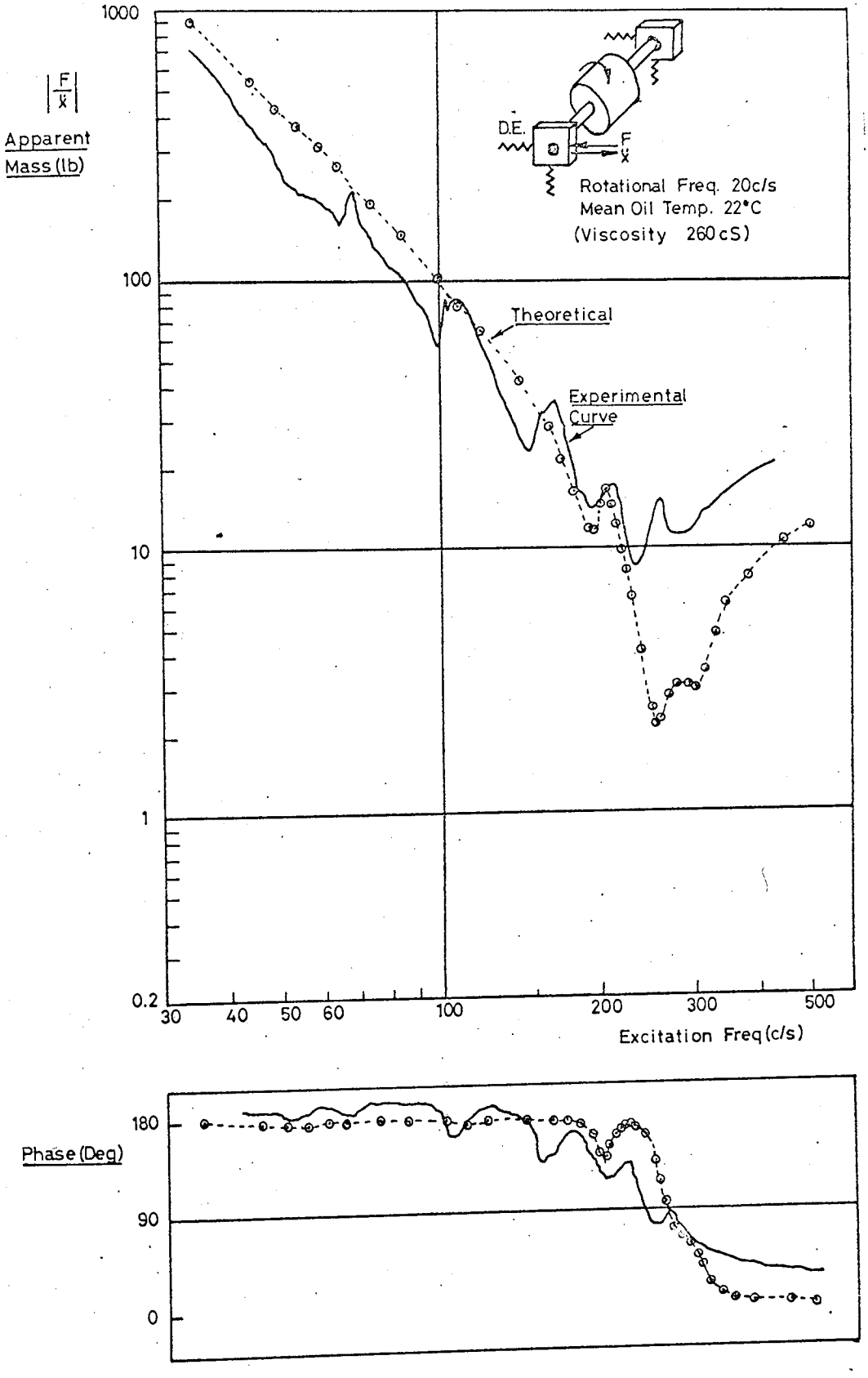

FIG.633. HORIZONTAL DRIVING POINT IMPEDANCE. D.E. SUPPORT. MODEL RIG 24 CRS IN JOURNAL BEARINGS. ROTOR SPEED 20c/s.

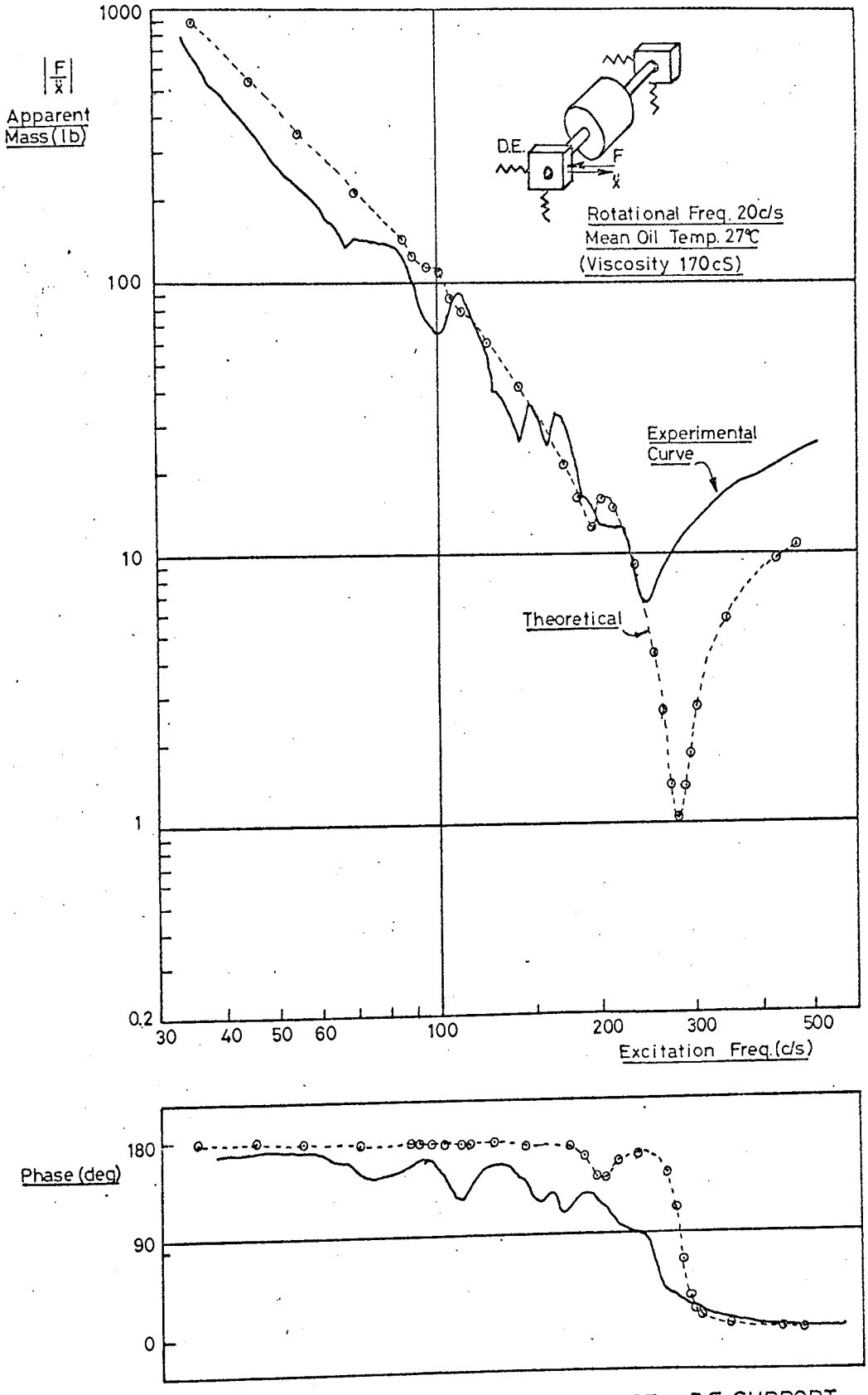

FIG.6.34. HORIZONTAL DRIVING POINT IMPEDANCE. D.E. SUPPORT MODEL RIG 20 CRS. IN JOURNAL BEARINGS. ROTOR SPEED 20c/s.

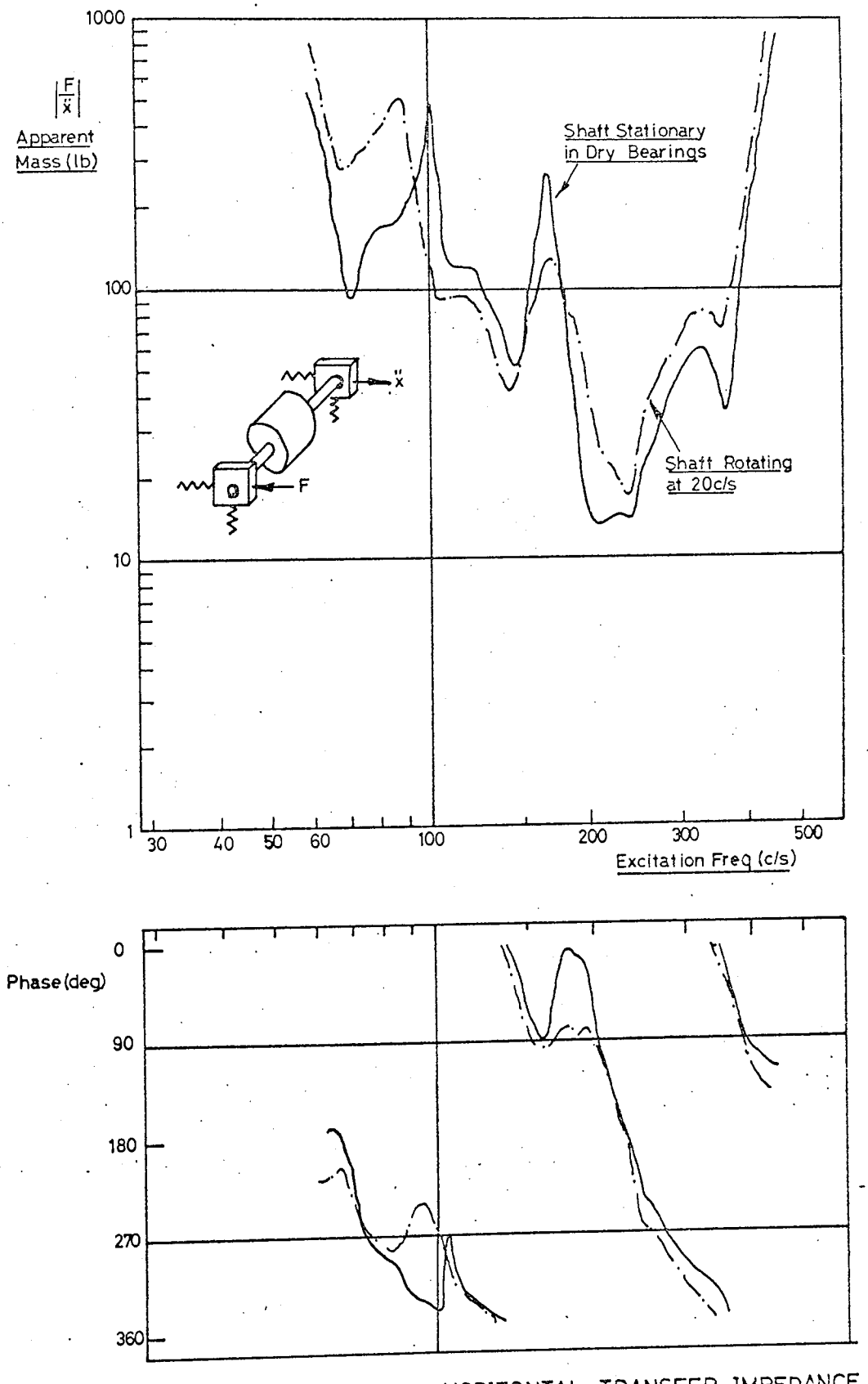

FIG. 6.35. COMPARISON BETWEEN HORIZONTAL TRANSFER IMPEDANCE WITH STATIONARY AND ROTATING SHAFT. MODEL RIG 20"CRS IN JOURNAL BEARINGS.

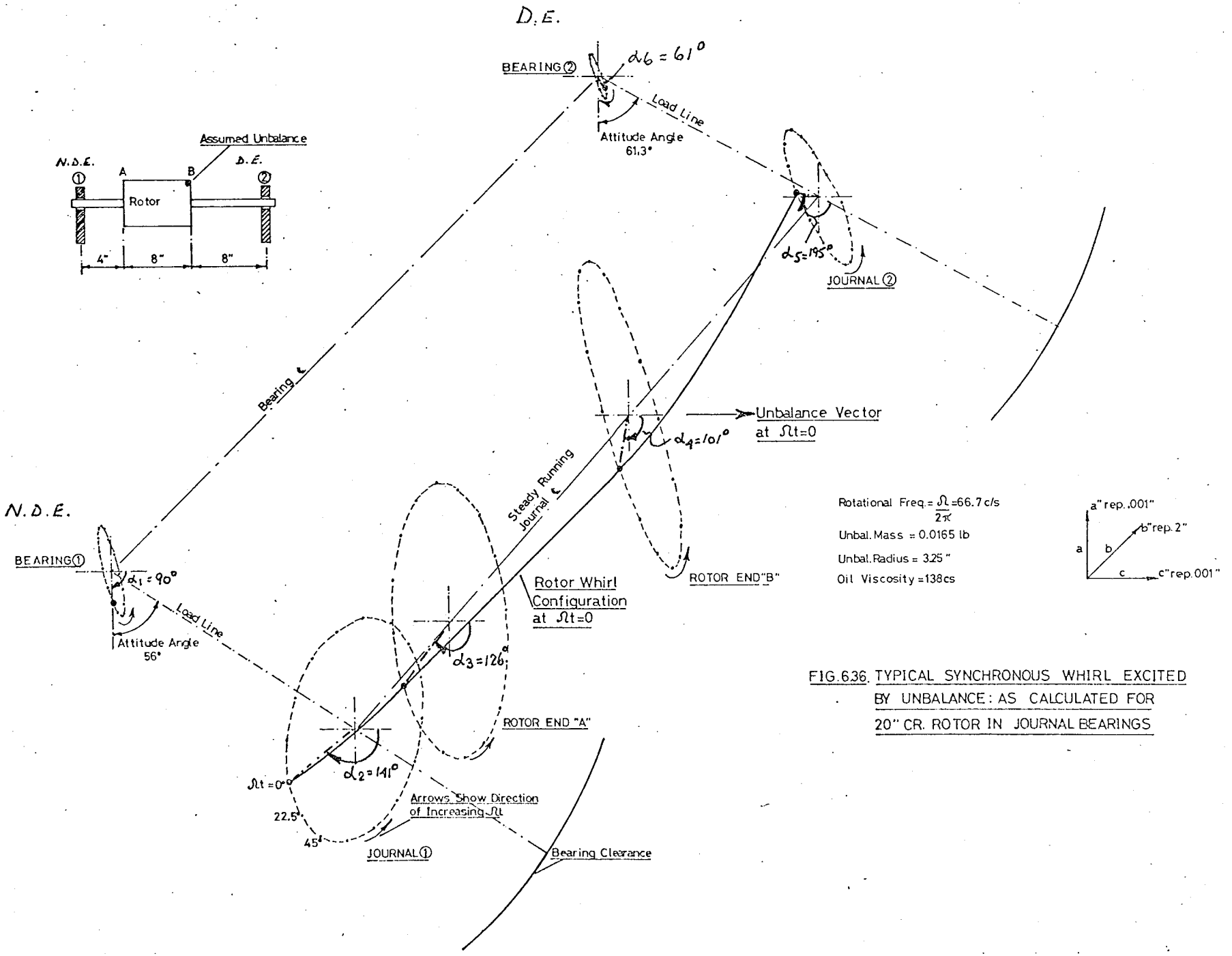

FIG. 6.36. TYPICAL SYNCHRONOUS WHIRL EXCITED BY UNBALANCE: AS CALCULATED FOR 20" CR. ROTOR IN JOURNAL BEARINGS

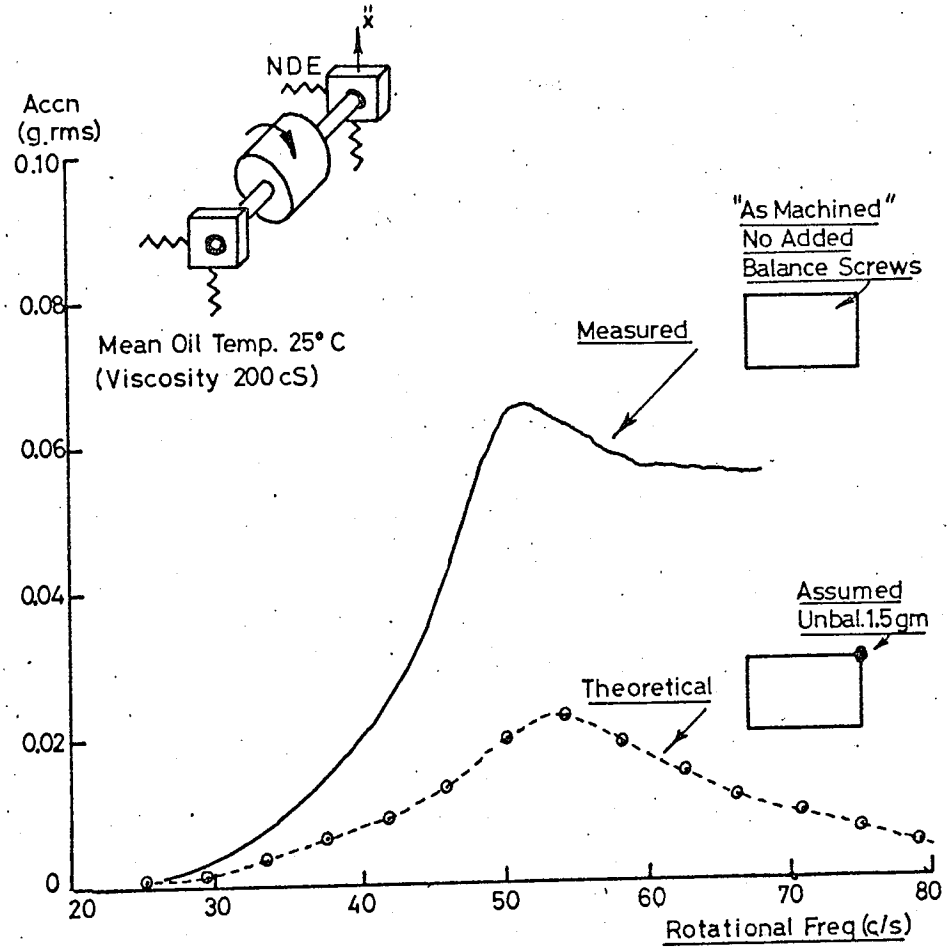

FIG 6.37 VERTICAL UNBALANCE RESPONSE N.D.E. SUPPORT. MODEL RIG 24"CRS IN JOURNAL BEARINGS

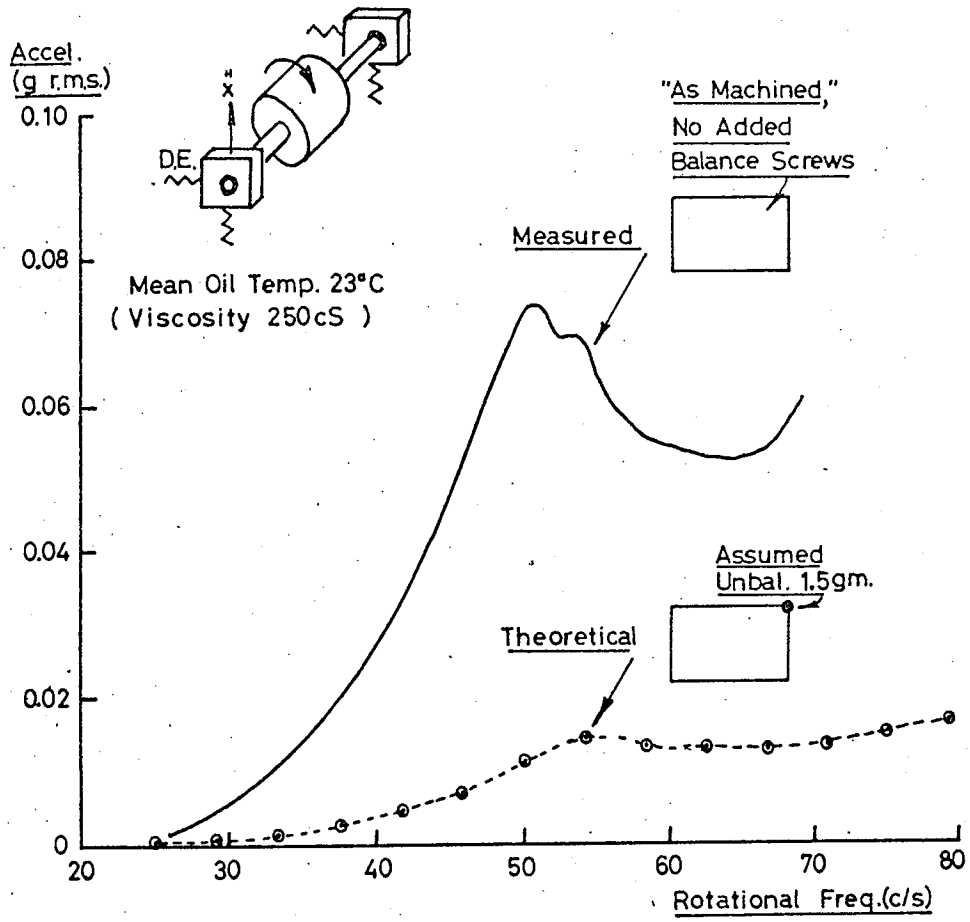

FIG. 6.38. VERTICAL UNBALANCE RESPONSE D.E. SUPPORT. MODEL RIG 24"CRS IN JOURNAL BEARINGS.

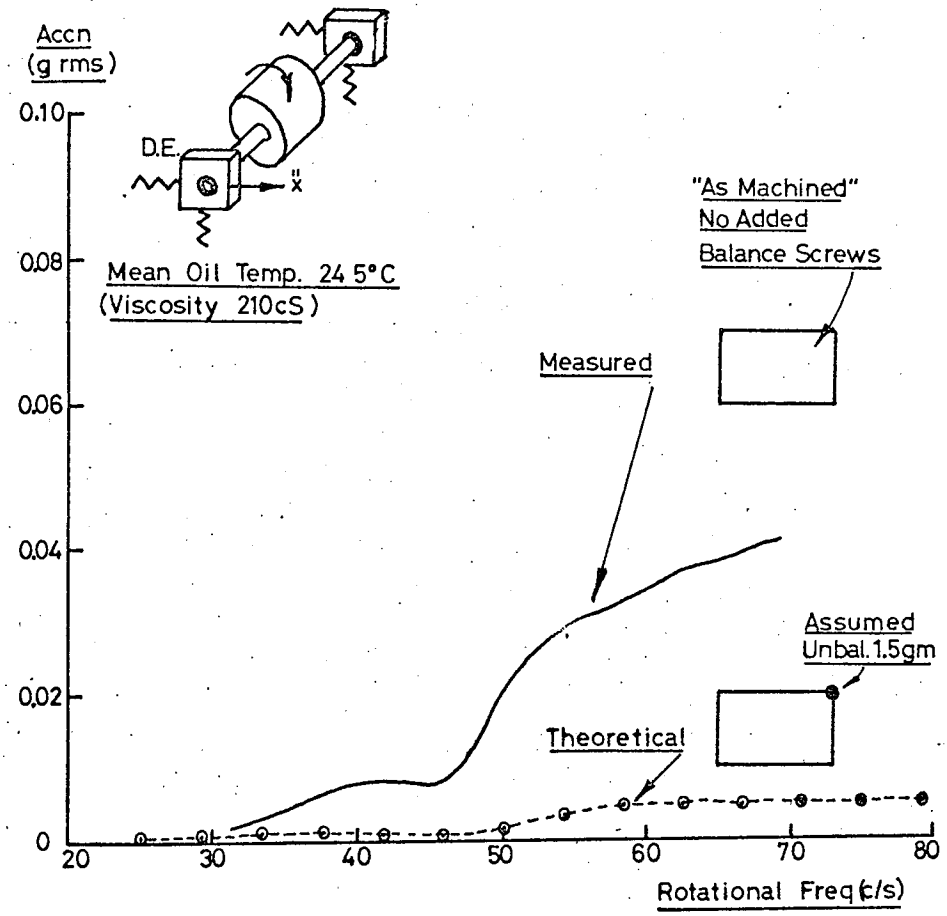

FIG.6.39. HORIZONTAL UNBALANCE RESPONSE. D.E. BEARING SUPPORT. MODEL RIG 24"CRS IN JOURNAL BEARINGS.

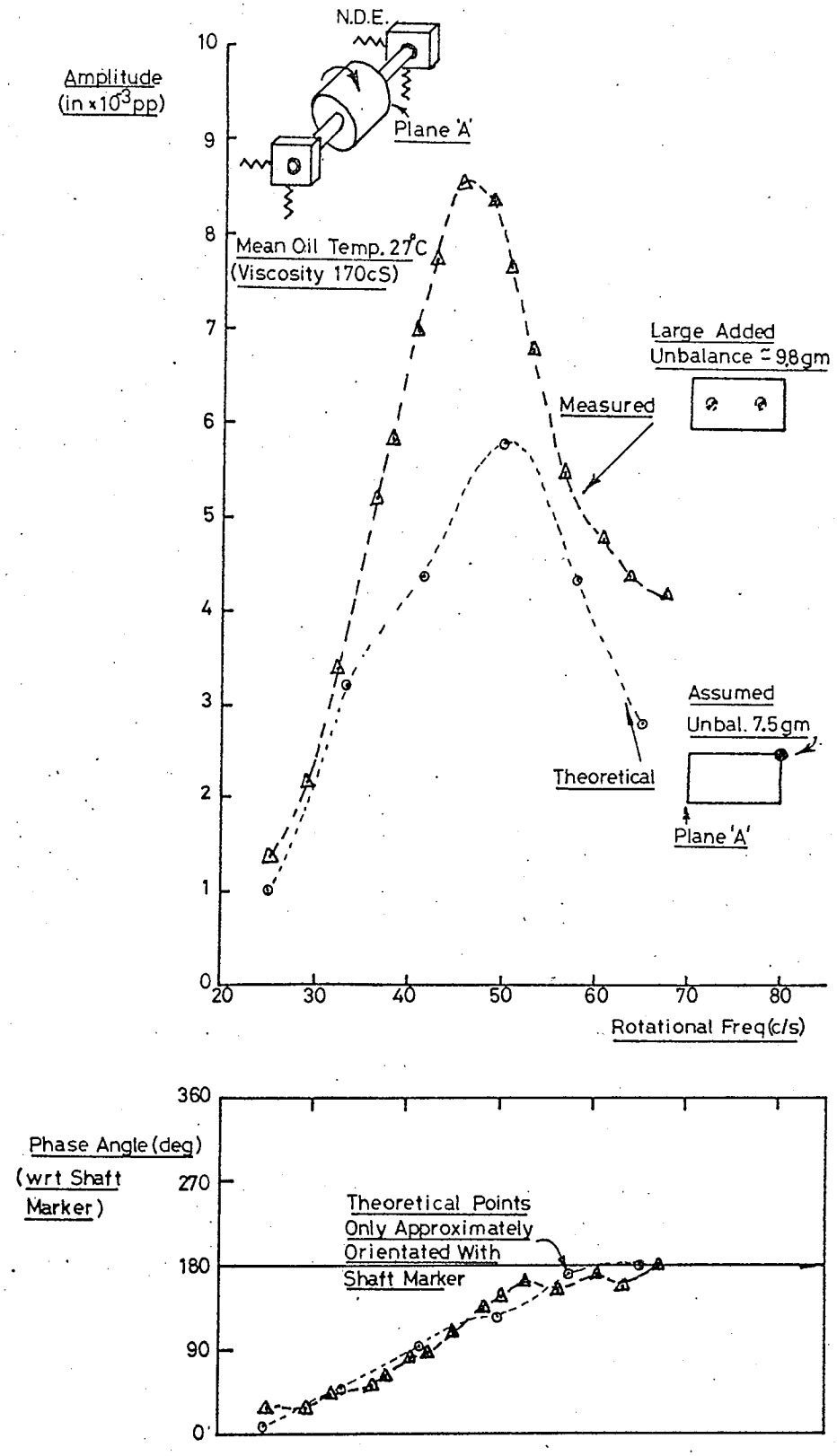

FIG.6.40. ROTOR UNBALANCE RESPONSE VERTICAL PLANE 'A'
MODEL RIG 24"CRS IN JOURNAL BEARINGS

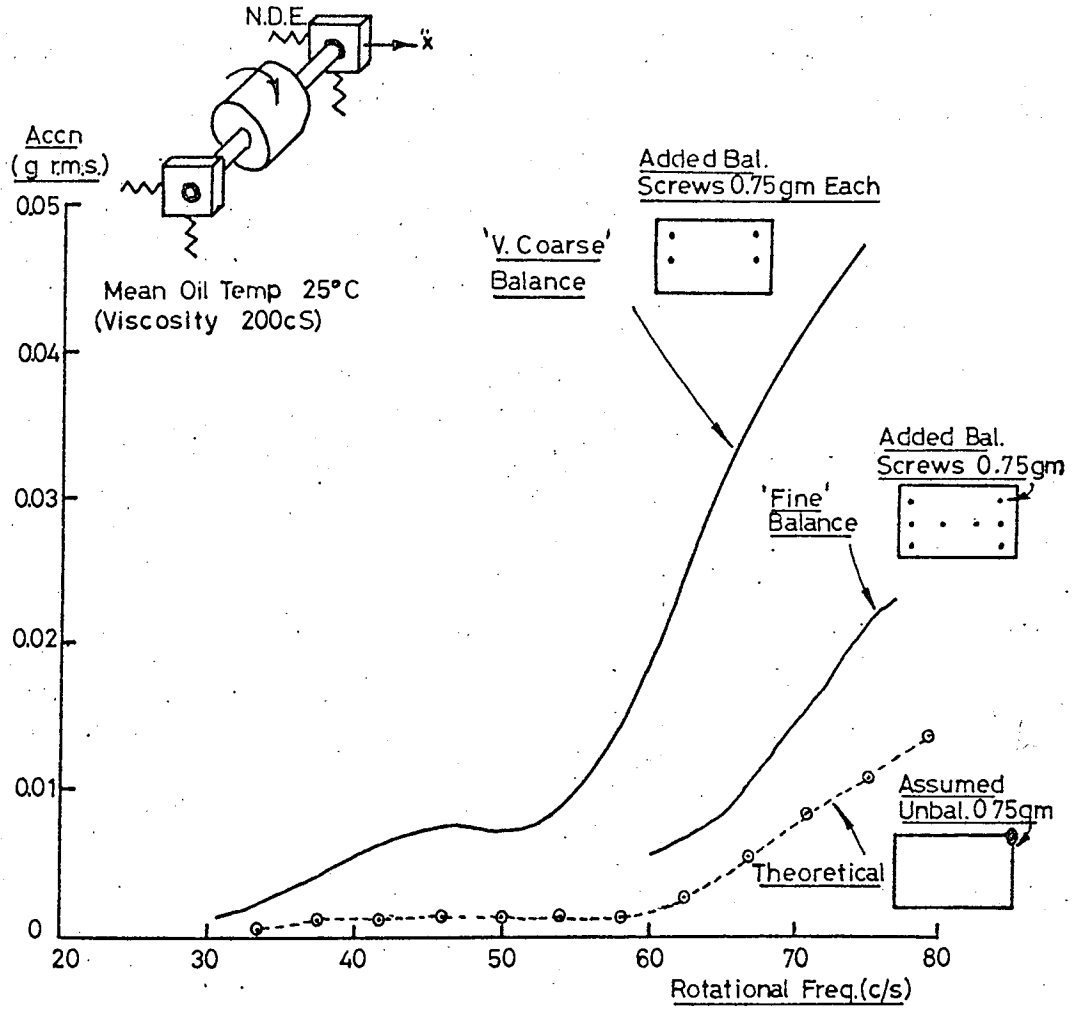

FIG 6.41. HORIZONTAL UNBALANCE RESPONSE, N.D.E. SUPPORT. MODEL RIG 20CRS IN JOURNAL BEARINGS

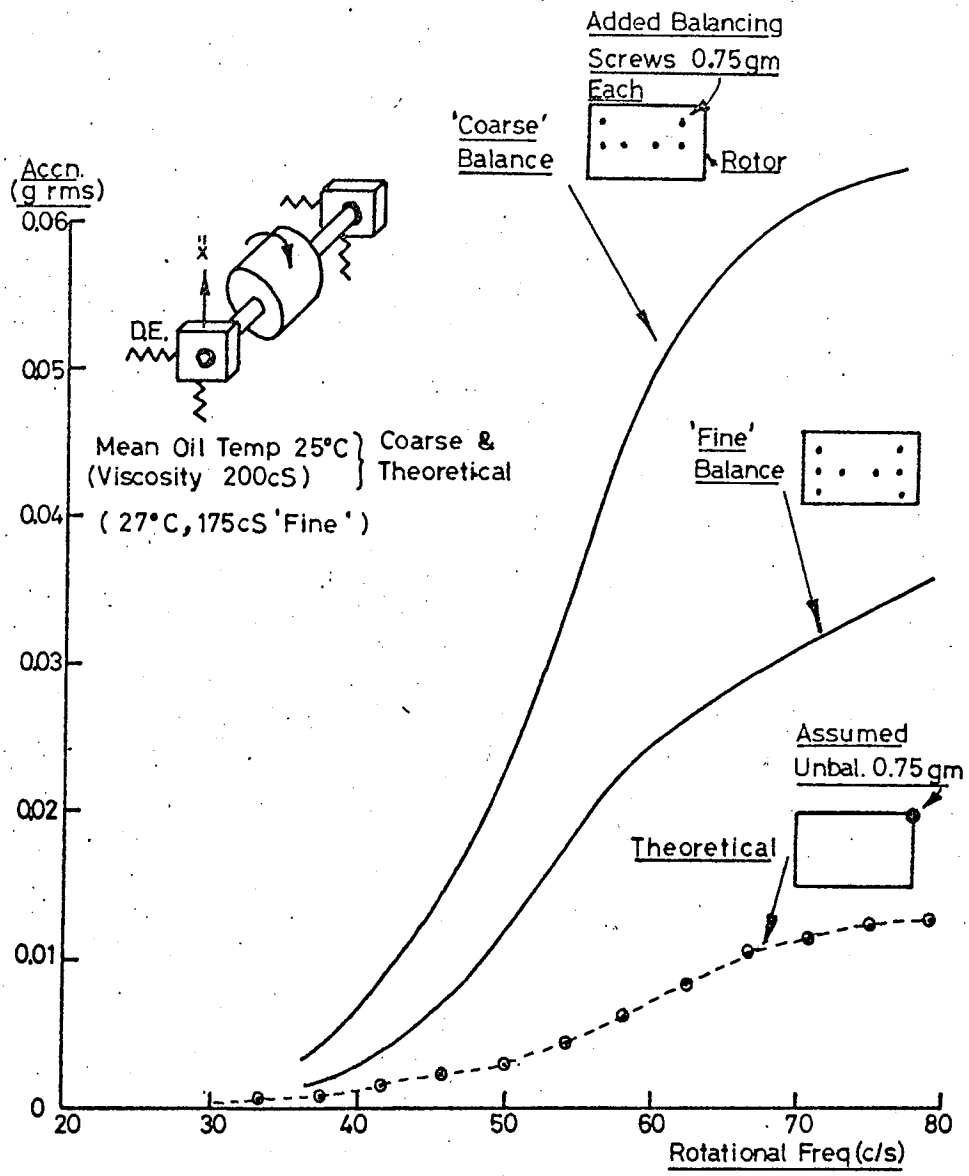

FIG 6.42 VERTICAL UNBALANCE RESPONSE. D.E. SUPPORT. MODEL RIG 20 CRS IN JOURNAL BEARINGS.

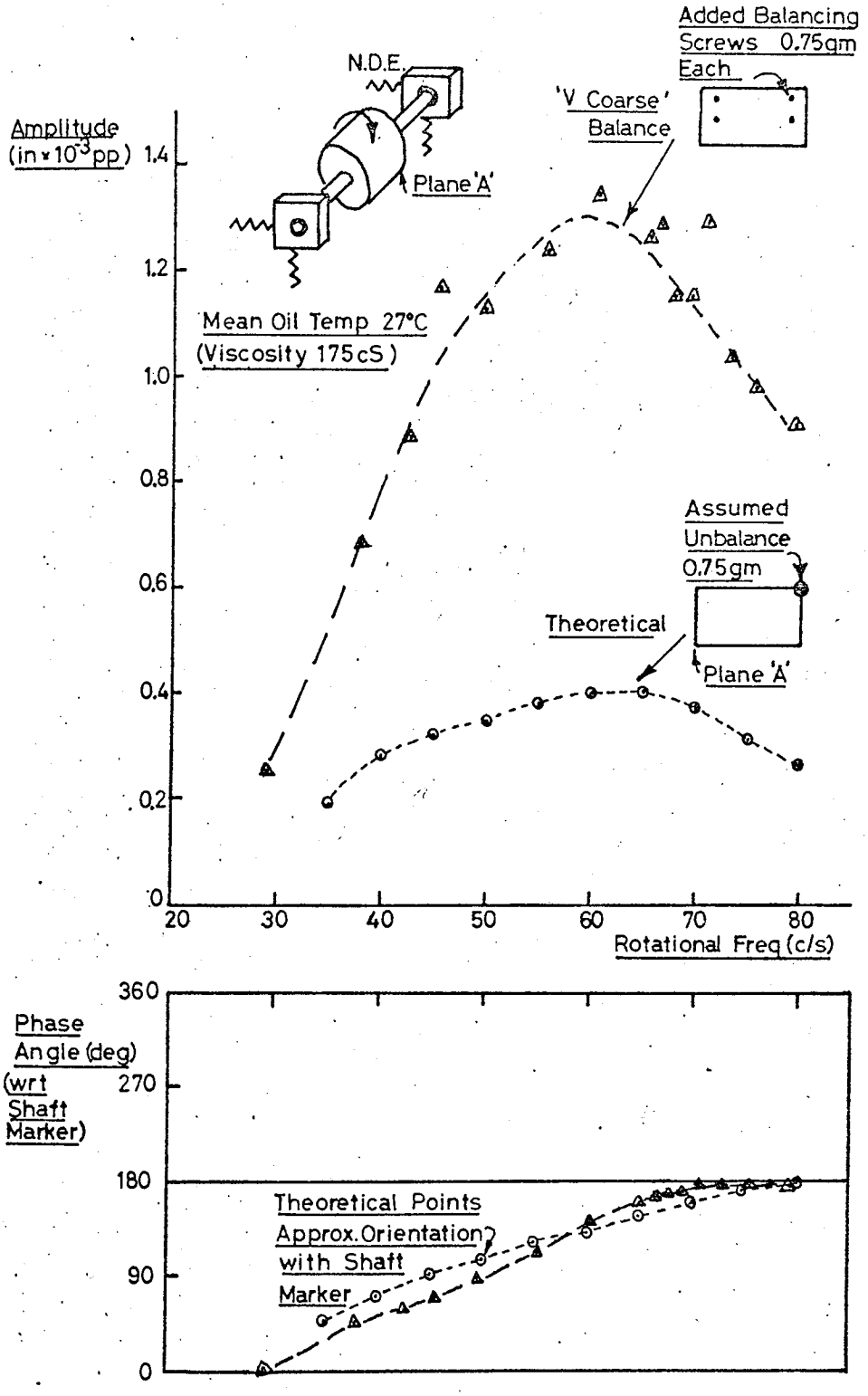

FIG. 6.43. ROTOR UNBALANCE RESPONSE. VERTICAL PLANE 'A' MODEL. RIG 20" CRS IN JOURNAL BEARINGS

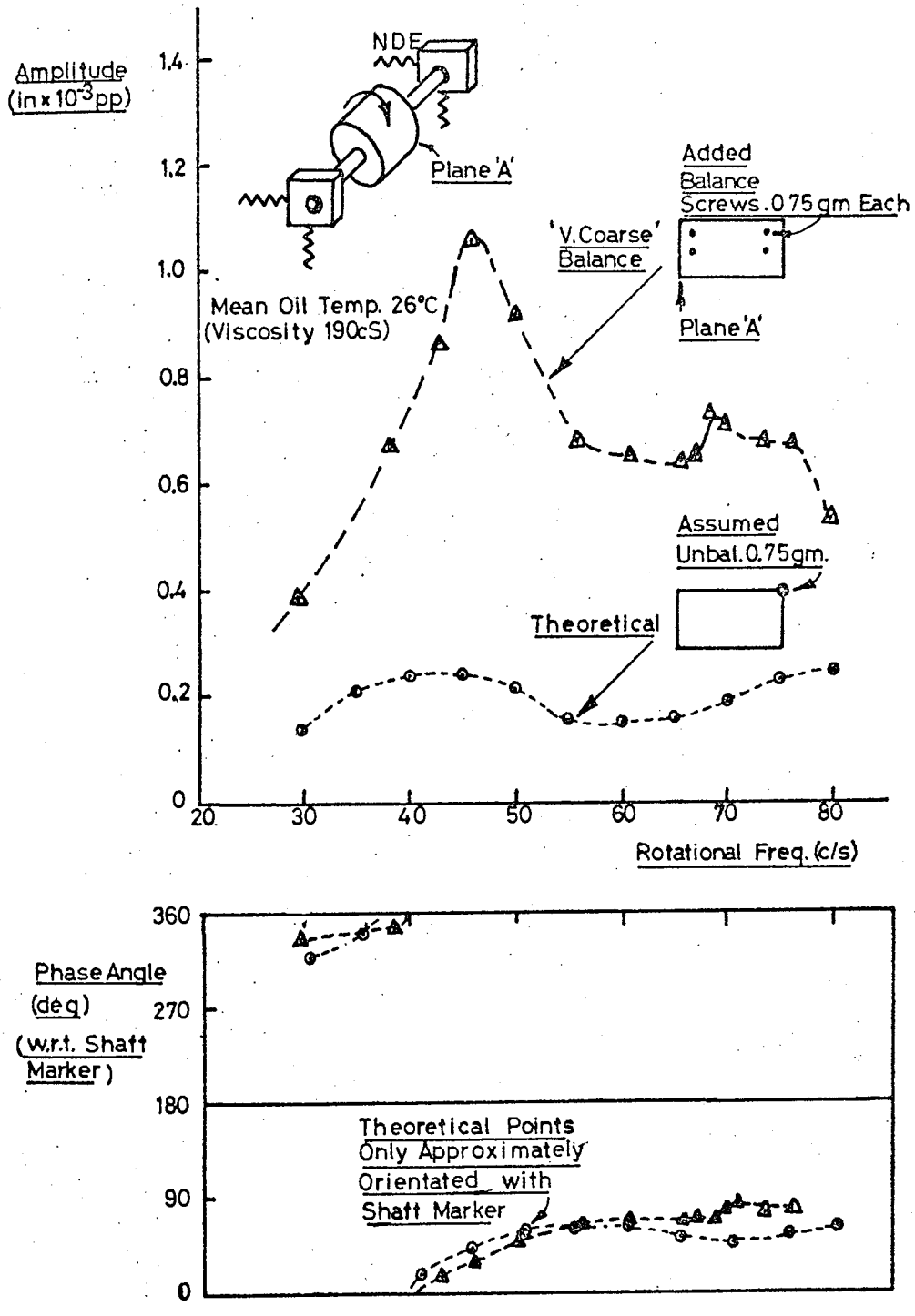

FIG. 6.44. ROTOR UNBALANCE RESPONSE HORIZONTAL PLANE 'A' MODEL RIG 20" CRS IN JOURNAL BEARINGS

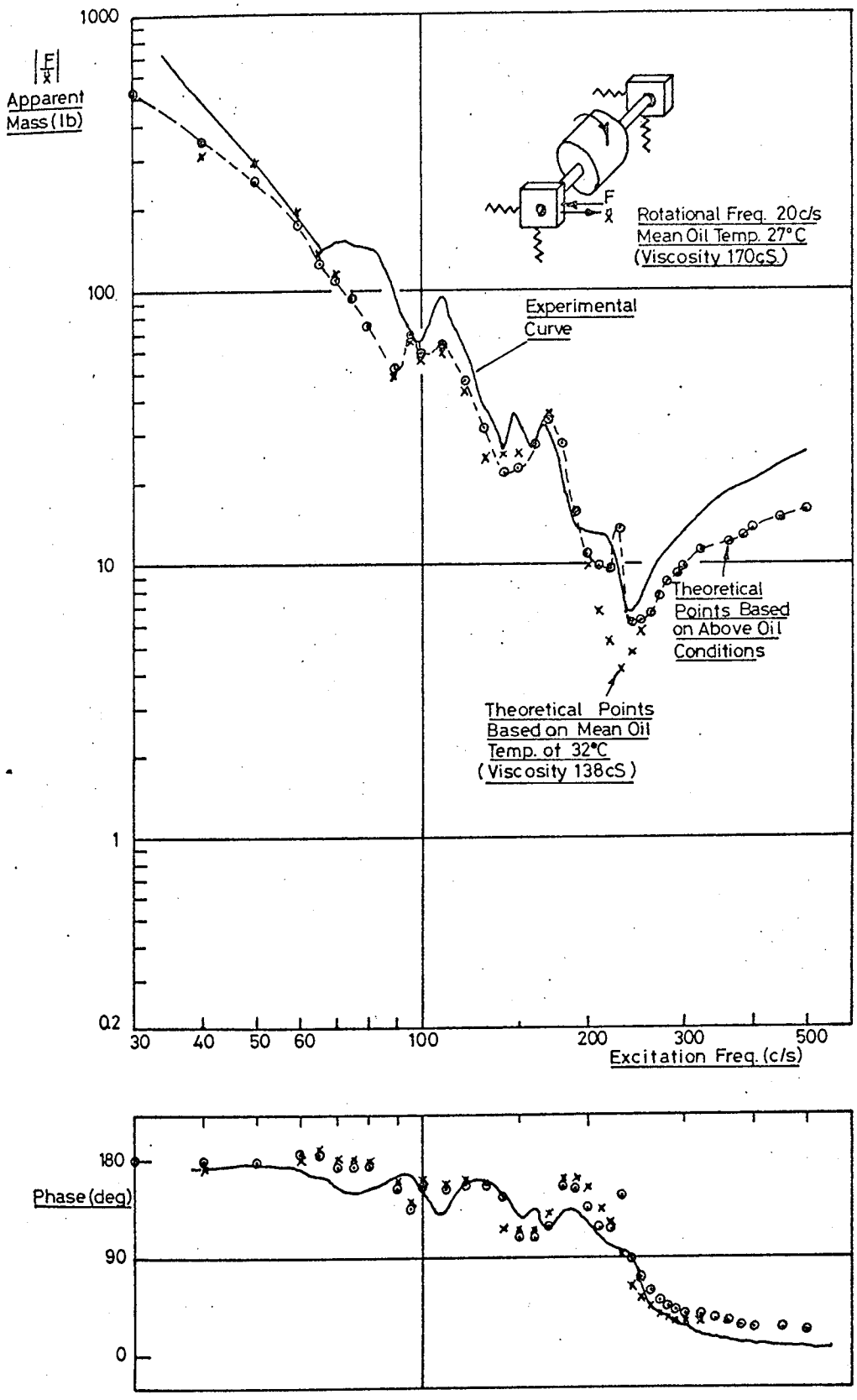

FIG.6.45. HORIZONTAL DRIVING POINT IMPEDANCE DE SUPPORT COMPARED WITH THEORETICAL BASED ON MEASURED $Z_{yy_1}, Z_{xx_1}, Z_{yy_2}$ & Z_{xx_2}.
MODEL RIG 20CRS IN JOURNAL BEARINGS

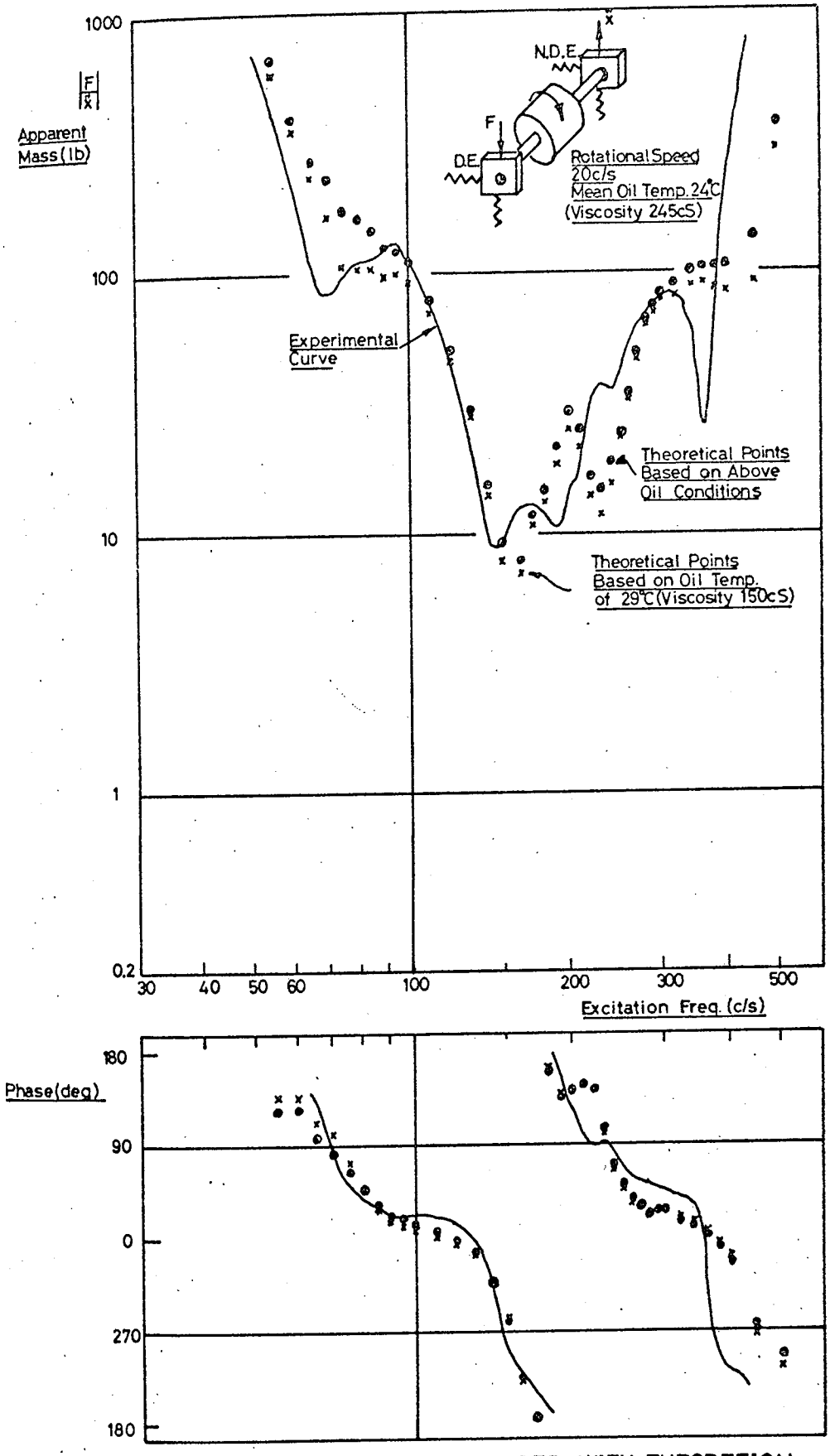

FIG. 6.46. TRANSFER IMPEDANCE COMPARED WITH THEORETICAL BASED ON MEASURED Z_{xx_1} Z_{yy_1} Z_{xx_2} & Z_{yy_2} MODEL RIG 20" CRS IN JOURNAL BEARINGS.

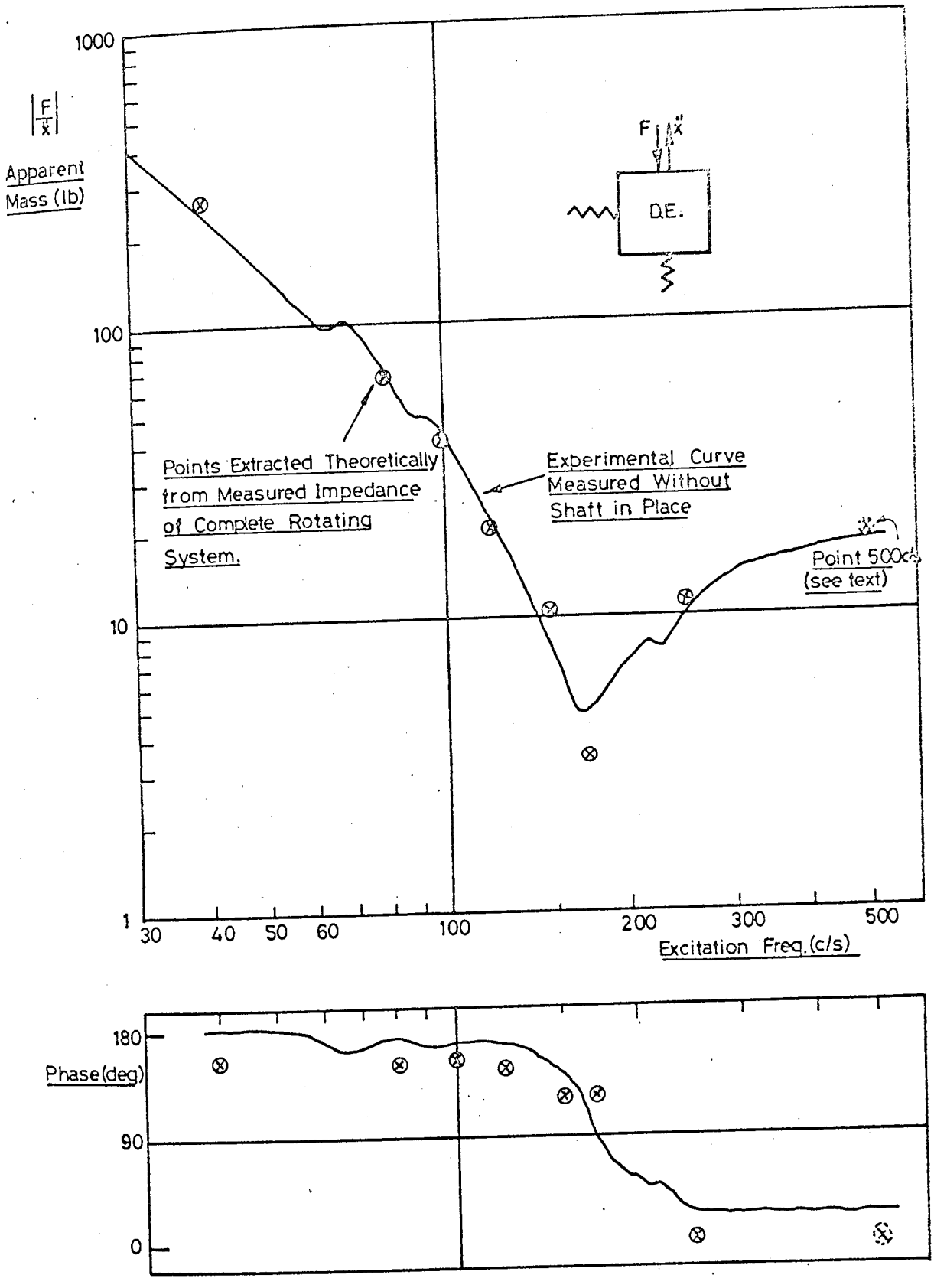

FIG.6.47 DRIVING POINT IMPEDANCE D.E. SUPPORT EXTRACTED FROM EQUIVALENT MEASUREMENT ON ROTATING SYSTEM. MODEL RIG 20" CRS IN JOURNAL BEARINGS.

Chapter 7.

Experiments on a Large Rotary Converter

7.1 Introduction

A large rotary converter, installed in the Electrical Department of the University, provided an opportunity of examining experimental techniques for the measurement of bearing support impedances on a full scale machine. The converter, a photograph of which is shown in fig 7.1, was about 70 years old and had a shaft which weighed nearly 3 tonf. The maximum running speed of the shaft was well below the first flexural critical and it therefore behaved predominantly as a 'rigid' rotor.

It was found that the controlling stiffnesses of the bearing pedestals were about 10^6 lbf/in - the same order that was expected from the industrial compressors of Chapter 10.

No drawings, details of the shaft dimensions, its weight, critical speeds, bearing clearance, and the like were available due to the machine's age. Also, since there was no adequate craneage in the laboratory, the machine could not be dismantled and all information had to be obtained experimentally, often by using very approximate methods. Despite the inaccuracies in the data, particularly those regarding the shaft dynamics, a measure of agreement was obtained between the theoretically calculated behaviour of the complete rotating system and that observed in practice.

It was also possible to measure unbalance responses of the bearing supports for various added unbalance masses. These experiments confirmed the measured controlling stiffnesses of the supports within the running frequency range and, conversely, confirmed that the measured support vibration amplitudes in conjunction with the support impedances indicated the correct bearing forcing levels.

7.2 Construction of the Rotary Converter.

Fig 7.2 shows a sketch of the machine from which it may be seen that the shaft was supported in separate bearing pedestals at about 7ft centres. Both pedestals were mounted on a common, cast-iron bedplate which in turn was Rawlbolted to the floor. The mean diameter of the shaft was approximately 7 in and it carried a large wound rotor near its mid-span, and a commutator assembly towards the non-drive end (N.D.E.). The shaft ran in plain, white-metalled journal bearings which were partly immersed in oil baths. Oil was carried to the top of the journals by loosely-mounted, eccentric steel rings rotating with the shaft.

On the overhung portion of the shaft at the N.D.E. was mounted an exciter rotor whose corresponding stator and casing had been removed for these experiments. The drive-end (D.E.) of the shaft was similarly overhung and at this end a sheave of vee-belt pulleys was mounted through which the shaft was driven from a D.C. motor.

The maximum shaft speed was 800 r.p.m. (13.3 c/s)

7.3 Estimation of Shaft Mass and Bearing Dimension.

In the absence of suitable craneage, the mass of the shaft was estimated using a hydraulic jack of known ram area in conjunction with a precalibrated pressure gauge. The jack can be seen in the foreground of the photograph fig 7.1.

With the jack positioned outside the N.D.E. bearing pedestal the shaft was jacked clear of the N.D.E. bearing and the jacking force required and the axial position of the jack noted. This procedure was repeated with the jack at the D.E. of the shaft.

From these two measurements the total shaft mass was estimated to be 6190 lb whilst its centre of gravity was approximately 35 in. from the centre line of the N.D.E. pedestal. The position of the centre of

gravity thus obtained is indicated in fig 7.2.

Since it was not possible to remove the shaft from its bearings no direct accurate measurement of the journal and bearing diameters could be obtained. The diametral clearance was estimated, however, by jacking each journal to the top of its bearing housing and noting the deflection of the shaft relative to the pedestal. The error due to the slope of the shaft within the bearing length was small in this case since large diametral clearances of between .034 & .036 in were recorded. The total width of each bearing was $7\frac{1}{8}$ in, this consisting of two similar plain white-metalled sections having a nominal diameter of 5 in.

It is of some historical interest to note that although the bearing clearances were several times larger than those which would normally be used today, the overall bearing dimensions result in capacity numbers, C, according to Ockvirk's theory (Chapter 4 section 4.3(i)) of 2.5 and 3.4 for the D.E. and N.D.E. bearings respectively. (These figures being based on a kinematic viscosity of 280cS as measured for a sample of the lubricating oil at 19°C). The quoted load numbers indicate journal eccentricities of 0.47 and 0.53 respectively, again according to Ockvirk's theory, which are the same order as would be aimed at in normal modern design practice. They must have been obtained empirically, however, at the time, or even before, the first successful attempt by Osborne Reynolds to explain the nature of hydrodynamic lubrication.

7.4 General Dynamic Behaviour of the Machine.

Because much of the shaft's length was inaccessible, it was not possible to measure shaft dimensions to a sufficient order of accuracy to justify an attempt at detailed calculation of its dynamic behaviour (for instance by using the transfer matrix methods which had been used for the design calculations on the model rig of Chapter 6.). It was considered more instructive to measure the natural frequencies and approximate modal shapes of the complete structure.

For this purpose the bearing pedestals of the machine were vibrated harmonically using techniques similar to those discussed in Chapter 5 section 5.5 (iii). A Savage 1 kw electromagnetic vibrator, having a maximum thrust of 250 lbf, was used to provide the excitation, this vibrator being shown coupled to the N.D.E. pedestal in fig 6.1. With the lifting tackle available it was only possible to provide horizontal excitation since the vibrator weighed some 350 lbf.

Measurements of shaft amplitudes were made using a magnetically-attached, piezoelectric accelerometer.

With the shaft lying stationary in its bearings, the machine exhibited a complex response and the 'modes' referred to below were not pure, horizontal responses. Damping in the system and coupling with motion in the vertical plane, due largely to the geometry of the bearings, meant that phase angles between the exciting force and the measured responses showed only approximate 180° changes as nodes were traversed. For the sake of simplicity the measured modal shapes of fig 7.3 are plotted according to whether the response was predominantly in-phase or in antiphase with the exciting force.

Predominant modes detected during horizontal excitation at the N.D.E. pedestal are illustrated in fig 7.3. The fundamental modal shape corresponding to a natural frequency of 34 c/s (75 lbf r.m.s. force) is shown in the upper diagram. The significant influence of the pedestal flexibilities can be seen whilst the shaft amplitude within the bearings is about 25% greater than that of the pedestal. Like all responses measured on the machine with the shaft stationary in its bearings, this mode was heavily damped. It also showed evidence of a weak 'softening' nonlinearity (fig 7.4) as the excitation force was increased - very similar to the type of response associated with hysteritic damping forces (74). Some investigations into the nature of the non-linear effects of journal bearing geometry are given in Appendix I.

The first overtone mode at 65 c/s again demonstrates the powerful influence of pedestal impedances on the shaft's behaviour. The modal shape shown in fig 7.3 corresponds to the familiar 'S' form associated with rigid supports.

At higher frequencies the effect of the overhung masses (driving pulley at the D.E. exciter rotor at the N.D.E.) was increasingly apparent, as is demonstrated by the shape of the fourth mode shown in fig 7.3 at 155 c/s.

The resonance at 244 c/s (mode 5, fig 7.3) involved, predominantly, motion of the exciter rotor, this being effectively 'cantilevered from the overhung shaft. Amplitudes elsewhere along the shaft are not shown, these being less than 10% of the exciter rotor amplitude at the D.E.

It would seem from fig 7.3 that a further mode, between those shown at 65 c/s and 125 c/s and having two nodes along the shaft, should have been present. That this was not detected was possibly due to the axial position of the exciting force, the vibrator always being attached at the bearing pedestals.

7.5 Impedance Measurements on the Bearing Pedestals.

The mechanical driving point impedances of the bearing pedestals were measured in the horizontal plane using the techniques of Chapter 5, section 5.5 (iii) (i.e. by tape recording the basic data for subsequent analysis on the 'Spectral Dynamics' equipment).

In order to uncouple the pedestals from the shaft the latter was jacked within the bearing clearance until no contact could be detected between it and the bearing. This procedure, like the approximate method used for estimating the shaft mass, was only possible due to

the large bearing clearances (0.35 in diametral). Even with these clearances it often required three of four attempts to obtain a truly vertical 'lift' to place the journal in the centre of its bearing.

The lowest frequency at which the pedestal impedances could be measured was governed by the vibrator's ability to react the exciting force. Without damaging the vibrator or detracting from the direct, horizontal forcing otherwise obtained, this limit was reached at about 20 c/s which, unfortunately, was above the maximum rotational frequency of the shaft.

Fig 7.5 shows the measured driving point impedance at the N.D.E. pedestal. The low frequency controlling stiffness of this pedestal varied between 0.6 and 0.9 x 10^6 lbf/in and it responded, predominantly, in a single degree of freedom up to about 250 c/s. The resonant frequency in this mode was 112 c/s. At lower frequencies the controlling stiffness decreased slightly whilst around 45 to 48 c/s a minor resonance was apparent as can be seen from fig 7.5. This response was attributed to coupling between the pedestals via the bedplate and corresponded to the second overtone of the shaft. When supported in its own bearings the resonant frequency was 65 c/s (see fig 4.3), the reduction in frequency being due, presumably, to the increased support centres consequent on jacking the shaft outside the N.D.E. pedestal.

Although the pedestals themselves were of almost identical design, that at the drive end carried the A.C. brush gear cantilevered from its inside face. In measurements on this pedestal the spring-loaded carbon brushes were wedged clear of the sliprings to prevent unwanted mechanical coupling with the shaft. The effect of the heavy brush carriers on the pedestal behaviour may be seen in fig 7.6 in which the horizontal driving point impedance is shown. In this diagram the D.E. pedestal

shows two main resonant minima at 102 c/s and approximately 190 c/s respectively. At low frequencies the pedestal impedance was asymptotic to a line representing a stiffness of 1.5×10^6 lbf/in - approximately twice the horizontal controlling stiffness of the N.D.E. pedestal.

Over most of the frequency range 20 to 250 c/s the transfer impedance measured at the pedestals between horizontal and vertical planes was at least ten times greater than the horizontal driving point impedance (fig 7.7). In the immediate vicinity of the fundamental and first overtone modes, however, occurring at 20 and 45 c/s respectively, with the shaft jacked at the N.D.E. coupling reduced the transfer impedance to the same order as the horizontal driving point impedance. Comparing figs 7.5 and 7.7 for example, at the 45 c/s resonance the transfer impedance was 6300 lb (1.10×10^6 lbf/in) whilst the driving point impedance was 3300 lb (0.57×10^6 lbf/in).

With the shaft jacked clear of the bearings, coupling at low frequencies between the two pedestals ($Zx_1x_2 = Zx_2x_1$) was spring controlled and of rate 2×10^6 lbf/in, i.e. 3.3 and 1.3 times greater than the low frequency horizontal driving point impedances of the N.D.E. and D.E. pedestals respectively. The effect of this coupling on the horizontal transfer impedance between supports, obtained with the shaft lying in its bearings, can be seen in fig 7.8. In this diagram the coupling below 25 c/s approaches 2×10^6 lbf/in, rather than the theoretically infinite value obtained for 'pinned' shaft supporting conditions. This effect may be compared with the corresponding measurements on the model rig (Chapter 6, Section 6.5(ii)(b) and figs. 6.19 and 6.35) in which the supports were effectively uncoupled in the absence of the shaft.

7.6 Unbalance Response at the Bearing Pedestals.

First order pedestal responses to deliberately introduced unbalances were measured using the harmonic tracking techniques discussed in Chapter 5 section 5.5 (ii). The tracking (tuning)

signal was derived in these tests from an E.M.I. stroboscope which was triggered photoelectrically from equispaced white marks arranged around the exciter rotor.

The only convenient place to attach unbalance masses was at the non-drive end of the commutator assembly where there were existing tapped holes. The axial plane of the added unbalance was therefore $9\frac{1}{4}$ in from the centre line of the N.D.E. pedestal, whilst the radius of the attachment point was $10\frac{1}{2}$ in.

Fig 7.9 shows the measured response at the N.D.E. pedestal to the inherent shaft unbalance and after adding two unbalance masses of 2.94 and 5.69 lb respectively - both these being attached at the same point.

The effective impedance modulus of the pedestal was calculated from these responses by assuming the rotor behaved in a rigid manner. This assumption was justifiable since the first natural frequency of the shaft when rotating was about twice the maximum running speed. At 12 c/s (720 r.p.m.), for example, the difference in pedestal response for the two unbalance masses m_1 and m_2 was 0.0097 g r.m.s., which was assumed to be due to a mass m at $10\frac{1}{2}$ in radius. Thus:-

$$m = (m_1 - m_2) = (5.69 - 2.94) = 2.75 \text{ lb.}$$

Assuming the length of the shaft to be $l = 84$ in (see fig 7.2) and the axial distance of the unbalance plane from the pedestal to be $l_1 = 9\frac{1}{4}$ in, then the exciting force F, at the N.D.E. pedestal was

$$F = (m_1 - m_2).\, r\Omega^2\left(\frac{l - l_1}{l}\right)$$

or $F = 2.75 \times 10.5 \times (2\pi \times 12)^2 .\, \frac{(84-9.25)}{84} \text{lb.in.} \frac{\text{rad}^2}{\text{s}^2}$ $\left[\frac{\text{lbf.s}^2}{386 \text{ lb.in.}}\right]$

or $F = 379$ lbf.

The effective pedestal impedance, Z, was therefore

$$Z = \frac{F}{\ddot{x}} = \frac{379}{(.0097 \times 1.414)} \frac{lbf}{g} = 27,730 \frac{lbf}{g}$$

A similar calculation at the maximum running frequency of 13.3 c/s (800 rpm) gave the effective acceleration impedance as 25,420 lbf/g.

These points are plotted on fig. 7.5 for comparison with the swept-sine experimental results. As can be seen from this figure by extrapolating the swept sine result down to the lower frequencies, both methods give approximately the same value for the driving point impedance.

Although the above calculations are approximate, in that they neglect coupling due to the journal bearings and the structure itself, the order of agreement was encouraging bearing in mind the stiff nature of the system. Conversely, these results confirmed that the measured support impedance could be used to provide a realiable measure of bearing force levels.

7.7 Measurements of Bearing Pedestal Impedances with the Shaft Rotating

Swept-sine impedance measurements were made on the pedestals with the machine running at its full speed of 800 r.p.m. A typical experimental result is shown for the N.D.E. pedestal by the full line of fig 7.10. In this figure the fundamental mode appears as a heavily damped resonant minimum at approximately 22 c/s, this frequency being nearly 30% lower than that obtained with the shaft lying stationary in its bearings (fig 7.7) This resonance is followed by an anti-resonance, corresponding to a series resonance of the shaft system of the type discussed in Chapter 3 section 3.2.. The impedance curve of fig 7.10 may also be compared in the region of the fundamental with the results obtained from the model rig, for example, fig 6.32..

Parts of the experimental curve of fig 7.10 are shown dashed where mean lines have been drawn through irregularities caused by periodic 'noise', due mainly to vibration at harmonics of the running frequency.

An attempt has been made to compare the experimental results of fig 7.10 with a calculated impedance derived using the analytic approach of Chapter 4. For this purpose the lumped parameters defining the shaft dynamics were estimated very approximately from the geometry of the system and the measurements reported above.

Since it was apparent from the measured modal shapes (fig 7.3) that the distributed mass of the shaft was becoming increasingly important above about 100 c/s, this was taken as the upper frequency for the Atlas computer solution.

Recalling the analysis given in Chapter 4, the parameters required to define the shaft's behaviour were:-

Shaft mass = M. 'Diametral' rotor inertia = I

Polar rotor inertia = I_3

Shaft stiffness = k_1, k_2 Shaft lengths = l_4, l_5

It was assumed that the rotor and commutator were rigid and that the half-shaft stiffness k_1 and k_2 were governed by the shaft between the pedestals and rotor at the D.E., and between the pedestal and commutator at the N.D.E. Based on mean shaft diameters of 7.25 in at the D.E. and 7.0 in at the N.D.E., with l_4 = 29 in. and l_5 = 44.5 in., values of $k_1 = 3.59 \times 10^5$ lbf/in and $k_2 = 1.43 \times 10^5$ lbf/in were obtained.

The mass M was taken as the total shaft mass of 6190 lb whilst the equivalent inertia I, about the centre of gravity was estimated as 8×10^5 lbf in^2. This estimate was based on an assumption that the rotor and commutator could be considered as point masses separated by a massless shaft.

Whence $I = m_R^2 l_R^2 + m_C l_C^2$, where:-

m_R = concentrated rotor mass

m_C = concentrated commutator mass

l_R = distance of c.g. rotor from c.g. of complete shaft

l_C = distance of c.g. of commutator from c.g. of complete shaft.

For simplicity, and since there was no way of estimating it, the polar inertia I_3, was assumed to be zero. The effect of this assumption was to neglect 'gyroscopic' coupling between the horizontal and vertical planes - a factor of secondary importance in the frequency range considered.

Bearing dimensions for the computation were those discussed in section 7.3 above, whilst the oil viscosity (280 cS) was estimated from the mean oil temperatures at both bearings at the beginning and end of the run ($19^{\circ}C$). The measured pedestal impedances were 'read in' as data as outlined in Chapter 4, section 4.4.

The results of this calculation are shown in fig 7.10 as circled points. Not surprisingly, in view of the approximations made, considerable differences etween theory and experiment are apparent. For instance the calculated fundamental resonance is about 11% lower than that measured whilst the 'first' overtone is nearly 18% too high. Between the predominant resonances the impedance modulus is up to twice the value measured (6200 lb and 3500 lb at 37 c/s respectively).

7.8 General Conclusions

The experiments on the rotary converter gave a useful indication of the order of bearing support impedances to be expected on full scale machines. The machine was also useful in providing a representative system for the development of the transient impedance techniques of Chapters 8 & 9.

An important conclusion reached in the unbalance response measurements was the confirmation of the swept-sine, driving-point impedance measurements made on the 'uncoupled' support (shaft jacked). The converse of this - that the measured vibration amplitudes at the supports indicated the bearing forcing levels satisfactorily - was also of particular significance.

The degree of coupling between the pedestals (due to their common bedplate) indicated that to interpret measured vibration levels correctly it may be necessary on full scale machines operating at higher rotational frequencies to include the transfer impedances Zx_1x_2, Zy_1y_2, in an analytic treatment. This would present no theoretical difficulties since the measured transfer impedances could be incorporated in the system matrix equations in a similar manner to that already used for the driving point impedances of the bearing supports. Similarly the transfer impedances Zxy_1, Zxy_2, between horizontal and vertical planes could be incorporated.

However, in practice, the measurement of the relevant impedances (eight separate measurements) using swept sine techniques would be out of the question in most industrial situations due to the time required. Even with multi-channel recording facilities at least four changes in the position of the vibrator would be necessary.

In this respect the transient excitation techniques (Chapters 8 & 9) offer a distinct advantage in that the initial data may be obtained quickly and with the minimum of equipment.

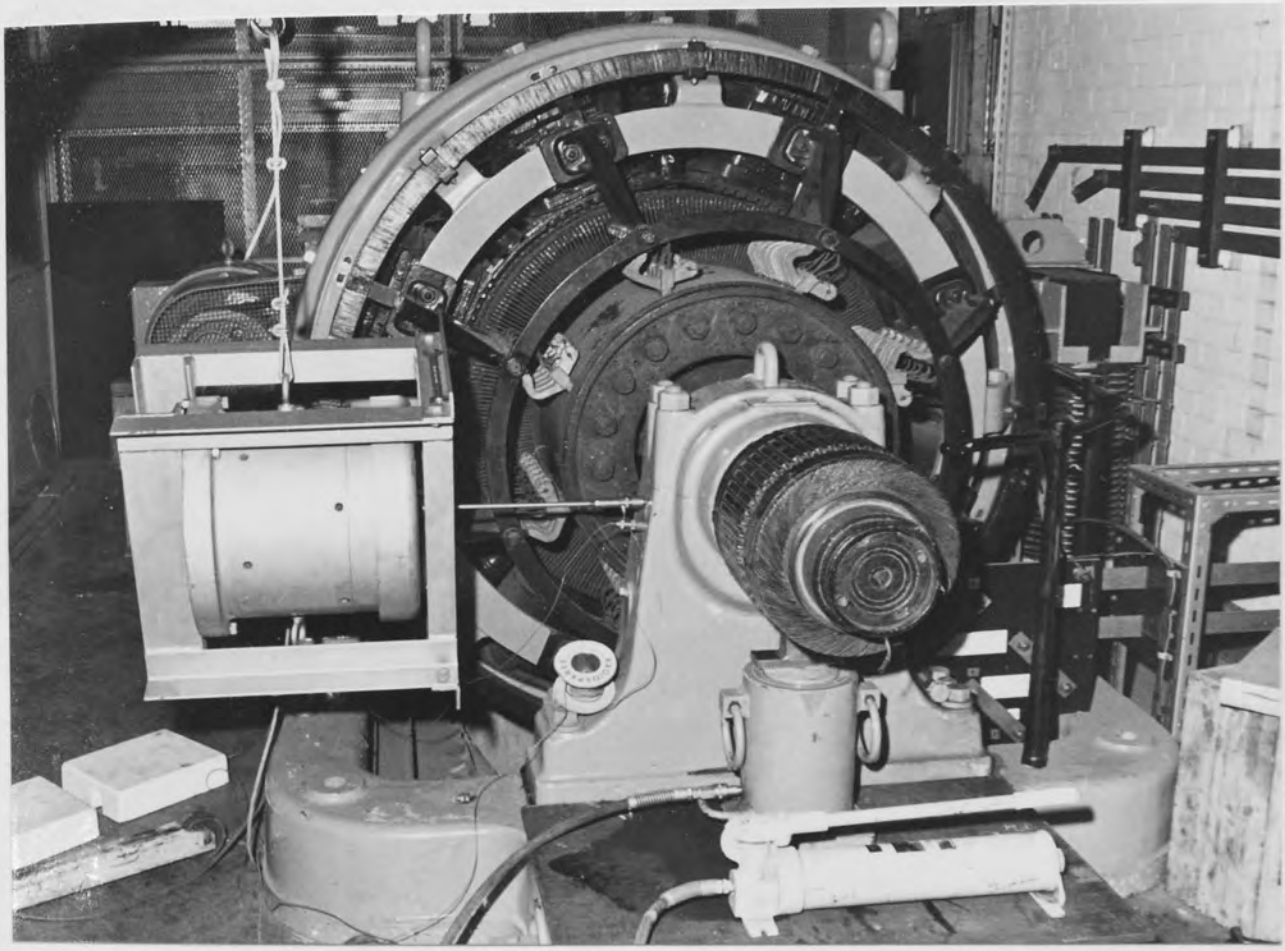

FIG. 7.1. ROTARY CONVERTER

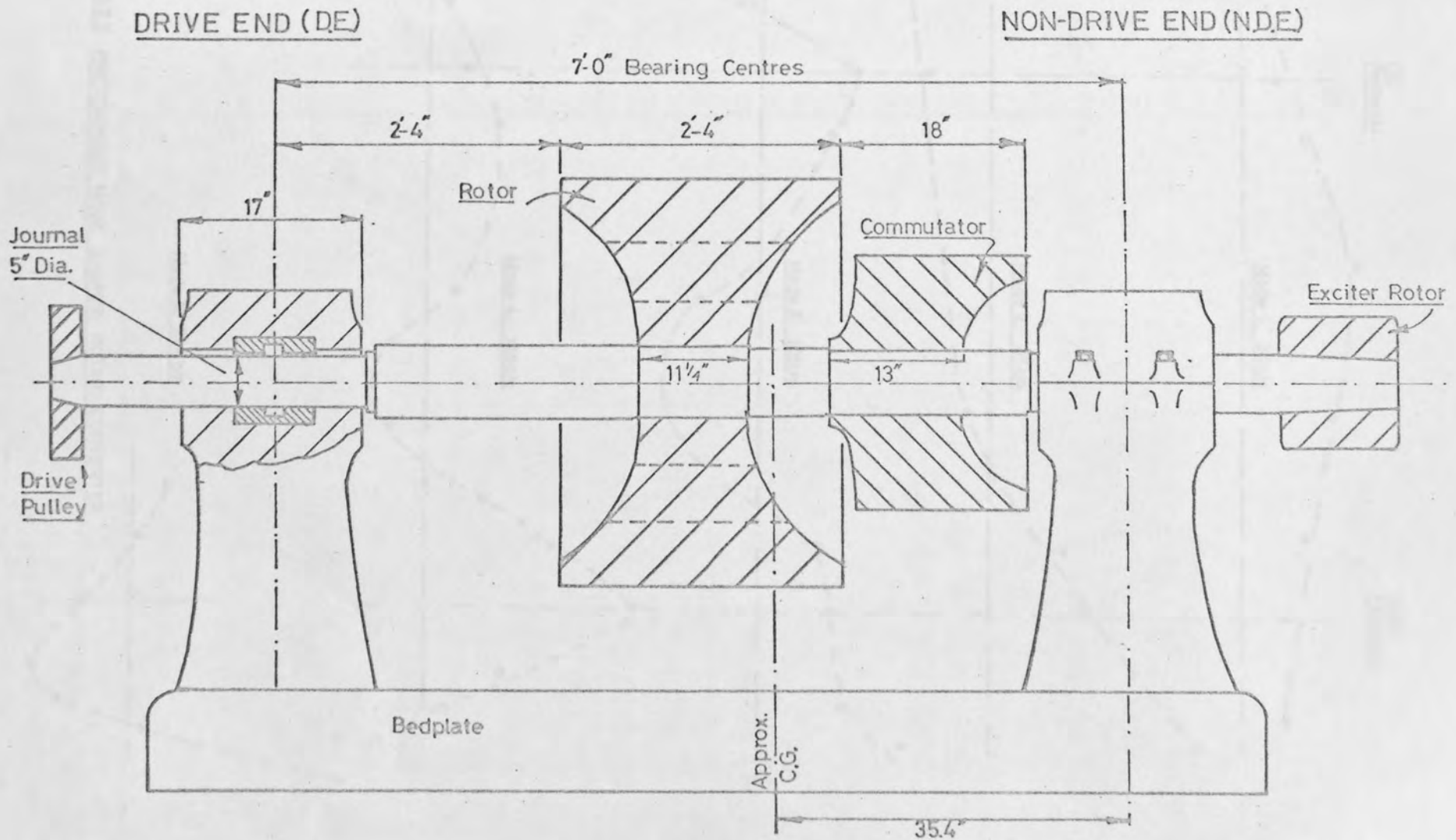

FIG. 7.2. APPROXIMATE CONSTRUCTION OF ROTARY CONVERTER

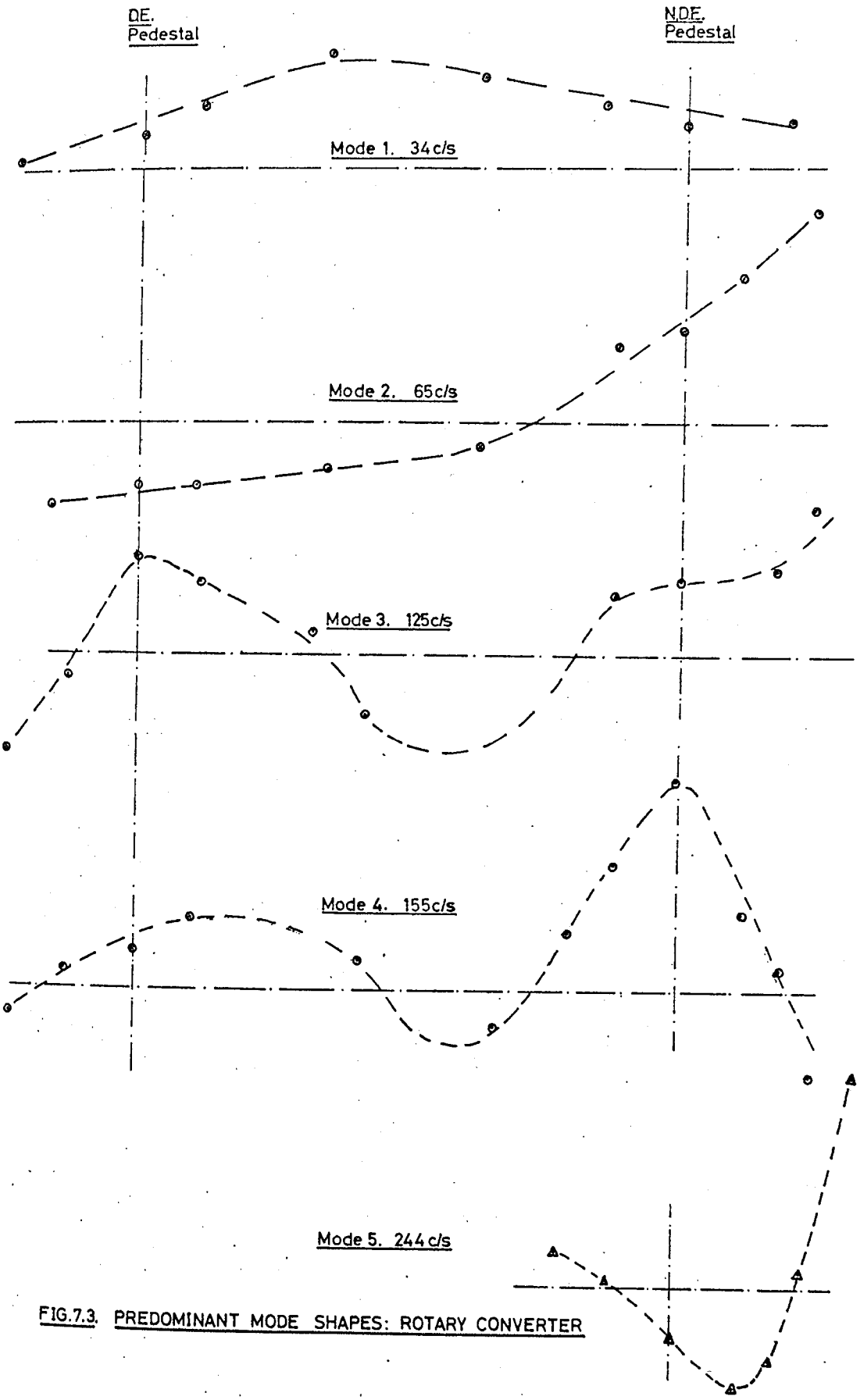

FIG.7.3. PREDOMINANT MODE SHAPES: ROTARY CONVERTER

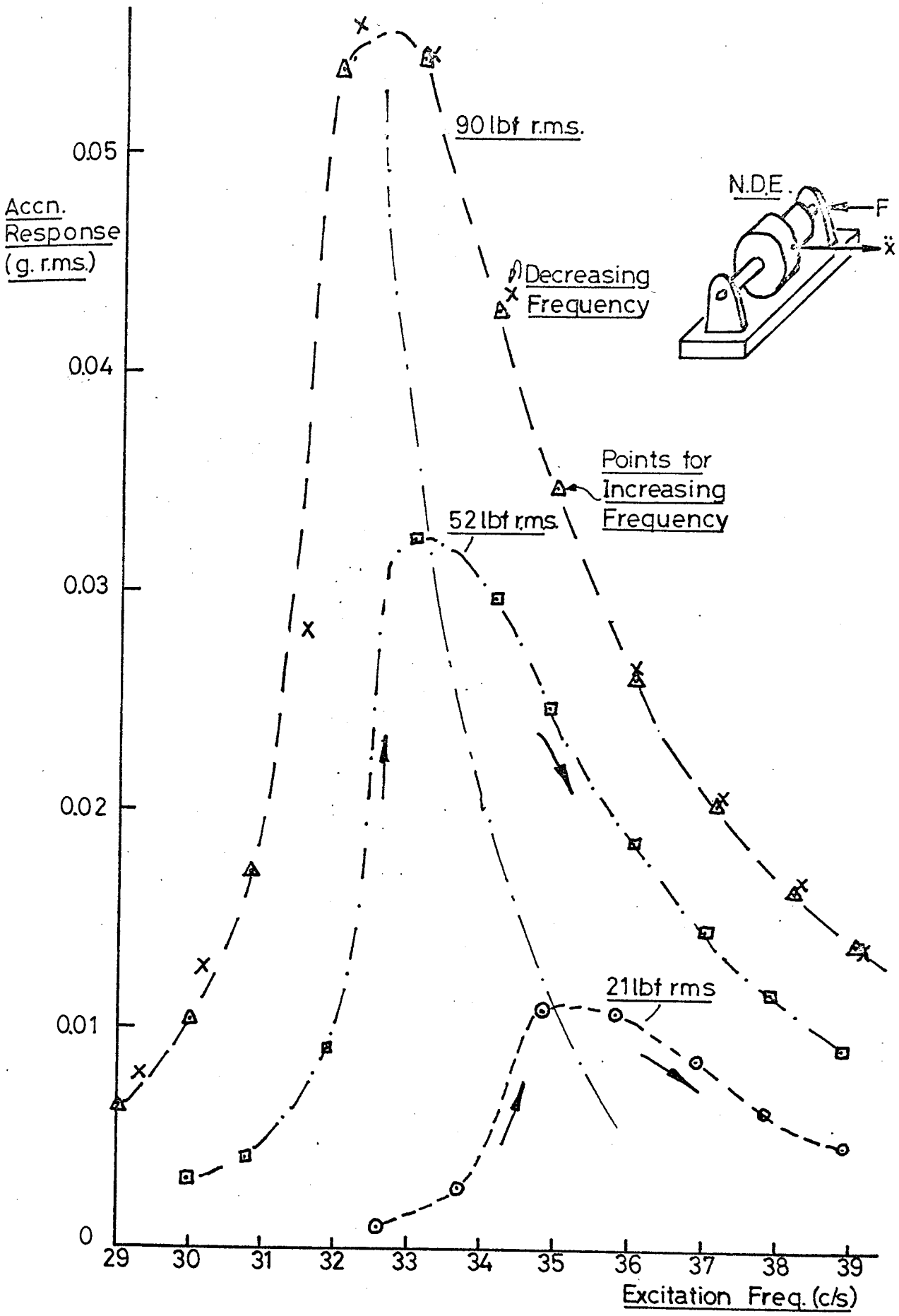

FIG.7.4. NON-LINEAR FUNDAMENTAL MODE RESPONSE

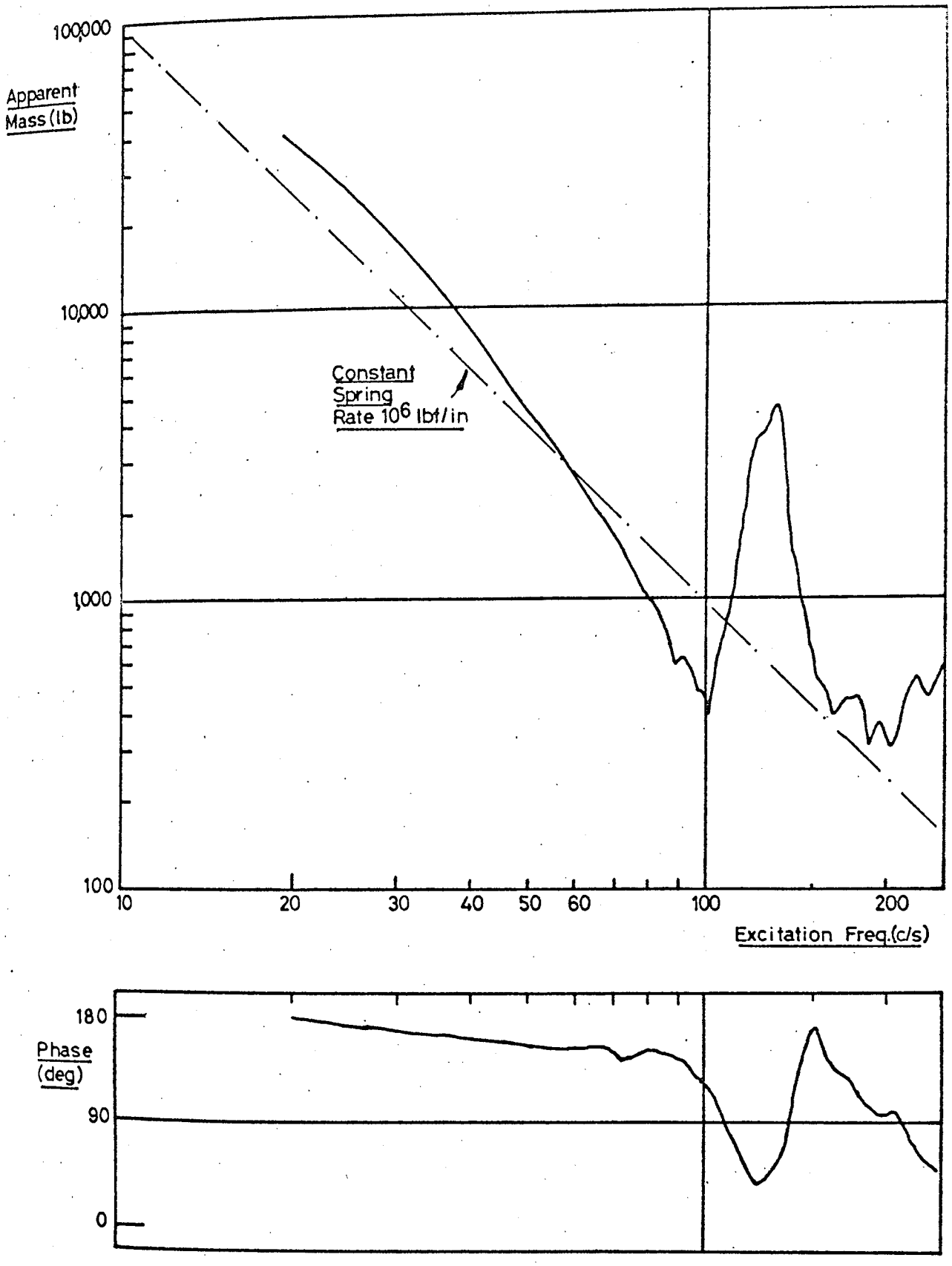

FIG.7.6 HORIZONTAL DRIVING POINT IMPEDANCE. D.E. PEDESTAL ROTARY CONVERTER. SHAFT JACKED CLEAR OF BEARING.

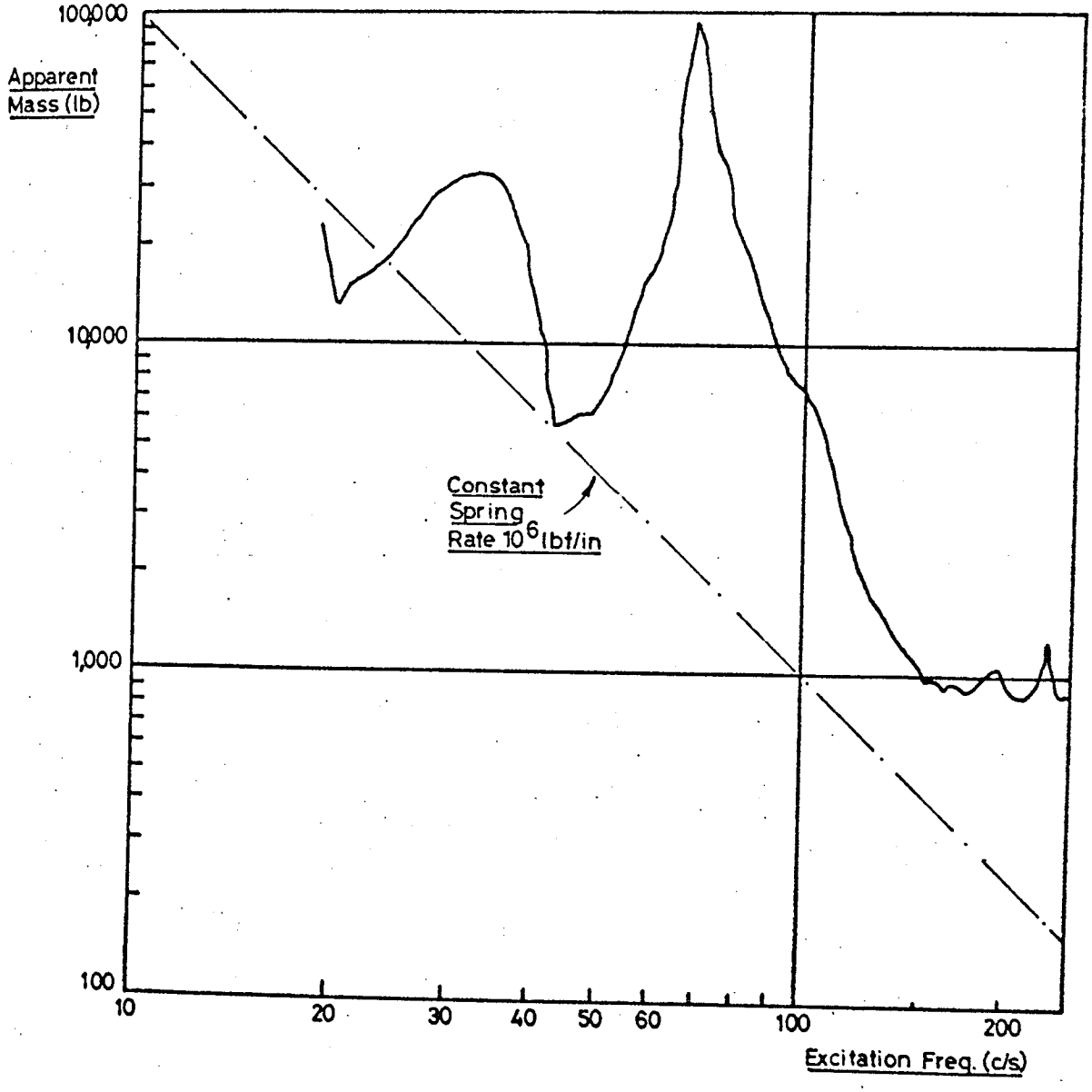

FIG.7.7 TRANSFER IMPEDANCE. N.D.E. PEDESTAL . ROTARY CONVERTER. SHAFT JACKED CLEAR OF BEARING.

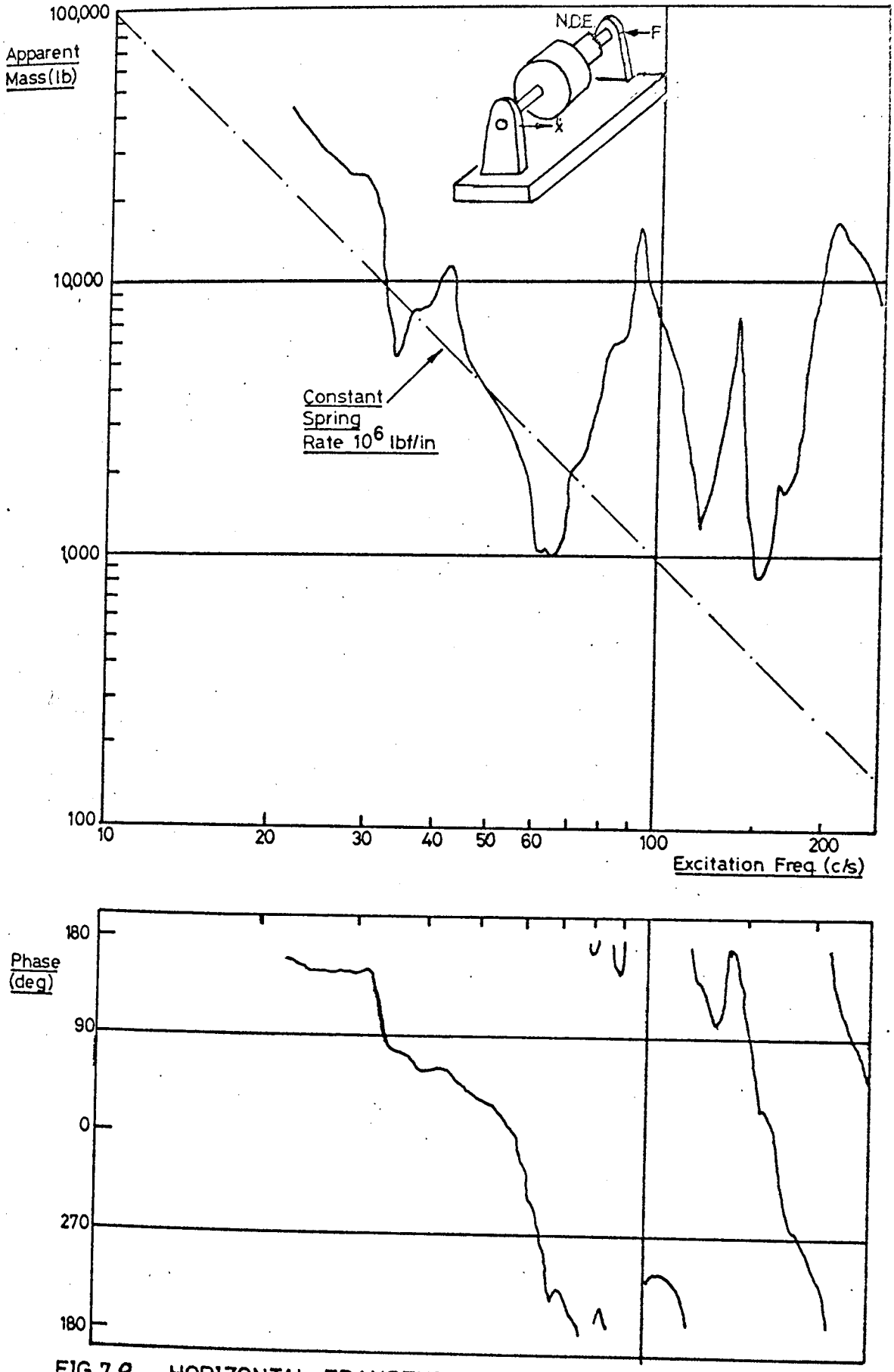

FIG. 7.8 HORIZONTAL TRANSFER IMPEDANCE. ROTARY CONVERTER. SHAFT LYING STATIONARY IN BEARINGS.

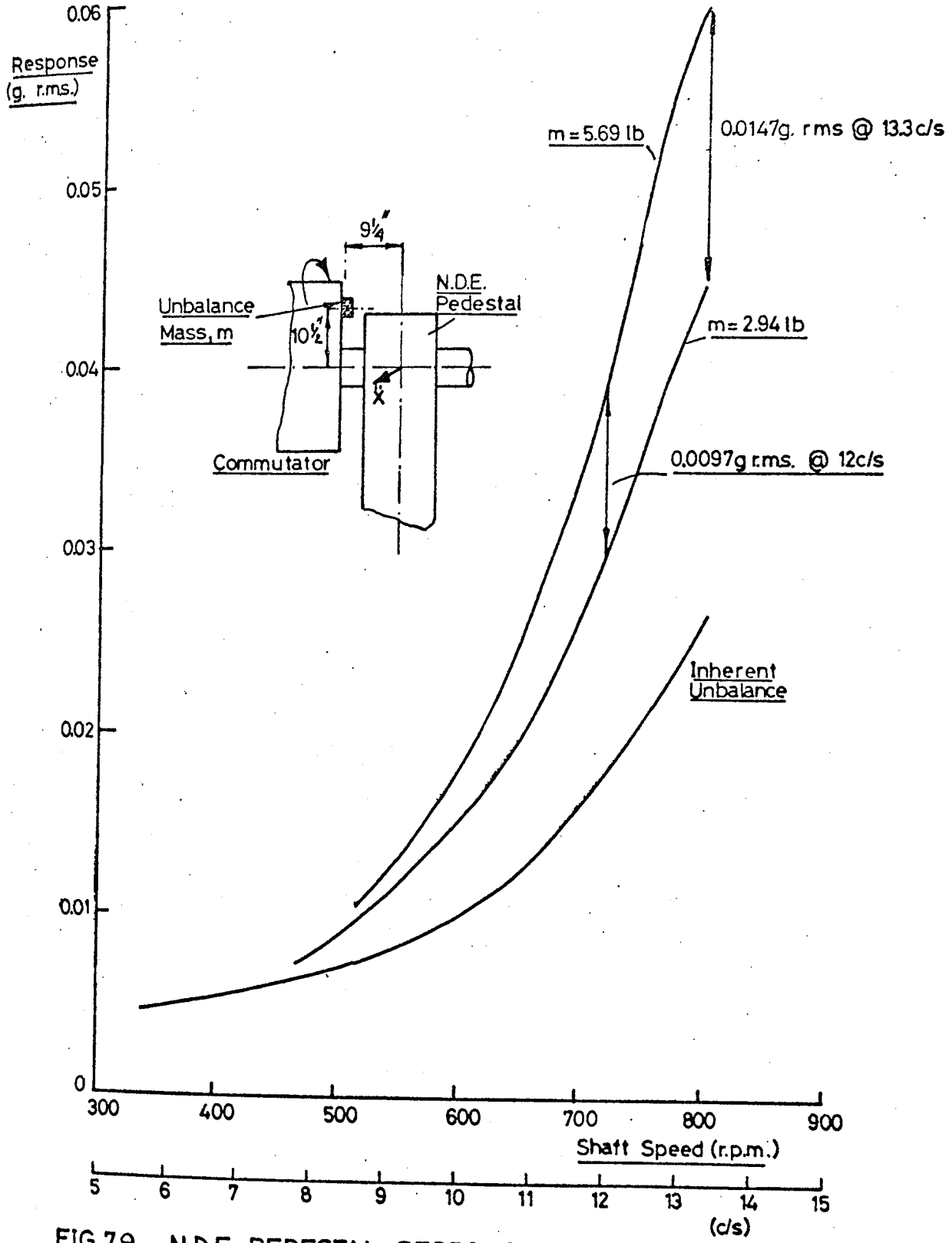

FIG. 7.9. N.D.E. PEDESTAL RESPONSE TO VARIOUS ADDED UNBALANCES. ROTARY CONVERTER.

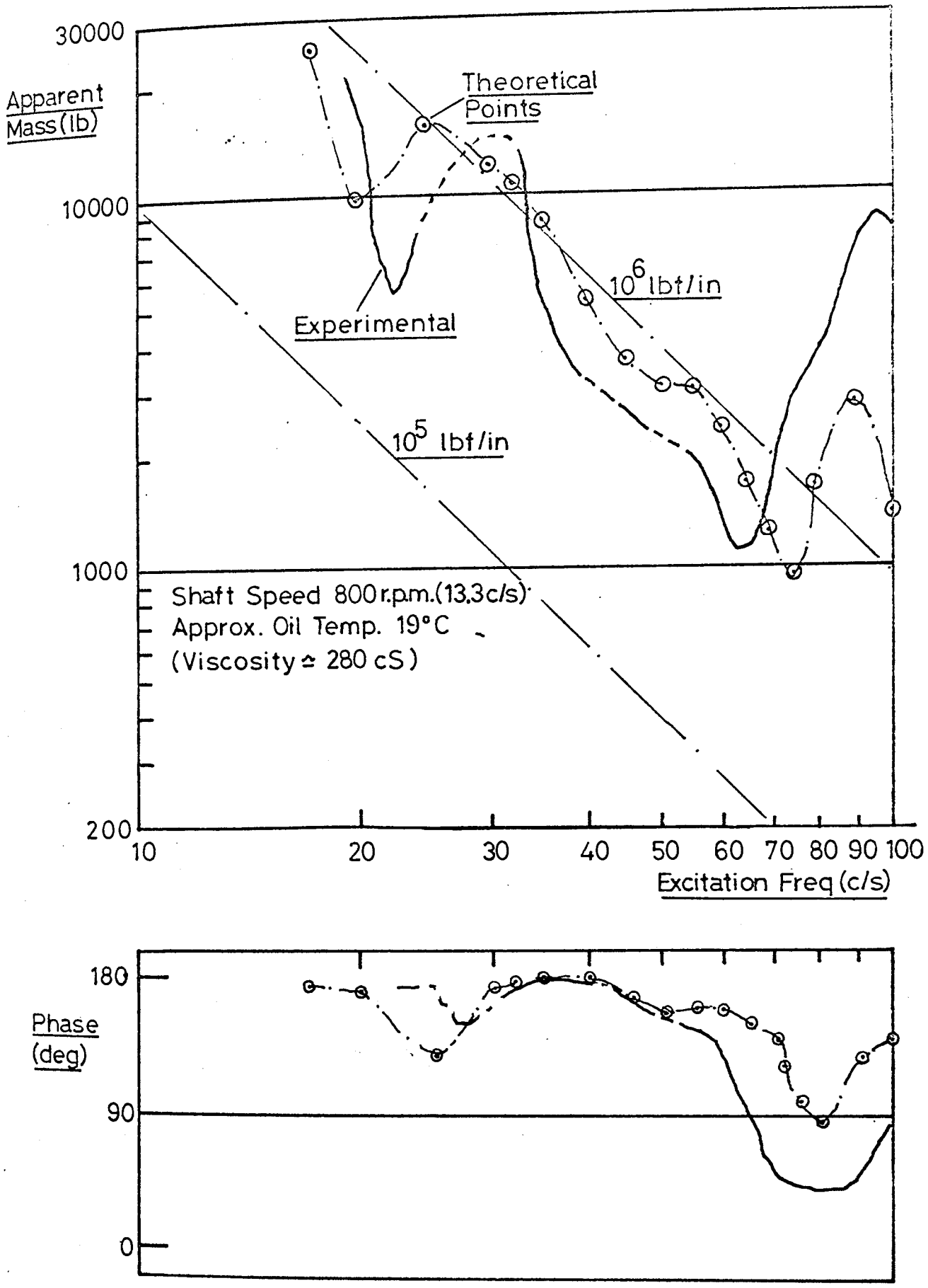

FIG. 7.10 HORIZONTAL DRIVING POINT IMPEDANCE NDE BEARING PEDESTAL. ROTARY CONVERTER SHAFT ROTATING AT 800 R.P.M.

Chapter 8.

Measurement of Mechanical Impedance Using Transient Excitation.

8.1 Introduction

In order to investigate further the feasibility of using measured bearing support impedances in conjunction with corresponding vibration amplitudes on a method of assessing the acceptability of rotating machinery vibration, it was planned to investigate the dynamic properties of several industrial centrifugal compressors (See Chapter 10.).

Due to the nature of the plant and the working fluids of these compressors the use of standard harmonic excitation techniques to perform impedance measurements on site was virtually precluded. In particular, the limited time available for tests during plant shutdown meant that the use of electrodynamic vibrators was impractical. Early tests with a pneumatically driven rotary out-of-balance vibrator also proved unsatisfactory, partly due to the high speeds required to be compatible with the running speed of the compressors i.e. up to 20,000 r.p.m.

Attention was therefore turned towards transient excitation as a practical means of measuring mechanical impedance of large structures in the field. It is the object of this chapter to outline the writer's experience in using such a technique both on model rigs and on the large rotary converter discussed in Chapter 7. In both cases it was possible to check the accuracy of the results against more conventional swept-sine measurements made using the procedures discussed in Chapter 5.

Although no claim to theoretical originality is suggested it would seem that the use of transients in mechanical vibration measurements is a somewhat neglected field capable of providing useful information where other methods are not feasible.

8.2 Analysis of Transients in Linear Systems.

The literature on transients in linear systems is extensive, an excellent introduction to the subject being provided by Jacobsen & Ayre(81). This text also includes a comprehensive bibliography of the earlier work relating to transients. A somewhat more advanced treatment is given by Weber (82). The majority of published material deals with the analytic prediction of system response to given transient inputs. In particular the solution of the differential equation of the simple damped oscillator

$$m\ddot{x} + b\dot{x} + kx = F(t) \qquad (8.1)$$

where $F(t)$ is an aperiodic input function, is widely covered because of its obvious practical significance (See, for example, (83)). Methods of solution commonly employed where the input is analytically defined include the Laplace transformation and the superposition integral (Duhamel's Integral) (84) (85). Where the excitation is of more general form, given either numerically or graphically, system responses can be evaluated using the phase-plane-delta method. ((81) Chapter 67). Because this method involves stepwise approximations it is suitable for the solution of non-linear transient vibration problems. Systems having many degrees of freedom may be tackled by writing the equations of motion in normalised form and solving for the response of the uncoupled normal co-ordinates. Analytical treatment of continuous systems responding to transient excitation is also covered, the more modern work often with reference to the dynamic behaviour of aircraft and spacecraft structures (86). Both mechanical and electrical analogue methods of analysis are widely discussed. Such techniques involve the use of a mechanical or electrical system possessing a degree of equivalence to the practical arrangement under investigation and the measurement of the response quantity of interest resulting from a prescribed input function (87).

Since, in practice the occurence of shock excitation of mechanical structures is normally unwanted, the bulk of work dealing with such

transients is aimed solely at predicting the maximum deformations, forces of stresses involved. The results of the methods of calculation outlined above are therefore often presented in terms of a shock or response spectrum. In its two dimensional form, the shock spectrum is a plot of maximum response under the influence of a given forcing function against the natural frequency of the responding system. Such a shock spectrum is shown in fig 8.1 for a simple oscillator subject to a one half cycle sine wave force pulse.

8.3 Fourier Integral

It is demonstrated in Chapter 9 that an approximate estimate of mechanical impedance may be obtained from the shock spectrum of electrical filter circuits (wave analysers) subject to the voltage analogues at the mechanical system input and response. A more accurate estimate of impedance might be expected to be obtained from the Fourier spectra of these transients.

Considering an input function whose time history is given by $f(t)$ the corresponding Fourier or Frequency Spectrum $\overline{F(\omega)}$ is given by

$$\overline{F(\omega)} = \int_{-\infty}^{+\infty} f(t)\, e^{-j\omega t}\, dt \qquad (8.2)$$

i.e. the Fourier transform of the function.

$\overline{F(\omega)}$ as given by eqn (8.2) is complex and may therefore be expressed in terms of its real and imaginary components

$$\overline{F(\omega)} = R_e\left[\overline{F(\omega)}\right] + j\, I_m\left[\overline{F(\omega)}\right] \qquad (8.3)$$

where

$$R_e\left[\overline{F(\omega)}\right] = \int_{-\infty}^{+\infty} f(t) \cos \omega t\, dt \qquad (8.4)$$

and

$$I_m\left[\overline{F(\omega)}\right] = -\int_{-\infty}^{+\infty} f(t) \sin \omega t\, dt \qquad (8.5)$$

The absolute value of $\overline{F(\omega)}$ may be obtained from the real and imaginary parts as

$$F(\omega) = \sqrt{Re\left[\overline{F(\omega)}\right]^2 + Im\left[\overline{F(\omega)}\right]^2} \qquad (8.6)$$

whilst the phase angle is given by

$$\theta(\omega) = \tan^{-1} \frac{Im\left[\overline{F(\omega)}\right]}{Re\left[\overline{F(\omega)}\right]} \qquad (8.7)$$

Since it is convenient to consider the start of measured transients as occurring at zero time the limit $t = 0$ may be used in place of $-\infty$ in eqns. (8.4) and (8.5), whilst for time histories obtained experimentally the upper limit may be determined either by the total duration of the record or by the time after which accurate measurement becomes impossible. (See Appendix II).

In contrast to the Fourier series representation of periodic functions where components occur at discrete frequencies, the Fourier spectrum of a transient is a continuous function of frequency.

Further, if $f(t)$ is an input transient and $r(t)$ the corresponding time history of the response then the mechanical transfer function is given by

$$\overline{Z(\omega)} = \frac{\overline{F(\omega)}}{\overline{R(\omega)}} \qquad (8.8)$$

where $\overline{F(\omega)}$ and $\overline{R(\omega)}$ are the Fourier transforms of the input and output transients respectively.

If $f(t)$ and $r(t)$ are given by simple mathematical expressions then the integration indicated by equation (8.2) or by equations (8.4) and (8.5) may be performed directly. For example the single half sine wave pulse defined by

$$f(t) = \begin{cases} F \sin\left(\frac{\pi t}{\tau}\right) & 0 < t < \tau \\ 0 & t < 0 \; ; \; t > \tau \end{cases} \qquad (8.9)$$

yields the Fourier spectrum

$$\overline{F(\omega)} = \int_0^{\tau} F \sin\left(\frac{\pi t}{\tau}\right) e^{-j\omega t}\, dt \qquad (8.10)$$

whose modulus and phase angle are given by

$$F(\omega) = \frac{2F\tau}{\pi}\left|\frac{\cos(\omega\tau/2)}{1-\left(\frac{\omega\tau}{\pi}\right)^2}\right| \quad \omega \neq \frac{\pi}{\tau} \qquad (8.11)$$

or $$F(\omega) = \frac{F\tau}{2} \qquad \omega = \frac{\pi}{\tau}$$

and $$\theta(\omega) = -\frac{\omega\tau}{2} + n\pi$$

where n is the smallest integer which prevents $|\theta(\omega)|$ exceeding $\frac{3\pi}{2}$

These functions are sketched in Fig 8.2

Alternatively, where the time history is defined by graphical or numerical data, any applicable method of numerical integration may be used. (See section 8.6 (iv) Data Analysis).

A detailed discussion of Fourier transformations including their relationship to Laplace transforms and complex Fourier series expansions of periodic phenomena is given by H.P.Hsu (88). This reference also includes statement and proof of the sampling theorems of communications theory, the results of which are referred to or implied in the following discussion.

8.4 The Measurement of transient vibration.

Although the sinusoidal frequency response function and the unit impulse response are directly related theoretically - in fact they form a Fourier transform pair - practical measuring techniques for periodic and transient vibrations require rather different approaches. For example, a poor low-pass filter which has a tendency to resonate at its

cut-off frequency may perform satisfactorily under steady state conditions, whilst when used in an instrumentation chain for transient measurements the same filter would produce a spurious output due to 'ringing', sufficient to swamp the signal required. Similarly, since most transients occurring in engineering practice have finite Fourier Spectra down to zero frequency, accelerometers are the only mass-spring type of transducer suitable for shock measurement.

In common with many other technologies vibration research has received considerable impetus from the development of missiles and it is from organisation concerned with this field that much of the modern literature on transient instrumentation comes. For instance, Boucha(89) Stathopoulos (90), and Riedel (91) discuss the application of accelerometers, amplifiers, filters and magnetic tape recorders to shock measurement.

Papers concerned specifically with the measurement of mechanical impedance using transient excitation have also been published. Blake and Belshein (67) (95) describe what they refer to as the 'tap' method. Although, in essence, their method is similar to that described below, they give few experimental or analytical details useful where full scale structures are concerned. Becker (96) describes experiments performed on a Hopkinson pressure bar apparatus with the object of developing a transient impedance measuring technique. He used the two identical cylindrical bars, one acting as hammer, the other as waveguide, to produce a force pulse which approximated to a step function at the end of the waveguide. Such a transient input has the advantage of good high-frequency content and, as the author remarks, this facility would be of use in the dynamic investigation of mechanism elements.

Although the method is of somewhat limited general application Becker does report in another paper (97) an interesting series of experiments aimed at measuring the mechanical impedance at the end of

a rock drill. In these tests the drill shaft itself acted as waveguide. Unfortunately no other experimental or analytical estimate of the impedance is presented to confirm the values obtained by thetransient technique.

Viner (98) reports tests performed using small rocket motors to provide transient excitation of some simple beam-like structures under water. In this paper two very pertinent recommendations are made. Firstly, that further development of laboratory transient data analysis techniques is required, and secondly that a study should be undertaken of transient loading problems as applied to large, complex structures. It is hoped by the writer that the current discussion is in the spirit of these recommendations.

8.5 Experimental Investigations

8.5(i) Problem Outline.

In theory (Section 8.3) it should be possible to obtain the mechanical impedance of a structure from a knowledge of the time histories of input and response transients. The question was whether, in practice, the limitations of time and technique would permit useful data to be obtained on site. A clear idea was also required of the difficulties imposed by the complexity of practical engineering structures. Requirements of any method developed were that the basic data should be obtainable in a matter of minutes and that the analysis of the data to obtain mechanical impedance should if need be require a minimum of specialised equipment.

8.5 (ii) Choice of Forcing Transient.

From an analysis viewpoint it was found convenient to have a forcing transient whose time history approximated to a simple analytic function. A pulse approximating to a single half sine wave was found to result from a hammer blow. Consider the freely falling hammer mass-spring system at the moment of contact with a rigid test structure. From the complemen-

function solution of equ. (8.1) we obtain, with intitial conditions

$$X_o = 0$$

$$\dot{X}_o = V$$

$$x = \left(V / \sqrt{\frac{k}{m}} \right) . \sin \sqrt{\frac{k}{m}} . t \qquad (8.12)$$

as the time history of the distortion of the spring.

From which the force applied to the structure is

$$F = kx = \left(kV / \sqrt{\frac{k}{m}} \right) . \sin \sqrt{\frac{k}{m}} . t \qquad (8.13)$$

When $t = \pi \sqrt{\frac{k}{m}}$, that is half the period of the simple system, the force becomes zero. Separation between spring and test structure therefore occurs and, providing no rebound is permitted, a single half sine force pulse is delivered. The maximum value of the applied force for constant initial velocity of the mass, m, is proportional to $\sqrt{k}$, whilst it can be seen from Fig. 8.2 that the Fourier spectrum of a half sine pulse is at a maximum at zero frequency (D.C.) having amplitude proportional to both the height and duration of the pulse. Since the pulse duration is inversely proportional to the square root of the spring stiffness the D.C. Fourier spectrum amplitude is a constant for constant initial velocity of the mass. The frequency at which the Fourier spectrum first becomes zero, however, increases with decreasing pulse duration. Altering the spring rate therefore has a similar effect to altering the upper cutoff frequency of the spectrum.

Preliminary experimental tests to generate a single half sine pulse were conducted using an ordinary hand hammer modified as shown in fig 8.3 (a). The faces of the hammer were ground flat and then drilled and tapped. On one face a helical spring could be fixed terminated by a washer type piezo electric load cell and a light aluminium anvil.

With this system the force pulse experienced by the load cell approximated closely to that imparted to the structure under test, appreciable errors only occurring at frequencies approaching those at which wave effects in the anvil and load cell became important. By altering the stiffness of the spring the pulse duration could be adjusted. In the limiting case the spring and load cell were removed completely, the latter being replaced by a piezo electric accelerometer fixed to the other hammer face as shown in fig 8.3 (b), and also the photograph fig 8.11. Particular interest centred on this arrangement, concerning both the type of pulse delivered and whether the hammer could be considered as a pure mass and hence its measured acceleration used as an estimate of force delivered to the test structure. (see section 8.6(i)).

The force pulse shape was naturally modified by the impedance of the system excited. This effect was most pronounced in the case of relatively light flexible systems (such as the models discussed in Section 8.6 (ii) (iii)) since the driving point impedance at the hammer face was appreciable compared with the structural impedance being measured. In addition the magnitude of the force pulse clearly depended on the amount of energy expended by the operator. These two factors meant that it was necessary in all tests to monitor the force pulse applied by the hammer. The captive bolt gun described in Section 8.6 (i) has been investigated as a possible method of providing large, repeatable force pulses, which, due to the small bolt mass, should not be materially modified by the test structure's impedance.

For much of the later work on the industrial compressors (Chapter 10) a large hammer, which could be suspended as a pendulum, has been used to provide the forcing transient. This device is shown in use in the photograph of fig 8.4. The hammer was made from a length of 6 in. diameter steel bar having a mass of approximately 37 lb, and, like the

hand hammer mentioned above, it had a copper anvil attached to one face and an accelerometer to the other. Half-sine force pulses of 2000-3000 lbf amplitude having durations of about 1 ms were readily obtainable. Because of the method of suspension this arrangement was much less tiring to use than the hand hammer and the magnitude of the force pulse was also more accurately controllable, being governed by the initial displacement of the 'pendulum' from the vertical.

8.5 (iii) Instrumentation.

As in the measurement of all transient phenomena considerable care in the choice and use of instrumentation was necessary to obtain meaningful results. When dealing with single frequency periodic signals as in normal resonance testing, distortions due to faulty transducer mounting, loose connections, amplifier overloading and the like are normally apparent when, say, monitored by an oscilloscope. In the case of response time histories resulting from the transient excitation of a multi-degree of freedom system, however, spurious distortion due to these defects is difficult to detect by visual inspection of the wave form. For this reason passing a transient of known time hostory through the complete measuring system was found to be a useful check. The half sine pulse generated by the hammer blow was normally used for this purpose. Typical instrumentation used during laboratory investigations is shown in fig 8.5.

For data acquisition on site or where further analysis was required both force and response transients were recorded on the Ampex F.M. magnetic tape recorder. As indicated in Chapter 5, this instrumentation recorder had, at the fastest tape speed, a flat frequency response characteristic up to 20 kc/s whilst the signal to noise ratio was of the order of 44 db.

8.5 (iv) Data Analysis using Fourier Integral.

Due to the linear nature of the Fourier transform given by equation (8.2) it is possible to approximate the time history of a transient by a series of rectangular pulses (staircase function) and to sum their Fourier spectra to obtain the spectrum of the complete function (fig 8.6). Thus the Fourier spectrum of the n th rectangle is obtained from equation (8.2) as

$$\overline{F_n(\omega)} = \int_{t_{n-1}}^{t_n} A_n e^{-j\omega t}\, dt \qquad (8.14)$$

where A_n is the amplitude of the n th rectangle

t_{n-1}, t_n are the elapsed times at beginning and end of the ractangle.

which may be expressed in real and imaginary parts as

$$Re\left[\overline{F_n(\omega)}\right] = A_n . \Delta t \left[\frac{\sin\phi . \cos(2n-1)\phi}{\phi}\right] \qquad (8.15)$$

$$Im\left[\overline{F_n(\omega)}\right] = -A_n \Delta t \left[\frac{\sin\phi . \sin(2n-1)\phi}{\phi}\right] \qquad (8.16)$$

where $\phi = \frac{\omega . \Delta t}{2}$

Summation of real and imaginary parts over all n rectangles yields the total Fourier spectrum component.

Tabulated values of the functions enclosed in square brackets in equations (8.15) and (8.16) are available to simplify hand calculation(99). The majority of analysis of filmed transients reported in this chapter, however, was performed with the aid of an Elliott 803 digital computer.

Typical times required on this machine to evaluate Fourier spectra of force and response transients, and hence the impedance and phase characteristics, were of the order of 45 minutes.

Literature available on the analysis of recorded transients to obtain Fourier Spectra includes various methods of a graphical nature suitable for use where more sophisticated methods are not practicable or where only a limited amount of data is to be analysed. In this connection Samulon (93) suggests a graphical method based on the use of sampling function, $\frac{\sin x}{x}$, approximations to the given transients whilst Rosenbrock (94) puts forward a technique for obtaining frequency response directly from a measured transient response.

Although filmed oscilloscope traces provide a straightforward method of recording short duration transients, some limitation is imposed on the dynamic frequency range over which the Fourier spectrum can be computed. The upper frequency at which accurate analysis is possible is determined by the sampling rate. For example, fig (8.7) shows a decaying sinusoid representing the response of a simple oscillator to an impulsive input transient i.e. a pulse whose duration is much less than the natural period of the responding system. If the length of the record represents τ seconds and it is uniformly sampled n times then, theoretically the maximum frequency accurately defined is $n/2\tau$ c/s (Nyquist Frequency).

In practice this upper frequency should be reduced to $n/3\tau$ or $n/4\tau$ to eliminate the possibility of 'aliasing' errors (100). Since the duration of the record is governed by the oscilloscope time base and the value of n is determined by the minimum spacing of the individual sampling points that can easily be measured, reducing the value of τ to enable a high frequency pulse to be defined often means in practice truncating the lower frequency components of a complex response. The effect on Fourier spectrum analysis of this type of error is discussed in more detail in Appendix II.

8.6 Experimental Impedance Measurements.

As mentioned by way of introduction, transient excitation was first considered as a method of measuring the mechanical impedance of the bearing support structures and industrial machines in the absence of any practical alternatives. Since such field measurements would be largely uncorroborated a programme of experimental work was conducted to ascertain the shortcomings and limitations of the technique in which four test systems of increasing dynamic complexity were investigated. These were a seismically suspended mass, an arrangement closely resembling an 'ideal' single degree of freedom system, the model rotating machine rig described in chapter 6 (which had eight degrees of freedom in the frequency range of interest) and the large rotary converter discussed in chapter 7.

8.6 (i) Seismic Mass

A steel cube supported by long wires may be considered to behave as a pure mass in the frequency range bounded by the natural frequency of the system as a pendulum and the lowest natural frequency of the cube considered as a continuous medium. Such an arrangement consisting of a steel cube having a mass of 17.18lb & a pendulum natural frequency of less than 0.5 c/s was found to be mass-like up to at least 10 kc/s. (First extensional mode natural frequency 12.5 kc/s approximately). These limits were acceptable since the frequency range over the dynamics of the rotating machinery were to be investigated was from about 10 c/s to 1000 c/s.

The seismic mass was used to determine the type of force pulse delivered by both hand hammer and captive bolt gun.

Hand Hammer.

Tests confirmed that a single, repeatable force pulse which approximated to the theoretical half sine wave was obtainable from the hammer. These tests also provided a method of measuring the effective

mass of the hammer in terms of the force delivered and the hammer acceleration. Minimum pulse durations of between two and three hundred microseconds were found to be readily obtainable with amplitudes of around 1500 lbf. Figs (8.8(a) and (b) show, respectively, typical unfiltered pulse shapes where soft and hard effective springs were interposed between hammer and testpiece.

For the test shown in fig 8.8(a) the spring rate was 1000 lbf/in giving a pulse duration of 9.5 m sec. A high frequency oscillation superimposed on the predominant half sine wave corresponded approximately to the first natural frequency of the helical spring between parallel plates. The calculated value for this mode was 720 c/s that observed being 800 c/s. (See for example (70) chapter 34.) Forcing consequent on this oscillation was impressed on the seismic mass and can be seen in its measured acceleration response. On separation between hammer anvil and testpiece a vibration persisted as recorded by the hammer loadcell, at the natural frequency of the helical spring with an additional end mass due to the loadcell and anvil.

To obtain a pulse whose Fourier spectrum is sensibly flat over a wide frequency range, the duration must be as short as possible (section 8.5 (ii)). The minimum force pulse duration would be achieved by using a hardened steel anvil on both hammer and test structure thus involving maximum stiffness and the minimum of plastic deformation ((67) chapter 8). However since during field tests it was frequently necessary to apply hammer blow to finish machined surfaces, a copper anvil was used to prevent damage thereto. Some distortion due to the imperfectly elastic nature of the impact resulted, as can be seen from the unfiltered force pulse shown in fig 8.8 (b). This defect was imperceptible, however, when low-pass filtering with a cut-off frequency of less than 3 kc/s was used and its effect on measurements up to 1000 c/s was therefore unimportant. The results of a test conducted to determine

the effective hammer mass using this arrangement are shown in fig 8.9. The filtered records of hammer and seismic mass acceleration responses were measured by hand to obtain sampled values at uniform time intervals. About eighty samples were used for the full film width corresponsing to one millimetre intervals. Digital computer evaluation of the required real and imaginary Fourier spectrum components for both responses enabled the effective hammer mass to be calculated from their ratio and the known seismic mass.

Intermediate spring stiffnesses have also been achieved by the use of Belleville washer stacks. These devices have markedly non-linear force-displacement characteristics which were of the 'softening' type for the washers used. The resulting force pulse was therefore somewhat distorted but nevertheless accurately repeatable.

Although satisfactory results were obtained using the hammer, the need to monitor the force pulse because of its shape and amplitude variation mentioned above might, in some circumstances, be disadvantageous. Also, the rather crude appearance of expensive machinery being struck by a hammer created some opposition to the experiments on the part of plant operators.

Captive Bolt gun

One method investigated with the aim of obtaining large, repeatable force pulses was the use of a captive bolt pistol of the type used for the humane slaughter of animals.* A sketch of the arrangement used is shown in fig 8.10 (a) and in the photograph of fig 8.11.

The gun consisted of a steel bolt of mass 170 gm which was fired by a .22 calibre blank cartridge. As in the case of the hand hammer it was

---

* Note:- These pistols are classified as firearms under the 1937 Act and therefore the appropriate certificate must be obtained from the police.

intended to shape the force pulse delivered by the addition of spring-like elements between the bolt (which may be considered as the mass, m, of section 8.5) and the test structure. Apart from the control of the force frequency spectrum so obtained, some flexibility was necessary since the very large force amplitudes otherwise developed were sufficient to damage the test structure or, as happened on one occasion, to bend the bolt of the gun.

Various arrangements have been considered for providing this flexibility but the most convenient was a bonded-rubber shaft coupling. This was relatively easy to attach to the heat-treated bolt and could be quickly and cheaply replaced. Simple compression tests on these couplings indicated that their spring rate was, as might be expected, noticeably non-linear and increased with increasing deflection. In itself this was no disadvantage and only meant that the resulting force-pulse would differ from the linear, half-sine shape. Peak forces were also limited by firing the bolt from a partly-extended position thereby increasing the breech volume and decreasing the muzzle velocity. In this case an adjustable stop was incorporated to re-locate the bolt before each firing.

It should be mentioned here that no reliable figure could be obtained for the energy delivered by the standard cartridges. The gun makers quoted 110 lbf.ft for the bolt energy but 50 ft/sec for the bolt velocity when fired from the design position i.e. minimum breech volume. If the quoted velocity was approximately correct, as appeared to be the case from the subsequent tests, then the value given for the bolt energy was about twice as high as that calculated on the basis of the measured bolt mass. The lack of reliable information meant that it was not possible, with any degree of accuracy, to estimate analytically the height of the resulting force pulse. Although it is felt that the captive bolt gun provides, in principle, a useful method for transient excitation, the tests conducted

to date have produced disappointingly inconsistent results. In test firings against the seismic mass two peculiarities were encountered. Firstly, the amplitude of the force pulse, as recorded by the accelerometer attached to the mass, was not constant from one firing to the next. Secondly, for about one firing in three the accelerometer charge amplifier output would indicate a very large, fast-rising forcing transient with an impossibly long apparent duration (>50 Ms).

Fig 8.10 (b) shows four filtered force pulses (seismic mass accelerometer outputs) obtained from the more reliable test firings. The low-frequency content, below 500 c/s, was observed to be a half-sine pulse having a duration of about 2.5 ms. As the filter cut-off frequency was increased, however, two distinct pulses became evident, the first being of shortest duration. It was originally thought that this effect was due to the hot gases propelling the bolt acting as a 'spring' whose rate would vary rapidly with time due to cooling and leakage. In this case, unlike the hammer blow discussed in the previous section, a restoring force due to the gas pressure would act on the bolt in the direction of the testpiece after the initial separation. But although this effect must certainly modify the pulse shape it did not explain the wide variation in amplitude encountered.

In order to examine the type of distortion undergone by the rubber coupling when fired at the seismic mass a series of high-speed films were taken using a 'Fastax' prism camera. This camera had a magazine for 100 ft reels of 16mm film, whilst a nominal film speed of 4000 frames per-second was used for the majority of tests. This meant that the complete film was exposed in about one second and accurate timing of the firing with respect to starting the camera was necessary.

For this purpose a small micro-switch was fixed to the butt of the gun and actuated by the trigger mechanism, the arrangement being visible

in the photograph of fig 8.11. The instant of closure of the switch was compared on an oscilloscope with the initial contact between the bolt and the seismic mass - as indicated by the accelerometer attached thereto. The delay between switch closure and bolt impact was adjusted by trial and error until it was estimated that the impact would occur somewhere in the middle of the film's exposure. This made sure that the film would accelerate to its rated speed whereupon the time interval per frame would be known.

The developed films were analysed frame-by-frame by projecting them on to a screen and measuring both the distance travelled by the bolt and the compression of the rubber coupling. The known bolt diameter was used as a reference to estimate the overall magnification of the projected images. Fig 8.12 shows four frames from one such film and illustrates the type of coupling deformation that was observed when the bolt was fired from a position 0.7 inches extended.

Fig 8.13 (a) shows a plot of the measured longitudinal deformation versus time from which it can be seen that the total time during which the bolt was in contact with the mass was very nearly 2.5 ms. This figure agreed with that obtained from the low-frequency acceleration content of the mass as illustrated in fig 8.10 (b).

By plotting the measured bolt displacement versus time the mean bolt velocity before contact with the seismic mass was estimated to be about 343 in/s. Rather surprisingly the bolt was found to travel at very nearly constant velocity (fig 8.14), which suggested that the energy transfer to it from the cartridge occurred very rapidly i.e. impulsive.

From the filmed results it was apparent that the coupling deformation was not a simple compression. As can be seen from fig 8.12 the rubber coupling was not only compressed axially but also tended to

buckle. In addition the maximum axial deformation suggested that, for this particular test, the two steel end cones, to which the rubber was bonded, came into contact.

It was concluded that the lack of repeatability reported above arose from the arbitrary mode of deflection experienced by the coupling. This was borne out by further static compression tests which showed that widely different effective stiffnesses were obtained for slight amounts of shearing action or buckling. Typical results for these tests are shown in fig 8.13 (b). Also plotted in this figure is the mean apparent coupling stiffness based on the observed pulse duration and the effective bolt mass i.e. bolt mass + $\frac{1}{2}$ x coupling mass.

It was also inferred from the filmed results that the first portion of the transient force pulse, of the type shown in fig 8.10 (b), was due to the initial contact between the anvil and seismic mass. In this case the combined mass of the anvil and steel end cone of the coupling (about 40 gm) was 'unsprung', the pulse width being determined by the local stiffness of the anvil and testpiece.

The other effect mentioned above, that of the large transient with, apparently, a very long duration, was attributed to contact between the two steel end cones of the coupling which resulted in a large, fast acceleration transient of the seismic mass sufficient to seriously overload the charge amplifier. This effect was simulated by giving the accelerometer a sharp blow and was found to produce an effect similar to a momentary D.C. amplifier drift.

It was found possible to overcome this particular problem by clamping a 'Jubilee' clip around the rubber coupling and hence increasing its axial stiffness, but the lack of repeatability due to buckling remained.

Despite these setbacks, providing some suitable spring-like device can be developed to shape the force pulse, the captive bolt gun is a light, compact device capable of delivering large forcing transients. It is hoped that further work will be undertaken in the future.

8.6 (ii) Single degree-of-freedom system.

An arrangement consisting of a cantilever with an additional end mass which responded predominantly in a single mode up to 300 c/s was used to check the validity of the experimental technique and of the data analysis methods used. This structure was in fact the model bearing support used for the non-linear system of Appendix I.

Fig 8.15 shows the force and response transients recorded during a test in which the hand hammer was used to provide excitation. The computed Fourier spectra of force and acceleration responses are also shown, whilst plots of mechanical impedance modulus and relative phase angle obtained therefrom are given in Fig.8.16. These curves are compared with those obtained using normal swept sine excitation with the automatic impedance measuring system manufactured by the Spectral Dynamics Corporation, discussed in Chapter 5, section 5.5 (iii).

8.6 (iii) Rotating Machine Model.

The rotating machine model discussed in chapter 6 provided a useful test facility. Since, with the shaft carried in ball bearings, very little damping was present in the system, the dynamic range of typical impedance plots was of the order of 50 db between alternate anti-resonant maxima and resonant minima. Any effects due to the limited dynamic range of the transient method could therefore be readily observed. Fig 8.17 shows a typical driving point impedance measurement taken at one of the bearing supports with the shaft stationary in self-aligning ball races. Force and response transients and impedance curves are shown, the latter again compared with a standard swept sine test result.

8.6 (iv) Transient measurements in the presence of periodic noise.

Transient measurements of mechanical impedance were also made on the model machine whilst it was rotating i.e. Similar measurements to those discussed in Chapter 6 section 6.5(ii). Since in the case of the transient method, the photographed acceleration responses contained information throughout the whole frequency passband of interest for the particular test, periodic vibrations generated by the machine within this passband were contained in the records. In particular, synchronous out-of-balance forcing and bearing harmonics were in evidence.

By virtue of the linear properties of the Fourier transform ((88) Chapter 4) it is theoretically possible for the purpose of evaluating this transform to consider any complex time history of finite duration to be constructed from an algebraic summation of simpler ones. (The convolution or Duhamel integral in effect implies this property, the fundamental time history from which more general functions are constructed being either the unit impulse or the unit step function.) The accuracy with which this process could be employed in practice to eliminate the unwanted contribution of the periodic noise signals from the response Fourier Spectrum was therefore investigated using the rotating machine model.

With the geometry of the model arranged such that its dynamic response did not vary appreciably with rotational speed in the frequency range of interest, that is minimum gyroscopic effect, records of bearing support vibration were taken at constant speed. A typical time history obtained whilst the model was running at 42.9 c/s (2574 r.p.m.) is shown in fig 8.18. This particular record is seen to consist primarily of a periodic component at very nearly six times the fundamental rotational frequency, this being a bearing harmonic related to the ball passage frequency.

Before the unwanted signal could be eliminated from a measured response due to an applied transient force it was necessary to identify their phase relationship. For the majority of tests made the periodic component component was reasonably large compared with the transient portion of the record and phase identification could be performed by simply comparing the periodic and complex records graphically. Fig 8.18 illustrates the application of this procedure to a transient impedance measurement made at the non-drive end bearing support of the rig. The results are compared with the equivalent swept sine test measurement made with the shaft stationary. Fig 8.19 shows the results of two transient driving-point impedance measurements taken on the model. In the first test the model was stationary whilst in the second it was rotating at about 6000 r.p.m. The effect of the synchronous frequency component on the impedance can be seen in the latter case. For cases where further identification of a periodic component was necessary the method shown diagrammatically in fig 8.20 has been investigated. Using this arrangement a once-per-revolution signal obtained from an inductive transducer was passed through a variable time delay R.C. network constructed around a 'Burr-Brown' operational amplifier. The delayed marker signal was then compared on an oscilloscope with the ambient acceleration signal. By varying the time delay, coincidence could be obtained between the marker and the maxima of the synchronous acceleration. Whence superimposing the delayed marker signal on the force pulse recorded during a subsequent impedance measurement enabled the position of the maxima to be determined within the complex response.

8.6 (v) Rotary Converter.

The model systems discussed above were small compared with the industrial compressors on which it was hoped eventually to make impedance measurements. However, the large rotary converter discussed in Chapter 7 having a rotor of approximate mass 6,100 lb and 7 ft bearing centres,

provided a system whose dynamic characteristics were of the same order as those expected on site. For example, the bearing supports behaved as pure springs of approximate rate 10^6 lbf/in at frequencies below about 100 c/s when isolated from the rotor system. Minimum measured apparent masses at the supports of this machine were around two hundred times greater than those measured on the models. A more severe test of the sensitivity of the transient method was therefore available.

Fig 8.21 shows force and response transients obtained during the measurement of the driving point impedance of a bearing pedestal whilst the shaft was lying stationary in the bearings. Impedance curves computed from the time histories are also shown together with the corresponding measurement obtained using swept sine excitation.

8.7 Discussion of Results. Limitations of the Method.

The simplest case, that of the seismic mass, provided a useful system for checking the transient performance of transducers, amplifiers, filters and recording equipment, and a method of measuring force transients. Good performance in close agreement with theoretical estimations was achieved after some initial development. The largest mass used during these tests weighed 35 lbf but the maximum pure mass whose impedance may be measured using accelerometers and half sine excitation is naturally governed solely by the sensitivity and resolution of the measuring equipment. To take a practical example, an overall acceleration sensitivity of 500 mv/g using a recording device which enables a half sine pulse of height 2 mv to be defined, means that a mass of 2.5×10^5 lb (more than 100 tons) can be estimated using a force pulse of height 1000 lbf. Such a pulse could be readily obtained even with the simple hand hammer arrangement discussed above.

The determination of the effective hammer mass shown in fig 8.9, illustrates several features of interest. Firstly the effect of low

pass filtering the acceleration pulses can be seen. The pulse duration was increased and regions of opposite sign were introduced due to the removal of the high frequency portion of the total Fourier spectrum. The change in pulse shape was most pronounced near the discontinuity where the pulse height returns to zero (Gibb's Phenomenon). Secondly, the effect of some mismatching of the low pass filters used can be seen in the apparent mass and phase plots. The filters used for force and response transients in the experiments reported here left something to be desired from the point of view of matching. For maximum accuracy in impedance measurements it was therefore necessary to weight the Fourier spectra of the force and response transients to allow for the difference in the filter frequency responses. Although the results for the single degree-of-freedom systems (figs 8.15, 8.16) illustrated the general validity of the transient method, some of the difficulties associated with lightly damped structures were apparent. Thus, since the quality factor, Q, for the system was between 55 and 60, truncation of the response on the fixed length filmed record was inevitable if a useful upper sampling frequency limit was to be maintained. This resulted in some scatter of results particularly at the lower end of the spectrum (see appendix II). The small irregularity in the impedance and phase plots around 65 c/s was due to some coupling between the predominant bending mode of the cantilever and another mode related to the fixing of the complete structure to its base. (see Appendix I).

A single degree-of-freedom structure provides a useful basis for estimating the range of system parameters over which impedance measurements may be performed using transient technique. Assuming a half sine forcing function, and that an accelerometer is used for response measurement, the required estimate may be obtained from the absolute maximum (Maximax) value of the acceleration response of the simple structure. For small fractions of critical damping in the

system maximax responses do not differ greatly from those occurring with zero damping. The maximax response may occur during either the forced or residual vibration eras. During the forced era the maximum acceleration of the undamped system is given by

$$\ddot{X}_{m_F} = \omega_n^2 \cdot \frac{F}{K} \cdot \frac{1}{\left(1-\frac{\omega}{\omega_n}\right)} \cdot \sin\left(\frac{2n\pi\omega}{\omega_n+\omega}\right) \qquad (8.17)$$

where n may assume any positive integer value (see, for example, (81) Chapters 3 & 4). During the residual era the maximum acceleration is

$$\ddot{X}_{m_R} = 2\omega_n^2 \cdot \frac{F}{K} \cdot \frac{\omega}{\omega_n} \cdot \sin\left(\frac{N\pi(\omega_n+\omega)}{2\omega}\right) \qquad (8.18)$$

For force pulse durations less than half the responding system natural period the maximax response occurs in the residual era i.e. $\ddot{X}_{max} = \ddot{X}_{m_r}$, whilst as the pulse duration is still further decreased the system response becomes essentially impulsive. The hammer having a copper anvil always produced pulses less than 500 μs duration when applied to the structures tested and could therefore be expected to give maximax acceleration response in the residual era for modes having natural frequencies up to at least 1 kc/s. As a guide to the useful limits of the transient method under discussion it can be seen from fig 8.1 that the ratio $\ddot{X}_{max}/(F/m)$ increases approximately linearly up to a value of unity at a period ratio given by $\frac{\tau}{T} \simeq 0.53$. Using conservative values for force pulse height and accelerometer sensitivity a typical operating range for a single degree-of-freedom system is shown shaded in fig 8.22.

For the tests on the rotating machine model shown in figs. 8.17, 8.18 and 8.19 the hand hammer had been modified using the helical

spring-load cell arrangement. The approximate half sine force pulse so produced had a first Fourier spectrum zero around 160 c/s and a second at 280 c/s, whilst the maximum practicable sampling rate imposed an upper frequency limit on the measurements of 380 c/s for the time base used. Since it was unreasonable to expect great accuracy at frequencies where the force content was very small, estimates of impedance were not normally considered above the first zero in the force Fourier spectrum. Due to the very small high frequency component in the shaped force pulse, filtering of it and the resultant response transient was not normally required.

Bearing in mind the relatively crude method of subtracting the periodic noise component from the complex transient response signal as illustrated in fig 8.18 reasonable agreement was obtained between the impedance values computed from the corrected response and the swept sine test curve. The test result shown, however, provided a severe test for the method since the Fourier Spectrum of the force pulse was small in the region of the frequency of the periodic component. Errors around that frequency are therefore particularly significant. Unwanted periodic noise present during the spectral analysis of harmonic excitation test data simply produced peaks in the response whose bandwidth is governed by the filters used, whilst no effect is evident outside this bandwidth. In the case of transient measurements, however, the periodic noise contained in the response record may have a significant content over a wide frequency range. The errors introduced have sampling function, $(\frac{\sin x}{x})$, form which characteristic can be seen in fig 8.19 where the 100.1 c/s noise component affects the transient impedance results over a considerable band of frequencies.

The tests reported on the large rotary converter suggested that the transient method was capable of providing useful information on the structural impedance of large complex industrial structures. The tests

in fig 8.21 were conducted with the shaft-rotor assembly lying stationary in the cylindrical journal bearings. This condition produced some variation from test to test, thought to be partly due to the variation in damping at the bearings consequent on lubricant viscosity change and partly due to the non-linear coupling between shaft and supports. (See Appendix I). These effects were most pronounced in the region of a mode at resonance around 65 c/s which was primarily a flexural vibration of the shaft. Additional errors between swept sine and transient measurements resulted from a compromise between the useful upper frequency adequately sampled and that time scale which produced truncation of the complete response.

8.8 Conclusions

The exploratory work reported in this Chapter indicated that the transient method of measuring mechanical impedance was capable of yielding viable results even on large structures.

The essential equipment required for filmed oscilloscope records was minimal and sufficiently portable to be useful in many industrial situations where vibrators, their associated power supplies and amplifiers could not be used. This had particular application in solving the problem of impedance data acquisition from the industrial compressors discussed later in Chapter 10.

The ordinary hand hammer was useful over a surprisingly wide dynamic range whilst the larger 'pendulum' hammer increased this range still further. In the case of the captive bolt gun, despite the initial difficulties of obtaining repeatable results, it is hoped that this method will be developed to provide large force pulses without the need for force monitoring.

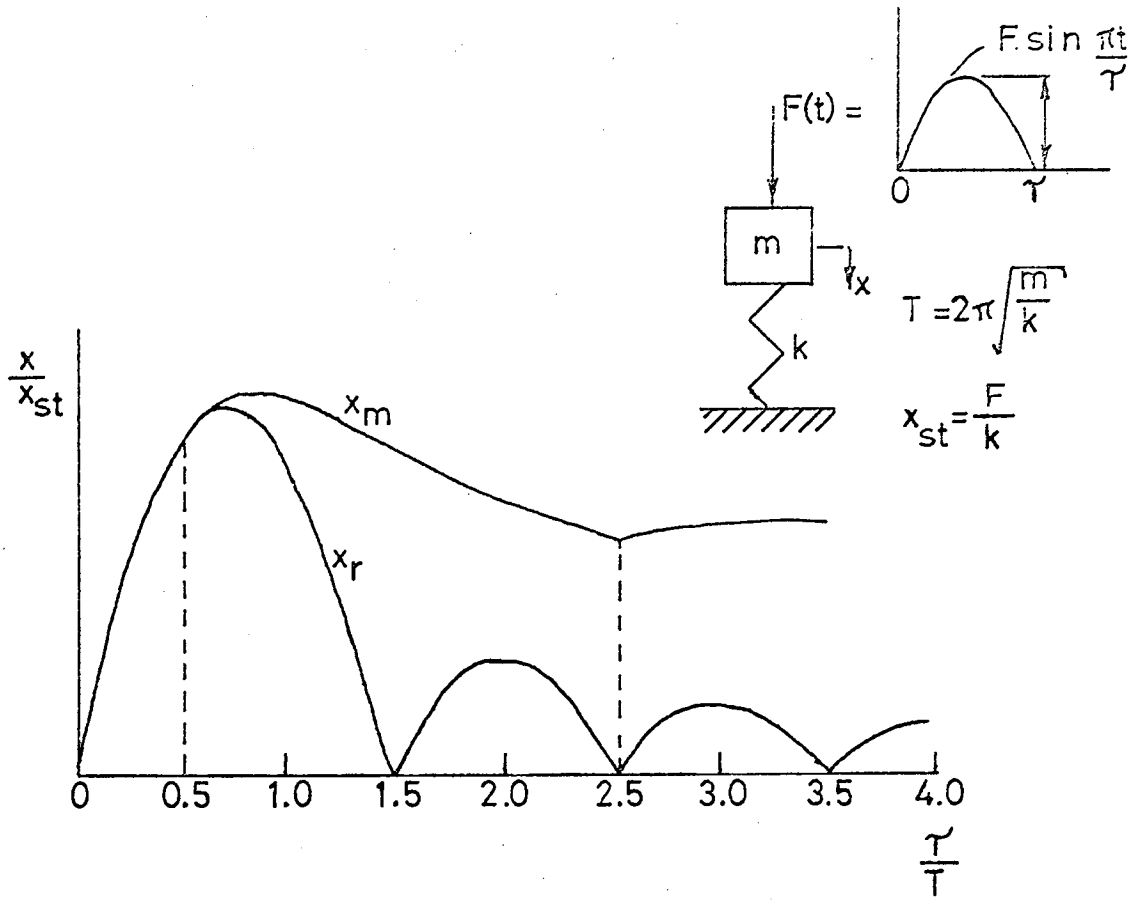

FIG.8.1 SHOCK SPECTRUM. UNDAMPED SIMPLE OSCILLATOR. HALF-SINE FORCE PULSE.

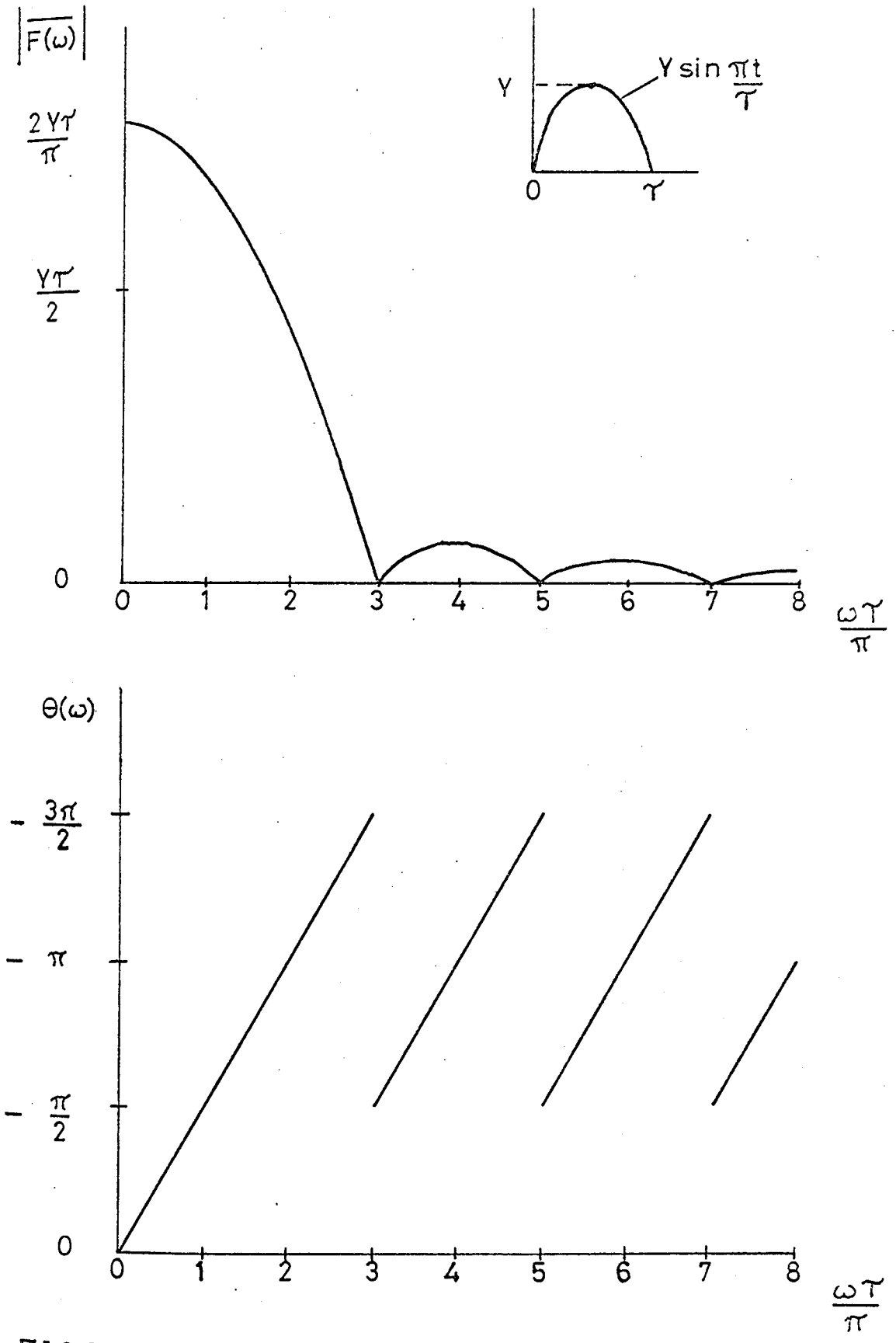

FIG 8.2 FOURIER SPECTRUM MODULUS & PHASE HALF-SINE PULSE

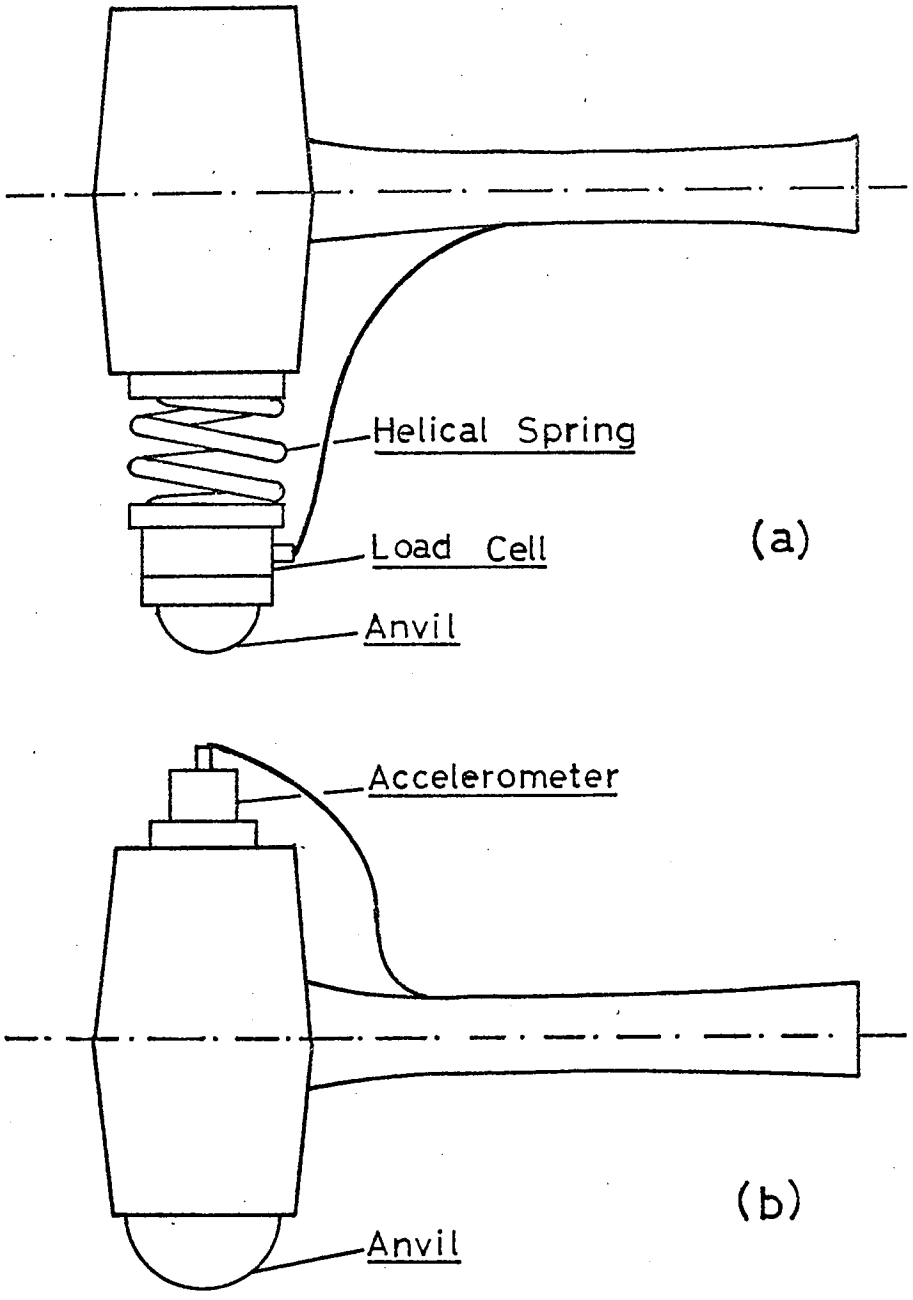

FIG.8.3 HAMMER MODIFICATIONS

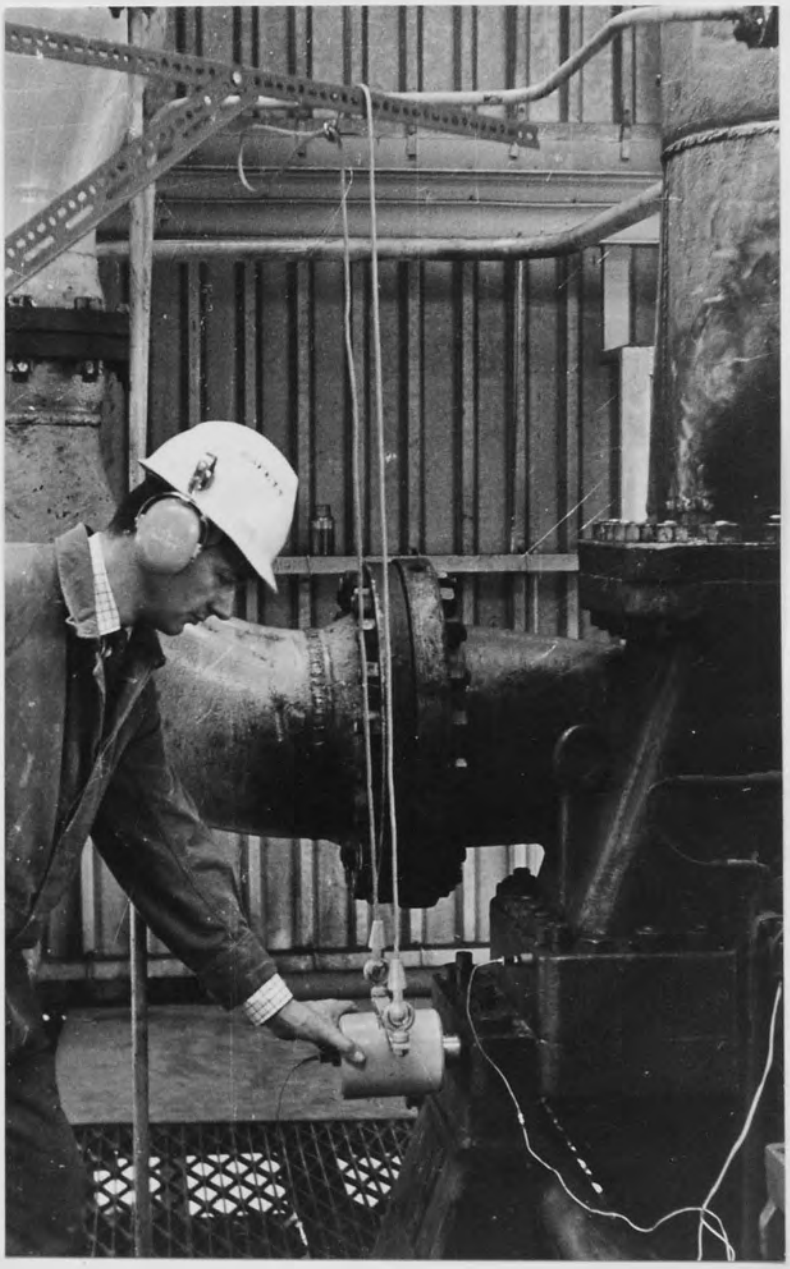

FIG. 8.4. "PENDULUM" HAMMER

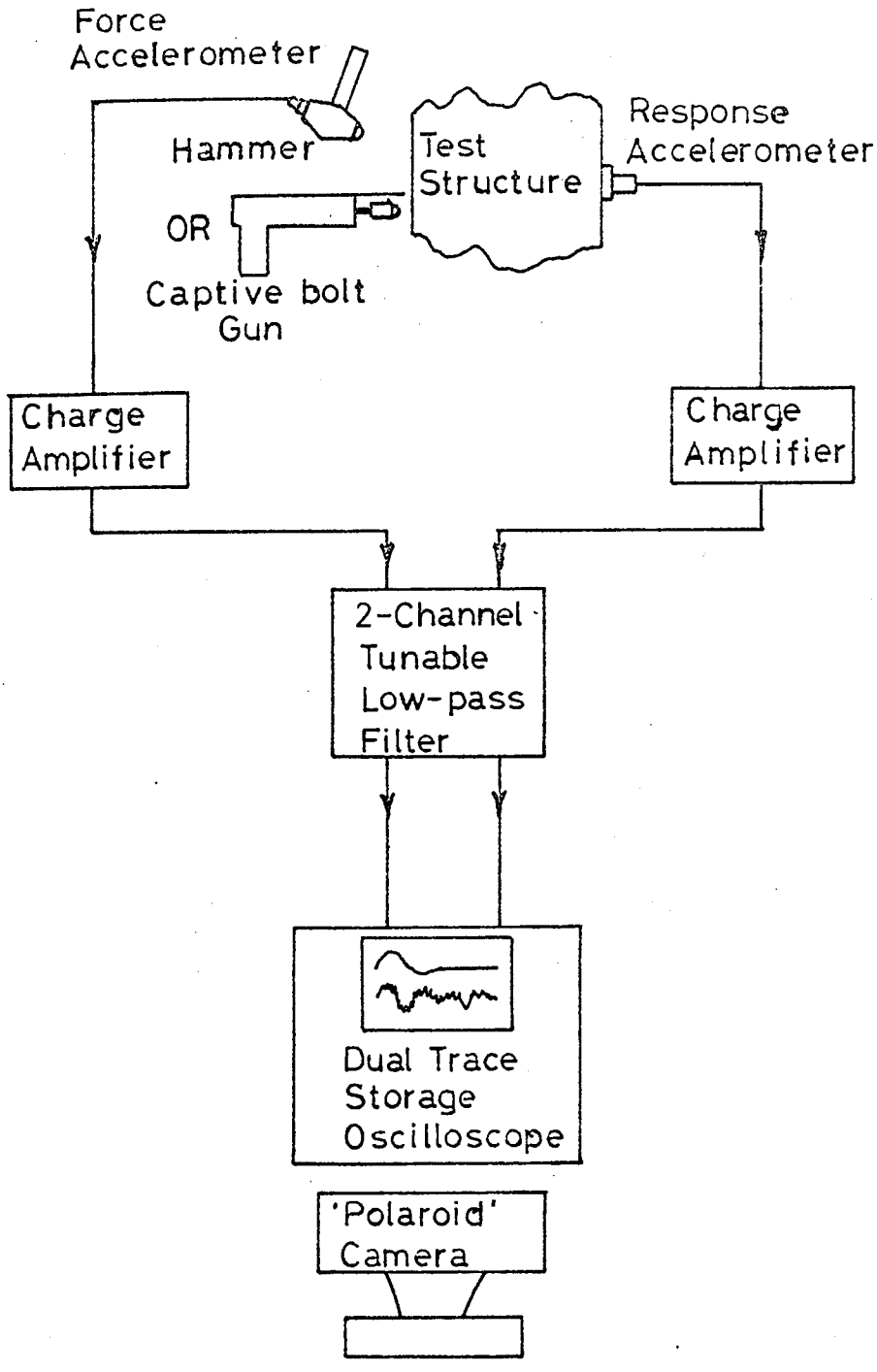

FIG.8.5 INSTRUMENTATION FOR LABORATORY TESTS.

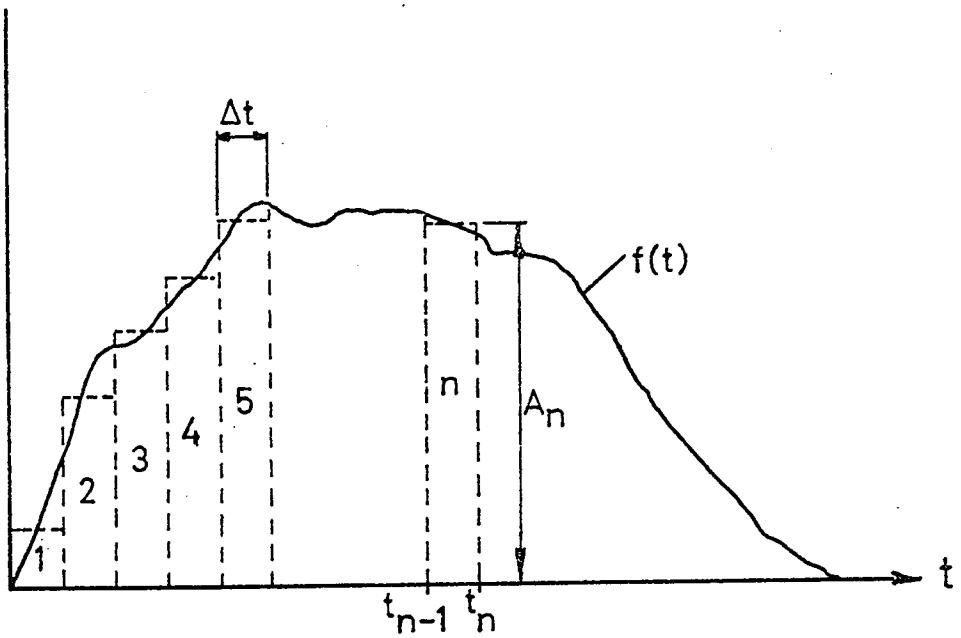

FIG.8.6 STAIRCASE FUNCTION APPROXIMATION OF TRANSIENT FOR FOURIER TRANSFORM EVALUATION.

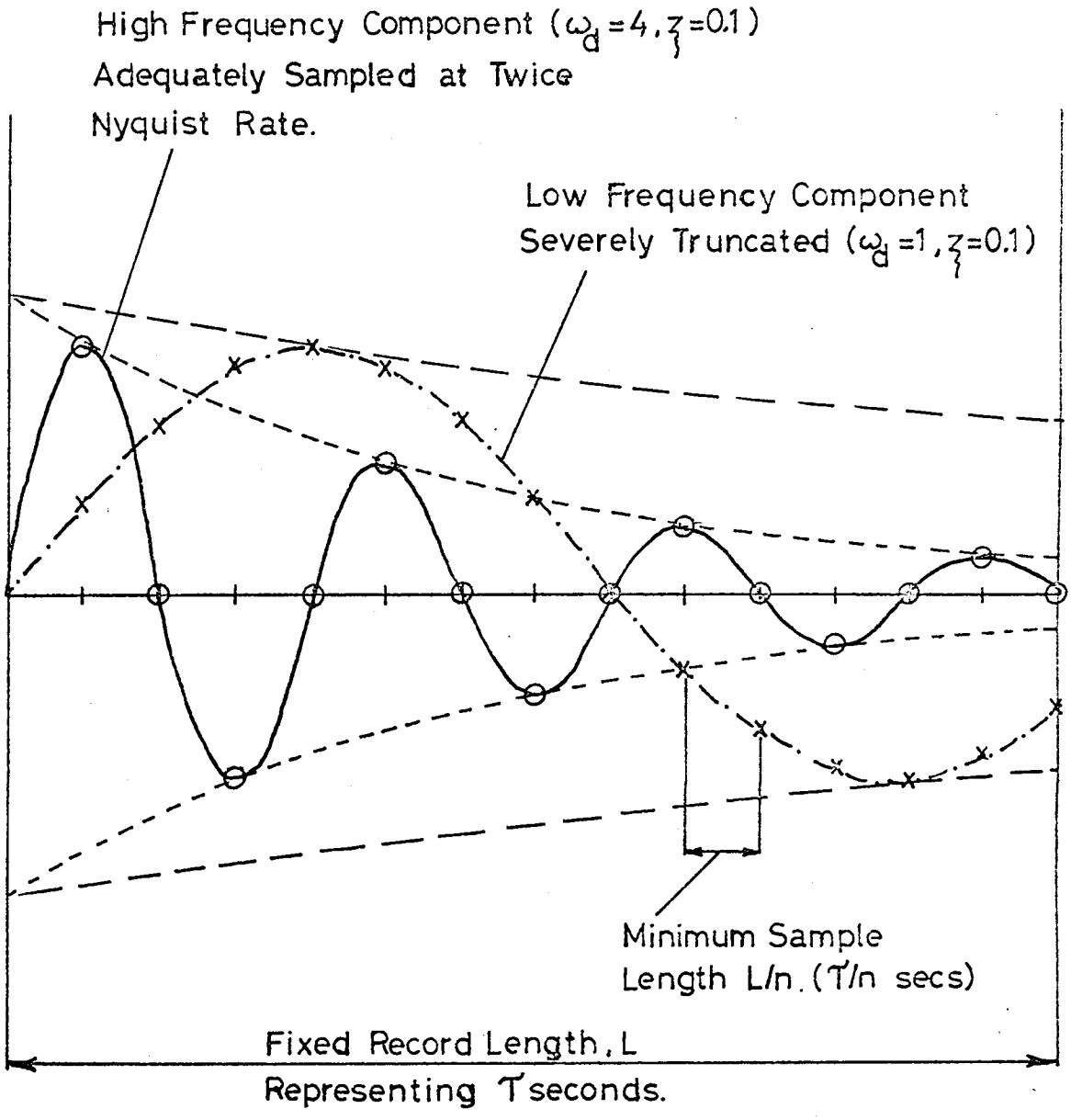

FIG8.7 SAMPLING LIMITATIONS.
OSCILLOSCOPE RECORD.

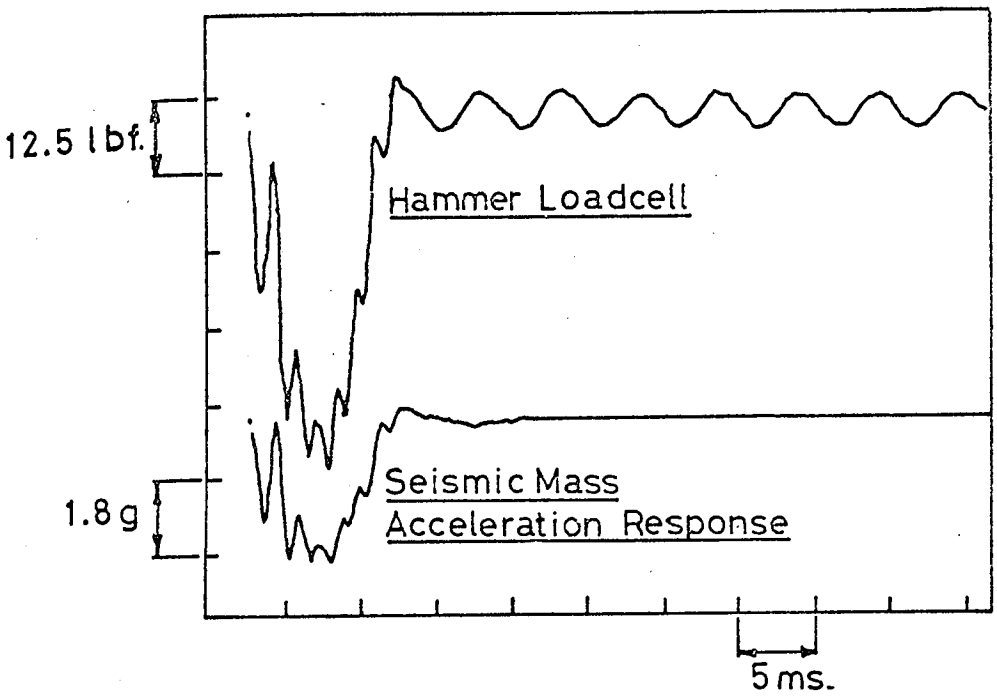

FIG.8.8(a) 17.18 lb. SEISMIC MASS RESPONSE. HAMMER SPRING 1000 lbf/in.

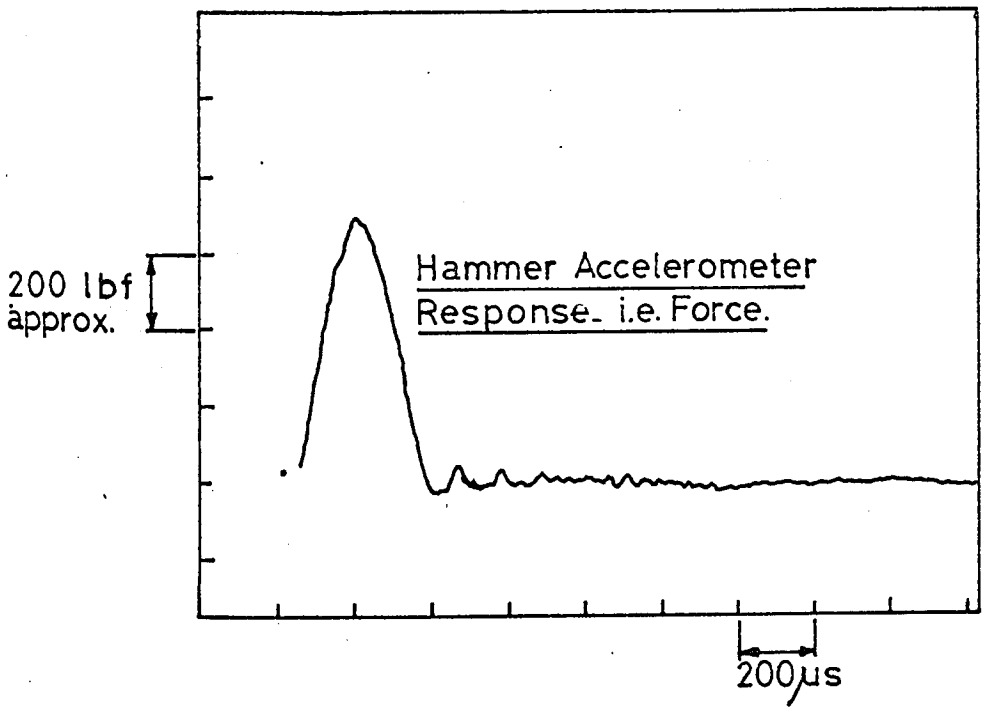

FIG. 8.8(b) TYPICAL EFFECTIVE FORCE PULSE. HAMMER WITH COPPER ANVIL.

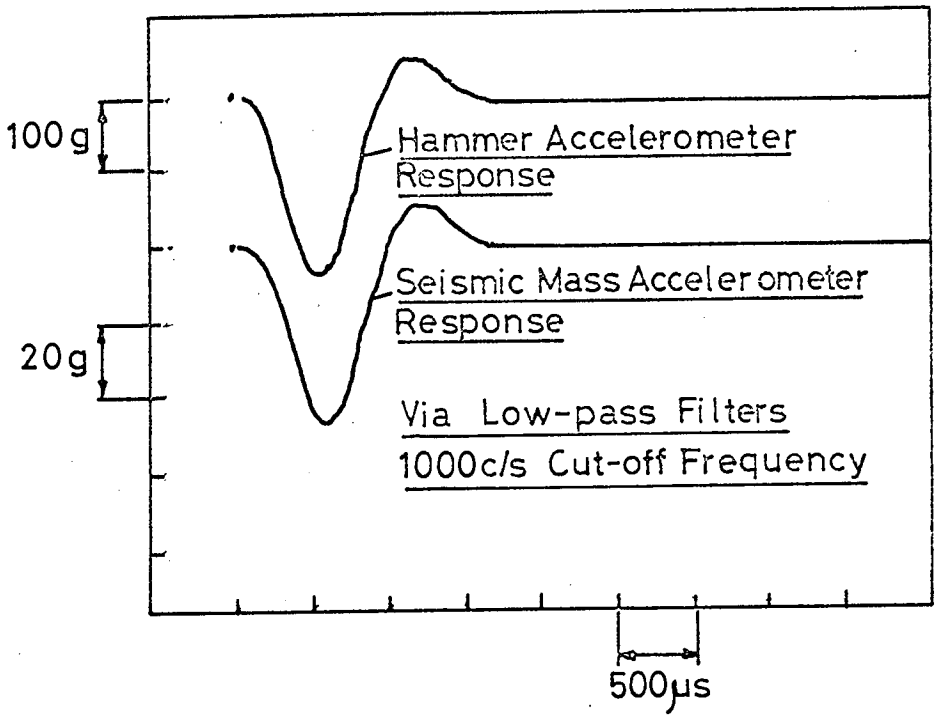

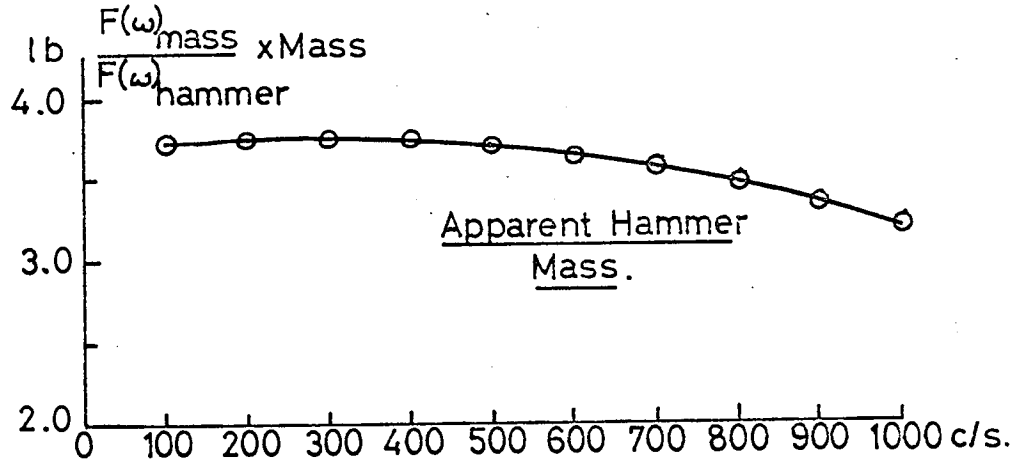

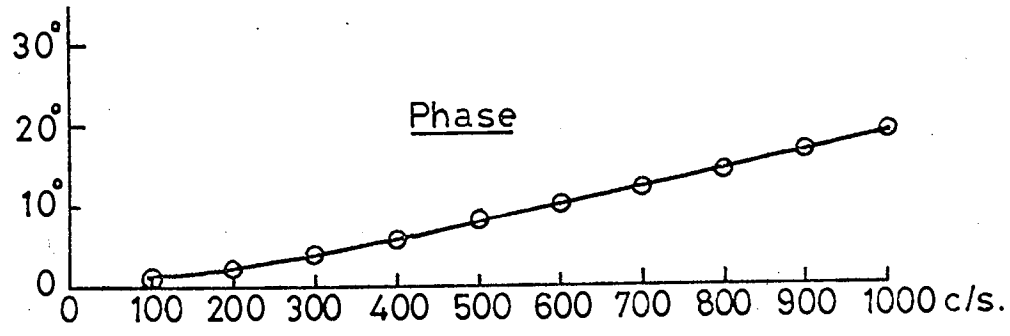

FIG.8.9 DETERMINATION OF EFFECTIVE HAMMER MASS USING 17.18lb SEISMIC MASS.

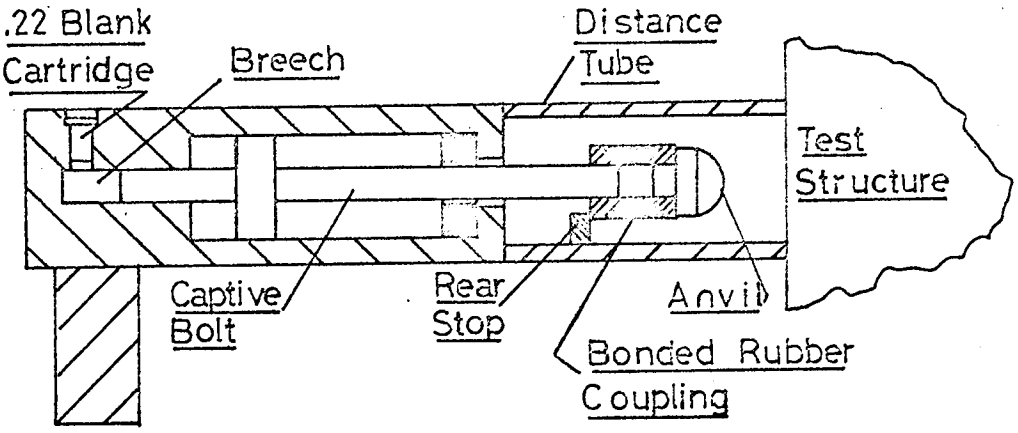

FIG.8.10(a) MODIFIED CAPTIVE BOLT GUN.

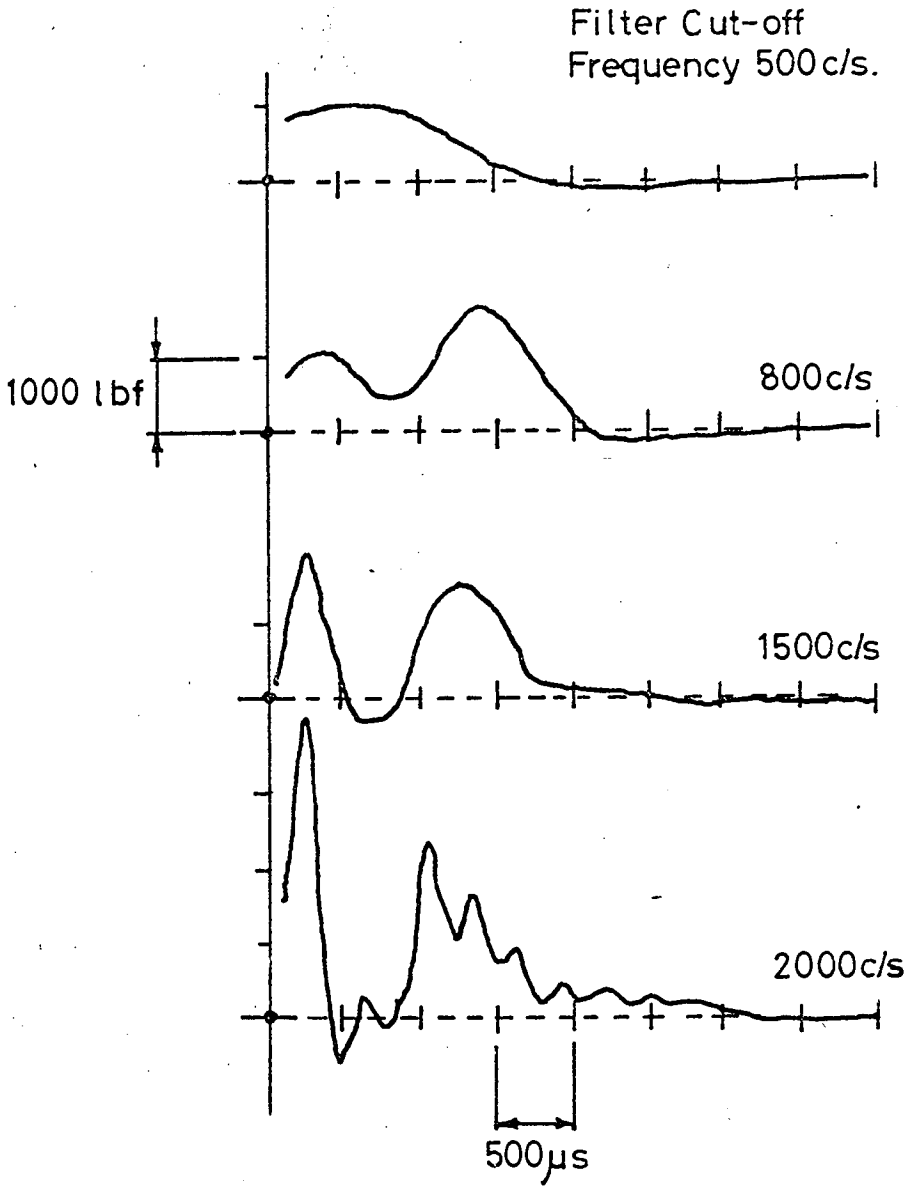

FIG.8.10(b) FILTERED FORCE PULSES.
BOLT INITIALLY EXTENDED .7 IN.

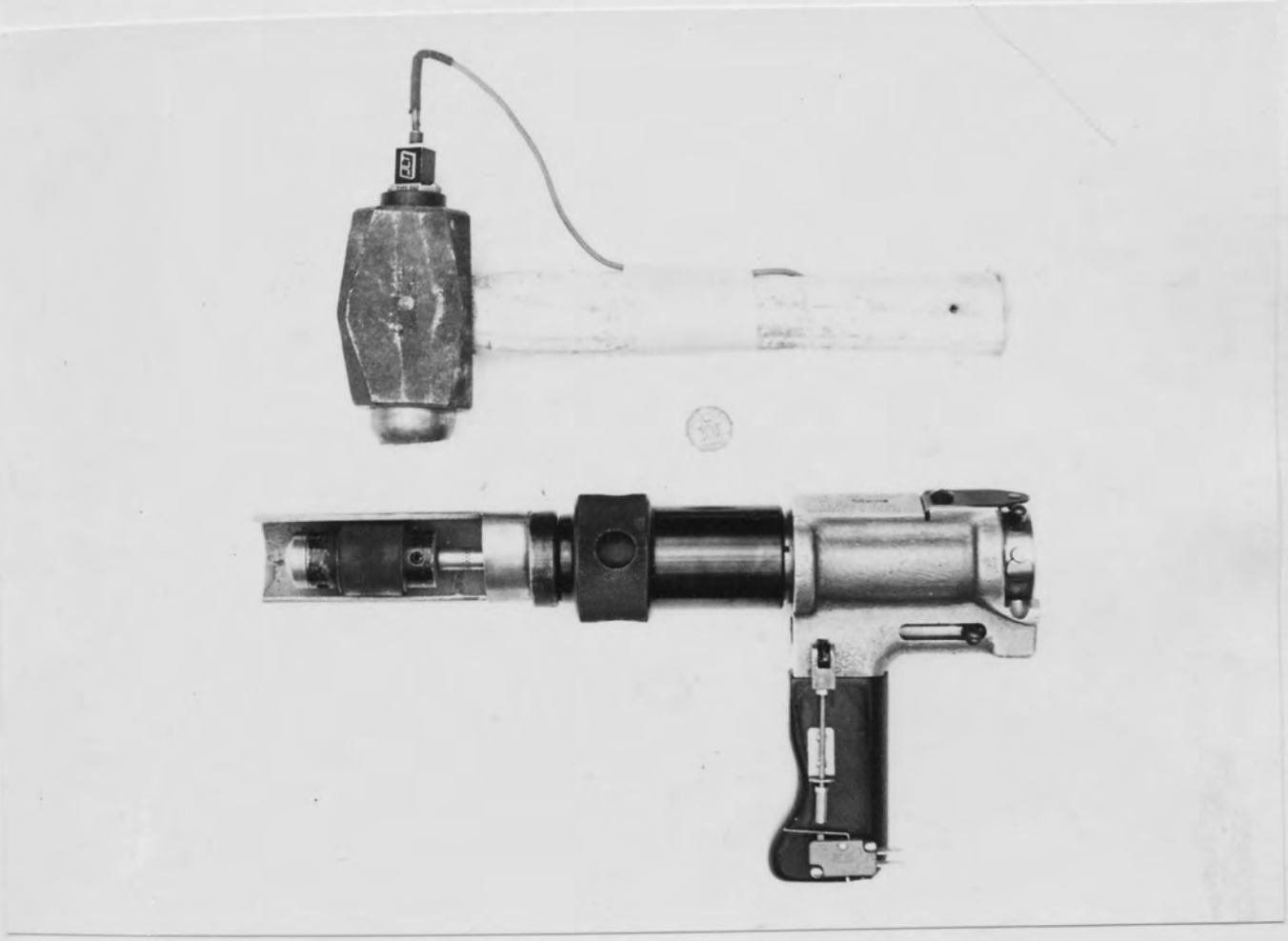

FIG.8.11. HAND HAMMER & CAPTIVE-BOLT GUN.

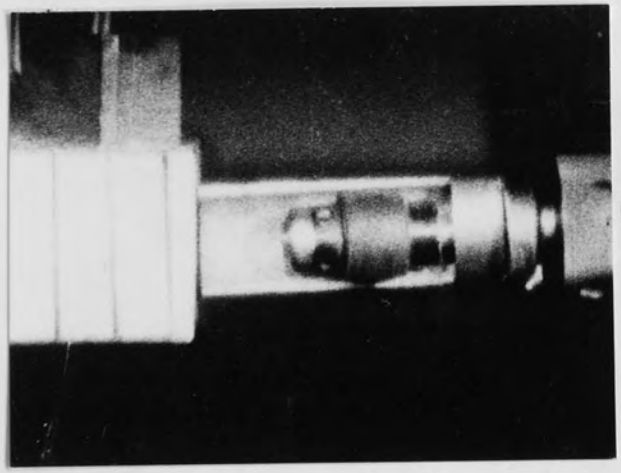

Frame 1
(.0000s)

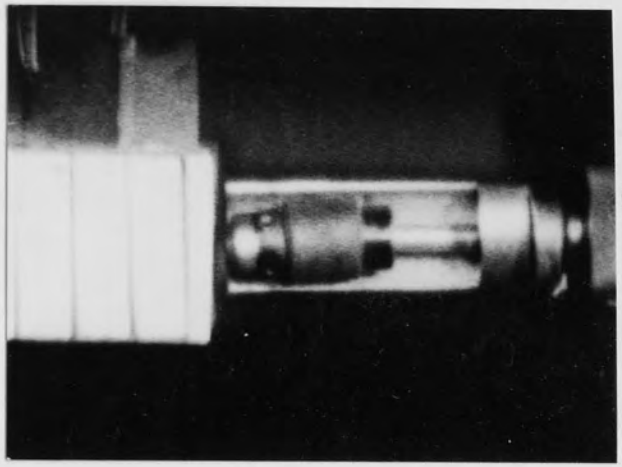

Frame 16
(.0040s)

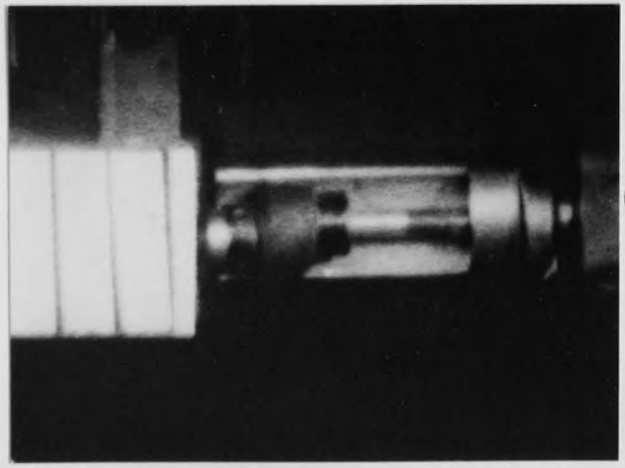

Frame 25
(.0063s)

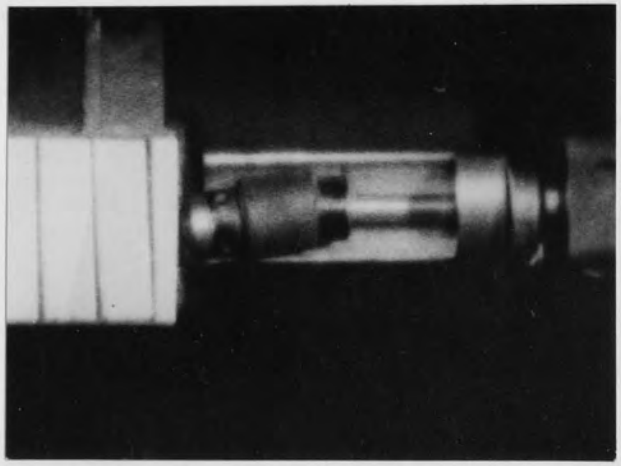

Frame 32
(.0080s)

FIG.8.12. H.S. FILM OF CAPTIVE BOLT-GUN

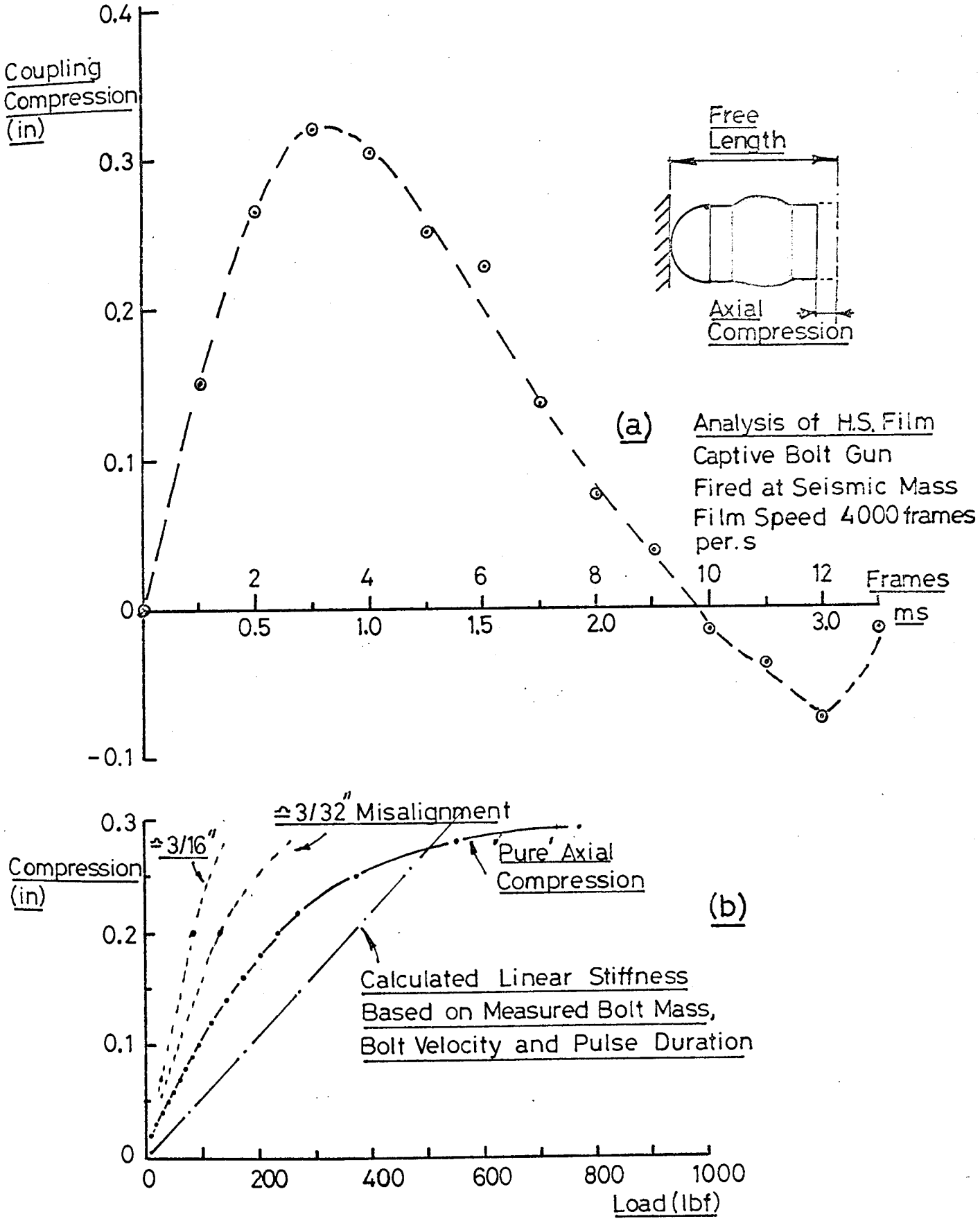

FIG 8.13. HIGH SPEED FILM ANALYSIS OF CAPTIVE BOLT GUN TEST FIRING. & STATIC STIFFNESS TESTS ON RUBBER COUPLING.

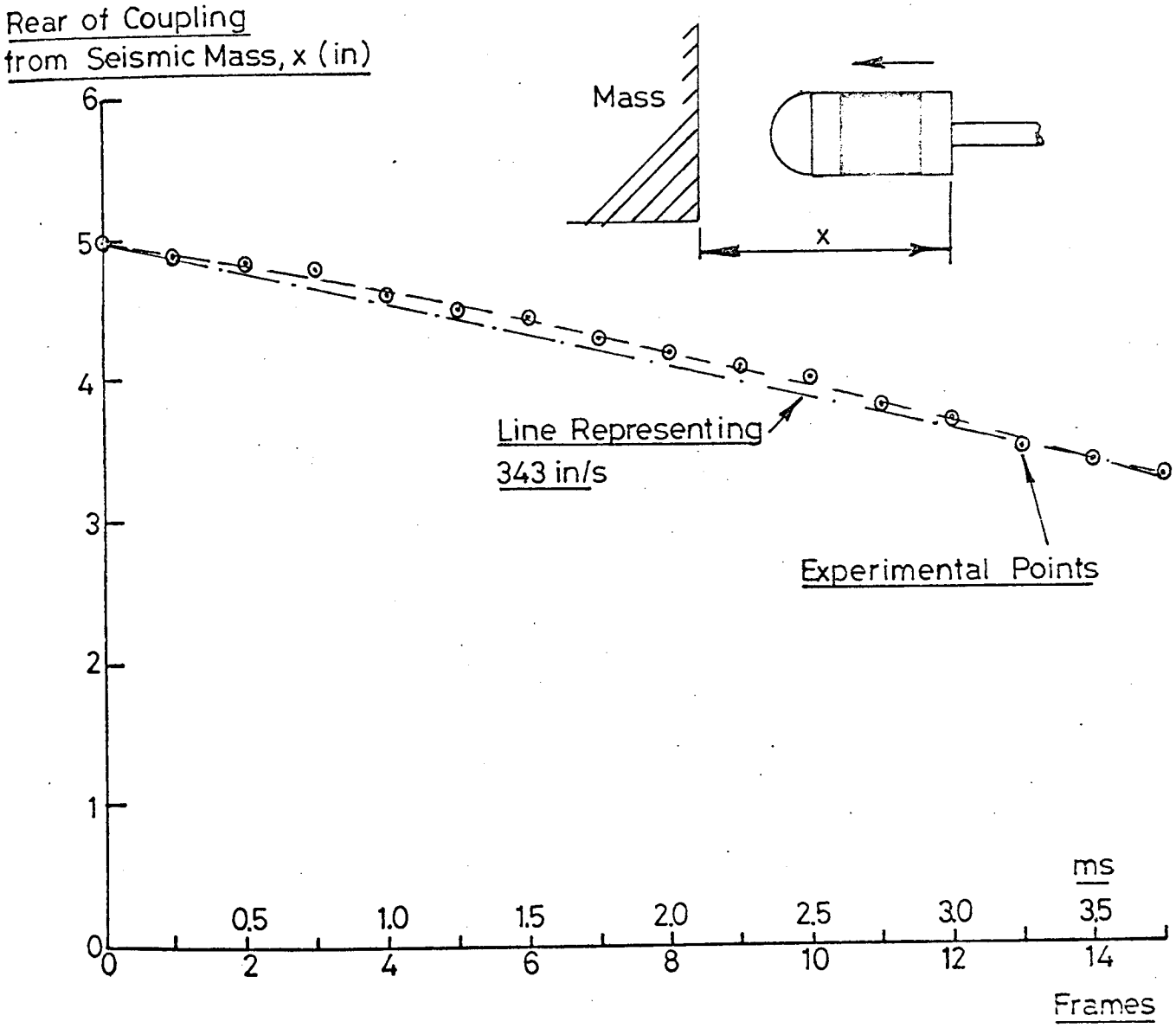

FIG.8.14. CAPTIVE BOLT VELOCITY FROM HIGH SPEED FILM. BOLT INITIALLY EXTENDED 0.7 IN FROM BREECH.

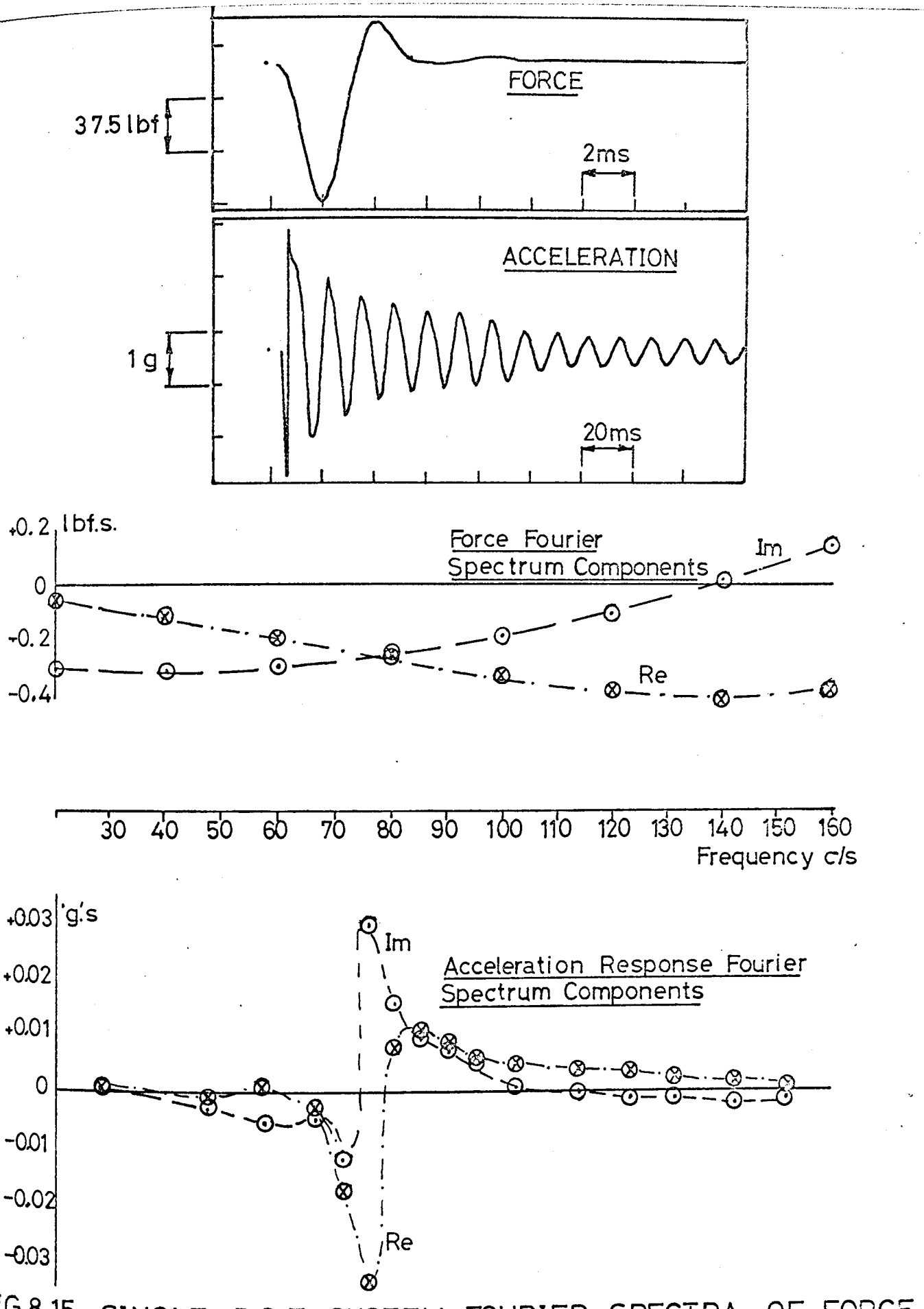

FIG.8.15. SINGLE D.O.F. SYSTEM. FOURIER SPECTRA OF FORCE AND RESPONSE TRANSIENTS

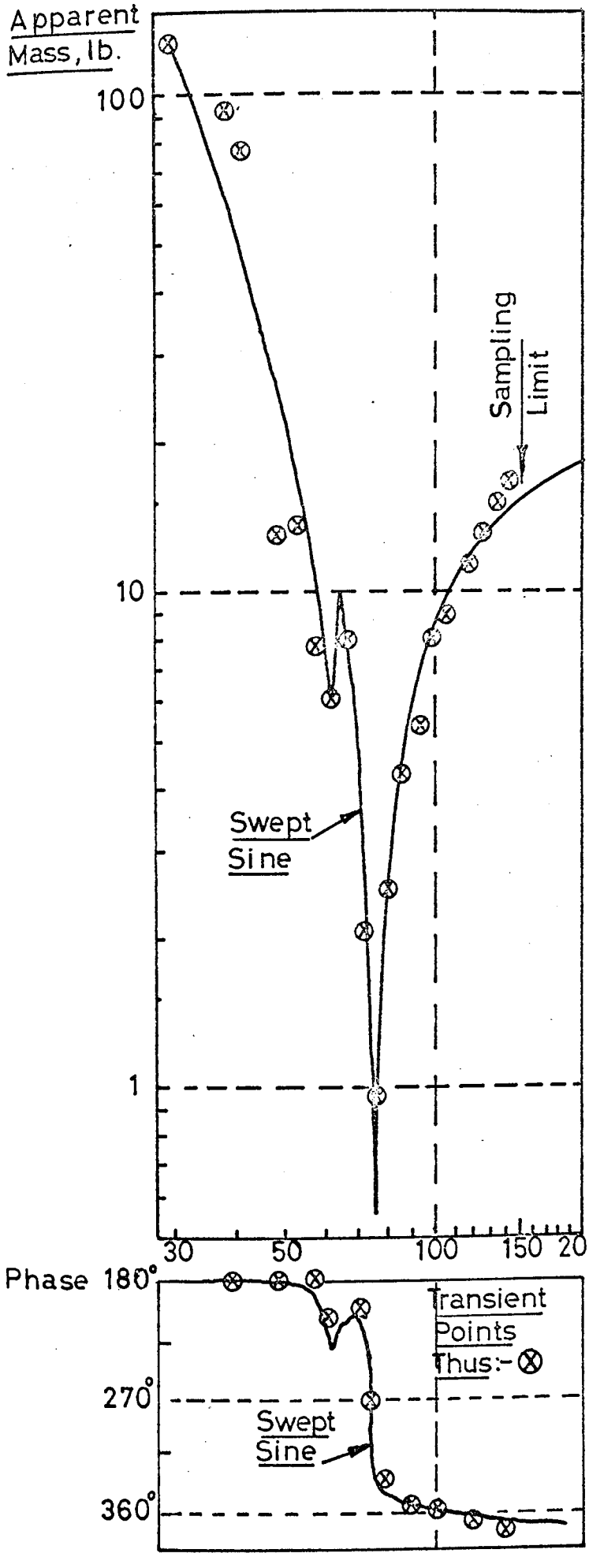

FIG.8.16 SINGLE D.O.F. SYSTEM. TRANSIENT IMPEDANCE METHOD.

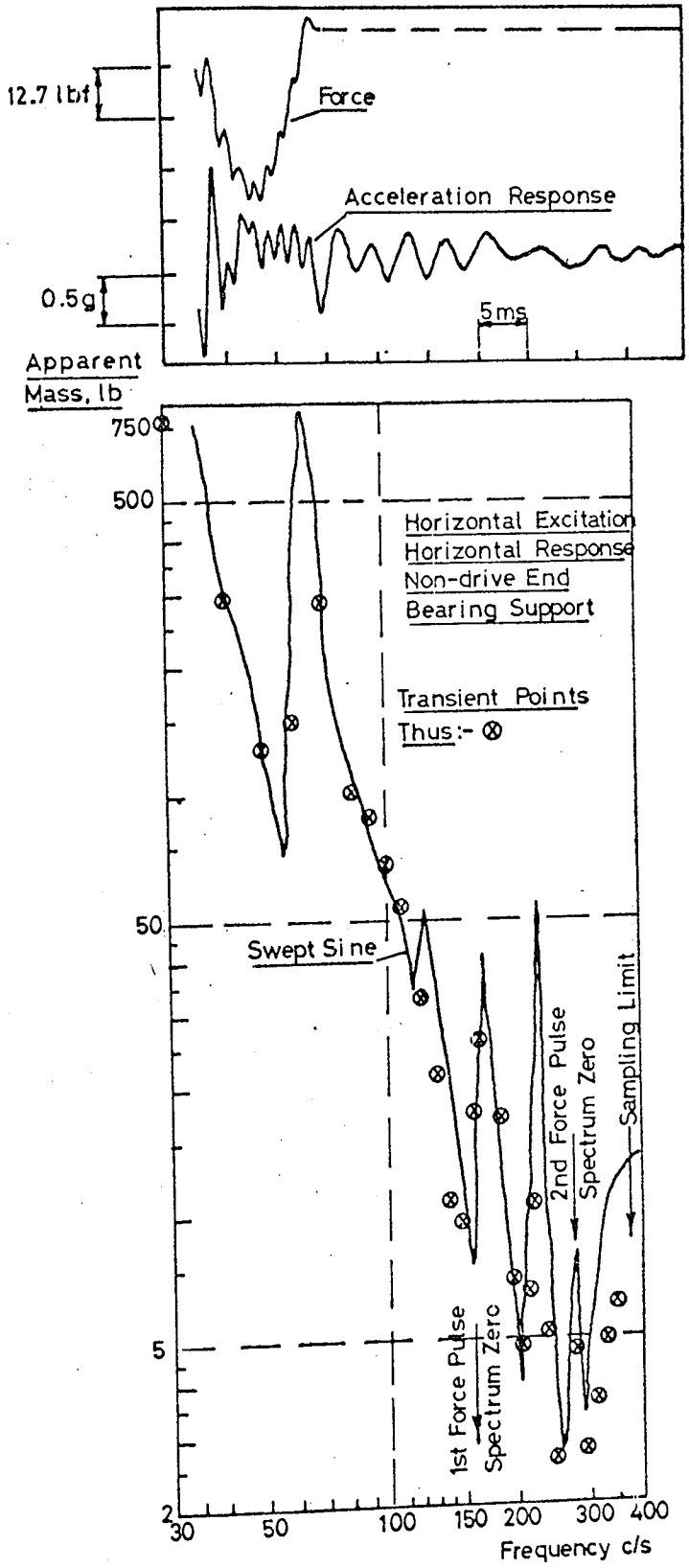

FIG.8.17 TESTS ON ROTATING MACHINE MODEL. FORCE AND RESPONSE TRANSIENTS. IMPEDANCE CURVE.

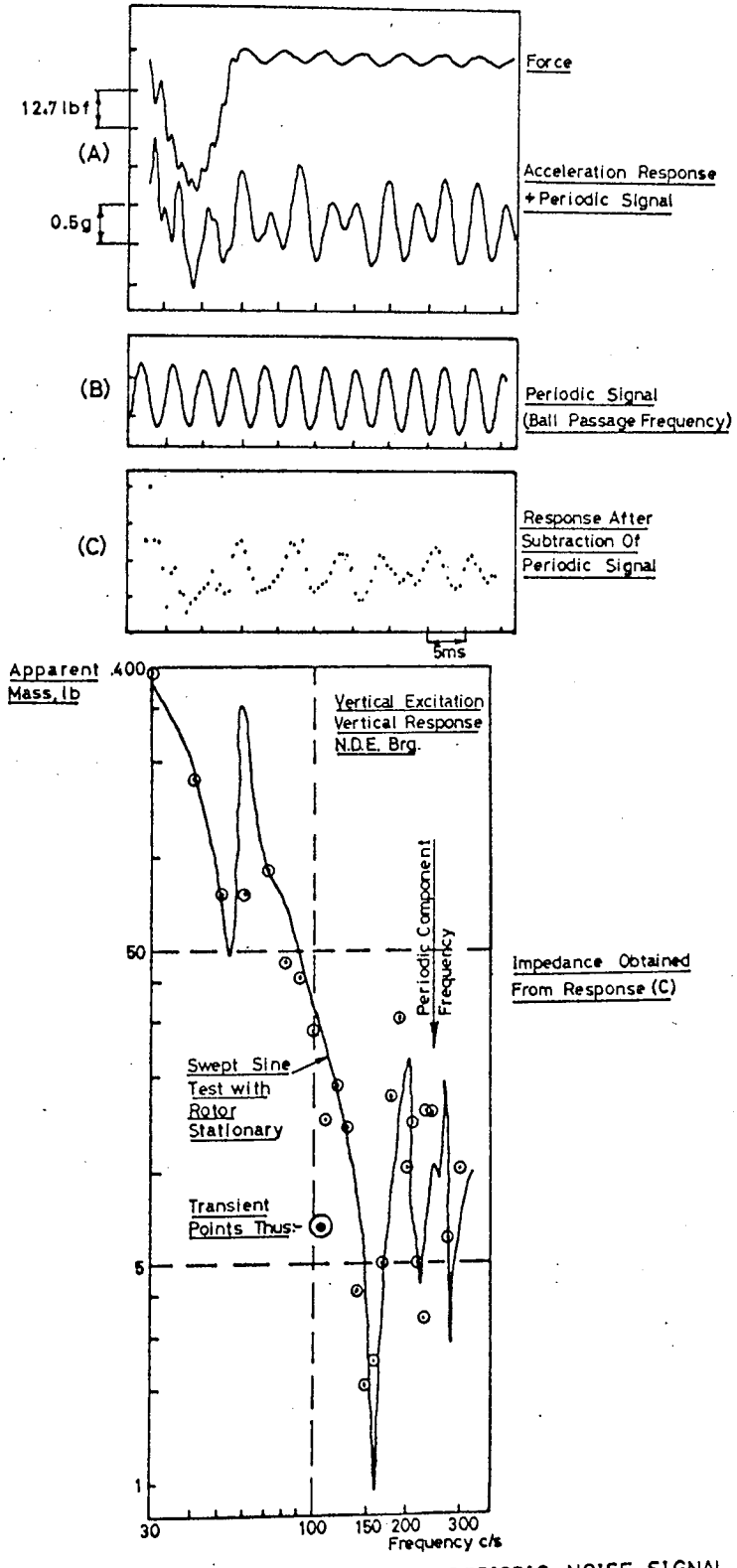

FIG.8/8 METHOD OF SUBTRACTING PERIODIC NOISE SIGNAL FROM TRANSIENT RESPONSE.
TESTS ON ROTATING MACHINE MODEL.

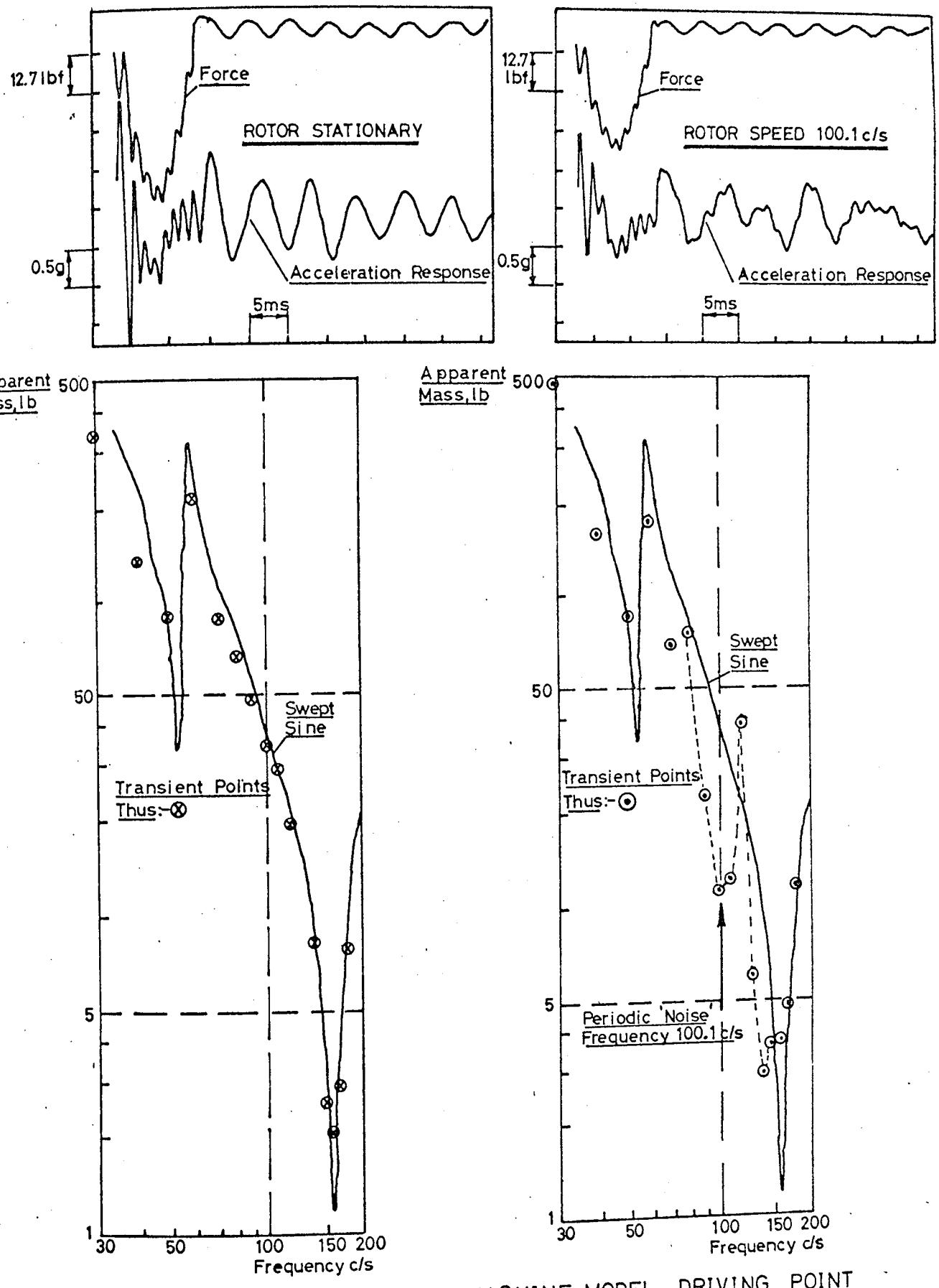

FIG.8.19. TESTS ON ROTATING MACHINE MODEL. DRIVING POINT IMPEDANCE AT BEARING SUPPORT SHOWING EFFECT OF PERIODIC NOISE.

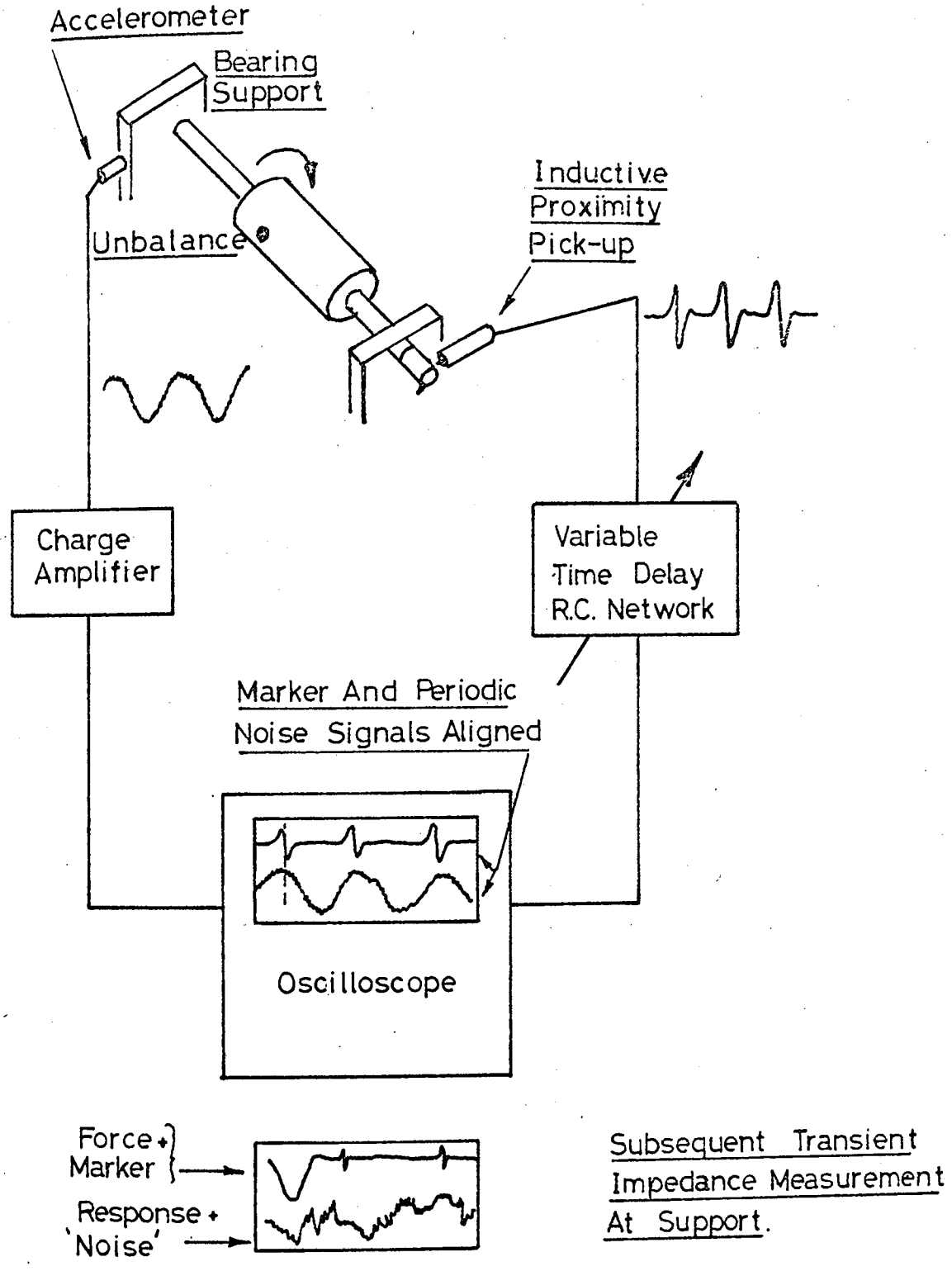

FIG.8.20 METHOD FOR IDENTIFICATION OF PERIODIC NOISE SIGNAL PHASE RELATIONSHIP.

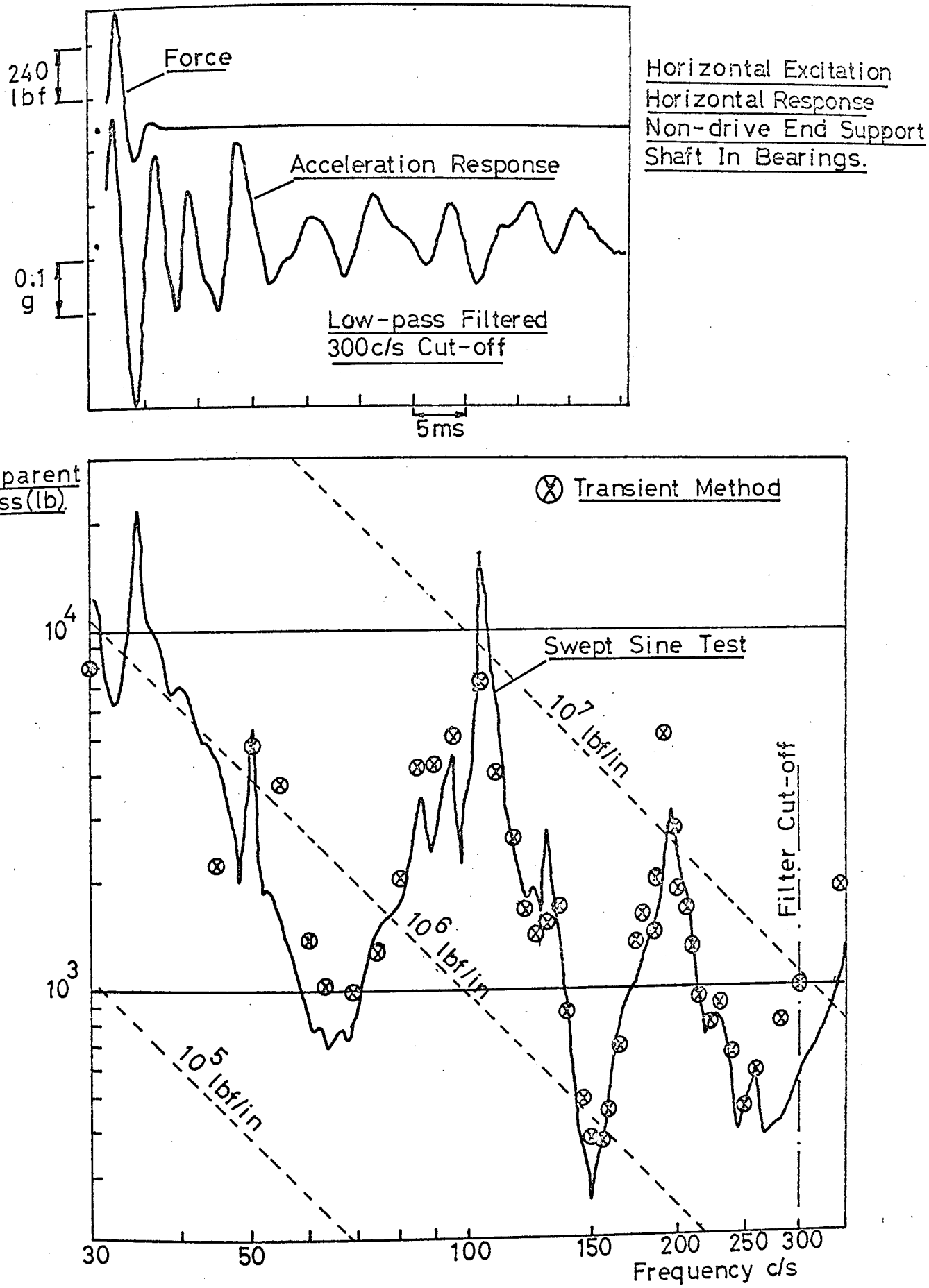

FIG8.21 FORCE & RESPONSE TIME HISTORIES.
IMPEDANCE MODULUS. ROTARY CONVERTER.

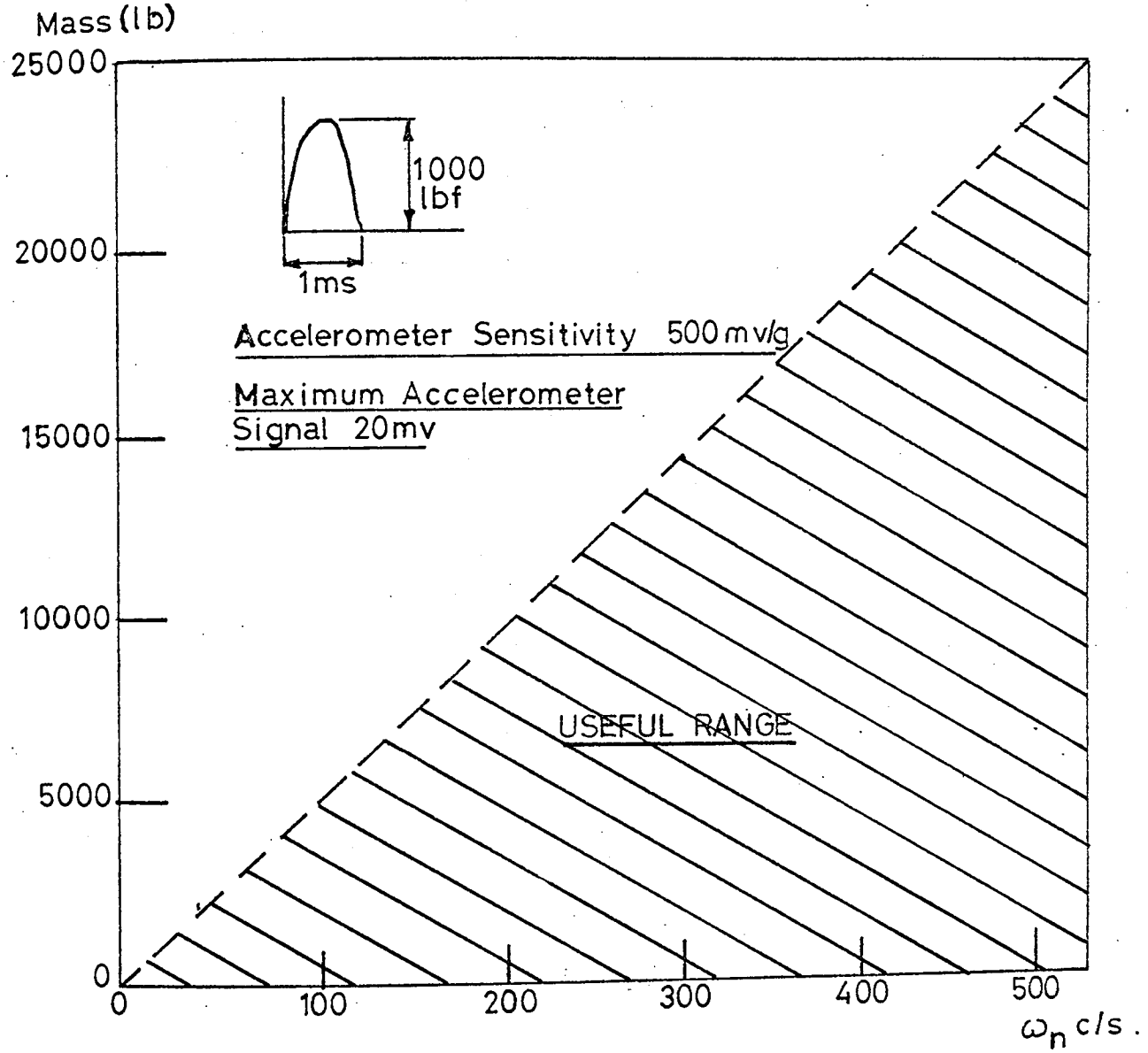

FIG.8.22. USEFUL RANGE OF TRANSIENT METHOD FOR TYPICAL OPERATING CONDITIONS. SINGLE D.O.F. SYSTEM RESPONDING TO HALF-SINE FORCE PULSE

Chapter 9.

Investigations into other methods of Transient Data Analysis

1. Introduction

The oscillographic recording of transient data considered in Chapter 8 and the subsequent evaluation of the Fourier transform from hand-sampled values at uniform time intervals requires the minimum of specialised equipment. Although hand calculation can be employed (see Chapter 8 Section 4 (iv)) a digital computer is a necessity where large amounts of information are involved. Three alternative methods of analysis have been investigated and are outlined below, which find application where conventional vibration data-reduction equipment is available. Two, correctly applied, yield "exact" results in the theoretical sense, whilst the other is approximate and intended for 'quick look' applications.

In section 9.2 the analysis of a transient signal by the synthesis of a periodic function is discussed. Although the possibility of using this approach is sometimes mentioned in the literature (for example reference (101)) very little information on experimental technique is available. In this respect the present work is believed to be original.

In order to try to overcome the inaccuracies inherent in the sampling by hand of filmed transients, a method has been investigated which makes use of a low-speed (10 samples per second maximum) digital data logger. The method required the successful slowing-down of the data by a factor of about 1000, and this was satisfactorily accomplished using standard F.M. magnetic tape-recording equipment. These experiments are discussed in section 9.3.

The third transient analysis procedure, reported in section 9.4, is thought to be original, no similar published work being known. The procedure relied on the measurement of the maximax response of a heterodyning wave-analyser to the transient signal. An automatic analysis system is described which has been found particularly useful in the analysis of transients recorded for the measurement of bearing support impedances of the industrial compressors of Chapter 10.

9.2 Periodic synthesis of transient data.

One method of deriving the Fourier integral representation of a transient is to consider the limiting case of the complex Fourier series expansion of a periodic signal as the fundamental period tends to infinity.

Consider, for example, the periodic signal consisting of a series of half-sine pulses shown in fig 9.1 (a) and defined by

$$f(t) = \left| \begin{array}{ll} Y \sin \frac{\pi t}{\tau} & 0 < t < \tau \\ 0 & \tau < t < T \end{array} \right\} \qquad (9.1)$$

The complex Fourier series representation of this signal is

$$f(t) = \sum_{n=-\infty}^{\infty} c_n e^{jn\omega_0 t} \qquad (9.2)$$

where $\omega_0 = 2\pi/T$ (9.3)

and $$c_n = \frac{1}{T} \int_0^T f(t) e^{-jn\omega_0 t} . dt \qquad (9.4)$$

Substituting from equation (9.1) into equation (9.4) yields

$$C_n = \frac{1}{T}\int_0^{\tau} Y \cdot \sin\frac{\pi t}{\tau} \cdot e^{-jn\omega_0 t} \cdot dt \qquad (9.5)$$

giving $$C_n = \frac{Y}{T}\left[\frac{e^{-jn\omega_0 t}}{\left(\frac{\pi^2}{\tau^2} - n^2\omega_0^2\right)} \cdot \left(-jn\omega_0 \sin\frac{\pi t}{\tau} - \frac{\pi}{\tau}\cdot\cos\frac{\pi t}{\tau}\right)\right]_0^{\tau} \qquad (9.6)$$

or $$C_n = \frac{Y\tau}{\pi T\left(1-\left(\frac{n\tau\omega_0}{\pi}\right)^2\right)} \cdot \left(e^{-jn\omega_0\tau} + 1\right) \qquad (9.7)$$

From which the amplitude spectrum is obtained as:-

$$|C_n| = \frac{Y\tau}{\pi T\left(1-\left(\frac{n\tau\omega_0}{\pi}\right)^2\right)} \sqrt{2\left(1+\cos n\omega_0\tau\right)} \qquad (9.8)$$

or $$|C_n| = \frac{2Y\tau}{\pi T\left(1-\left(\frac{n\tau\omega_0}{\pi}\right)^2\right)} \cdot \left|\cos\left(\frac{n\omega_0\tau}{2}\right)\right| \qquad (9.9)$$

A plot of the frequency spectrum for the particular signal parameters $\tau/T = 0.2$, $T = 1$ is shown in fig 9.1(b), from which it can be seen that the function only exists at integer multiples of the fundamental frequency 0, ω_o, $2\omega_o$, $3\omega_o$, etc. Thus as the period is increased the number of spectral lines per unit frequency increases whilst their amplitude decreases pro rata. If this process is continued, in the limit the spectrum becomes a continuous function of frequency. In fact the envelope of the line spectrum is the modulus of the Fourier transform of the single half sine pulse scaled in the ratio 1/T.

From the above, the possibility of analysing a given transient signal by first constructing a periodic signal from it appears attractive. Thus by recording the single transient on a continuous magnetic tape loop and replaying the resultant periodic signal through a wave analyser, a line spectrum may be plotted whose envelope contains the required information. Several conflicting requirements occur in practice, however,

For example, to obtain maximum frequency resolution the tape loop period must be as long as possible (i.e. spectral lines close together), whilst to obtain the maximum line spectrum amplitude this period should be at a minimum. One overriding limitation is governed by the minimum loop period attainable (i.e. maximum tape speed, minimum tape length) and the narrowest effective filter bandwidth available. The filter must only pass a single harmonic of the fundamental loop passage frequency.

With the equipment available to the writer (E.M.I.2500 loop deck, see chapter 5) the maximum tape passage frequency that could be achieved using a tape speed of 120 in/sec was of the order of 4 c/s, although

these conditions produced very rapid tape wear. The short loop also meant that the tape was incorrectly supported during its passage over the record and replay heads such that considerable signal distortion occurred at fast tape speeds. Some compromise was therefore necessary, but the most reliable analyses resulted from the use of tape speed at 60 in/sec and a loop passage frequency of about $2\frac{1}{4}$ c/s.

Considerable errors in the analysis can occur due to the inclusion in the synthesised signal of tape joint and switching transients. Some improvement in results could be obtained by arranging to 'squelch' the signal during passage of the tape joint past the replay heads but no ideal method has yet been found by the writer suitable where very short tape lengths are used. Fig. 9.2. illustrates the effect of unwanted signals on the analysis of a force pulse obtained during tests on the rotary converter discussed in Chapter 7. For the sake of comparison, values at discrete frequencies of the modulus of the Fourier transform of the single pulse, multiplied by the scaling factor I/T, as calculated on the digital computer are also shown. In these tests the pulse was first recorded, after low pass filtering, on the Ampex FR 1300 F.M.tape recorder and then re-recorded on to the continuous tape loop. The Quantech Model 304 wave analyser (see Chapter 5) was used for the line spectrum analysis, the narrowest filter bandwidth of 1 c/s being necessary to ensure satisfactory rejection of adjacent loop-frequency harmonics.

Fig 9.3 shows the acceleration response time history resulting from the force pulse discussed above together with the synthesised periodic signal obtained on re-playing the continuous tape loop. By using a new tape loop and ensuring a good quality joint little error was introduced into the analysis, as can be seen from the comparison with the computed discrete points for the single pulse.

The apparent mass of the machine support obtained from the envelope of the response line spectra of fig 9.3 and the 'correct' force pulse spectra is shown in fig 9.4. These results are compared with the swept sine test results.

9.3 Analysis of Transients using Low-speed Digital Data Logger

Two drawbacks of the methods discussed in Chapter 8 for the analysis of transients from filmed oscillographic records were the limited dynamic range and the errors introduced by truncation of the response time history due to the finite record length (see Appendix II).

These problems could be largely overcome by using the high-speed digital data-sampling instruments now available commercially. Such equipment normally uses electronic switching and binary-coded core-type 'memories' giving the extremely fast handling rates associated with digital computers. Since sampling can be performed at several thousand samples per second, data having a significant frequency content up to at least 1 Kc/s can be processed 'on-line'. In addition a very wide dynamic range is available limited only by the resolution of the detector and the size of the memory or store.

Unfortunately, no equipment of this type was available to the writer but a series of experiments were performed to assess the feasibility of using an existing, low-speed data logger whose maximum sampling rate was 10 per second. This instrument was manufactured by Dynamco Ltd. and had been designed around a D.M.2022 digital voltmeter, the latter having 5-digit resolution. Mechanical (relay) sampling of the input data was incorporated, the digital voltmeter reading being encoded in binary form and punched onto paper tape for each sampling operation.

Due to the low sampling rate the absolute maximum data frequency that could be adequately resolved was about 5 c/s, based on the Nyquist criterion. To obtain reliable results without the possibility of aliasing errors this frequency was effectively reduced to 2.5 c/s, i.e. four samples per cycle. Attention was therefore directed at slowing down the original tape-recorded data so as to increase the 'real-time' sampling rate (see fig 9.5).

Contrary to expectation it was found possible to achieve overall data speed reductions of up to about 1000:1 with only a slight increase in signal to noise ratio. This was accomplished by successive transcription from the Ampex FR 1300 tape recorder onto the E.M.I. loop deck and back again. (see Chapter 5 for details of these instruments).

Apart from the limitations imposed by the quality of the recorded signal, the maximum possible speed reduction was governed by the length of the tape loop if truncation of the transient was to be avoided. This represented a maximum loop period of approximately 25 seconds at 15 ins/s tape speed. The table below illustrates a typical series of speed reductions used and indicates the resulting duration of an assumed 100ms, 'real-time', response transient after each recording.

Tape Recorder	Record		Replay		Speed Reduction Overall
	Tape Speed in/s	Transient Duration sec	Tape Speed in/s	Transient Duration sec	
E.M.I.Loop	60	0.1	15	0.4	4
Ampex	60	0.4	$1\frac{7}{8}$	12.8	128
E.M.I.Loop	15	12.8	15	12.8	128
Ampex	60	12.8	$7\frac{1}{2}$	102.4	1024

Fig 9.6 shows an acceleration response transient, recorded during tests on one of the centrifugal compressors of Chapter 10, as replayed from the original site recording, and after a speed reduction up to 1024:1, according to the sequence indicated in the above table. Apart from a slight 'blurring' of the wave form, caused by high frequency noise, the final recording is seen to be of good quality.

As in all instrumentation tape recording this quality was only achieved by careful attention to detail. Perfectly clean, demagnetised record and reproduce heads, together with a well made joint in the tape-loop, were found to be essential. For, since any defects in the recordings were cumulative as the speed reduction process was continued, it was discovered in earlier tests that the original transient could become completely unrecognisable by the time the final recording operation had been reached.

With the transient successfully slowed-down by 1000:1, the digital logger was used to give sampling up to a maximum frequency limit of 2.5 Kc/s referred to the original input data. The punched tape output was then processed on the University's Elliott 803 computer to obtain the Fourier Transform of the transient waveform in a manner similar to that discussed with reference to filmed records in Chapter 8 section 2 (iv).

9.4 Approximate Method-Wave Analyser Response Spectrum

In general, the calculation of the shock response spectrum of a linear system from its known transfer function and the known Fourier spectrum of the input transient is an irreversible process. A measure of correlation does exist, however, for example the Fourier spectrum of a unit impulse input function is a constant (a line parallel to the frequency axis), whilst the maximax response of a simple oscillator

to this input increases in a linear fashion as its natural frequency increases

More specifically, the after-shock response of a simple undamped oscillator is related to the input spectrum. For example, consider the response of a single mass-spring system of natural frequency ω_n to the acceleration transient $a(\tau)$ of duration T. If the transient is imagined to be divided into a series of step functions spaced at intervals $\Delta\tau$ then the change in input velocity, Δv , per step is

$$\Delta v = a(\tau).\Delta\tau \tag{9.10}$$

By applying the principle of superposition in the form of Duhamel's integral the total response V at time t after the transient has occurred is

$$V = \int_0^T h(t-\tau).\, a(\tau)\, d\tau \tag{9.11}$$

where $h(t-\tau)$ is the unit step response function for the system. For the single degree of freedom system considered this is

$$h(t-\tau) = 1 - \cos\omega_n(t-\tau) \tag{9.12}$$

when substituting in equation (9.11)

$$V = \int_0^T \left[1 - \cos.\omega_n(t-\tau)\right] a(\tau).\, d\tau \tag{9.13}$$

Since the input transient is considered zero outside the range 0 to T the limits of integration in equation (9.13) may be replaced by $-\infty$ to $+\infty$ without affecting the result.

Thus

$$V = \int_{-\infty}^{\infty} \left[1 - \cos \omega_n (t-\tau)\right] . a(\tau) . d\tau \qquad (9.14)$$

or $$V = \int_{-\infty}^{\infty} a(\tau) . d\tau - \int_{-\infty}^{\infty} a(\tau) . \cos \omega_n (t-\tau) . d\tau \qquad (9.15)$$

The first integral in equation (9.15) must be zero for a transient waveform and hence

$$V = -\int_{-\infty}^{\infty} a(\tau) \cos \omega_n (t-\tau) . d\tau \qquad (9.16)$$

The R.H.S. of equation (9.16) is an expression for the Fourier spectrum of the input transient as anticipated (see Chapter 8 section 2)

Since it is often convenient to have an approximate measure of mechanical impedance without resorting to full scale analysis a method of obtaining such an estimate has been investigated which relies basically on the measurement of the maximax response of tunable electronic filter circuits to the force and response transients. The method described only yields values of the modulus of impedance with no corresponding phase angle, but since this is frequently all that is required it may warrant some consideration.

Ideally, the response spectrum of a given filter circuit could be calculated for particular input transients. Typical commercially available wave analysers, however, are specifically designed to have very steep filter "skirts" often giving rejections outside the intended pass band of the order of 30 to 40 db. per octave. Since they are

then described only approximately even by fourth or fifth order transfer functions, little reliable quantitative information can be gained from the analytical treatment of the circuit as a simple resonator. On the other hand, even if the transfer function is known analytically, extensive calculations using the more exact function are time consuming. In practice 'calibration' of the maximax analyser response for known pulse shapes has been found the best course of action.

It might be argued that the use of simpler filter circuits would be the most sensible approach, particularly as active networks can be readily constructed using modern, solid-state, operational amplifiers. Wave analysers of the heterodyne type, however, have been found to give response spectra for simple transients more nearly proportional to the corresponding Fourier spectra.

One arrangement that has been used satisfactorily is illustrated in fig 9.7(a) . The peak value memory circuit shown had been developed to give very fast rise times, compatible with those encountered at high filter centre frequencies, whilst having a long delay time constant to enable the maximum value to be measured.

The operation of this circuit is shown in fig 9.7 (b) where the circuit input, a filter response time history, is illustrated together with the corresponding output. For analysis of transients using this method the Quantech Model 304 wave analyser (see Chapter 5) has been used extensively since this instrument could be easily transported. Another filter system used occasionally was the Spectral Dynamics SD 101A tracking filter. Initial tests to obtain mechanical impedance were conducted by adjusting the filter to the centre frequency of interest, passing the voltage analogue of the forcing transient through the filter, and measuring the maximum filter response. This procedure was then

repeated for the acceleration response analogue of the mechanical system under investigation. To ensure constant amplitude force pulses where the modified hand hammer was used, the latter was supported as a pendulum and released from rest from a predetermined height. A plot of the estimated mechanical impedance at discrete filter centre frequencies was then obtained from the maximum filter response due to the forcing transient and that due to the acceleration transient. The results obtained by this means for the single degree of freedom system (Chapter 8, Section 5 (ii)) are shown in fig 9.8.

A development of the above method has also been used to provide automatic plotting of maximax response whilst the filter centre frequency is swept continuously throughout a range of interest. This facility was particularly useful where a wave analyser response was to be calibrated for given input transients. The arrangement used is sketched in fig 9.9 from which it can be seen that the transient of interest was recorded on a magnetic tape loop. The repetition period of the loop was made as long as practicable such that the filter response was sensibly due to the passage of a single transient. Loop periods of around 25 seconds were found to be satisfactory. Since the filter centre frequency was slowly increasing, its maximax response due to each successive passage of transient differed, in general, from the previous one. It was therefore necessary to discharge the peak value memory circuit after each maximum had been recorded by the X - Y plotter. To produce a well defined plot and to minimise the effect of pen overshoot and unwanted tape-joint transients, it was also necessary to lift the plotter pen after each maximum had occurred. These switching operations were effected by G.P.O. type Uniselector triggered via a single stage amplifier from pulses recorded on another track of the magnetic tape.

The sequence of events therefore involved discharging the memory circuit immediately before passage of the recorded transient and "pen down", "pen up" commands after the filter, memory circuit and plotter had responded. In practice, since the number of indexed positions on the Uniselector was not exactly divisible by the number of operations required, redundant pulses were also recorded to ensure continuous correct switching. The results of so analysing force and response transients obtained during tests on the rotary converter of Chapter 7 are shown in fig 9.10. The estimated impedance plot obtained by direct division of force and response points is also shown and compared with the corresponding swept sine test results.

It may be mentioned here that future work is anticipated to develop the above method for use on the Spectral Dynamics mechanical impedance system discussed in Chapter 5. In this case it is hoped to use the maximax responses of the SD 101A tracking filters as inputs to the logarithmic converters. It should then be possible to obtain the impedance of the test structure directly and plot this automatically to a logarithmic scale, thereby greatly increasing the dynamic range of the measurement.

9.5 Conclusions

The three methods of transient data analysis presented in this chapter have all been been successfully for obtaining the mechanical impedance of bearing support structures of the centrifugal compressors of Chapter 10.

A reasonably fast analysis time (about 20 minutes) and the most straightforward data preparation were achieved with the filter shock spectrum method of section 9.4, although no phase relationship was obtainable.

Phase could be obtained from the slow-speed data logger technique of section 9.3, but this method was very tedious and the resulting data still required processing on the digital computer.

Acceptable analysis times of between 15 and 30 minutes were also possible with the method involving synthesis of a periodic signal (section 9.2) and with some modification phase could also be obtained. However, the difficulties involved in achieving good recordings at the requisite tape-loop speeds tended to detract from the method.

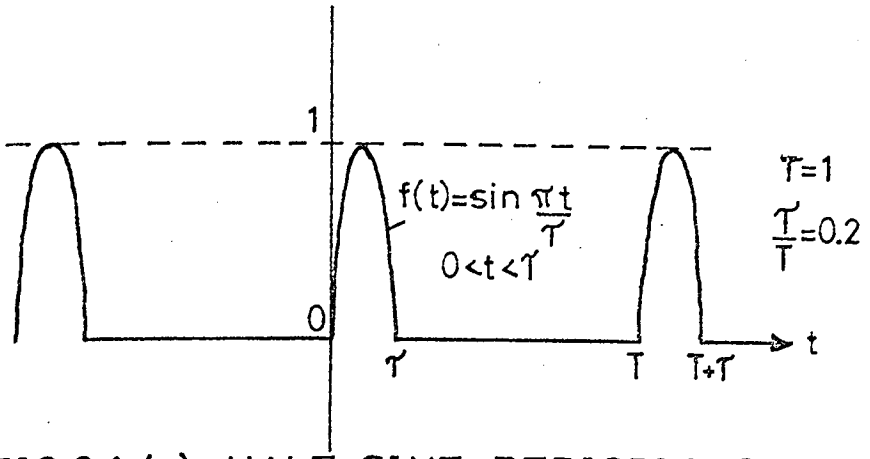

FIG.9.1 (a) HALF-SINE PERIODIC SIGNAL.

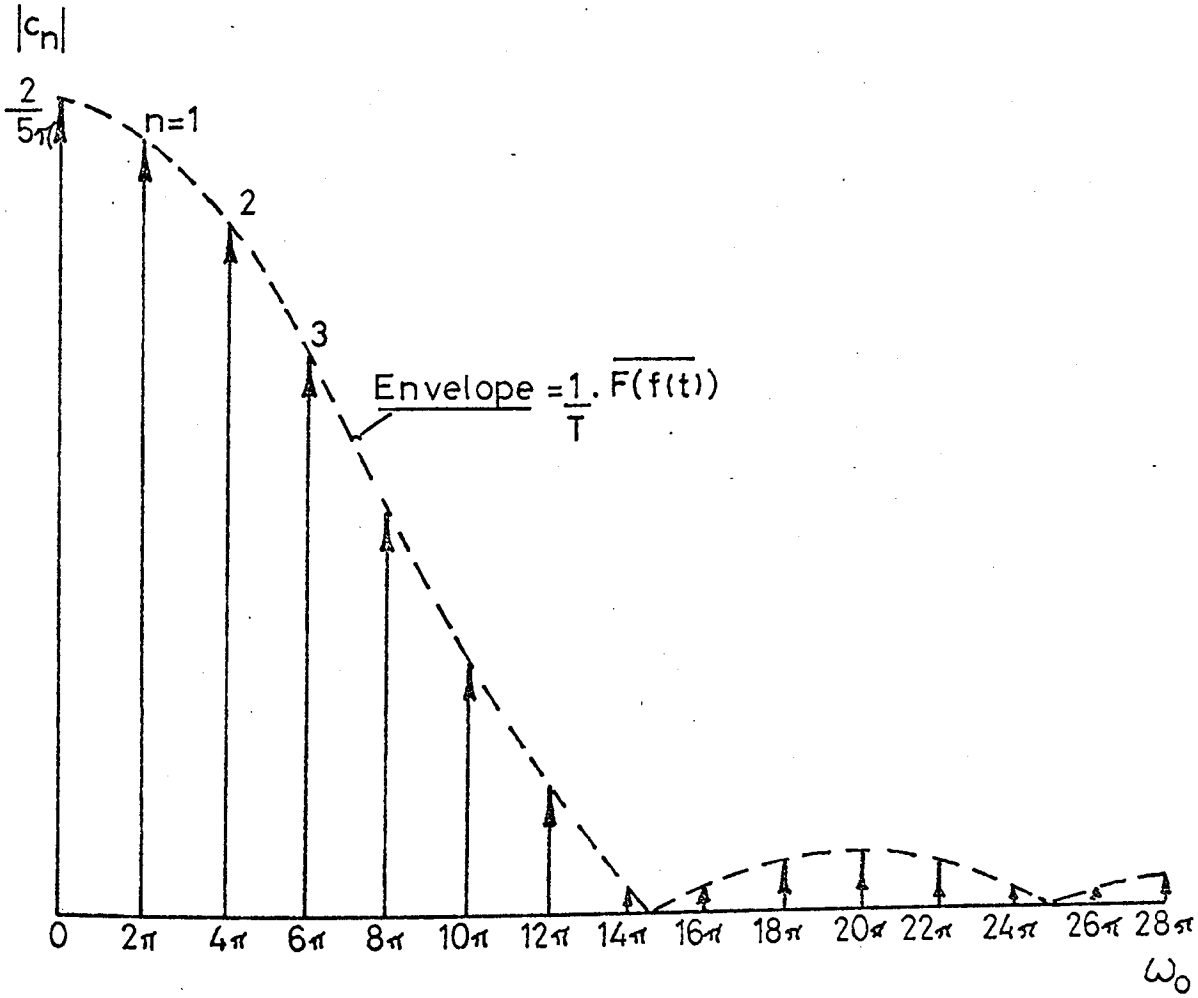

FIG.9.1 (b) COMPLEX FOURIER SERIES AMPLITUDE SPECTRUM.

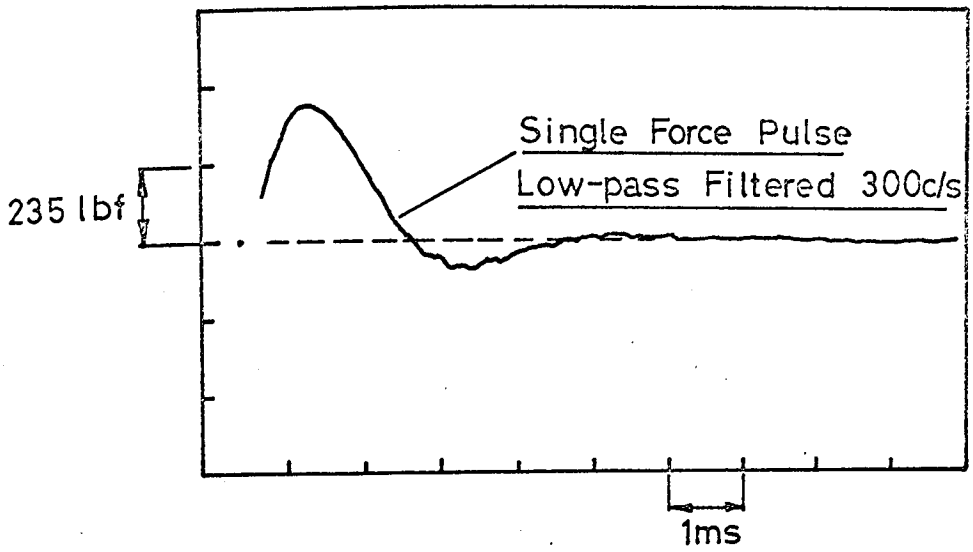

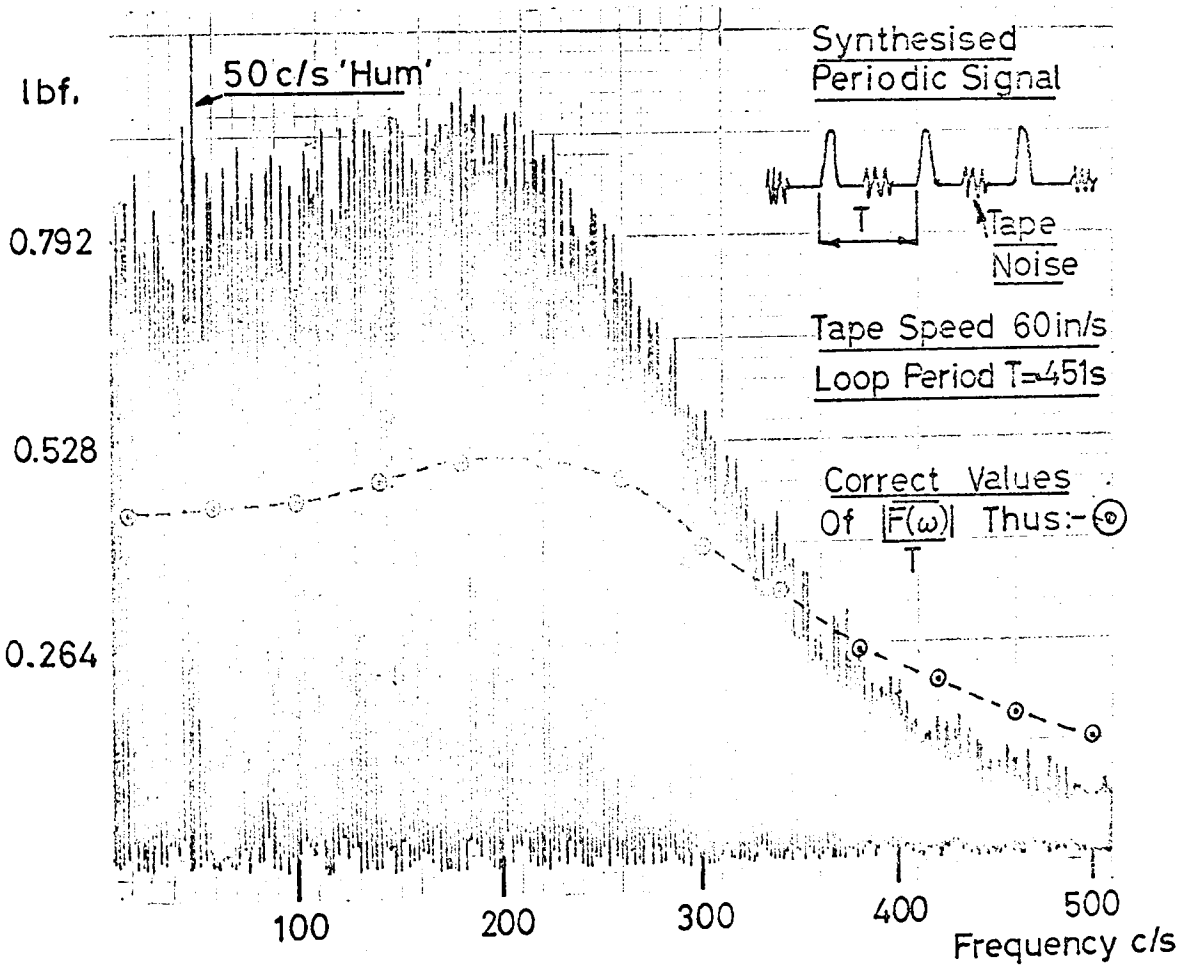

FIG.9.2 TESTS ON ROTARY CONVERTER. SINGLE FORCE PULSE AND LINE SPECTRUM OF SYNTHESISED PERIODIC SIGNAL CONTAINING TAPE NOISE.

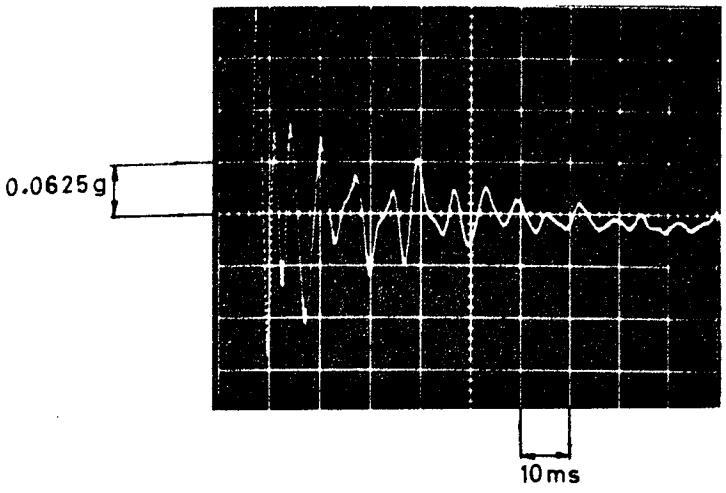

SINGLE ACCELERATION RESPONSE TRANSIENT

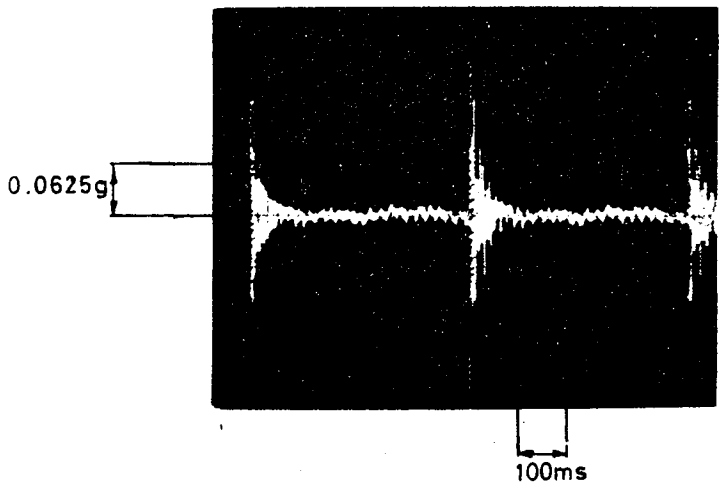

SYNTHESISED PERIODIC SIGNAL

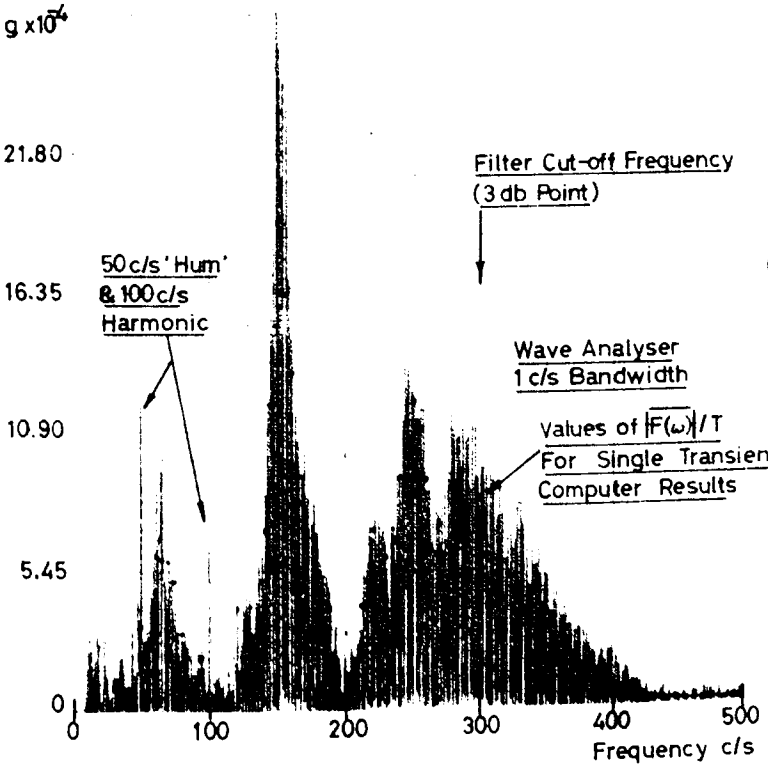

FIG.9.3 TESTS ON ROTARY CONVERTER. ANALYSIS OF RESPONSE TRANSIENT

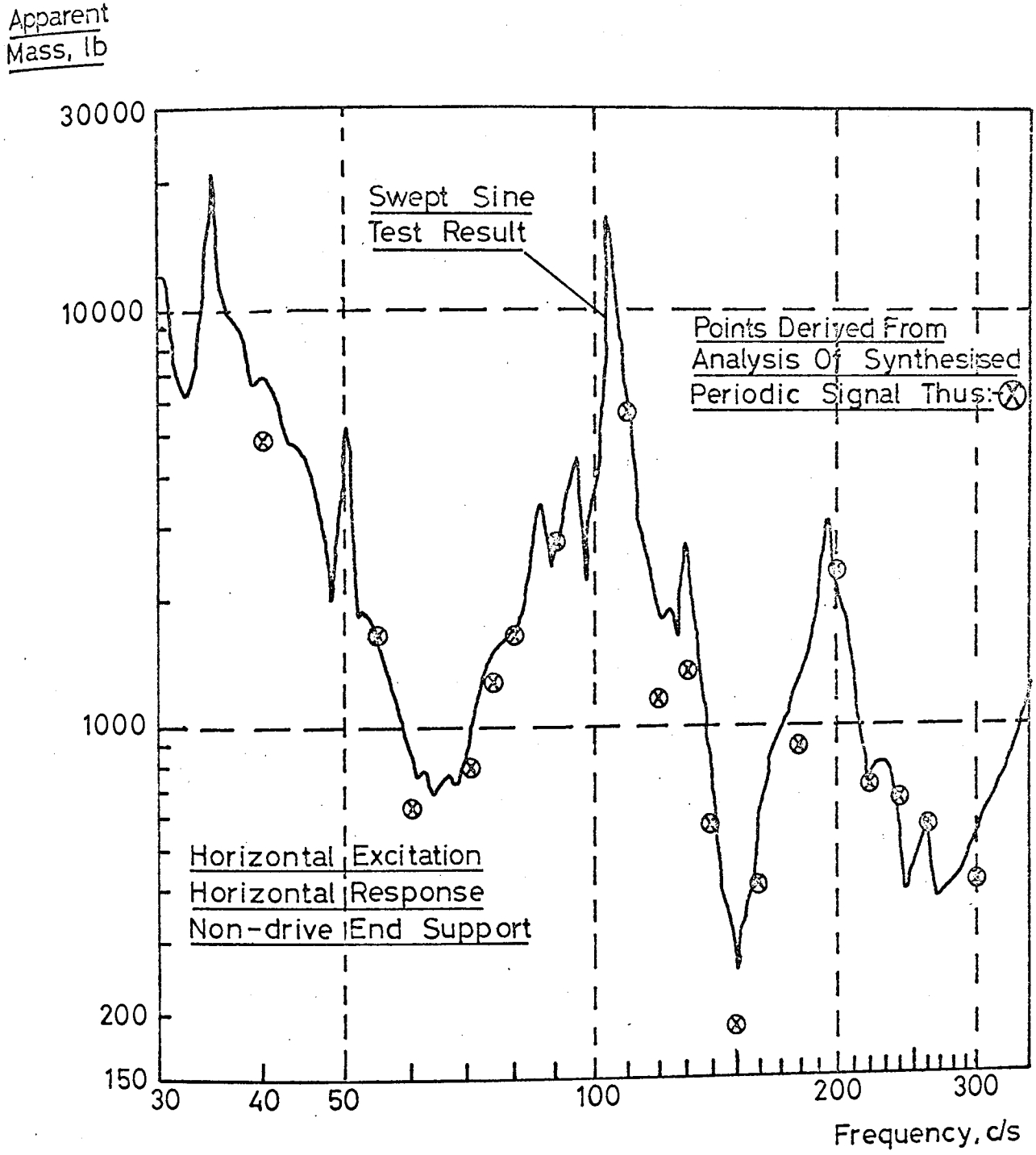

FIG.9.4 TESTS ON ROTARY CONVERTER. SUPPORT IMPEDANCE OBTAINED FROM LINE SPECTRUM OF SYNTHESISED PERIODIC ACCELERATION RESPONSE SIGNAL.

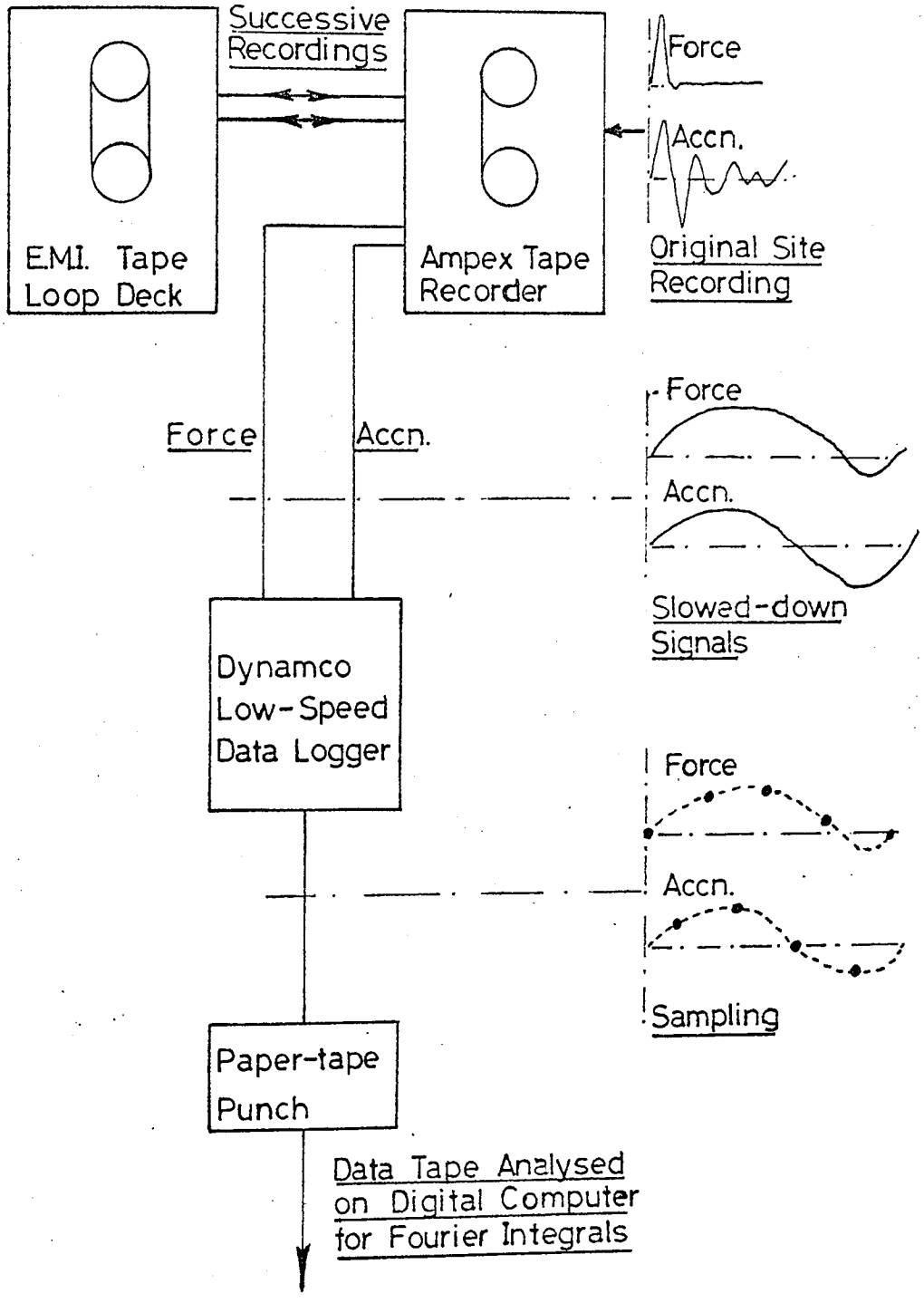

FIG.9.5. METHOD OF LOW SPEED DATA LOGGING OF FORCE AND RESPONSE TRANSIENTS.

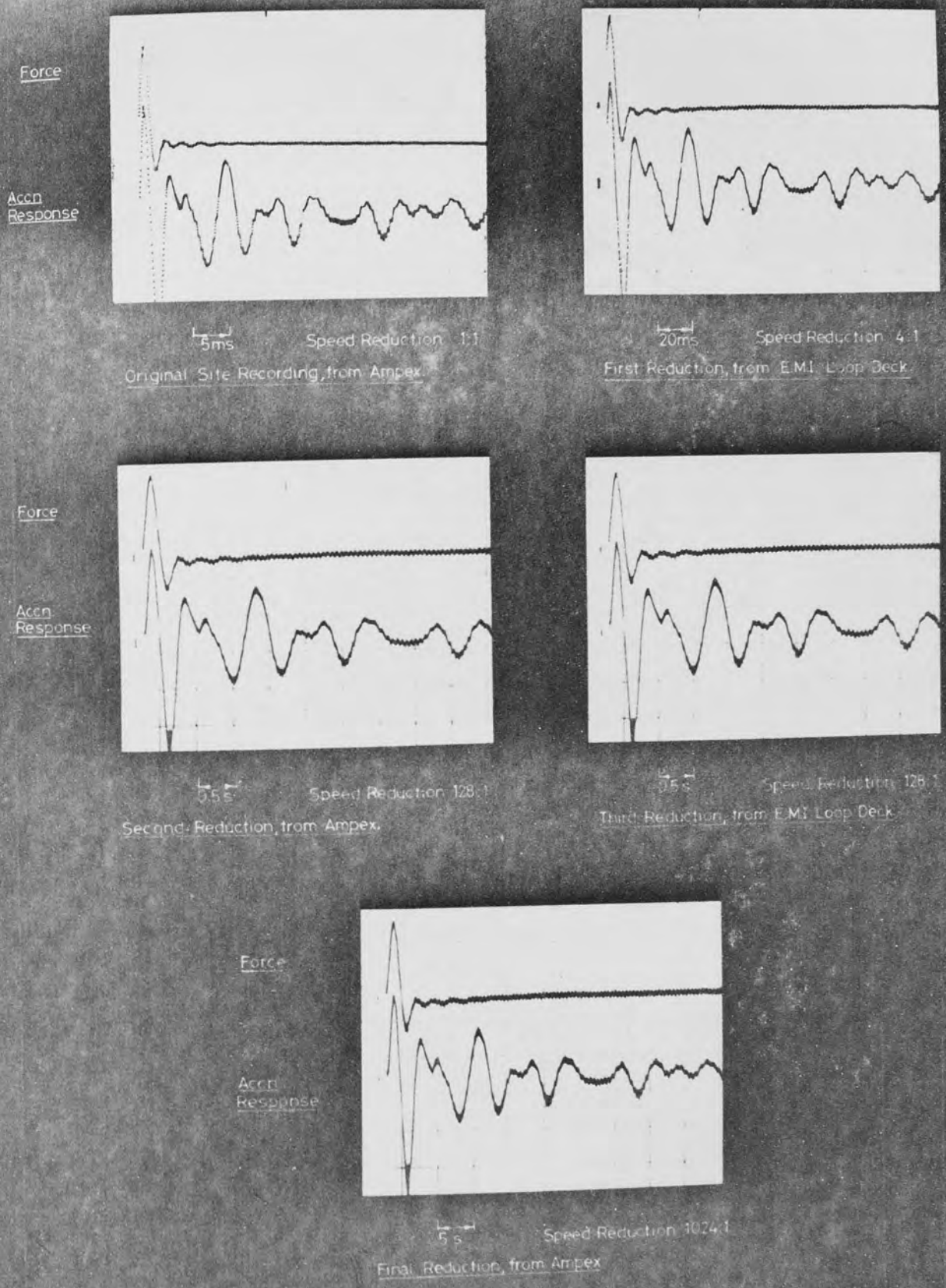

FIG 9.6 SLOWING DOWN OF FORCE AND RESPONSE TRANSIENTS USING AMPEX TAPE RECORDER AND E.M.I. LOOP DECK

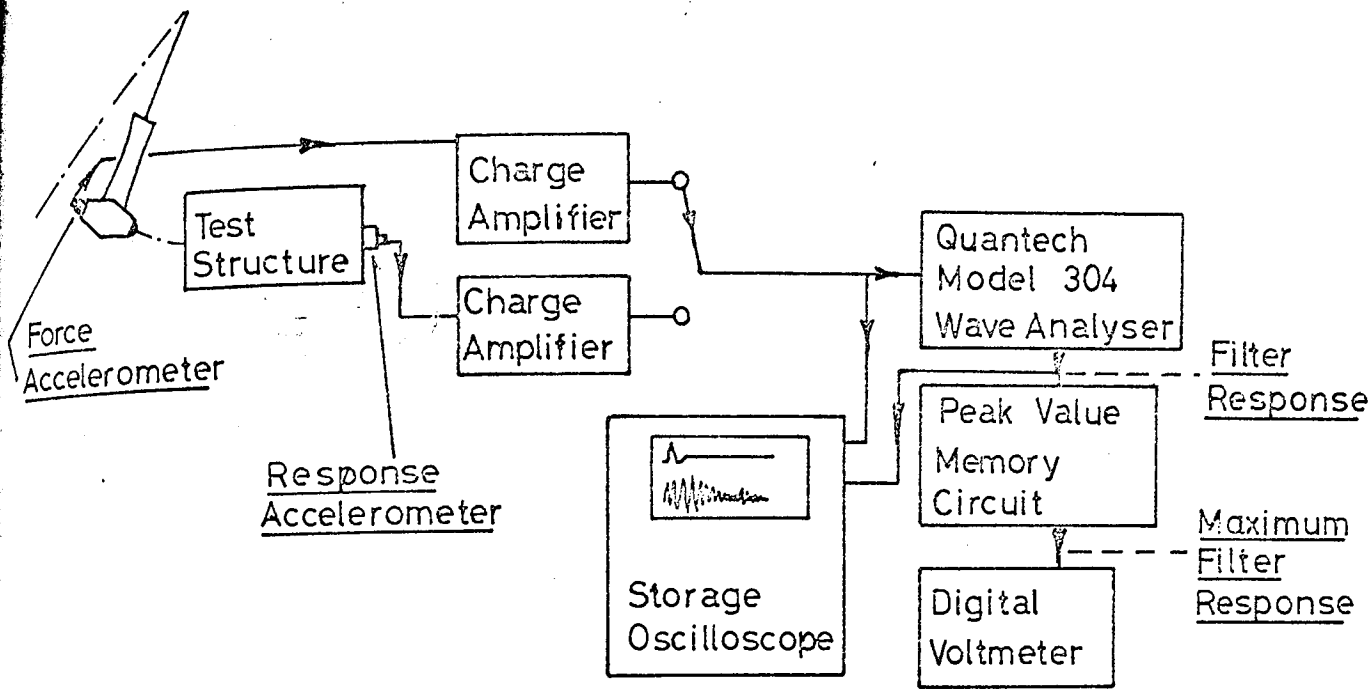

FIG.9.7 (a). METHOD UTILISING SHOCK SPECTRUM MEASUREMENT OF HETERODYNING WAVE ANALYSER.

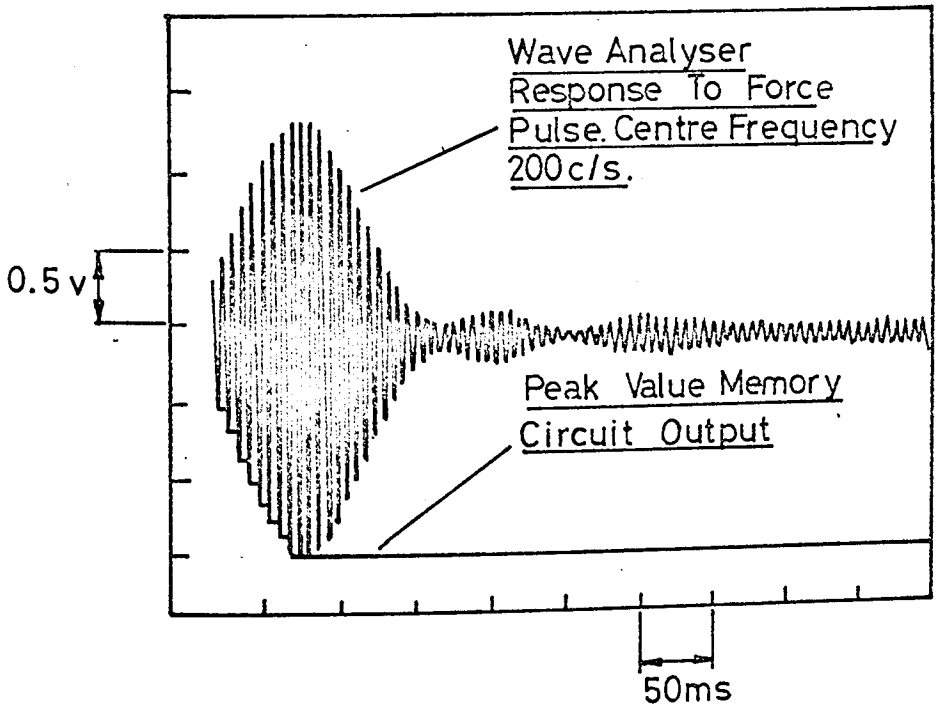

FIG.9.7.(b). OPERATION OF PEAK VALUE MEMORY CIRCUIT.

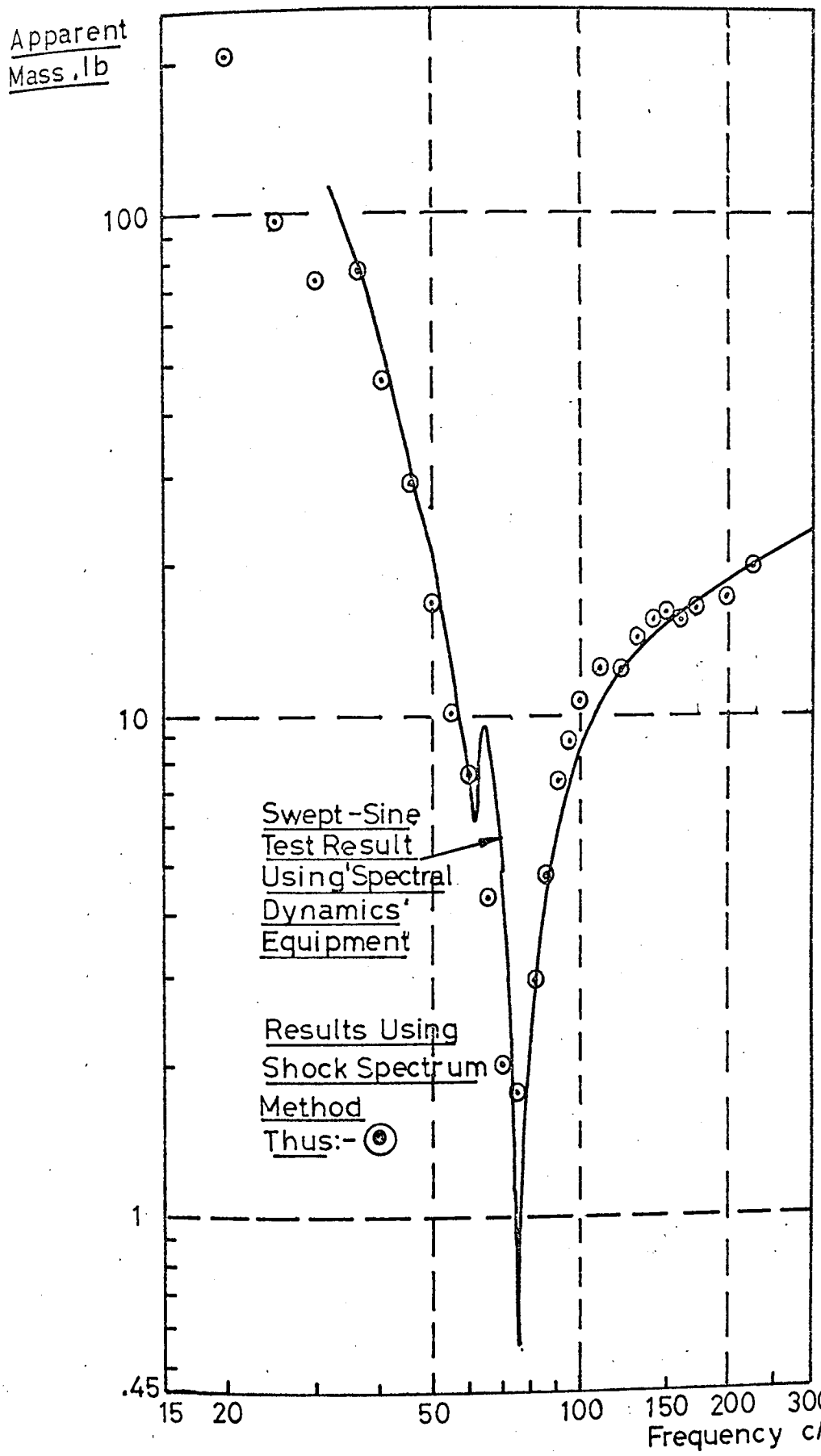

FIG. 9.8.. TESTS ON SINGLE D.O.F. SYSTEM. IMPEDANCE DERIVED FROM WAVE ANALYSER SHOCK SPECTRA

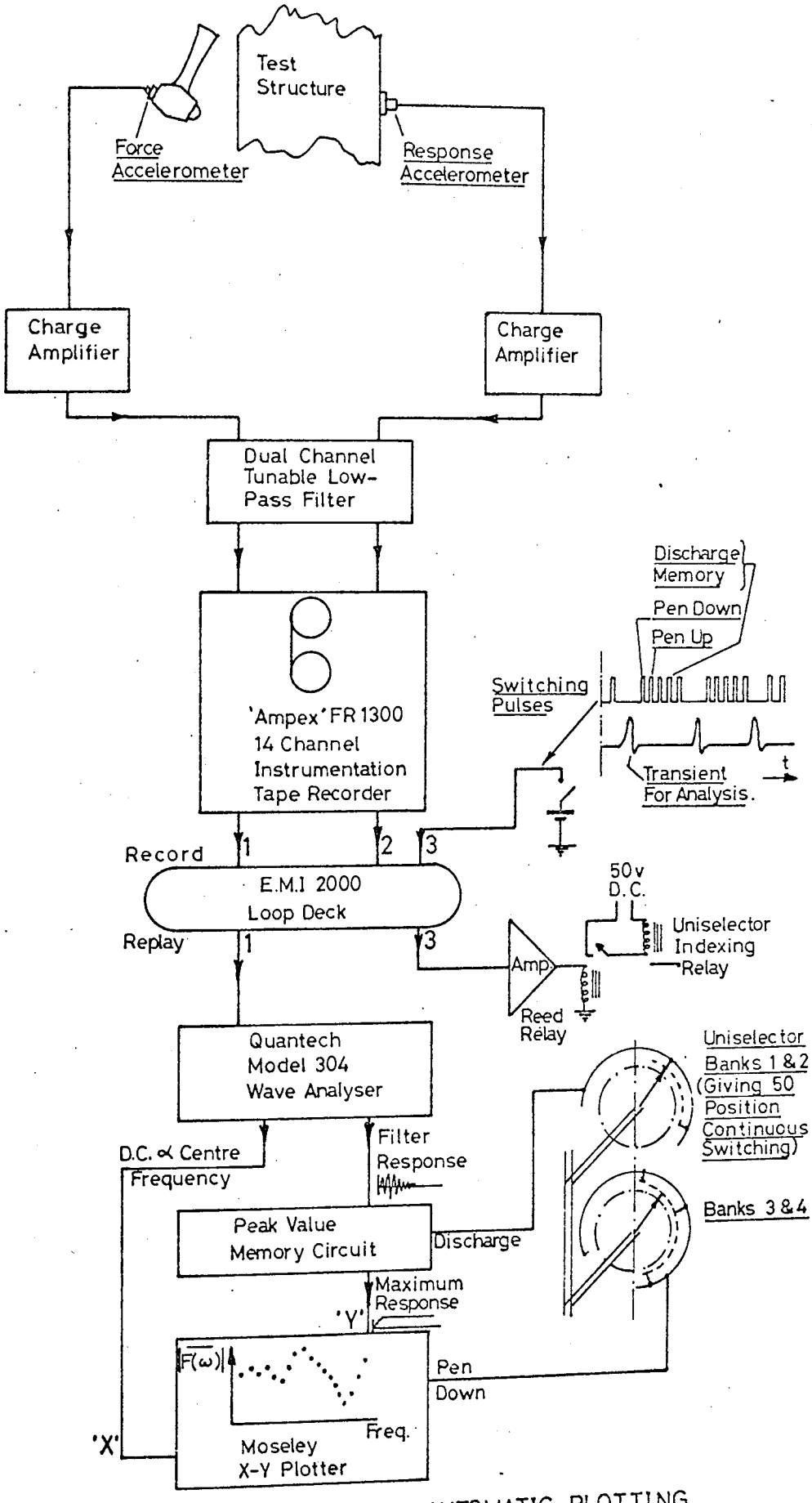

FIG 9.9. ARRANGEMENT USING AUTOMATIC PLOTTING. HETERODYNING WAVE ANALYSER SHOCK SPECTRUM METHOD FOR TRANSIENT ANALYSIS

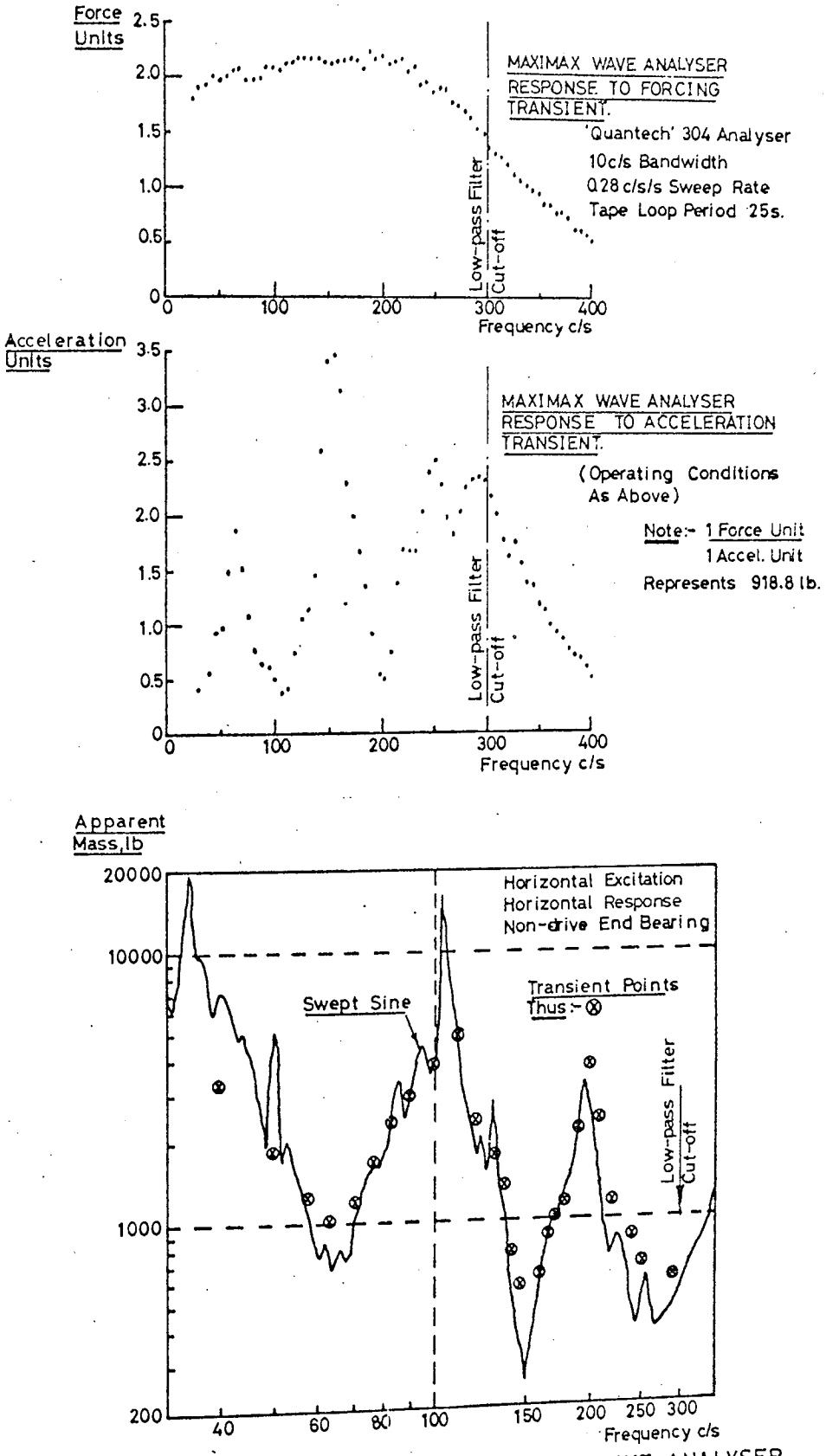

FIG 9.10 TESTS ON ROTARY CONVERTER. WAVE ANALYSER SHOCK SPECTRUM METHOD USING AUTOMATIC PLOTTING SYSTEM.

Chapter 10.

Experiments on Six Industrial Centrifugal Compressors.

10.1 Introduction

This chapter describes a series of vibration measurements made on six centrifugal compressors which formed part of a large petrochemical processing plant.

The aim of the experiments was to investigate the possibility of measuring the dynamic properties of the machines on site so that these properties could be used to interpret observed vibration levels on a more realistic basis than by comparison with existing vibration criteria (see Chapter 2 Section 2.5).

Due to the inevitable practical difficulties encountered, the information on any particular machine was rarely comprehensive, but the advantages of comparing measured vibration levels throughout the speed range of a machine with corresponding measurements of bearing support impedance were clearly demonstrated.

The transient excitation technique for measuring mechanical impedance, discussed in Chapters 8 and 9, was found to be very useful. It would have been impossible in the time available for each test to obtain impedance information by using conventional means.

In section 10.2 below, the general layout and construction of the machines is discussed. Details of the performance and dimensions of these machines are tabulated in Appendix V for reference.

Section 10.3 describes the experimental approach used on site to record machine-generated vibration and the 'raw' impedance data.

The results of support impedance measurements and the variation in vibration levels with running speed are presented in section 10.4

and 10.5 for each of the six machines. In most cases only first-order, 'unbalance' vibration components are considered, these being the most significant. For one machine, however, (K107 section 10.4 (i)) the identification and behaviour of a journal instability is discussed together with the cure effected by changing the bearing design.

The influence of the machines' foundations on the properties of the bearing support structures are also considered.

The final section 10.6 summarises the main conclusions reached during the course of this work. In this section the bearing support impedances measured on the compressors are compared with values published by other authors for a variety of rotating machines.

With regard to the scope of this investigation, it should be mentioned here that one of the original intentions was to examine the behaviour of the complete shaft/bearing/support systems of these machines. Neither the time nor the opportunity to obtain all the necessary experimental information was available to complete this task. The lack of shaft and bearing details also precluded this approach.

10.2 General Layout

The six compressors were all of the multiwheel, centrifugal type and comprised two main groups. The first group of three compressors had been installed for about ten years as process machines in a complex referred to as 'Ethylene II'. Each of these machines was driven via a step-up gearbox by a large induction motor

Installation of the second group of machines, serving a new plant 'Ethylene III', has been completed over the last three years. Many of the measurements on these machines have been taken during the commissioning of the plant. The compressors on Ethylene III were all driven by directly-coupled steam turbines.

The machines are subsequently referred to by their plant identification numbers, compressors K 107, K 105 and K 101 being part of Ethylene II and compressors K1, K2 and K3 serving Ethylene III. K 105, K 107, K2 and K3 each had a single casing whilst K 101 and K1 had both low and high pressure casings (L.P. & H.P.). In the case of K1 these were driven in tandem via an intermediate gearbox whilst for machine K 101 the L.P. and H.P. shafts were directly coupled. Photographs of the machines are shown in figs 10.1 and 10.2

The shafts of all the compressors ran in journal bearings. The bearing housings of the machines on Ethylene III were bolted to the ends of the casing whilst those on Ethylene II were cast integral with the casing itself. The complete casing assemblies were mounted on the foundation by either two or four individual supports. The foundations were all of reinforced concrete and consisted of a series of portal frames carrying a massive table. In each case the complete lineout - prime mover, gearbox (if used) and compressor - was mounted on the same foundation.

All the compressors incorporated flexible shafts, their normal running speed being between the first and second flexural critical speeds. In most cases the running speed was close to twice the first critical speed.

10.3 Experimental Approach

Many of the experiments on the compressors were conducted during a period when the plant had been shut-down for maintenance or, in the case of the new plant Ethylene III, during a pause in construction work.

Since the date and duration of these shutdowns were rarely predictable with any degree of certainty, information on any particular machine has often been collected piecemeal over a period of several months.

Whenever an opportunity arose to experiment with the transient impedance measuring technique or to monitor the vibration levels of a machine during start-up this opportunity was taken.

The initial data from all tests was recorded on the Ampex FR 1300 tape recorder (see Chapter 5, section 5.3) for future analysis. The recorder, together with other essential equipment such as charge amplifiers and an oscilloscope, were operated in a Land Rover. A general view of the instrumentation used on site is shown in fig 10.3.

Due to the nature of the working fluid of the compressors, rigid fire precautions were normally in force on the plant, so the Land Rover was normally parked some distance from the compressor house. Miniature, screened, low-noise cables about 200 yards in length were used between the accelerometers on the compressor and their associated charge amplifiers.

The general approach used to examine the behaviour of each machine may be conveniently divided under three main headings:-

(a) Initial survey of vibration levels throughout the complete lineout - normally with the machine running at full speed. Recordings were made of the accelerations at the bearing housings, casing supports and foundations and line spectrum analyses were subsequently performed to identify the major frequency components.

(b) Measurement of bearing support impedances using the transient method.

(c) Recording overall accelerations during a run-up or rundown of the machine. The variation with shaft speed of selected frequency components were subsequently obtained using the harmonic tracking method.

10.4 Machines in 'Ethylene II' Compressor House

10.4 (i) Compressor K 107

10.4 (i) (a) General

The maximum design power requirement of the compressor was 2300 H.P. and its rated speed 10,400 r.p.m. (173.3 c/s). The induction motor speed was nominally 1482 r.p.m. (24.7 c/s).

The makers quoted the first flexural speed of the compressor shaft as 5250 r.p.m. (87.5 c/s) i.e. very nearly half the normal running speed. The basis for the makers' figure is not known but it was presumably a calculated, 'simply-supported' value.

Apart from the unbalance, first-order vibration, this machine exhibited a large-amplitude vibration which was identified as a journal bearing instability. Altering the bearing design cured this defect.

10.4 (i) (b) Line Spectra and Relative Amplitudes

Fig 10.4 shows a line spectrum of the vibration present at the N.D.E. bearing housing of the compressor whilst it was running at full speed in shaft bearings of the same pattern as those supplied by the makers. Components at the motor frequency, compressor frequency and their harmonics are identified in this diagram, but these are seen to be small compared with a large component at about 82 c/s.

The vibration criteria proposed by Rathbone (63) are also sketched in this and several of the subsequent diagrams in this chapter. (It is emphasised that these curves are shown to provide a guide to the reader more familiar with such criteria, and not to condone their assessments of the acceptibility of machine vibration).

From a series of line spectra, similar to fig 10.4, the amplitudes at several points throughout the lineout were obtained for the first-order motor, first-order compressor and the bearing instability

frequencies. These are illustrated in figs 10.5 and 10.6, the plane of measurement (horizontal or vertical) and the amplitude of vibration being represented, respectively, by the direction and length of the arrows.

With regard to the influence of the foundation, it was observed from these results that the transmission of vibration from the machine generating the vibration to other parts of the foundation decreased with increasing frequency. At the induction motor frequency (24.7 c/s) for example, the amplitude at the foundation was often as large as the corresponding pedestal amplitudes. At the compressor unbalance frequency (173.3 c/s) however, the foundation amplitudes were normally less than 10% of the bearing housing levels.

10.4 (i) (c) Bearing Support Impedance Measurements.

Measurements of impedance were made in the horizontal plane at the bearing housings of the compressor and at the pedestals of the induction motor using the transient method. In both cases the shaft of the machine concerned was lying stationary in its bearings. Presumably due to its relatively small mass, the stationary compressor shaft had no measurable influence on the behaviour of the machine casing, so that the fundamental critical was not apparent in the impedance plot. In the measurements on the induction motor pedestals, the details of the shaft dynamics were not known but by comparison with tests on the rotary converter (Chapter 7), which was of similar general construction, the low-frequency controlling stiffness and the 'uncoupled' pedestal resonances would be only slightly affected by the presence of the shaft.

Fig 10.7 shows two driving point impedance measurements taken, respectively, at the D.E. and N.D.E. bearing housings of the compressor.

It may be seen that the controlling stiffness at the D.E. housing was approximately 10^6 lbf/in with a pronounced resonance at 122 c/s. At the N.D.E. of the machine a further resonance was detected at close to 50 c/s, the controlling stiffness being approximately 0.7×10^6 lbf/in. The lower resonance is thought to be a predominantly translational rigid body mode of the casing. It was noted that the approximate casing mass of 8,900 lb, obtained from the shipping specifications, would result in a fundamental rigid body mode at 45 c/s for a single degree-of-freedom approximation having a spring stiffness 1.7×10^6 lbf/in.

An interesting axial driving point impedance measurement on the induction motor pedestal remote from the compressor is shown in fig 10.8. This pedestal had caused some concern previously in that it showed vibration amplitudes of around 2.0×10^{-3} in r.m.s. at the running speed of 24.7 c/s. By existing criteria this level of vibration would be judged unsatisfactory - "rough, needs correction" according to Rathbone (63.) However , as may be seen from fig 10.8 the controlling stiffness of the support was very low, being approximately 1.5×10^5 lbf/in, so that the apparent forcing level was only 300 lbf r.m.s. - small compared with the bearing load due to the shaft weight.

The axial driving point impedance discussed above showed the lowest controlling stiffness recorded anywhere on bearing support structures throughout the plant.

10.4 (i) (d) Journal Bearing Instability

The first indication of unsatisfactory running conditions was obtained when an initial survey was conducted by the writer into the general vibration levels on the machine (October 1966). The line spectrum shown in fig 10.4 is an analysis of one of the records obtained.

The proximity of the observed 82 c/s vibration component with the fundamental critical frequency quoted by the makers, and the fact that the machine was running at approximately twice this frequency (173.3 c/s), suggested a journal bearing instability might be the cause.

The machine had a history of bearing failures, the bearing shells requiring replacement at each maintenance shutdown. The bearing at the N.D.E. of the machine appeared to be particularly susceptible to damage showing extensive fatigue failure of the white metal lining. The makers' specification for the bearing stipulated an 'anti-whirl' design and, although the exact geometry used is unknown, they appeared to be of 'elliptic' section i.e. bored with shims between the top and bottom halves.

An interesting characteristic of the (assumed) instability was that it apparently increased to a maximum intensity after several days continuous running and subsequently diminished. A check made on the machine some five weeks after the initial survey mentioned above showed similar first-order, unbalance levels but no evidence of the instability. It is thought that this behaviour may havebeen caused by the stabilising effect of the deformed bearing surfaces which resulted from a period of unstable operation. In this connection almost any departure from plain cylindrical bearing geometry would probably enhance stability. (see Tondl (18) and chapter 2 section 2.4 (ii)).

Following an overhaul of the machine during which the bearing shells had again been replaced (November 1967), the opportunity arose to record the compressor bearing housing vibrations during start-up of the machine. Unfortunately, just before the machine was due to be started, the stroboscope used to provide a tracking signal for the subsequent analysis developed a fault which made it unusable. In the absence of any other tracking signal the overall accelerations were recorded by themselves.

To analyse the vibration during the compressor's acceleration to maximum speed, a method was devised which involved recording the complete run-up on a magnetic tape lopp (see chapter 5 section 5.3(ii)) and playing the recording through a fixed centre-frequency, constant-bandwidth filter. By plotting the filter response versus time-using the time-base of an X-Y plotter - for a series of different centre frequencies, the variation of particular vibration components with shaft speed was extracted.

Fig 10.9 shows examples of the analyses for both the first-order and unstable whirl components. From the first-order component the increase of shaft speed with time was obtained, this being shown in the upper diagrams. The acceleration of the machine was very nearly linear, maximum speed being reached in 10 second.

It may be seen from fig 10.9 that the unstable whirl appeared very suddenly just before the machine reached full speed. Its frequency, when first extablished, was 73 c/s which decreased to 70 c/s four seconds after full speed had been reached. The frequency of the unstability then increased again to about 72 c/s at which frequency it remained during the period of the test i.e. approximately ten minutes.

The acceleration response at the N.D.E. bearing housing showed a gradual rise in amplitude from 0.094 g. rms. when first fully established, to 0.2 g. r.m.s. at the end of the test. The corresponding maximum response at the D.E. bearing housing was 0.041 g. r.m.s. or 20.5% of the level at the N.D.E. Based on the measured driving point impedances at the bearing housings (fig 10.7) - that is neglecting the transfer impedance which was not measured on this machine - these accalerations represent bearing force amplitudes of 304 lbf r.m.s. and 99 lbf r.m.s. at the N.D.E. and D.E. housings respectively.

Assuming the shaft weight of 400 lbf to be equally distributed between the bearings, the above levels represent oscillatory bearing forces of 76% and 23.8% of the steady bearing load.

It is interesting to note that in the original tests, when different bearing shells were in use, although the whirl frequency differed from the test discussed above (82 c/s compared with 72 c/s) the relative horizontal amplitudes were similar, the D.E. bearing housing level being 17% of that at the N.D.E. (fig 10.5). Since the measured driving point impedances did not differ appreciably between these two frequencies the whirl configuration was presumably similar. The variation in whirl amplitude and frequency between the two tests may have been caused by slight differences in bearing conditions, in particular the effective clearance.

After discussions with the compressor manufacturer it was decided to install bearings of a design more resistant to instability. The bearings finally chosen were of the tilting-pad type. Recordings of the vibration at the bearing housings of the machine made after these bearings had been installed showed no evidence of the instability (May 1968), although an increase in the unbalance vibration was apparent.

10.4 (i) (e) First-order, Unbalance Vibration.

Fig 10.10 (a) shows the horizontal first-order acceleration response measured at the D.E. bearing housing when the shaft was running in the tilting-pad replacement bearings. The response shows a maximum in the region of 120-130 c/s and a comparison with fig 10.7 shows this to be the region of minimum driving point impedance. Maximum bearing force levels are also shown in fig 10.10 (a), these being based on the measured driving point impedance.

The first-order response at the N.D.E. bearing housing is shown in fig 10.10 (b). In this diagram the response with the tilting pad replacement bearings in place was obtained using the harmonic tracking

techniques of chapter 5 section 5.5.(ii). Also shown in fig 10.10 (b) are points indicating the response at the N.D.E. housing with the original bearings in place. These were obtained from the analysis illustrated in fig 10.9. Like the D.E. housing, the acceleration response at the N.D.E. housing showed a maximum around 120 c/s corresponding to the minimum impedance region in fig 10.7. A further maximum in the response at 170 c/s was also consistent with the measured driving point impedance. The oscillatory bearing force levels based on the measured impedance are indicated in fig 10.10 (b) together with the corresponding percentage of the approximate steady bearing load.

As illustrated in fig 10.10 (b) the unbalance responses with the tilting-pad bearings in place appeared to be less well damped than those obtained with the original shaft bearings - particularly in the region of 120 c/s. This is the reverse of that which the writer would have expected intuitively in view of the improved stability of the tilting pad design.

None of the unbalance response curves showed any evidence of the 'fundamental' critical speed, the makers' figure for which is marked on figs 10.10 (a) and 10.10 (b). Presumably this was because either the shaft was so well balanced in the fundamental mode that it failed to excite the system (which seems improbable) or the dynamic characteristics of the journal bearings were such as to mask its existence. The latter explanation is consistent with the behaviour of the model rig discussed in chapter 6 section 6.6(ii).

10.4 (ii) Compressor K 105

10.4 (ii) (a) General

The design speed of the compressor was 10,800 r.p.m. (180 c/s) at which speed the power required was 1710 H.P. The nominal induction

motor rating was 2000 H.P. the machine running at 1482 r.p.m. (24.7 c/s). The makers quoted the first and second flexural critical speeds of the compressor as 5260 r.p.m. (87.67 c/s) and 18470 r.p.m. (307.8 c/s) respectively. As in the case of compressor K 107, above, the assumption made in obtaining these figures are not known but it is assumed that they were calculated values for the shaft based on simply-supported end conditions.

As far as the writer is aware this machine has run quite satisfactorily since it was commissioned in 1959. It is interesting to note that this machine, installed at the same time as K 107, also ran close to twice its first flexural critical speed (2.06 times for this machine, 1.98 for K 107). Unlike K 107, however, this machine was fitted with a tilting-pad journal bearing at the N.D.E., presumably in order to counteract journal bearing instability.

10.4 (ii) (b) Line Spectra and Relative Amplitudes

An example of a series of line spectrum analyses made on recordings of vibrations throughout the lineout is shown in fig 10.11 for the N.D.E. bearing of the compressor in the horizontal plane. The only components of vibration detected were at the first order motor and compressor frequencies and at twice the compressor rotational frequency. A further component at close to 50 c/s (second-order motor) may have been partly due to mains 'hum'.

Similar analyses from this initial survey (September 1966) were used to obtain the diagrams in fig 10.12 in which amplitudes at the bearing supports and foundation are shown for both motor and compressor running frequencies.

As in the case of K 107 (section 10.4(i)(a) above) the influence of the foundation on the behaviour of the bearing supports of the machine

generating the vibration showed a general decrease with frequency. The coupling between the supports at the bearing centre-line, however, was very noticeable and in the case of the compressor unbalance vibration resulted in amplitudes of a comparable magnitude at the induction motor pedestals.

10.4 (ii) (c) Bearing Support Impedance Measurements.

Fig 10.13 shows two impedance measurements taken at the N.D.E. pedestal of the induction motor. The transient methods of chapter 8 and 9 were used to obtain these results which show, respectively, the driving point impedance at the bearing centre-line and the transfer impedance between this point and a point close to the joint between the pedestal and the foundation. Thus the greater the separation between these two curves, the greater the contribution of the pedestal itself to the impedance at the bearing centre-line. It may be seen from fig 10.13 that at low frequencies ($<$ 70 c/s) the transfer impedance was approximately 150 to 200% greater than the driving point impedance. At higher frequencies, and in particular around the compressor running frequency of 180 c/s, the transfer impedance was approximately six times greater. At these frequencies, therefore, the support impedance 'seen' by the shaft was influenced very little by the impedance of the foundation. Similarly shaft generated vibration at this frequency would be strongly attenuated at the foundation - which effect was apparent from the survey of fig 10.12. Conversely, however, small displacements of the foundation induced by some other machine in the lineout would be amplified at the bearing centre-line.

Further measurements on the induction motor pedestals showed very low axial controlling stiffnesses similar to those on K 107. An example is given in fig 10.14 from which it can be seen that the

controlling stiffness was about 4×10^5 lbf/in. The heavily damped characteristics of the resonance at approximately 150 c/s was presumably due to the fact that the shaft was lying in the bearings. (cf fig 10.8 for K 107).

Fig 10.15 shows the measured driving point impedance of the D.E. bearing housing of the compressor. The resonances at 65 c/s, 120 c/s and 180 c/s were all within the speed range of the compressor. The low frequency stiffness is seen to be approximately 0.9×10^6 lbf/in.

Also shown in fig 10.15 is the transfer impedance between the bearing housings. It is interesting to note that in this case the coupling was spring-controlled and of the same order of magnitude as the driving point impedance at the D.E. bearing housing. This indicated that the compressor casing was behaving as a rigid body.

An attempt was also made on this machine to measure the driving point impedance at the N.D.E. bearing housing using transient excitation. Above 70 c/s this measurement was successful but at lower frequencies the impedance was so high that the acceleration response spectrum was masked by instrumentation 'noise'.

To assess the effect of the ambient noise on the transient measurement the response was first analysed over the duration of the transient in the manner discussed in chapter 9 section 9.3 (i.e. low-speed data logging followed by digital computation). The 'apparent' impedance so obtained is indicated in fig 10.16.

A section of the recording immediately before the transient, and of the same duration, was then analysed in an identical manner. The impedance calculated from the response channel noise spectrum so obtained is also shown in fig 10.16, to the same scale as the impedance obtained from the transient.

Except for small discrete tones - at the mains frequency of 50 c/s, for example - the noise was apparently random so that the above method of analysis was only approximate. A more exact analysis of the spectrum of the random noise would have required sampling several similar short records taken over a period of time and averaging the results for particular sampling rates - roughly equivalent in digital terms to analogue power spectral density measurements.

However, the method used indicated the approximate characteristics of the noise and it may be seen from fig 10.16 that its effect decreased with increasing frequency up to about 300 c/s, approximately following a square-law. This behaviour was attributed to the charge amplifiers used in the acceleration measurement which, due to the capacitive-feedback arrangement employed, amplified internal noise according to a 12 db/octave law.

Above 300 c/s the noise content of the signal again increased due to an increase in acceleration 'noise' level on the machine. This effect has been observed repeatedly in the case of line spectrum analyses, but its influence on the transient was normally small since the acceleration impedance tended to decrease with frequency.

Where measurements were to be taken on structures having very high low-frequency impedance increasing the gain of the charge amplifier to obtain greater overall accelerometer sensitivity also increased the noise level. Since the low-frequency noise spectrum decreased with frequency and the required transient response spectrum increased with frequency, an amplifier gain was reached at which the noise level was as high as the required signal.

The limit on the low-frequency capability of the transient method was always well below the running frequency of the compressors but it has sometimes restricted investigations into the rigid-body behaviour

of the casings, particularly where they were very massive (see chapter 8, section 8.7). It is hoped that in future the problem may be overcome, either by using a forcing transient with a much larger low-frequency content or by increasing the sensitivity of the accelerometer itself.

In the first case a 'step' forcing transient would be most suitable but would be difficult to generate. Increasing the accelerometer sensitivity, on the other hand, should be relatively straightforward and could be achieved by increasing the mass of the seismic element. In this respect the resonant frequency of the conventional accelerometers used for the experiments reported here was unnecessarily high, being about 11 kc/s. Since the upper frequency of interest for the impedance measurements on the machines was normally about 500 c/s, a resonant frequency of approximately 3 K c/s would be adequate - providing the force pulse was suitably shaped - and would enable an increase in gain of 25 to be achieved.

Returning attention to fig 10.16, the controlling stiffness at the N.D.E. housing was estimated to be about 5.5×10^6 lbf/in. The 120 c/s and 180 c/s casing resonances detected in the measurement at the D.E. housing are also apparent in this figure.

10.4 (ii) (d) First-order, Unbalance Vibration

An opportunity arose to record the acceleration response of the machine when it was started up following an overhaul. Unfortunately no tracking signal was available with which to tune the analysis equipment and the responses were therefore analysed by playing the complete recording through a fixed centre frequency, constant bandwidth filter in a similar manner to that discussed in section 10.4 (i) (d) above. The maximum first order levels at each centre frequency (shaft rotational frequency) are shown in fig 10.7 for the D.E. and N.D.E. bearing supports of the compressor.

The response at the N.D.E. support is seen to contain a peak in the region of 70 c/s and another around 120 c/s. These peaks correspond to the resonances detected in the impedance measurements (fig 10.16)

No conclusive evidence of the fundamental critical speed could be seen, however, although a slight rise in vibration level between 85 and 105 c/s may havebeen significant.

It should be mentioned that the rapid acceleration to full speed of the induction motor driven machines would tend to increase the frequency and decrease the amplitude of the resonant peaks (see chapter 2, section 2.2 (iv)) due to the non-stationary nature of the unbalance excitation. From the mechanical standpoint this effect was small since the acceleration during start-up of K 105 and K 107 was about 18 c/s/s, whilst the resonant bandwidths (-3db points) were normally greater than 15 c/s. In this case accelerations of about 55 c/s/s would be considered the limit for near-steady-state responses to be achieved. Care was necessary, however, in selecting the bandwidths of the filters used in the analysis (see Chapter 5 section 5.5 (i)).

The first-order response at the D.E.bearing housing, shown in the lower diagram of fig 10.17, contained a very broad peak between 55 c/s and 105 c/s, which frequency range included both the casing resonance detected during the impedance measurements and the first flexural critical speed. For this housing, however, the only evidence of the 120 c/s casing resonance was a slight peak in an otherwise decreasing response curve.

In fig 10.17 the 'apparent' bearing forces, based on the measured driving point impedances, are indicated at the points of maximum response. For the stiff N.D.E.housing this calculation indicated a maximum bearing force of 235 lbf r.m.s. at a shaft frequency of 75 c/s. However, since

the transfer impedance between supports was of a comparable magnitude to the driving point impedance (less in the case of the N.D.E.) this estimate is liable to considerable error.

Since the relative phase angle of the responses at the two bearing housings was not available the contribution of the transfer impedance could not be accurately assessed. But a calculation based on the assumption that, at 75 c/s, the casing response was a rigid-body, 'in-phase' motion (known from the impedance measurements) and the shaft generated bearing forces were also in phase (reasonable, due to the proximity of the fundamental critical) indicated that the bearing forces were 63 lbf r.m.s. and 55 lbf r.m.s. at the D.E. and N.D.E. housing respectively.

At the normal running speed of the compressor of 10,800 r.p.m. (180 c/s) the bearing forces, based on the driving point impedances, were 44 lbf r.m.s. and 64 lbf r.m.s. at the N.D.E. and D.E. bearings respectively. Making allowance for the transfer impedance, using the assumptions given above for the 75 c/s calculation, the levels were 18 and 50 lbf r.m.s. respectively.

10.4 (iii) Compressor K 101

10.4 (iii) (a) General

The design speed for the shafts of both L.P. and H.P. casings of this machine was 7575 r.p.m. (126.3 c/s). The nominal power delivered by the induction motor was 5000 H.P. representing 2200 to 2800 H.P. for the L.P. casing and 1900 to 2200 H.P. for the H.P. casing.

The makers quoted the first flexural critical speed for the low pressure casing as 5200 r.p.m. (86.7 c/s) and an approximate total casing mass of 16,950 lb (shipping specification). Corresponding values given for the H.P. casing were 6500 r.p.m. (108.3 c/s) and 9,600 lb respectively.

10.4 (iii) (b) Line Spectra and Relative Amplitudes

Two line spectra, obtained from an analysis of the vibration at the N.D.E. of the low pressure casing and at an induction motor support, whilst the machine was running at its normal speed, are shown in fig 10.18. Components detected at the induction motor running frequency, the running frequency of the compressors and harmonics thereof are identified in this diagram.

From a series of similar analyses the levels at various points throughout the structure were obtained at the first order compressor and induction motor frequencies. The results of this survey are illustrated in fig 10.19.

As in the case of compressors K 105 and K 107, the influence of the foundation was most pronounced at the induction motor frequency (24.7 c/s). Attenuation of the motor-generated unbalance vibration down the bearing pedestals in the horizontal plane suggested that the effective pedestal impedance was reduced by about 30% at the bearing centre line due to motion of the foundation. This behaviour is illustrated in fig 10.19 by the result of a series of amplitude measurements taken down the N.D.E. motor pedestal. In the vertical plane the effect was even more pronounced and at least 50% of the pedestal motion apparently resulted from motion of the foundation to which it was attached.

At the induction motor running frequency, because the impedance of the compressor supports was predominantly spring controlled (i.e. below their rigid body resonance), the vibration amplitudes at the bearing housings of the compressors were similar to the foundation amplitudes at that end of the lineout.

At the compressor running frequency, however, the foundation amplitudes as may be seen from fig 10.19, were only about 10% of those at the compressor bearing housings. It was concluded that at this higher frequency the foundation impedance was very high and that the behaviour of the bearing housings was largely determined by the impedance of the supporting structure between the housings and the foundation.

10.4 (iii) (c) Bearing Support Impedance Measurements.

Two examples of impedance measurements taken at the induction motor pedestals using transient excitation are shown in fig 10.20. This figure shows the horizontal driving point impedance at the bearing centre-line of the D.E. pedestal and the transfer impedance measured between the bearing centre-line and a point, close to the foundation, on the fabricated steel box structure on which the pedestal stood. In both cases the shaft was lying stationary in its bearings.

This pedestal, in common with the one at the N.D.E. of the machine, was much stiffer at low frequencies than those of K 107 and K 105 and had a controlling stiffness of approximately 6×10^6 lbf/in. At 60 c/s, the lowest frequency at which the measurement was reliable due to instrumentation noise, the transfer impedance was approximately 2.5 times greater than the driving point impedance. This figure was in reasonable agreement with the observed attenuation of unbalance vibration down the pedestal.

Since no details of the motor shaft assembly were available, its influence on the measured impedances was unknown, but it is possible that the minimum impedance detected around 80 c/s was due to a resonance of the system corresponding to a natural frequency of the simply supported shaft. Similarly it is thought that the resonance at 150 c/s corresponded to a predominant resonance of the uncoupled pedestal.

In this respect the driving point impedance of fig 10.20 may be compared with the behaviour of the rotary converter pedestals discussed in chapter 7, which were of similar design (see fig 7.10 for example).

It is interesting to note that at frequencies above about 300 c/s the modulus of the transfer impedance down the pedestal approached the same value as the driving point impedance, whilst at 500 c/s they were equal. This effect is attributed to the fact that the response accelerometer in the transfer impedance measurement was some 2 to 3 in. from the concrete foundation. At high frequencies this distance would no longer be negligible compared with the wavelength of flexural vibration in the fabricated pedestal supporting structure.

Tests on the bearing housings of both L.P. and H.P. compressor casings have shown these structures to be very stiff at low frequencies. Their impedances were so high that, even with the large pendulum hammer (Chapter 8, section 8.5 (ii)), at frequencies below approximately 80 c/s instrumentation noise masked the transient response spectrum (see section 10.4 (ii) (c) above).

This effect is illustrated by the measurement at the N.D.E. of the high pressure casing shown in fig 10.21. At the normal running frequency (126.3 c/s) of the compressor the driving point acceleration impedance at the N.D.E. was approximately 15,000 lb (2.5×10^7 lbf/in) - or ten times higher than the corresponding measurement at the same frequency on compressor K 105 (1500 lb) and 14.3 times greater than the impedance at the N.D.E.bearing of K 107. (see figs 10.16 and 10.17 respectively.)

The driving point impedances measured at the bearing housings of the L.P.compressor were also very high. Fig 10.22 shows the result

obtained for the N.D.E. bearing housing, from which it can be seen that the controlling stiffness was approximately 10^7 lbf/in whilst the acceleration impedance at the running frequency was 13,000 lb.

10.4 (iii) (d) First-order, Unbalance Vibration

No opportunity has arisen to track the first-order vibration levels throughout the speed range of the machine. At the normal running speed, however, it was apparent that although the measured amplitudes (figs. 10.18, 10.19) were acceptable on the basis of existing criteria (just above the 'fair' assessment given by Rathbone (63)), due to the high impedances at the bearing housings they suggested considerable oscillatory bearing forces.

As a provisional estimate using the driving point impedance given in figs.10.21 and 10.22, for example, the measured vibration amplitudes at the N.D.E. housings of the low-and high-pressure casings (0.13 g. r.m.s. in both cases) represent bearing forces of 1690 lbf r.m.s. and 1950 lbf r.m.s. respectively.

Although the above figures may be considerably modified due to the effect of the (unknown) coupling between the bearing planes, the conclusions regarding the interpretation of measured amplitudes were largely confirmed following a recent maintenance shutdown. On dismantling the H.P. casing of the machine it was found that the last stage rotor wheel had disintegrated at some time during the previous running period due to erosion of parts of the riveted assembly. Presumably the shaft was therefore considerably out of balance. However, routine vibration measurements taken by the company's own technical staff immediately before the shutdown had shown amplitudes which were acceptable on the basis of existing criteria.

10.5 Machines in Ethylene III Compressor House

10.5 (i) Compressor K3

10.5 (i) (a) General

The design running speed of this machine was 13,370 r.p.m. (222.8 c/s) - the highest speed for the machines covered in this chapter. The duty horsepower at the compressor coupling was 2215 H.P., this being supplied by a direct-coupled steam turbine.

The makers quoted the first flexural critical speed of the compressor shaft as 5900 r.p.m. (98.33 c/s) and the shaft mass as 750 lb.

The total mass given for the complete compressor and bedplate was 6.2 tonnes (13,670 lb) and it was assumed from this that the casing mass was approximately 10,000 lb.

The casing supporting structure on this and the other machines of Ethylene III differed from that of the Ethylene II machines. For the compressor under consideration the casing was supported from the foundation by four concrete-filled, box-section, fabricated steel supports, inclined at about 10° to the vertical. These supports may be seen in fig. 10.2. The reason for filling the casing supports with concrete was not known but since they were already apparently of adequate strength it is assumed that this was some attempt to minimise vibration amplitudes.

Unlike the machines of Ethylene II, the bearing housings of this compressor were individual assemblies bolted to the casing. Being relatively light, stiff structures they were spring controlled relative to the casing up to frequencies of about 400 c/s.

10.5 (i) (b) Support Impedance Measurements.

Fig 10.23 shows the horizontal driving point impedance measured at the D.E.casing support together with the transfer impedance measured

between the N.D.E. and D.E. supports. These impedances are seen to be spring controlled, approximately equal and in phase below the first major resonant frequency at 70 c/s.

This indicated that the casing was behaving as a rigid 'point mass' at low frequencies, as distinct from a rigid body with pinned-flexible supports at each end. Presumably the relatively large sectional area of each support at the point of attachment of the casing tended to create encastré end conditions.

As for all the machines in this chapter, no evidence of a resonance corresponding to the fundamental natural frequency of the shaft was detected, presumably because of the large casing mass compared with that of the shaft (ratio approximately 13.3:1.).

The impedance at the N.D.E. casing support is shown in fig 10.24 and on this curve is sketched one branch of the impedance curve 'looking into' the shaft. To obtain the shaft impedance shown it was assumed that the shaft could be represented by an undamped, single degree-of-freedom system having a mass, m = 750 lb and natural frequency f_n = 98.33 c/s, i.e. the makers quoted values.

Referring to the inset sketch in fig 10.24 the shaft acceleration impedance Z_s, is given by:-

$$\frac{1}{Z_s} = \frac{-\omega^2}{k_s} + \frac{1}{m} \qquad (10.1)$$

or

$$Z_s = \frac{k_s \, m}{(k_s - m\omega^2)} \qquad (10.2)$$

Hence writing $k_s = m\omega_n^2$

$$Z_s = \frac{m^2 \, \omega_n^2}{(k_s - m\omega^2)} \qquad (10.3)$$

It may be seen from fig. 10.24 that the intersection between the shaft impedance curve and the measured casing support impedance modulus curve is only slightly below the rigid bearing first flexural critical frequency, f_n, This implies that the 'resonance-antiresonance' combination relating to the natural frequency of the complete system would be of very narrow bandwidth and explains why, due to the effect of damping, the resonance was not detectable in the casing impedance measurement. A similar argument applies to thebehaviour of the bearing housings. (See also chapter 3 section 3.3).

At higher frequencies the modes of vibration of the casing were more complicated. At the N.D.E. of the casing (fig.10.24) a resonance at approximately, 160 c/s was apparent but at the D.E. this resonance was much less pronounced. (fig. 10.23). Conversely a resonance at 200 c/s detected in the measured impedance at the D.E. of the casing was absent from the N.D.E.plot. Both resonances were detected in the transfer impedance measured between supports.

It would seem from the impedance measurements and from the first-order responses, discussed in section 10.5 (i) (c) below, that the 200 c/s resonance was a mode involving appreciable coupling between the horizontal and vertical planes.

Up to 250 c/s, driving point impedances measured at the bearing housings of the compressor were approximately a factor of two lower than the corresponding casing support impedances. For the D.E. bearing housing, for example, the impedance of which is shown in fig.10.25, the low frequency controlling stiffness was approximately 1.6×10^6 lbf/in compared with the value of 3.7×10^6 obtained from the casing support impedance measurement shown in fig.10.23.

Above 300 c/s the impedance of the housing decreased rapidly, compared with that of the casing support - showing a resonance at 500 c/s. Both bearing housings exhibited the 160 c/s and 200 c/s casing resonances.

Ignoring a slight difference in height between the horizontal centreline of the housing and that of the casing support, the stiffness of the housing relative to the casing was estimated, from the low frequency stiffness of the complete system, to be about 2.9×10^6 lbf/in.

10.5 (i) (c) First-order, Unbalance Response.

Opportunities to record the vibration levels on the machine whilst it was running arose on two separate occasions nearly twelve months apart. Fig 10.26 shows the first-order response at the D.E. casing support, obtained by the harmonic tracking method, for 'Test 1' (July 1967) and for 'Test 2' (July 1968). In the period between these tests the shaft had been removed from the casing on at least one occasion.

It may be seen from fig 10.26 that although the responses at the 200 c/s casing resonance were of similar magnitude for the two tests, those at lower frequencies differed considerably. Major variations in amplitude around the 160 c/s casing resonance, the 'fundamental' critical and the 70 c/s lower rigid-body casing resonance were apparent.

Similar variations between the two tests were observed at the N.D.E. casing support as is shown in fig 10.27. In this case the maximum in the response at the 160 c/s casing resonance (corresponding to the minimum in the impedance plot of fig 10.24) was of much lower amplitudes in the latter test, whilst the resonance in the region of the 70 c/s casing resonance and the fundamental critical was more pronounced in the earlier test.

Since reliable transfer impedance between the horizontal and vertical planes have not been obtained to date, only approximate values of the shaft-generated unbalance forces can be calculated. However, the information available so far enables several reasonable estimates to be made at particular shaft frequencies.

In the region of the 70 c/s casing resonance, for example, the unbalance forces may be assumed to be predominantly in phase since this frequency is close to the 'fundamental' critical. Also, it is known from the impedance measurements that the casing behaved as a 'point mass' in this mode with nearly equal, in phase motion at each end of the casing. The total oscillatory bearing force may therefore be calculated on the basis of the measured driving point impedances at this frequency. The forces obtained for the two tests are indicated in figs 10.27 and 10.28.

Similar assumptions were used in the calculation of the bearing forces at the fundamental critical. In the case of 'test 2' it may be seen that although the total force was approximately 800 lbf r.m.s. or about 150% of the shaft weight, the vibration amplitude would be classified as 'good' according to Rathbone (63).

In the impedance measurements on K3 discussed above, it may be seen from fig 10.23 that at 200 c/s the horizontal transfer impedance ($Z_{21} = Z_{12}$) between the casing supports was at least five times larger than the driving point impedances at the N.D.E. and D.E. supports. If, neglecting the coupling with the vertical plane, the responses at the N.D.E. and D.E. supports are written

N.D.E. $$\ddot{x}_1 = \frac{F_1}{Z_1} + \frac{F_2}{Z_{12}} \qquad (10.4)$$

D.E. $$\ddot{x}_2 = \frac{F_1}{Z_{12}} + \frac{F_2}{Z_2} \qquad (10.5)$$

Providing $\ddot{x}_1$ and $\ddot{x}_2$ are of the same order and $Z_{12} \gg Z_{22}$, $Z_{12} \gg Z_{11}$

then $$\ddot{x}_1 \simeq \frac{F_1}{Z_1} \qquad (10.6)$$

$$\ddot{x} \simeq \frac{F_2}{Z_2} \qquad (10.7)$$

i.e. the forces may be obtained from the driving point impedances alone.

The force levels at 200 c/s based on these assumptions are indicated in figs 10.22 and 10.28.

10.5 (ii) Compressor K2

10.5 (ii) (a) General

The makers gave the mass of the large, single casing of this machine as 16,350 lb. The shaft mass was quoted as 2540 lb. The normal running speed of the machine was 5620 r.p.m. (93.8 c/s) whilst the value quoted for the first flexural critical speed was 2165 r.p.m. (35.2 c/s). The rated power requirement was 8380 H.P., this being supplied by a directly coupled steam turbine.

10.5 (ii) (b) Support Impedance Measurements.

Due to the large casing mass difficulty was experienced in obtaining reliable transient impedance measurements below about 70 c/s. An extensive series of tests performed using the hand hammer (see Chapter 8 section 8.5 (ii)) had to be discarded since the instrumentation noise level was of a similar order of magnitude to the transient response spectrum amplitude. More success was achieved with the large pendulum hammer, however, since it normally delivered a transient force pulse having a spectrum some 20 db above that of the small hand hammer.

An example of such a measurement taken at the N.D.E. casing support is shown in fig 10.29. The approximate instrumentation noise level is

also sketched in this diagram. The most significant feature of the measured impedance is seen to be a resonance at 90 c/s - slightly below the normal running frequency. Despite the resonant condition the impedance was still high at this frequency being 5200 lb on an acceleration basis (4.3×10^6 lbf/in). From this measurement, a corresponding one at the D.E. support, and the transfer impedance between supports, the mode was found to involve rigid body motion of the casing with in-phase displacements at each end.

The amplitude at the N.D.E. was about 140% of that at the D.E.

Since the bearing housings were somewhat more receptive measurements of impedance could be made down to a lower frequency. These measurements suggested the presence of a further rigid-body casing resonance at approximately 60 c/s as is illustrated in fig.10.30 for the N.D.E. bearing housing.

10.5 (ii) (e) First-order, Unbalance Responses

It has only been possible on one occasion to record the vibration levels on the machine over its full speed range. These recordings were obtained during the early stages of commissioning the machine and their analysis was hampered by the effects of a violent, aerodynamic surging of the compressor - caused by a filter left accidentally in the suction line.

Examples of the analyses made are shown in figs. 10.31 and 10.32 for the first order responses at the D.E. and N.D.E. casing supports respectively. Portions of the response curves shown in dashed lines are those which were masked by the compressor surge.

Considering the D.E. response, it may be seen that the casing resonance at 90 c/s resulted in a considerable increase in the level of vibration near the normal running speed. A peak in the response at about 43 c/s occurred somewhat above the fundamental critical frequency

quoted by the makers. A further peak occurred in the vicinity of 65 c/s which is thought to be related to the 60 c/s casing resonance detected during the impedance measurements.

The first order response at the N.D.E. casing support (fig 10.32) showed peaks at the same frequencies as at the D.E. but, contrary to the information obtained from the impedance measurements, the response at the 90 c/s casing resonance was less pronounced than that at the D.E. It seemed that appreciable coupling existed between the vertical and horizontal planes. This is illustrated by the large vertical response of the N.D.E. casing support at the 90 c/s resonance shown in fig 10.33. Whether this coupling was due predominantly to the structure itself or the journal bearing dynamic characteristics is not known.

Tentative figures for the unbalance forces at 90 c/s, based on the horizontal driving point impedances alone, were 355 lbf r.m.s. at the D.E. of the casing and 148 lbf at the N.D.E.

10.5 (ii) (d) Casing Resonances Excited by Compressor Surge.

Confirmation of the resonant frequencies detected during the transient impedance measurements was obtained from the response of the compressor casing to the aerodynamic surge mentioned above. Examples of the response measured at the N.D.E. casing support whilst the machine was running at a nominal speed of 5000 r.p.m. are given in fig 10.34.

From the upper photograph it may be seen that large, peak accelerations of about 1 g. r.m.s. were produced during each surge whilst the repetition rate of the surges was approximately 0.5 per second. A portion of the record is shown to an expanded time base in the second photograph and a component frequency at approximately 90 c/s is identified. This agrees with the casing resonant frequency seen in the impedance plots of figs 10.29 and 10.30.

A further component in the record at about 67 c/s agrees with the resonance in the unbalance responses in figs 10.31 and 10.32, although higher in frequency than the minimum in the impedance modulii. It is probable that this discrepancy was due to the coarse increments chosen (10 c/s) for the digital computer evaluation of the transient spectra in the impedance measurements.

The final photograph of fig 10.34 shows a portion of the response to a higher gain and with the majority of the 67 c/s and 90 c/s components filtered out. A component at about 40 c/s is indicated in this record which is assumed to relate to the 'fundamental' natural frequency of the shaft. This may be compared with the resonance at the same frequency in the unbalance response plots of figs 6.31 & 6.32.

10.5 (iii) Compressor K1

10.5 (iii) (a) General

On this machine the low-pressure compressor was coupled directly to the steam turbine and the H.P. compressor was driven from the far end of the L.P. shaft via a step-up gear box. The L.P. design shaft speed was 5600 r.p.m. (93.3 c/s) whilst the makers quoted a first flexural critical speed of 2400 r.p.m. (40 c/s). For the H.P. casing the design speed and first flexural critical were given as 11,300 r.p.m. (188.3 c/s) and 4170 r.p.m. (69.5 c/s) respectively. The total power required for the two casings under normal conditions was 10,170 H.P., consisting of 4850 H.P. for the low pressure stages and 5320 H.P. for the high pressure stages.

10.5 (iii) (b) Support Impedance Measurements.

The supports for both low and high pressure casings on this machine were continuous along the length of the casing as may be seen in fig 10.2. Like the casing supports used on K2 and K3 they were of fabricated construction and were filled with concrete.

Impedance measurements on the high pressure compressor showed a rigid body resonance at 50 c/s in which the casing was in phase at each end. The horizontal driving point impedances at the N.D.E.and D.E. of the casing were nearly equal at this frequency and both had low-frequency controlling stiffnesses of approximately 2×10^6 lbf/in. These impedances are shown in fig 10.35.

It was noted that the 50 c/s casing resonance was compatible with a single degree-of-freedom having a mass equal to the casing mass of 16,350 lb and a spring stiffness of 4.3×10^6 lbf/in i.e. very nearly equal to the sum of the measured casing support stiffness.

It may be seen from fig 10.35 that above the antiresonance at 100 c/s the impedance characteristics at each end of the casing differed considerably, and whilst the N.D.E. showed a pronounced resonance at 130 c/s a much smaller variation in the impedance modulus was detected at the D.E. Apparently this mode involved a rotation of the casing with a node at some point outside the D.E. of the casing. Inevitably, some coupling with the vertical plane existed and in this connection the resonance at 95 c/s and 180 c/s (the latter close to the normal running frequency) are thought to be predominantly in the vertical plane.

Driving point impedances measured at the bearing housings of the H.P. casing showed similar characteristics to those measured on the other machines of Ethylene III, i.e. they behaved, in the frequency range of interest, as single degree-of-freedom systems attached to the casing. The measured acceleration impedance at the N.D.E.bearing housing for example, shown in fig 10.36, was a factor of 2 to 3 lower than the corresponding casing impedance up to approximately 200 c/s. Above this frequency it decreased in a spring controlled fashion being resonant at 470 c/s.

Because of its large mass it was found that, even with the large pendulum hammer, impedances at the low pressure casing could not be measured much below 70 c/s. A rigid-body casing resonance was detected, however, at approximately 90 c/s - just below the design running speed. This resonance may be seen in the horizontal driving point impedance measured at the N.D.E. casing support shown in fig 10.37. Despite the resonant conditions at this frequency, the impedance was still very high being 8000 lb on an acceleration basis or roughly 25% of the total casing mass.

10.5 (iii) (c) Vibration Monitored During Bearing Failure.

During the early stages of commissioning this machine (May 1967) the turbine and low-pressure compressor were run by themselves. During the run-up recordings were made of vibration levels at various points on the two units. The speed was increased in stages, in the normal way, particular speeds being held for ten to twenty minutes.

When the machine had been running for about ten minutes at 5,900 r.p.m. (98.3 c/s), or 5% overspeed, the N.D.E. bearing of the low-pressure casing was found to be overheating. On dismantling it was found that, apparently due to rubbing at the bearing seals, the white-metal surface of the bearing had been largely destroyed due to the heat generated.

Subsequent analysis of the first order vibration on the compressor clearly showed the onset of the failure. Fig 10.38 illustrates the variation in response at the N.D.E. casing support during the period when the speed was being increased, the rise in level consequent on the bearing failure, and the much-increased amplitudes during run-down.

The growth of vibration during the period immediately preceeding the shutdown is illustrated in fig 10.39 from which it may be seen that an increase of 450% occurred over about $2\frac{1}{4}$ minutes.

A less dramatic, but nevertheless significant, rise in first order vibration was also detected in the recording made whilst the machine was running at a constant speed of 3900 r.p.m. (65 c/s). This is shown in fig 10.39 and is thought to indicate the incipient bearing failure.

The mechanism by which the first order vibration increased during the failure of the bearing is not definitely known but it was presumably a thermal unbalance phenomenon caused by non-uniform heating of the shaft due to its contact with the bearing seal.

Referring to the first-order vibrations at the N.D.E. casing support shown in fig 10.38, it may be seen that a large peak in the response occurred between 90 and 95 c/s. This is attributed to the casing resonance detected in the measured support impedances (see fig 10.37). As mentioned above the driving point impedance was still very high at this frequency and the maximum response following the bearing failure represents a force level, ignoring coupling effects, of:-

$$F_1 = \ddot{x}_1 . Z_1 = 0.186 \times 8000 \text{ lbf} = 1490 \text{ lbf}$$ or 47% of the total shaft weight.

It is interesting to note that, on the basis of existing vibration criteria, the machine would still have been considered satisfactory at 5900 r.p.m. ('fair', Rathbone (63)) even after the considerable rise in amplitude at that speed.

10.5 (iii) (d) First-order Vibration, Complete Line-out

The only start-up of the complete lineout recorded to date was curtailed before normal running speed was reached due to a failure elsewhere on the plant.

Confirmation of the 50 c/s and 130 c/s H.P. casing resonances was obtained however. For example fig 10.40 shows the horizontal response the D.E. of the H.P. compressor casing, the peaks in which may be compared with the 50 c/s resonance in the impedance measurement of

fig 10.35 and the makers' quoted fundamental flexural critical. The general increase in vibration above 120 c/s was also consistent with the measured impedance characteristics.

10.6 General Conclusions

Fig 10.41 illustrates the range of driving point impedance moduli measured at the casing supports and bearing housings of the six machines discussed above.

For comparison, impedances quoted by various authors in published material are also shown. The machinery considered by these authors varied from large turbogenerators to marine line-shafting thrust blocks. All the impedances were quoted in connection with the determination of critical speeds of non-rigidly supported shafts.

The range of impedances given by Caruso (68) was obtained by comparing the observed fundamental critical speed of several steam turbines with values calculated for assumed support impedances. Only three 'standard' designs of support were considered by Caruso although the turbines' shaft capacity varied from 2000 H.P. to 7000 H.P. Because of the method by which they were obtained, these values include the effect of the (unknown) journal bearing dynamic characteristics and are 'real' quantities i.e. they ignore damping.

Dimentberg (17) obtained his impedance value ("dynamic stiffness") by horizontal excitation of a 1500 r.p.m. turbogenerator bearing pedestal. Details of the size of the pedestal were not given.

In Morton's (45) experience the controlling stiffness of the bearing supports of the large turbogenerators with which he was concerned varied between 1.54×10^6 lbf/in and 10^7 lbf/in. Although not specifically stated in his paper, it is assumed that Morton was referring to the frequency range up to 80 c/s since the machines had a maximum normal running frequency of 60 c/s.

The results of a direct experimental measurement of the impedance of a 350 MW turbine bearing pedestal installed at Tilbury 'B' power station have been given by Grant (71). From details of the procedure given by the author it was found that the values as presented were in error by a factor corresponding to the gravitational acceleration, g, (386 in/s^2) and the curve sketched in fig 10.41 has been corrected accordingly.

The limits given by Couchman (75) for the variation in stiffness of large line-shafting bearing blocks for five ships on which experiments had been conducted are also shown in fig 10.41.

Hagg and Sankey (39) have quoted a value of 1.35×10^7 for the vertical stiffness of a turbogenerator bearing pedestal for frequencies up to 35 c/s. The pedestal considered housed a 16 in diameter bearing but no details were given on how the stiffness was derived.

All the above authors, with the exception of Caruso, have been concerned with machines whose running speed was below that of the compressors considered in this chapter. No other published quantitative information on the dynamic characteristics of bearing supporting structures of high speed machinery is known to the writer. The present results suggest that between 100 and 200 c/s (6,000 to 12,000 r.p.m.) variations in driving point impedance by a factor between 100 and 300 are not uncommon.

With regard to the machines of Ethylene II and III, despite the necessity to obtain the information under less than ideal experimental conditions, it has been shown that:-

(a) the transient excitation technique for obtaining the mechanical impedance of bearing support structures was of considerable value. To overcome the remaining difficulty of measuring impedances of massive structures at low frequencies it is proposed to experiment with accelerometers having a very high sensitivity and a relatively

low natural frequency compared with those available commercially (see section 10.4 (ii) (c)).

(b) good correlation was achieved between the observed variations in vibration with shaft speed and the measured impedance characteristics of the compressor casings.

(c) the very wide variations in the measured impedances at the various running frequencies support the argument against the use of any acceptance criterion based on the vibration amplitudes alone.

Although the oscillatory shaft force transmitted to the bearings of the machine have in many cases been based on the driving point impedance alone it would be necessary for more reliable estimates to be obtained to include the effect of coupling between the bearing planes of the casing (and, perhaps, between the casings themselves), together with measurements of the phase of the response. In the light of the results obtained from the model rig (Chapter 6) and the rotary converter (Chapter 7), for machines having 'rigid' casings of the type considered it is thought that the transfer impedances $Zx_1\ x_2$, $Zy_1\ y_1$, $Zx_2\ y_2$, between axial planes of measurement would suffice. But since, by using the transient approach, the time required to obtain the initial data for such impedance measurements is relatively short, there seems no reason why more extensive measurements should not be made if necessary.

K107

K105

K101

FIG. 10.1 CENTRIFUGAL COMPRESSORS ; "ETHYLENE II"

FIG. 10.3. SITE INSTRUMENTATION.

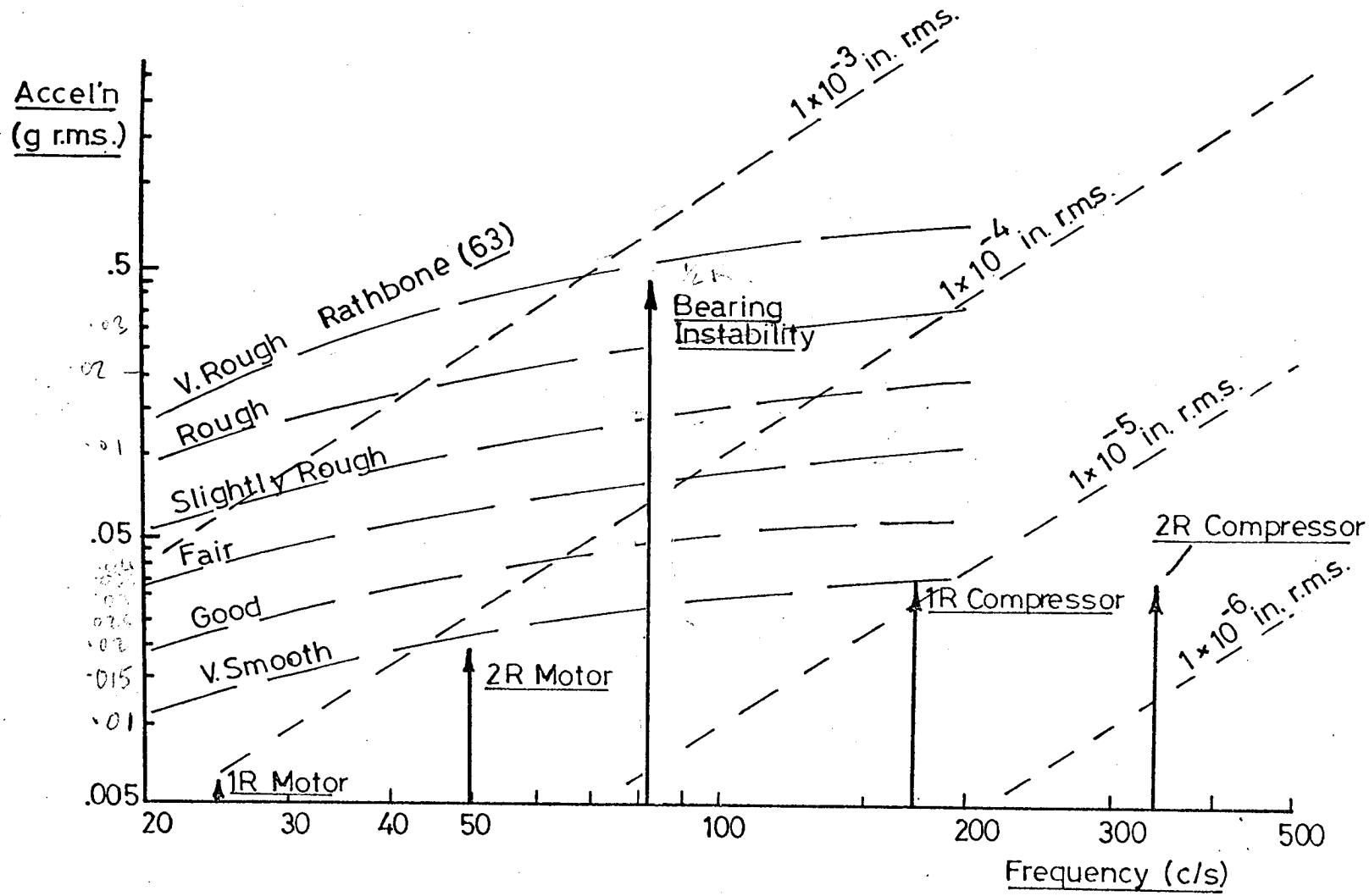

FIG. 10.4. LINE SPECTRUM OF VIBRATION AT N.D.E. BEARING HOUSING. COMPRESSOR K107.

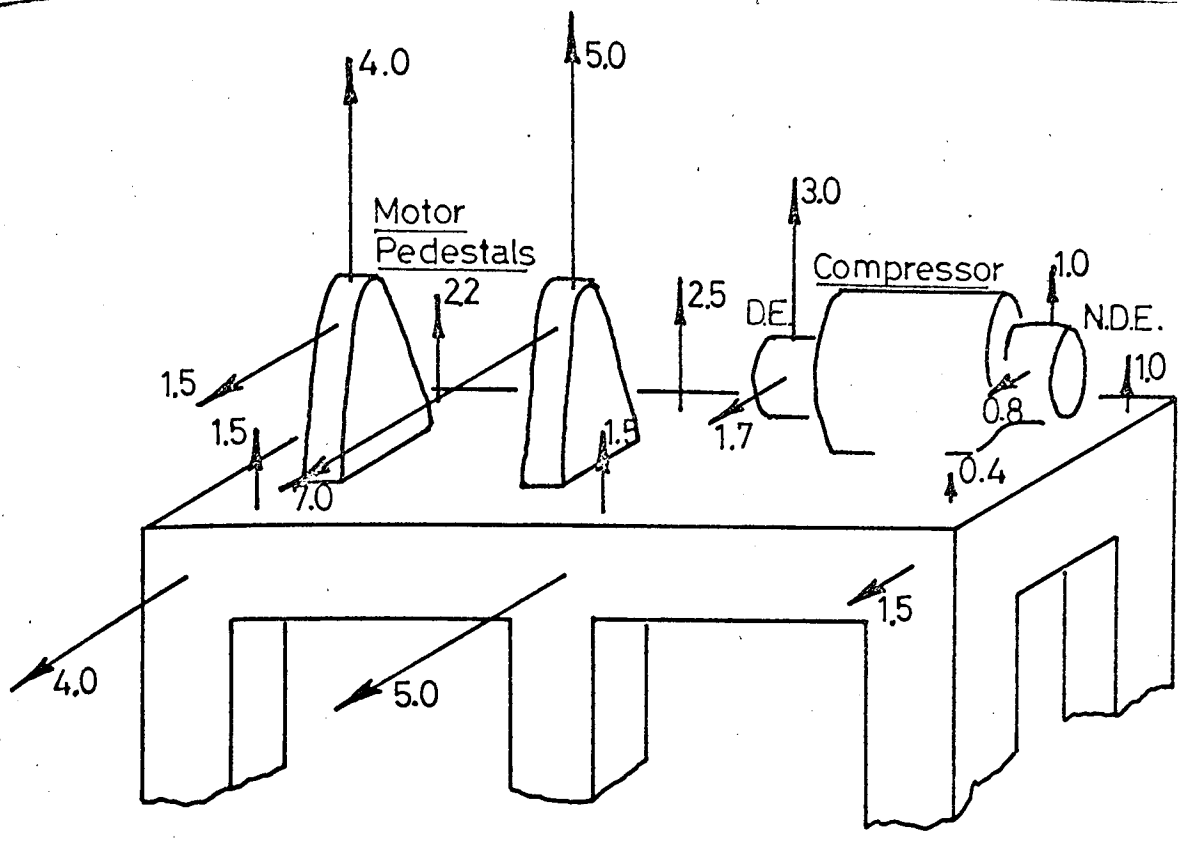

ALL AMPLITUDES $\times 10^{-4}$ in r.m.s.

MOTOR FREQUENCY
24.7 c/s

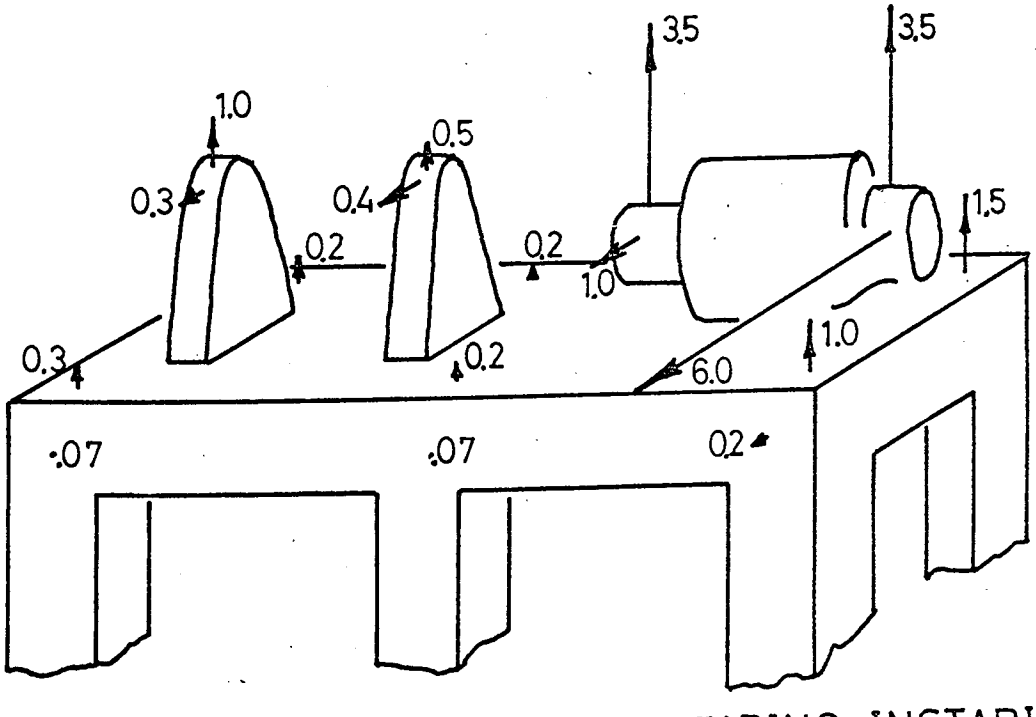

BEARING INSTABILITY
FREQUENCY 82 c/s

FIG. 10.5 VIBRATION AMPLITUDES
COMPRESSOR K107

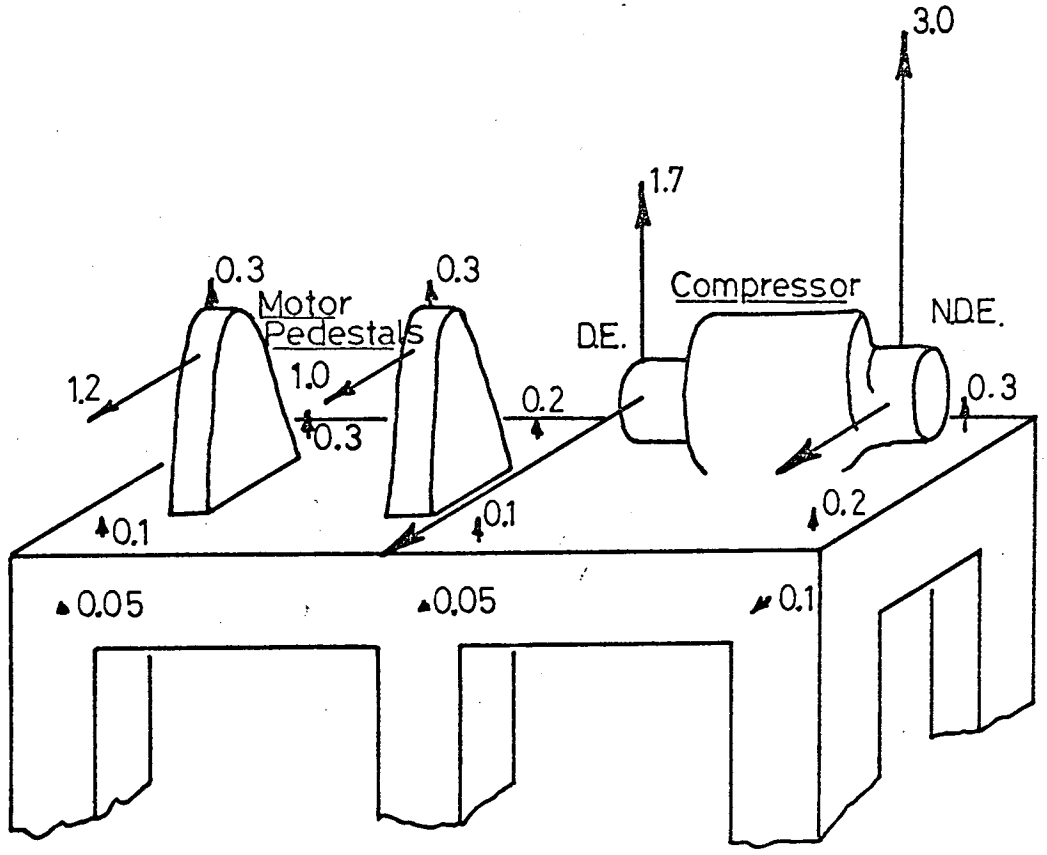

1st ORDER COMPRESSOR
FREQUENCY 173.3 c/s.

ALL AMPLITUDES $\times 10^{-4}$ in. r.m.s.

FIG. 10.6. VIBRATION AMPLITUDES. COMPRESSOR K107.

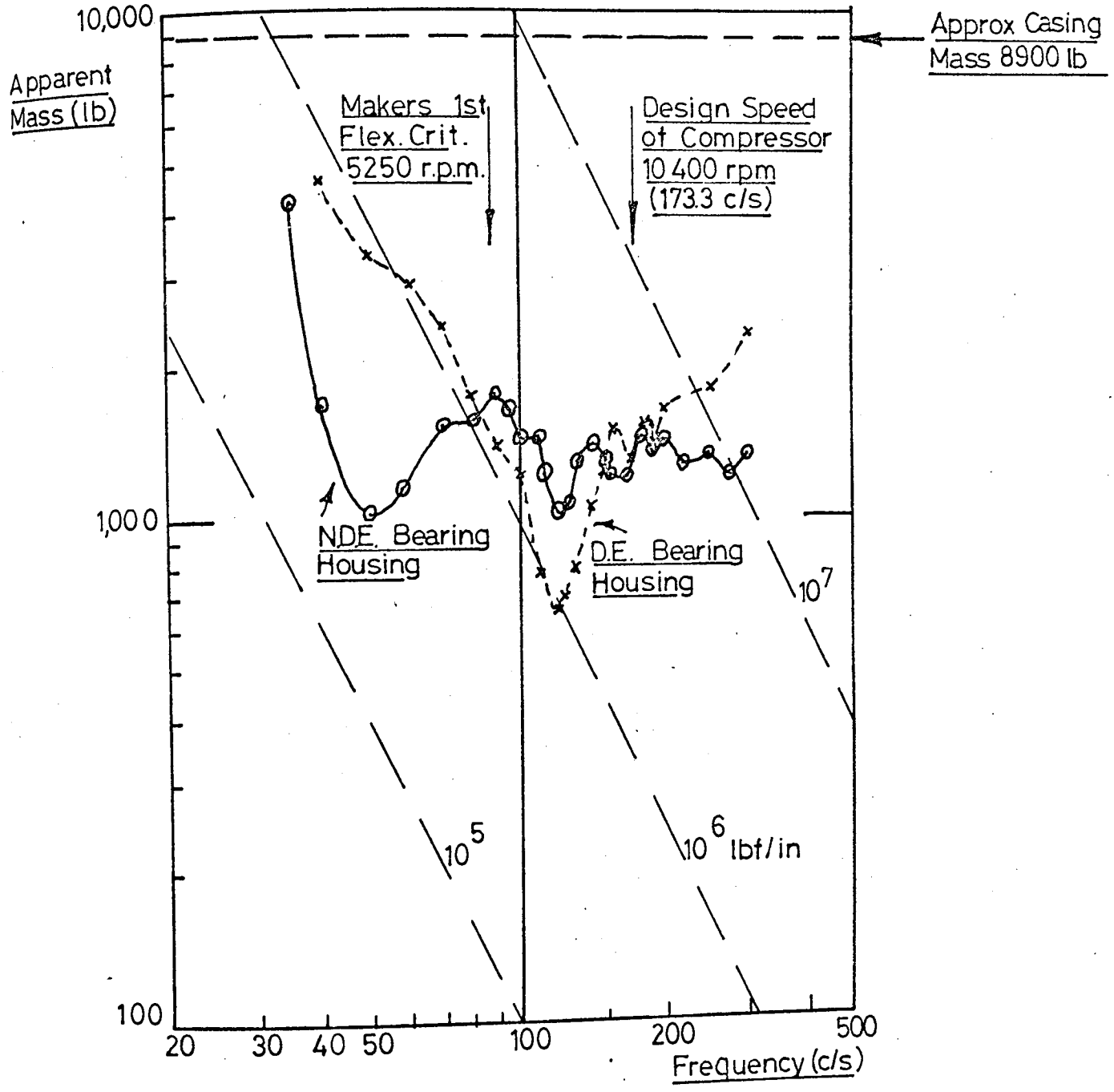

FIG. 10.7. DRIVING POINT IMPEDANCES MEASURED AT BEARING HOUSINGS OF COMPRESSOR K 107. IN HORIZONTAL PLANE

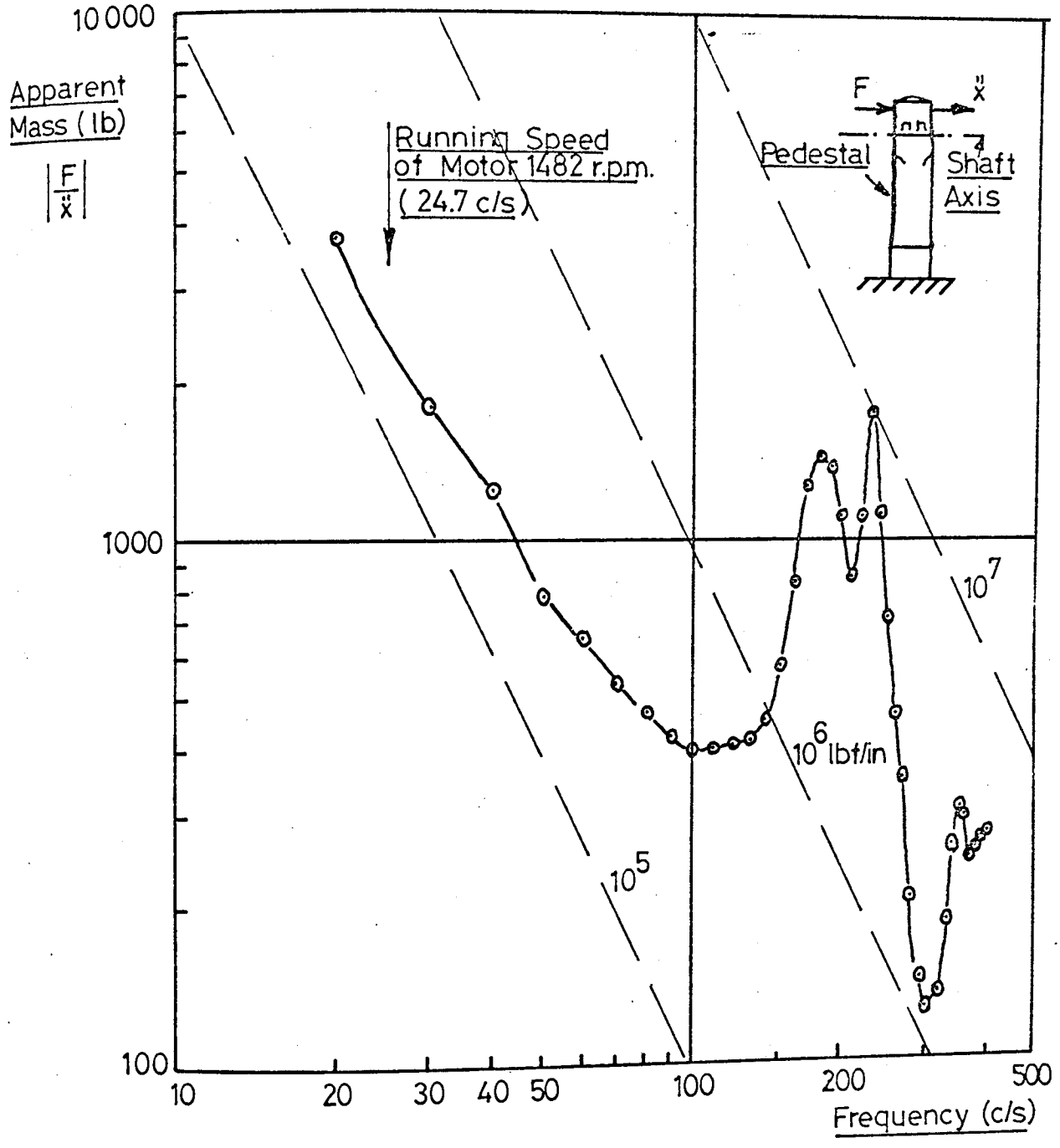

FIG. 10.8. AXIAL DRIVING POINT IMPEDANCE OF MOTOR PEDESTAL REMOTE FROM COMPRESSOR CASING, K107

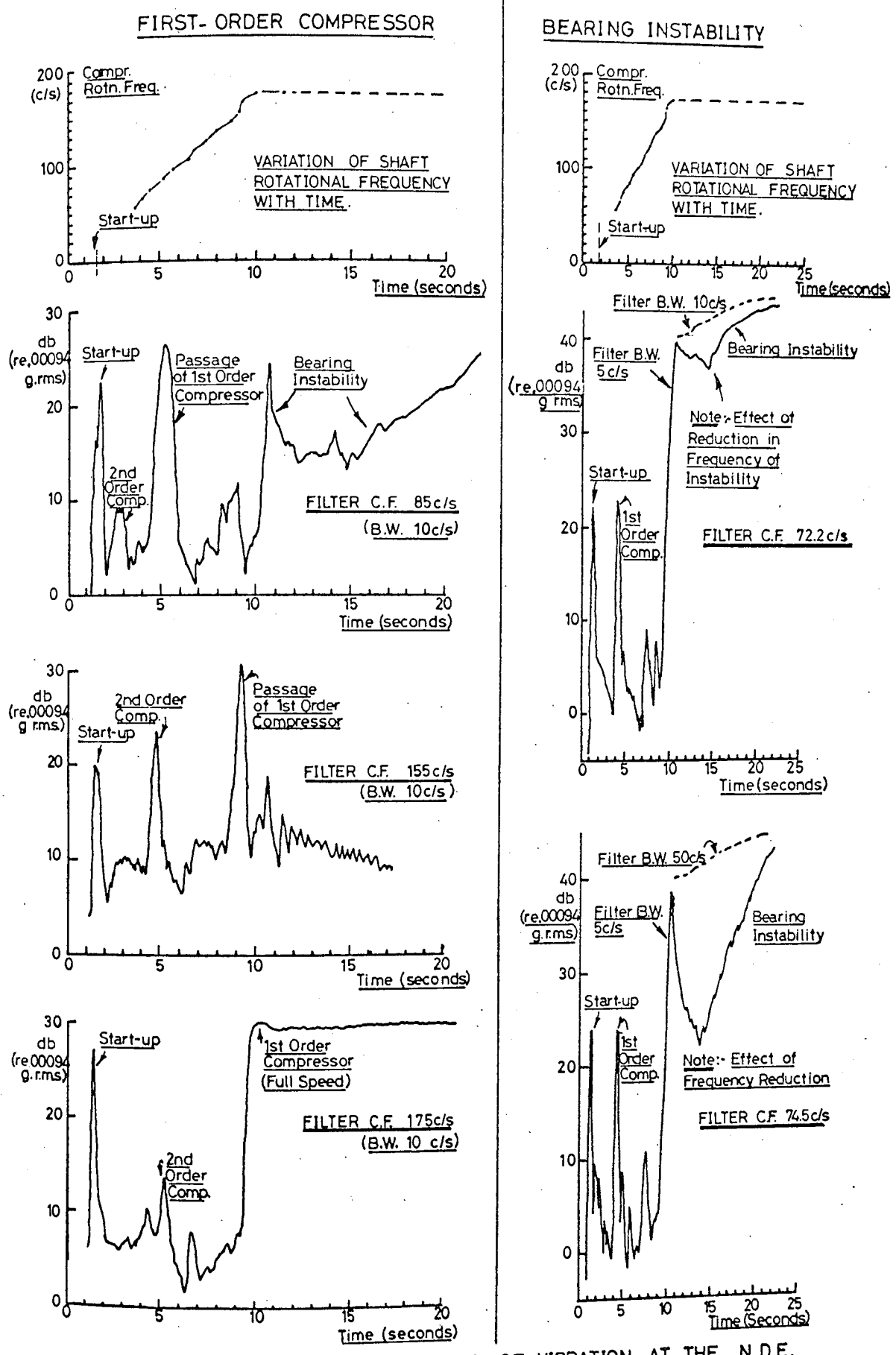

FIG. 10.9. EXAMPLES OF THE ANALYSIS OF VIBRATION AT THE N.D.E. BEARING HOUSING OF COMPRESSOR K107. (HORIZONTAL PLANE)

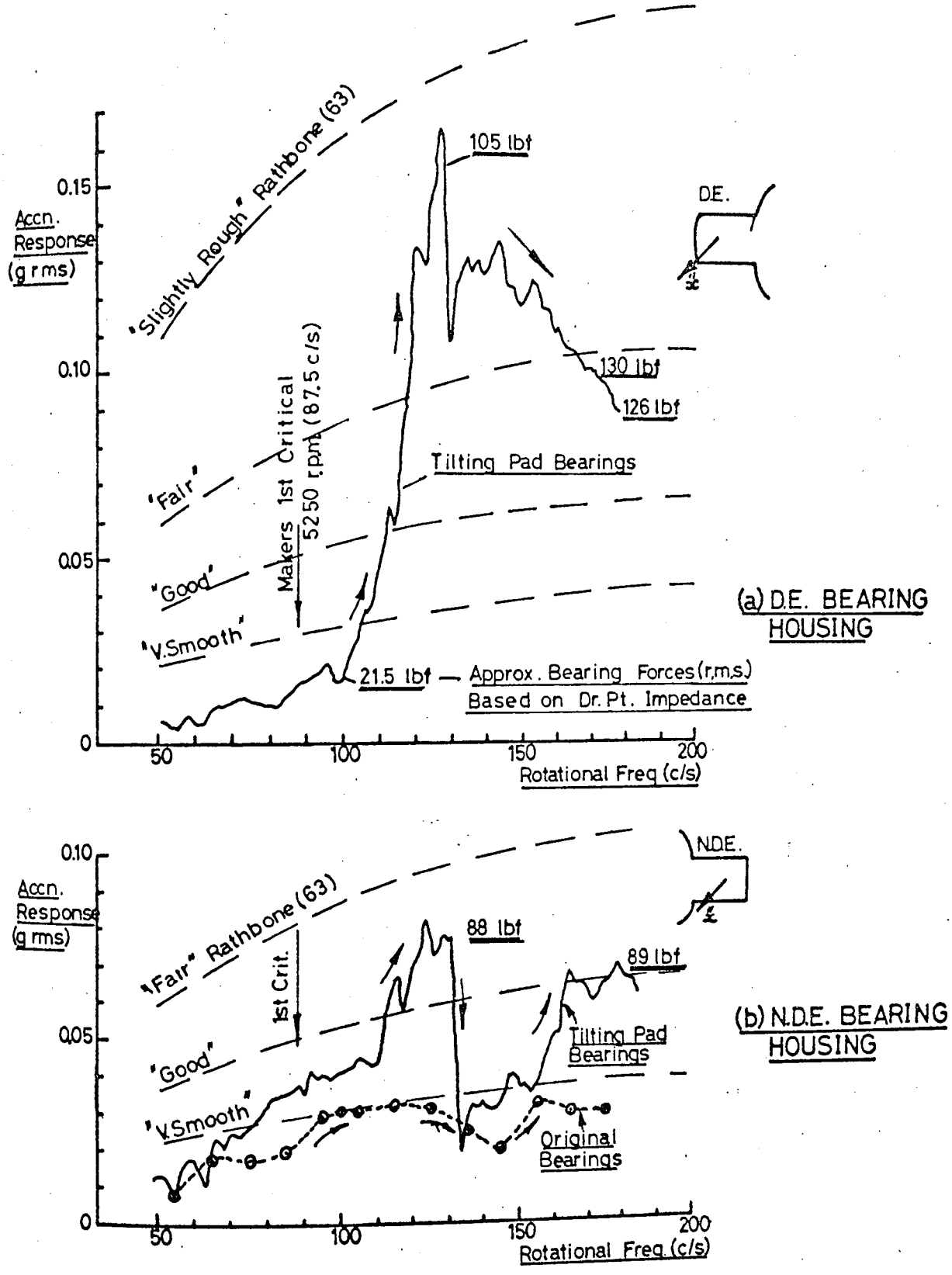

FIG. 10.10. FIRST-ORDER VIBRATION AT BEARING HOUSINGS OF COMPRESSOR K107, (HORIZONTAL PLANE)

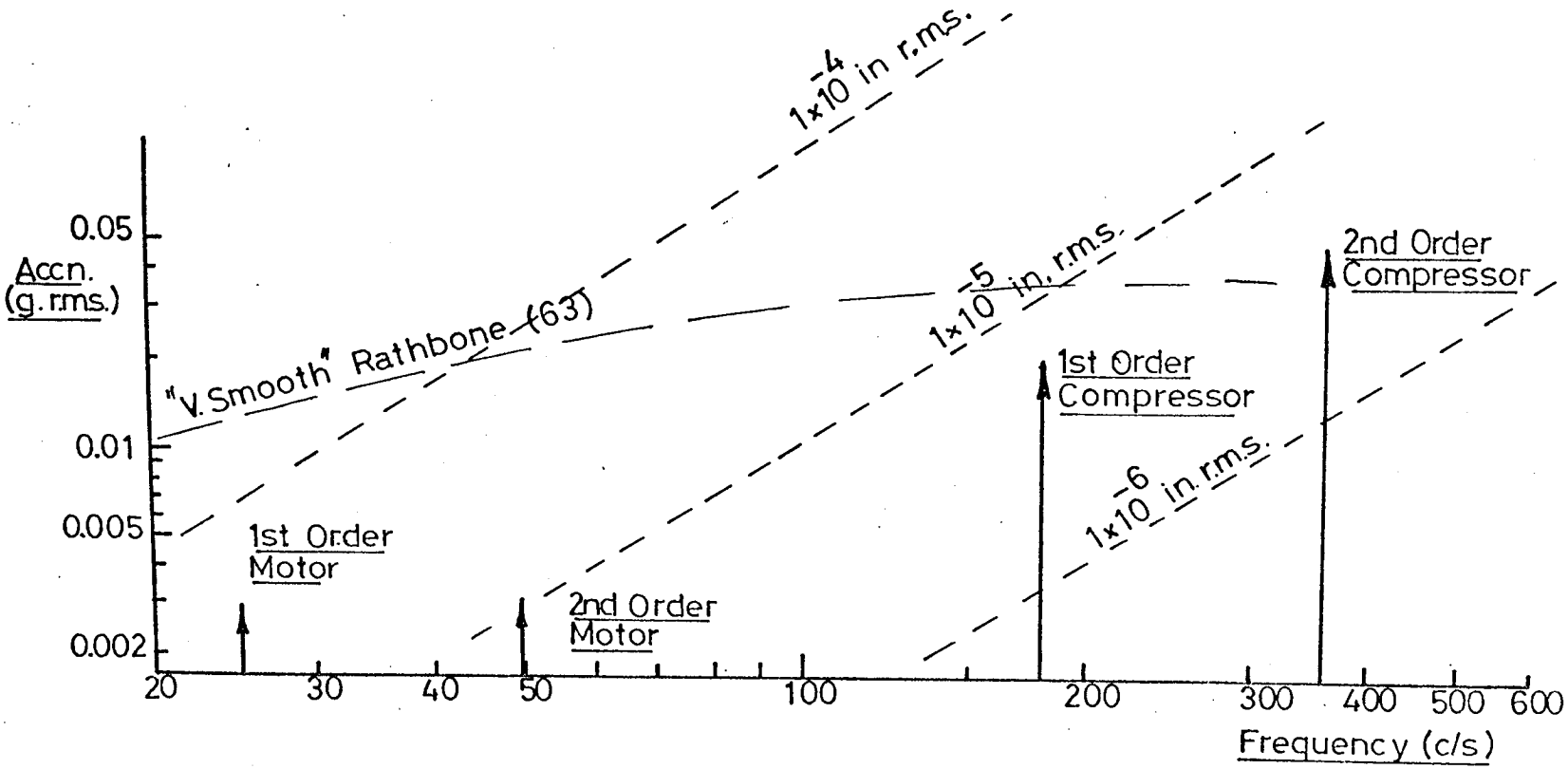

FIG. 10. 11. LINE SPECTRUM OF VIBRATION AT D.E. BEARING HOUSING OF COMPRESSOR K105. (HORIZONTAL PLANE).

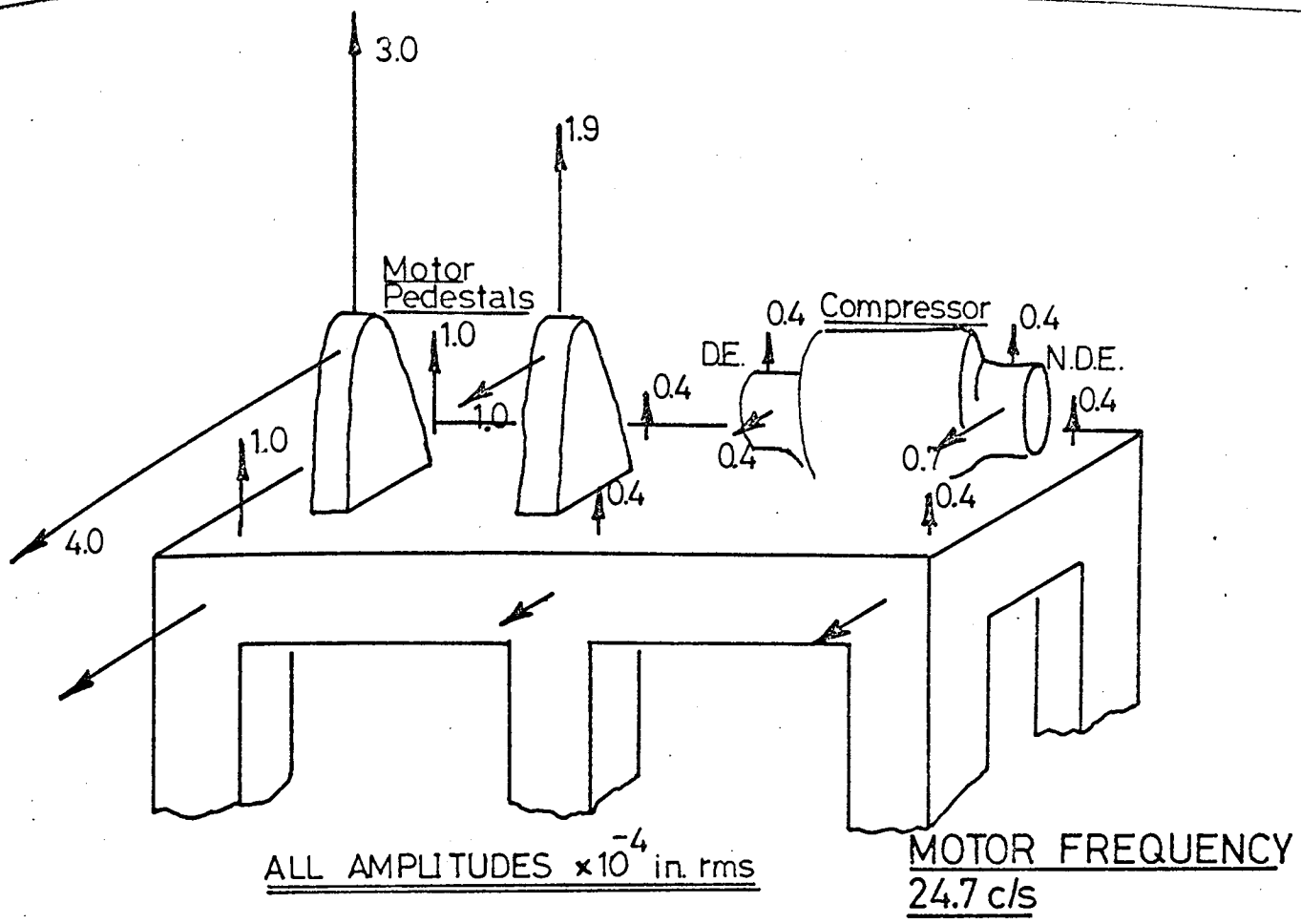

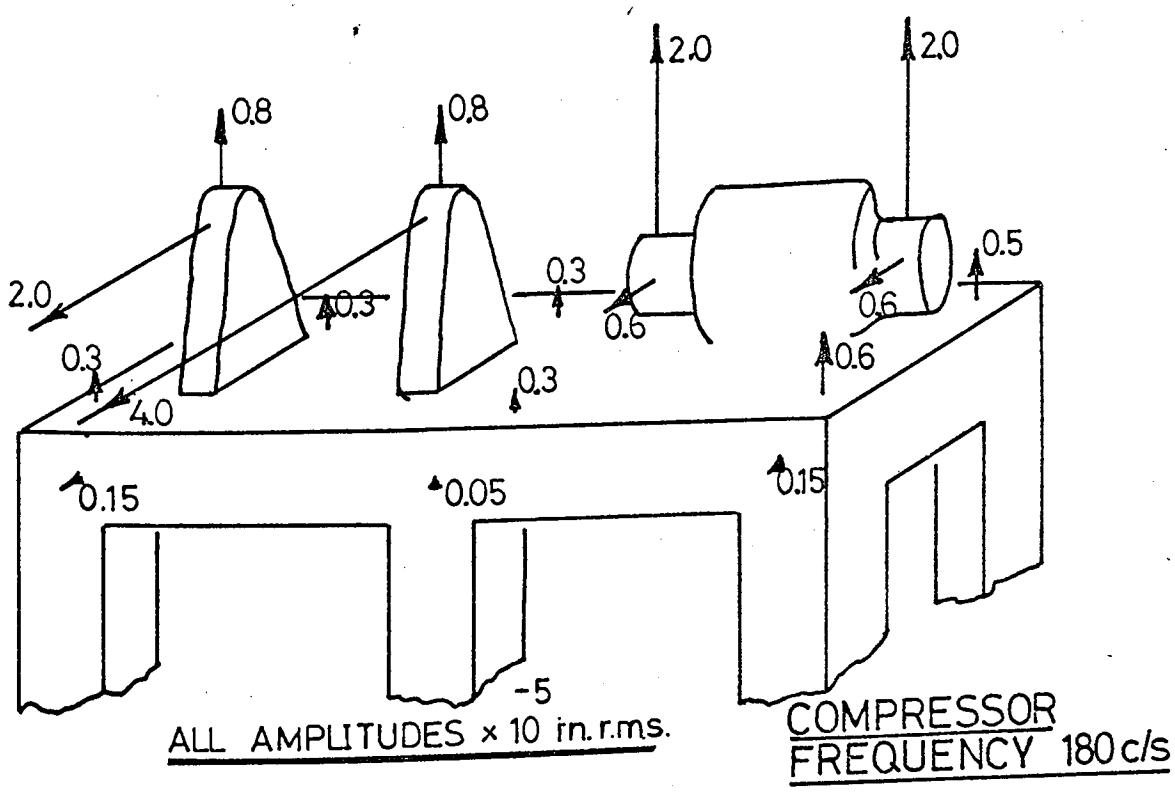

FIG.10.12. VIBRATION AMPLITUDES. COMPRESSOR K105.

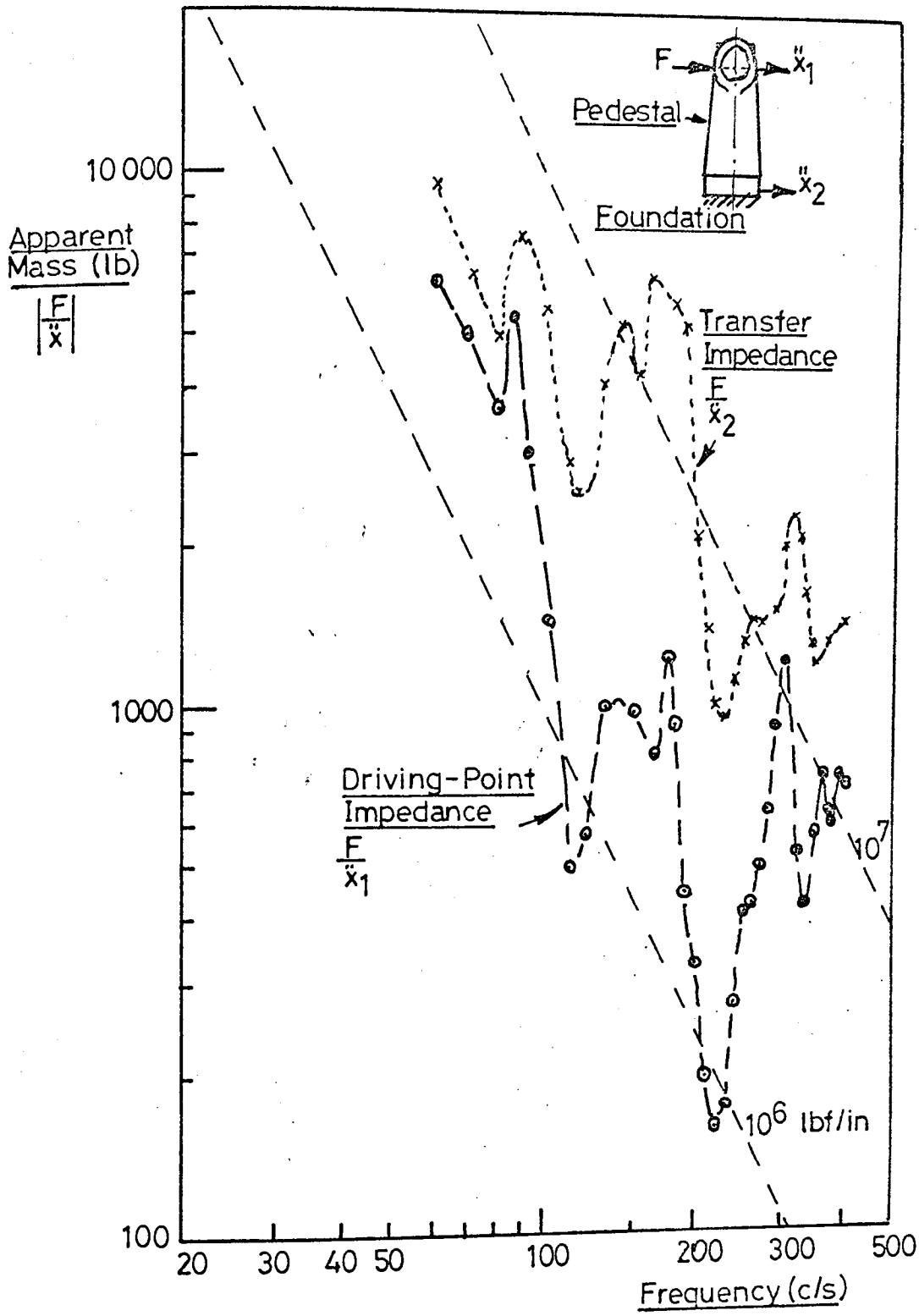

FIG.10.13. DRIVING POINT & TRANSFER IMPEDANCES MEASURED ON MOTOR PEDESTAL REMOTE FROM COMPRESSOR. K105.

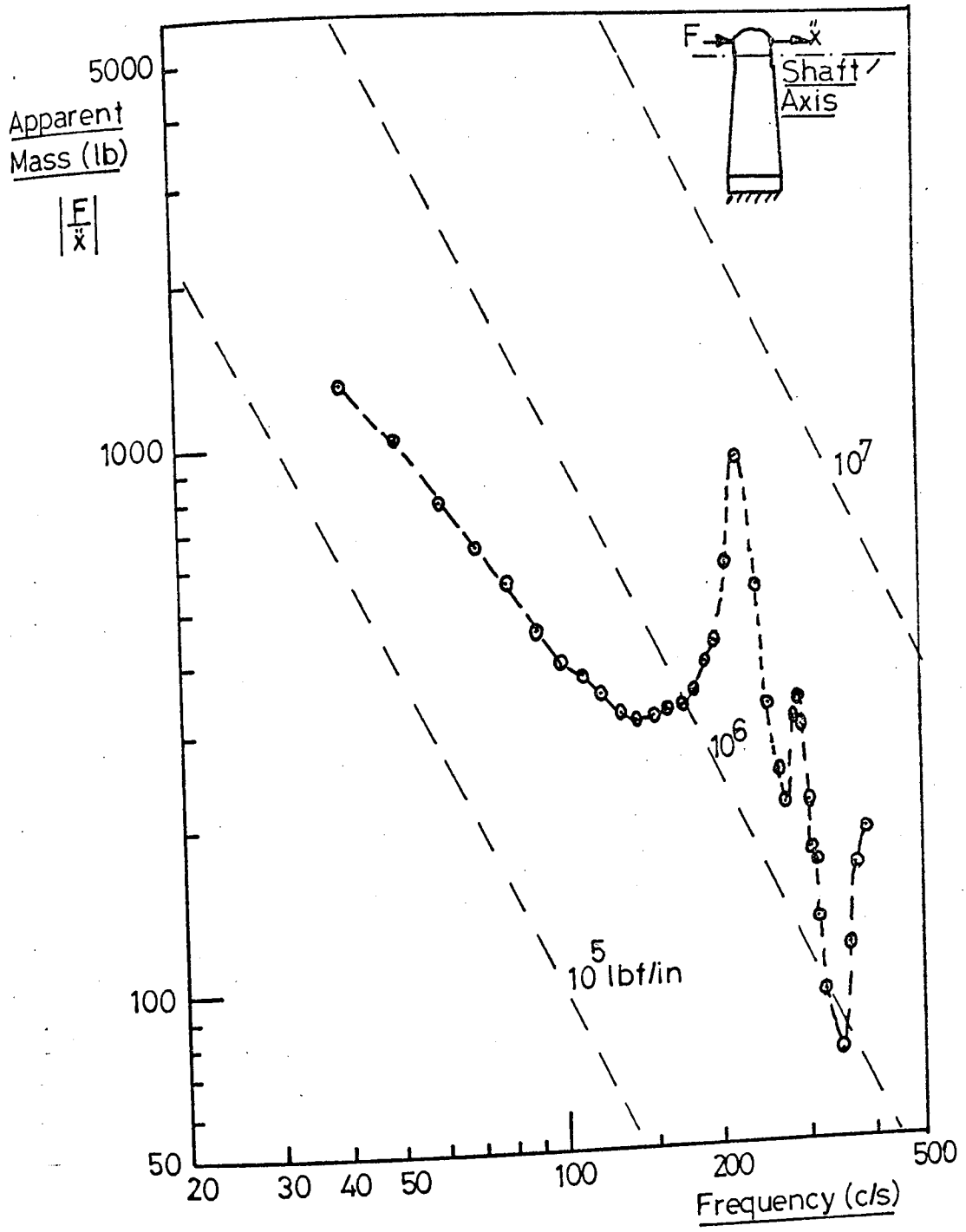

FIG. 10.14. AXIAL DRIVING POINT IMPEDANCE OF MOTOR PEDESTAL REMOTE FROM COMPRESSOR CASING, K105

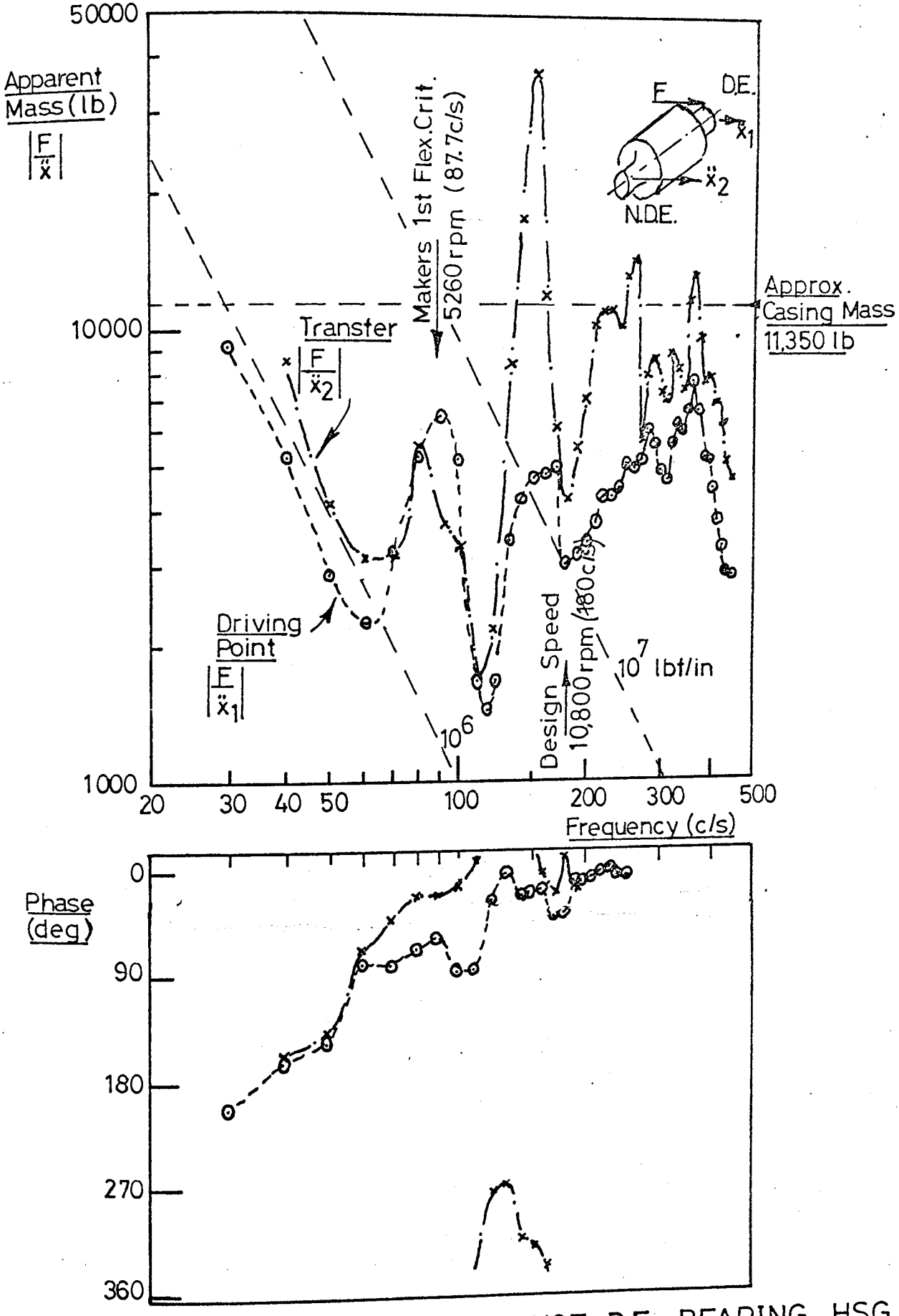

FIG. 10.15. DRIVING POINT IMPEDANCE D.E. BEARING HSG. & TRANSFER IMPEDANCE. COMPRESSOR K105.

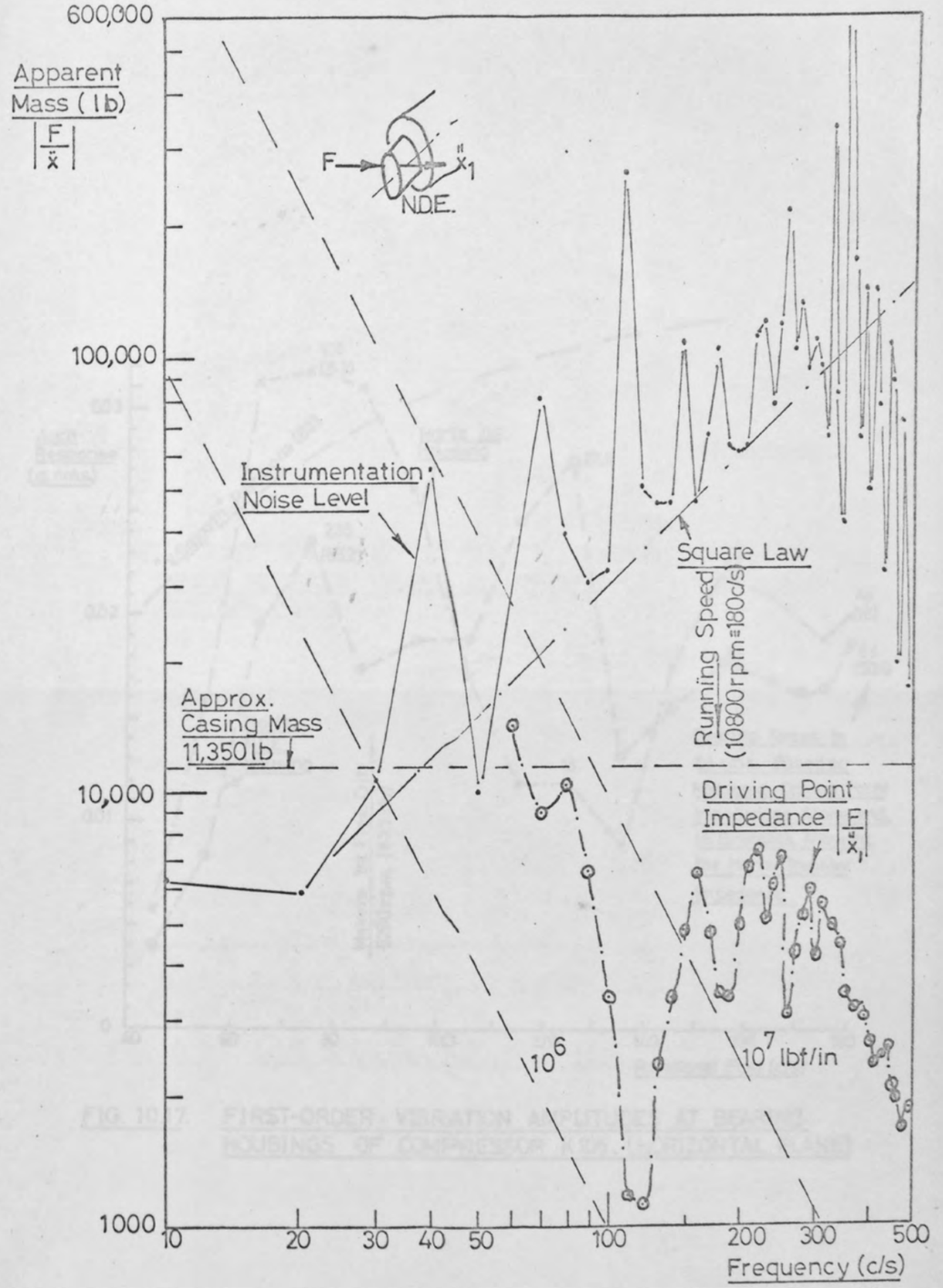

FIG. 10.16. DRIVING POINT IMPEDANCE NDE BEARING HOUSING. COMPRESSOR K105.

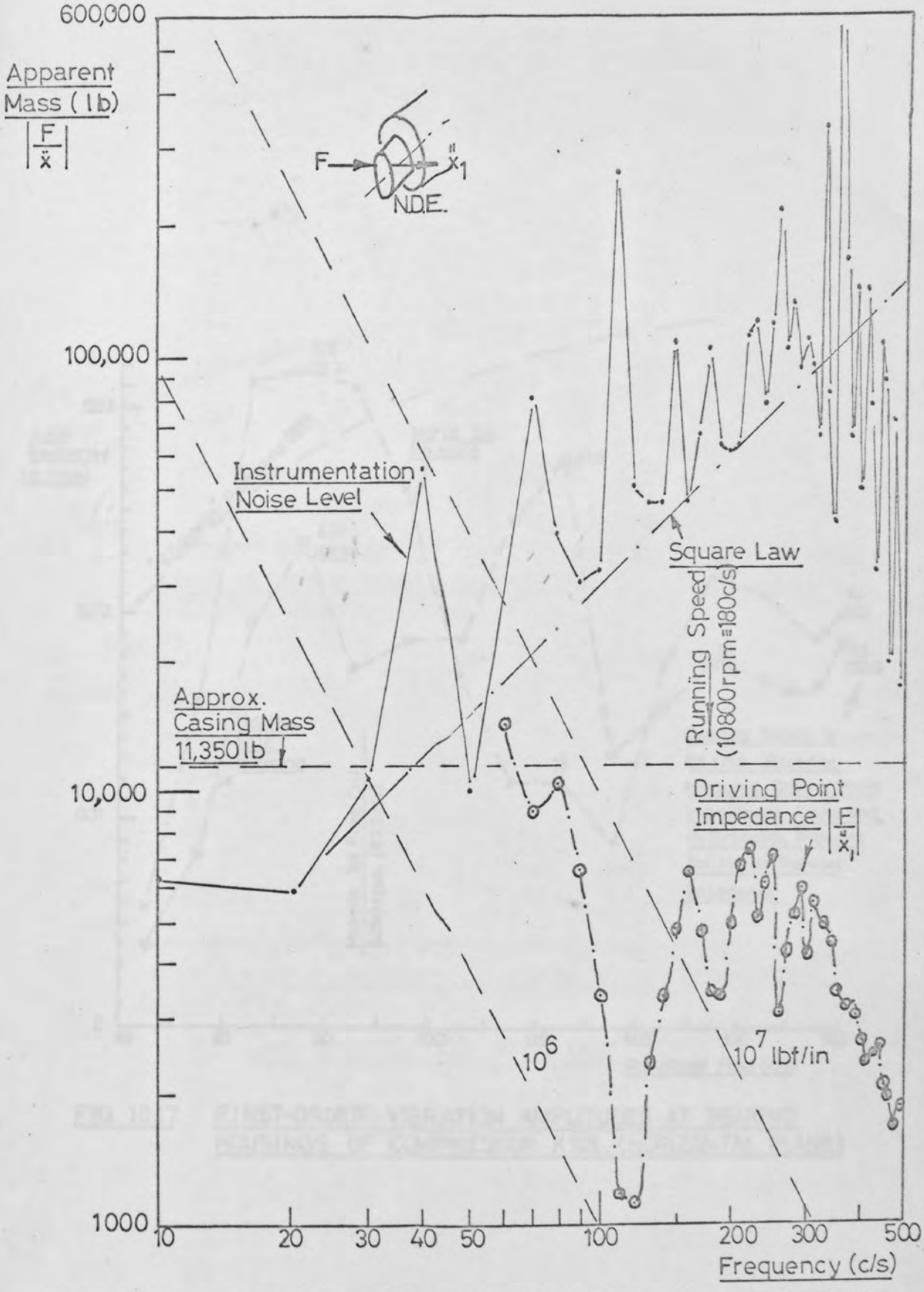

FIG. 10.16. DRIVING POINT IMPEDANCE NDE BEARING HOUSING. COMPRESSOR K105.

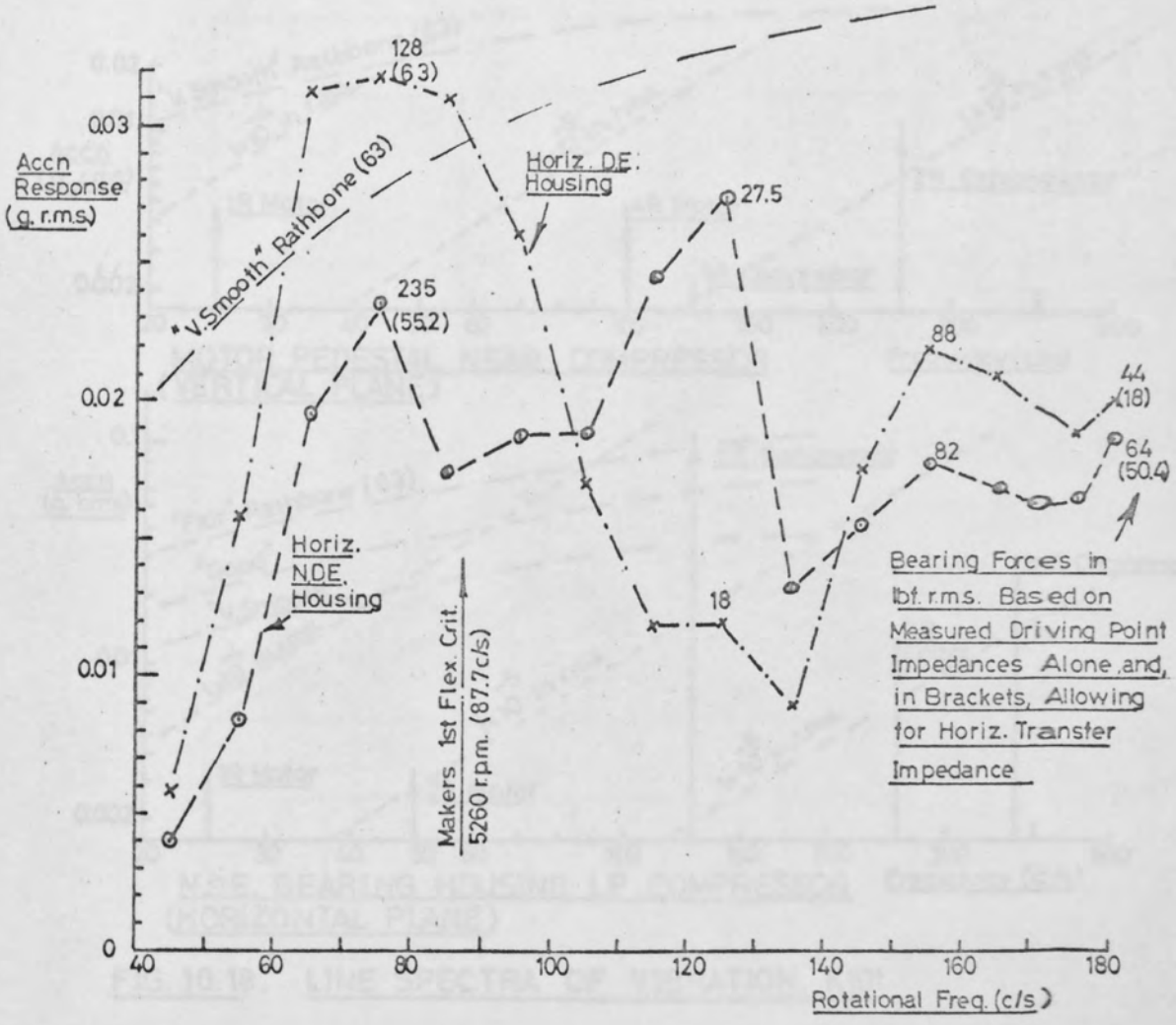

FIG. 10.17. FIRST-ORDER VIBRATION AMPLITUDES AT BEARING HOUSINGS OF COMPRESSOR K105. (HORIZONTAL PLANE)

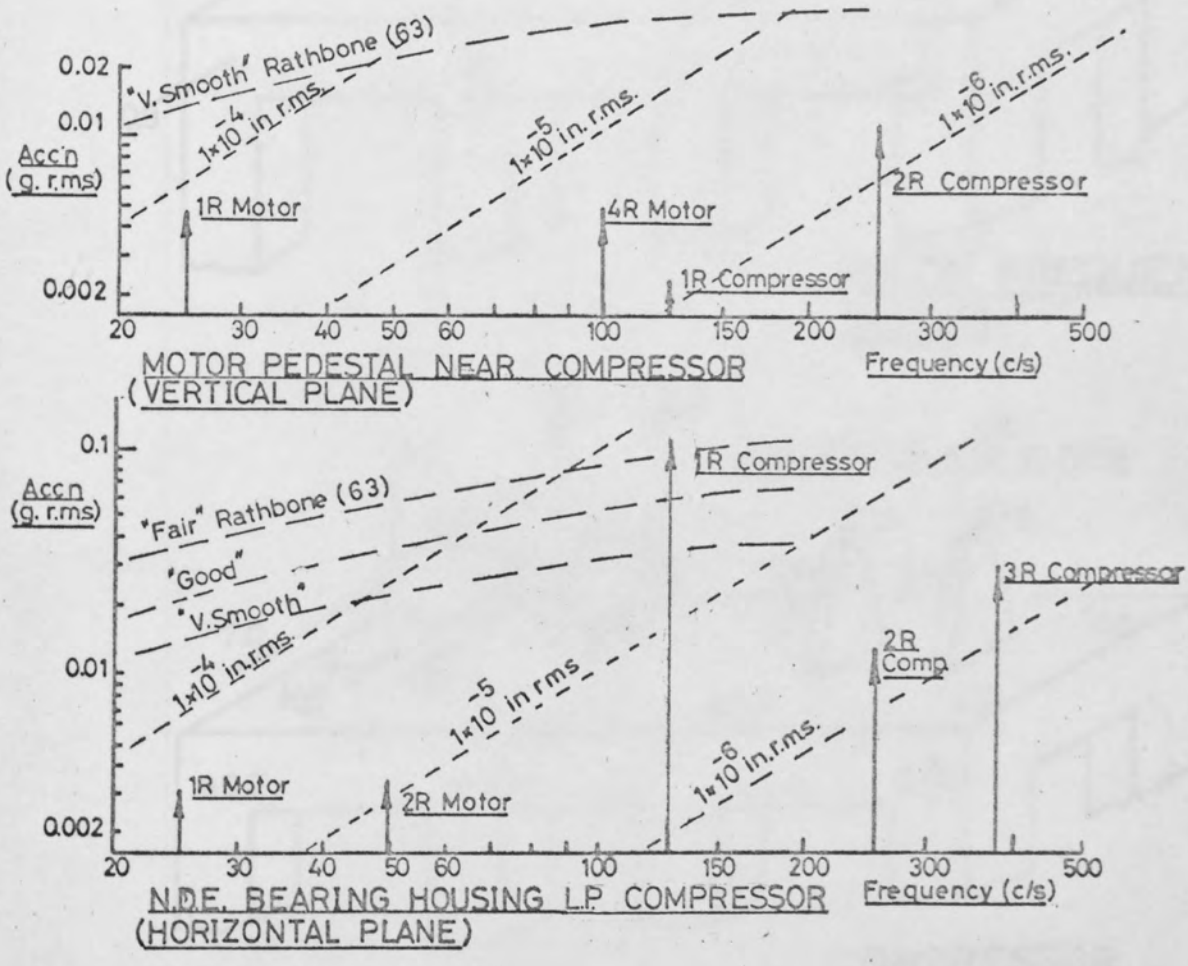

FIG. 10.18. LINE SPECTRA OF VIBRATION, K101

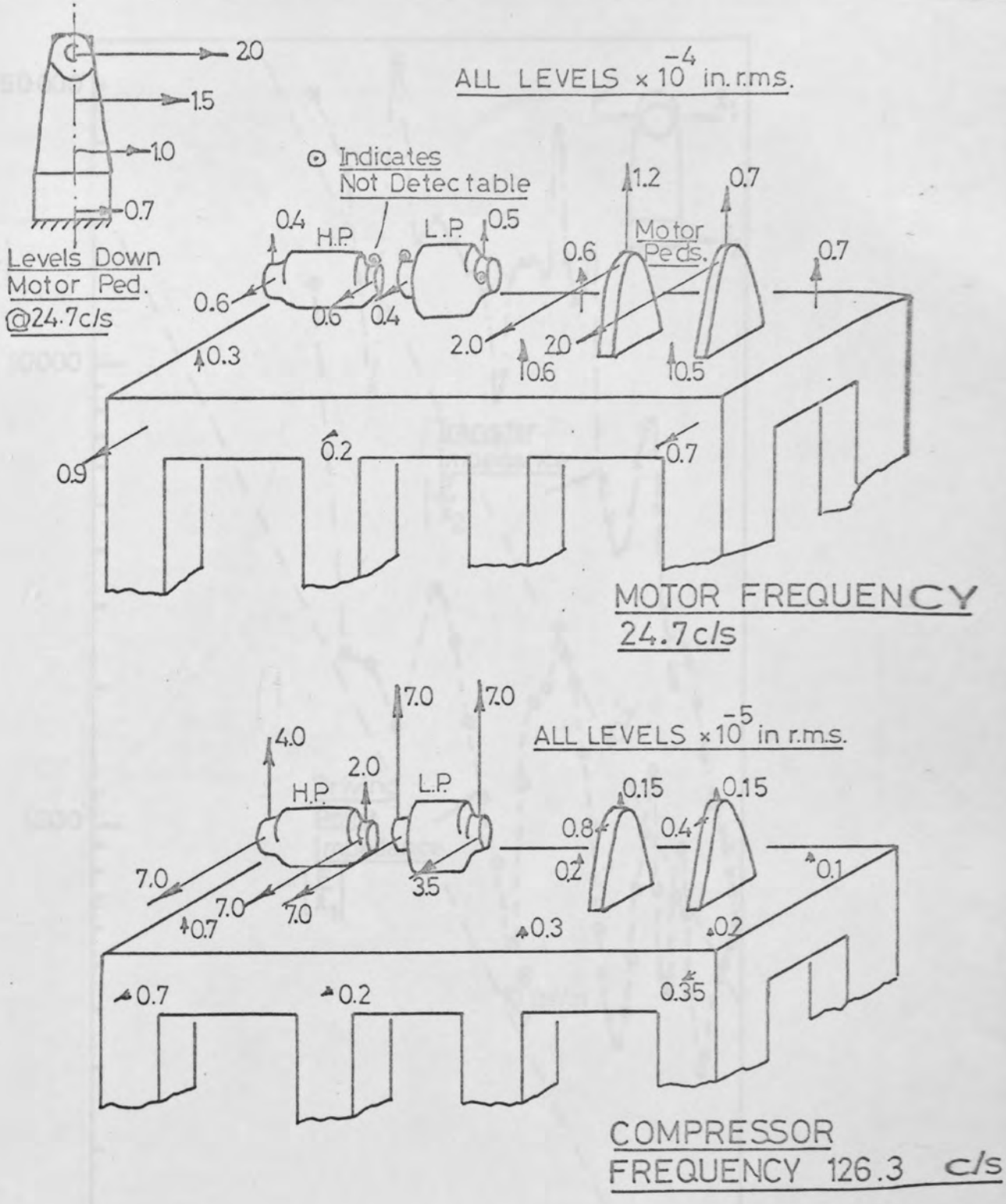

FIG.10.19. VIBRATION AMPLITUDES COMPRESSOR K101.

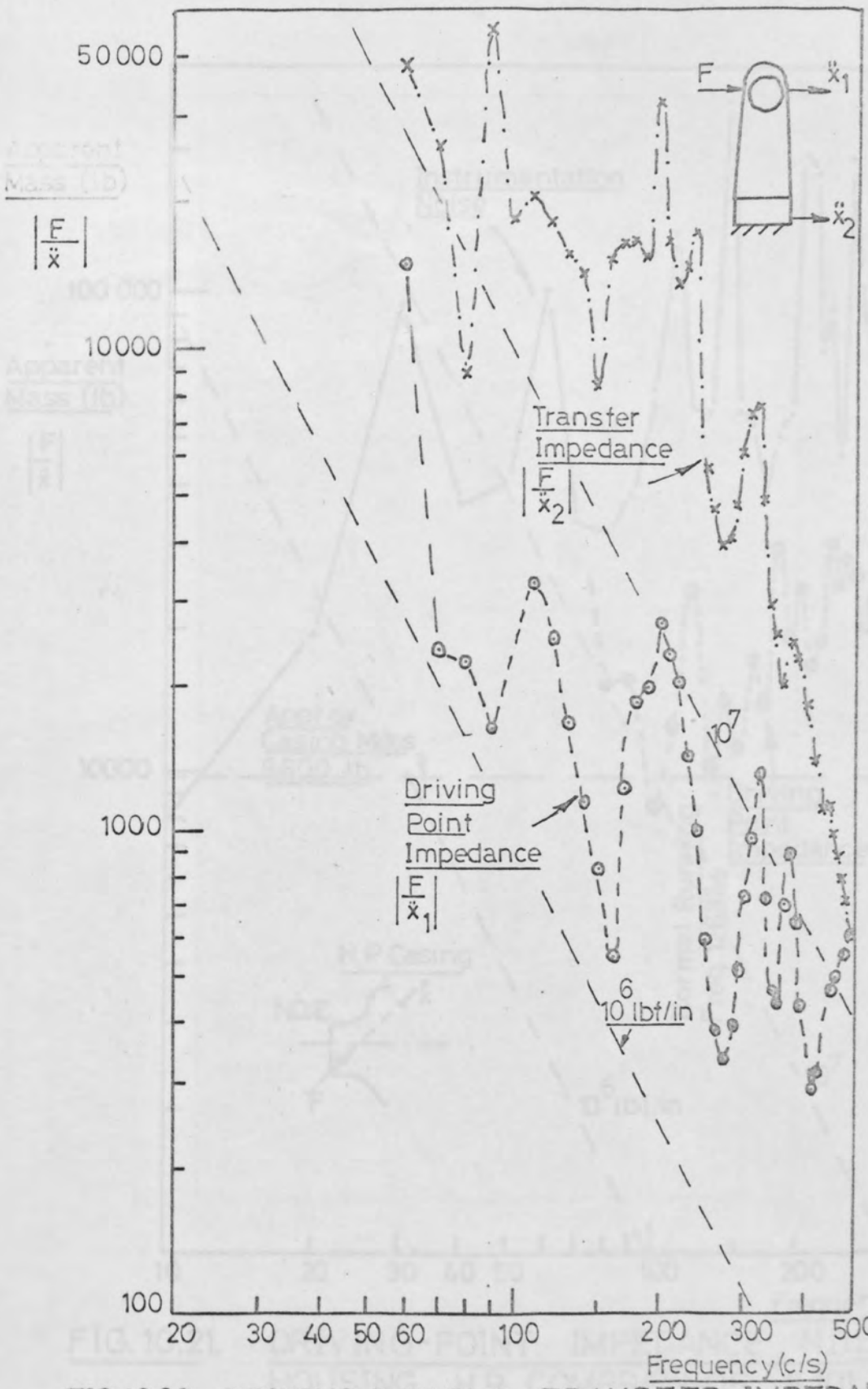

FIG.10.20. DRIVING-POINT & TRANSFER IMPEDANCES MOTOR PEDESTAL NEAREST COMPRESSOR, K101

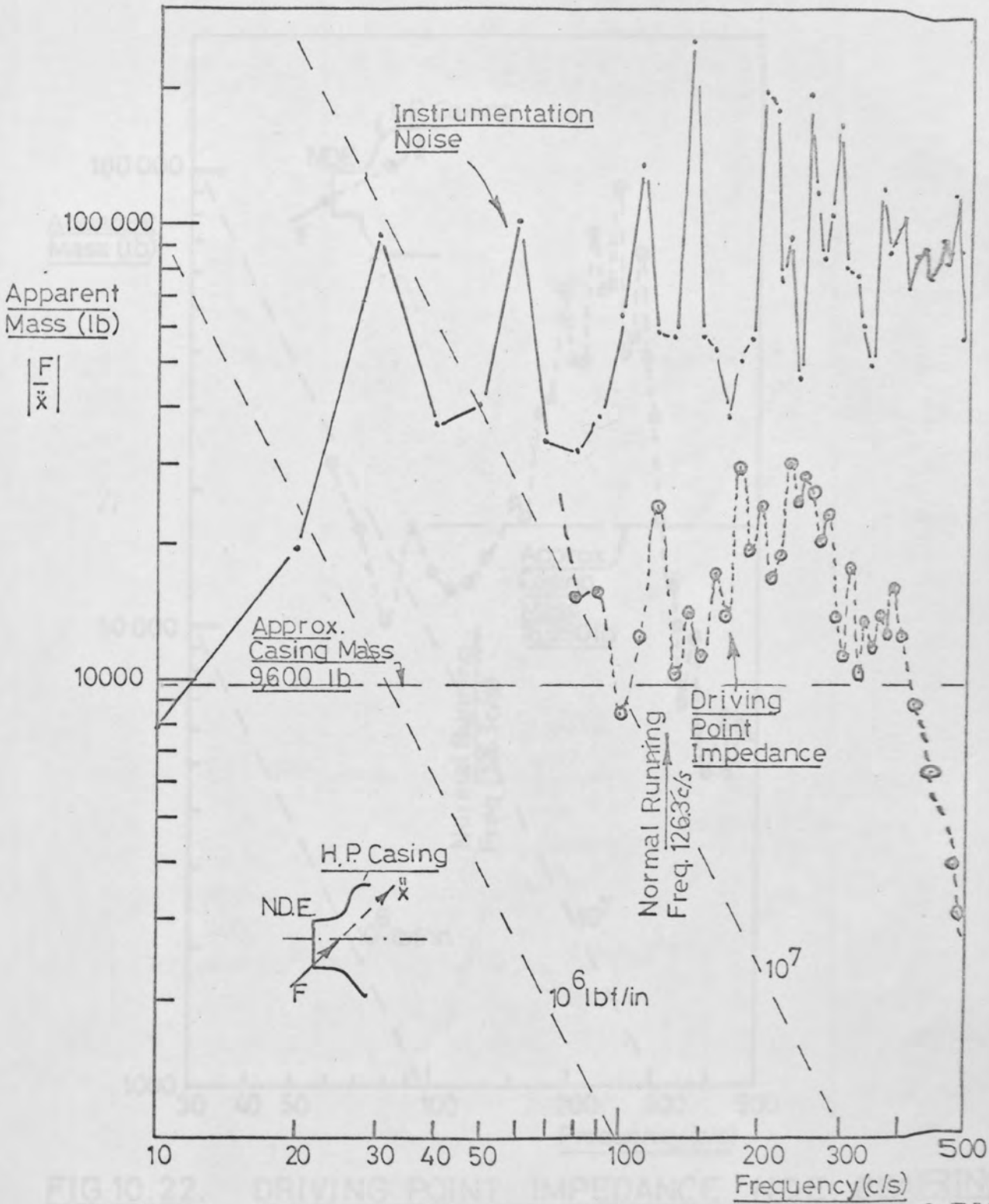

FIG. 10.21. DRIVING-POINT IMPEDANCE N.D.E. BEARING HOUSING H.P. COMPRESSOR, K101. (HORIZONTAL PLANE)

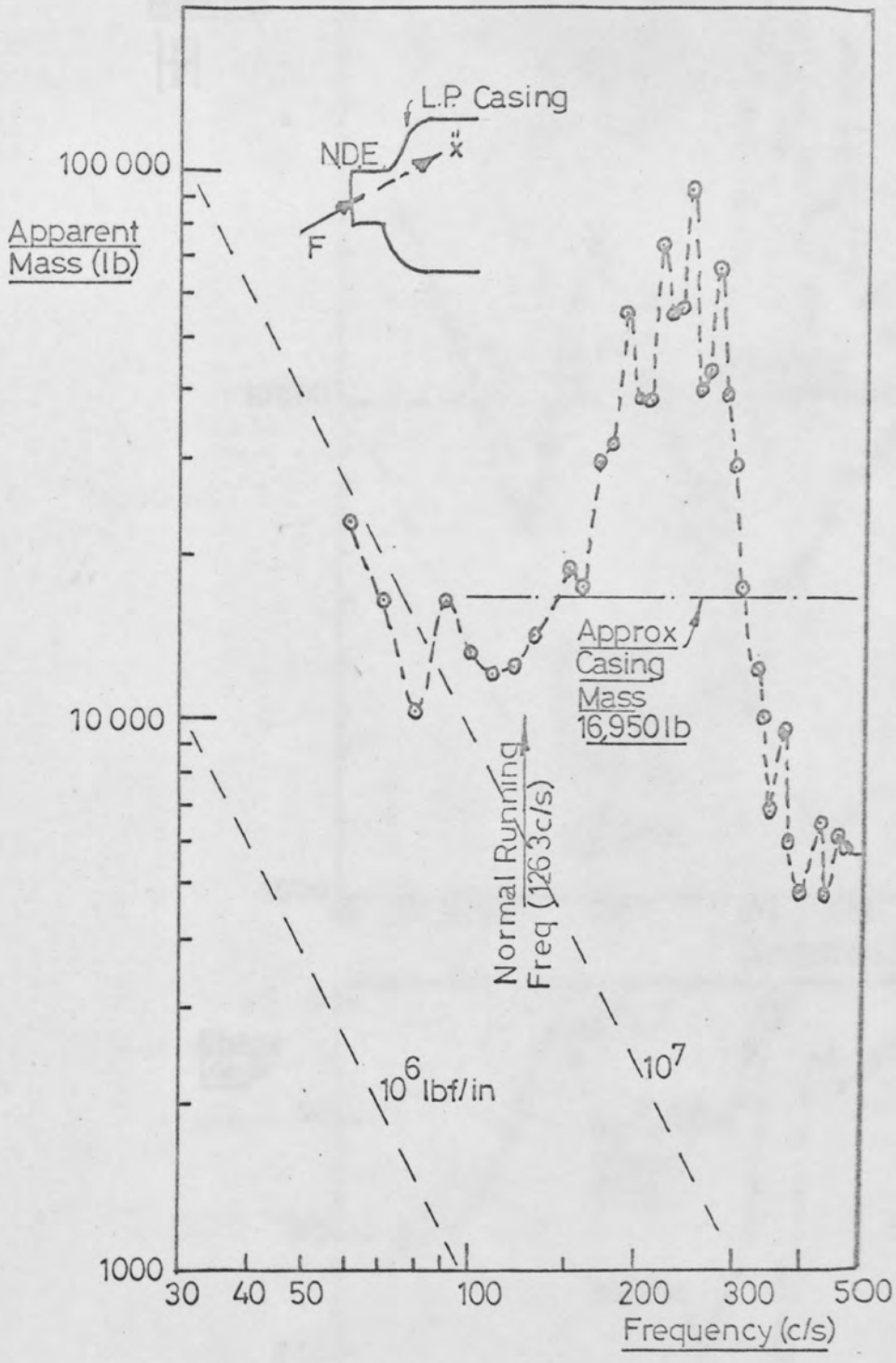

FIG.10.22. DRIVING POINT IMPEDANCE N.D.E. BEARING HOUSING L.P. COMPRESSOR, K101. (HORIZONTAL PLANE)

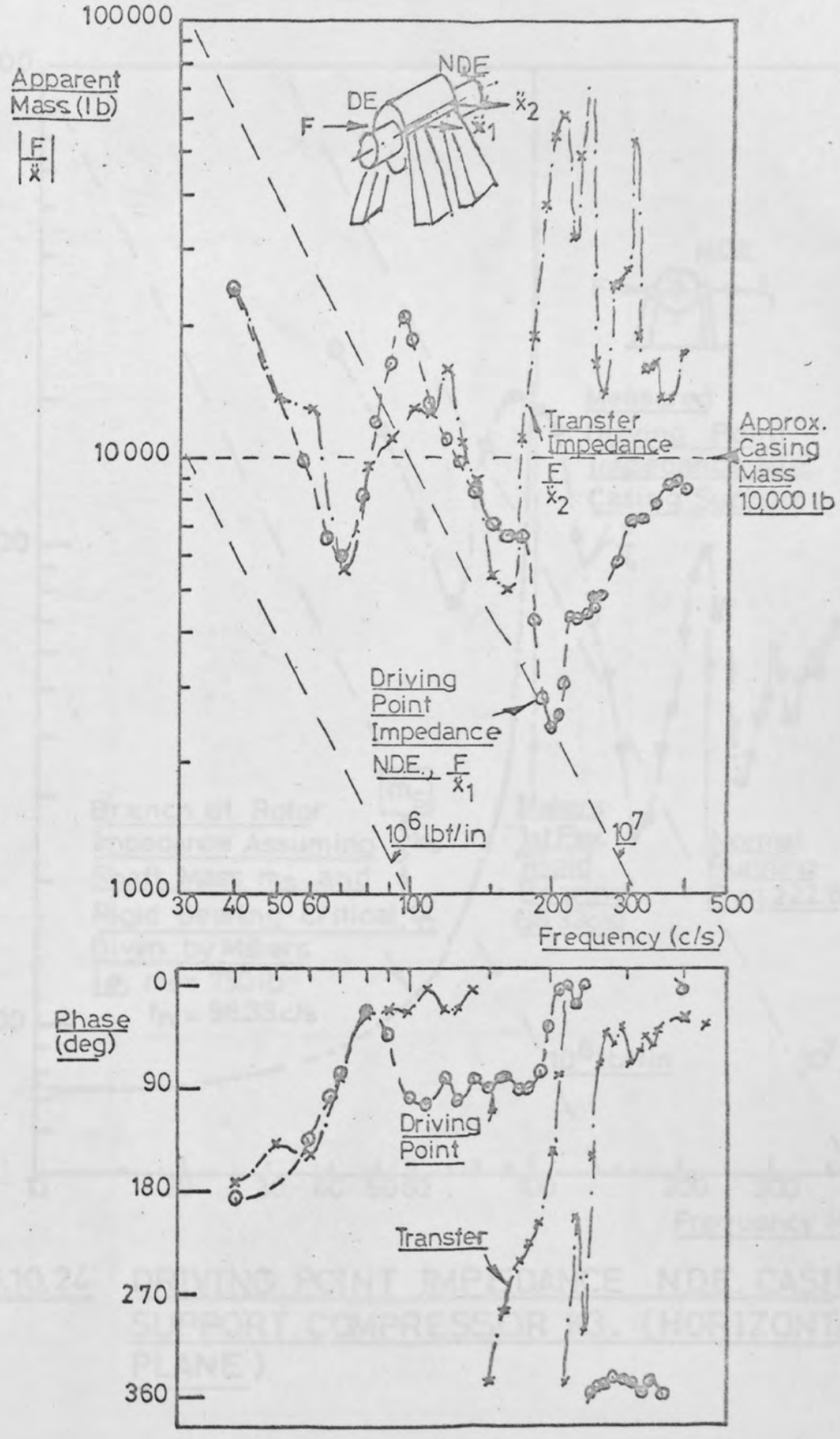

FIG.10.23. DRIVING POINT & TRANSFER IMPEDANCES AT CASING SUPPORTS OF COMPRESSOR K3

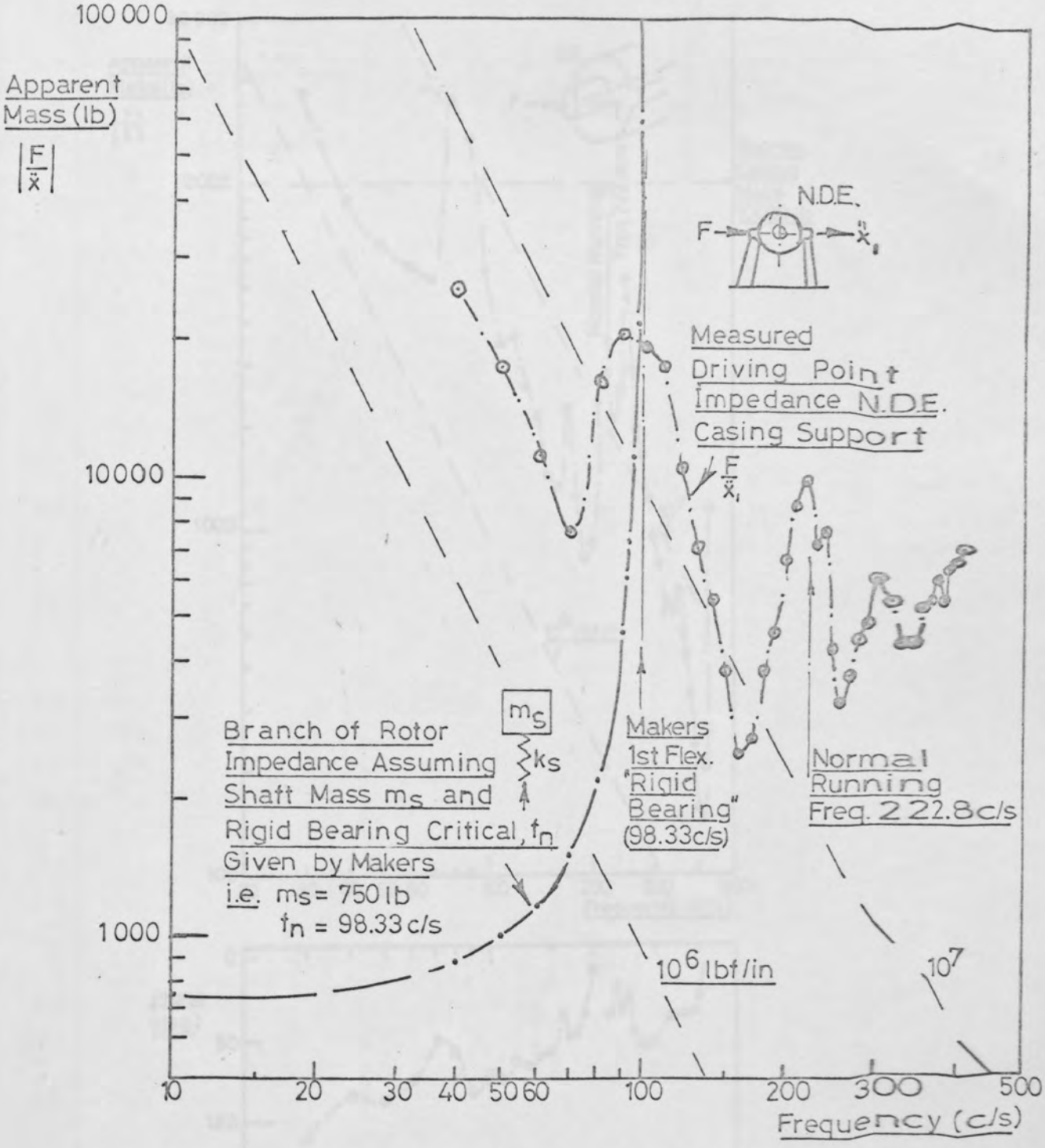

FIG.10.24. DRIVING POINT IMPEDANCE N.D.E. CASING SUPPORT, COMPRESSOR K3. (HORIZONTAL PLANE)

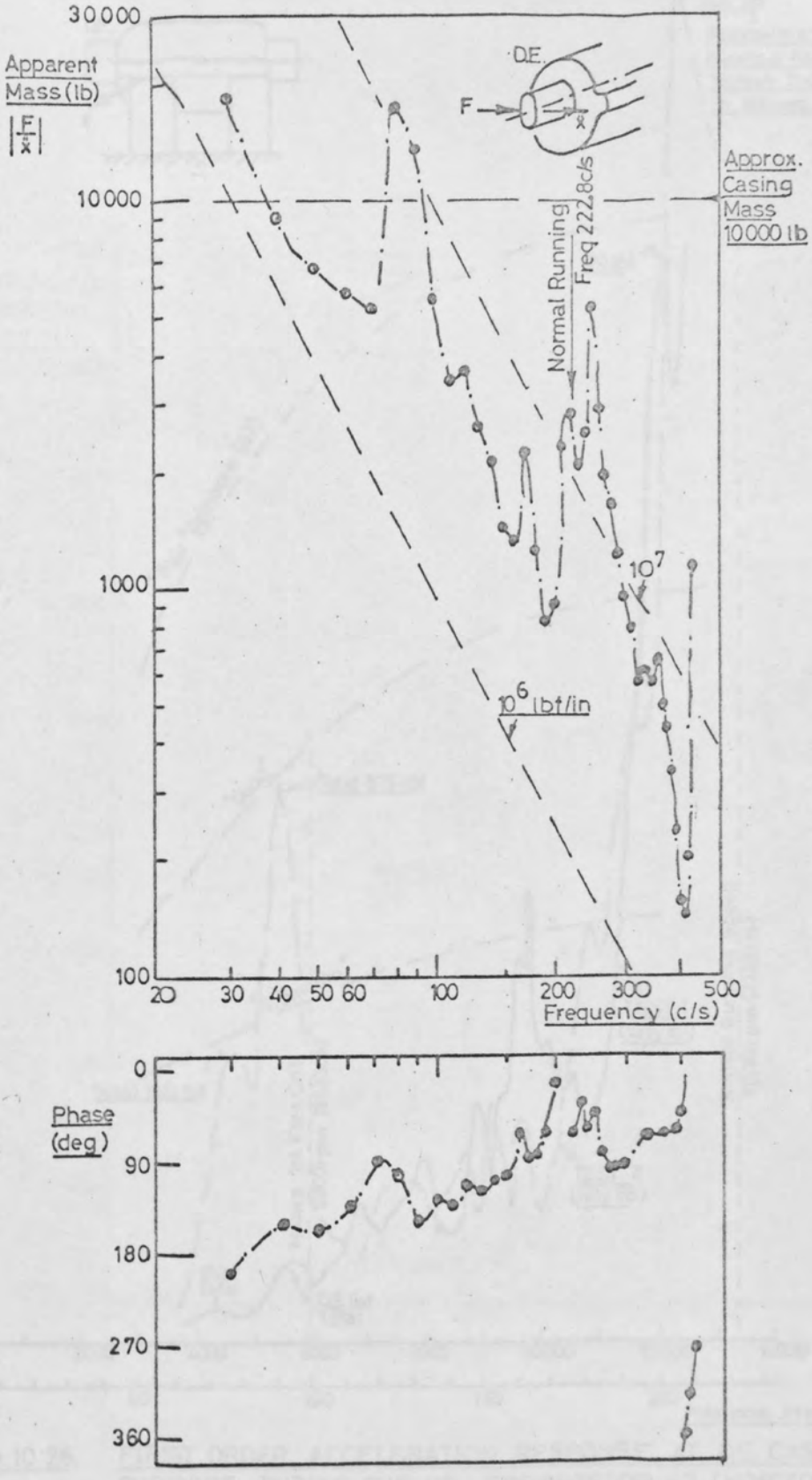

FIG. 10.25. DRIVING POINT IMPEDANCE D.E. BEARING HOUSING, COMPRESSOR K3. (HORIZONTAL PLANE)

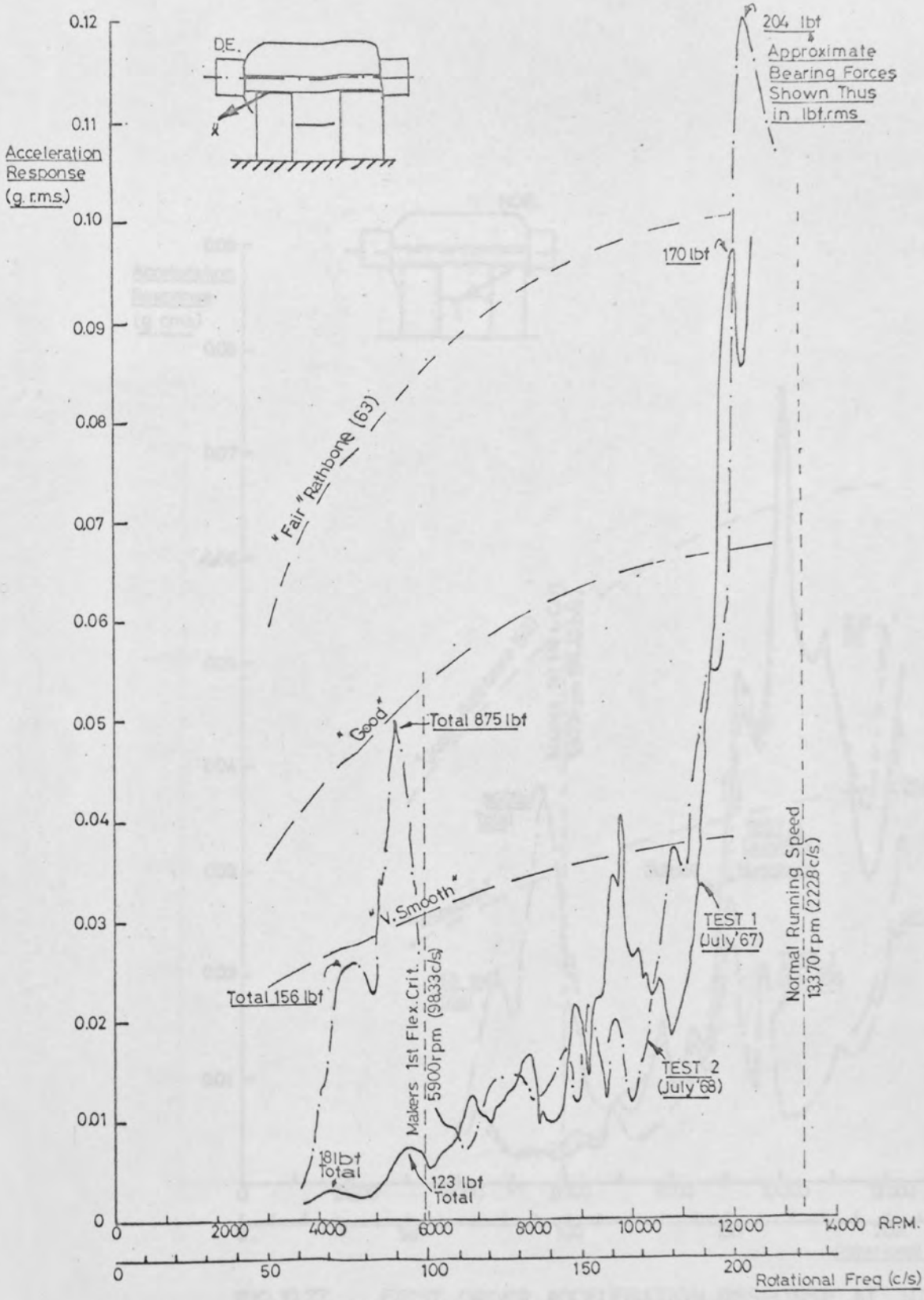

FIG. 10 26. FIRST ORDER ACCELERATION RESPONSE AT D.E. CASING SUPPORT DURING RUN-UP ; COMPRESSOR K3 (HORIZONTAL PLANE)

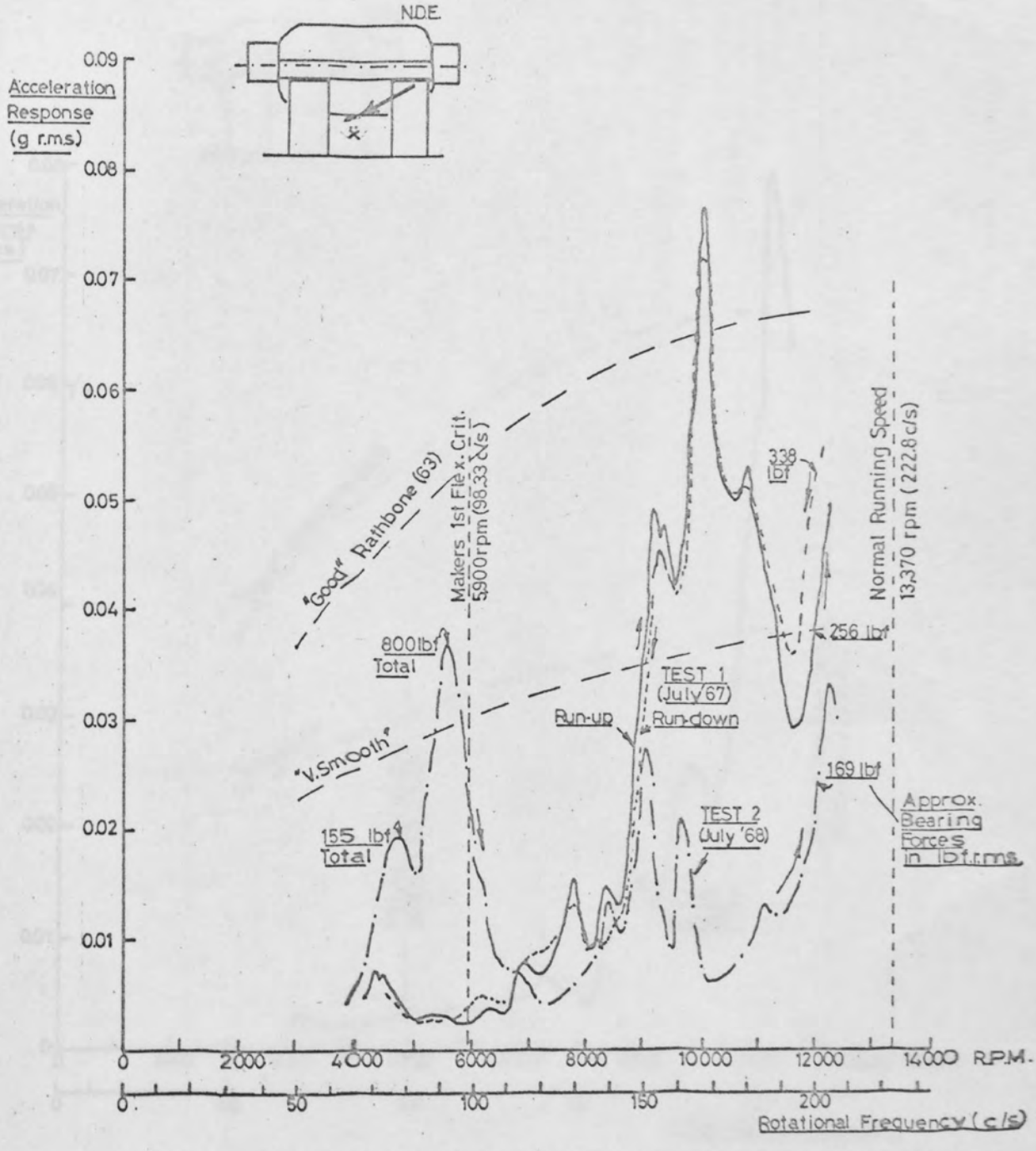

FIG.10.27. FIRST ORDER ACCELERATION RESPONSE AT N.D.E. CASING SUPPORT OF COMPRESSOR K3 (HORIZONTAL PLANE)

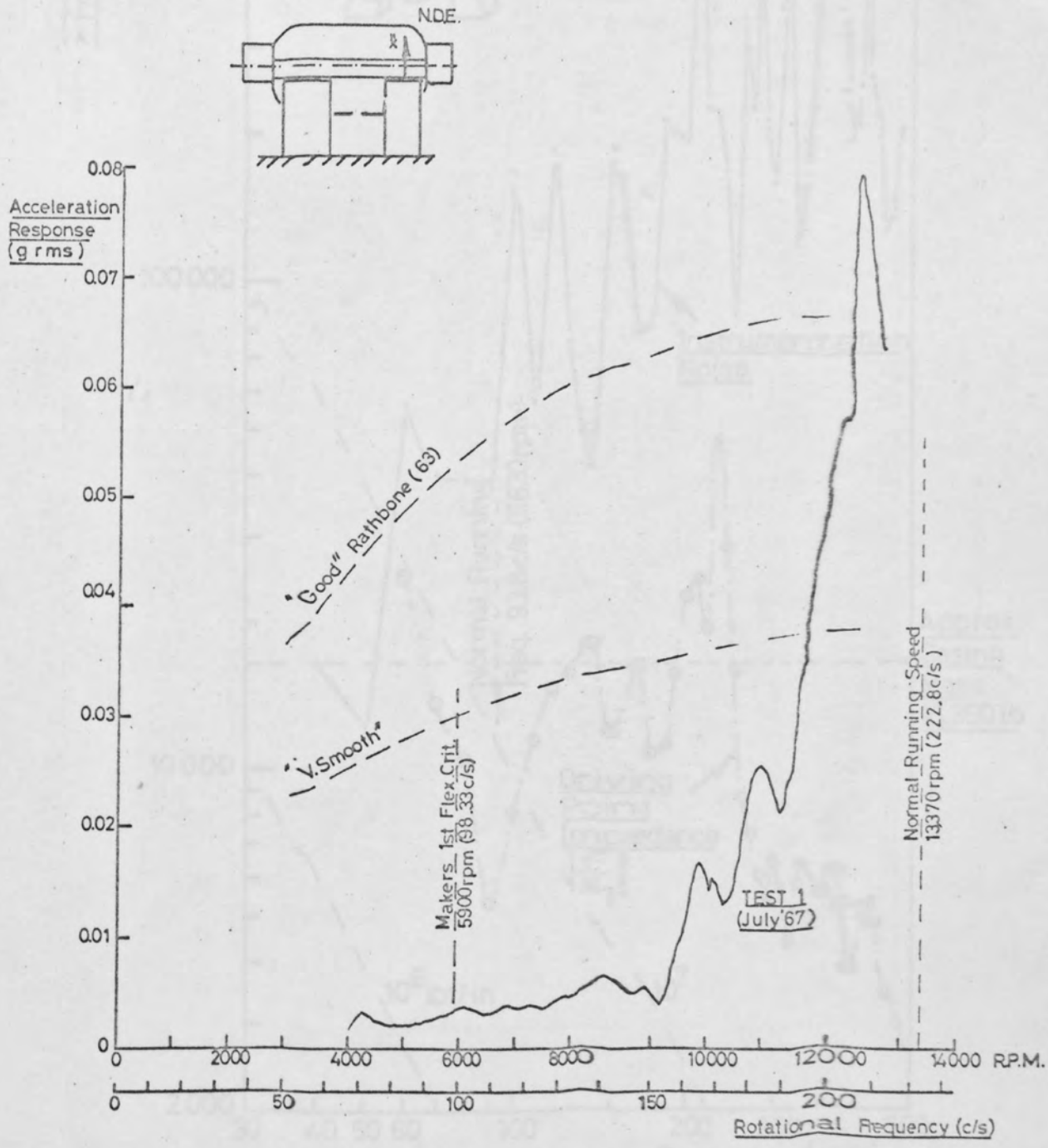

FIG.10.28. FIRST ORDER ACCELERATION RESPONSE AT N.D.E. CASING SUPPORT DURING RUN-UP, COMPRESSOR K3 - (VERTICAL PLANE)

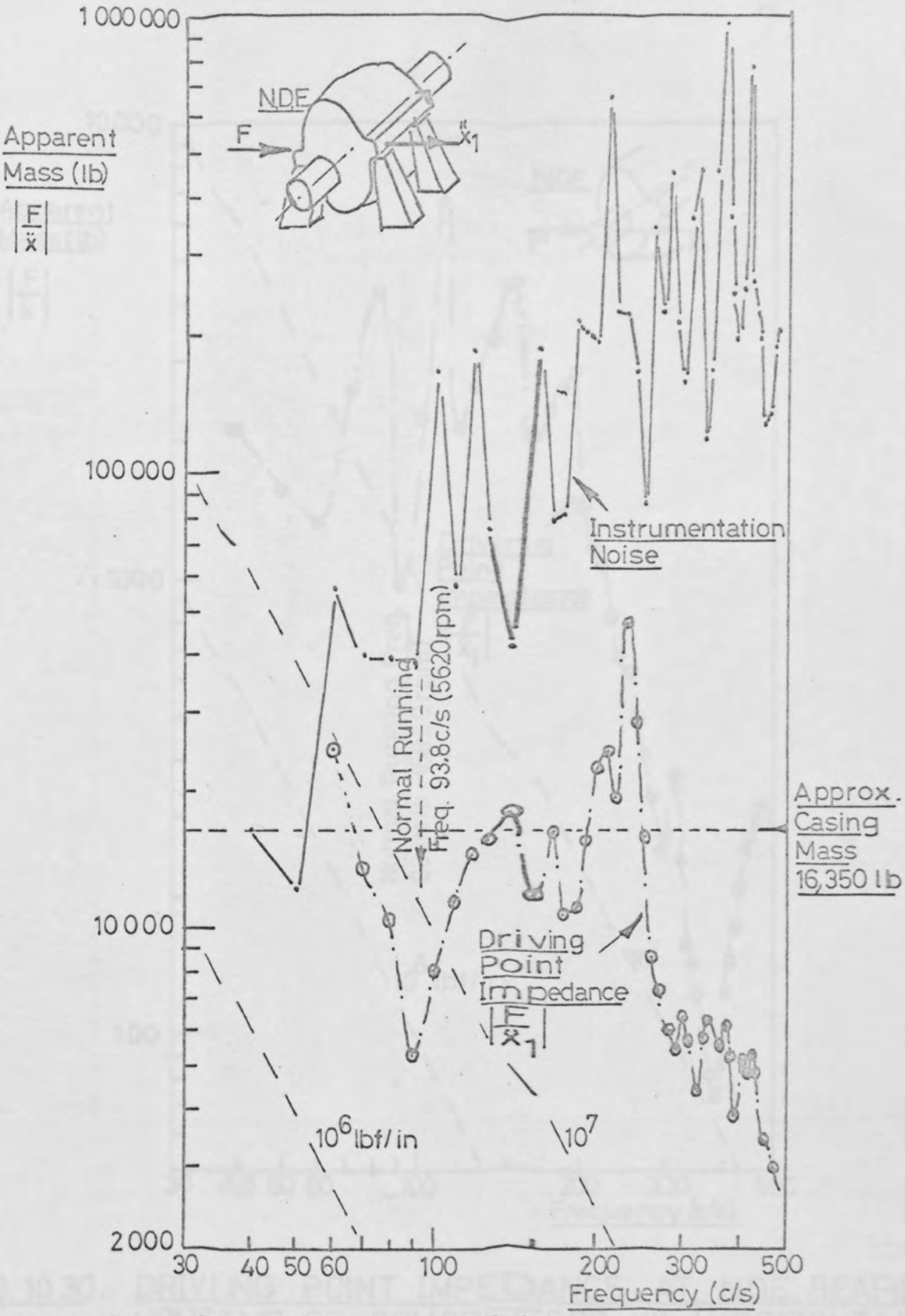

FIG. 10.29. DRIVING POINT IMPEDANCE AT N.D.E. CASING SUPPORT, COMPRESSOR K2. (HORIZONTAL PLANE)

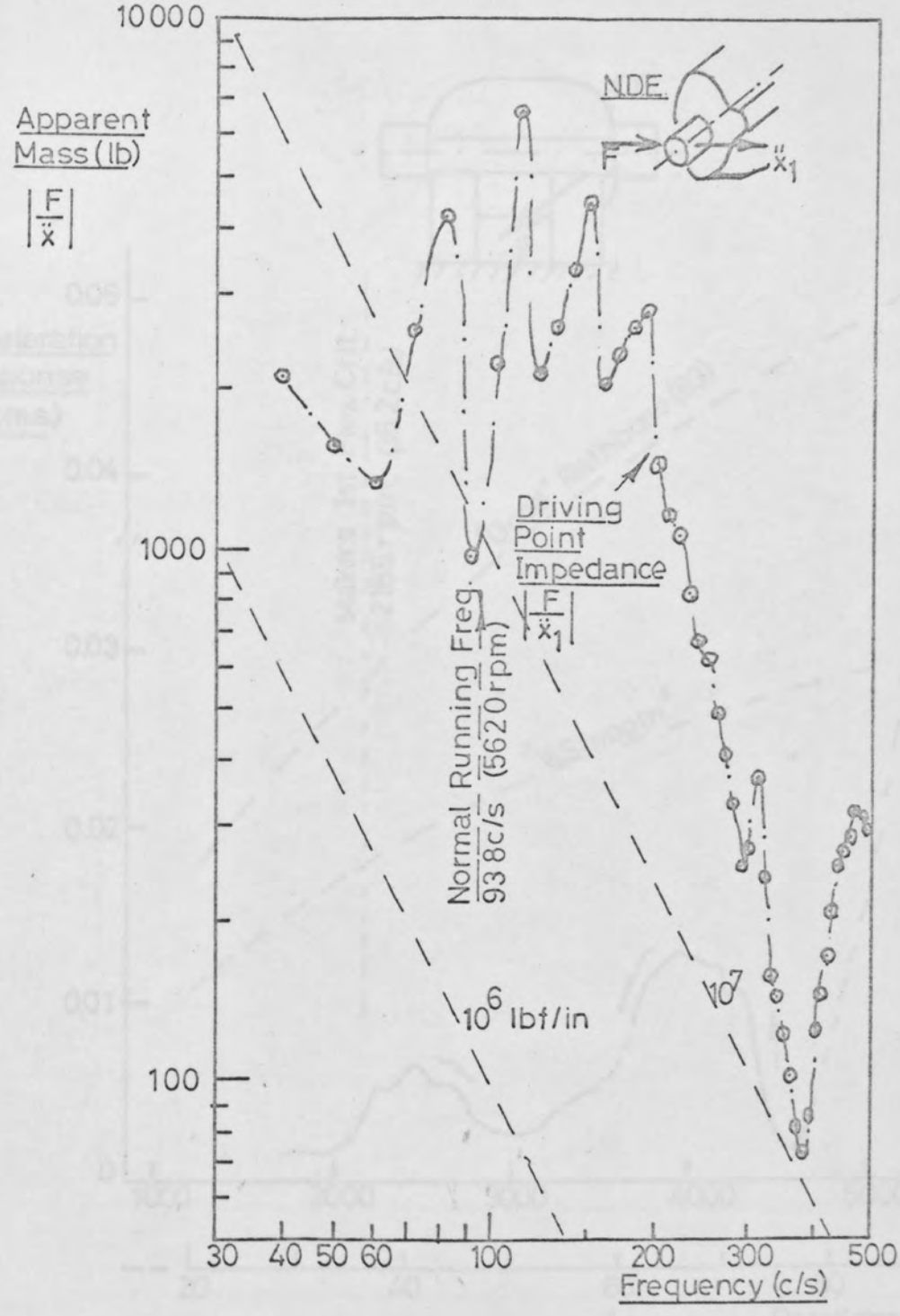

FIG. 10.30. DRIVING POINT IMPEDANCE AT N.D.E. BEARING HOUSING OF COMPRESSOR K2 (HORIZONTAL PLANE)

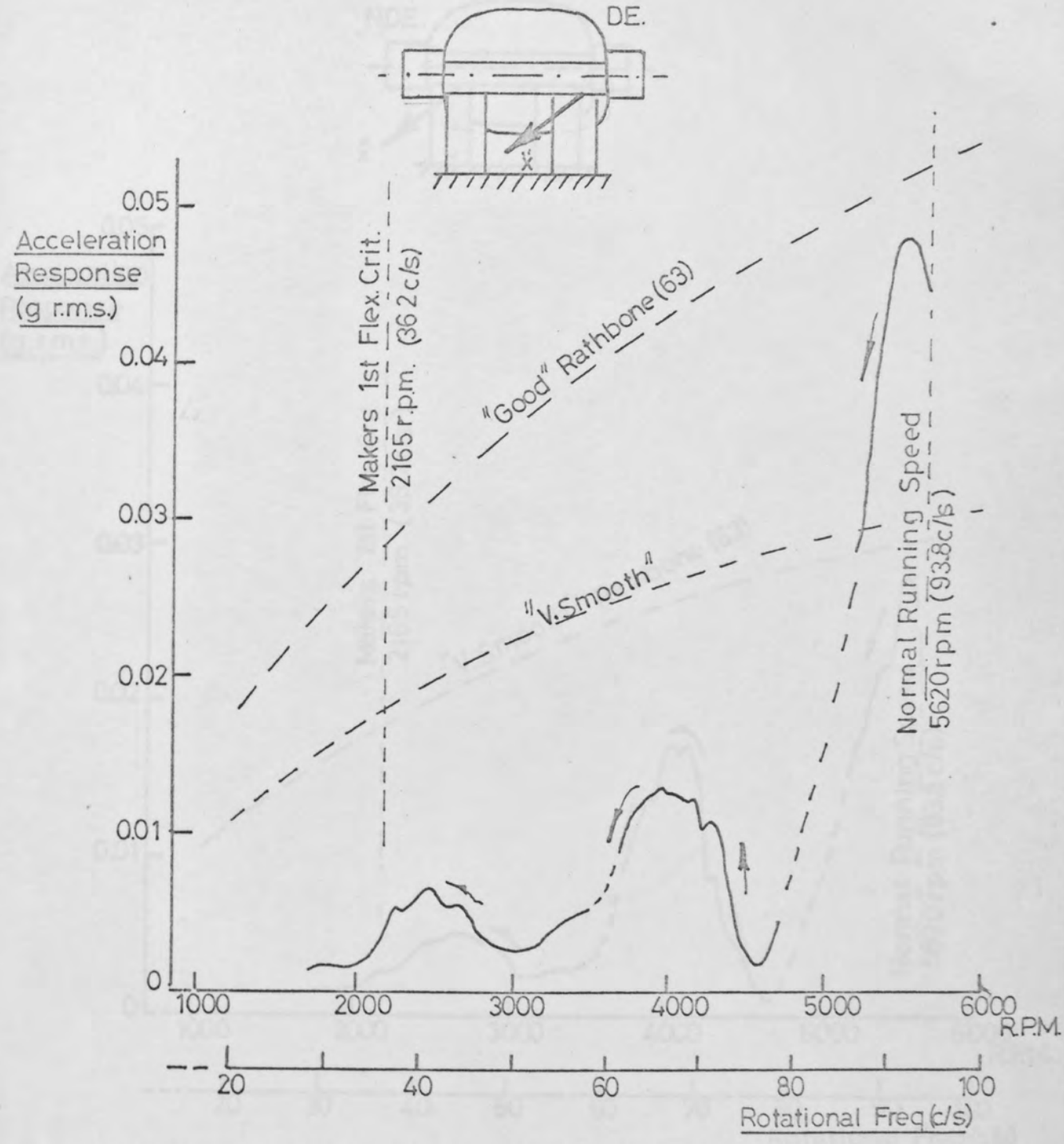

FIG. 10.31. FIRST ORDER ACCELERATION RESPONSE AT D.E. CASING SUPPORT OF COMPRESSOR K2. (HORIZONTAL PLANE).

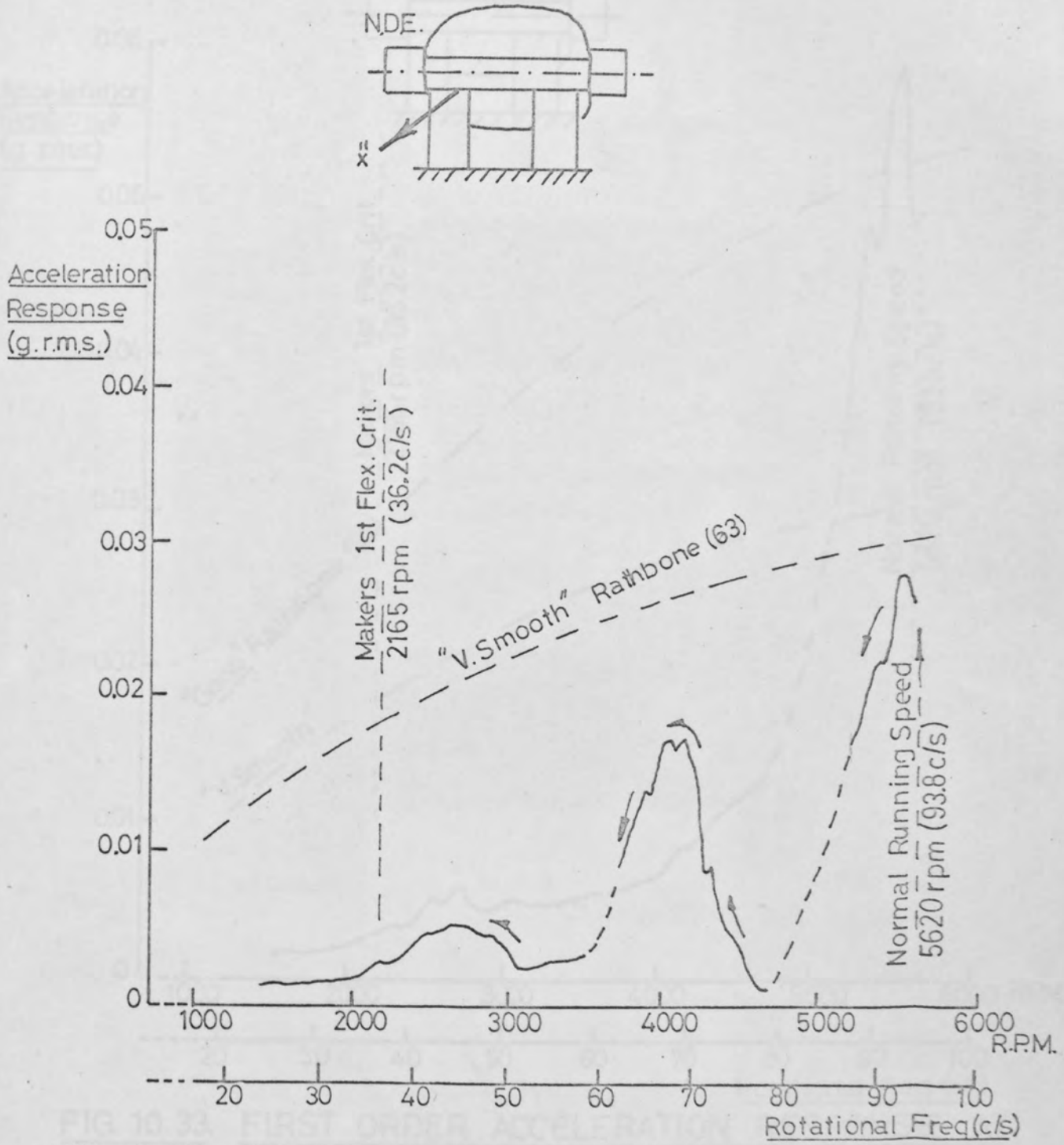

FIG. 10. 32 FIRST ORDER ACCELERATION RESPONSE AT N.D.E. CASING SUPPORT OF COMPRESSOR K2. (HORIZONTAL PLANE)

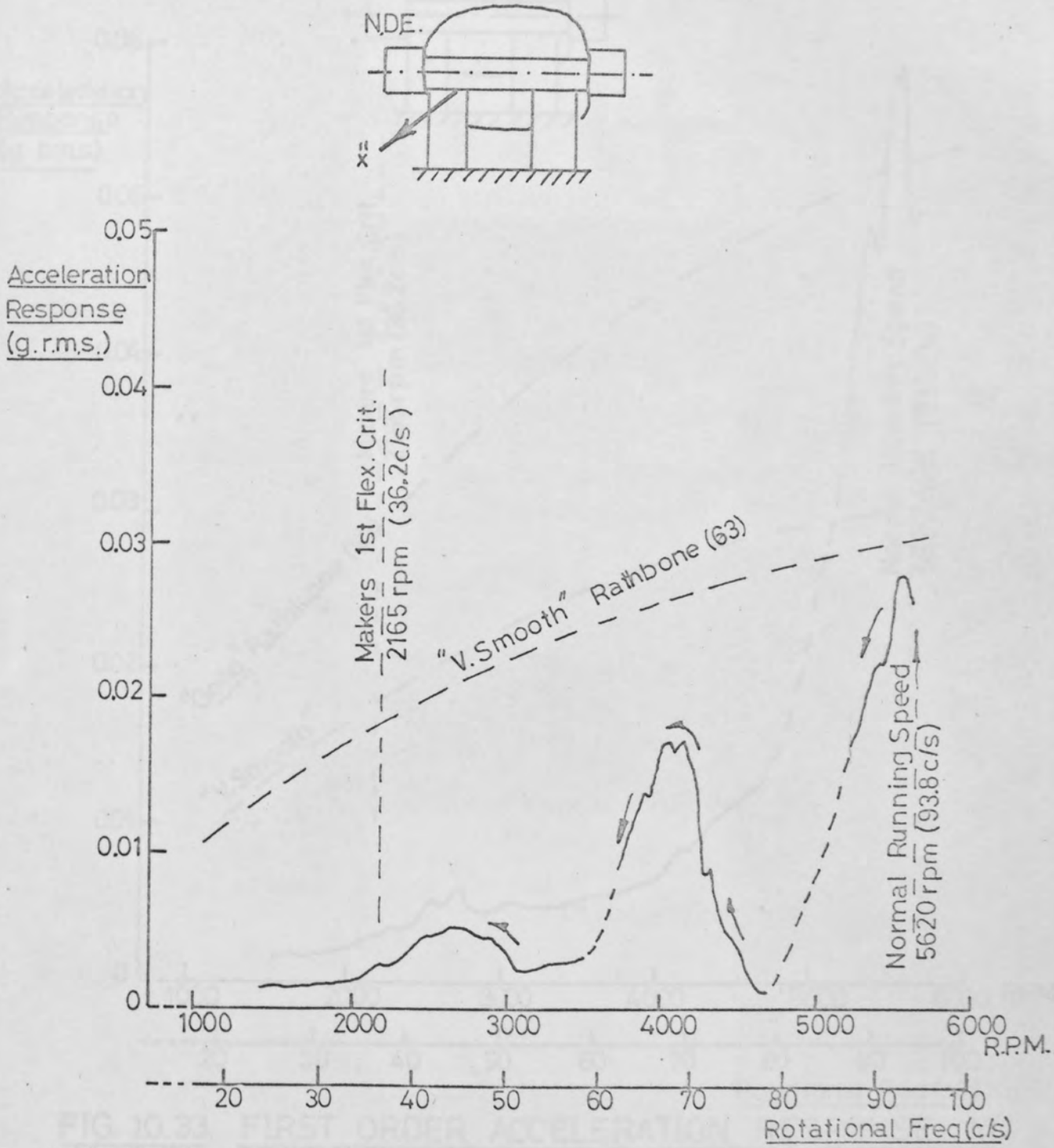

FIG. 10. 32 FIRST ORDER ACCELERATION RESPONSE AT N.D.E. CASING SUPPORT OF COMPRESSOR K2. (HORIZONTAL PLANE)

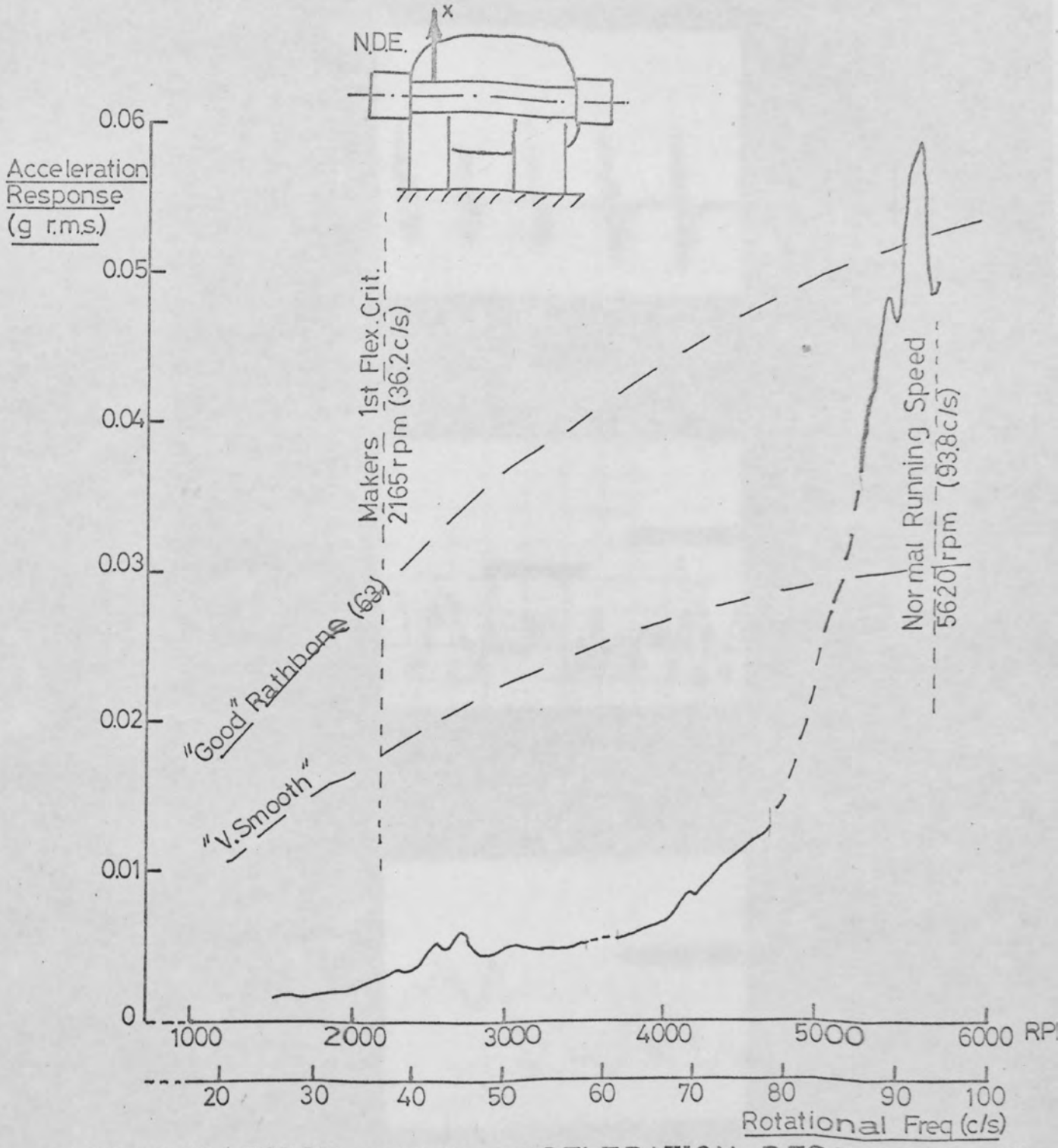

FIG. 10.33. FIRST ORDER ACCELERATION RESPONSE AT NDE CASING SUPPORT OF COMPRESSOR K2 (VERTICAL PLANE)

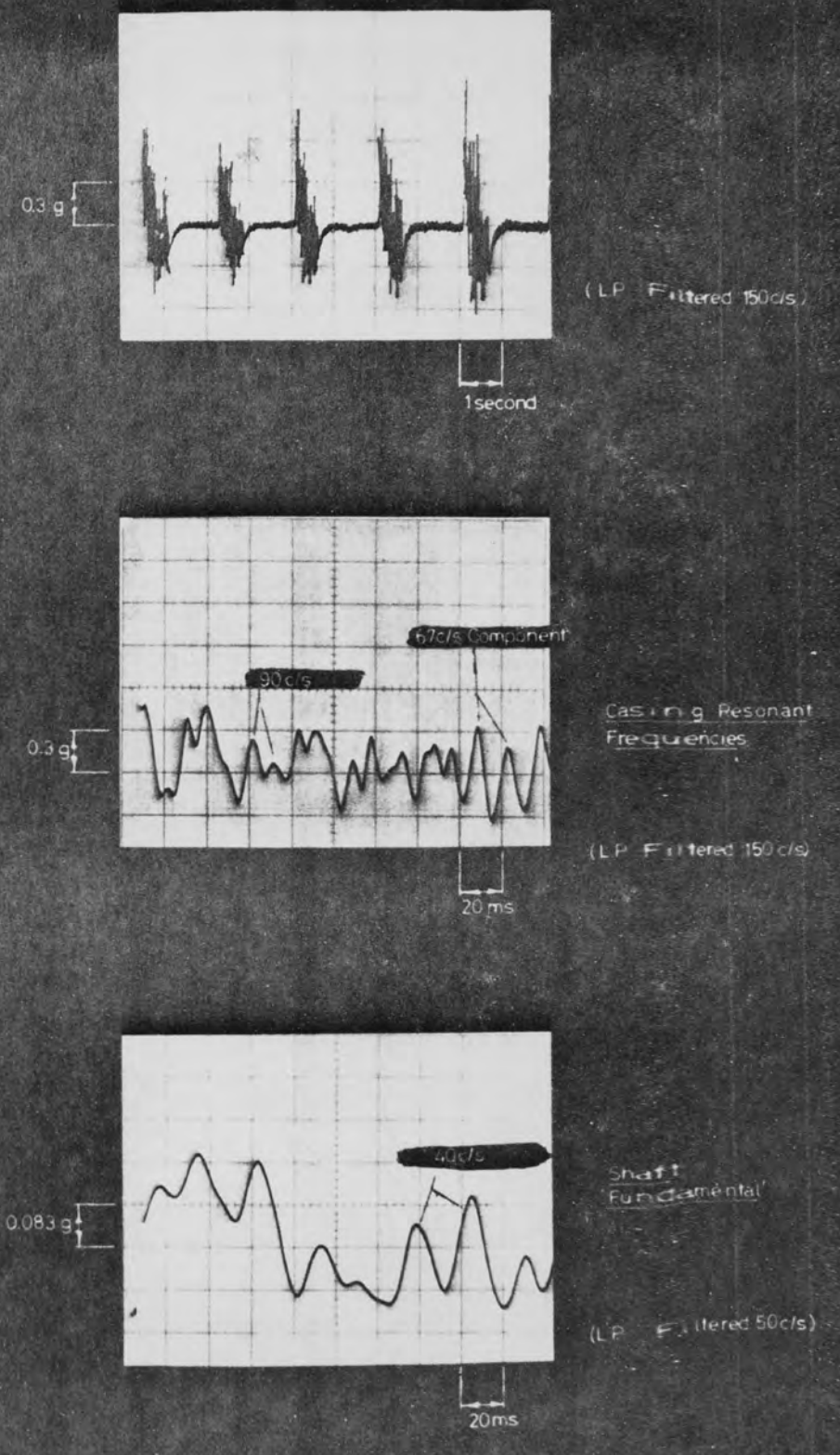

FIG 10.34 ACCELERATION RESPONSE AT N.D.E. CASING SUPPORT OF COMPRESSOR K2 TO AERODYNAMIC SURGE. (HORIZONTAL PLANE)

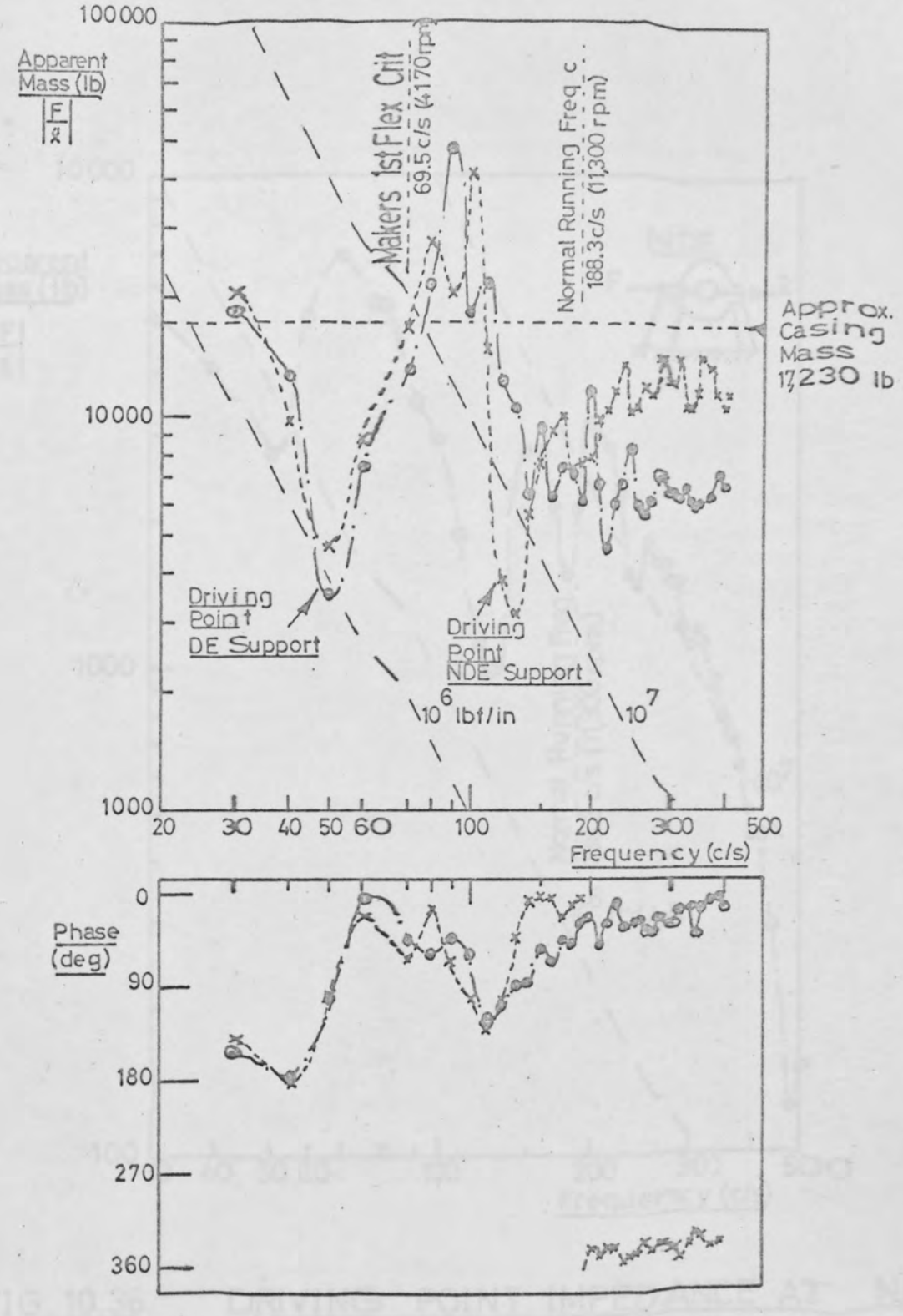

FIG. 10.35. DRIVING POINT IMPEDANCES AT D.E. & NDE. CASING SUPPORTS OF H.P. COMPRESSOR K1. (HORIZONTAL PLANE)

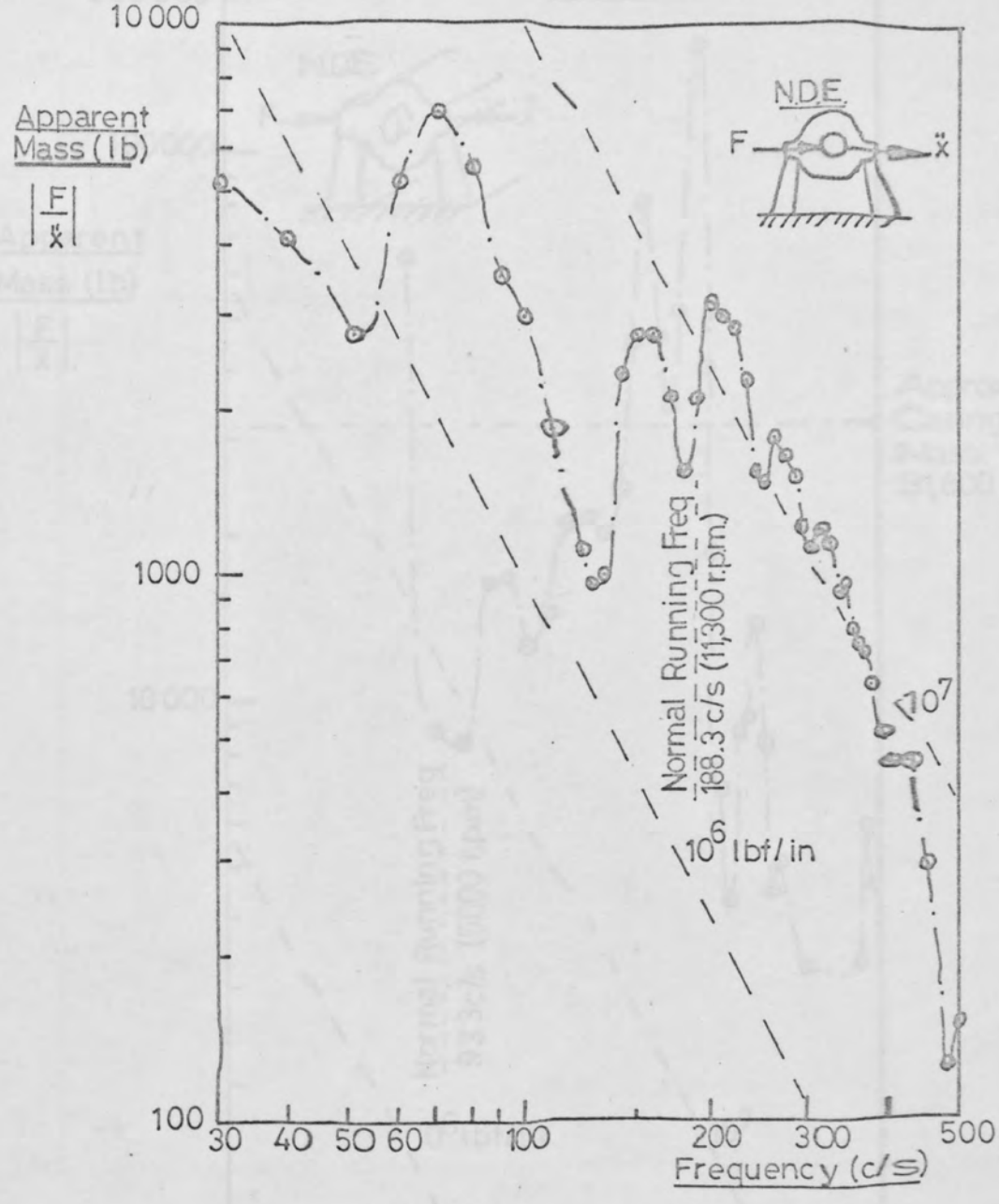

FIG. 10.36. DRIVING POINT IMPEDANCE AT N.D.E. BEARING HOUSING OF H.P. COMPRESSOR K1. (HORIZONTAL PLANE)

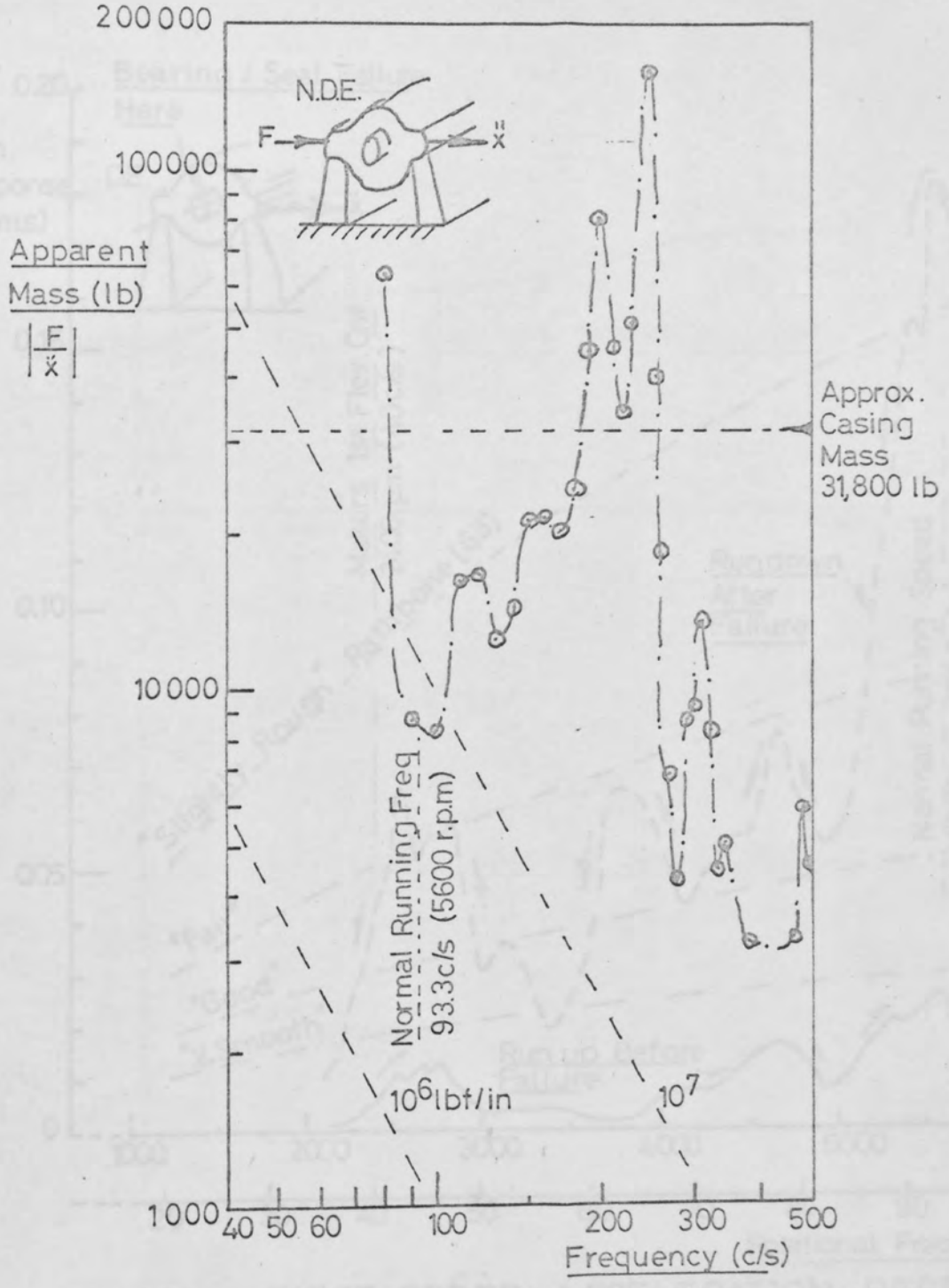

FIG. 10.37. DRIVING POINT IMPEDANCE AT N.D.E. CASING SUPPORT OF L.P. COMPRESSOR K1 (HORIZONTAL PLANE)

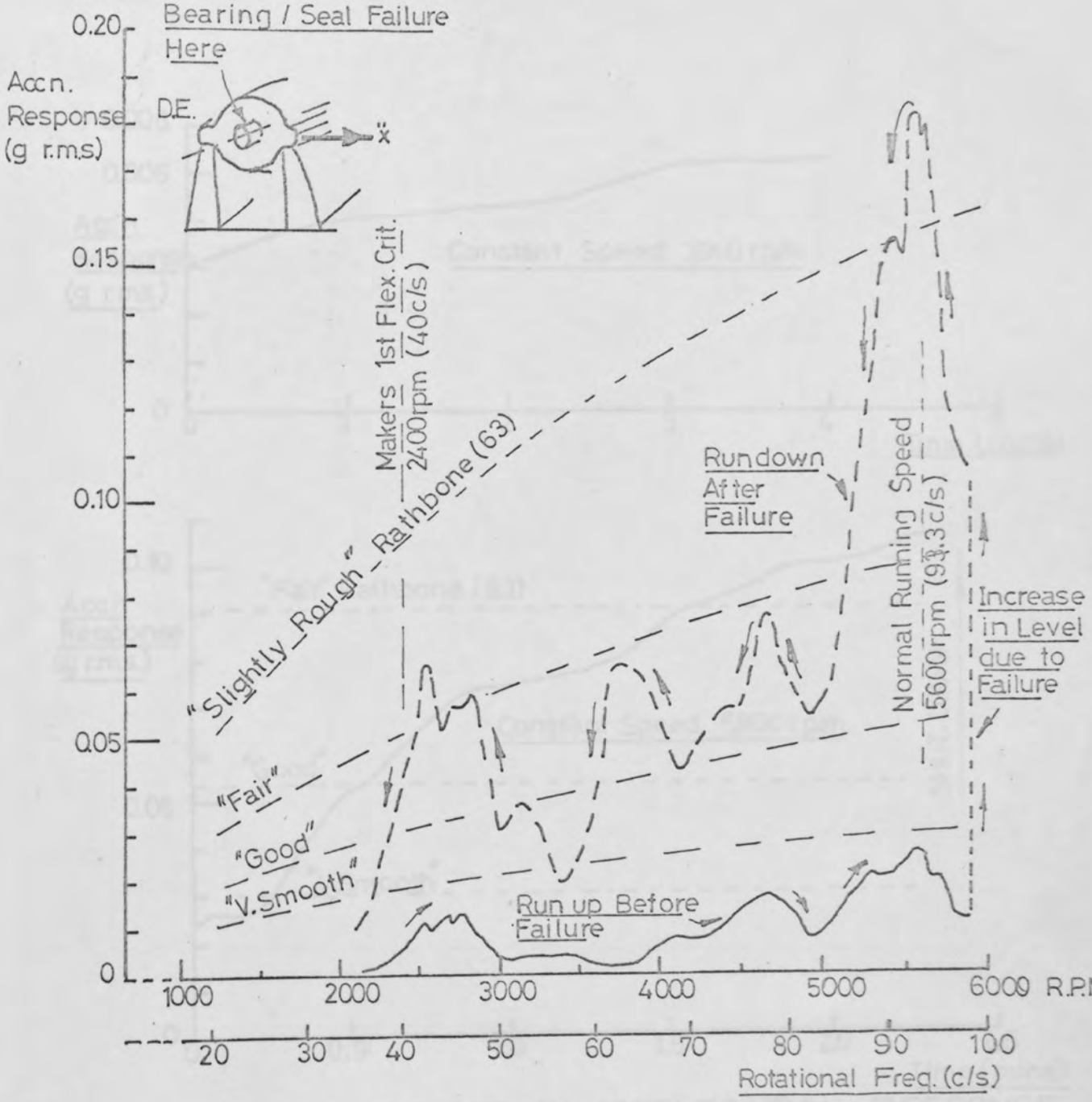

FIG. 10.38. FIRST-ORDER ACCELERATION RESPONSE AT D.E. CASING SUPPORT OF L.P. COMPRESSOR SHOWING EFFECT OF BEARING/SEAL FAILURE.

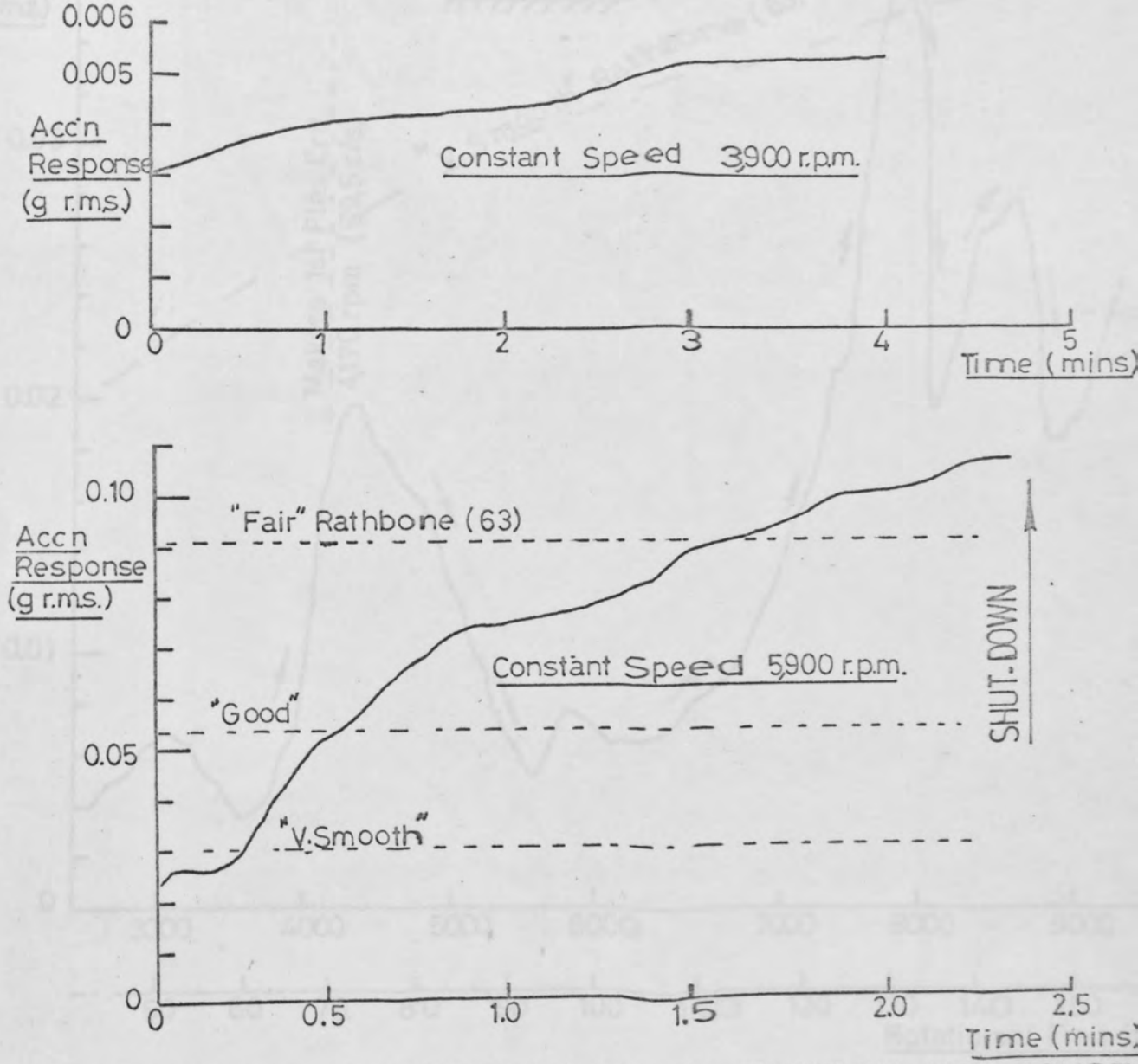

FIG.10.39. INCREASES IN ACCELERATION RESPONSE AT D.E. CASING SUPPORT OF LP COMPRESSOR K1 DURING BEARING FAILURE

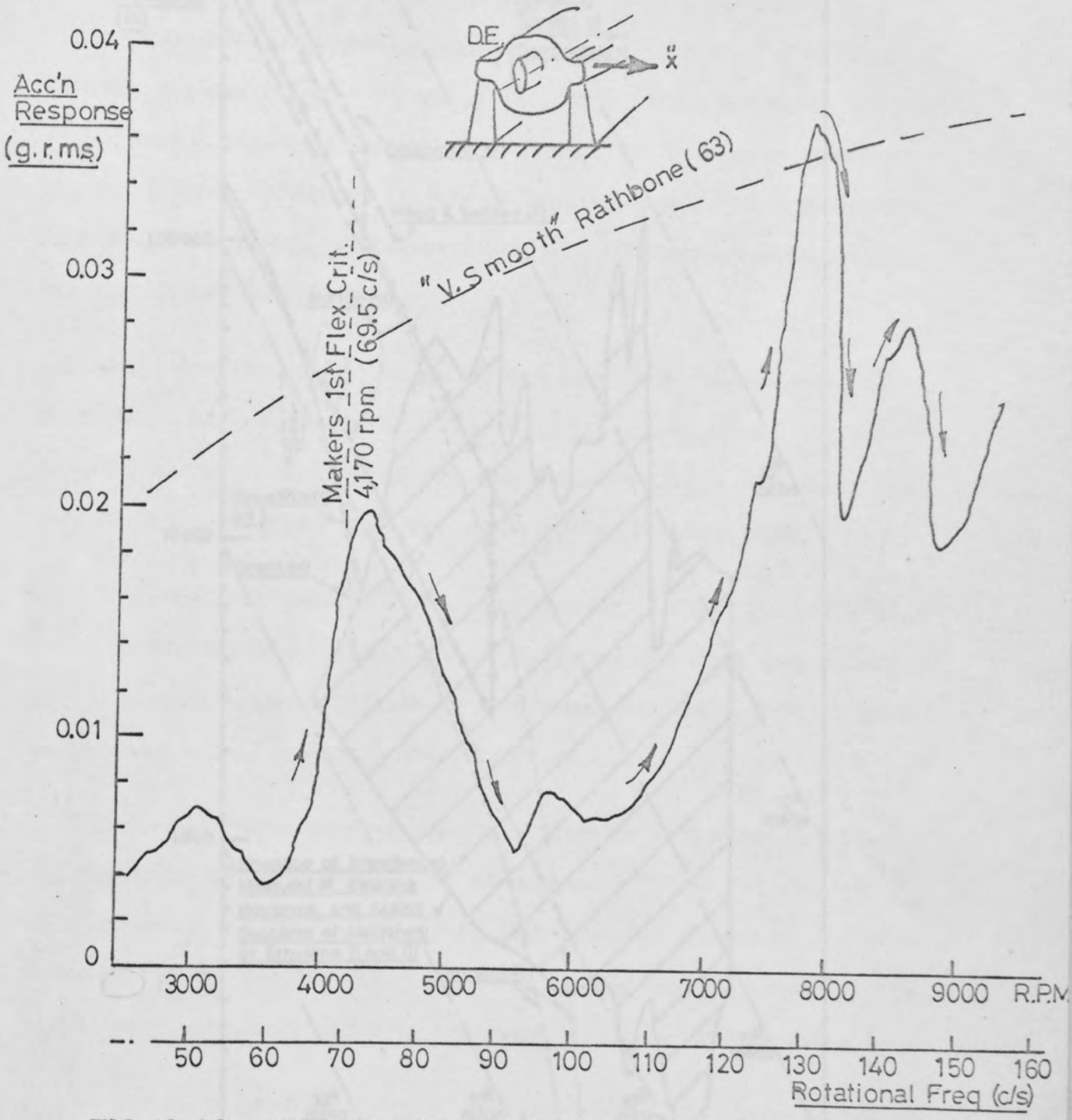

FIG. 10.40. FIRST-ORDER ACCELERATION RESPONSE AT D.E. CASING SUPPORT OF H.P. COMPRESSOR K1 (HORIZONTAL PLANE)

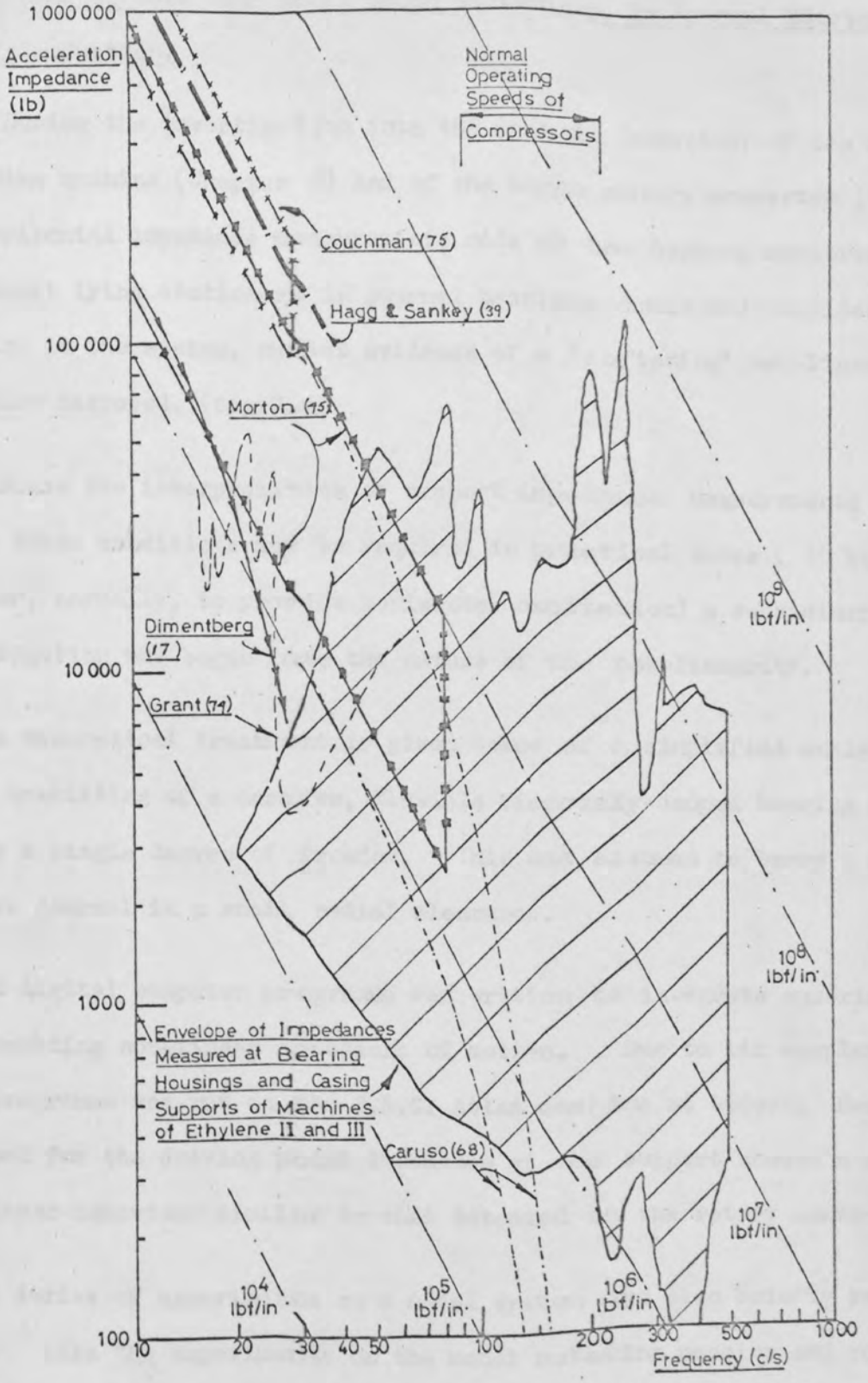

FIG. 10.41. MEASURED IMPEDANCES OF BEARING SUPPORT STRUCTURES OF MACHINES OF ETHYLENE II & III COMPARED WITH VALUES GIVEN BY SEVERAL AUTHORS FOR DIFFERENT MACHINES.

APPENDIX I

Non-linear effects with Shaft Lying Stationary in Journal Bearings

1.1 Introduction.

During the investigation into the dynamic behaviour of the model rotating machine (Chapter 6) and of the large rotary converter (Chapter 7) horizontal impedance measurements made at the bearing supports with the shaft lying stationary in journal bearings indicated considerable damping in the system, whilst evidence of a 'softening' non-linearity was also detected. (fig 7.4)

Since the interpretation of support impedance measurements made under these conditions may be required in practical cases (it being simpler, normally, to provide horizontal excitation) a subsidiary investigation was begun into the nature of the non-linearity.

A theoretical treatment is given below of a simplified analytic model consisting of a massive, flexible viscously-damped bearing support having a single degree of freedom. This was assumed to carry a rigid, massive journal in a small radial clearance.

A digital computer programme was written to integrate numerically the resulting non-linear equations of motion. Due to its complexity this programme was run on the S.R.C. Atlas machine at Didcot. Results obtained for the driving point impedance at the support showed a softening non-linear behaviour similar to that detected on the rotary converter.

A series of experiments on a model system are also briefly reviewed below. Like the experiments on the model rotating machine and rotary converter, these tests indicated an increased level of damping in the system with the journal in the support. Although the model system behaved in a non-linear manner, similar to that predicted theoretically the effect was much more pronounced in the practical case. This

behaviour, together with difficulties experienced in obtaining repeatable results, were attributed to the influence of minor, local irregularities in the bearing material.

I.2 Theoretical Analysis of Simplified System.

The practical situation during a horizontal impedance measurement on a bearing support is shown in fig 1.1 (a). At the support under consideration the shaft journal lies at the bottom of its bearing. In fig I.1(b) a simplified dynamic model is shown, consisting of a journal, mass m, polar moment of inertia I, and radius r. The journal was assumed to be supported in a bearing of radius R whose housing was flexibly supported (linear spring stiffness k) and subject to viscous damping of constant b.

It was required to find the mechanical driving point impedance at the support ($Z = F/\ddot{x}_2$) when the bearing clearance was small

i.e. $\frac{r}{(R-r)} \gg 1.$

It may be noted that for a more complete analysis of a practical configuration:-

a) the journal mass, m, should be replaced by the frequency-dependent shaft impedance,

b) the journal inertia, I, should be replaced by the equivalent torsional impedance of the shaft.

I.2 (i) Equation of Motion

Referring to fig I.1 (b) the support is shown displaced from its equilibrium centre C a distance x_2 to the right, whilst the journal angular displacement is ϕ.

The arc $O\,O' = r\,\phi$

Thus $OC'O' = \frac{r\,\phi}{(R-r)}$

so the vertical displacement, y, of the journal is

$$y = (R-r)\left(1 - \cos\left(\frac{r\,\phi}{R-r}\right)\right) \qquad (I.1)$$

whence $$\dot{y} = r \sin\left(\frac{r\,\phi}{R-r}\right).\dot{\phi} \qquad (I.2)$$

The absolute displacement of the journal centre in the horizontal direction is:-

$$x = x_2 + (R-r)\sin\left(\frac{r\,\phi}{R-r}\right) \qquad (I.3)$$

where $$\dot{x} = \dot{x}_2 + (R-r)\cos\left(\frac{r\,\phi}{R-r}\right).\left(\frac{r}{R-r}\right).\dot{\phi} \qquad (I.4)$$

or $$\dot{x} = \dot{x}_2 + r.\cos\left(\frac{r\,\phi}{R-r}\right).\dot{\phi} \qquad (I.5)$$

The Kinetic energy, T, of the complete system is given by

$$T = \tfrac{1}{2} m\dot{x}^2 + \tfrac{1}{2} M\dot{x}_2^2 + \tfrac{1}{2} m\dot{y}^2 + \tfrac{1}{2} I\dot{\phi}^2 \qquad (I.6)$$

Substituting in equation (I.6) for $\dot{x}$ and $\dot{y}$ from equ.(I.5) and (I.6)

$$T = \tfrac{1}{2}\left(M\dot{x}_2^2 + m\left[\dot{x}_2^2 + 2\dot{x}_2\dot{\phi}r\cos\left(\frac{r\,\phi}{R-r}\right) + \dot{\phi}^2 r^2\cos^2\left(\frac{r\,\phi}{R-r}\right)\right]\right.$$

$$\left. + mr^2\sin^2\left(\frac{r\,\phi}{R-r}\right).\dot{\phi}^2 + I.\dot{\phi}^2\right) \qquad (I.7)$$

The potential energy, V, is given by:-

$$V = \tfrac{1}{2} kx_2^2 + mgy \qquad (I.8)$$

or $$V = \tfrac{1}{2} kx_2^2 + mg\,(R-r)\left(1-\cos\left(\frac{r\,\phi}{R-r}\right)\right) \qquad (I.9)$$

---

whilst the dissipation function, $D = b\,\dot{x}_2^2$

From equations (I.7) and (I.9) the Lagrangian Function L = T−V is obtained as

$$L = \tfrac{1}{2}\left\{ m\left[\dot{x}_2^2 + 2\dot{x}_2\dot{\phi}\, r\cos\left(\frac{r\phi}{R-r}\right) + r^2\dot{\phi}^2 \right] - kx_2^2 + I\dot{\phi}^2 + M\dot{x}_2^2 \right\} - mg(R-r)\left(1-\cos\left(\frac{r\phi}{R-r}\right)\right) \qquad (I.10)$$

In the co-ordinate x_2 the equation of motion is:-

$$\frac{d}{dt}\left(\frac{\partial L}{\partial \dot{x}_2}\right) - \frac{\partial L}{\partial x_2} + \frac{\partial D}{\partial \dot{x}_2} = F(t) \qquad (I.11)$$

where F(t) is the external forcing function.

Performing the differentation indicated in eqn.(I.11), and assuming the excitation to be sinusoidal, the equation of motion in x_2 is:-

$$(M+m)\ddot{x}_2 + Kx_2 + mr\ddot{\phi}\cos\left(\frac{r\phi}{R-r}\right) + b\dot{x}_2 - \left(\frac{mr^2}{(R-r)}\right)\cdot\sin\left(\frac{r\phi}{R-r}\right)\cdot\dot{\phi}^2 = F\sin\omega t \qquad (I.12)$$

Similarly, in the co-ordinate ϕ the equation of motion is

$$\frac{d}{dt}\left(\frac{\partial L}{\partial \dot{\phi}}\right) - \frac{\partial L}{\partial \phi} + \frac{\partial D}{\partial \dot{\phi}} = 0 \qquad (I.13)$$

which is found to be

$$(I+mr^2)\ddot{\phi} + mr\cos\left(\frac{r\phi}{R-r}\right)\ddot{x}_2 + mgr\sin\left(\frac{r\phi}{R-r}\right) = 0 \qquad (I.14)$$

As far as the writer is aware, no general analytic solution exists to the simultaneous, non-linear, second-order differential equations (I.12) and (I.14)

Solutions have been obtained, however, by using numerical methods as outlined below.

I.2 (ii) Solution of the Equation of Motion using Digital Computation

Fig I.2 shows diagramatically the structure of the digital computer programme written to obtain solutions of equations (I.12) and (I.14). The main operations in the computation were:-

a) step-by-step integration of the equations for a sinusoidal forcing function. The integration procedure used (procedure (ii) fig I.2) was of the Runge-Kutta type, this being ideally suited for digital computation.

b) Fourier analysis (procedure (iii) fig I.2) of the response waveforms to obtain their fundamental (forcing frequency) content in terms of the sine and cosine coefficients A_1, B_1.

c) Calculation of the moduli of the responses and their phase angles with respect to the forcing function from the previously evaluated Fourier coefficients.

Runge-Kutta Integration

In general, n simultaneous second order equations may be rewritten as 2n simultaneous first order equation of the form:-

$$\frac{dyi}{dx} = F_i\ (x,\ y_1,\ y_2,\ \ldots\ldots\ y_i) \qquad (I.15)$$

where $i = 2n$

x = independent variable

y_i = dependent variables

Eqns. (I.12) and (I.14) may therefore be written as four such equations ($i = 4$) in time, t, as the independent variable.

Thus putting

$$\frac{dx_2}{dt} = Z, \text{ say} \qquad (I.16)$$

$$\frac{d\phi}{dt} = \psi, \text{ say} \qquad (I.17)$$

and making the following further substitutions to simplify the algebra:-

$$\lambda^2 = \left(\frac{k}{M+m}\right) \qquad A_1 = \frac{mr}{(M+m)}$$

$$A_2 = \frac{mr^2}{(R-r)(M+m)} \qquad A_3 = \frac{mr}{(I+mr^2)}$$

$$A_4 = \frac{mgr}{(I+mr^2)} \qquad A_5 = \frac{b}{(M+m)}$$

$$\frac{r}{(R-r)} = \alpha \qquad \frac{F}{(M+m)} = P$$

Eqns. (I.12) and (I.14) become

$$\frac{d\dot{z}}{dt} + \lambda^2 x_2 + A_5.\dot{z} + A_1 \cos c\phi . \frac{d\psi}{dt} - A_2 \sin c\phi . \psi^2 = P\sin\omega t \qquad \text{(I.18)}$$

$$\frac{d\psi}{dt} + A_3 \cos c\,\phi . \frac{d\dot{z}}{dt} + A_4 . \sin c\,\phi = 0 \qquad \text{(I.19)}$$

Substituting for $\frac{d\dot{z}}{dt}$ from eqn. (I.19) into eqn. (I.18) yields, after some manipulation

$$\frac{d\psi}{dt} = \frac{(P\sin\omega t - \lambda^2 x_2 - A_5.\dot{z} + A_2.\sin c\,\phi.\psi^2)\,A_3\cos c\,\phi + A_4 \sin c\,\phi}{(A_1 A_3 \cos^2 c\,\phi - 1)} \qquad \text{(I.20)}$$

and by re-substituting back into eqn. (I.19) from eqn. (I.20)

$$\frac{d\dot{z}}{dt} = \frac{P\sin\omega t - \lambda^2 x_2 - A_5.\dot{z} + A_2.\sin c\,\phi.\psi^2 + A_1 A_4 \sin c\,\phi \cos c\,\phi}{(1 - A_1 A_3 \cos^2 c\,\phi)} \qquad \text{(I.21)}$$

Eqns. (I.16) and (I.17) together with eqns.(I.20) and (I.21) above are of the form

$$\begin{aligned} y_1 &= \dot{x}_2 = Z \\ y_2 &= \dot{Z} = F_a(x_2, \phi, \psi, t) \\ y_3 &= \dot{\phi} = \\ y_4 &= \dot{\psi} = F_b(x_2, \phi, \psi\ t) \end{aligned} \qquad \text{(I.22)}$$

In the digital computer programme (fig I.2) procedure (ii) was based on the Runge-Kutta method of integration (see Hawgood (102) for instance) and involved a four-step routine to obtain, for each function on the R.H.S. of eqns. (I.22), the quantities:-

$$k_{1_i} = \Delta t.\ F_i\ (t,\ y_i)$$

$$k_{2_i} = \Delta t.\ F_i\ \left(t + \frac{\Delta t}{2},\ y_i + \frac{k_{1_i}}{2}\right)$$

$$k_{3_i} = \Delta t.\ F_i\ \left(t + \frac{\Delta t}{2},\ y_i + \frac{k_{2_i}}{2}\right)$$

$$k_{4_i} = \Delta t.\ F_i\ (t + \Delta t,\ y_i + k_{3_i})$$

and hence the new y_i values at time $(t + \Delta t)$ from a weighted average to give

$$(\text{new})\ y_i = (\text{old})y_i + \frac{k_{1_i} + 2k_{2_i} + 2k_{3_i} + k_{4_i}}{6} \qquad \text{(I.23)}$$

Procedure (i) in fig I.2 evaluated the R.H.S's of eqns.(I.22) for each step of the Runge-Kutta integration.

It should be mentioned here that, in the first programme written to perform this integration, the modified five-step routine due to Merson was used. This incorporated a self-checking facility to alter the integration step length (Δt) so that the accuracy at the 'new' points was within a preset limit. This procedure was found to be of little value, however, since no obvious criterion was apparent, before computation, with which to assess the absolute numerical accuracy required

In the first attempts at running the computer programme the integration of eqns. (I.22) was started at the convenient initial values $x_2 = z = \phi = \psi = 0$. However, due to the small amount of damping in the system (normally $\zeta = 0.01$) this meant that large transient responses at the natural damped frequencies were sometimes induced when the steady

state responses at $t = 0, 2\pi, 4\pi$, etc. differed appreciably from zero.

Although it would have been possible to continue the integration until steady state conditions were eventually reached, this would have greatly increased the computing time required. In some cases evidence of numerical instability in the solutions was also apparent when the initial values were very inaccurate.

To overcome these problems, approximate initial values were obtained from steady state solutions of linearised versions of eqns. (I.12) and (I.14). Thus by neglecting the term

$$-\frac{mr^2}{(R-r)} \cdot \sin \frac{r\phi}{R-r} \cdot \dot{\phi}^2$$

and putting $\cos\left(\frac{r\phi}{R-r}\right) = 1, \quad \sin\left(\frac{r\phi}{R-r}\right) = \frac{r\phi}{R-r}$

eqns. (I.12) and (I.14) could be written:-

$$(M+m)\ddot{x}_2 + b\dot{x}_2 + Kx_2 + mr\ddot{\phi} = F\sin\omega t \qquad (I.24)$$

$$(I+mr^2)\ddot{\phi} + mr\ddot{x}_2 + \frac{mgr^2}{(R-r)} \cdot \phi = 0 \qquad (I.25)$$

Whence by substituting assumed harmonic solutions of the form

$$x_2 = X_{2_s} \cdot \sin\omega t + X_{2_c} \cdot \cos\omega t$$

$$\phi = \Phi_s \cdot \sin\omega t + \Phi_c \cdot \cos\omega t$$

together with corresponding time derivatives $\dot{x}_2$, $\ddot{x}_2$, $\ddot{\phi}$ into eqns. (I.24) and (I.25), values of x_2, $\dot{x}_2$ $(= z)$, ϕ, $\dot{\phi}$ $(= \psi)$ were obtained in the usual manner. The use of these values as initial conditions ($t = 0$) for the numerical integration considerably decreased the amount of computation required.

Fig I.3 shows a typical solution for the support displacement response x_2, evaluated at an excitation frequency of 80 c/s with support damping ratio $\zeta = 2\sqrt{km} = .01$ and a radial clearance of the journal of 0.002 in. In this particular case the linearised initial displacement was approximately 16% in error and some 110 cycles were required before the response amplitude was constant between successive cycles within 1%. The first and the last two cycles are shown in fig I.3.

Fourier Analysis

Procedure (iii) in the computer programme (fig I.2) performed a Fourier analysis of the system responses over the last complete cycle of the sinusoidal exciting force.

The coefficients A_o, A_1, B_1 of the Fourier series

$$f(t) = A_o + A_1 \cos\omega t + A_2 \cos 2\omega t + \ldots\ldots$$
$$+ B_1 \sin\omega t + B_2 \sin 2\omega t + \ldots\ldots$$

were obtained from:-

$$A_o = \frac{1}{N} \sum_{o}^{N} Y_i$$

$$A_1 = \frac{2}{N} \sum_{o}^{N} Y_i \cos\left(\frac{\pi . n}{N}\right)$$

$$B_1 = \frac{2}{N} \sum_{o}^{N} Y_i \sin\left(\frac{\pi . n}{N}\right)$$

where the Y_i's were successive values of the functions x_2, Z, ϕ and ψ, N was the total number of integration steps, n the particular step under consideration.

The value of A_o, the 'D.C.' component – which should have been zero over a full period due to the symmetric nature of the system - was used as a check on the solution.

The modulii of the fundamental responses were then found from

$$|Y_i| = \sqrt{A_1^2 + B_1^2}$$

whilst their phase angles, θ_i, with respect to the exciting force were obtained from

$$\theta_i = \tan^{-1} \frac{B_1}{A_1}$$

The driving point impedance, Z, at the support and the horizontal (x) and vertical (y) displacements of the journal were also evaluated, the latter according to eqns. (I.1) and (I.3).

I.3 Theoretical Results

All theoretical solutions to date have been based on bearing support and journal parameters approximately equal to those of the model system investigated experimentally and discussed in section I.4 below i.e. M = 27 lb, K = 1.5 x 10^4 lbf/in, R = 1.5 in with radial clearances of (R-r) = .002, .010, .0625 in. The journal masses were those measured for the model whilst their polar inertias were calculated assuming the journals to be perfect cylinders i.e. $I = \frac{mr^2}{2}$. Damping at the support was assumed to be $\zeta = c/2\sqrt{Mk} = 0.01$.

Fig I.4 shows the calculated driving point impedances at the support for a journal radial clearance of 0.002 in. The linearised solution (according to eqns. (I.24), (I.25)) are shown together with the non-linear results. In the latter case the amplitude of the force was assumed to be 1 lbf.

Two resonances occur in the impedance diagram of fig I.4, the upper one, corresponding to the support resonance in the absence of the journal, being most sensitive to the non-linear bevahiour in terms of

frequency separation. The single anti-resonance is related to the series resonance of the journal when supported in a rigid housing and occurs at 57.1 c/s in the linearised case i.e. at $f_{AR} = \frac{1}{2\pi}\sqrt{\frac{2g}{3(R-r)}}$.

The 'softening' non-linear behaviour may be seen more clearly in fig I.5 in which the response of the support is plotted to a linear scale for force amplitudes of 0.5 and 1.0 lbf.

The influence of journal diameter is illustrated in fig I.6 in which the non-linear driving point impedance $(F/\ddot{x}_2)$ is shown for two journals whose clearances are 0.002 in and 0.010 in respectively. It may be seen that for a given force amplitude, a decrease in journal clearance (increased mass and inertia) raises both the resonant frequencies and decreases the apparent mass 'looking into' the support at higher frequencies.

Results obtained for the support impedance with much larger journal clearances showed little evidence of the non-linear behaviour. For example, with a radial clearance of 0.0625 in (R = 1.5 in, r = 1.4375 in) the maximum variation in support impedance modulus detected in the non-linear solution for a force amplitude of 0.5 lbf was about 1% of the linearised values. This compares with nearly 100% variation (at 53 c/s) for the 0.002 in radial clearance journal.

I.4 Experiments on a Model Bearing Support Rig.

A sketch of the small model used in a series of experiments is shown in fig I.7. This consisted of a steel 'bearing housing' mounted on top of a cantilever beam. Three cylindrical steel journals were manufactured having radial clearances of 0.002, 0.010, 0.0625 in respectively, relative to the 3.0 in diameter housing.

In an attempt to simulate the conditions in real bearings the housing of the model was lined with Babbit metal, this being cast into the housing before final boring.

It was intended that the support, without the journal in position, should respond in a single degree of freedom up to about 500 c/s, with a fundamental resonance at approximately 250 c/s. However, due to the effect of fixing flexibilities at the junctions between the bearing block and the cantilever and between the cantilever and baseplate, the effective low-frequency stiffness was reduced to less than 10% of the design value. Thus the approximate measured stiffness was 1.5×10^4 lbf/in, that calculated from the dimensions of the cantilever being about 2.2×10^5 lbf/in.

Although the support still responded predominantly in a single degree of freedom, resonant at 77.5 c/s, a minor resonance was also encountered at approximately 60 c/s due, apparently, to a mode involving motion of the complete cantilevered assembly against the base fixing.

The response of the support was linear, however, for the forcing amplitudes used, as is demonstrated by the acceleration response curves for 1.0 lbf r.m.s. and 0.5 lbf r.m.s. shown in fig I.8.

With the journals in the bearing housing the responses were distinctly non-linear. As predicted by the theoretical treatment above, the non-linearity was of the 'softening type', the 'backbone' of the resonant peaks decreasing in frequency with increasing exciting force. This characteristic is illustrated in fig I.9 in which the support response to varying force levels is shown for the journal giving the largest clearance (0.0625 in). However, the non-linearity was more pronounced than that predicted theoretically.

With the smaller bearing clearances, difficulty was experienced in obtaining completely repeatable results. Although, with a given journal in the housing, the responses were repeatable from one test run to the next, appreciable differences, particularly close to resonances, were

found if the journal was removed and then replaced. This behaviour persisted even after careful degreasing at each change of journal.

The reason for the non-repeatability was not conclusively established but it is thought that it arose due to changes in the local supporting conditions between the journal and the relatively soft Babbit metal bearing surface. In this connection slight brinelling and scoring of the bearing material could have been significant - particularly with the 0.002 in clearance journal.

Fig I.11 shows the theoretical non-linear response of the journal and support for a 0.010 in radial clearance journal with a typical result obtained experimentally for the journal of the same nominal clearance. Although the two cases are not exactly comparable, since the assumed damping in the theoretical result (ζ = 0.01) was somewhat lower than that observed in the model ($\zeta \simeq$ 0.015), a reasonable agreement might be expected.

In practice, however, the lower-frequency resonance, theoretically around 26 c/s, was not detectable at all - the maximum horizontal acceleration of the journal relative to the support occurred at about 55 c/s. The reason for this discrepancy was not clear since the exact nature of the response was confused by the fact that the support itself did not respond in a 'pure' single degree of freedom.

In general, however, the results were compatible with a decrease in the effective journal clearance, again possibly due to local irregularities in the bearing surface. In this respect the theoretical results for the .010 in clearance journal, from which fig I.11 was plotted, indicated a maximum angular rotation, ϕ, of the journal of about 6×10^{-4} radian (3.44×10^{-2} deg) with corresponding maximum vertical journal amplitudes (y) of 3×10^{-5}in - or 0.3% of the radial clearance.

With regard to the large amount of damping observed in the tests on the model rotating machine of Chapter 6 and the rotary converter (Chapter 7) when the shaft was lying in the bearings, the tests on the model support also showed a considerable increase in the absolute damping in the system when the journal was in place. This effect can be seen in the typical support impedance measurements of fig I.10 where the damping at the main resonance ($\simeq$ 75 c/s) increased by about 30% when the small journal (0.0625 in clearance) was in the housing. With the journal having a nominal 0.010 in clearance in place the damping controlling this resonance was nearly five times that obtained for the support alone.

No indication of the increase in damping was obtained from the non-linear solution and it was concluded that this was due to interface effects between journal and housing.

General Conclusions

The theoretical analysis accounted qualitatively for the softening non-linearity observed during support impedance measurements on the rotary converter. In the tests on the model bearing support the effect was more pronounced than predicted theoretically. This behaviour and the poor repeatability suggested that the effective clearance was reduced by local irregularities in the bearing surface.

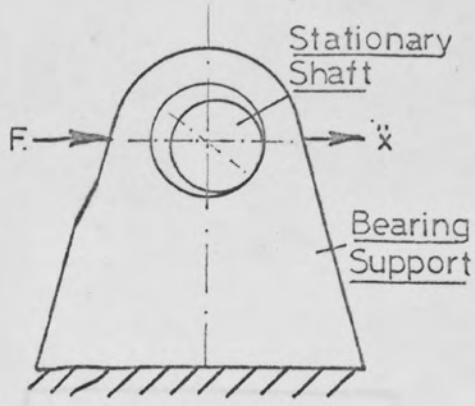

FIG. I.1.(a) PRACTICAL SITUATION

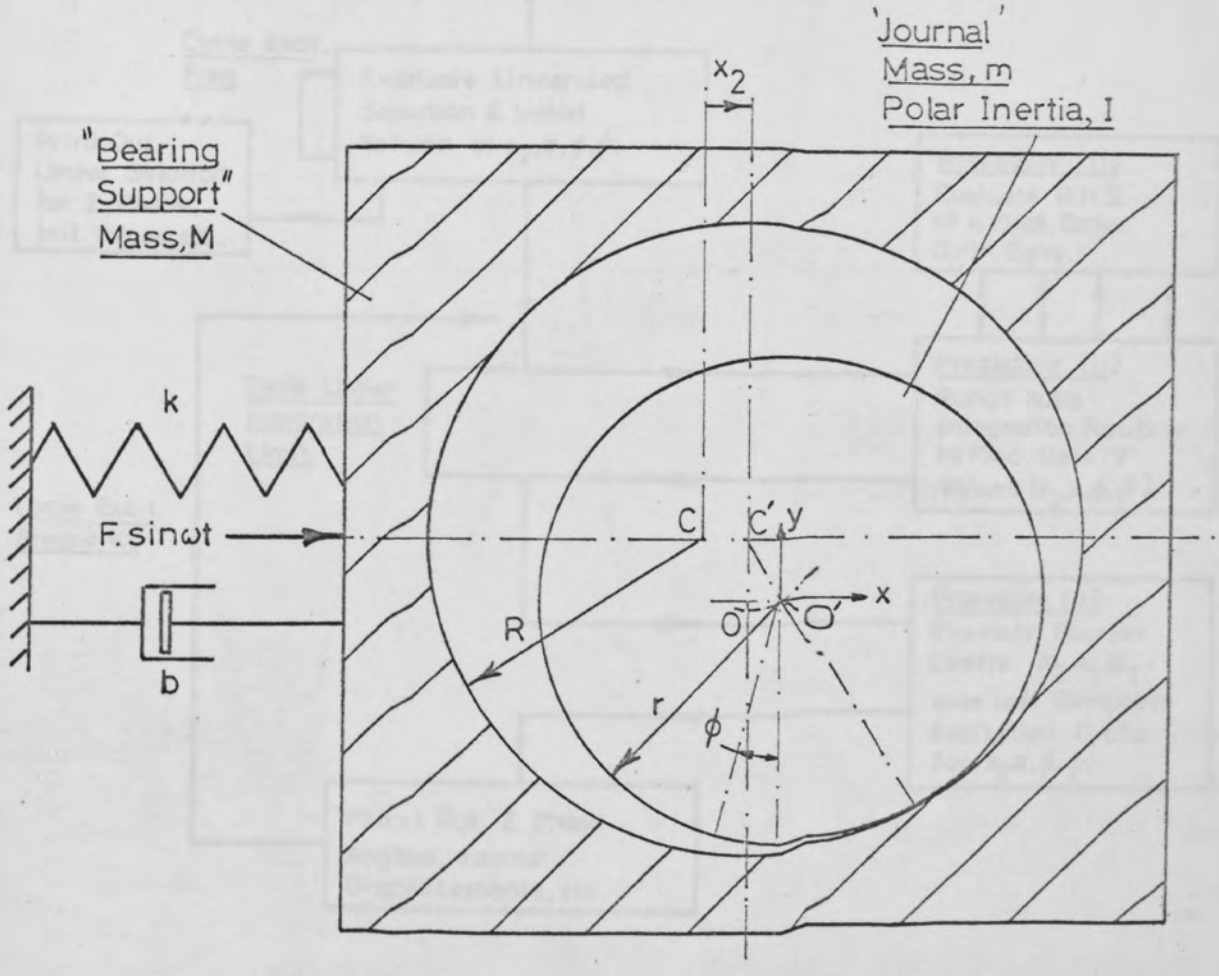

FIG. I.1.(b) ANALYTIC MODEL

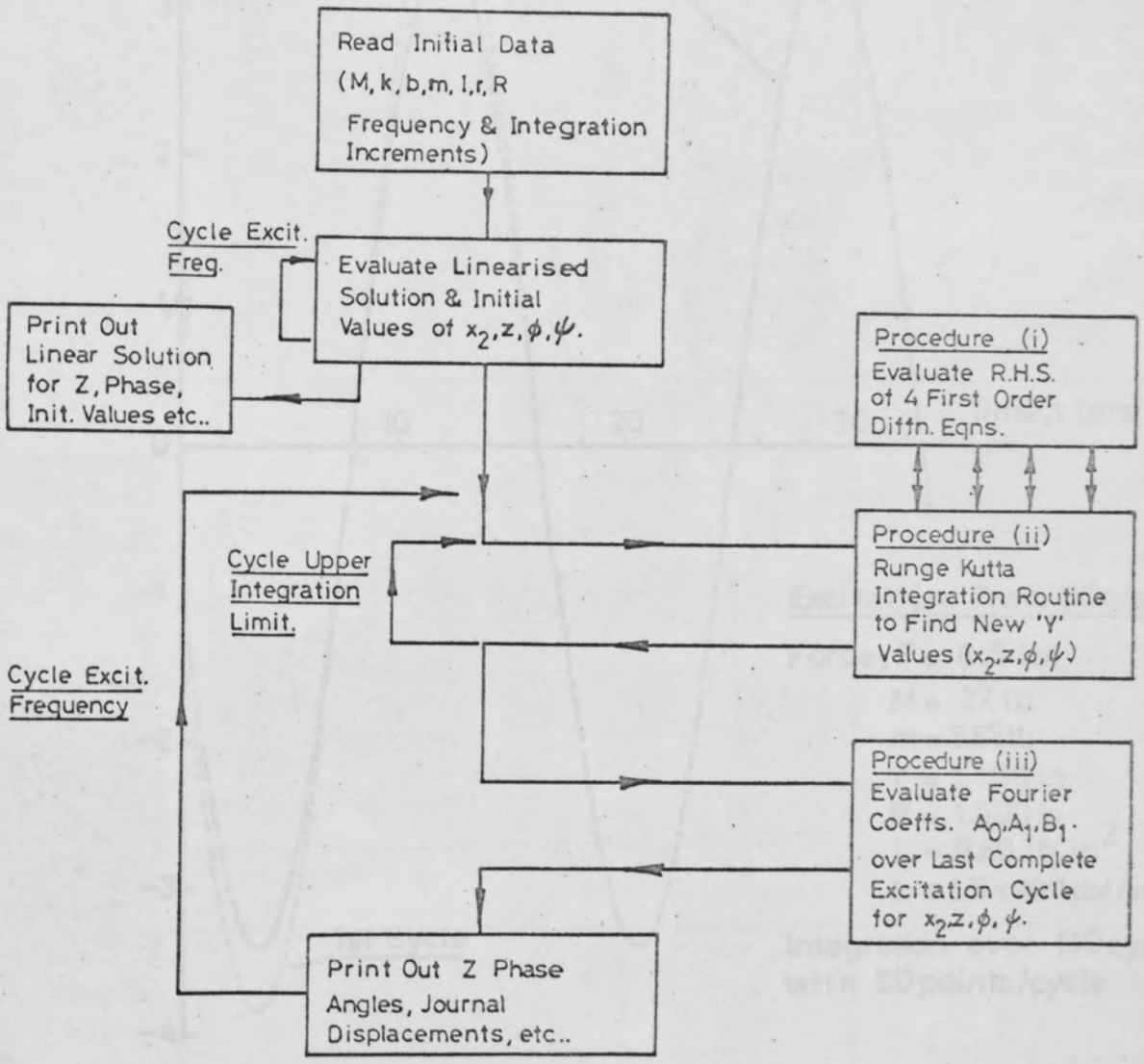

FIG. I.2. 'ATLAS' COMPUTER PROGRAMME TO SOLVE NON-LINEAR EQUATIONS OF MOTION.

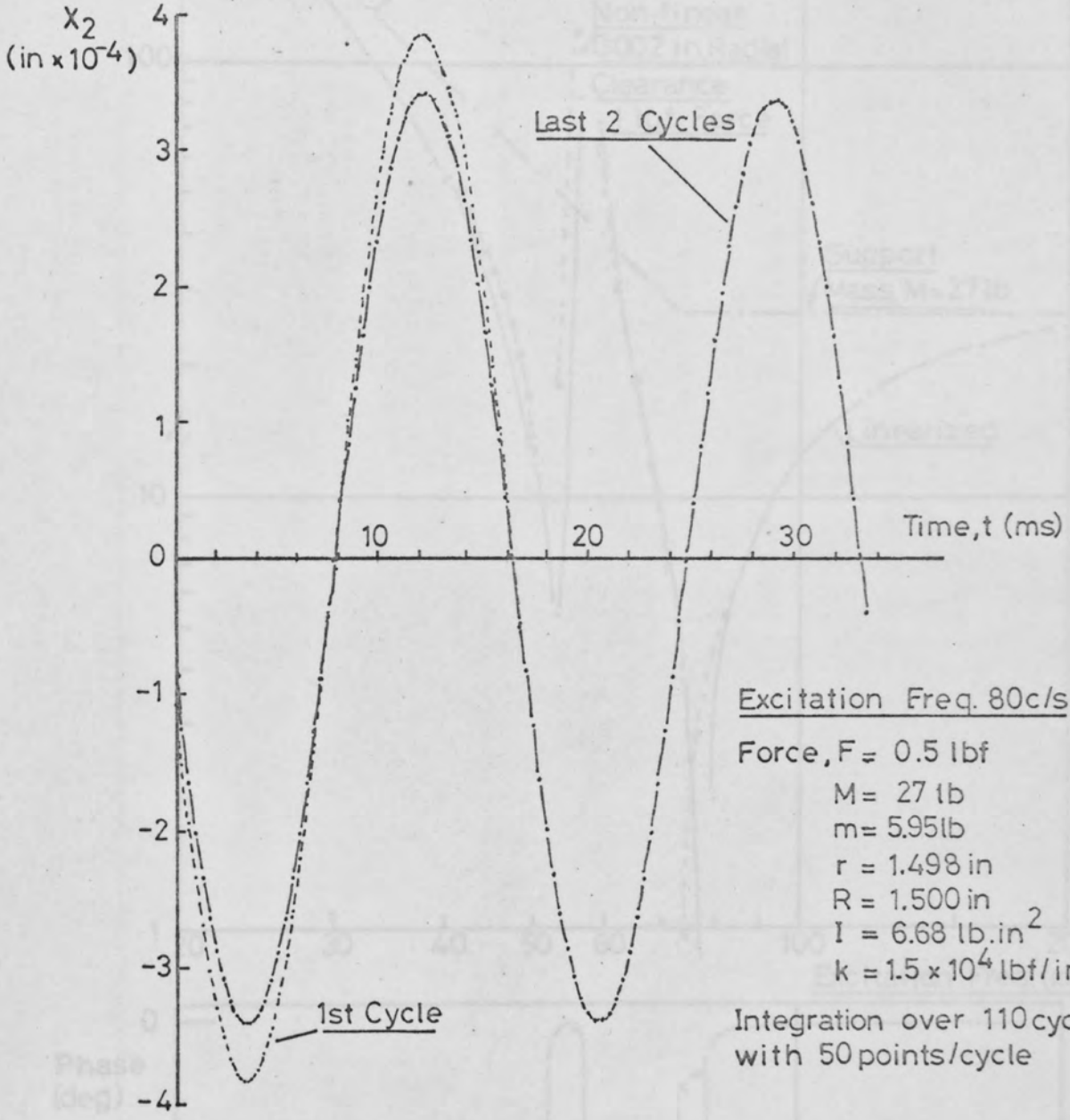

FIG.I.3. COMPUTER SOLUTION FOR BEARING SUPPORT DISPLACEMENT.

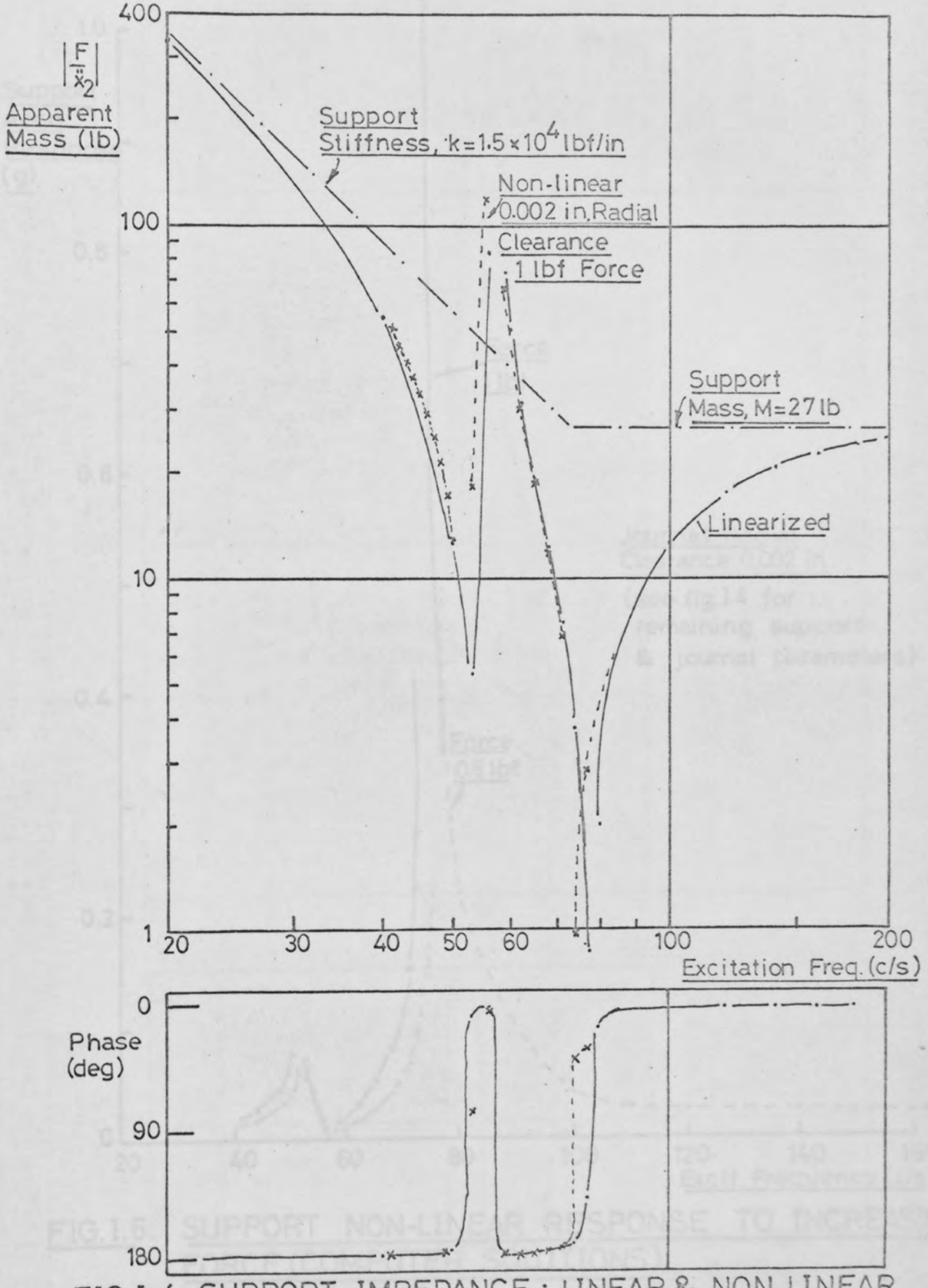

FIG. I. 4. SUPPORT IMPEDANCE : LINEAR & NON LINEAR SOLUTIONS

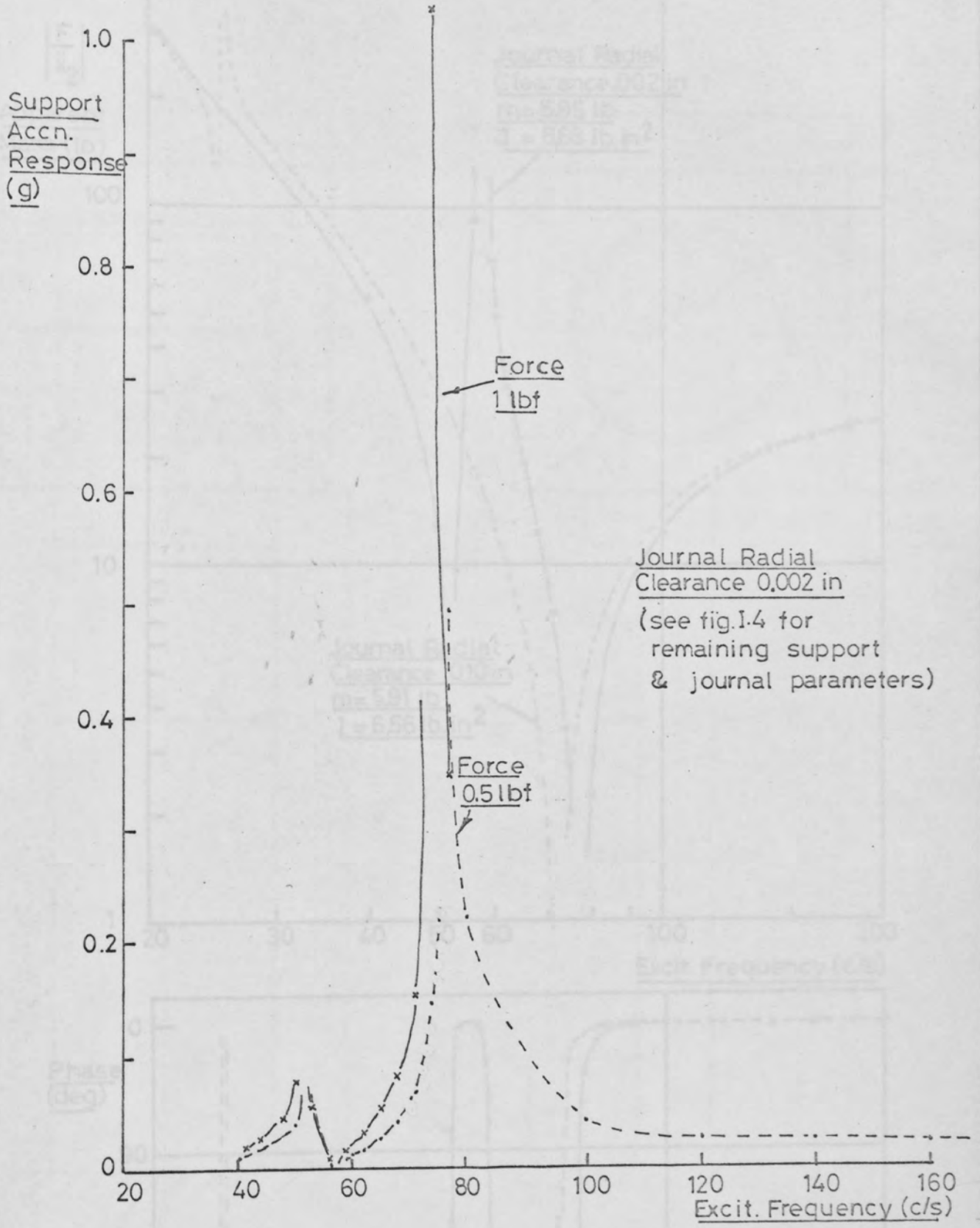

FIG. I.5. SUPPORT NON-LINEAR RESPONSE TO INCREASING FORCE (COMPUTER SOLUTIONS)

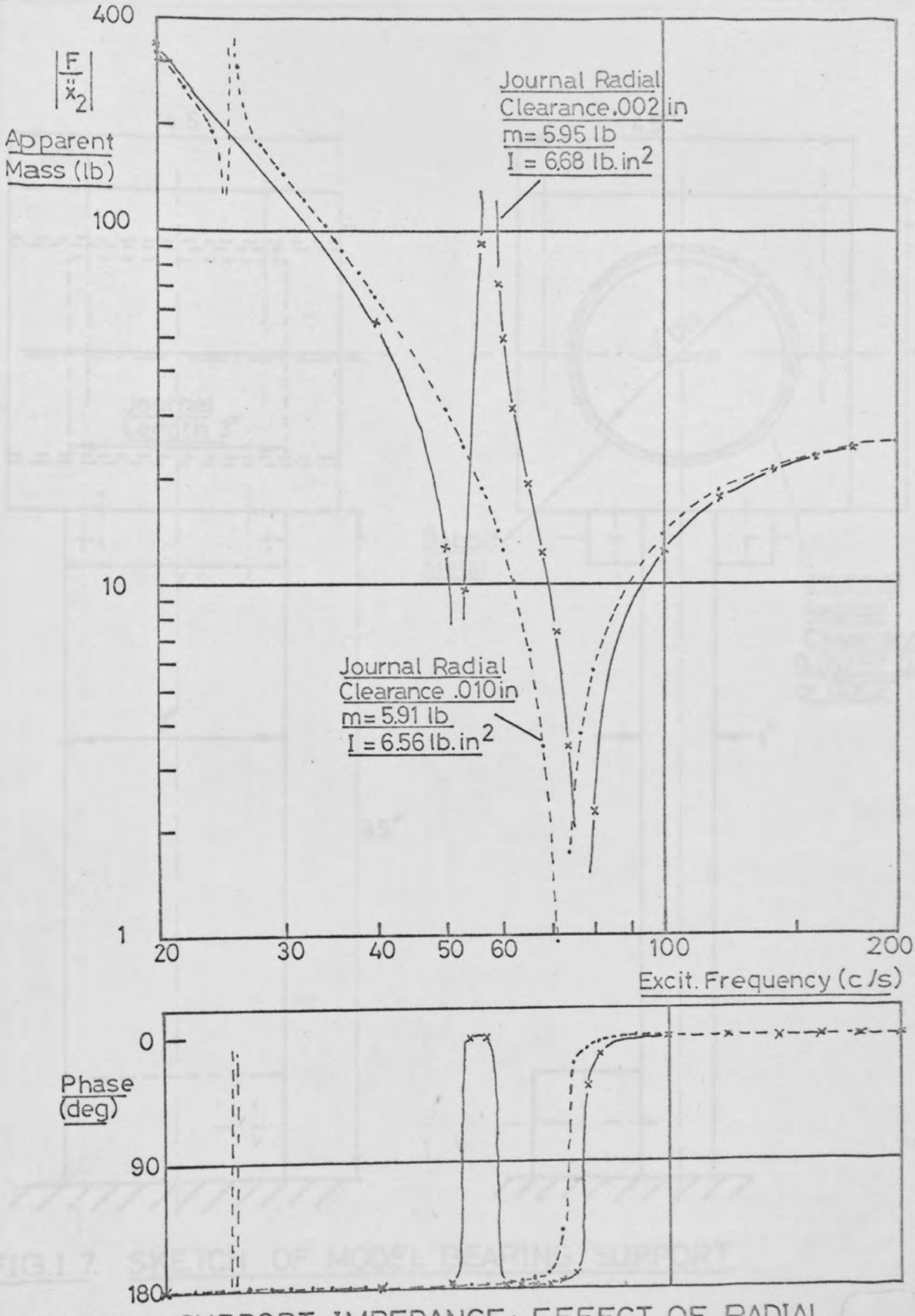

FIG. I. 6. SUPPORT IMPEDANCE: EFFECT OF RADIAL CLEARANCE (COMPUTER SOLUTIONS)

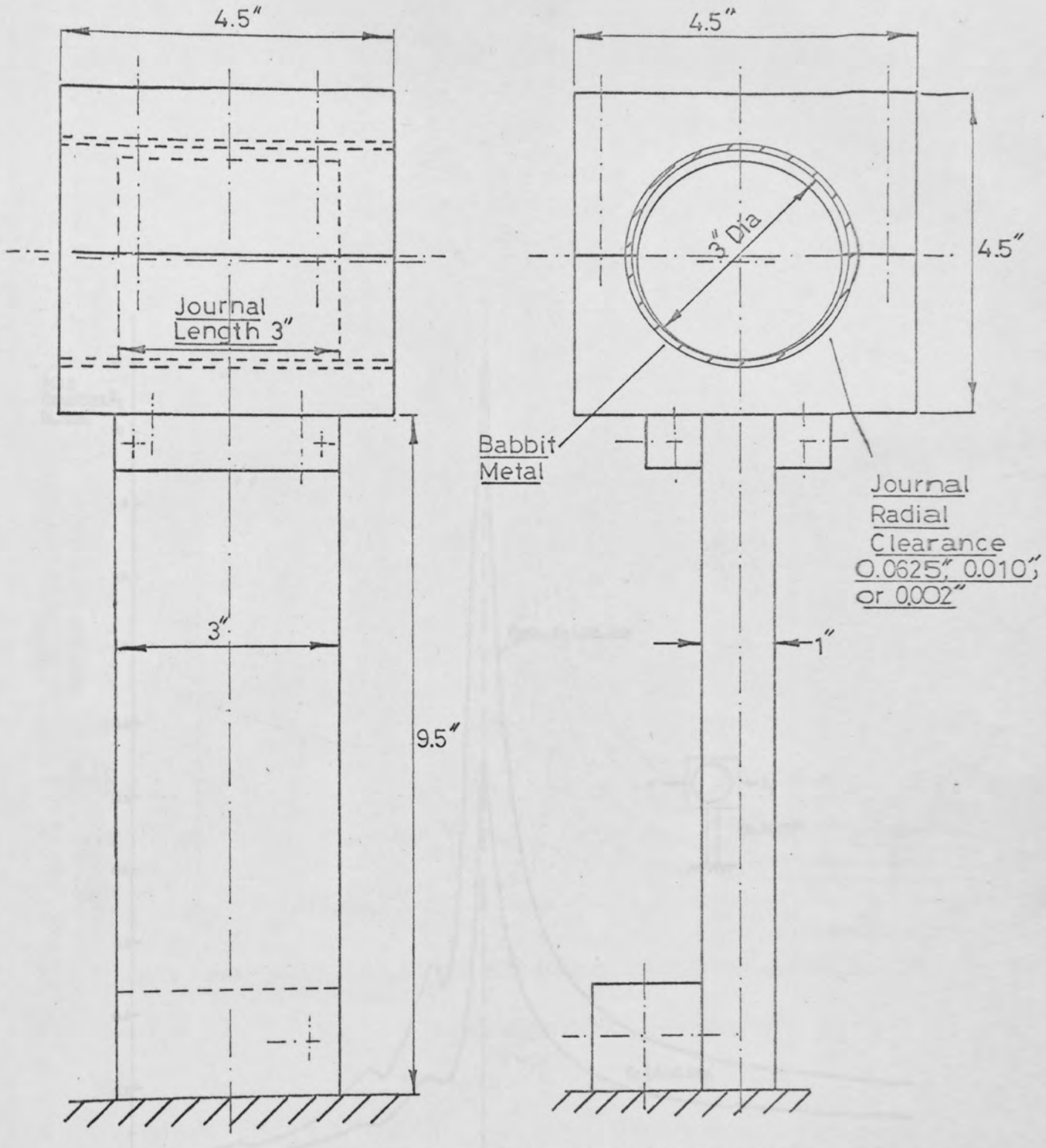

FIG.I.7. SKETCH OF MODEL BEARING SUPPORT

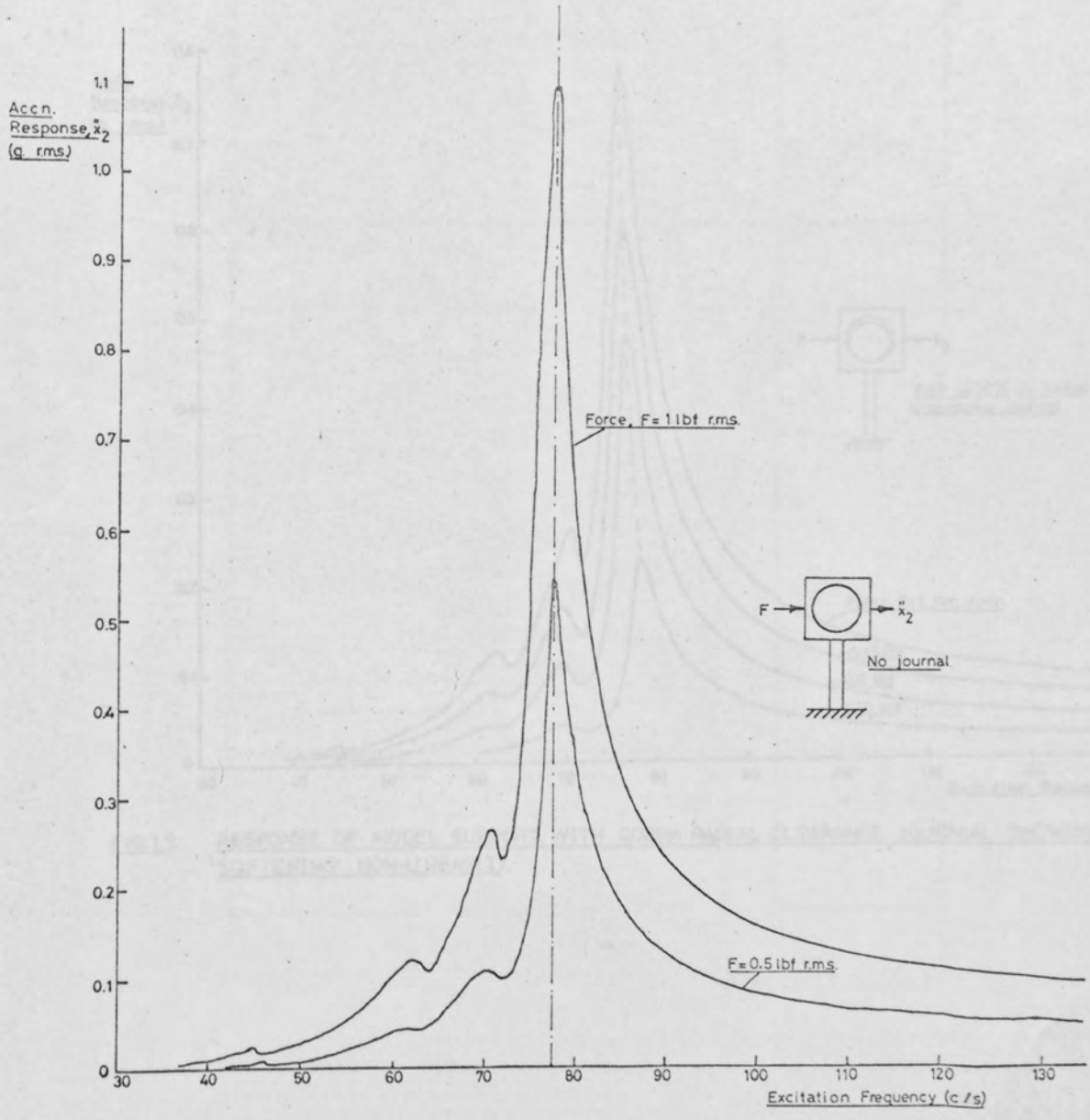

FIG.I.8. RESPONSE OF MODEL SUPPORT ALONE SHOWING INHERENT LINEARITY.

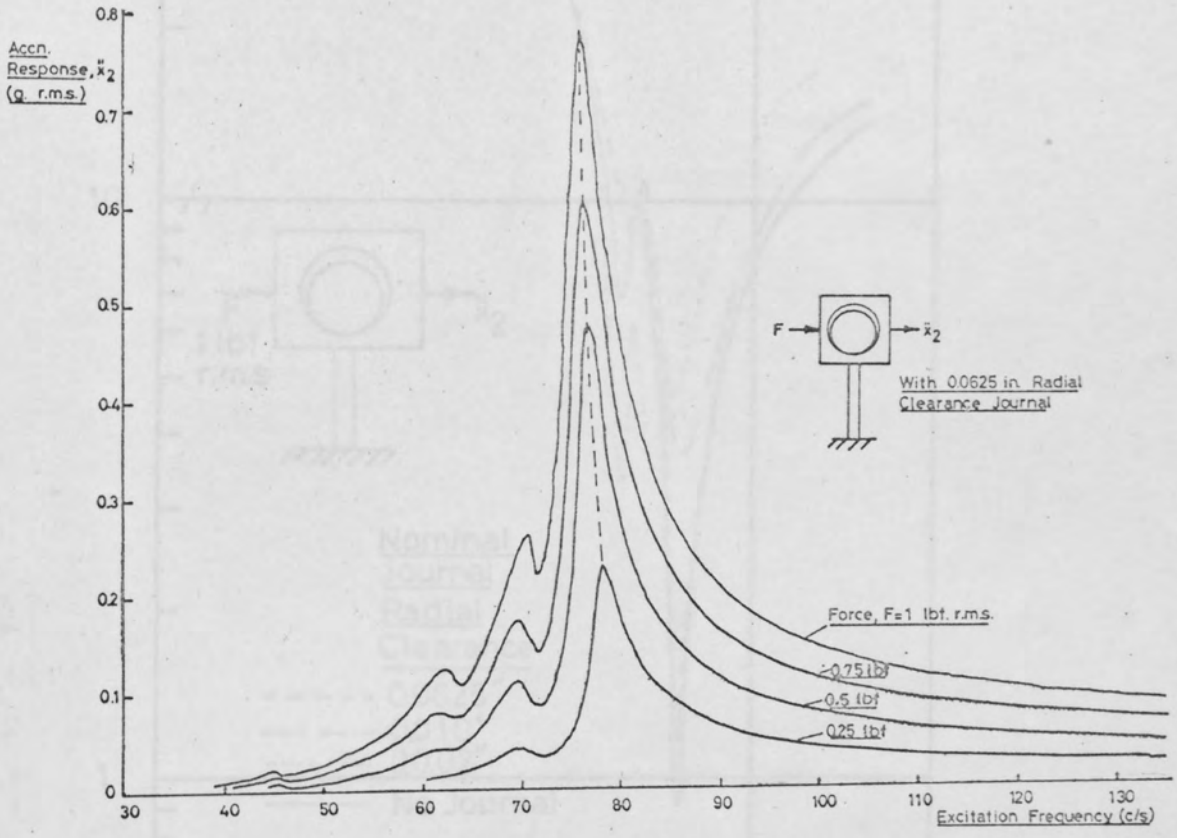

FIG. 1.9. RESPONSE OF MODEL SUPPORT WITH 0.065in RADIAL CLEARANCE JOURNAL SHOWING 'SOFTENING' NON-LINEARITY.

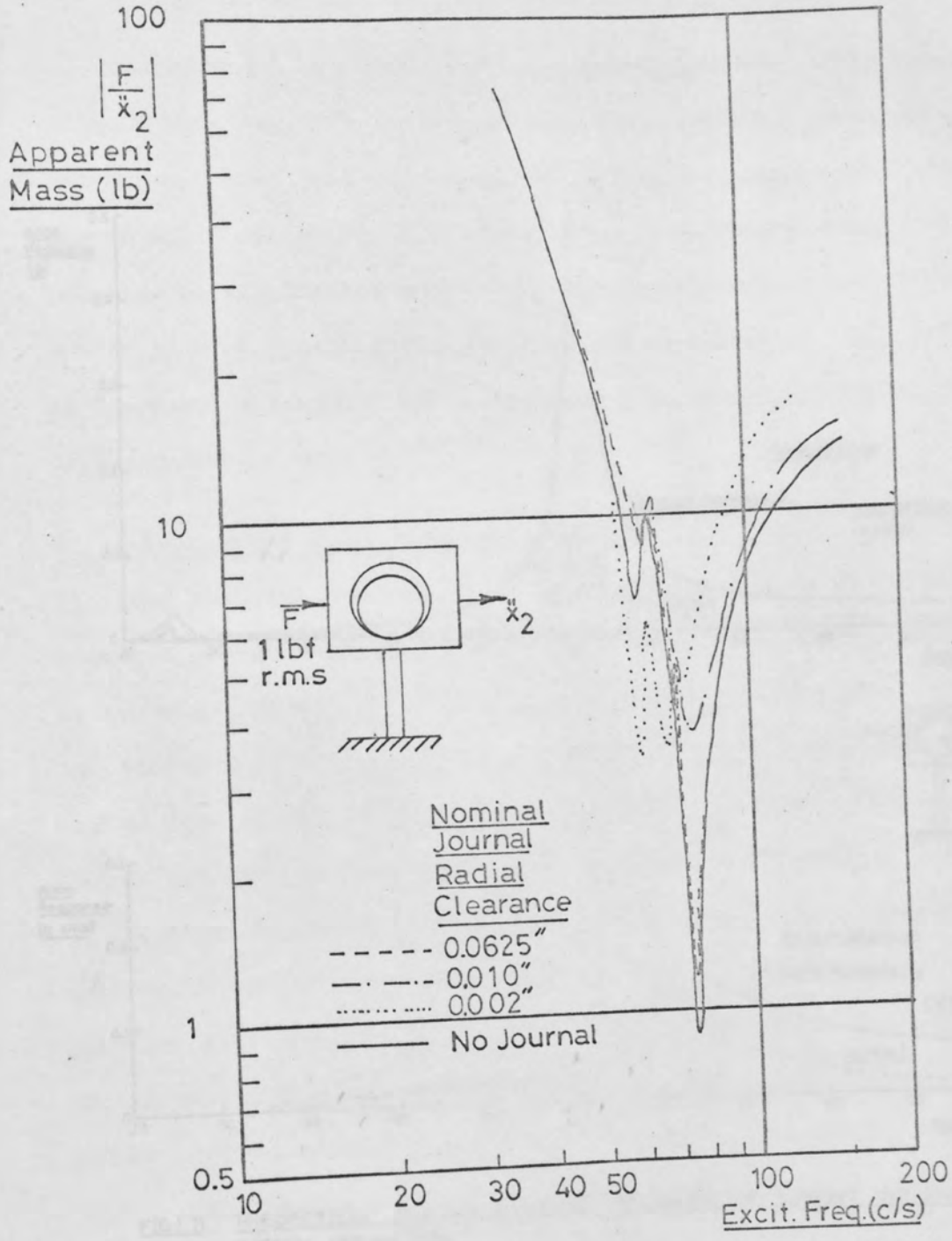

FIG. I. 10. MEASURED SUPPORT IMPEDANCES FOR VARIOUS JOURNAL DIAMETERS.

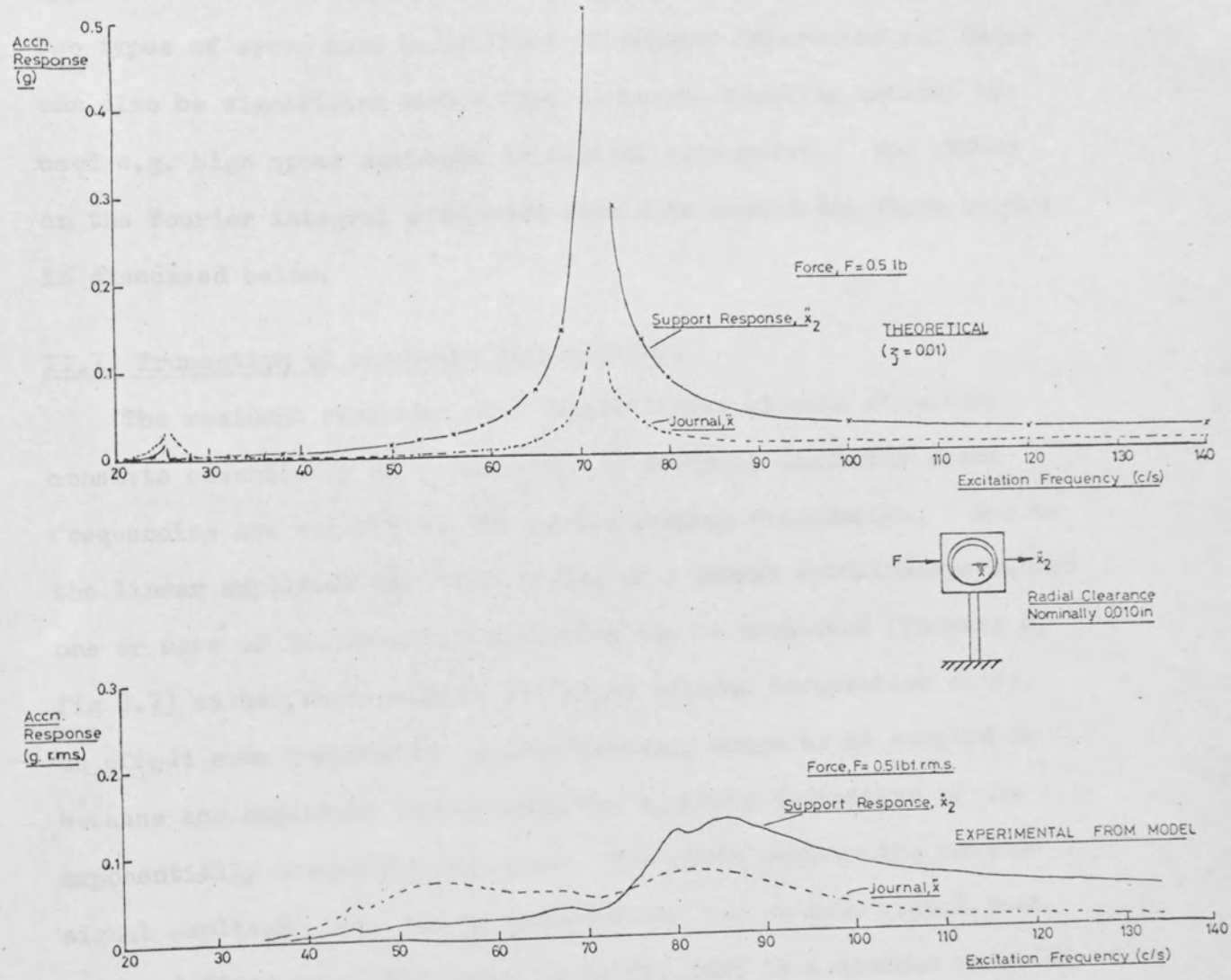

FIG.1.11. THEORETICAL AND EXPERIMENTAL RESPONSES OF SUPPORT AND JOURNAL FOR SIMILAR SYSTEM PARAMETERS.

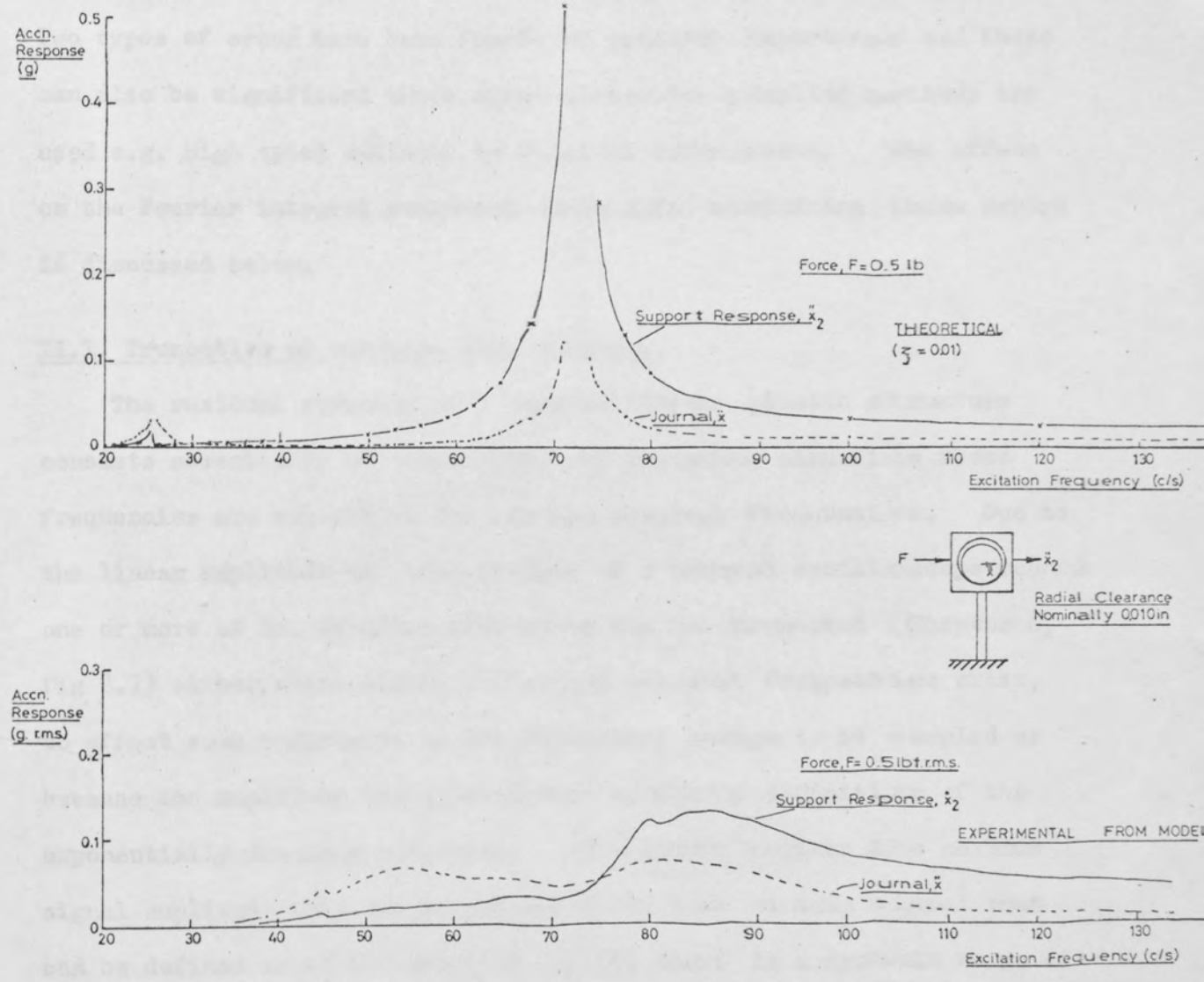

FIG.I.11. THEORETICAL AND EXPERIMENTAL RESPONSES OF SUPPORT AND JOURNAL FOR SIMILAR SYSTEM PARAMETERS.

APPENDIX II

Errors in analysis of Transients from photographed records

Although a camera and oscilloscope provide the simplest method of recording transient time histories (see Chapter 8) a degree of approximation is naturally involved in taking measurements therefrom. Two types of error have been found of primary importance and these can also be significant where more elaborate sampling methods are used e.g. high speed analogue to digital conversion. The effect on the Fourier integral evaluated from data containing these errors is discussed below.

II.1. Truncation of response time history.

The residual response of a damped linear elastic structure consists essentially of a summation of decaying sinusoids whose frequencies are related to the system natural frequencies. Due to the linear amplitude and time scales of a normal oscilloscope record one or more of the decaying sinusoids may be truncated (Chapter 8, fig 8.7) either, where widely different natural frequencies exist, to effect some compromise in the frequency range to be sampled or because the amplitude scale precludes complete definition of the exponentially decaying responses. The ratio between the maximum signal amplitude that can be recorded and the minimum signal that can be defined is of the order of 1: 50, that is a dynamic range of 34 db. The maxima of the unit initial amplitude decaying sine wave

$$y = e^{-\zeta \omega_n t} \cdot \sin \omega_d t \qquad \text{(II.1)}$$

can therefore only be measured until

$$e^{-\zeta \omega_n t} = \frac{1}{50} \qquad \text{(II.2)}$$

that is for the number of cycles, n, given by

$$n = (\log_e 50) / \zeta . 2\pi$$

or $$n = \frac{3.9119}{2\pi . \zeta} \qquad \text{(II.3)}$$

Consider the acceleration response of a single degree of freedom system to be defined by

$$\ddot{x} = \ddot{X}_o e^{-\zeta \omega_n t} \sin \omega_d t \qquad \text{(II.4)}$$

which for small damping may be written

$$\ddot{x} = \ddot{X}_o e^{-\zeta \omega_n t} . \sin \omega_n t \qquad \text{(II.5)}$$

$$(i.e.\ \omega_n \triangleq \omega_d)$$

The Fourier transform of this function is given, from eqn.(II.2) by

$$\overline{F(\omega)} = \int_{-\infty}^{\infty} X_o e^{-\zeta \omega_n t} . \sin \omega_n t . e^{-j\omega t} . dt \qquad \text{(II.6)}$$

The approximation arising from the truncation of the response is tantamount to introducing a finite upper limit of integration in Eqn. (II.6), whether this is due to the record being of limited length or immeasurable beyond that limit.

Eqn. (II.6) thus becomes

$$\overline{F(\omega)} = \ddot{X}_o \int_o^{\tau} e^{-\zeta \omega_n t} . \sin \omega_n t . e^{-j\omega t} \qquad \text{(II.7)}$$

or $$\overline{F(\omega)} = \ddot{X}_o \int_o^{\tau} e^{-(\zeta \omega_n + j\omega)t} . \sin \omega_n t . dt \qquad \text{(II.8)}$$

Performing the indicated integration and writing the complex exponentials in trignometric form yields

$$\overline{F(\omega)} = R_e\left(\overline{F(\omega)}\right) + j I_m\left(\overline{F(\omega)}\right) \qquad \text{(II.9)}$$

where

$$R_e\left(\overline{F(\omega)}\right) = \ddot{X}_o \Bigg[\left((1+\zeta^2) - \left(\frac{\omega}{\omega_n}\right)^2 \right) + e^{-\zeta\omega_n\tau} \Bigg\{ \left(-\zeta(1+\zeta^2) - \zeta\left(\frac{\omega}{\omega_n}\right) \right) \cdot \sin\omega_n\tau \cos\omega\tau +$$

$$\left\{ -(1+\zeta^2) + \left(\frac{\omega}{\omega_n}\right)^2 \right\} \cdot \cos\omega_n t \cdot \cos\omega t +$$

$$\left\{ -\left(\frac{\omega}{\omega_n}\right)(1-\zeta^2) + \left(\frac{\omega}{\omega_n}\right)^3 \right\} \cdot \sin\omega_n\tau \sin\omega\tau +$$

$$\left\{ 2\zeta\left(\frac{\omega}{\omega_n}\right) \right\} \cos\omega_n\tau \sin\omega\tau \Bigg\} \Bigg] \Bigg/$$

$$\omega_n \left\{ \left\{ (1+\zeta^2) - \left(\frac{\omega}{\omega_n}\right)^2 \right\}^2 + 4\zeta^2\left(\frac{\omega}{\omega_n}\right)^2 \right\} \qquad \text{(II.10)}$$

and

$$I_m\left(\overline{F(\omega)}\right) = \ddot{X}_o \Bigg[-2\zeta\left(\frac{\omega}{\omega_n}\right) + e^{-\zeta\omega_n\tau} \Bigg[\left\{ \zeta^2\left(\frac{\omega}{\omega_n}\right) - \left(\frac{\omega}{\omega_n}\right) + \left(\frac{\omega}{\omega_n}\right)^3 \right\} \cdot$$

$$\sin\omega_n\tau \cos\omega\tau +$$

$$2\zeta\left(\frac{\omega}{\omega_n}\right) \cos\omega_n\tau \cos\omega\tau +$$

$$\zeta \left\{ (1+\zeta^2) + \left(\frac{\omega}{\omega_n}\right)^2 \right\} \sin\omega_n\tau \sin\omega\tau +$$

$$\left\{ (1+\zeta^2) - \left(\frac{\omega}{\omega_n}\right)^2 \right\} \cos\omega_n\tau \sin\omega\tau \Bigg] \Bigg] \Bigg/$$

$$\omega_n \left\{ \left\{ (1+\zeta^2) - \left(\frac{\omega}{\omega_n}\right)^2 \right\}^2 + 4\zeta^2\left(\frac{\omega}{\omega_n}\right)^2 \right\} \qquad \text{(II.11)}$$

These expressions have been evaluated on a digital computer for various upper limits of integration, τ, The three dimensional surface of the modulus of the Fourier transform having axes $|F(\omega)|, \omega$, n is sketched in fig II.1 for the case ωn = 100 c/s, ζ = 0.1 to show both high and low-frequency aspects. It can be seen that the effect of truncating the response in the time domain is similar to decreasing the magnification factor (Q) at resonance in the frequency response plot, whilst the flanks of the curve become distorted due to the exclusion of some of the sampling function components required for complete definition.

For the decaying response whose Fourier transform is plotted (ω_n = 100 c/s. ζ = 0.1) the amplitude limitation suggested in eqn. (II.3) is reached when n = 6.2 cycles. The maximum error in the transform modulus is then about 3% of the correct value i.e. for n = ∞ If the full amplitude range is not used the errors incurred are naturally greater, thus if only 28 db are available (ratio 1:25) then only 5.12 cycles of the same waveform may be sampled. The maximum error in $|F(\omega)|$ is then 5%.

It may be mentioned here that where systems having widely differing natural frequencies are to be investigated, the use of a non-linear time scale for photographed records could be of value. Exponential time bases employing R.C. circuitry are readily constructed and would enable the accurate sampling of high frequency components without truncation of the more slowly decaying low frequency ones.

II.2. Trace Misalignment

Where hand measurements are made from filmed records slightly inaccurate location of the zero level may occur. This results in the inclusion in the sampled data of a ramp function as shown in fig II.2

and defined by

$$f(t)\Big|\begin{matrix} y\cdot\frac{t}{\tau} & t \le \tau \\ 0 & t \le 0\ ;\ t > \tau \end{matrix}\Big\} \qquad \text{(II.12)}$$

where, as above, τ is the duration of the record.

The Fourier transform of this function is

$$\overline{F(\omega)} = \frac{1}{\tau}\int_0^{\tau} t \cdot e^{-j\omega t}\, dt \qquad \text{(II.13)}$$

A sketch of the Fourier transform surface obtained by adding the effect of a misalignment of 20% of the initial amplitude ($y = 0.2\ \ddot{X}_o$) to that caused by truncating the response is shown in fig II.3 The parameters ω, ζ of the decaying sinusoid in this figure are identical to those used to plot fig II.1 thus the differences between the surfaces are solely due to the misalignment. On comparing the two diagrams it can be seen that very large errors in the modulus of the Fourier spectrum have been introduced by the assumed misalignment. These errors are worse away from the 'resonant' frequency $\omega = \omega_n = 100$ c/s, and reach values of the order of 300%. Although the assumed misalignment of 20% is larger than should occur with careful measurement, errors of this type have been found significant where much smaller misalignments were possible and were responsible in the majority of cases where an unacceptable scatter of results had been obtained in experimental transient impedance measurements.

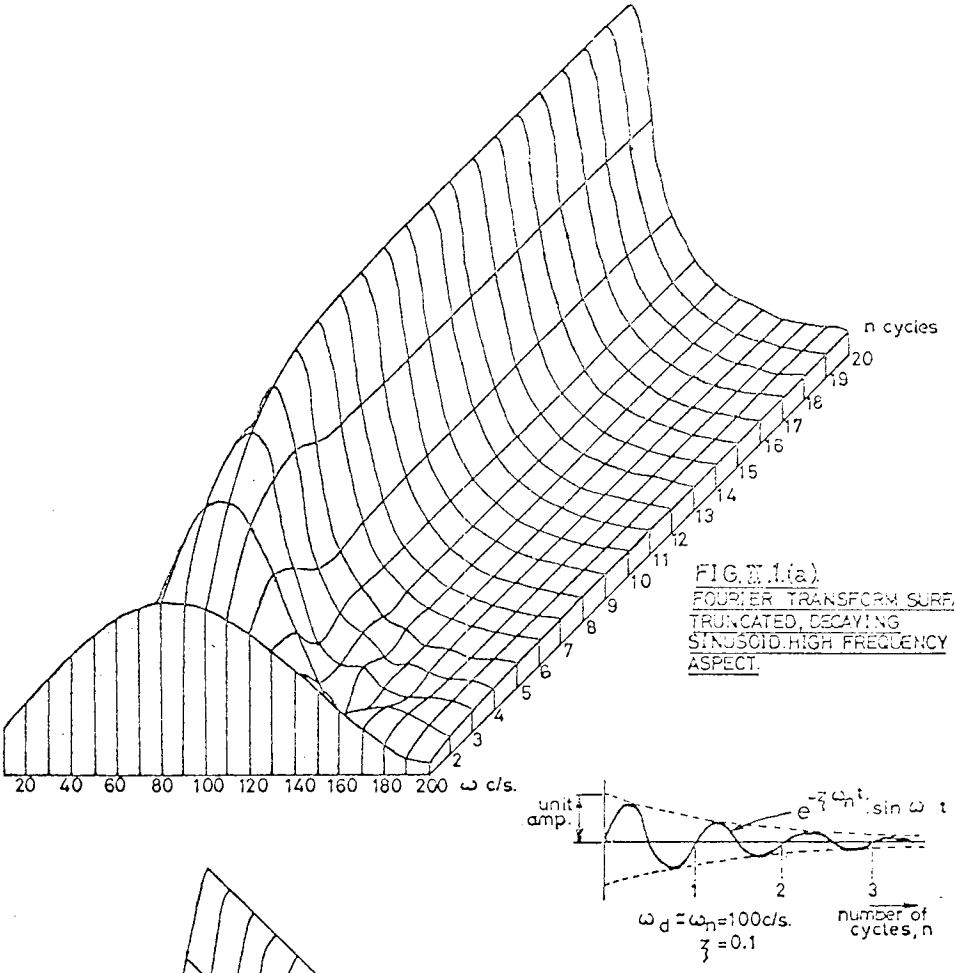

FIG. II.1.(a).
FOURIER TRANSFORM SURFACE TRUNCATED, DECAYING SINUSOID. HIGH FREQUENCY ASPECT.

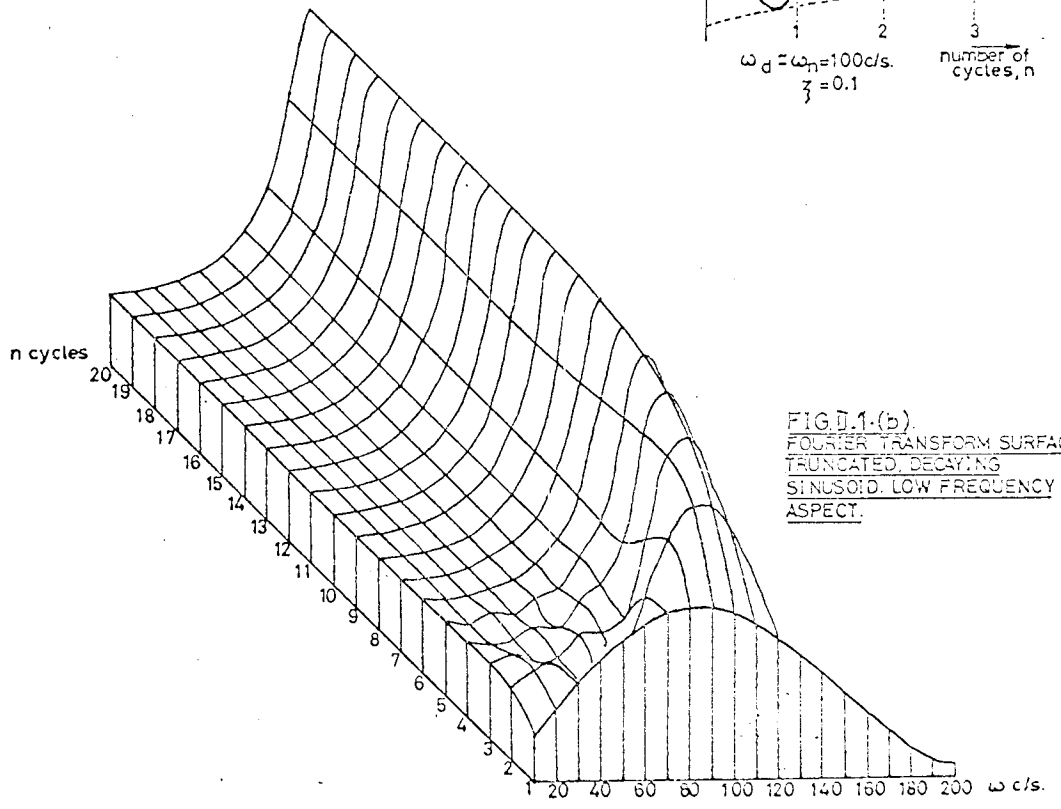

FIG. II.1.(b).
FOURIER TRANSFORM SURFACE TRUNCATED, DECAYING SINUSOID. LOW FREQUENCY ASPECT.

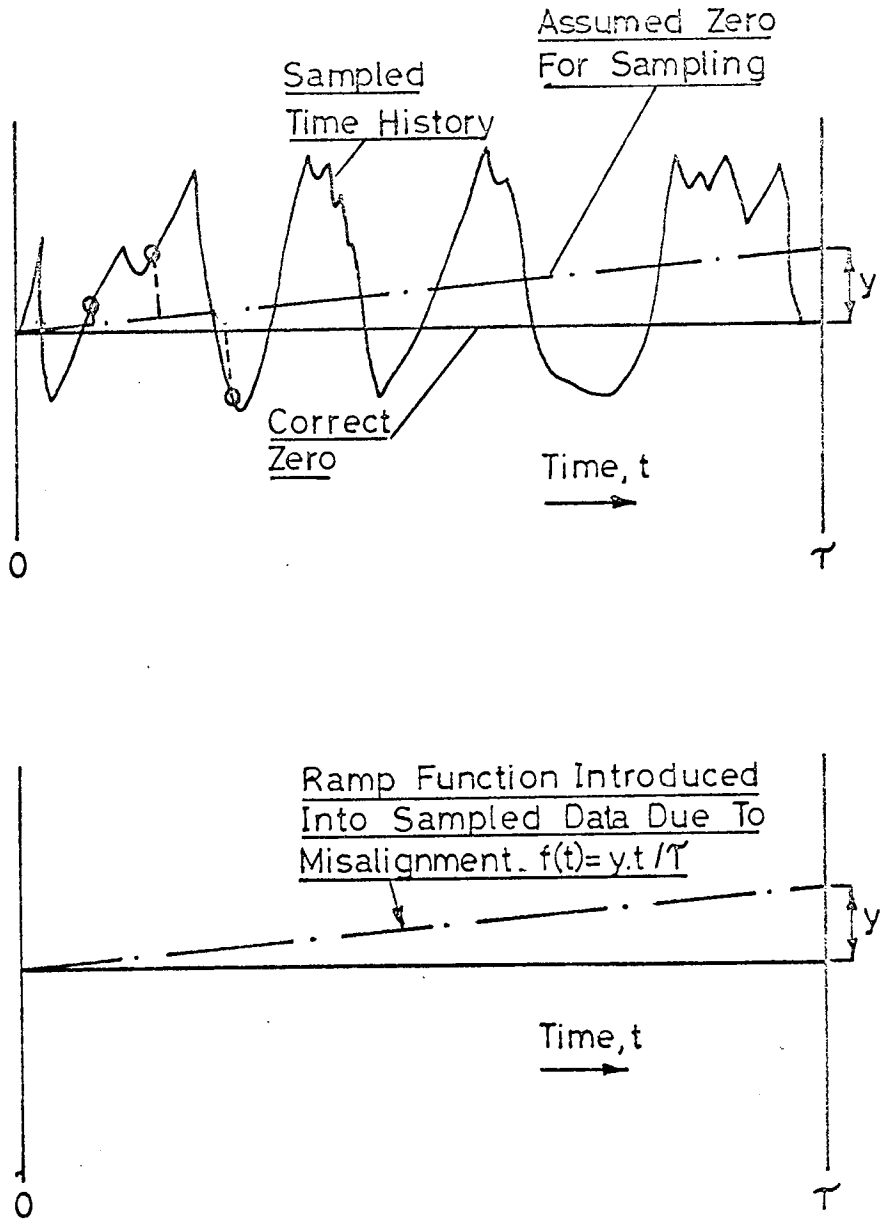

FIG.II.2. RAMP FUNCTION ERROR

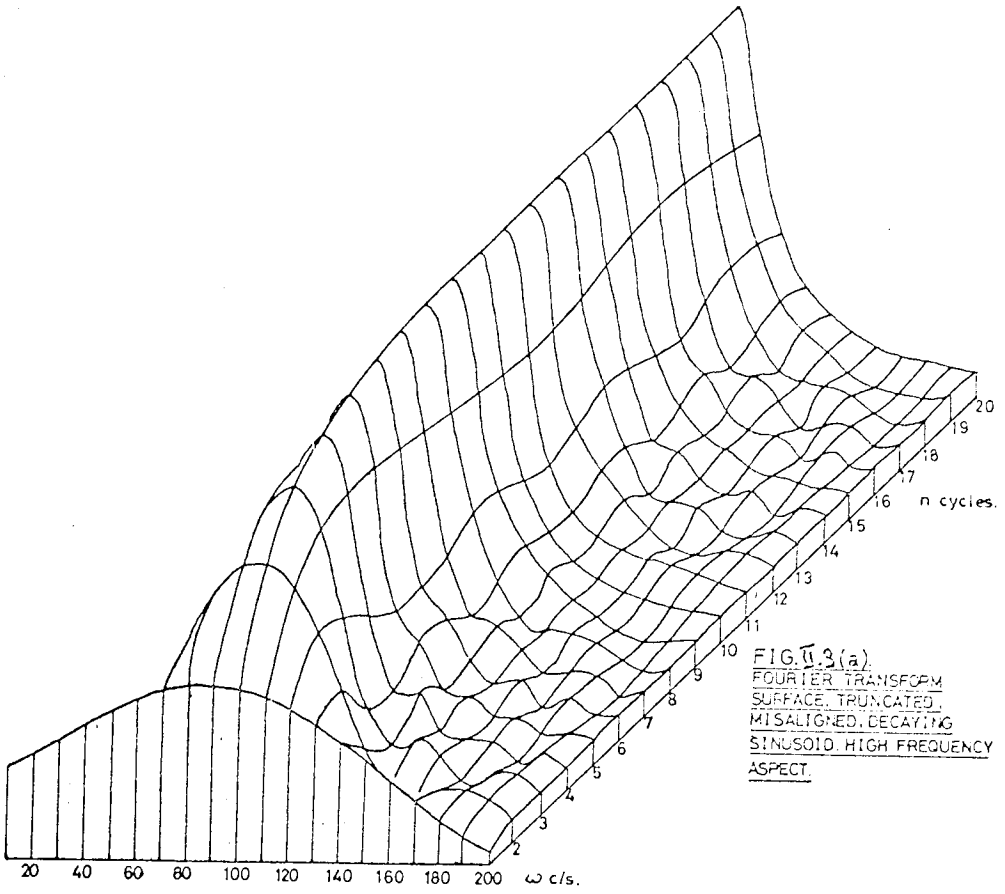

FIG. 3 (a).
FOURIER TRANSFORM SURFACE, TRUNCATED, MISALIGNED, DECAYING SINUSOID. HIGH FREQUENCY ASPECT.

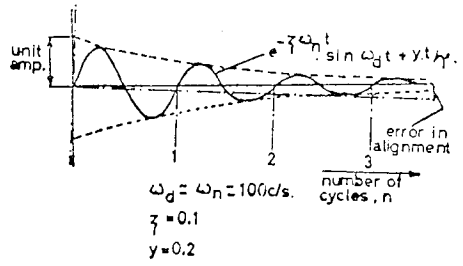

FIG. 3 (b).
FOURIER TRANSFORM SURFACE, TRUNCATED, MISALIGNED, DECAYING SINUSOID. LOW FREQUENCY ASPECT.

APPENDIX III

Ball and Journal Bearing Disturbances on the Model Rig.

III.1 Introduction

During the course of the investigations into the dynamic behaviour of the model rig (Chapter 6), significant non-synchronous vibrations were detected with both the ball-and-journal bearing configurations. In this appendix a series of measurements are reported which were made to identify the cause of the disturbances and estimate their severity in terms of bearing force levels. They are also believed to be of general interest from the point of view of vibration diagnosis in full-scale machines.

With the shaft carried in ball-bearings, vibrations due to geometric irregularities of the outer bearing tracks were observed which excited a series of natural frequencies of the system as the shaft speed was increased i.e. critical speeds. In some cases the bearing force levels, as determined from the measured support impedances, were in excess of 25% of the steady bearing loads due to the shaft's weight. They were therefore of a comparable magnitude to the forces resulting from the residual unbalance of the system. Examples of the experimental results are given in section III.2 below.

In section III.3 a series of noise measurements are presented which were made whilst the rig was running. These measurements showed how the bearing 'noise' was selectively amplified by the shaft assembly near its predominant 'ringing' frequencies.

As reported in Chapter 6, section 6.6 (i), the journal bearings used for the model rig gave rise to a violent instability above a certain rotational speed. The nature of this unstable behaviour and the bearing forces it produced are discussed in section III.4 (i). The possibility of predicting the threshold of instability by using an extension of the theoretical approach of chapter 4 is considered in

III.2 Displacement Excitation due to Ball Bearings

Apart from the inevitable first-order unbalance vibrations, measurements of acceleration responses at the bearing supports of the model rig showed a series of discrete-frequency disturbances at non-integer multiples of the running frequency. These disturbances were found, from line spectrum analyses, to be at 5.74 times the rotational frequency, f_{rot}, and at harmonics thereof.

A typical line spectrum of the D.E. bearing support acceleration response is shown in fig III.1 for a shaft speed of 9.3 c/s. The components at 5.74 f_{rot}, 11.48 f_{rot}, 17.2 f_{rot} ... etc., are identified in this diagram.

It was concluded, from a consideration of the geometry of the bearings used, that the component at 5.74 f_{rot}, could only have arisen from an irregularity in the outer track of one (or both) of the bearings. Thus, referring to the inset diagram of fig III.1, the linear velocity of the inner track, Vi, is:-

$$V_i = 2\pi . f_{rot} . r_i \qquad \text{(III.i)}$$

So that the cage velocity (i.e. velocity of the centre of the balls) is:-

$$Vc = \frac{V_i}{2} = \pi f_{rot} . r_i \qquad \text{(III.2)}$$

Therefore, the passage frequency, f_p, of a single ball past an irregularity in the outer track is:-

$$f_p = \frac{V_c}{2\pi r_c} = \frac{Vc}{2\pi(r_i + \frac{r_i + r_o}{2})} \qquad \text{(III.3)}$$

Substituting for Vc from (iii.2)

$$f_p = \frac{\pi . f_{rot} . r_i}{2\pi(r_i + \frac{r_i + r_o}{2})} = f_{rot} . \frac{ri}{(r_i + r_o)} \qquad \text{(III.4)}$$

or, for n balls, the passage frequency is

$$f_p = \frac{n.r_i}{r_i+r_o} \cdot f_{rot} \qquad \text{(III.5)}$$

For the Hoffman UMS 12 double-row, self aligning ball bearings used, the nominal dimensions were:-

$$r_i = 0.8986 \text{ in.}, \; r_o = 1.3206 \text{ in.} \qquad \text{(III.6)}$$

there being 14 balls/row.

So that the passage frequency past an irregularity in the outer track was:-

$$f_p = \frac{14 \times .8986}{1.3206 + .8986} = 5.7 \qquad \text{(III.7)}$$

which agrees with that observed experimentally.

This type of excitation may be compared with others reported by Yamamoto (36), for instance. (See Chapter 1, section 2.4 (i)).

An interesting characteristic of the ball passage frequency and its harmonics was that each harmonic was not of constant amplitude but exhibited a 'beating' phenomena. The period of the beats was not constant but was dependent on the shaft speed and in some cases was as long as 30 seconds. Fig III.2 shows typical amplitude variations recorded for the 5.74 f_{rot} vibration at various rotational speeds with the 24 in bearing centre configuration.

It is thought the beats arose due to slight differences in the excitation frequency at each bearing - possibly due to small differences in their dimensions - although no conclusive evidence was found. Fig. III.3 (a) shows the variation in amplitude of the beats at 5.74 f_{rot} as a function of rotational speed whilst fig III.3 (b) shows the variations in beat frequency with rotational speed. It can be seen from the latter

diagram that, although the beat frequency showed a general increase with increasing rotational speed no simple linear relationship was apparent as would be expected for a given difference in the dimensions of the two bearings. The results were repeatable, however, within about 5% of the values shown, which tended to discount slippage effects in determining the general pattern. Very slow variations in rotational speed were also discounted since the frequency of the 'tracked' harmonics ($5.74\ f_{rot}$) was observed to be within 0.3 c/s, whilst those slight variations which did occur were always in a fixed direction i.e. normally very slight decreases in shaft speed.

Several measurements were made of the variation with rotational speed of the mean level of vibration at the bearing harmonic frequencies. Examples of such measurements are given in figs III.4 and III.5 for the $5.74\ f_{rot}$ disturbances. In these measurements the 'harmonic tracking' methods of Chapter 5 section 5.5 (ii) were used. In order to obtain readable records in the presence of the beating phenomenon, averaging of between 10 and 100 seconds was used in the analysis system.

The vertical response at the N.D.E. bearing support for the 24 in bearing centre configuration (See Chapter 6, section 6.2 (i) and fig 6.1) is shown in fig III.4. The frequencies of the peak responses in this plot agree closely with the impedance minimum measured previously (compare with figs 6.20 and 6.21) on the complete rotating system - including those resonances due to gyroscopic coupling with the horizontal plane. The bearing forces corresponding to each peak in fig III.4 are also shown, based on the support impedance measurements made without the shaft in place. The maximum mean force of 9.04 lbf r.m.s. is seen to occur at a rotational frequency of 48.5 c/s (excitation frequency 278 c/s) whilst at the maximum beat amplitude the forcing at

this frequency rose to about 11.8 lbf r.m.s. This may be compared with the maximum unbalance forcing of 14 lbf r.m.s. indicated by the measured response at the N.D.E. pedestal to the 'fine' balance condition at a rotational frequency of 52.5 c/s, discussed in Chapter 6, section 6.5 (iii). In this configuration (24 in centres) the steady load at each bearing due to the shaft weight was 35 lbf.

With the 20 in bearing centre configuration a maximum mean forcing level, at the 5.74 f_{rot} frequency, of 16.7 lbf r.m.s. was observed, this being indicated in fig III.5. This may be compared with the 14.4 lbf r.m.s. at rotational speed of 65 c/s obtained at the N.D.E. support with the 'fine' balance condition, and with the steady shaft load of 42 lbf at this support. Also shown in fig III.5 is the response at the D.E. support to the 5.74 f_{rot} excitation, the corresponding forcing levels being indicated at the resonant peaks.

It may also be seen in fig III.5 that the bearing disturbances were dependent on the amount of unbalance (first-order) vibration. Thus between rotational frequencies of about 58 to 79 c/s (fundamental critical range) the effect of increasing the unbalance was to reduce the amplitude of the high frequency vibration. Although, presumably, the reason for this non-linearity was a cyclic variation in bearing load in the radial plane containing the irregularity in the outer bearing track, no evidence of modulation could be seen in the line spectra of the support response. It might be expected that a modulation of the 5.74 f_{rot} bearing excitation with the rotational frequency f_{rot} would produce sidebands in the spectrum at 6.74 f_{rot} and 4.74 f_{rot} respectively.

III.3 Noise Measurements.

During the experiments performed with the shaft supported in ball bearings it was noticed that a distinctive, high frequency noise was generated by the rig, similar in quality to that of a siren.

The variation in overall 'near field' noise level with rotational frequency is illustrated in fig III.6 for the 20 in bearing centre configuration, from which it can be seen that the maximum level of 107 db (re .0002μbar) occurred at about 80 c/s (4800 r.p.m.).

The character of the noise was predominantly random and therefore approximate levels were obtained using the Quantech wave analyser (see Chapter 5, section 5.4) with a 10 c/s constant bandwidth filter together with some additional averaging. A more accurate analysis would have required calibration of the amplitude scale in terms of power spectral density (P.S.D.), but the method used gave a good qualitative description of the noise spectrum.

It was thought at first that the noise was generated by the balancing holes acting as acoustic resonators but this was discounted after they had been covered with adhesive tape. It can be seen from fig III.7 that no significant change in the spectrum occurred between these two conditions.

Throughout the shaft speed range 30 - 90 c/s the noise spectrum showed a distinct maximum whose frequency depended on the location of the microphone. With the microphone close to the D.E. half-shaft the maximum occurred between 2000 and 2500 c/s, the frequency tending to increase with increasing rotational speed. With the microphone close to the N.D.E. half-shaft a maximum in the noise spectrum was encountered between 3500 and 4500 c/s. The peak at about 2150 c/s in the spectrum shown in fig III.7 illustrates this behaviour - in this case the microphone was close to the D.E. half-shaft.

From the relatively small variation in the frequencies at which the peaks in the spectrum occurred with much larger variation in shaft speed and from the appearance of the spectra themselves, small levels of bearing noise were apparently being 'selectively' amplified by the mechanical and acoustic properties of the system.

A series of tests were performed to try to identify the cause of the amplification, in which the half-shafts of the model were subjected to a transient mechanical excitation. For this purpose the half-shafts were struck with an ordinary steel spanner which had been bound over most of its length with several layers of adhesive tape. The spanner therefore delivered a fast, impulsive mechanical transient to the shaft whilst the spanner's own response was very heavily damped.

The unfiltered acoustic (microphone) response of the system to this excitation is shown in fig III.8. In fig III.8 (a) the microphone was placed close to the D.E. half-shaft, in a similar position to that used for obtaining the noise spectrum of fig III.7, and it may be seen that the response is predominantly at a single frequency of about 2100 c/s i.e. close to the peak in the spectrum of fig III.7.

The response at the N.D.E. half-shaft to similar excitation is shown in fig III.8 (b) and in this case the predominant acoustic response is seen to be at a frequency of about 4000 c/s - again close to the frequencies at which peaks in the spectrum were obtained with the shaft rotating.

It was therefore concluded that the peaks in the measured noise spectrum of the model whilst running were due to amplification of the bearing 'noise' at frequencies where the half-shafts acted as efficient acoustic radiators.

III.4 (i) Measured Characteristics of Journal Bearing Instability.

With the model shaft running in plain journal bearings (Chapter 6, section 6.6) a severe unstable whirl developed as the shaft speed was increased above some limiting value. This boundary of instability was affected by the oil conditions, but, for the range of oil viscosities

used, was between shaft rotational frequencies of 85 and 98 c/s for the 20 in bearing centre configuration and between 75 and 80 c/s when the bearings were 24 in apart. The instability was independent of the rotor unbalance in the range of residual balances considered.

In both 20 and 24 in bearing centre configurations the establishment of full instability was preceded by a narrow range of speeds in which a 'quasi-stable' whirl was apparent, and in which the whirl centre coincided approximately with the line of centres of the steady running journal positions. At the upper end of this region a small increase in speed was followed by a large, rapid increase in the whirl amplitude.

When fully established the whirl amplitude was apparently governed by the full bearing clearances whilst its frequency was between 0.45 and 0.47 of the shaft's rotational frequency about its own axis.

Fig III.9 (a) shows the vertical acceleration response of the D.E. support for the 20 in bearing centre configuration as the rotational speed was increased. To obtain this type of plot the 'harmonic tracking' technique (Chapter 5, section 5.5 (ii))was used, the Quantech analyser centre frequency being maintained at 0.45 f_{rot}. By using a 10 c/s filter bandwidth the whirl frequency could vary from 0.4 to 0.5 of the rotational frequency and the corresponding response still be within the filter bandwidth throughout the speed range up to 100 c/s.

For the test shown in fig III.9 (a) the mean oil temperature was 40°C (artificially raised in this case by using an immersion heater in the oil header tank), the corresponding oil viscosity being approximately 80 cS. Under these conditions it may be seen that the full instability developed suddenly at a shaft frequency of 96.6 c/s

and persisted, on decreasing the shaft speed, down to approximately 82 c/s. (This hysteresis or 'inertia' effect has been reported by several investigators - see Chapter 2, section 2.4(ii) and, for example, Tondl (18), Morton (46)). In similar tests, as the mean oil temperature was decreased (increased viscosity, decreased bearing load numbers, decreased bearing eccentricities) the unstable speed was reduced so that at a mean oil temperature of 30°C (viscosity 140 cS) the full instability developed at a rotational frequency of 90 c/s and died out at 80 c/s when the shaft speed was reduced. The 'inertia' effect was therefore more pronounced the higher the speed at which full instability first occurred. However, the 'quasi-stable' region was extended with the higher unstable speeds.

Fig III.9 (b) shows the U.V.recordings of the rotor whirl amplitudes at a rotational speed of 96.6 c/s corresponding to the support response measurements of fig III.9 (a). The unstable whirl is seen to be such that each end of the rotor was in phase whilst the whirl frequency was 0.45 times the rotational frequency. Since the maximum instantaneous rotor whirl amplitudes, when viewed from the D.E.,occurred in the sequence 'left, up, right, down ' the rotation was clockwise and in the same direction as the shaft rotation (forward whirl). Also, since the whirl amplitudes in the horizontal and vertical planes were very nearly equal, each end of the rotor precessed in a circular path. The diameter of the whirl was 16.6×10^{-3} in. at the N.D.E. (Plane A) and 20×10^{-3} in. at the D.E. (Plane B).

In fig III.9 (a) the maximum support response was 0.185 g. r.m.s. at the whirl onset rotational frequency of 96.6 c/s. Since the measured vertical driving point impedance at the D.E. support (fig 6.10) at the whirl frequency of $0.45 \times 96.6 = 43.5$ c/s was 210 lb, the bearing force level was apparently $0.185 \times 210 = 39$ lbf. r.m.s.

An approximate, independent check may be made on the validity of this apparent force level from the measured rotor whirl amplitudes and the known system geometry. Referring to the sketch in fig III.10, the radius of the circular whirl at the rotor centre of gravity was calculated, from the known amplitudes at each end, to be 9.15×10^{-3} in.

The force required to constrain the rotor in this circular path would be approximately:-

$$F = Mr\omega^2 \qquad \text{(III.8)}$$

where M = rotor mass = 70 lb

r = whirl radius = 9.15×10^{-3} in.

ω = angular frequency of whirl.

Since $\omega = 2\pi(.45 \times 96.6)$ rad/s = 273.5 rad/s (III.9)

$$F = 70 \times (9.15 \times 10^{-3}) \times (273.5)^2 \ \frac{\text{lb.in}}{\text{s}^2} \quad \frac{\text{lbf. s}^2}{386 \text{ lb.in}} \qquad \text{(III.10)}$$

or F = 124 lbf.

So that from the geometry of the system the force F_2, at the D.E. support would be

$$F_2 = F \times \frac{8}{20} = 124 \times \frac{8}{20} = 49.5 \text{ lbf.}$$

$$\text{or } F_2 = \frac{49.5}{1.414} = 35 \text{ lbf r.m.s.} \qquad \text{(III.11)}$$

which, in view of the approximations made, is in reasonable agreement with the 39 lbf r.m.s. obtained above from the measured support impedance.

It is interesting to note that the decrease in acceleration response at the support shown in fig III.9 (a), was consistent with a constant amplitude rotor whirl whose frequency was decreasing - which behaviour

was observed from the measured rotor amplitudes. In this respect the dashed line in fig III.9 (a) shows the decrease in acceleration response, based on the measured support impedance, that would occur for a whirl of constant amplitude and frequency 0.45 f_{rot}. This is compared with the response for a constant support acceleration impedance.

It was stated above that the unstable whirl appeared to involve motion of the journals limited only by the bearing clearance. This may be deduced approximately from the apparent force at the D.E. support, the rotor amplitudes and the system geometry. Thus, referring to fig III.10 it is known from the tests of Chapter 6 section 6.3, that the stiffness of the D.E. half shaft was $k_2 = 1.419 \times 10^4$ lbf/in. If the support motion is neglected and it is assumed that the D.E. journal was executing circular whirl of radius r_{j_2}, in phase with the rotor, then the deflection, σ, of the D.E. half-shaft relative to the rotor would be, from the measured rotor amplitudes:-

$$\sigma = \left\{(10 + 1.7) \times 10^{-3} - r_{j2}\right\} \text{ in.pk} \qquad \text{(III.12)}$$

So that the force on the D.E. half-shaft at the bearing centre line required to restrain the shaft in this motion would be $k_2\,\sigma$.

Based on the observed apparent force (F_2 = 39 lbf r.m.s.) at the support, σ may be obtained from:-

$$F_2 = k_2 \cdot \sigma \qquad \text{(III.13)}$$

$$\text{or } \sigma = \frac{F_2}{k_2} \qquad \text{(III.14)}$$

$$\text{whence } \sigma = \frac{39}{1.419 \times 10^4} \quad \frac{\text{lbf. r.m.s. in.}}{\text{lbf}}$$

$$\text{or } \sigma = 2.75 \times 10^{-3} \text{ in. r.m.s.}$$

$$\text{or } \sigma = 3.88 \times 10^{-3} \text{ in. pk} \qquad \text{(III.15)}$$

Substituting for S from eqn. (III.12)

$$r_{j_2} \simeq (11.7 - 3.88) \times 10^{-3} \text{ in.pk}$$

or journal whirl radius $r_{j_2} \simeq 7.81 \times 10^{-3}$ in pk

which is close to the design radial clearance of 7.5×10^{-3} in. Had the support motion (1.4×10^{-3} in pk) been included in the above calculations the journal amplitude would have been 6.4×10^{-3} in or about 85% of the design clearance.

III.4 (ii) Theoretical Estimation of the Boundary of Journal Bearing Instability.

Although it was highly probable, in view of the plain circular bearing design used, that a rotor speed existed at which unstable oil whirl would occur, the low rotational speed at which it appeared in practice (less than 50% above the fundamental flexibly-supported critical frequencies) warranted some further investigation.

Various methods have been suggested in the literature for estimating the boundary of unstable operation. Some authors, like Morrison (43), adopt a classical approach to investigate the nature of the roots of the characteristic equation of the system whilst others, like Morton (46), have considered speeds at which the effective bearing oil-film impedance changes from a complex quantity and positive (dissipative) damping to a real quantity (undamped) and subsequently to the negative damping condition (see also Chapter 2, section 2.4(ii)).

In this section an approximate method is outlined which makes use of the same digital computer programme that was developed to obtain the responses of the system to its own unbalance (Chapter 4, section 4.3(vi)).

Recalling the method used in that programme, the linear dynamic coefficients of the journal bearings - kxx_1, kxy_1 ..... kxx_2, kxy_2 ..... bxx_1, bxy_1 ..... bxx_2, bxy_2 ..... - were obtained for each shaft speed based on certain assumptions due to Morrison. The system matrix equation (4.80) were then solved for the unbalance excitation $mr\Omega^2$, Ω being the angular velocity of the shaft.

To estimate the shaft speed at which unstable whirl will occur, use is made of two known characteristics of the phenomenon:-

(i) the whirl was in the same direction as the shaft's rotation about its own axis (i.e. forward), and was therefore presumed to be readily excited by external forcing rotating in that direction.

(ii) the frequency of the whirl was close to half the shaft's rotational frequency.

In the computer calculation, therefore, the bearing coefficients were first derived for a particular rotational speed and the system equations were then solved to obtain the responses to a force vector rotating at some fraction, η, of the shaft speed. Due to the existing layout of the programme it was convenient to assume the force to be of the form

$$F = m\,r\,(\eta\,\Omega)^2 \qquad \text{(III.16)}$$

i.e. an 'unbalance' type of force equivalent to a small mass in rotating at angular frequency $\eta\,\Omega$ at radius r, large compared with the resulting whirl radius. The calculated responses therefore showed the susceptibility of the complete system (bearings, supports, rotor and shaft) to whirl at the assumed frequency $\eta\,\Omega$.

In the computations performed on the S.R.C. Atlas computer to date the bearing support impedances (Zxx_1, Zyy_1, Zxx_2, Zyy_2) used have been the approximate undamped, single degree-of-freedom values based on the

original measurements made with the ball bearings in housings (Chapter 6, section 6.4).

Fig III.11 shows the results obtained for the 20 in bearing centre configuration, experimental results for which were discussed in section III.4 (i) above. It may be seen from fig III.11 that for the assumed oil condition (viscosity = 140 cS) the system was theoretically most responsive to excitation at values of η between 0.525 and 0.475, the maxima occurring in the region of a shaft frequency of 75 c/s. This may be compared with the frequency of 90 c/s at which full instability developed under similar experimental conditions. The peak theoretical response to excitation at η = 0.45 however, (the frequency of the whirl observed in practice) was closer to the observed unstable speed.

Similar results were obtained for the 24 in bearing centre configuration, the calculated maximum response occurring at a shaft speed of 70 c/s (η = 0.525 - 0.475), the observed instability in practice being at 79.5 c/s for similar oil conditions.

It is thought that the reduced resistance to fractional shaft speed excitation predicted theoretically may be due in part to the assumption of undamped (real) support impedances used in the calculations. The positive damping provided by the bearing supports in practice may serve to enhance stability. It is intended, in the near future, to include the measured complex driving point support impedances in a similar series of computations.

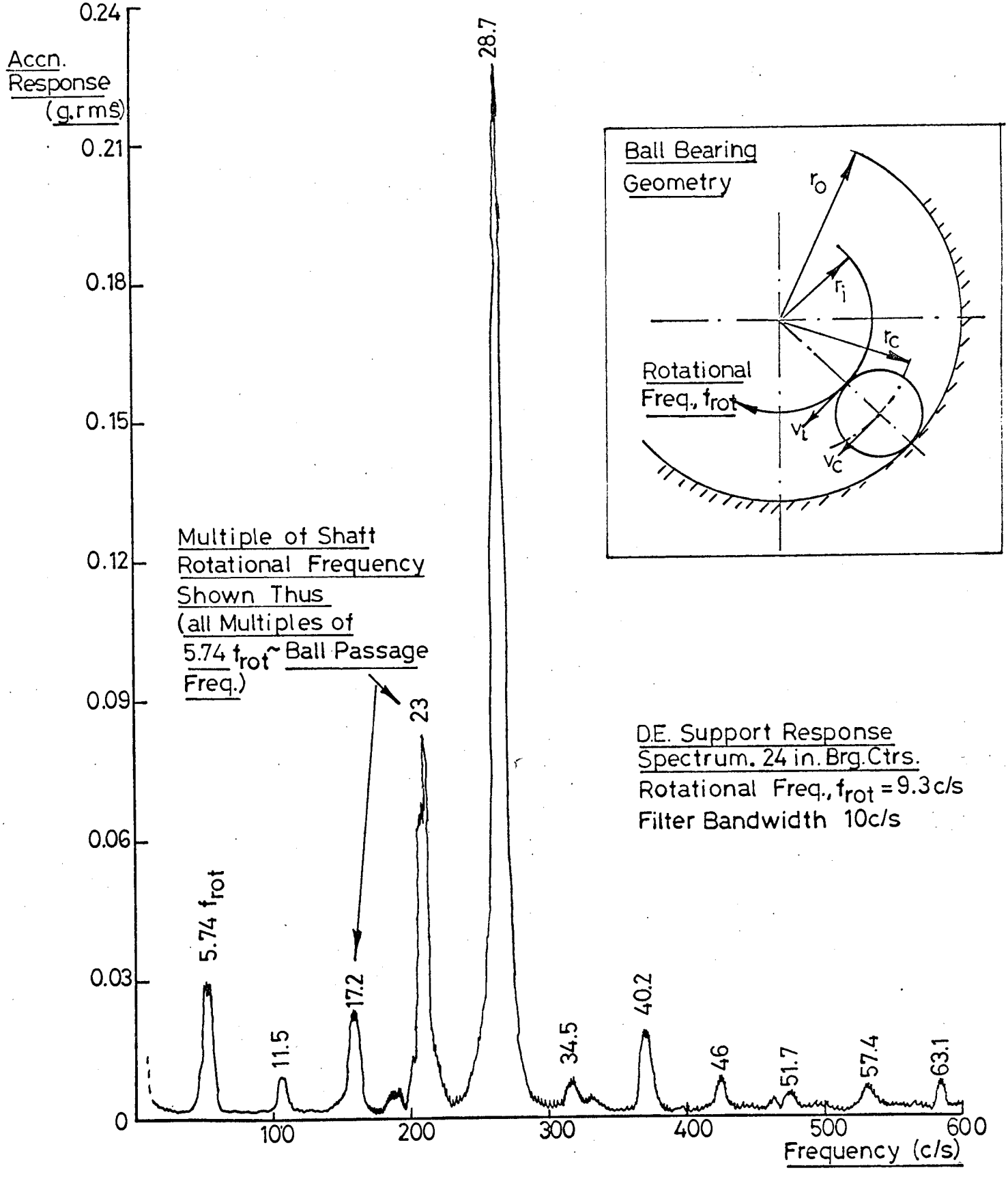

FIG. III.1. LINE SPECTRUM OF D.E. SUPPORT VIBRATION. MODEL RIG 24" BRG. CENTRES. BALL BEARINGS.

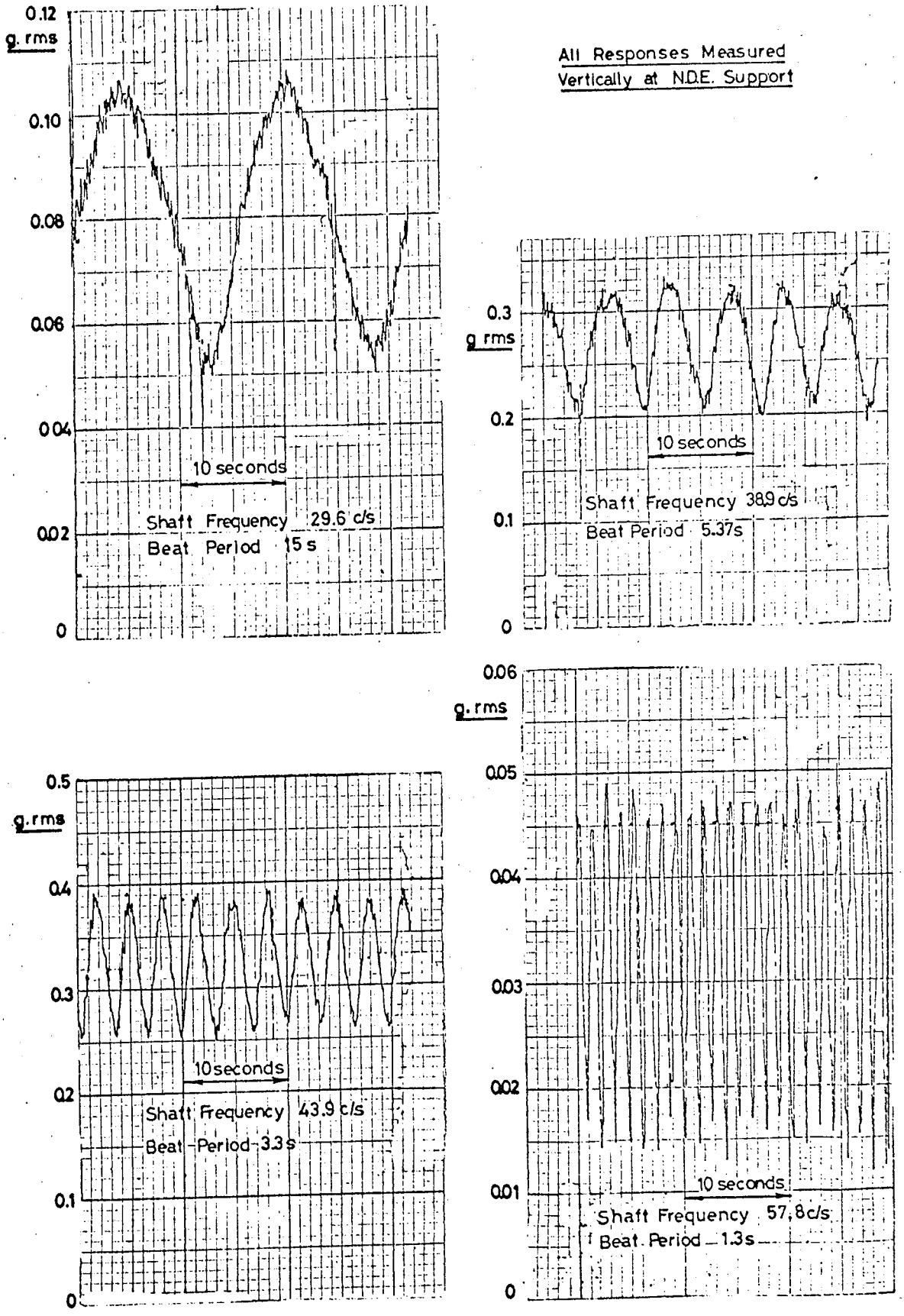

FIG. III. 2. BEATING OF BEARING DISTURBANCE AT 5.74 x SHAFT FREQUENCY. MODEL RIG 24" CRS IN BALL BEARINGS

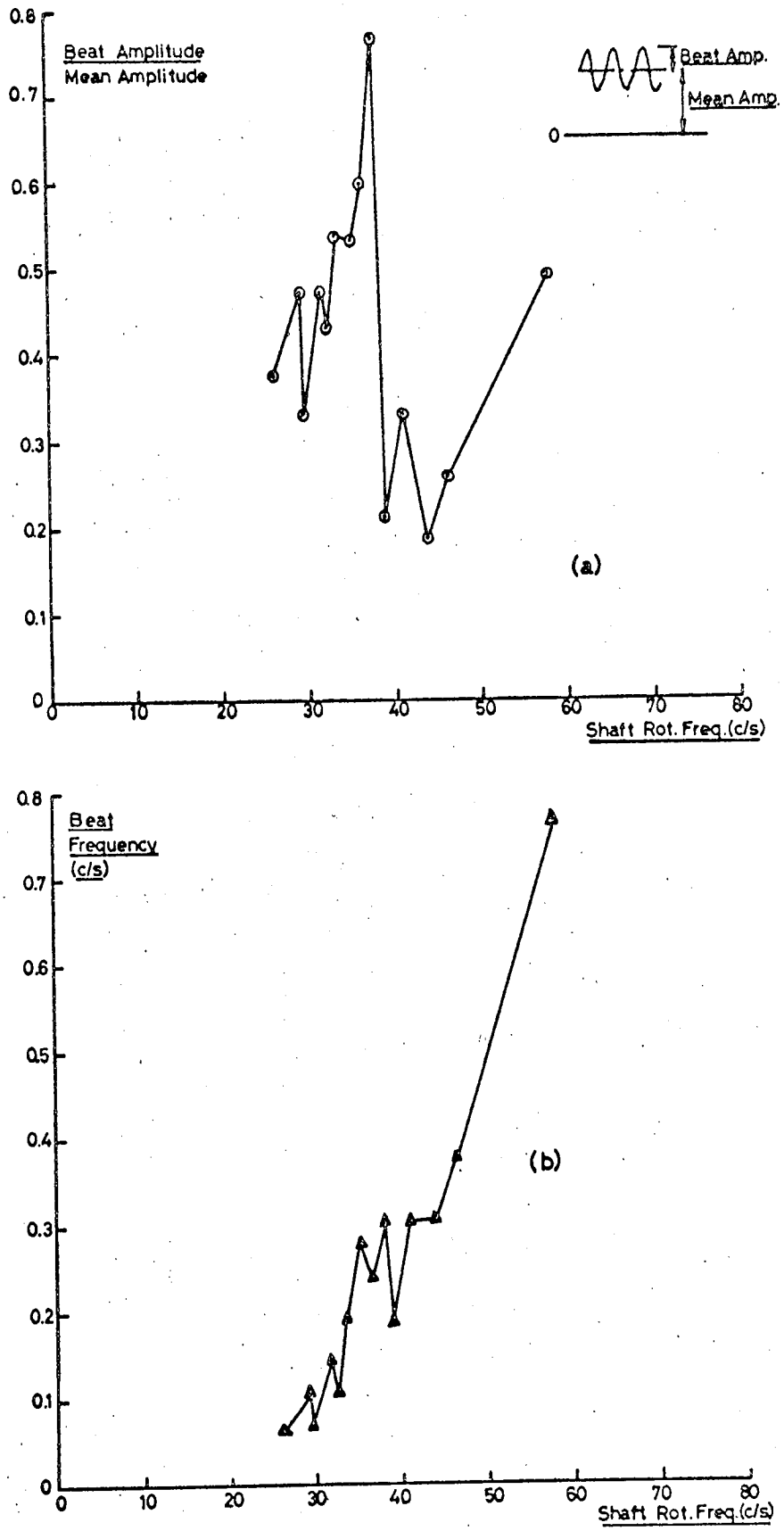

FIG. III.3. AMPLITUDE AND FREQUENCY CHARACTERISTICS OF BEATS. BEARING DISTURBANCE AT 5.74 x SHAFT FREQUENCY. MODEL RIG 24" BRG. CTRS.

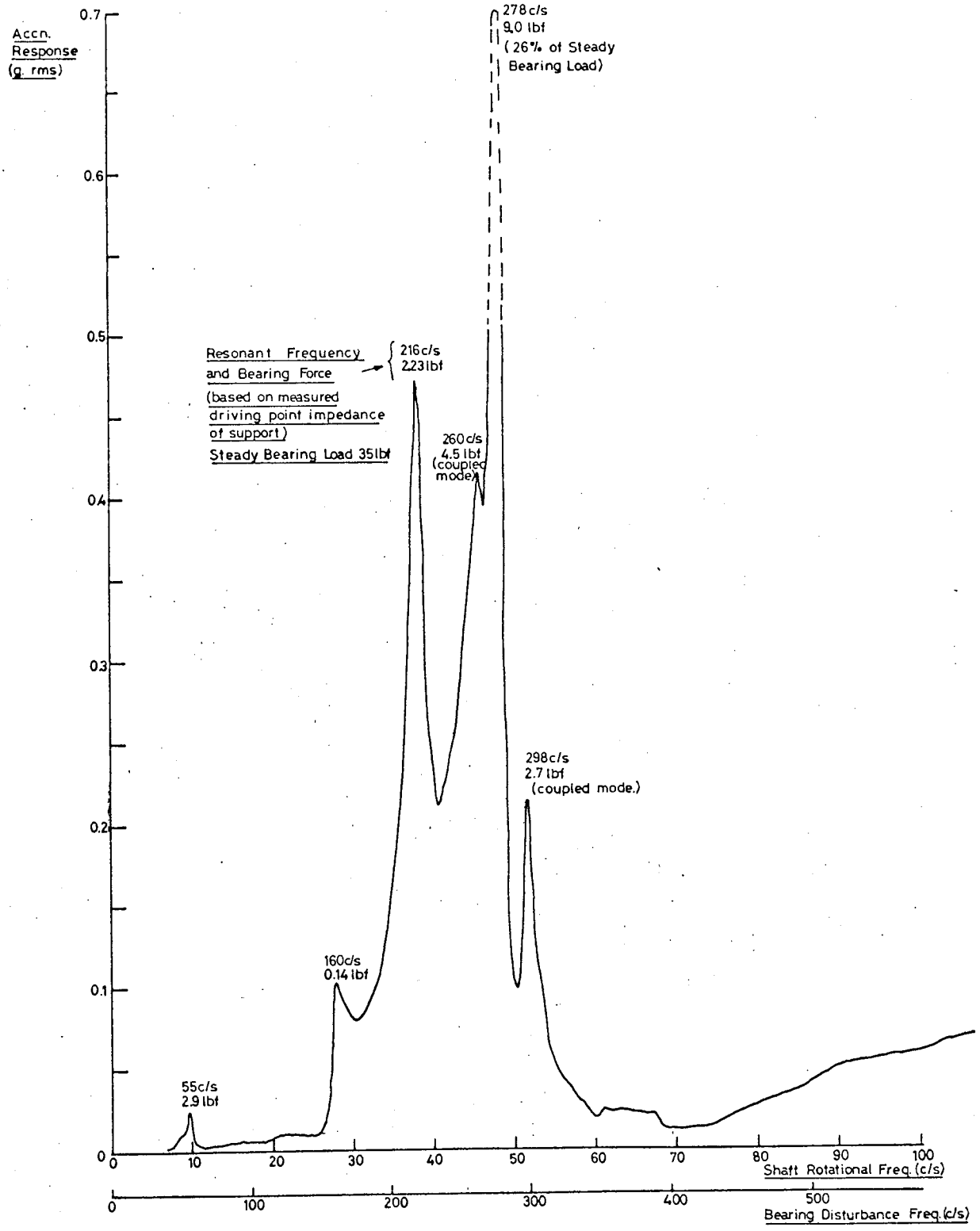

FIG. III. 4 VERTICAL RESPONSE AT D.E. SUPPORT TO 5.74 x SHAFT FREQUENCY BEARING DISTURBANCE. MODEL RIG 24" BRG. CRS

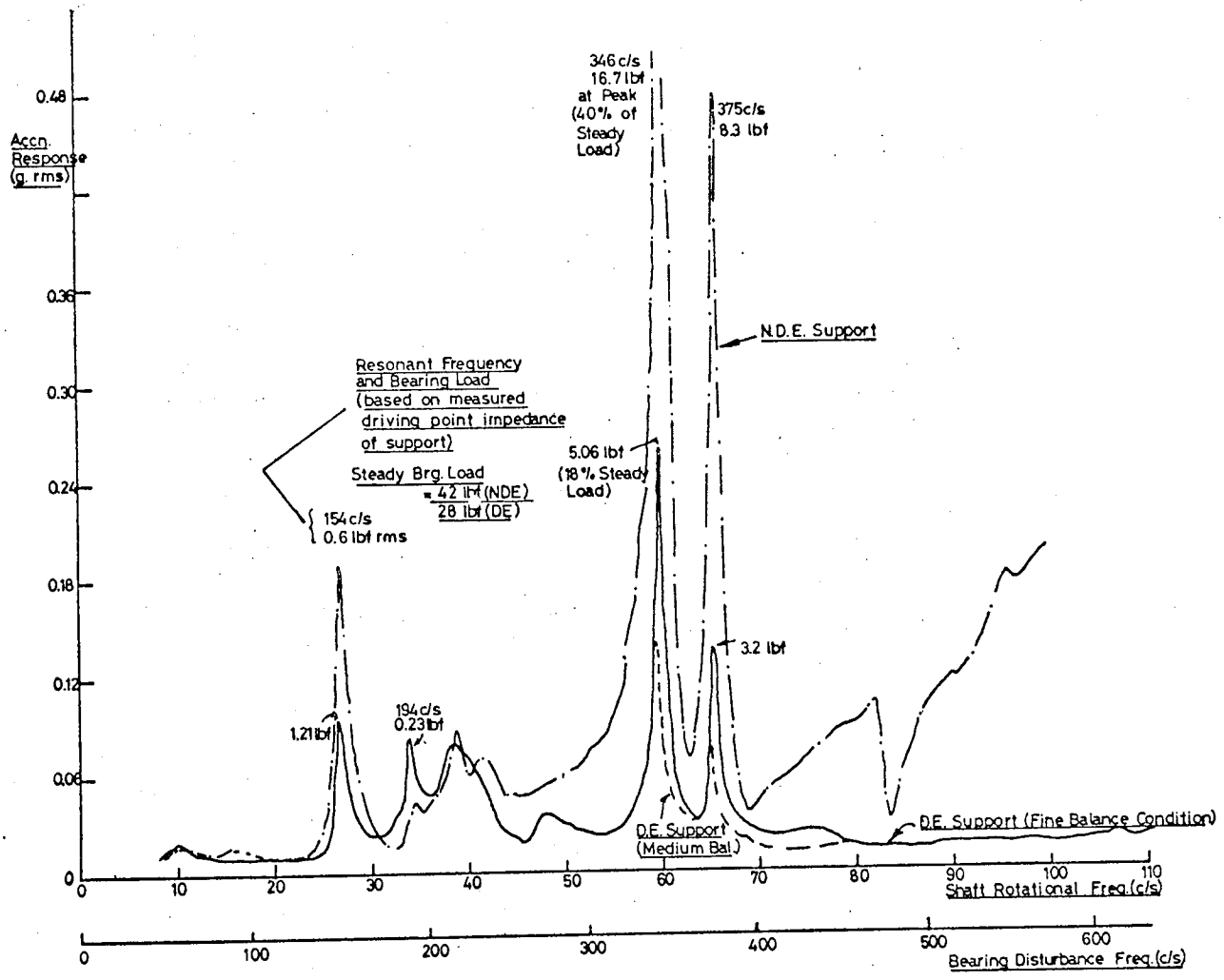

FIG. III.5. VERTICAL RESPONSE AT D.E. & N.D.E. SUPPORTS TO 5.74" SHAFT FREQUENCY BEARING DISTURBANCE. MODEL RIG 20" BRG. CRS.

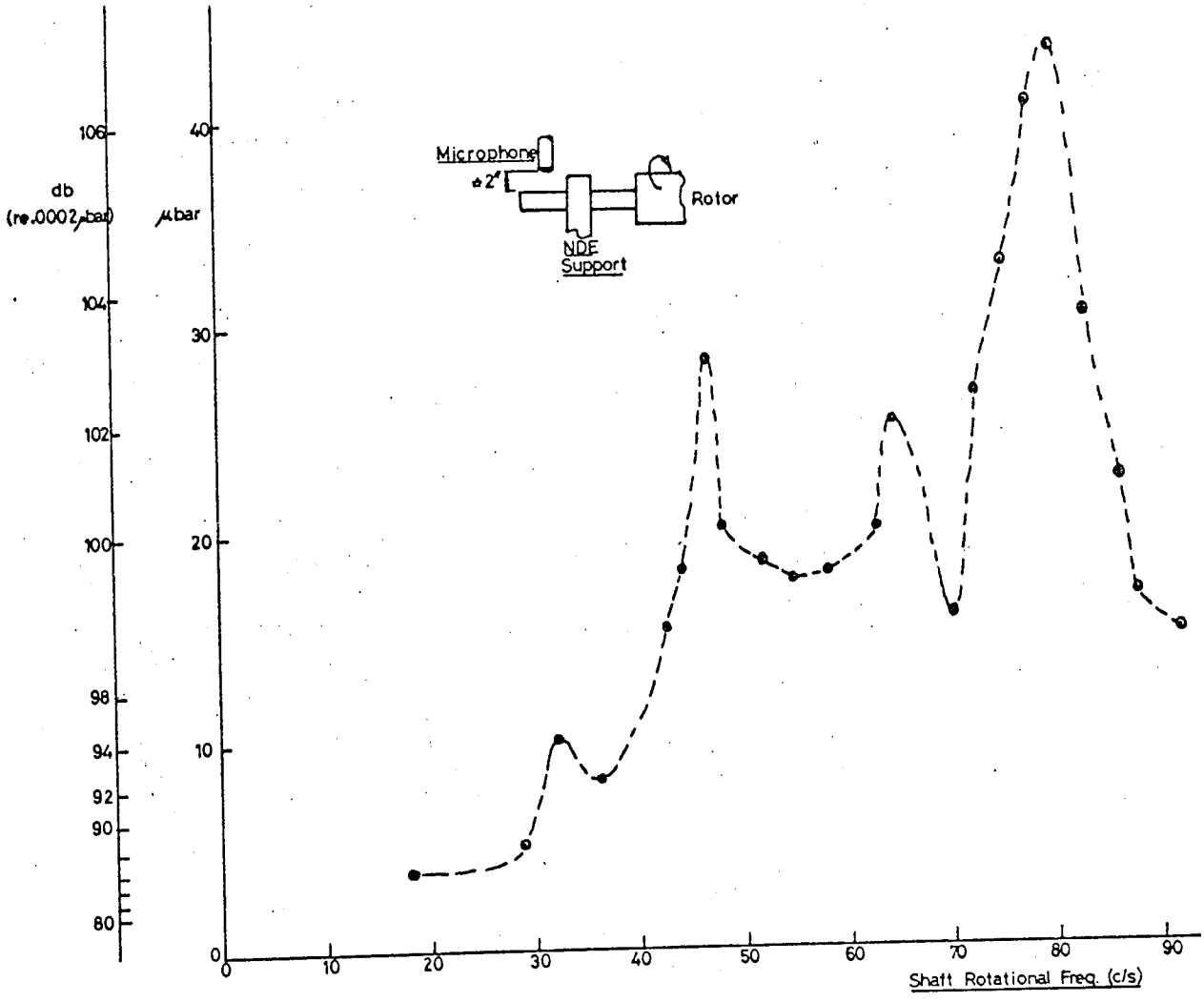

FIG. III.6. OVERALL NEAR-FIELD NOISE LEVEL. MODEL RIG 20" BRG. CRS. BALL BEARINGS

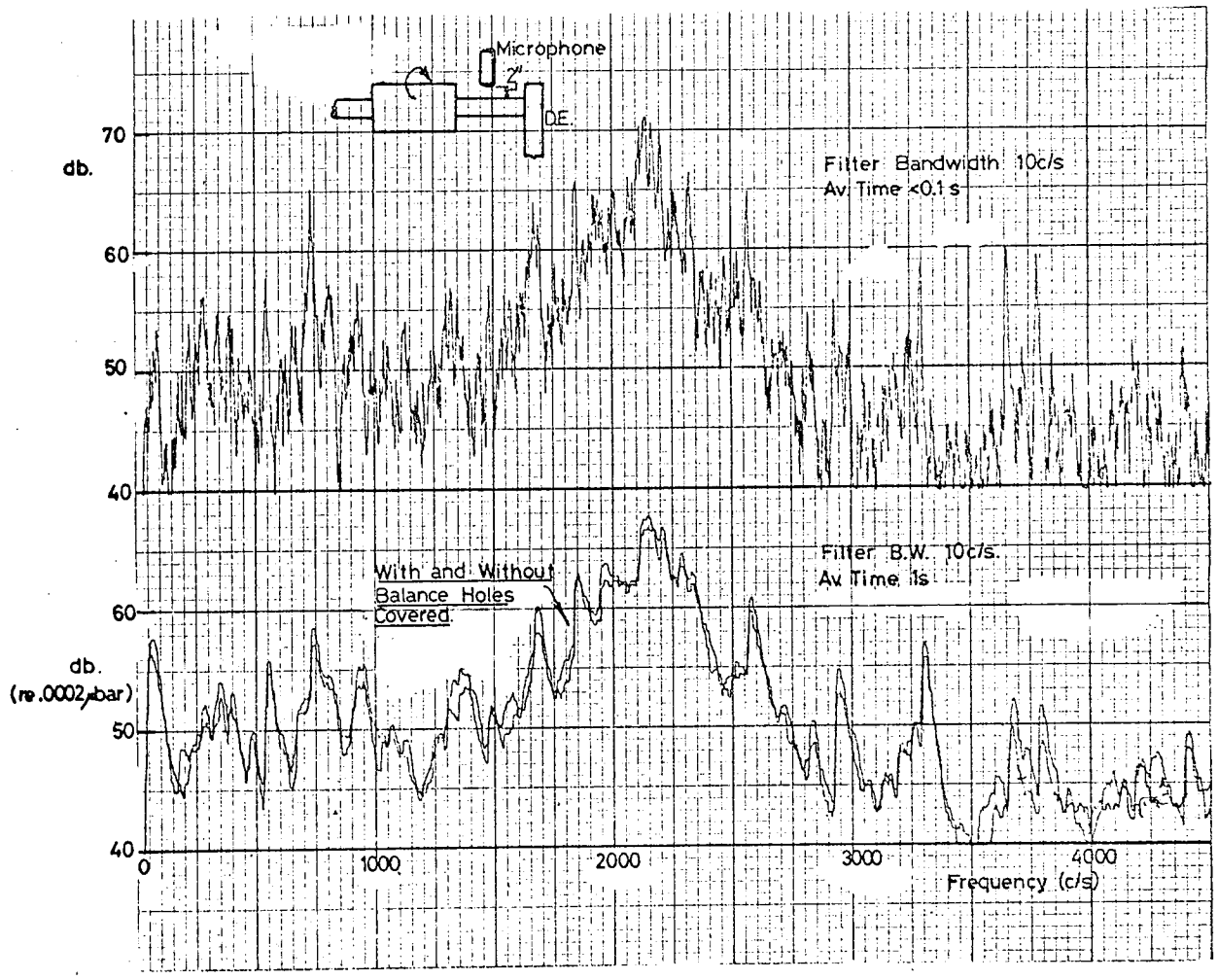

FIG. III. 7. SPECTRUM OF NOISE CLOSE TO D.E. HALF SHAFT AT SHAFT ROTATIONAL FREQUENCY OF 63.8 c/s. MODEL RIG 20" BRG CRS

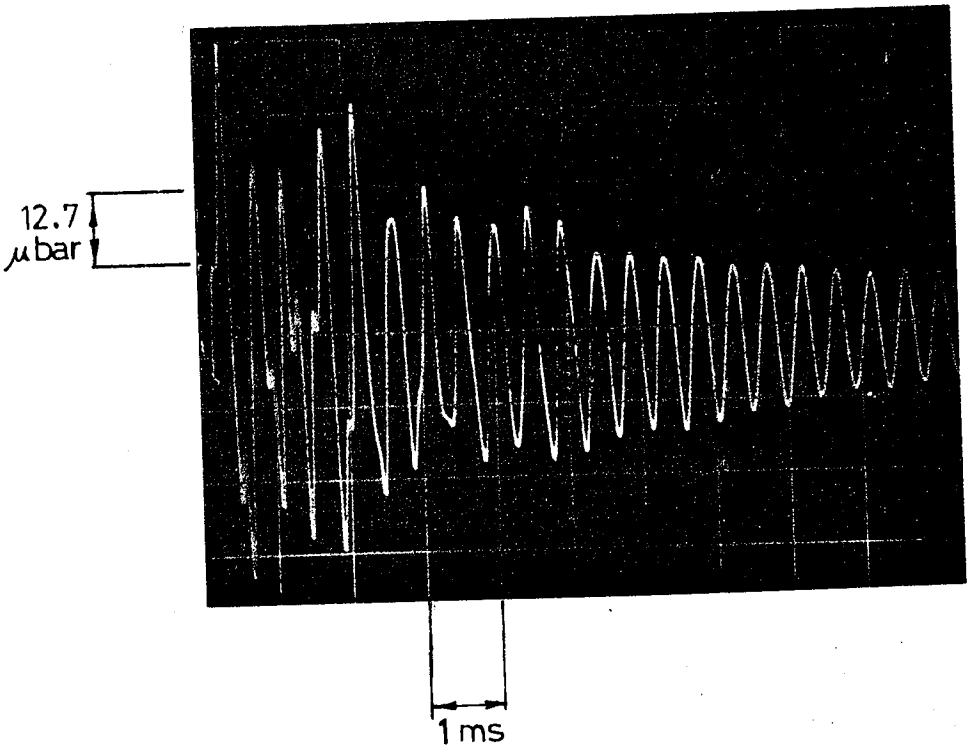

(a)

Mic. close to
D.E. Half-Shaft

Predominant
Freq. ≐ 2100 c/s

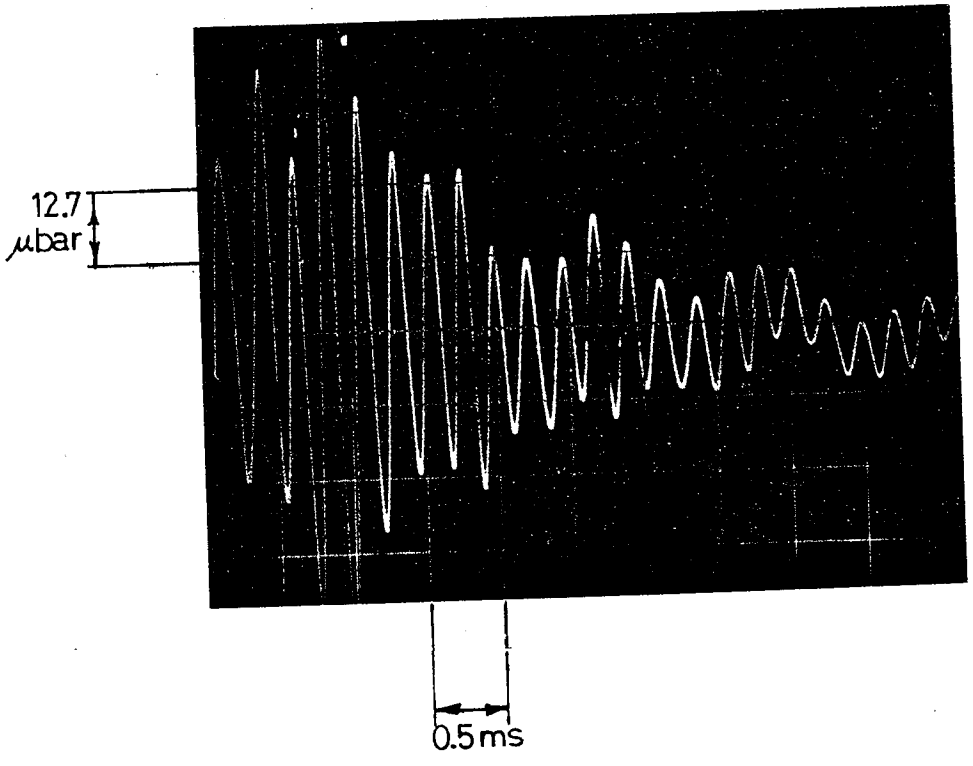

(b)

Mic. close to
N.D.E. Half-Shaft

Predominant
Freq. ≐ 4400 c/s

FIG. III.8. ACOUSTIC RESPONSE OF SHAFT TO TRANSIENT MECHANICAL EXCITATION. MODEL RIG 20" BRG. CRS.

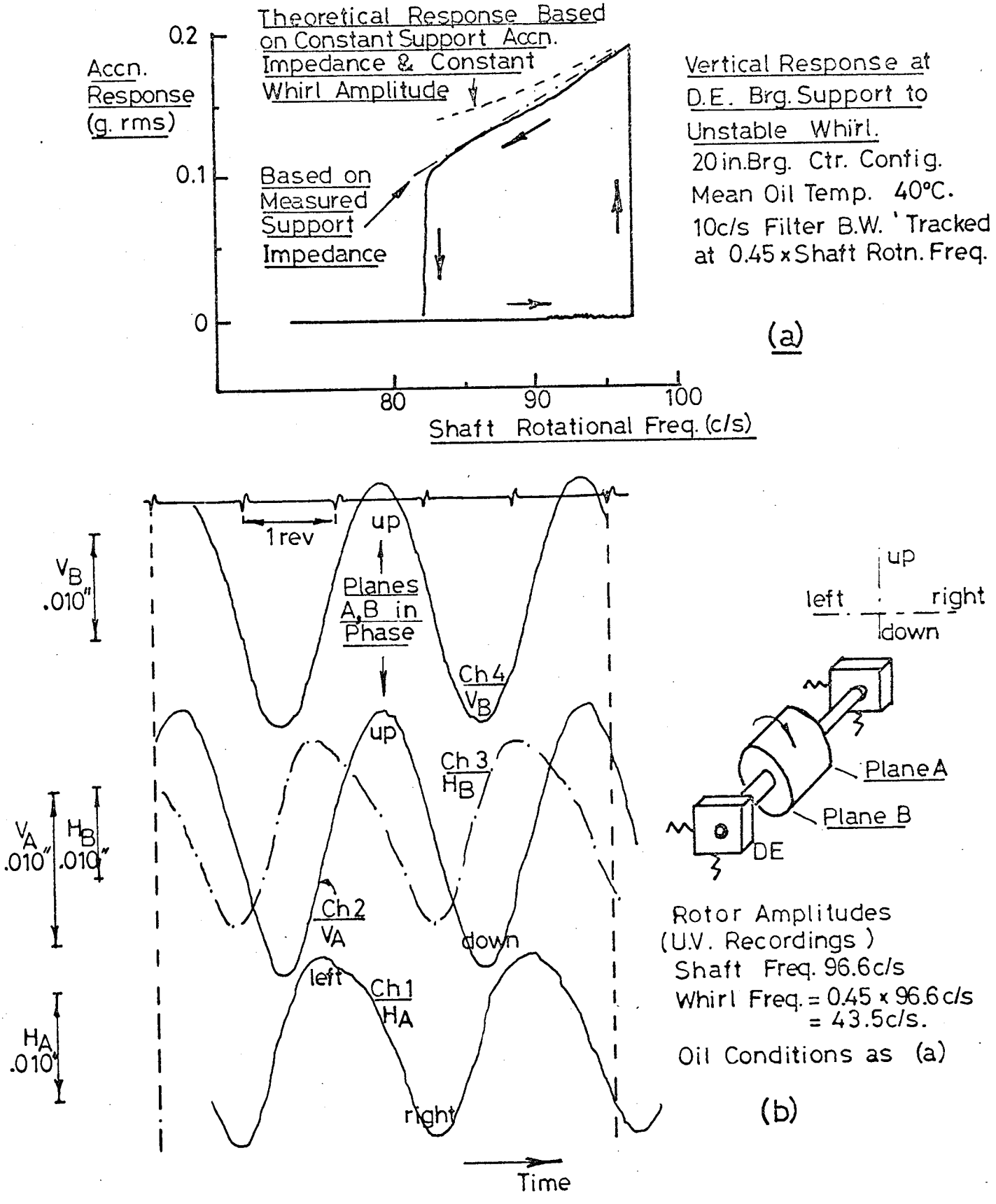

FIG. III.9. JOURNAL BEARING UNSTABLE WHIRL. MODEL RIG.

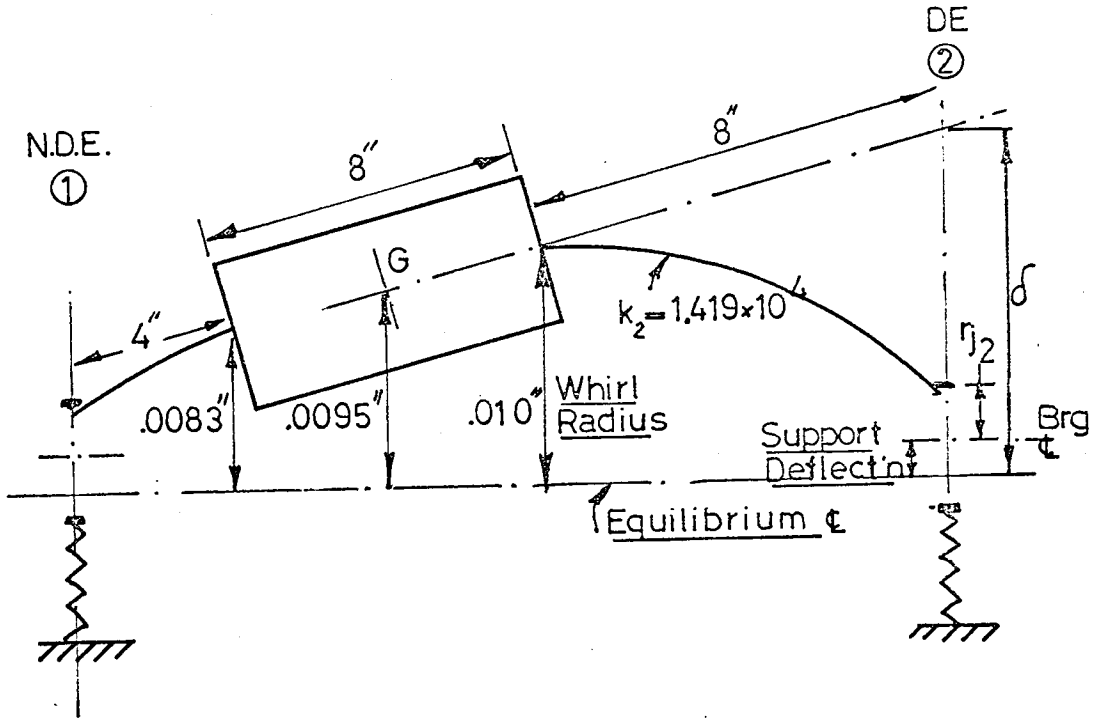

FIG. III.10 APPROXIMATE GEOMETRY OF WHIRLING SHAFT. MODEL RIG 20″ BRG. CRS.

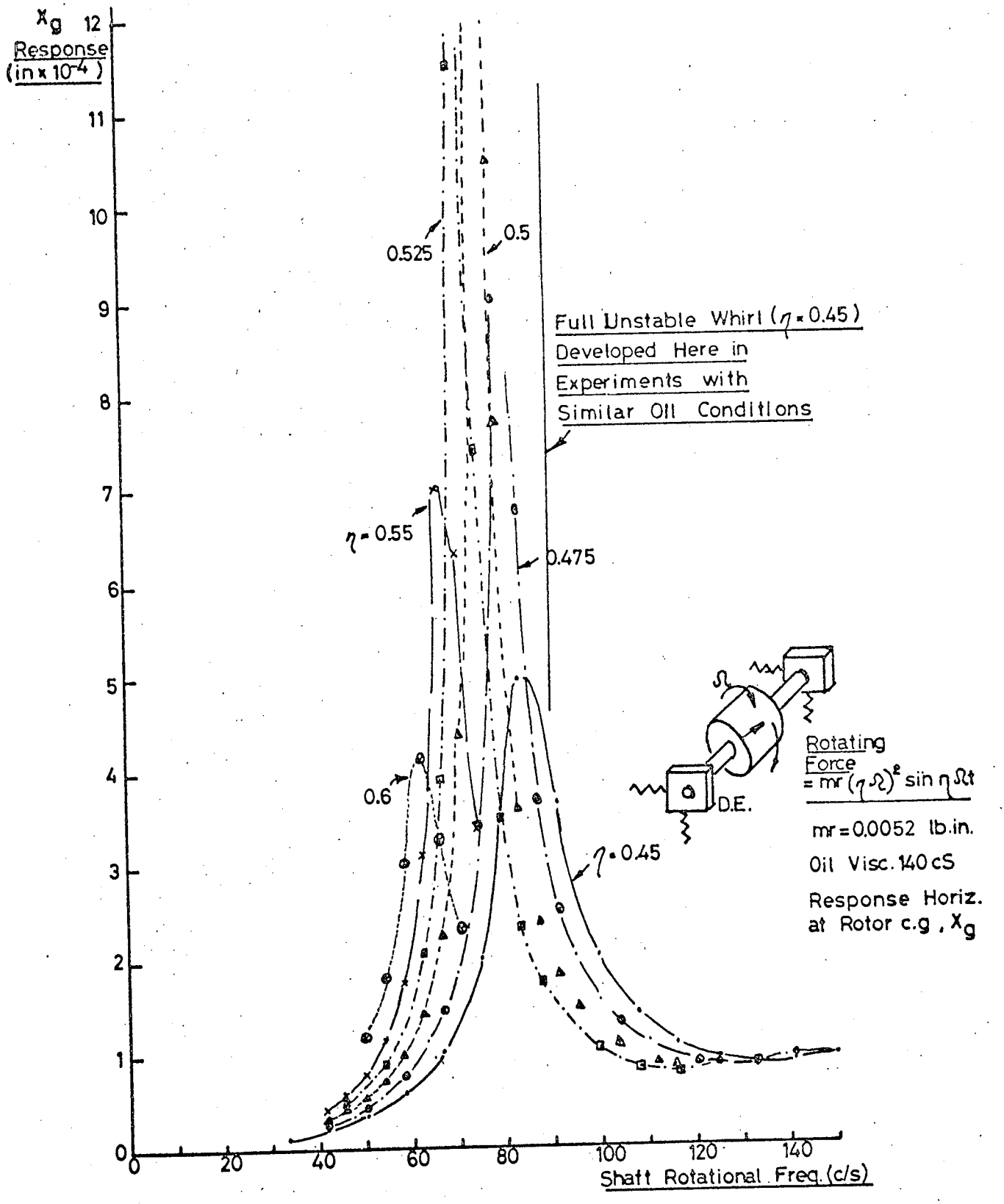

FIG. III.11 THEORETICAL RESPONSE OF MODEL SYSTEM TO ROTATING FORCE AT FRACTION, η, OF SHAFT FREQUENCY. 20° BRG. CTR. CONFIGURATION.

APPENDIX IV - Coupling between Planes at Bearing Supports

In the discussion given in the preceeding chapters of the experimental impedance measurements made at bearing supports, reference has been made to evidence of coupling between the planes of measurement. In this appendix the behaviour of a simple analytic model is considered to illustrate the nature of impedances measured under conditions where the principal planes of the structure differ from those in which exciting forces act and responses are measured.

The upper diagram of fig IV.1(a) shows a bearing support in which the convenient planes of measurement (horizontal, X, and vertical Y) differ from the principal planes 1 and 2. For simplicity, the planes of measurement X, Y and the principal planes 1, 2 are assumed to intersect at a single point (displacement coupling only) whilst the uncoupled behaviour in the principal planes may be represented by a single degree-of-freedom, viscously damped system.

Referring to fig IV.1(b) the acceleration impedances Z_1 and Z_2 in the principal planes are therefore:-

$$Z_1 = -\frac{k_1}{\omega^2} + m\omega^2 - \frac{j\, b_1}{\omega} \qquad \text{(IV.1)}$$

$$Z_2 = -\frac{k_2}{\omega^2} + m\omega^2 - \frac{j\, b_2}{\omega} \qquad \text{(IV.2)}$$

where ω = angular excitation frequency (rad/s)

When excited by the harmonic force F, in plane X, the acceleration responses $\ddot{x}_1$, $\ddot{x}_2$ in the principal planes are:-

$$\ddot{x}_1 = \frac{F_1}{Z_1} = -\frac{F\cos\theta}{Z_1} \qquad \text{(IV.3)}$$

$$\ddot{x}_2 = \frac{F_2}{Z_2} = \frac{F\sin\theta}{Z_2} \qquad \text{(IV.4)}$$

where F_1, F_2 are the components of the excitation in the principal planes and θ is the angle included between the plane of measurement X and the

The acceleration response in plane X is therefore $\ddot{x}_x$ where:-

$$\ddot{x}_x = -\ddot{x}_1 \cos\theta + \ddot{x}_2 \sin\theta \qquad \text{(IV.5)}$$

Substituting for $\ddot{x}_1$ and $\ddot{x}_2$ from equations (IV.3) and (IV.4)

$$\ddot{x}_x = \frac{F \cos^2\theta}{Z_1} + \frac{F \sin^2\theta}{Z_2} \qquad \text{(IV.6)}$$

The driving point impedance Zx in plane X is therefore

$$Zx = \frac{F}{\ddot{x}_x} = \frac{Z_1 Z_2}{Z_2 \cos^2\theta + Z_1 \sin^2\theta} \qquad \text{(IV.7)}$$

Since Z_1 and Z_2 are complex, Z_x is also complex and equation (IV.7) is of the form:-

$$Z_x = \frac{(A - jc)(B + jD)}{B^2 + D^2} \qquad \text{(IV.8)}$$

where

$$A = \left\{\left(-\frac{k_1}{\omega^2} + m\right)\left(-\frac{k_2}{\omega^2} + m\right) - \frac{b_1 b_2}{\omega^2}\right\} \qquad \text{(IV.9)}$$

$$B = \left\{\left(-\frac{k_1}{\omega^2} + m\right)\sin^2\theta + \left(-\frac{k_2}{\omega^2} + m\right)\cos^2\theta\right\} \qquad \text{(IV.10)}$$

$$C = \left\{\left(-\frac{k_2}{\omega^2} + m\right)\frac{b_1}{\omega} + \left(-\frac{k_1}{\omega^2} + m\right)\frac{b_2}{\omega}\right\} \qquad \text{(IV.11)}$$

$$D = \left\{\frac{b_2}{\omega}\cos^2\theta + \frac{b_1}{\omega}\sin^2\theta\right\} \qquad \text{(IV.12)}$$

So that the real and imaginary parts of Zx are:-

$$\text{Re}\,(Zx) = \frac{AB + CD}{B^2 + D^2} \qquad \text{(IV.13)}$$

$$\text{IM}\,(Zx) = \frac{AD - CB}{B^2 + D^2} \qquad \text{(IV.14)}$$

The modulus and argument of Zx have been calculated according to

$$Zx = \sqrt{Re\,(Zx)^2 + Im\,(Zx)^2} \qquad \text{(IV.15)}$$

$$\theta = \tan^{-1}\left\{\frac{Im(Zx)}{Re(ZX)}\right\} \qquad \text{(IV.16)}$$

for the case m = 1, k_1 = 1, k_2 = 16, b_1 = 0.2, b_2 = 0.8

(i.e. $\omega_{n_1} = 1.0, \omega_{n_2} = 4.0$)

The results of these calculations are shown in fig IV.2 for various angles of inclination θ. For $\theta = 90^\circ$ the planes of measurement are uncoupled and Zx = Z_2. As θ is reduced the coupling increases and the resonant minimum around $\omega = \omega_{n_i} = 1$ becomes more significant. The separation between the antiresonance and the coupled resonance at = 1 increases with the amount of coupling between planes X and Y.

This behaviour may be compared with the measurement on the bearing supports of the rotating machine model where the axial, horizontal and vertical planes exhibited some degree of coupling (figs 6.9, 6.10, for example).

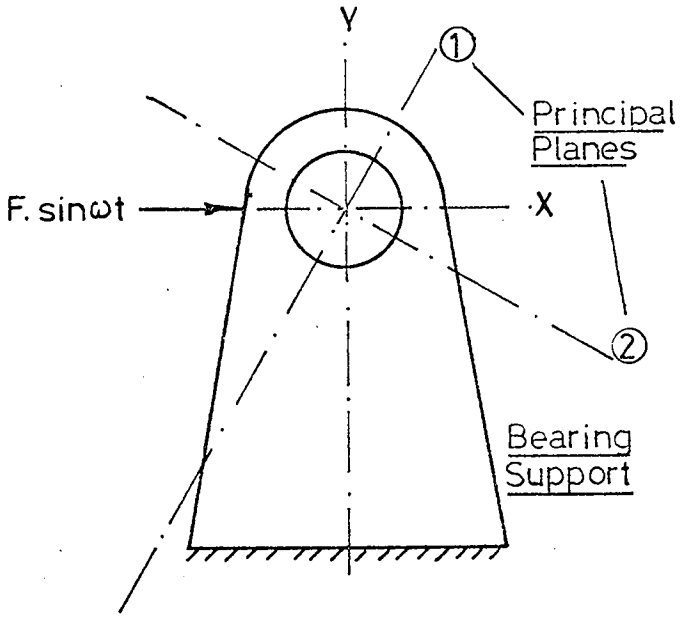

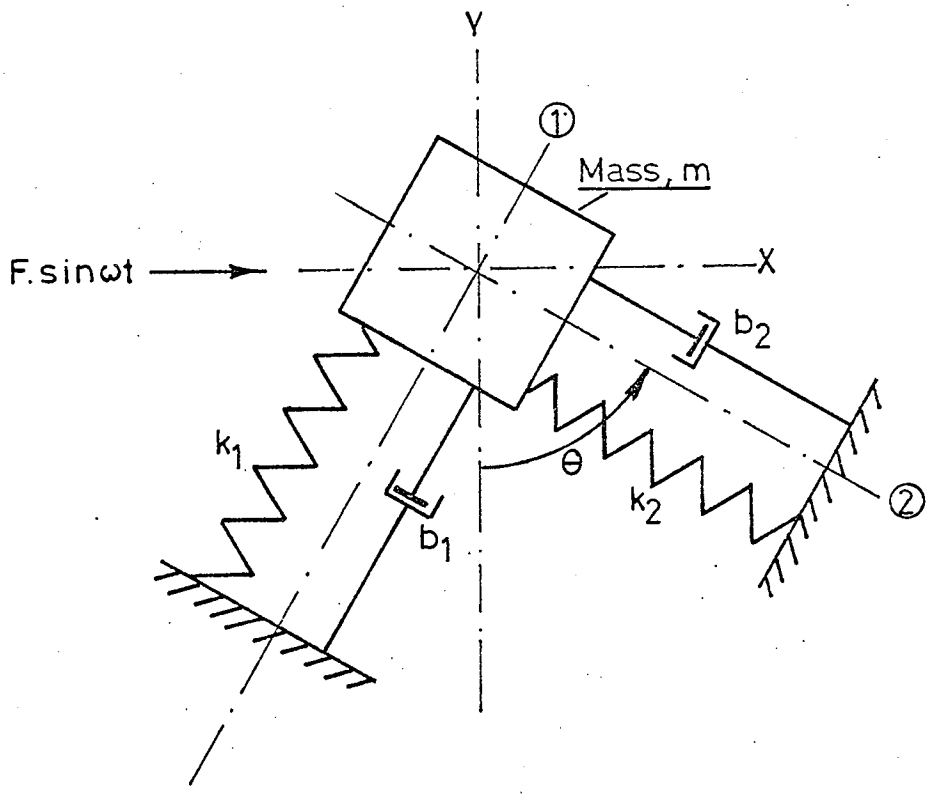

FIG. IV.1 SIMPLIFIED MODEL TO ILLUSTRATE COUPLING BETWEEN PLANES X, Y OF BEARING SUPPORT.

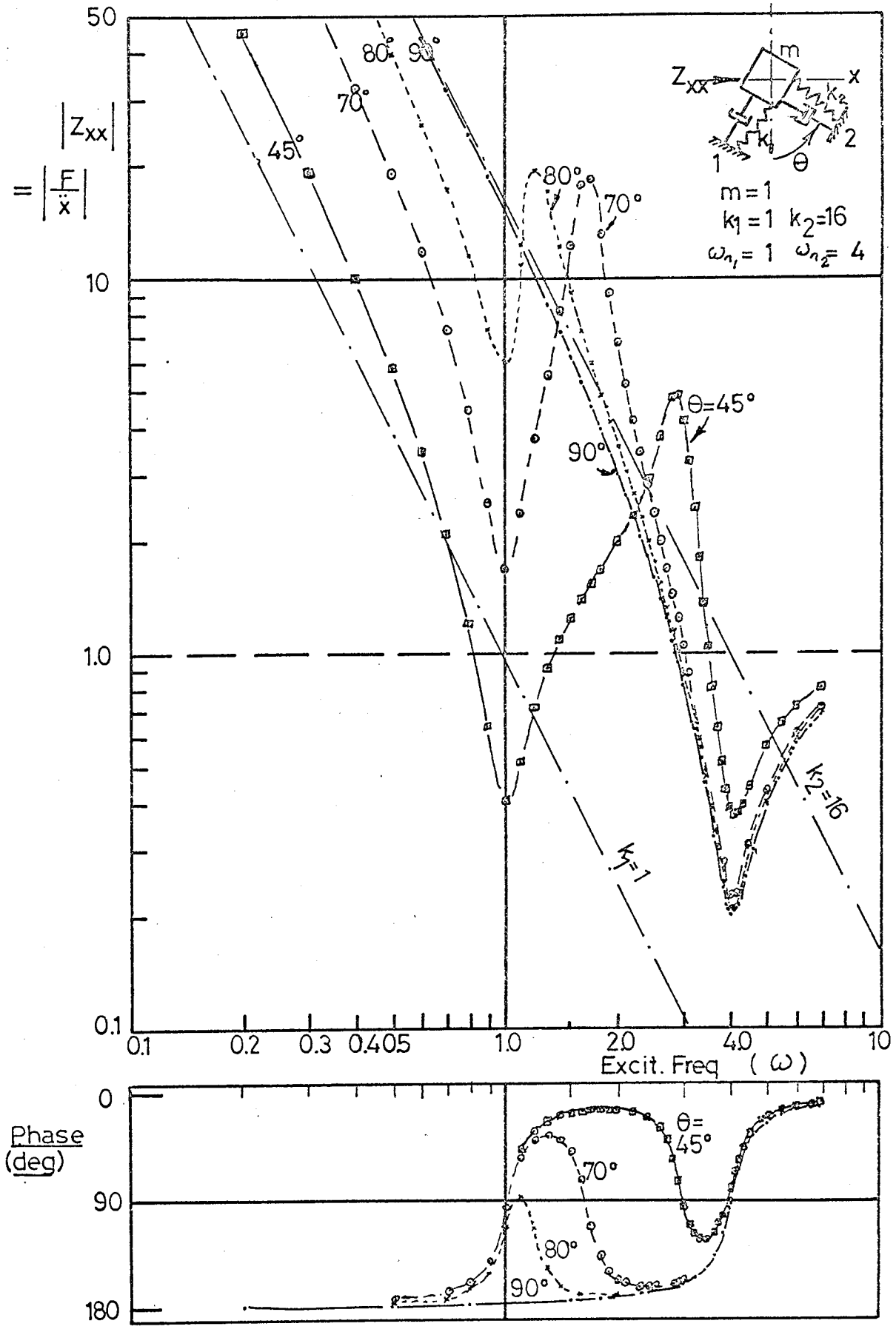

FIG. IV. 2. EFFECT OF INCLINATION, θ, OF PRINCIPAL PLANES ON DRIVING POINT IMPEDANCE Z_{xx}

APPENDIX V

Details of Centrifugal Compressors Discussed in Chapter 10.

Compressor	K 107	K 105
Plant	Ethylene II	Ethylene II
Number of Casings	1	1
Lineout Arrangement	Induction Motor/ G'box/Compressor	Induction Motor/ G'box Compressor
Motor Normal Speed (r.p.m.)	1482	1482
Motor Rotn. Freq. (c/s)	24.7	24.7
Compressor Speed (r.p.m.)	10,400	10,800
Rotn.Freq.,f_r (c/s)	173.3	180
Power Required (H.P.) (design conditions)	2300	2000
Casing Mass, m_c (lb)	8,900	11,350
Shaft Mass, m_s (lb)	400	670
Ratio m_s/m_c	.045	.059
1st Flex.Crit.Compressor (r.p.m.)	5250	5260
" " " " fc_1 (c/s)	87.5	87.7
2nd Flex.Crit.Compressor (r.p.m.)	Not known	18,470
" " " " fc_2 (c/s)	-	307.8
Ratio fr/fc_1	1.98	2.06
Ratio fc_2/fc_1	-	3.51

Compressor	K 101	
Plant	Ethylene	
Number of Casings	2 (H.P. & L.P.)	
Lineout arrangement	Induction Motor/G'box/ L.P.Casing/H.P.Casing	
Motor Normal Speed (r.p.m.)	1480	
Rotn. Freq. (c/s)	24.7	
	L.P.Casing	H.P.Casing
Compressor Speed (r.p.m.)	7575	7575
Rotn.Freq. f_r (c/s)	126.25	126.25
Power Required (H.P.	2200-2800	1900-2200
(design conditions)	(Total 5000 Max.)	
Casing Mass, m_c (lb)	16,950	9,600
Shaft Mass, m_s)lb)	950	500
Ratio m_s/m_c	.056	.052
1st.Flex.Crit.Compressor (r.p.m.)	5200	6500
" " " "fc_1 (c/s)	86.7	108.3
2nd.Flex.Crit.Compressor (r.p.m.)	Not known	Not known
" " " " fc_2 (c/s)	-	-
Ratio fr/fc_1	1.46	1.17
Ratio fc_2/fc_1	-	-

Compressor	K3	K2
Plant	Ethylene III	Ethylene III
Number of Casings	1	1
Lineout arrangement	Steam Turbine/ Compressor	Steam turbine/ Compressor
Turbine Normal Speed (r.p.m.)	13,370	5,620
Rotn. Freq. (c/s)	22.8	93.8
Compressor Speed (r.p.m.)	13,370	5,620
Rotn.Freq.f_r (c/s)	22.8	93.8
Power Required (H.P. (design conditions)	2215	8380
Casing Mass, m_c (lb)	10,000 approx.	16,350
Shaft Mass, m_s (lb)	750	2540
Ratio m_s/m_c	.075	.155
1st.Flex.Crit.Compressor (r.p.m.)	5,900	2,165
" " " " fc_1 (c/s)	98.33	36.2
2nd.Flex.Crit.Compressor (r.p.m.)	22,000	9.030
" " " " fc_2 (c/s)	366.7	151
Ratio fr/fc	2.26	2.59
Ratio fc_2/fc_1	3.73	4.16

Compressor	K1	
Plant	Ethylene III	
Number of Casings	2 (L.P. & H.P.)	
Lineout Arrangement	Steam turbines/L.P.Compressor/ G'box/H.P.Compressor	
Turbine Normal Speed (r.p.m.)	5,600	
Rotn.Freq. (c/s)	93.3	
	L.P.Casing	H.P.Casing
Compressor Speed (r.p.m.)	5,600	11,300
Rotn.Freq.f_r (c/s)	93.3	188.3
Power Required (H.P.) (design conditions)	4850 (Total 10,170)	5320
Casing ΣMass, m_c (lb)	31,800	17,230
Shaft Mass, m_s (lb)	3,140	849
Ratio m_s/m_c	.099	.049
1st.Flex.Crit.Compressor (r.p.m.)	2400	4170
" " " fc_1 (c/s)	40	69.5
2nd.Flex.Crit.Compressor (r.p.m.)	9800	17,900
" " " " fc_2 (c/s)	163.3	298.3
Ratio fr/fc_1	2.33	2.7
Ratio fc_2/fc_1	4.08	4.29

Appendix VI. Design of Journal Bearings for the Model Rig.

VI.1. Steady Running Conditions.

The dimensions of the journal bearings were intended to give journal eccentricity ratios in the range 0.45 to 0.75 for the anticipated running conditions. The design calculations were based on Ockvirk's (76) "short bearing" theory, the relevant relationships given by that author being:-

$$\text{Capacity Number, } C = \frac{P}{\eta U}\left(\frac{c}{r}\right)^2\left(\frac{d}{b}\right)^2 \qquad \text{(VI.1)}$$

$$\text{and} \qquad C = \frac{\pi \varepsilon}{(1-\varepsilon^2)^2}\sqrt{1 + .622\varepsilon^2} \qquad \text{(VI.2)}$$

The non-dimensional expression for the capacity number (duty parameter) given in eqn. (VI.1) is the Sommerfield variable $S = \frac{P}{\eta U}\left(\frac{c}{r}\right)^2$ multiplied by the diameter-breadth ratio squared, whilst eqn. (VI.2) gives a unique value for ε, in the range $\varepsilon = 0$ to 1, for the given capacity number.

The fixed parameters of the model system were taken to be:-

(a) Shaft diameter, d = 1.25 in.

(b) Bearing load, W, due to rotor weight. For the symmetric 24 in bearing centre configuration. W = 35 lbf for both bearings whilst for the 20 in centre configuration W = 42 lbf at the N.D.E. bearing and 28 lbf at the D.E. bearing.

(c) Maximum shaft speed 6000 r.p.m. (100 c/s)

(d) Lubricating oil, Talpa 20, the makers' viscosity curve being shown in fig (VI.1) (a).

The above conditions were such that for 'conventional' clearances of around .001 inch per inch of diameter the bearing width would have been impractically small ($\simeq$ .050 in) to realise the eccentricity

ratios required. A convenient width for the bearings from a machining viewpoint was around 0.75 in since this enabled the oil supply groove to be formed with comparative ease.

The bearing dimensions finally chosen were width, b = 0.788 in, radial clearance, c = .0075 in. The use of relatively large clearances had the incidental advantages that the bearings were insensitive to temperature effects and to small angular misalignments of the journal.

The calculated characteristics of these bearings are illustrated in figs(VI.1)(b) and (VI.1)(c). A sample calculation is given below for the 20 in bearing centre configuration, the assumed oil temperature being 30°c and the shaft speed 5000 r.p.m. (83.3 c/s). Under these conditions the load per unit width of the bearing is

$$P = \frac{35}{0.788} = 44.4 \text{ lbf/in} \qquad \text{(VI.4)}$$

whilst the tangential velocity of the journal, U , is given by

$$U = rN = \frac{d}{2}.\ N = 0.625 \times 5000 \ \frac{\text{rev}}{\text{min}} \text{ in} \left[\frac{2\pi.\text{rad}}{\text{rev}}\right] \left[\frac{\text{min}}{60\text{s}}\right]$$

$$\text{or} \qquad U = 327.5 \text{ in/s} \qquad \text{(VI.5)}$$

The kinematic viscosity of the oil at 30°C is from fig (VI.1)(a), 140 cS and its specific gravity 0.905. The absolute viscosity is therefore

$$\eta = 140 \times .905 \text{ cP}$$

or in British units

$$\eta = 140 \times .905 \text{ cP} \left[\frac{\text{Reyns}}{6.9\text{x}10^{6}\text{cP}}\right] \left[\frac{\text{lbf.s}}{\text{Reyn.in}^2}\right]$$

$$\text{i.e.} \qquad \eta = 1.835 \times 10^{-5} \ \frac{\text{lbf.s}}{\text{in}^2} \qquad \text{(VI.6)}$$

$$\text{Also } \left(\frac{c}{r}\right)^2 = \left(\frac{.0075}{0.625}\right)^2 = 1.44 \times 10^{-4} \qquad \text{(VI.7)}$$

$$\text{and } \left(\frac{d}{b}\right)^2 = \left(\frac{1.25}{0.788}\right)^2 = 2.51 \qquad \text{(VI.8)}$$

Substituting the values given by eqns. (VI.4) to (VI.8) in eqn.(VI.1), the capacity number C is obtained as

$$C = \frac{P}{\eta U}\left(\frac{c}{r}\right)^2\left(\frac{d}{b}\right) = \frac{44.4 \times 1.44 \times 10^{-4} \times 2.51}{1.835 \times 10^{-5} \times 327.5} \quad \frac{\text{lbf.in}^2\text{.s}}{\text{in.lbf.s.in}}$$

giving $C = 2.68$.

From the curve of fig (VI.I)(c) this is seen to represent an eccentricity ratio, ε, of 0.475.

In the non-symmetric configuration (20 in bearing centres), for the same oil conditions and shaft speed, the capacity numbers at the N.D.E. and D.E. were $\frac{42}{35}$ and $\frac{28}{35}$ of the values obtained for the symmetric configuration. The capacity numbers for these bearing loads are also plotted in fig (VI.I) (b).

VI.2 - Dynamic Characteristics

In Chapter 4 section 4.3 (iii) expressions were derived for the full set of eight journal bearing coefficients in the horizontal and vertical co-ordinate axes x, y. The displacement and velocity coefficients were of the form $k = \frac{W}{c}.k'$, $b = \frac{W}{c\Omega}.b'$ respectively, k', b' being non-dimensional functions of the attitude angle ψ. The values of the non-dimensional coefficients $k'xx$, $k'yy$ ....., $b'xx$, $b'yy$ ..... are compared in figs VI.2 and VI.3 with similar coefficients given by Smith (37) for very wide ($\ell/d = \infty$) and very narrow ($\ell/d = 0$) bearings. It is not clear from Smith's paper exactly how he obtained the coefficients but, apparently, he based his calculations for the narrow bearings on the original theoretical expressions given by Ockvirk (76) and for the wide bearings on the work of Cameron and Wood.

The differences between Smith's $\ell/d = 0$ curves and those based on the analysis of Chapter 4 are presumably due to the assumptions made in the derivation of the latter. These assumptions, originally proposed by Morrison (43), were that:-

(a) the journal deflection path was circular

i.e. $\varepsilon = \cos \psi$ (VI.9) and hence $\frac{\partial \psi}{\partial \varepsilon} = \frac{-1}{\sin \psi}$ (VI.10.)

and

(b) the variation of load with eccentricity, obtained by Morrison by replotting Ockvirk's experimental results, was given by

$$\frac{\partial W}{\partial \varepsilon} = 4.6\, W \qquad \text{(VI.11)}$$

For comparison it may be noted that the 'exact' expression given by Ockvirk for the journal deflection path was

$$\tan \psi = \frac{\pi}{4} \left(\frac{1 - \varepsilon^2}{\varepsilon} \right)^{\frac{1}{2}} \qquad \text{(VI.12)}$$

so that

$$\frac{\partial \psi}{\partial \varepsilon} = - \frac{4\pi}{\varepsilon^2 (16 - \pi^2) + \pi^2} \qquad \text{(VI.13)}$$

Similarly partial differentation of Ockvirk's analytic expression for the capacity number (eqn. (VI.2) above) gives, after some manipulation

$$\frac{\partial W}{\partial \varepsilon} = \frac{1 + 4.244\, \varepsilon^2 + 1.244\, \varepsilon^4}{(1 - \varepsilon^2)(1 + .622\, \varepsilon^2)} \qquad \text{(VI.14)}$$

By comparing the values of $\frac{\partial \psi}{\partial \varepsilon}$ given by eqns. (VI.10) and (VI.13) it has been found that Morrison's assumption is within 20% of the exact value in the range $\varepsilon = 0.2$ to $\varepsilon = 0.65$. Outside this range the two expressions diverge rapidly so that at $\varepsilon = 1.0$, $\frac{\partial \psi}{\partial \varepsilon} = \infty$ according to Morrison's assumption, and 0.786 according to Ockvirk.

Similarly it has been found that Morrison's $\frac{\partial W}{\partial \varepsilon}$ (eqn.VI.11) is within about 20% of that given by eqn. (VI.14) up to $\varepsilon = 0.65$. Thus

although the effect of differences in the values of $\frac{\partial \phi'}{\partial \varepsilon}$ and $\frac{\partial \omega}{\partial \varepsilon}$ influence the resulting coefficients in x, y axes in a complicated manner, it might be expected that Smith's coefficients and those obtained in the present analysis would be in closest agreement in the range ε = 0.2 to 0.65. This is in fact the case as can be seen from figs (VI.2) and (VI.3).

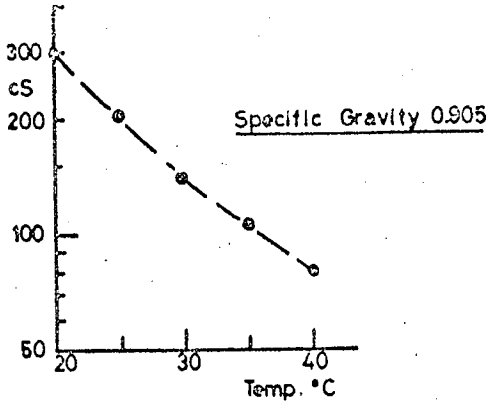

FIG. VI. 1 (a) KINEMATIC VISCOSITY OF LUBRICATING OIL USED (TALPA 20)

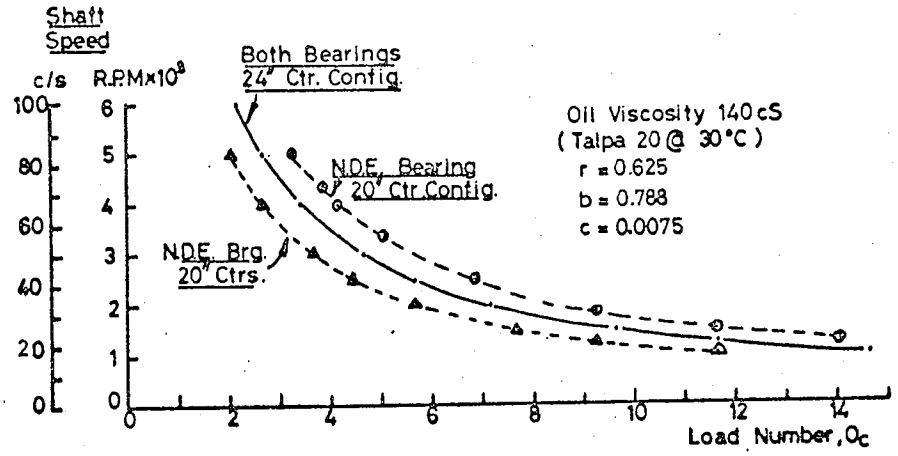

FIG. VI. 1. (b). BEARING LOAD NUMBERS.

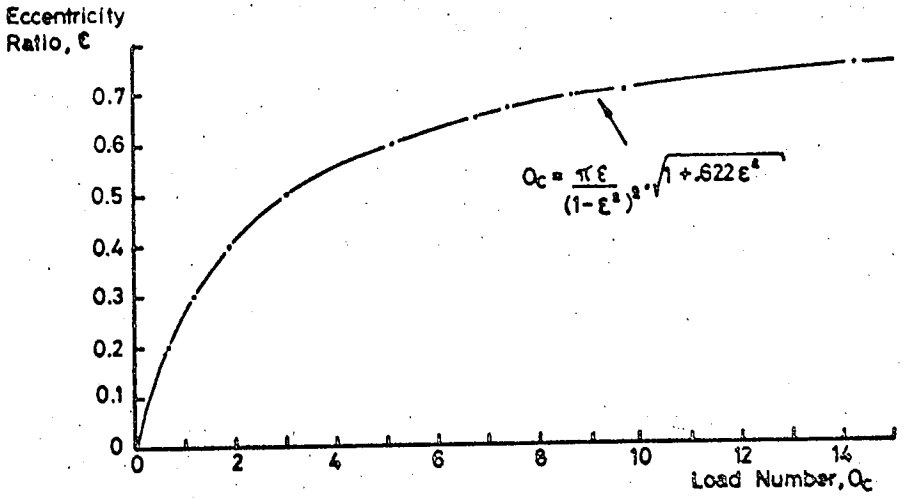

FIG. VI. 1 (c) JOURNAL ECCENTRICITY ACCORDING TO OCKVIRK'S 'SHORT BEARING' THEORY.

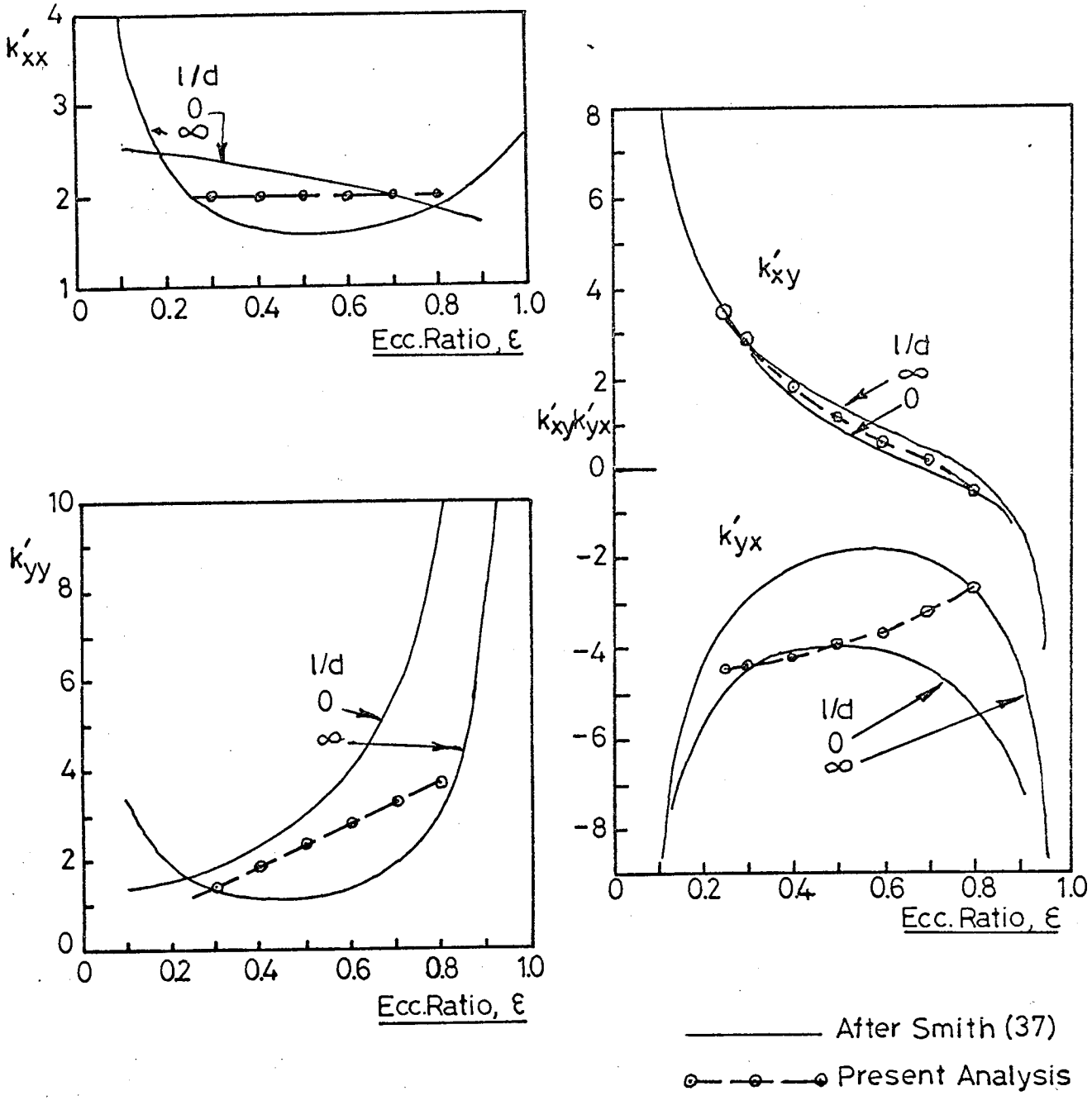

FIG.VI.2 NON-DIMENSIONAL JOURNAL BEARING DISPLACEMENT COEFFICIENTS.

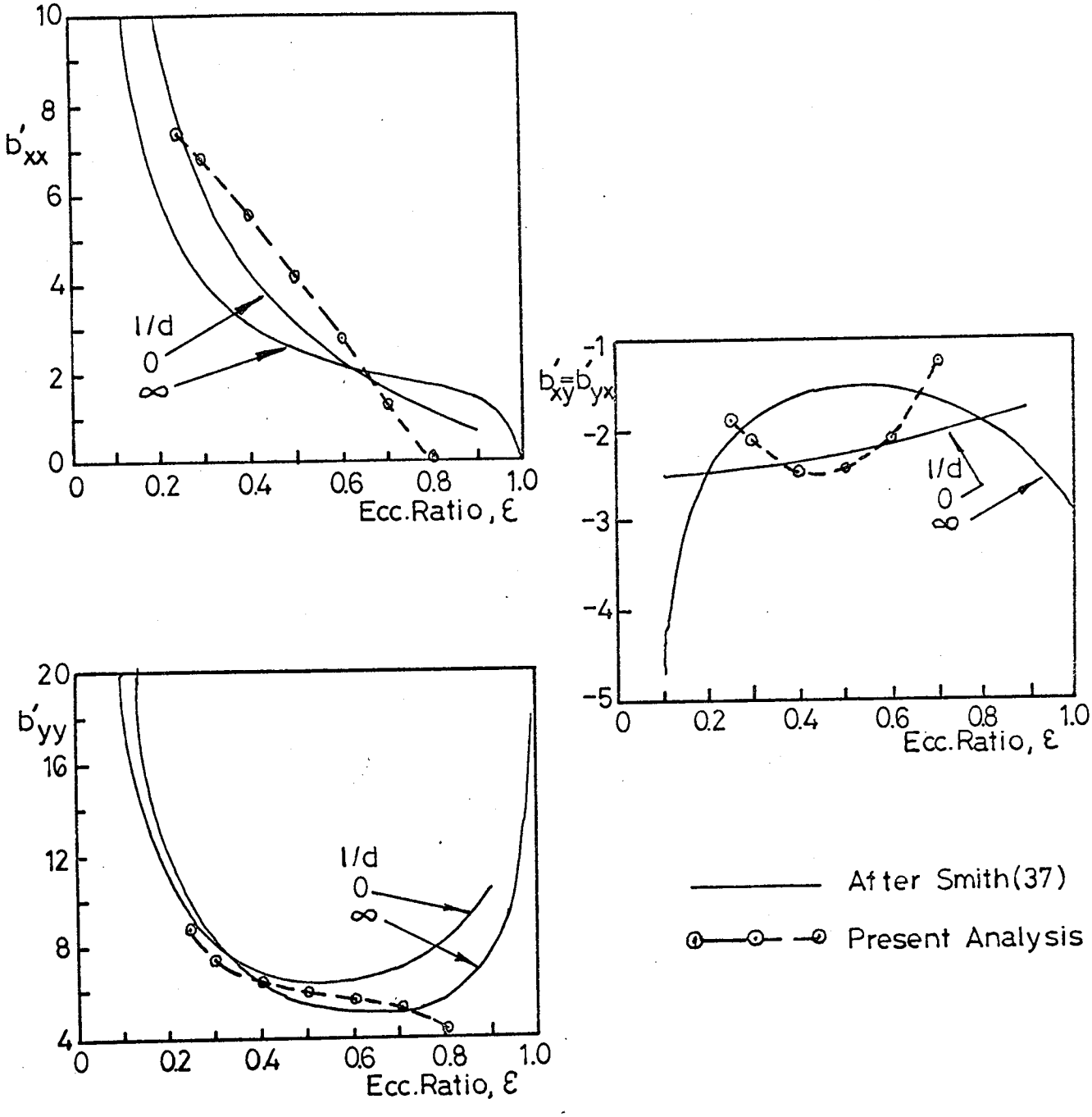

FIG. VI.3. NON-DIMENSIONAL JOURNAL BEARING VELOCITY COEFFICENTS.

APPENDIX VII - BIBLIOGRAPHY.

1. Rankine, W.J. 'On the Centrifugal Force of Rotating Shafts'. The Engineer, Vol. 27, 1869 p.249.

2. Greenhill, A.G. 'On the Stability of a Rotating Shaft Subject to Thrust and Twisting'. Proc. I.Mech.Eng. April 1883. p.182.

3. Dunkerley, S. 'On the Whirling and Vibration of Shafts'. Phil. Trans.A. June 1894. p.279.

4. Chree, C. 'The Whirling and Transverse Vibrations of Rotating Shafts'. Phil. Mag. Vol.7, No.41. 1904 p.504.

5. Jeffcott, H.H. 'The Lateral Vibration of Loaded Shafts in the Neighbourhood of a Whirling speed'. Phil. Mag. Vol.37. March 1919. p.304.

6. Stodola, A. 'Steam and Gas Turbines'. McGraw-Hill 1927.

7. Kimball, A.L. & Hull, E.H. 'Vibration Phenomena of a Loaded Unbalanced Shaft while passing through its Critical Speed'. Trans. A.S.M.E. Vol.47. 1925 p.673

8. Morris, J. 'The Strength of Shafts in Vibration'. Crosby Lockwood, London 1929.

9. Morris, J. 'The Escalator Method in Engineering Vibration Problems'. Chapman & Hall. London 1947.

10. Robertson, D. 'The Whirling of Shafts'. The Engineer, Vol. 158. No. 228 1934 p.216

11. Newkirk, B.L. 'Shaft Whipping'. Gen. Elect. Review 1924 Vol.27 p.169

12. Kimball, A.L. 'Internal Friction Theory of Shaft Whirling'. Gen. Elect. Review 1924 Vol.27 p.244.

13. Newkirk, B.L. & Taylor, H.D. 'Shaft Whipping due to Oil Action in Journal Bearings'. Gen. Elect. Review 1925 Vol.28 p.559.

14. Tang, J.M. & Trumpler, P.R. 'Dynamics of Synchronous Precessing Turborotor with particular reference to Balancing'. Trans. A.S.M.E. Vol.86 1964 p.115.

15. Alford, J.S. 'Protecting Turbomachinery from Self-excited Rotor Whirl'. Trans.A.S.M.E. Jrl. Eng. Power. 1965 p.333.

16. Pisarenko, G.S. 'Dissipation of Energy during Mechanical Vibrations'. Vol.1, 2. Akademiya Nank Ukrainskoi 1962.

17. Dimentberg, F.M. 'Flexural Vibration of Rotating Shafts' Butterworth, London 1961.

18. Tondl, A. 'Some Problems of Rotor Dynamics'. Chapman & Hall 1965.

19. Smith, D.M. 'Vibration in Turbo-machinery'. Proc.Inst.Mech.Eng. Vol. 180 p.1.

20. Smith, D.M. 'The Motion of a Rotor Carried by a Flexible Shaft in Flexible Bearings'. Proc.Roy.Soc.A., 1933 Vol.1 142 p.92.

21. Bishop R.E.D.,& Mahalingam, S. 'Some Experiments in the Vibration of a Rotating Shaft'. Proc.Roy.Soc.Ser.A., 1966 p.537.

22. Lewis, F.M. 'Vibration During Acceleration through a Critical Speed'. Trans. A.S.M.E. Vol.54 1932 p.253.

23. Fernlund, I. 'Running through the Critical Speed of a Rotor'. Chalmers tek Högsk 1963 No.277.

24. Marples, V. 'Transition of a Rotating Shaft through a Critical Speed'. Proc.Inst.Mech.Eng. Vol.180 1966 p.8.

25. Downham, E. 'Theory of Shaft Whirling'. The Engineer, Vol.204 1957 Oct.11th,18th,25th, Nov.1st, 8th.

26. Bishop, R.E.D. 'The Receptances of Uniform and Non-uniform Rotating Shafts'. Jrl.Mech.Eng.Sci. Vol.1. 1959 p.78.

27. Prohl, M.A. 'A General Method for Calculating Critical Speeds of Flexible Rotors'. Jrl.App.Mech. Sept. 1945 p.A-142.

28. Uhrig, R. 'The Transfer Matrix Method sees as One Method of Structural Analysis Amongst Others'.

29. Pastel, E.C. & Leckie, F.A. 'Matrix Methods in Elastomechanics'. McGraw Hill. N.Y. 1963.

30. Fuhrke, H. 'Delta Matrix Method'. Ing. Archiv. Vol.25 No.27.

31. Hertz, H. 'The Contact of Solid Elastic Bodies' Leipzig 1895.

32. Longman, E.G. 'Movement in a Ball Bearing' Machine Design Eng. April 1965.

33. Longman, E.G. Ibid, May 1965.

34. Shimizu, H. & Tamura, H. 'Vibration of Rotor Based on Ball Bearing'. Bull. J.S.M.E. Vol.9, No.35 p.524.

35. Anon Bulletin 408. Illinois Engineering Experiment Station. 1965.

36. Yamamoto, T. 'On Critical Speeds of a Shaft Supported by a Ball Bearing'. Jrl. App.Mech. June 1959 p.199.

37. Smith, D.M. 'Dynamic Characteristics of Turbine Journal Bearings'. Trans.A.S.M.E. Lub.& Wear Conv. 1963 Paper 8.

38. Hummell, C. 'Kritische Drehzahlen als Folge der Nachgiebigkeit des Schmiermittels in Lager'. F.V.D.I. Vol. 287. No.1. 1926.

39. Hagg, A.C. & Sankey, G.O. 'Some Synamic Properties of Oil-Film Journal Bearings with Reference to the Unbalance Vibration of Rotors'. Jrl. App.Mech. June 1956. p.304.

40. Barwell, F.T. 'Lubrication of Bearings'. Butterworth, London 1956.

41. Sternlicht, B. 'Elastic and Damping Properties of Cylindrical Journal Bearings'. Trans.A.S.M.E. Vol.81, 1959 p.10.

42. Holmes, R. 'The Vibrations of a Rigid Shaft in Short Sleeve Bearings'. J.Mech.Eng.Sci. Vol.2 1960 p.337.

43. Morrison, D. 'Influence of Plain Journal Bearings on the Whirling Action of an Elastic Rotor'. Proc.Inst.Mech.Eng. Vol. 176 1962 p.542.

44. Smith, D.M. 'Journal Bearing Dynamic Characteristics - Effect of Inertia of Lubricant'. Proc.Inst.Mech.Eng. Vol.179 1965 p.37.

45. Morton, P. 'On the Dynamics of Large Turbo-Generator Rotors'. Proc.Inst.Mech.Eng. 1966 Vol.180 p.295.

46. Morton, P. 'The Influence of Coupled Asymmetric Bearings on the Motion of a Massive Flexible Rotor'. Proc.Inst.Mech.Eng. 1968 Vol.182.

47. Hagg, A.C. 'The Influence of Oil-Film Journal Bearings on the Stability of Rotating Machines'. Jrl. App. Mech. Sept. 1946.

48. Hori, Y. 'A theory of Oil Whip'. Jrl.App.Mech. June 1959, p.189.

49. Someya, T. 'Stability of a Balanced Shaft Running in Cylindrical Journal Bearings'. Proc. Inst.Mech.Eng. Vol.178 1964 p.196.

50. Huggins, N.J. 'Non-Linear Modes of Vibration of a Rigid Rotor in Short Journal Bearings'. Proc. Inst.Mech.Eng. Vol.178 Pt.3N. 1964.

51. Flint, I.J. — 'Plant Aspects of Turbine Generator Foundations'. Proc.Inst.Mech.Eng.Paper 1. Foundations for Turbo-machinery. May 1967 (Joint meeting with Inst.Civil.Eng.)

52. Haupt, L. & Probst, P.H. — 'Civil Engineering and Vibrational Aspects of Steam Turbine Generator Foundations in Germany'. Ibid. Paper 2.

53. Fitzherbert, W.A. & Barnett, J.H. — 'Causes of Movement in Reinforced Concrete Turbo-Blocks and Developments in Turbo-Block Design and Construction'. Ibid. Paper 3.

54. Major, A. — 'Foundations for Machines and Turbines'. Collet's London 1962.

55. Vesselowsky, S. — 'Experimental and Theoretical Investigation of a Turbine Foundation'. Jrl. App.Mech. June 1940 PA-63.

56. Hull, E.H. — 'The Effect of Foundation Stiffness on the Resonant Frequencies of Rotating Machines'. Jrl. App.Mech.Sept. 1941. PA-121.

57. Pust, L. — 'Determining the Resonance Frequencies of Forced Vibrations of Turbogenerators with Foundations'. Exptl. Mech. June 1967 p.265.

58. Weber, H. — 'The Combined Vibration Characteristics of Shaft and Foundations in Turbines'. V.D.I. Berichte. No.48 1961 p.55.

59. Schaff, K. & Krieb, K.H. — 'Vibration of Turbogenerators on Steel Bedplates'. V.D.I. Zeits. Vol.100, Nos.36 1958 p.1739.

60. Eastwood, W. — 'Vibrations in Foundations'. The Structural Engineer. March 1963, p.82.

61. Crockett J.H.A. & Hammond R.E.E. — 'The Dynamic Principles of Machine Foundations and Ground'. Proc.Inst.Mech.Eng. Vol.160 1949 p.512.

62. Jones, R. Lister, N.W. & Thrower, E.N. — 'The Dynamic Behaviour of Soils and Foundations'. Symp.Inst.Civil.Eng. Vibrations in Civil Engineering, 1965. Ed.B.O.Skipp.

63. Rathbone, T.C. — 'Vibration Tolerance'. Power Plant Engineering, 1939, Vol.43, p.721.

64. Reiher, H.J. & Meister, F.J. — 'Human Sensitivity to Vibrations'. Forsch, auf dem Geb.des Ing. Vol.2 1931 p.381.

65. Yates, H.G. — 'Vibration Diagnosis in Marine Geared Turbines'. Trans. North East Coast Inst. Eng. Shipbuilders. Vol. 65, 1949 p.225.

66. V.D.I. 2056 — 'Criterion for Evaluation of Mechanical Vibrations of Machines'. October 1957.

67. Plunkett, R. (Ed) Colloquium on Mechanical Impedance Methods'. A.S.M.E. 1958.

68. Caruso, W.J. 'Prediction of Critical Speeds of Steam Turbines by Dynamic Stiffness Method'. Paper 12, p.137 Ibid.

69. Firestone,F.A. 'Twixt Earth and Sky with Rod and Tube; The Mobility and Classical Impedance Analogies'. Jrl. Acous.Soc.Am. Vol.28 1956 p.1117.

70. Harris, C.M. & Crede, C.E. (Eds.) Chapter 10. Shock and Vibration Handbook. McGraw Hill 1960.

71. Church, A.H. 'Mobility and Impedance Concepts'. Machine Design 1960, Feb 19. p.130 and Mar.31. p.117.

72. Mahalingham, S. 'Displacement Excitation of Vibrating Systems' Jrl. Mech.Eng. Sci. Vol.10 No.1 1968 p.74.

73. Salter, J.P. Environment al Engineering Quarterly. No.14. May 1965

74. Grant, G.L. Paper 9. 'Vibration in Civil Engineering' I.C.E. Symposium (Ed. B.O.Skipp.) 1965.

75. Couchman,A.A.J. 'Axial Shaft Vibration in Large Turbine-Powered Merchant Ships'. I.Mar.E. Vol.37. pt.3 1965.

76. Ockvirk, F.W. 'Short-Bearing Approximation for Full Journal Bearings'. N.A.C.A. Tech.Note 2808, 1952.

77. Lindley,A.L.G. & Bishop,R.E.D. 'Some Recent Research on the Balancing of Large Flexible Rotors'. Proc.I.Mech.Eng. Vol.177 No.30 p.811. 1963.

78. Moore, L.S. & Dodd, E.G. 'Mass Balancing of Large Flexible Rotors'. G.E.C. Jrl. Vol.31. No.2.p.74 1964.

79. Kennedy, C.C. & Pancu, C.D.P. 'The Use of Vectors in Vibration Measurement and Analysis'. Jrl. Aero. Sci. 1947 Vol.14 p.603.

80. Pendered, J.W. & Bishop,R.E.D. 'A Critical Introduction to Some Industrial Resonance Testing Techniques'. Jrl. Mech.Eng.Sci. 1963 Vol.15 p.345.

81. Jacobsen, L.S. & Ayre R.S. 'Engineering Vibrations', McGraw Hill. 1958.

82. Weber, E. 'Linear Transient Analysis' John Wiley & Sons, New York 1956.

83. Mindlin, R.D. Bell System Technical Journal. Vol 24 1945.

84. Crandall, S.H. Vol.2 Random Vibration. John Wiley & Sons, New York 1963.